UNIVERSITÀ DEGLI STUDI DI MILANO

DOCTORATE SCHOOL OF CHEMICAL SCIENCES AND TECHNOLOGIES

DEPARTMENT OF CHEMISTRY

PHD COURSE IN CHEMICAL SCIENCES, XXV CYCLE

SYNTHESIS AND BIOLOGICAL EVALUATION OF POTENT INTEGRIN LIGANDS CONTAINING A DIKETOPIPERAZINE SCAFFOLD, AND OF THEIR CONJUGATES WITH CYTOTOXIC AGENTS

RAFFAELE COLOMBO

R08771

Tutor: Prof. Cesare GENNARI
Co-Tutor: Prof. Umberto PIARULLI (Università dell'Insubria)

Coordinator: Prof. Emanuela LICANDRO

A.Y. 2011/2012

The present work was led by:	Prof. C. Gennari and Prof. U. Piarulli	
Doctoral Final Oral Examination:	January, 11th 2013	
Examination Committee:	Chairperson:	Prof. F. Cozzi
	Second Member:	Prof. L. Colombo
	Third Member:	Prof. L. Panza

The work herein described was performed at the University of Milan at the Department of Chemistry in the period from January 2010 to December 2012 under the supervision of Prof. Cesare Gennari and Prof. Umberto Piarulli, whom I sincerely wish to thank.

"I never teach my pupils. I only attempt to provide the conditions in which they can learn"
A. Einstein

Thanks to those who have provided me the best learning opportunities.

TABLE OF CONTENTS

CHAPTER 1

SYNTHESIS AND CONFORMATIONAL ANALYSIS OF RGD-PEPTIDOMIMETICS CONTAINING A BIFUNCTIONAL DIKETOPIPERAZINE SCAFFOLD, AS INTEGRIN LIGANDS

1 - Targeting Integrins

Integrins are the major family of adhesion receptors known in the kingdom Animalia, being involved in cell adhesion to extracellular matrix proteins and also playing important roles in cell-cell adhesion. In addition to mediating cell adhesion, integrins make transmembrane connections to the cytoskeleton and activate many intracellular signaling pathways. Since the recognition of the integrin receptor family around 20 years ago,[1] they have become the best-understood cell adhesion receptors. Integrins and their ligands play key roles in the pathogenesis of inflammatory diseases, leukocyte traffic, aggregation, tumor progression as well as osteoporosis and macular degeneration. The role of integrins in pathological conditions makes them attractive as pharmacological targets.[2]

Research in the last two decades has been directed to the discovery and the development of integrin antagonists for clinical applications.[3] The early discovery of the structural basis of the recognition between integrins and their natural ligands by means of short amino acid sequences,[4] together with outstanding crystallographic, electron microscopy, and computational analyses[5,6] on selected integrin subfamilies provided a breakthrough for the rational design of a wide variety of class-selective or promiscuous integrin inhibitors.

1.1 - *Integrins: family, function, structure*

Integrins are heterodimeric membrane glycoproteins comprising non-covalently associated α- and β-subunits, mediating dynamic linkages between extracellular adhesion molecules and the intracellular actin cytoskeleton. They are expressed by all multicellular animals, but their diversity varies widely among species; for example, 18 α and 8 β subunit genes are present in mammals, encoding for 25 different heterodimers, whereas the Drosophila and Caenorhabditis genomes encode only five and two integrin α and β subunits, respectively.

Each integrin subunit consists of an extracellular domain, a single transmembrane region, and a short cytoplasmic region (~30–40 amino acids). Figure 1.1 depicts the mammalian subunits and their αβ associations; 8 β subunits can assort with 18 α subunits to form 24 distinct integrins.[7]

Figure 1.1. Integrin family

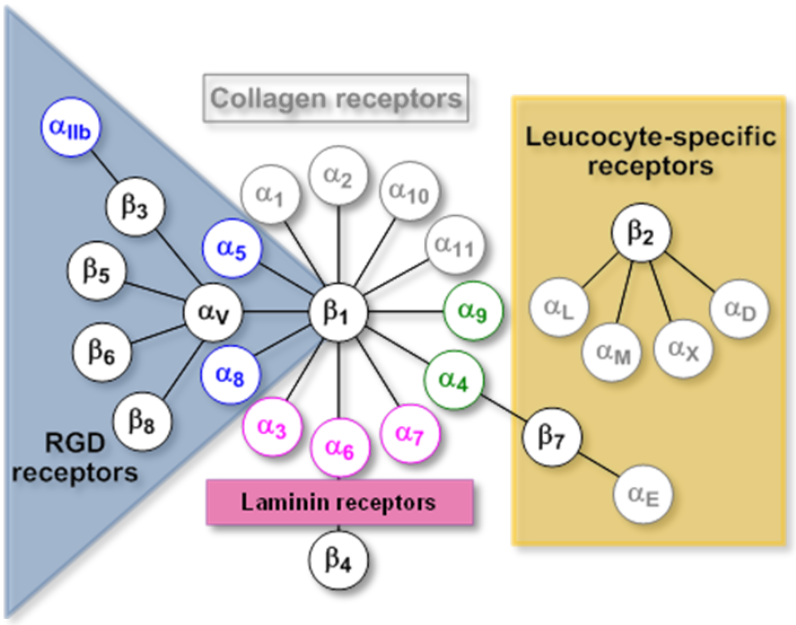

The N-terminus of the α-chain consists of a β-propeller domain that is formed by seven repeats of 60 amino acids each.[8] The β-propeller domain is linked to the transmembrane domain by three regions that have been named the Thigh, Calf-1, and Calf-2 domains (Figure 1.2 a). In addition, a highly flexible region is present between the Thigh and Calf-1 domains.[5] Half of all α-chains have an additional 200-amino acid inserted domain between repeats two and three of the β- propeller (the I-domain, Figure 1.2 a).[9] The I-domain functions as the major ligand-binding site in those integrins where it is present, whereas the β-propeller serves as the ligand binding in integrins without I-domains.[10] Cytoplasmic tail domains of individual α-subunits are well-conserved across species boundaries.[11]

The N-terminal region of the β-subunit consists of a cysteine-rich region termed the plexin-semaphorin-integrin (PSI) domain. C-terminal to this domain is an evolutionarily conserved I-like domain flanked on either side by immunoglobulin folds called hybrid domains. The membrane proximal region of the α-subunit contains four EGF-like repeats. The α-subunit also has a flexible "knee" region, which is formed by the hybrid domain and the first two EGF-like repeats (Figure 1.2 b).[10] The intracellular regions of the β-subunits are more conserved between subunits than are the α-subunit cytoplasmic tails.[12] These β-chain cytoplasmic tails play significant roles in regulating integrin activity.[5b]

Figure 1.2. Integrin structure[a]

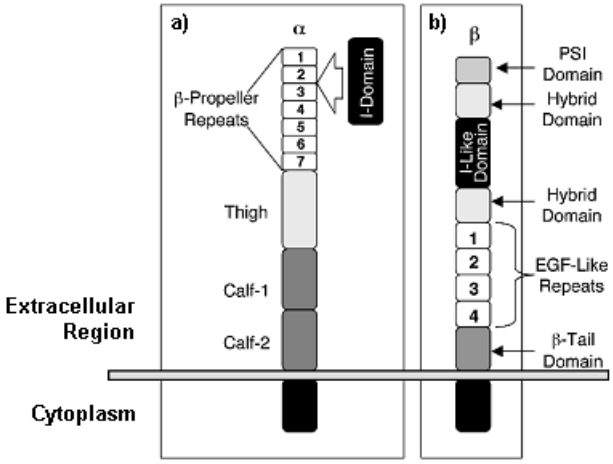

[a] **a**) Primary structure of integrin α-subunits. Half of the α-subunits also have an I-domain inserted between β-propeller repeats 2 and 3; **b**) Primary structure of integrin β-subunits.

Each α-chain combines with a β-chain to form a unique heterodimer with selectivity for ECM proteins, cell surface molecules, plasma proteins, or microorganisms.[13] Integrins bind to their ligands in a divalent cation-dependent fashion.[14] Although some integrins recognize primarily a single ECM protein ligand (e.g., $\alpha_5\beta_1$ recognizes primarily fibronectin), others can bind several ligands (e.g., integrin $\alpha_v\beta_3$ binds vitronectin, fibronectin, fibrinogen, denatured or proteolyzed collagen, and other matrix proteins). Many integrins recognize the tripeptide Arg–Gly–Asp (RGD) (e.g. $\alpha_v\beta_3$, $\alpha_5\beta_1$, $\alpha_{IIb}\beta_3$, $\alpha_v\beta_6$, and $\alpha_3\beta_1$), but sequences flanking the RGD peptide are also important for selectivity.[13a,b] Other integrins recognize alternative short peptide sequences (e.g., integrin $\alpha_4\beta_1$ recognizes Glu lle Leu Asp Val [EILDV] and Arg Glu Asp Val [REDV] in alternatively spliced CS-1 fibronectin and $\alpha_{IIb}\beta_3$ binds KQAGDV in the fibrinogen γ chain).[15] In addition, some integrins can also bind cell surface receptors to induce cell–cell adhesion.[13b,c]

The ligands bound by common integrins and integrin clinical targets are shown in Table 1.1.[16] Integrins are not constitutively active, but rather exist in multiple activation states (Figure 1.3).[17] Integrin activation status is regulated by the delicate balance in a bidirectional signaling mechanism which drives reversible changes in integrin conformation and affinity for their ligands. Both extra- and intracellular stimuli are allowed to regulate activation.[7,18]

Table 1.1. Integrin subfamilies cluster major therapeutic indications and main ligands

Integrin class	*Clinically targeted in?*	*Main ligands*[a]
α4- Family		
α4β1	MS, autoimmune, Crohn's, IBD	VCAM-1, FN
α4β7	MS, autoimmune, arthritis	MAd-CAM-1
α9β1	Cancer	VCAM-1, Opn, VEGF-C,-D
Leukocyte cell adhesion		
αLβ2	Inflammation, psoriasis, stroke, ischemia, fibrosis	ICAM-1,-2,-3
αMβ2	Inflammation, autoimmune	iC3b, Fbg
αXβ2	Inflammation	iC3b, Fbg
αDβ2	Inflammation	ICAM-3, VCAM-1
αEβ7	Inflammation	E-cadherin
RGD-binding		
gpIIbIIIa	Thrombosis, stroke, myocardial ischemia	Fbg, vWf
α5β1	Cancer, AMD	FN
α8β1	None	Npn, FN, VN
αnβ1	Cancer	VN, FN
αnβ3	Cancer, osteoporosis	VN, Opn, vWf, FN, Fbg[b]
αnβ5	Cancer	VN
αnβ6	Fibrosis, transplant rejection, cancer	FN, TGF-b1,-3
αnβ8	Cancer	FN, TGF-b1,-3
I domain: collagen binding		
α1β1	Fibrosis, cancer	Col
α2β1	Fibrosis, cancer	Col
α10β1, α11β1	None	Col
LN binding		
α3β1	None	LN-5
α6β1, α7β1	None	LN-1, -2
α6β4	None	LN-2, -4, -5

[a]Abbreviations: Col, collagens; Fbg, fibrinogen; FN, Fibronectin; LN, laminin; Npn, nephronectin; Opn, osteopontin; VN, vitronectin; vWF, von Willebrand factor.
[b]Among many other ligands.

Figure 1.3. Representation of integrin activation states

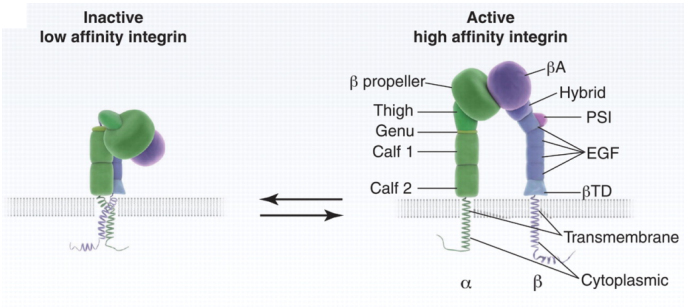

High affinity binding of integrins to ligands is promted in response to intracellular signaling events converging on the cytoplasmic domain that alter the tertiary and quaternary structure of the extracellular region, making the integrin ligand-competent (inside-out signaling).

Extracellular factors that influence integrin activation are ligand binding, divalent cation concentration, chemokine signaling and mechanical stress. Integrins transmit signals to the cell interior, which regulate organization of the cytoskeleton, activate kinase signaling cascades, and modulate the cell cycle and gene expression (outside-in signaling). Through this mechanism, integrins behave as mechanochemical transducers, orchestrating a synergic cross-talk with other extracellular matrix constituents and providing anchorage for endothelial cells.

The integrin tails serve as a site for the docking of various kinases and related adaptor proteins that comprise focal adhesions. Signals emanating from focal adhesions have been shown to promote survival, differentiation and proliferation.[19] In the absence of integrin ligation, these processes are abrogated, and therefore pharmacological inhibition of integrin ligation is of great interest for the therapy of numerous diseases resulting from aberrant integrin mediated signaling.

Integrins are transducing information both into and out of the cell to promote cell adhesion, spreading and motility. Disruption of focal adhesions prevents integrin-mediated cell adhesion and impairs cell motility and migration. Prolonged integrin inhibition in adhesion-dependent cells results in anoikis, apoptotic cell death due to ECM deprivation.[20]

1.2 - *Role in Angiogenesis*

Angiogenesis is the process whereby new vessels form from pre-existing vessels. The growth of new blood vessels promotes embryonic development, wound healing, the female reproductive cycle, and also plays a key role in the pathological development of solid tumors, hemangiomas, diabetic retinopathy, age-related macular degeneration, psoriasis, gingivitis, rheumatoid arthritis, and possibly osteoarthritis and inflammatory bowel disease.[21]

Several cell types within tumors, including tumor cells, monocytes, and fibroblasts, secrete growth factors, such as VEGF, that induce blood vessel growth into tumors (Figure 1.4).[22]

Studies have shown that angiogenesis plays a major role in tumor growth and that inhibiting angiogenesis can inhibit tumor progression and metastasis. Although growth factors and their receptors play key roles in angiogenic sprouting, adhesion to the ECM also regulates angiogenesis.

Formation of new vasculature requires endothelial cell attachment and migration on ECM proteins. One ECM protein, fibronectin, is associated with vascular proliferation.[23] As integrins are critical for the cell to bind ECM, many integrins play crucial roles in regulating vascular growth, both during embryonic development and in various pathologies. Proliferating endothelial cells express several integrins that are not expressed on quiescent blood vessels.

Recent studies suggest that inhibition of both $\alpha_v\beta_3$ and $\alpha_5\beta_1$ may be required for optimal effects on angiogenesis.[24]

Figure 1.4. Angiogenesis

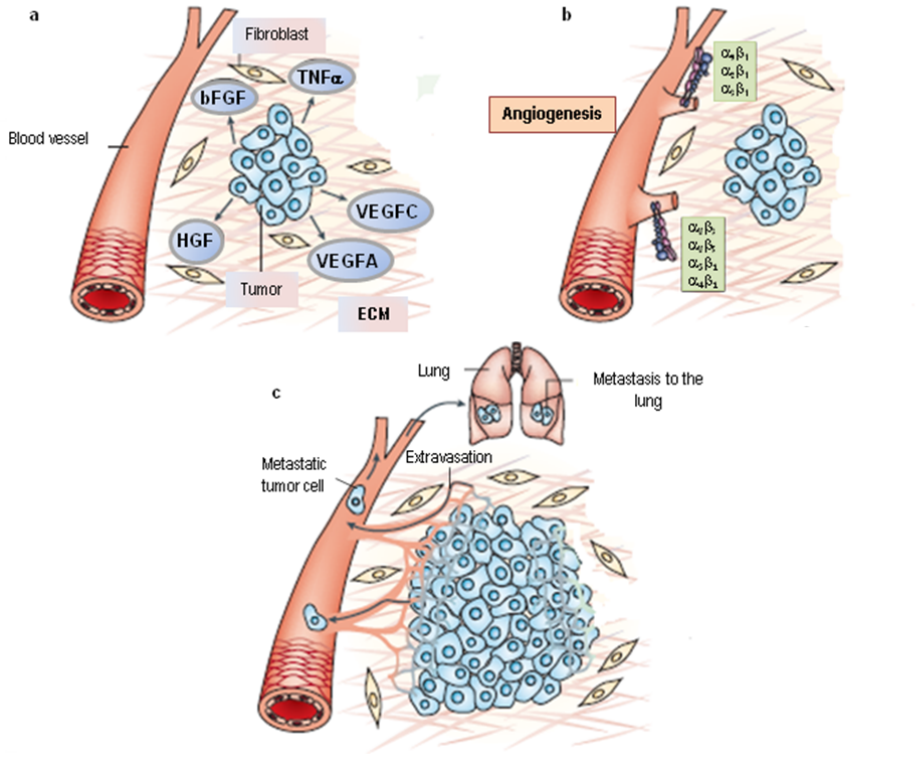

a) secretion of growth factors and Chemokines from tumor cells in vicinity of already existing blood vessels;
b) activation or expression upregulation of integrins such as $\alpha_1\beta_1$, $\alpha_2\beta_1$, $\alpha_4\beta_1$, $\alpha_5\beta_1$ and $\alpha_V\beta_3$ on blood vessels;
c) integrins promoting endothelial cell migration and survival during invasion of tumour tissue. New vessel sprouts are produced promoting tumour growth and providing a way to metastasis to local and distant sites, such as lung.

1.2.1 - *Integrins $\alpha_{IIb}\beta_3$*

$\alpha_{IIb}\beta_3$ integrin (GPIIa/IIIb) is highly expressed on the surface of platelets,[25] comprising approximately 80% of the total surface proteins found on platelets. The final common pathway in blood coagulation involves the engagement of this integrin induced by platelet activation. Under normal conditions integrin $\alpha_{IIb}\beta_3$ is maintained in the inactivated state. Soluble factors in the blood such as thrombin, bind their respective platelet receptors to activate inside-out signaling pathways that cause conformational changes in $\alpha_{IIb}\beta_3$ integrin.[25] Changes in conformation lead to increases in receptor affinity and avidity, which promote platelet aggregation and clot formation through increased cell-to-cell contacts and cell-matrix contacts. Aberrant platelet aggregation or thrombosis is central to the

pathophysiology of multiple Acute Coronary Syndromes (ACS), unstable angina, ischemic stroke and sickle cell anemia. Inhibition of $\alpha_{IIb}\beta_3$ prevents platelet aggregation and therefore has shown efficacy in the prevention of thrombosis for the treatment of ACS. Some $\alpha_{IIb}\beta_3$ integrin targeted drugs have already been approved so far.

The complete ectodomain structure of integrin $\alpha_{IIb}\beta_3$ was determined,[26] thus living information about its binding site, better understanding its binding mode and conformation (Figure 1.5). The binding mode of RGD-based $\alpha_{IIb}\beta_3$ antagonists was established through mutagenesis experiments[27] and crystallographic analysis of the platelet fibrinogen receptor.[28]

Figure 1.5. Crystal structure of the extracellular segment of integrin $\alpha_{IIb}\beta_3$.

1.2.2 - *Integrins $\alpha_v\beta_3$ and $\alpha_v\beta_5$*

Integrin $\alpha_v\beta_3$ is expressed on angiogenic blood vessels but not on resting vessels.[29] Inhibitors of $\alpha_v\beta_3$ antibody block angiogenesis in a variety of animal models. A key role of $\alpha_v\beta_3$ in vasculogenesis and angiogenesis has been outlined. Peptide and antibody antagonists of $\alpha_v\beta_3$ also block tumor angiogenesis and growth. Further analysis showed tumor regression related to apoptosis in the vasculature, induced by these antagonists.[30]

Different members of the integrin α_v subfamily transduce angiogenic signals by different growth factors. *In vivo* angiogenesis assays showed that bFGF or TNF-α depend on $\alpha_v\beta_3$ to initiate angiogenesis, whereas $\alpha_v\beta_5$ is required for TGF-α- and VEGF-mediated angiogenesis.[31] These data, taken together, have established a role for $\alpha_v\beta_3$ and $\alpha_v\beta_3$ integrins in angiogenesis and as important therapeutic targets.

One study showed that animals lacking β_3 or β_3 and β_5 subunits displayed increased tumor angiogenesis.[32] This led to the controversial conclusion that $\alpha_v\beta_3/\alpha_v\beta_5$ integrins might actually be involved in suppressing angiogenesis. However, it is likely that the apoptotic mechanism, which is generally induced by unligated integrins and controls tumor vascular growth, is responsible for the increased vascularization in β_3 - and β_5 -deficient tumors.[16,33]

The complete crystal structure of $\alpha_v\beta_3$ integrin ectodomain including an $\alpha\beta$ transmembrane fragment has been very recently determined.[34] The earlier determination of the crystal structure of the ectodomain of $\alpha_v\beta_3$ (ΔTM- $\alpha_v\beta_3$, Figure 1.6a) in the absence and presence of a prototypical RGD ligand (Cilengitide, Figure 1.6b), already revealed the modular nature of integrins and pivotal information on its divalent cation–mediated binding interactions with extracellular ligands.

Figure 1.6. Crystal structures of $\alpha_V\beta_3$ integrin[a]

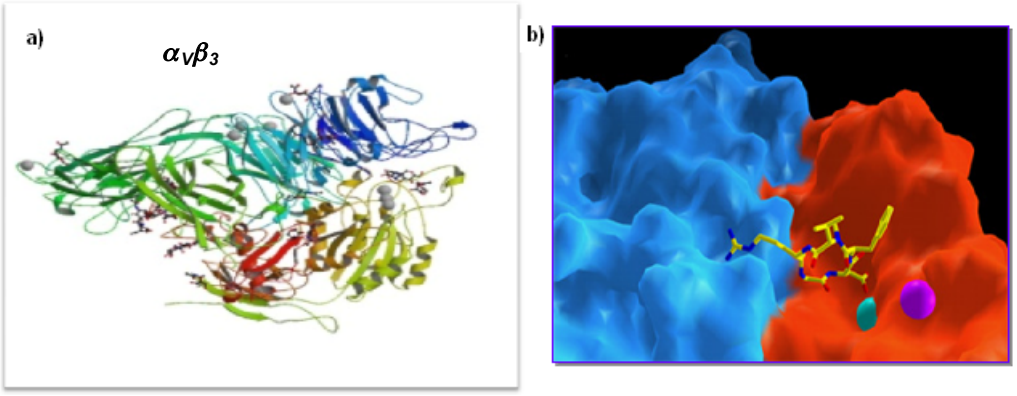

[a] a) Crystal structure of the extracellular segment of integrin $\alpha_V\beta_3$; b) Crystal structure of the extracellular segment of $\alpha_V\beta_3$ integrin in complex with the cyclic pentapeptide ligand Cilengitide, in its binding conformation.

A homology model for the closely related $\alpha_V\beta_5$ receptor was developed. The two integrins were found to mostly differ in the region comprising residues 159-188 in the β_3 subunit. A 'roof' was described for $\alpha_V\beta_5$ integrin featuring Tyr and Lys residues, which would hamper the binding of compounds containing bulky substituents nearby their Asp-mimicking group. Because of this difference, a few inhibitors of $\alpha_V\beta_3$ integrin displaying selectivity over $\alpha_V\beta_5$ have actually been found,[35] but specific inhibitors of $\alpha_V\beta_5$ integrins have not been described yet.

1.2.3 - *Integrin $\alpha_5\beta_1$*

Integrin $\alpha_5\beta_1$ is significantly upregulated in tumor angiogenesis in both mice and humans, but is not expressed on quiescent endothelium. Antagonists of $\alpha_5\beta_1$ also inhibited tumor angiogenesis in chicks and mice, thus leading to tumor regression.[23]

Integrin $\alpha_5\beta_1$-mediated adhesion promotes endothelial cell survival *in vivo* and *in vitro*[33] by suppressing the activity of protein kinase A (PKA). Integrin $\alpha_5\beta_1$ antagonists activate both PKA and caspase-8, thereby inducing apoptosis and inhibiting angiogenesis.[36] Although inhibition of integrin ligation can prevent cell attachment to the ECM, recent studies show that integrin $\alpha_5\beta_1$ antagonists also actively suppress signal transduction that leads to cell survival. Antagonists of $\alpha_5\beta_1$ suppress cell migration and survival on vitronectin, but not cell attachment to vitronectin, indicating that these antagonists affect the migration and survival machinery rather than integrin receptors for vitronectin.[16,37] The three-dimensional structure of the ligand-binding headpiece of integrin $\alpha_5\beta_1$ complexed with fragments of its physiological ligand fibronectin was determined by means of a molecular electron microscopy. The density map for the unliganded $\alpha_5\beta_1$ headpiece shows a 'closed' conformation similar to that seen in the $\alpha_V\beta_3$ crystal structure. By contrast, binding to fibronectin induces an 'open' conformation (Figure 1.7).[38]

Figure 1.7. Surface-rendered density maps of the $\alpha_5\beta_1$ headpiece[a]

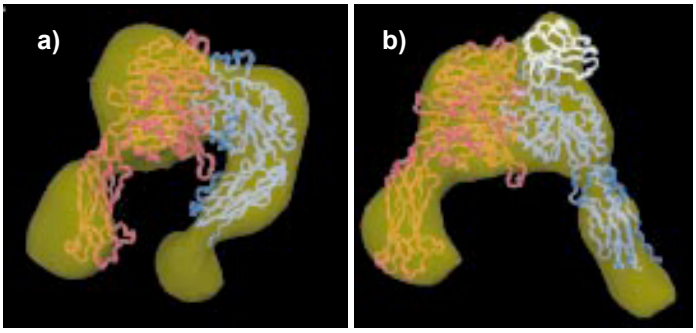

[a] a) the unliganded closed and b) the ligand-bound open conformation.

The lack of reliable structural data in the past, however, excluded $\alpha_5\beta_1$ as target for structure based drug design. However, the high homology between the different integrin subtypes makes them promising targets for homology modeling, which was achieved for $\alpha_V\beta_5$ integrin by Kessler and co-workers.[39,35b] Homology modeling of proteins is considered to be possible for a homology of 40% or greater.[40] This precondition is met by the integrins $\alpha_v\beta_3$ and $\alpha_5\beta_1$ with 53% homology for α_v/α_5 and 55% for β_3/β_1. Recently the $\alpha_5\beta_1$ crystal structure was published, providing the necessary knowledge for structure based drug design.[41] In particular Takagi and coworkers reported the crystal structure of a

ligand-binding fragment of human $\alpha_5\beta_1$ integrin, a prototypic integrin that functions as an RGD-dependent fibronectin receptor. The structure, solved as a complex with a Fab fragment of the anti-β_1 inhibitory antibody SG/19, revealed high similarity to the ligand unbound form of $\alpha_V\beta_3$ and $\alpha_{IIb}\beta_3$ integrins (Figure 1.8). Surprisingly, the RGD peptide can be introduced into the binding pocket by soaking, without causing any conformational change in integrin except for an ~1 Å shift of one residue and the dissociation of Ca^{2+} from the adjacent to the MIDAS (ADMIDAS). Docking simulations and structure-based mutagenesis identified a single α_5 residue responsible for the strong preference of $\alpha_5\beta_1$ for fibronectin, establishing a basis for the combinatorial roles played by each subunit during the specific recognition of protein ligands.

Figure 1.8. Structure of the $\alpha_5\beta_1$integrin headpiece in complex with SG/19 Fab[a]

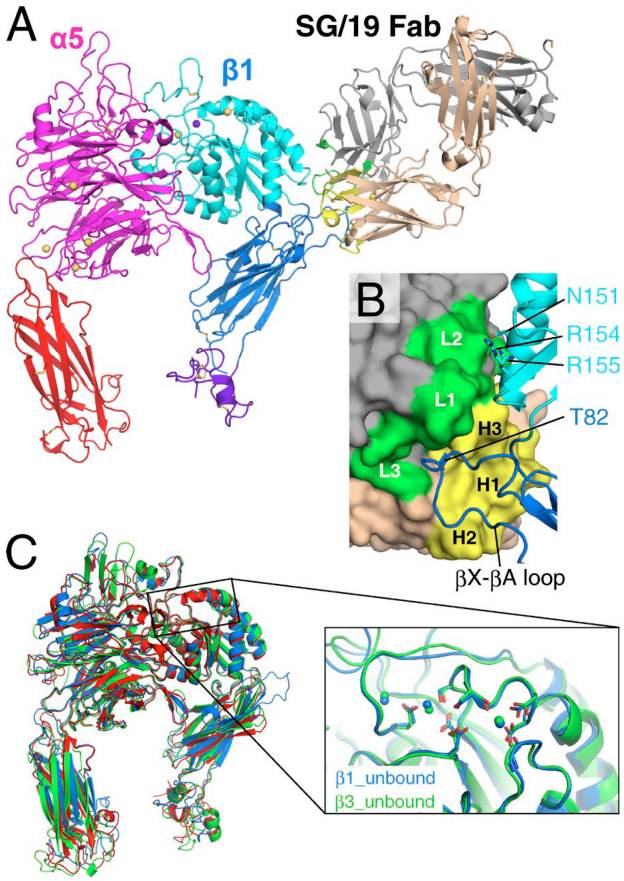

[a] A) Ribbon presentation of the overall structure with disulfide bonds in stick model. Individual domains are differently colored in magenta (β-propeller), red (thigh), cyan (βA), blue (hybrid), and purple (PSI), and bound metal ions are shown as spheres (yellow for Ca^{2+} and purple for Mg^{2+}). SG/19 Fab is colored in gray (light chain) and wheat (heavy chain), with their CDR loop regions highlighted in green and yellow, respectively. B) Close-up view of the SG/19-binding interface. SG/19 Fab and β_1 chain are shown in surface and ribbon presentations, respectively, with the same color code used in A. CDR regions and important interface residues are labeled. C) Superposition of three integrin headpiece structures in the ligand unbound form. Blue, $\alpha_5\beta_1$; red, $\alpha_v\beta_3$ (3IJE); green, $\alpha_{IIb}\beta_3$ (3FCS). On the right is a blowup of the region around the metal-binding sites in the β_1(blue) and β_3 (green; 3FCS) βA domains.

1.3 - *Role in hemostasis and thrombosis*

Thrombosis is a desease-related process consisting in the formation of a blood clot inside a blood vessel. It occurs when platelets adhere to damaged blood vessels and become activated.[42] These activated platelets recruit other platelets, resulting in the formation of a haemostatic plug. This is an essential mechanism for preventing blood loss, but inappropriate thrombus formation can lead to a stroke or to a heart attack. It is probably the first clearly integrin associated process.

In this context, integrin $\alpha_{IIB}\beta_3$ is responsible for platelet aggregation and this feature made it the first integrin to be identified as therapeutic target. In the 1990s, three $\alpha_{IIB}\beta_3$ integrin inhibitors were approved to reduce the risk of ischaemic events in patients with acute coronary syndromes and those undergoing percutaneous coronary intervention. They were the antibody fragment abciximab and the small-molecule inhibitors eptifibatide **1** and tirofiban **2** (Figure 1.9), all of which are administered intravenously.[43]

Figure 1.9. $\alpha_{IIB}\beta_3$ integrin inhibitors

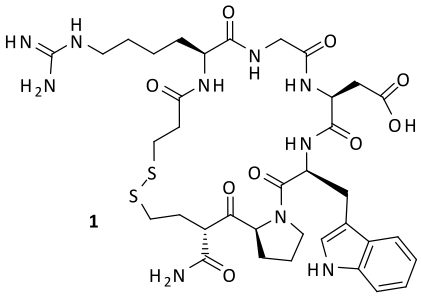

1

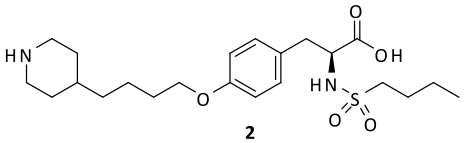

2

However, despite initial expectations that antagonists targeting this integrin would be blockbuster drugs, attempts to develop oral antagonists for more convenient administration were not successful, and the use of the approved intravenous inhibitors has largely been restricted to high-risk patients.

Instead, clopidogrel (commercially known also as PLAVIX®), an orally active ADP receptor antagonist, filled the market that was expected for $\alpha_{IIB}\beta_3$ integrin antagonists and became the second biggest-selling drug globally.[44]

The failure of oral $\alpha_{IIB}\beta_3$ antagonists was probably due to multiple factors.[45] There were severe problems, in particular a poor bioavailability and the lack complete understanding of the $\alpha_{IIB}\beta_3$ integrin role in thrombosis and signaling.

1.4 - *Immune system disorders*

Beside the studies on blood diseases, a great number of attempts have been made to find efficient antagonists of integrins involved in immune system disorders.

In particular, both β_1 and β_2 integrins are important in immune function, where they have essential roles in localizing the immune response to the site of inflammation.[46] Moreover a defect in β_2 integrins leads to a life-threatening immune dysfunction (that is, leukocyte adhesion deficiency).[47]

In this context, $\alpha_L\beta_2$ and $\alpha_4\beta_1$ have been the first integrins to be therapeutically targeted. In particular Karin and coworkers reported that $\alpha_4\beta_1$ integrin has a key role in the migration of lymphocytes to inflamed regions of the central nervous system in rodent models of multiple sclerosis.[48]

Monoclonal antibody binding the α_4 integrin subunit (natalizumab, approved in 2004) was effective in the treatment of multiple sclerosis, and also for the inflammatory bowel disorder Crohn's disease.[49] Although natalizumab showed substantial efficacy in clinical trials,[50] several patients developed a fatal progressive multifocal leukoencephalopathy after treatment,[51] and the drug was withdrawn from the market in 2005. However, after reassessment in 2010, the European Medicines Agency (EMA) concluded that the benefits outweighed the risks for patients treated with natalizumab, and it was re-approved with implementation of appropriate warning and safety measures. Several small-molecule inhibitors of α_4 integrins are in development as followers of natalizumab.

1.5 - *Osteoporosis*

Osteoporosis occurs when the balance between bone formation and degradation is disturbed. Integrins have an important role in the function of osteoclasts, which mediate bone resorption. Osteoclast $\alpha_1\beta_1$ integrin is responsible for the adhesion of osteoclasts to collagen.[52] The $\alpha_V\beta_3$ integrin is also important in osteoclast function, and polymorphisms in this receptor are also associated with increased rate of fracture.[53] An antagonist of this receptor (L-000845704) showed an increased bone density in postmenopausal women in a Phase II clinical study.[54] However, it seems that neither this antagonist or any other anti-integrin is currently in clinical development for osteoporosis.

1.6 - *RGD recognition motifs*

The arginine-glycine-aspartic acid (RGD) cell adhesion sequence (Figure 1.10) was discovered in fibronectin almost 30 years ago.[55] Other adhesion proteins such as vitronectin, fibrinogen, von Willebrand factor, thrombospondin, laminin, entactin, tenascin, osteopontin, bone sialoprotein and, under some conditions, collagens were then discovered to include RGD sites. It was soon confirmed

with regard to fibronectin and then extended to other proteins that the RGD sequence is the endogenous recognition motif for cell attachment to proteins.

Figure 1.10. Arg-Gly-Asp (RGD) tripeptide sequence

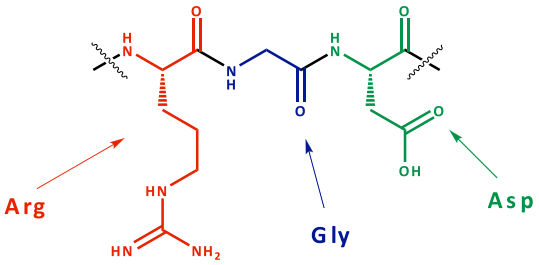

Cells expressing several α_V integrins (e.g. β_1, β_3, β_5, β_6 and β_8), as well as integrins $\alpha_{IIb}\beta_3$, $\alpha_5\beta_1$ and $\alpha_8\beta_1$, recognize the ubiquitous RGD sequence in their ligands. Naturally occurring integrin inhibitor proteins bearing the RGD motif are showing an extremely varied selectivity and potency in targeting RGD-recognizing integrins. Elucidations on their structure suggests that proper restriction of the RGD flexibility can lead to integrin inhibition.[56]

Hence, monomeric linear or confomationally constrained RGD-containing cyclic peptides, pseudo-peptides, and mimetics thereof displaying high potency and selectivity were conceived. The most significant advances in this field have led to the development of agents targeting $\alpha_{IIb}\beta_3$ integrin on platelets for inhibiting thrombosis[57] and inhibitors of $\alpha_V\beta_3$ and $\alpha_V\beta_5$ integrins against angiogenesis, cancer and bone resorption.[58] Among these, it is important to highlght the nanomolar $\alpha_V\beta_3/\alpha_V\beta_5$ binder cyclic pentapeptide c-RGD-(D-Phe)-N-methyl-V developed by Kessler (known as Cilengitide or EMD121974, which has recently entered phase III clinical investigation for patients with glioblastoma multiforme, *vide infra*).[58j]

As already mentioned, a crucial enhancement in this field was achieved with the crystal structure resolution of the ectodomain of $\alpha_V\beta_3$ integrin, both unligated and complexed with Cilengitide,[5b] as well as the better crystal structure resolution of $\alpha_{IIb}\beta_3$ integrin complexed with the synthetic anti-trombotic drug *Eptifibatide*.[6d,59]

Besides the well-defined RGD and other binding motifs, it has been proposed that the NGR and DGR sequences might also have a role in integrin recognition. Controversial results have however been reported. The importance of the *iso*DGR sequence as an integrin binding motif was serendipitously discovered by Corti research group (S.Raffaele/MolMed).[60]

The NGR sequence, present in several endogenous molecules as well as in fibronectin FN-I_5 and FN-I_7, can easyly deamidate (also *in vivo*) on asparagine, giving *iso*DGR and DGR (Scheme 1.1). Although protein modifications typically causes loss of activity/function, it was recently suggested

that *iso*DGR formation at NGR or DGR sites might result in a gain of function. The *iso*DGR sequence can in fact mimic RGD and interact with the RGD-binding site of integrins.[61]

Scheme 1.1. Formation of DGR and *iso*DGR sequences by asparagine deamidation

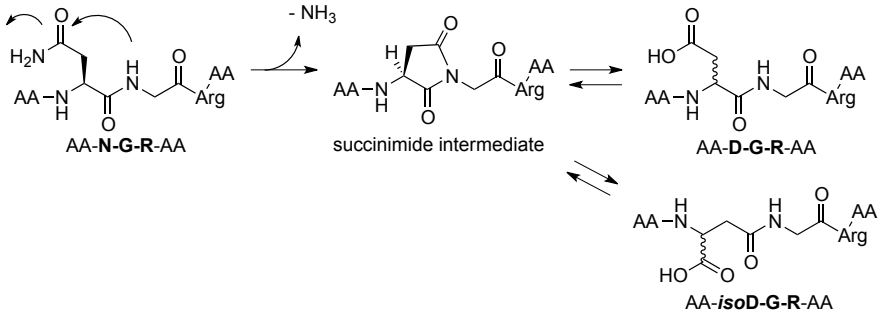

*Iso*DGR-containing peptides can recognize members of the RGD-dependent integrin family, such as **$\alpha_v\beta_3$, $\alpha_v\beta_5$**, $\alpha_v\beta_6$, $\alpha_v\beta_8$ and **$\alpha_5\beta_1$**, but not others.[62] Both affinity and specificity of the interaction between *iso*DGR and integrin binding site is reported to be highly dependent on the flanking residues. Notably, *iso*DGR docks onto the integrin binding site in an inverted orientation with respect to RGD. This orientation allows *iso*DGR to bind to the $\alpha_v\beta_3$ binding pocket maintaining all the typical electrostatic-clamp interactions of the RGD motif. The acidic and basic residues are at the correct distance and orientation to engage stabilizing interactions with the polar regions of integrin: the *iso*Aspartic carboxylic side chain is interacting with MIDAS, Asn^{215}, Tyr^{122} and Arg^{214}, while Arginine guanidinium interacts with Asp^{218}, Asp^{150} and Gln.^{180} Moreover, additional stabilizing interactions are present: glycine recognizes the receptor via polar interactions and an H-bond between its amide and carbonyl of Arg^{216}.[61] Therefore, *iso*DGR can be considered as a natural fit for the RGD binding pocket of $\alpha_v\beta_3$ integrin, suggesting that the naturally occurring transformation of NGR and DGR into *iso*DGR functions as a molecular switch able to activate integrin recognition.

Although *iso*DGR- and RGD-containing ligands can share the same integrin binding site, their effects on integrin finction might not be necessarily the same.[63] In a very recent paper, the MolMed group discovered an extremely interesting feature of the *iso*DGR ligands: when one of these ligands reaches the $\alpha_v\beta_3$ binding site, it is capable of blocking the integrin in the bent, inactive conformation.[64]

1.6.1 - *RGD integrin ligands: state of the art*

The potential of $\alpha_v\beta_3$ inhibitor EMD121974 (**3**, Cilengitide, Figure 1.11), developed by Kessler and co-workers, was soon recognized by various clinical programs opening the era of the integrin inhibitor class as investigational agents for antiangiogenic and anticancer therapies. The crystal structure

analysis of the ectodomain of $\alpha_v\beta_3$ complexed with Cilengitide offered the first clear picture of the RGD binding mode, which revealed a Cilengitide conformation featuring an inverse γ-turn centered on Asp, and a distorted βII'-turn with Gly and Asp at the *i*+1 and *i*+2 positions, respectively. A distance of 8.9 Å between the C_β of Asp and Arg, accounting for an almost extended conformation of the RGD motif were observed. The most important interactions between the ligand and the receptor involved the Arg guanidinium group, which was forming salt bridges with Asp150 and Asp218 in the α subunit, and the Asp carboxylic group of the ligand, which interacts with the Mn^{2+} ion at MIDAS (Metal-Ion-Dependent Adhesion Site) in the β subunit. Moreover, several hydrophobic interactions were engaging the Gly residue, positioned at the interface between the α and β subunits. An earlier example of RGD-based cyclic peptide had already been identified by Kessler, c(RGDfV) **4** (Figure 1.11),[65] which can be considered as an ancestor of Cilengitide. This compound is selectively active against $\alpha_V\beta_3$ integrin and is commercially available, which makes it useful as a reference standard.

Representative examples of semipeptidic $\alpha_V\beta_3$ inhibitors, bearing a non-peptidic and rigid turn-inducing motif to appropriately constrain the RGD motif, are reported in the literature. Classic bicyclic, but also monocyclic scaffolds and simple linear tethers have been used to properly fold the RGD sequence within a macrocyclic template, to better fit within $\alpha_V\beta_3$ integrin binding site.[66] Bicyclic heterocycles stand among the most popular constrained mimetics of natural amino acids in the structure-based design of peptidomimetics. Various successful examples of peptide are validating their use as preferred conformation-inducing scaffolds.[67] Kessler exploited azabicycloalkane and spyrocyclic systems, traditionally known as β-turn inducers, to prepare cyclic RGD-containing peptidomimetics.[68] The most active and less constrained compound of the series (ligand **5**, Figure 1.11) was a fully promiscuous antagonist.

Figure 1.11. Integrin ligands developed by Kessler and coworkers

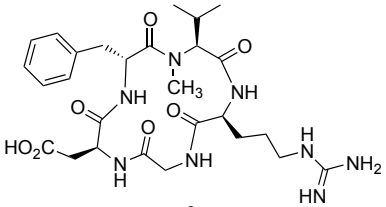

3
Cilengitide

$\alpha_V\beta_3$ 0.6 nM
$\alpha_{IIb}\beta_3$ 860 nM

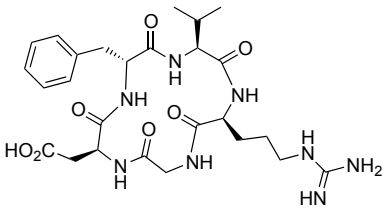

4
c(RGDfV)

$\alpha_V\beta_3$ 50 nM

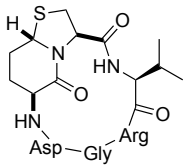

5

$\alpha_V\beta_3$ 43 nM
$\alpha_{IIb}\beta_3$ 550 nM

A stereoisomeric library of RGD pentapeptide mimetics incorporating 5,6- and 5,7-fused azabicycloalkane amino acids was generated by the group of Scolastico.[69] Among the high affinity

ligands found within the collection, the most active compounds (Figure 1.12) proved low nanomolar binders of $\alpha_V\beta_3$ and $\alpha_V\beta_5$ integrins. Ligand **7** was completely selective towards $\alpha_V\beta_3$ integrin with respect to $\alpha_{IIb}\beta_3$ and $\alpha_5\beta_1$ integrins. Moreover, significant antiangiogenic activity of this compound emerged from *in vitro* experiments, showing inhibition of the proliferation of endothelial cells.[70]

Figure 1.12. Azabicycloalkane RGD peptidomimetics

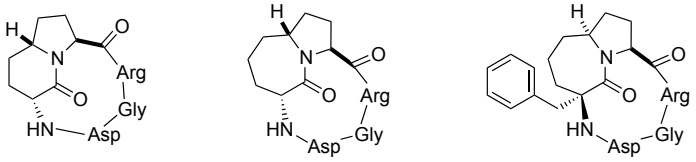

6

$\alpha_V\beta_3$ 14.3 nM
$\alpha_V\beta_5$ >10^3 nM

7
ST1646

$\alpha_V\beta_3$ 3.8 nM
$\alpha_V\beta_5$ 1.39 nM

8

$\alpha_V\beta_3$ 6.4 nM
$\alpha_V\beta_5$ 7.7 nM

A strong dependence of the overall conformation of the cyclic peptides on the lactam ring size and stereochemistry was revealed. Almost the same interactions observed in the crystal structure of $\alpha_V\beta_3$ complexed with Cilengitide **3** were maintained. An average distance between Arg and Asp C_β of 8.8 Å in the case of **6** and 8.5 Å in the case of **7** was observed, indicative of an almost extended conformation of the RGD sequence. Cyclopeptide **8** (Figure 1.12) emerged as a nanomolar antagonist of both $\alpha_V\beta_3$ and $\alpha_V\beta_5$ integrins comparable to ST1646 **7**. Docking studies revealed that the conformations containing an inverse γ-turn on Asp, conserved the main contacts observed in the X-ray crystal structure with Cilengitide **3**.[71]

Also monocyclic turn-inducing scaffolds were used in non-peptidic RGD-containing systems, based on βII'/γ arrangement with the γ-turn centred on Gly. Kessler inserted amino pyrrolidinone-based motifs to hold the RGD moiety, providing macrocycles **9a** and **9b** (Figure 1.13).[72] A βII' turn conformation with Gly at the *i*+1 position was unexpectedly observed for these compounds.

Figure 1.13. Pyrrolidinone RGD ligands

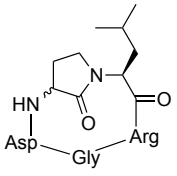

9a: (*S*) $\alpha_V\beta_3$ 40 nM
$\alpha_{IIb}\beta_3$ 2.8 μM

9b: (*R*) $\alpha_V\beta_3$ 0.8 nM
$\alpha_{IIb}\beta_3$ 8.5 nM

Ligand **9a** was a moderate and selective antagonist of $\alpha_V\beta_3$ integrin, while **9b** proved to be a more active $\alpha_V\beta_3$ inhibitor, even though aspecific. The main difference between the two analogues was the orientation of the lactam bond in the turn-motif, which was found to be rotated by 180° in the two isomers, and involved in a H-bond with the receptor in the case of **9b**.

D- and L-morpholines were exploited by Guarna and co-workers to replace the *N*-Me-Val motif of Cilengitide **3**, giving compounds **10** (Figure 1.14).[73] The different conformation of the peptide bond between D-Phe and the morpholine scaffold provided distinct structural arrangements for the two compounds. Ligand **10b** showed in particular a *cis* conformation in the docking analysis, with an RGD sequence arrangement comparable to that observed in the $\alpha_V\beta_3$-Cilengitide complex.

Figure 1.14. Morpholine-base RGD

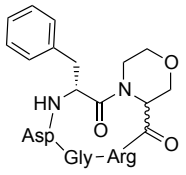

10a: (*S*) $\alpha_V\beta_3$ 157 nM
$\alpha_V\beta_5$ 15.1 nM

10b: (*R*) $\alpha_V\beta_3$ 32.6 nM
$\alpha_V\beta_5$ 21 nM

Kessler and Overhand designed several pyranoid and furanoid sugar δ- and ε-amino acid-based compounds. Due to their high flexibility, they proved to be aspecific antagonists of $\alpha_V\beta_3$ and $\alpha_{IIb}\beta_3$ integrins. This aspecificity was also supported by the conformational analysis of this compounds, which showed an arrangement standing in between the typical kinked conformation of $\alpha_V\beta_3$-selective antagonists and the extended one required for targeting $\alpha_{IIb}\beta_3$ integrin. The two most representative members of this class of compounds (ligands **11** and **12**) are sketched in Figure 1.15.[74,58k]

Figure 1.15. Pyranoid and furanoid RGD peptidomimetics

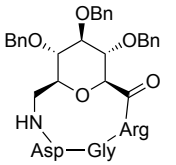

11

$\alpha_V\beta_3$ 25 nM
$\alpha_V\beta_5$ $>10^4$ nM
$\alpha_{IIb}\beta_3$ 13.4 nM

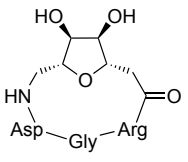

12

$\alpha_V\beta_3$ 1.49 μM
$\alpha_V\beta_5$ 0.38 μM

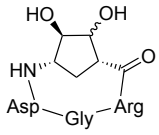

13

a (*S*): $\alpha_V\beta_3$ 51.4 nM
$\alpha_V\beta_5$ 165.5 nM

b (*R*): $\alpha_V\beta_3$ 44.7 nM
$\alpha_V\beta_5$ 125.4 nM

Casiraghi and colleagues, following an analogous inspiration, exploited furanoid carbasugar γ-amino acid equivalents to generate four stereoisomeric macrocycles (most active members **13**, Figure 1.15). Although an improvement in the affinity towards $\alpha_V\beta_3$ and $\alpha_V\beta_5$ was observed, surprisingly their activity proved to be almost irrespective of the configuration at the carbons bearing the amino acid functions. An inverted γ-turn, centered on Asp was revealed by NMR, displaying a C_β(Asp)- C_β(Arg) distance in the range of 8.0-8.4 Å.[75]

The same group incorporated 4-amino proline (Amp) scaffolds into a library of RGD peptides, to further extend these findings.[76] The compounds reported in Figure 1.16 (**14a-d**) displayed exceptionally high affinity towards $\alpha_V\beta_3$ and $\alpha_V\beta_5$ integrins. A picomolar activity was observed for $\alpha_V\beta_3$ integrin in the high affinity status. A preferential conformation featuring an inverse γ-turn motif around Asp for the macrocycles containing a *cis*-disposed γ-amino acid motif was detected by NMR conformational analysis. On the contrary, the macrocycles proved to be more flexible when a *trans* γ-amino acid was present. All the macrocycles showed a C_β(Asp)-C_β(Arg) distance in the 7.8-8.2 Å range. The most active analogues maintain the relevant key interactions observed for Cilengitide. Compound **14a** was stabilized by a strong H-bonding contact between the NH in the aminoproline motif and Tyr178. Quite interestingly, the alkyl and acyl chains of **14b** and **14c** provided additional contacts for binding, pointing towards a large hydrophobic hollow rich with aromatic residues.

Figure 1.16. Library of RGD peptides containing 4-amino proline or *cis*-β-aminocyclopropanecarboxylic acid

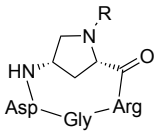

14

a: R= H	$\alpha_V\beta_3$	4.4 nM
	$\alpha_V\beta_5$	80.2 nM
b: R= n-Heptyl	$\alpha_V\beta_3$	2.84 nM
	$\alpha_V\beta_5$	36.1 nM
c: R= Propionyl	$\alpha_V\beta_3$	5.60 nM
	$\alpha_V\beta_5$	94.0 nM
d: R= Bz	$\alpha_V\beta_3$	5.15 nM
	$\alpha_V\beta_5$	86.6 nM

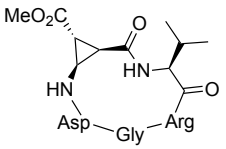

15

$\alpha_V\beta_3$	20 nM
$\alpha_5\beta_1$	1.5 μM

Pseudopentapeptides containing both enantiomers of *cis*-β-aminocyclopropanecarboxylic acid (β-Acc) were conceived, the most interesting (ligand **15**) is sketched in Figure 1.13.[58e] Compound **15** resulted more active towards both $\alpha_V\beta_3$ and $\alpha_5\beta_1$ integrins, with respect to the reference compound c(RGDfV) **4**. The C_β(Asp)-C_β(Arg) distance found for compound **15** resulted considerably shorter than expected (7.06 Å). Moreover, a γ-turn centered on Gly and a pseudo β-turn wherein (+)-β-Acc occupied the *i*+1 position were observed.

Despite the impressive work dedicated to the identification of semipeptide analogues, Cilengitide is the only investigational agent of this class that has been developed for clinical testing on cancer patients. The growth inhibitory activity of Cilengitide observed in the clinic is likely due to a

combination of multifaceted mechanisms. These might depend on whether the drug is administered alone or in combination, and include inhibition of angiogenesis, direct cytotoxic activity on tumor cells, increase of endothelial cell permeability, and inhibition of cell adhesion, migration and invasion.[66,77]

Our research group reported the synthesis of two cyclic peptidomimetic compounds **16** and **17**, containg the RGD sequence and bearing either **DKP1** or **DKP2** as a rigid scaffold (Figure 1.17).[78]

Figure 1.17. Cyclic RGD peptidomimetics **16** and **17** containing scaffolds **DKP1** and **DKP2** respectively.

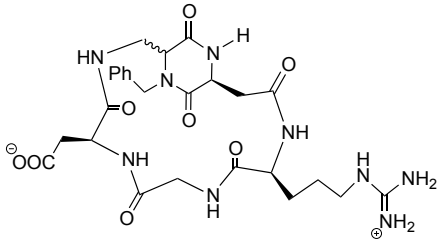

16: (*S*,*S*)
17: (*S*,*R*)

These compounds were examined *in vitro* for their ability to inhibit biotinylated vitronectin binding to the purified $\alpha_v\beta_3$ and $\alpha_v\beta_5$ receptors, giving strikingly different yet encouraging results. High micromolar IC_{50} values were obtained by compound **16** [IC_{50} ($\alpha_v\beta_3$): 3898 ± 418 nm; IC_{50} ($\alpha_v\beta_5$): > 10^4], while compound **17** gave low nanomolar values and demonstrated 50 times more selective for the $\alpha_v\beta_3$ integrin with respect to the $\alpha_v\beta_5$ ($\alpha_v\beta_3$ IC_{50}: 3.2 ± 2.7; $\alpha_v\beta_5$ IC_{50}: 114 ± 99).

2 - Cyclic [DKP-RGD] compounds

We decided to prepare a small library of cyclic DKP-RGD peptidomimetics (Figure 1.18), based on previous results obtained by our research group, mantaining the RGD sequence and fine tuning the diketopiperazine scaffolds (i.e. varying the configuration of the two stereocenters and the substitution at the diketopiperazinic nitrogen atoms). The aim of this study was to investigate activity, selectivity, and structure of these compunds, in order to identify new specific α_v-integrin ligands. Furthemore, we wanted to better understand the role of diketopiperazine building blocks as inducers of secondary structures in these peptidomimetics. These data were also a starting point for the synthesis of RGD-peptidomimetics bearing modified DKPs that allow the conjugation with Paclitaxel (see Chapter 2).

Figure 1.18. Cyclic RGD-peptidomimetics **16**-**23** containing bifunctional diketopiperazine scaffolds **DKP1**-**DKP8**.

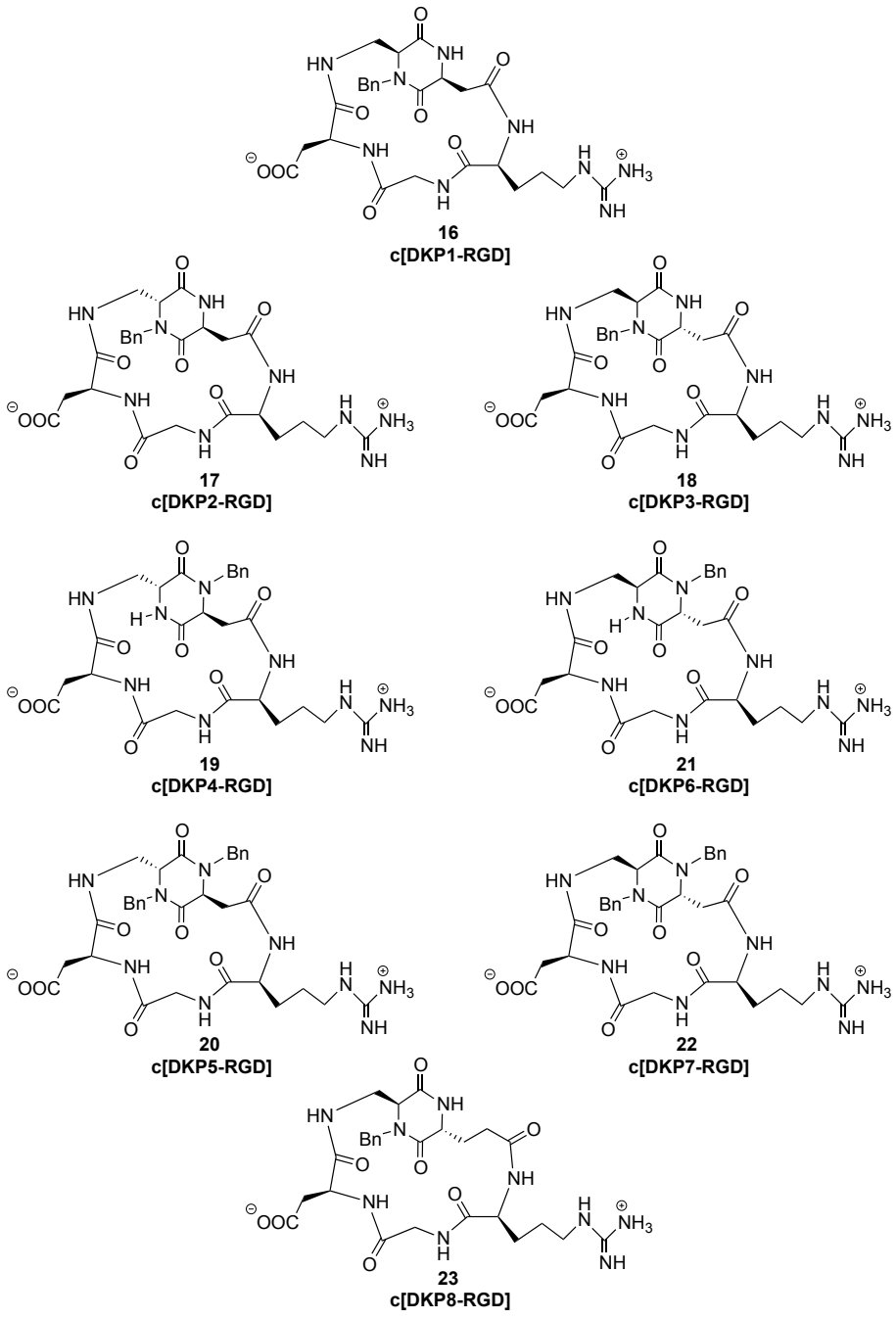

2.1 - *Diketopiperazines* [79]

Having emerged as privileged structures, diketopiperazines (DKPs) were used as templates capable of inducing a defined secondary structure in peptide sequences. This relevant application, which has gained importance in the last decade, inherently takes advantage from the synthesis of symmetrical

and unsymmetrical DKPs bearing reactive functionalities (e.g., NH_2, COOH) in the side chains of the amino acids. This let them being incorporated as peptidomimetic moiety.

These constrained heterocyclic scaffolds were used in receptors, for the selective recognition of small peptides and anions, and in peptidomimetics mimicking topologically relevant elements of the secondary structure of proteins (e.g., β-turns, β-hairpins, and α-helices).

2.1.1 - *DKPs as β-turn mimics*

A β-turn is defined as any tetrapeptide sequence, showing a typical 10-membered intramolecular H-bonded ring (Figure 1.19).

Figure 1.19. Example of a β-turn motif

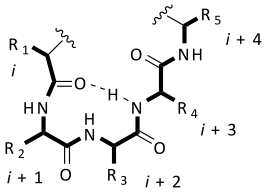

Although there has been much discussion in the literature on what constitutes a β-turn mimic and how different types of mimics are to be characterized,[80] these can be roughly classified into three broad classes, which are illustrated in Figure 1.20: a) internal β-turn mimics, b) β-hairpin mimics (where a rigid scaffold induces reversal of the peptide chain), and c) external β-turn inducers.

Figure 1.20. Classification of β-turn mimics.

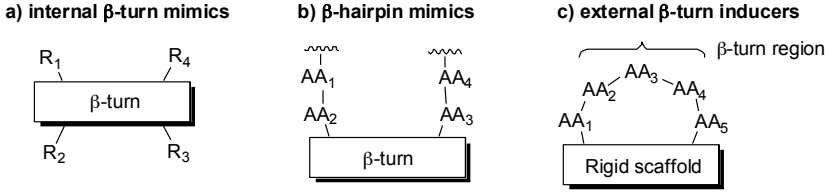

2.1.2 - *Internal β-turn mimics*

The first class of β-turn mimics includes scaffolds displaying side chains with trajectories mimicking a peptide reverse turn. Several examples of this type of DKP-based scaffolds are reported in the

literature. Golebiowski and co-workers developed a solid-supported high-throughput synthesis of bicyclic diketopiperazines, starting from racemic piperazine-2-carboxylic acid.[81] A library of β-turn mimics was prepared (general structure shown in Figure 1.21), in which the first two substituents (R^4 and R^5) were introduced via the Petasis reaction and subsequent amide bond formation, whereas R^1 and R^2 substituents were originated from an α-amino acid and were introduced in the amidation reaction.

Figure 1.21. Examples of DKP-based internal β-turn mimics.

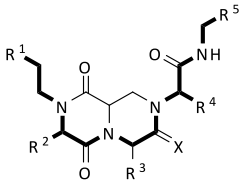

Later on, the same authors were able to introduce the missing R^3 substituent by developing a solid-phase protocol based on the Ugi reaction and using both L- and D-diaminopropionic acid as starting material, leading to two (complementary) epimeric series of β-turn mimics **24** (Figure 1.22).[82,83]

Figure 1.22 – Examples of DKP-based internal β-turn mimics.

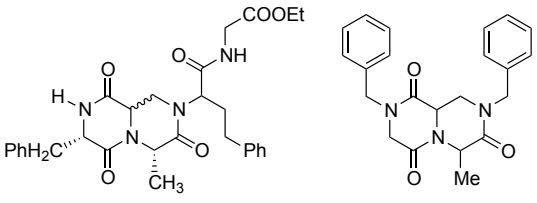

Simulated annealing calculations were performed on both epimers of structure **24** to determine their propensity to adopt a β-turn. The obtained data suggest that both *R*- and *S*- epimers of structure **24** fit more closely a type I β-turn.[83] Starting from simple α-amino acids, Kahn and co-workers have also reported the solution-phase synthesis of a conformationally restricted β-turn mimic **25**, based on a similar bicyclic diketopiperazine scaffold (Figure 1.22).[84]

Burgess and co-workers described the use of diketopiperazine scaffolds in antagonists of tropomysin receptor kinase C.[85] Selectivities for this particular receptor were achieved by using amino acid side chains corresponding to those present in the β-turn regions of the parent neurotrophin ligands. The

diketopiperazine scaffolds used in this work (Figure 1.23) are functionalized at the N-1 and C-3, and the substituents at these two positions were calculated to overlay well with the side chains of the *i*+1 and *i*+2 residues of a type-I β-turn.

Figure 1.23. DKP mimics of a type I β-turn.

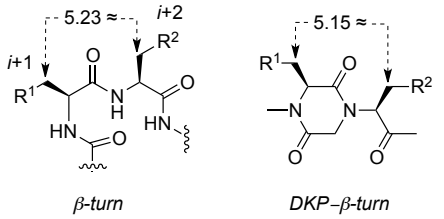

2.1.3 - *DKPs as β-hairpin inducers*

The second class of β-turn mimics consists of a rigid scaffold which, when incorporated into a peptide or pseudo-peptide chain, causes a reversal of the chain.[86] In strictest terms, these structures themselves should adopt a β-turn conformation, but quite often they lack substitution at the important *i*+1 and *i*+2 residues of the turn region or the means to introduce significant diversity at these positions. As β-hairpin inducers, the scaffolds can promote the formation of parallel or antiparallel β-sheets depending whether the side chains contain the same (e.g., two amine or carboxylic groups) or complementary functionalities (one amine and one carboxylic function). Gellerman and co-workers have reported the synthesis of orthogonally protected optically pure diketopiperazine scaffolds, starting from N_α-carboxymethyl ω-Alloc ornithine and orthogonally protected L-lysine.[87,88] The resulting non-symmetrical diketopiperazine scaffold **26** (Figure 1.24) bears two amine functionalities [AllocNH-$(CH_2)_3$, generated from Orn and FmocNH-$(CH_2)_4$, generated from Lys] in the arms of the DKP core and a complementary N_α-carboxymethyl group, which could be further manipulated via solid-phase organic chemistry.

Figure 1.24. Example of DKP-based β-turn mimic

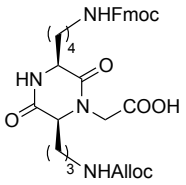

26

Alternatively, two different functionalities can be created in the lateral chains of the two amino acids forming the DKP core, such as an amine (e.g., derived from Lys, Orn or diaminobutyric acid) and a carboxylic acid (e.g., derived from Asp or Glu). Davies and co-workers performed some calculations on the minimum constraint requirement for a β-turn, which would fit tightly at the turn without causing steric hindrance, and preserve the polar backbone at the β-turn.[89] The result turned out to be a reverse *cis*-amide link in the form of a DKP ring containing an amino and a carboxylic groups in a *cis*-orientation, which would mimic a β-turn (correct angles and distances) and induce the formation of β-sheet structures.

2.1.4 - *DKPs in cyclic peptidomimetics, as external β-turn inducers*

In the case of external β-turn inducers, a rigid template is used to constrain the backbone of a cyclic peptide in order to stabilize the peptidic residue into a β-turn conformation. Notable examples of this type of β-turn mimic, based on a DKP scaffold, have been reported by Robinson and co-workers.[90]
The authors have reported an extensive investigation of proline-based diketopiperazine templates (Figure 1.25), that were used to stabilize turn and hairpin conformations in cyclic peptides containing the Asn-Pro-Asn-Ala (NPNA) sequence.

Figure 1.25. Examples of diketopiperazine-based scaffolds as "external" β-turn mimics.

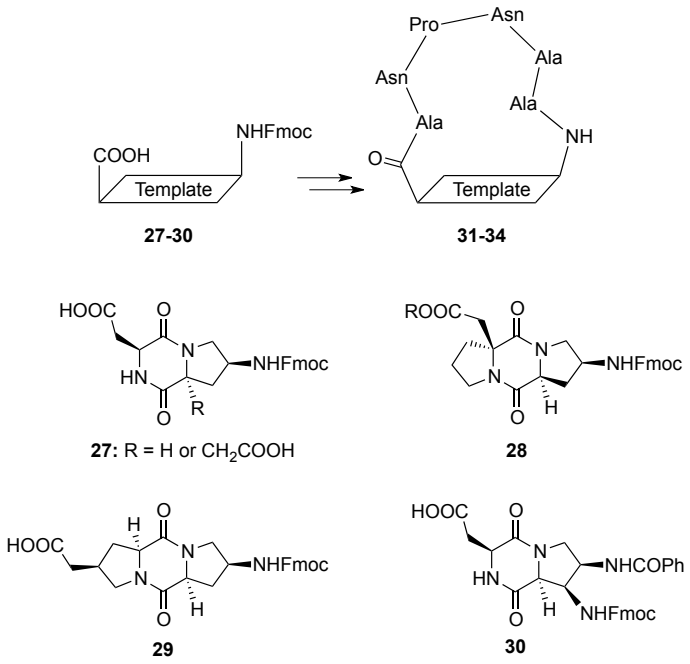

This tetrapeptide motif, which is found as a repeated unit in the circumsporozoite (CS) surface protein of the malaria parasite *Plasmodium falciparum*, has a tendency to adopt type-I β-turns in aqueous solution in linear peptides containing tandemly repeated NPNA sequence, and this secondary structure appears to be important for immune recognition of the folded CS protein. Several bifunctional bi- and tri-cyclic diketopiperazine scaffolds were prepared and inserted into cyclic peptides containing the ANPNAA sequence.

Scaffold **27** (R = H) was also introduced into the cyclic peptide **35** containing the Arg-Gly-Asp (RGD) sequence (Figure 1.26).[90]

Figure 1.26. Cyclic RGD peptidomimetics **35** containing bicyclic DKP template **27**.

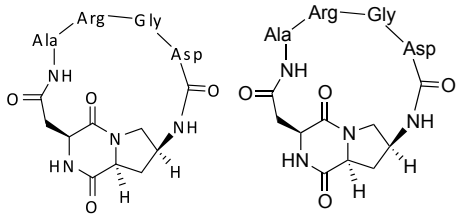

A conformational study to determine the three-dimensional presentation of the RGD motif in peptidomimetic **35** was performed by ^{1}H-NMR spectroscopy. However, no conclusive evidence of a defined conformation could be found, and it seems very likely that the peptide backbone of **35** is interconverting rapidly between two or more conformational states in aqueous solution.

In a similar approach, Royo, Albericio and co-workers prepared cyclic peptidomimetics containing *cyclo*[Lys-Asp] as a template (compounds **36a-c**, Figure 1.27).[91] The side arms of the diketopiperazine were used to link the amino and carboxy termini of three different peptides containing the RGD sequence (RGD, RGDG, and GRGDG), following a solid phase approach.

Figure 1.27. Cyclic RGD peptidomimetics containing *cyclo*[Lys-Asp].

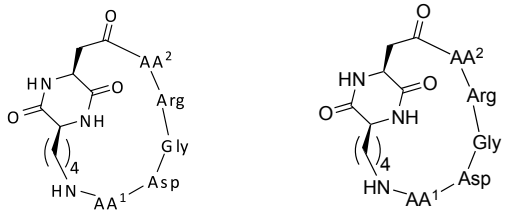

39 a: AA^1, AA^2 = not present
b: AA^1 = not present, AA^2 = Gly
c: AA^1, AA^2 = Gly

36 a: AA^1, AA^2 = not present
b: AA^1 = not present, AA^2 = Gly
c: AA^1, AA^2 = Gly

2.1.5 - *DKPs in helical structures*

Bis-peptides were recently introduced by Schafmeister and co-workers as "synthetic oligomers assembled from cyclic, stereochemically pure monomers coupled through pairs of amide bonds to form rigid spiroladder oligomers with predefined and programmable three-dimensional structures".[92] A "molecular rod" **37** (Figure 1.28) was synthesized starting from the "bis-amino acid" 4-amino-4-carboxy proline **38**.[93] This substituted proline was prepared in multi-gram quantities in nine synthetic steps from commercially available *trans*-4-hydroxy-L-proline. The synthesis of the "molecular rod" **37** occurred in two stages: a first "assembly" stage where the linear oligomer was grown, coupling the proline COOH to the primary amine in 4-position, by solid-phase peptide synthesis. A "rigidification" stage followed after cleavage from the resin. In this step, the diketopiperazines were cyclized by an intramolecular aminolysis reaction, in which the secondary amine of each monomer attacked the methyl ester of the previous monomer.

Figure 1.28. Molecular rod

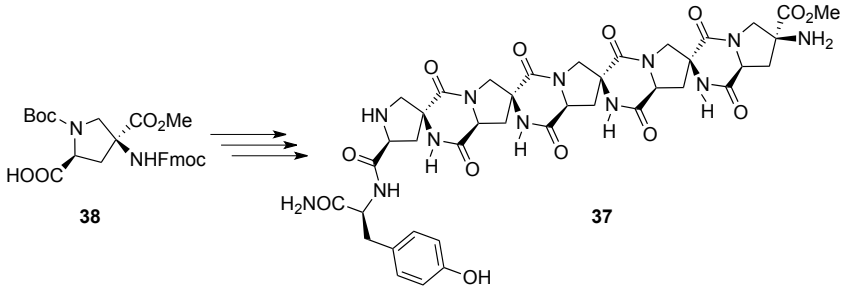

2.1.6 - *Previous work of our research group in the diketopiperazine field*

In 2008, our group reported the synthesis of a new class of bifunctional DKP scaffolds (**DKP1**, **DKP2**, Figure 1.29), formally derived from aspartic acid and 2,3-diaminopropionic acid, bearing a carboxylic acid and an amino functionality.[94] As a consequence of the absolute configuration of the two α-amino acids forming the cyclic dipeptide unit, the two reactive functionalities (amino and carboxylic acid) are locked in a *cis*- (**DKP1**) or *trans*-configuration (**DKP2**). In addition, while being derived from α-amino acids, these DKP scaffolds can be seen as a conformationally constrained dipeptide formed by two β-amino acids (see Figure 1.29), and in particular a β^2- and a β^3-amino acids (following Seebach's nomenclature).[95]

Figure 1.29. Structure of bifunctional DKP scaffolds highlighting the conformationally constrained β2–β3 dipeptide sequence.

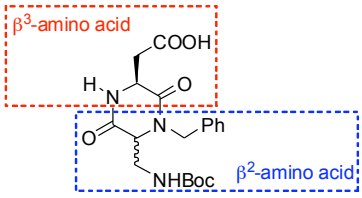

DKP1 (*S*,*S*)
DKP2 (*S*,*R*)

In particular, the bifunctional scaffold **DKP1**, derived from L-aspartic acid and (*S*)-2,3-diaminopropionic acid, bears the amino and carboxylic acid functionalities in a *cis* relationship and, as such, can be seen as a β-turn mimic and promoter of antiparallel β-sheet. In view of these potential properties, the synthesis of several peptidomimetics was performed by solution phase peptide synthesis (Boc strategy). Conformational analysis of these derivatives[94] was carried out by a combination of ^{1}H-NMR spectroscopy (chemical shift and NOE studies), IR spectroscopy, CD spectroscopy and molecular modeling, and revealed the formation of β-hairpin mimics involving 10- and 18-membered H-bonded rings and a reverse turn of the growing peptide chain (**39** and **40**, Figure 1.30). The β-hairpin conformation of the longer derivatives (**40a** and **40b**) was detected also in competitive, dipolar and even protic solvents such as dimethylsulfoxide and methanol, thus showing the high stability of these structures and the very good turn-inducing ability of the scaffold.

Figure 1.30. Peptidomimetics containing scaffold **DKP1**.

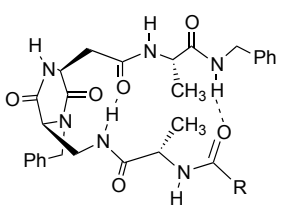

39 a: R = O-*t*Bu
b: R = CH_3

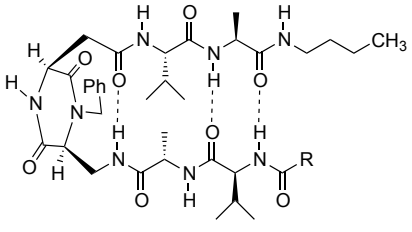

40 a: R = O-*t*Bu
b: R = CH_3

This attitude was further confirmed in the conformational analysis of two oligomers of **DKP1**, namely the trimer Boc-(**DKP1**)$_3$-NH*n*Bu **41** (Figure 1.31), and the tetramer Boc-(**DKP1**)$_4$-NH*n*Bu **42** (Figure 1.31).[96] The conformational preferences in solution of these foldamers were investigated by ^{1}H-NMR and CD spectroscopy and molecular modeling. In the case of the trimeric structure, the conformational studies suggest the possible formation of two turns for the first and third residues, while the tetramer

42 (Figure 1.31) is best described as a β-bend ribbon conformation, which is characterized by a succession of β-turns forming a linear peptide with a ribbon-like shape.

Figure 1.31. Structure of trimer **41** and tetramer **42**.

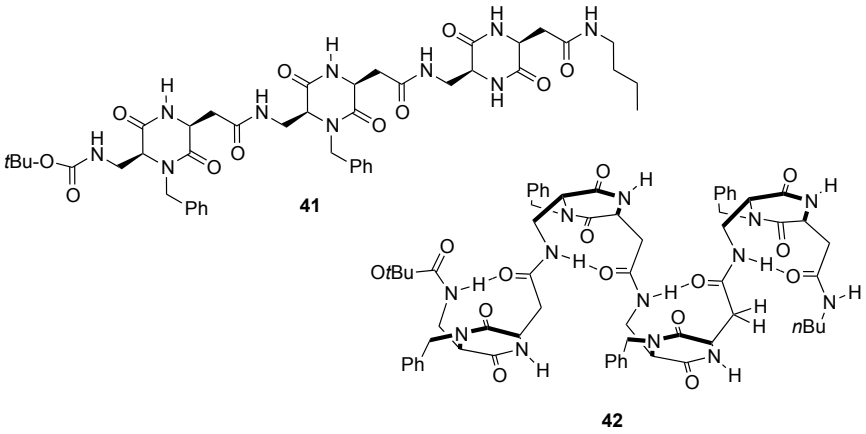

The most peculiar feature of the β-turn structure present both in the hairpin and β-bend ribbon are the CD spectra which display a rather strong minimum around 200 nm and a weaker one at 225 nm with a negative maximum at 215 nm (Figure 1.32). This was shown, by NMR studies, to adopt a turn-like conformation with a 10-membered H-bonded ring induced by the β^2–β^3 unit.

Figure 1.32. CD spectrum of the tetramer **42** and the hairpin peptidomimimetic **40a**. The data of the latter compound have been multiplied by a factor 10 to magnify the appearance of the curve.

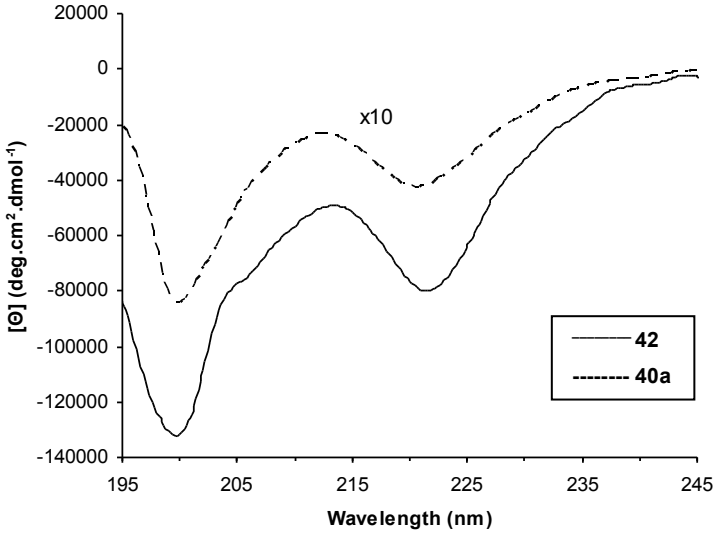

Finally, in 2009 our group reported synthesis, conformational analysis and investigation of the biological activity of cyclic RGD-peptidomimetics **16** and **17** (see Figure 1.17), containing the bifunctional diketopiperazine scaffolds **DKP1** (*cis*) and **DKP2** (*trans*).[97]

Conformational studies of these cyclic RGD peptidomimetics were performed by NMR spectroscopy (^{1}H-NMR and NOESY spectra of dilute 9:1 H_2O/D_2O solutions) and by computational methods [Monte Carlo/Stochastic Dynamics (MC/SD) simulations]. The RGD-peptidomimetic **16** exists in two different preferred conformations: one characterized by a γ-turn centered at the Gly residue and a βII'-turn at Gly-Asp, and the second featuring a γ-turn at Arg and a βII'-turn at Arg-Gly (respectively, **16A** and **16B** in Figure 1.33). In both cases, the RGD sequence displays a kinked, non-extended arrangement with a rather short (6.5-7.4 Å) C_β(Arg)–C_β(Asp) distance. This result is in good agreement with the low integrin affinity of compunds **16**. On the contrary, the high affinity ligand **17** adopts a single extended arrangement of the RGD sequence [C_β(Arg)–C_β(Asp) average distance = 9.3 Å] characterized by a pseudo β-turn at DKP-Arg and the formation of an inverse γ-turn at Asp (Figure 1.33).[97]

Figure 1.33. Preferred intramolecular hydrogen-bonded patterns proposed for compound **16** and **17** on the basis of spectroscopic data.

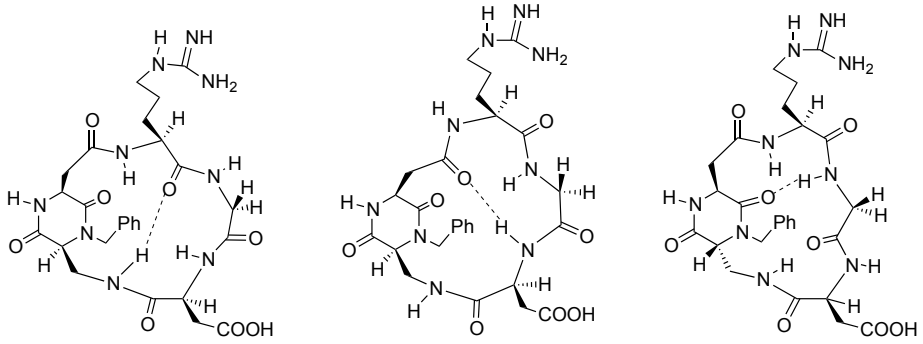

2.2 - *Library of DKP scaffolds*

On the basis of the goals previously achieved by our research group, a library of bifunctional diketopiperazines structurally similar to **DKP1** and **DKP2** (see Figure 1.29) was prepared, varying their stereochemistry and substitution pattern (**DKP3 - DKP8**, Figure 1.34).

Figure 1.34 – Library of bifunctional diketopiperazine scaffolds **DKP1-DKP8**

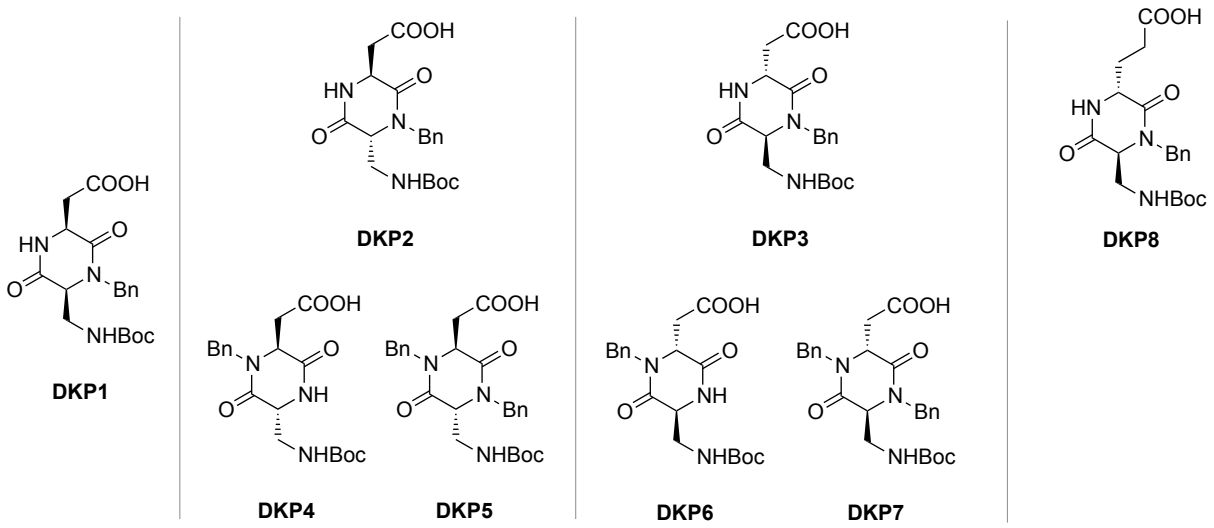

2.2.1 - *Conception of the library*

DKP1 and **DKP2** already revealed interesting and valuable constrained rigid scaffolds which, bearing a carboxylic acid and an amino functionalities. Tiny variations in their stereochemistry, ring substitutions or degrees of freedom, may dramatically change the behavior of these scaffolds when inserted into a peptidomimetic moiety. Having a wide range of scaffolds available may be of great impact, expecially when aiming at the modulation of a biological target.

A collection of eight diketopiperazines (**DKP1**–**DKP8**) was synthesized, varying their stereochemistry and substitution patterns (Figure 1.34). In particular the scaffolds differ in:

1) the relative stereochemistry, namely *cis* (**DKP1**) or *trans* (**DKP2**–**DKP8**);

2) the absolute stereochemistry of the *trans* scaffolds [3*R*,6*S* (**DKP2**, **DKP4**, **DKP5**) or 3*S*,6*R* (**DKP3**, **DKP6**, **DKP7**, **DKP8**)];

3) the substitution at the endocyclic nitrogen atoms, which can be either hydrogen or benzyl (**DKP2**, **DKP3**, **DKP4**, **DKP6**, **DKP8**) or dibenzyl (**DKP5**, **DKP7**);

4) the length of the side-arm bearing the carboxylic group, which can be either carboxymethyl (**DKP1**–**DKP7**) or carboxyethyl (**DKP8**).

2.3 - *Synthesis of DKP1-DKP8*

A solution phase Boc-strategy was chosen for the synthesis of all the scaffolds. Different synthetic approaches were devised depending on the diketopiperazine nitrogen substitution.

2.3.1 - *Synthesis of **DKP1** - **DKP3***

The synthesis of **DKP1**, **DKP2** and **DKP3** (bearing a benzyl group at nitrogen N-4, Figure 1.34) was performed according to procedures already developed in the group.[94] Hydroxymethyl diketopiperazine **43** was identified as a suitable precursor. The diketopiperazine ring was supposed to be provided by the cyclization of the dipeptide methylester derived from suitably protected and functionalized L- or D-aspartic acid and L- or D-serine (Scheme 1.2).

Scheme 1.2. Retrosynthetic approach to **DKP1-DKP3**.

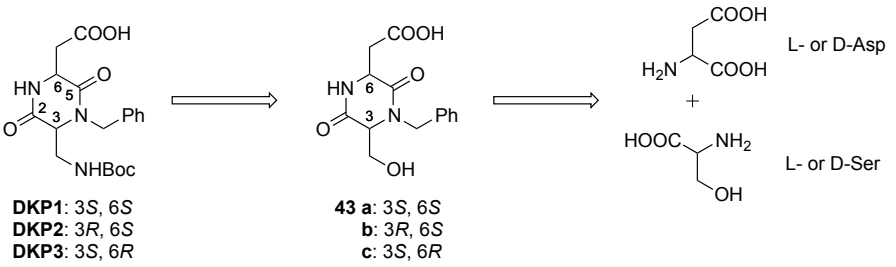

Initially, aspartic acid was protected as an allylester on the β carboxylic acid functionality, *i.e.* orthogonally to Boc and methyl ester. Either L- or D-aspartic acid were accordingly esterified by treatment with acetyl chloride in allyl alcohol to give aspartic acid β-allylester hydrochloride **44** (Scheme 1.3). The reaction of acetyl chloride with allyl alcohol generated HCl *in situ* leading to the formation of allyl acetate, which did not interfere with the reaction. This procedure is reported to be selective for the β-carboxylic group esterification, but some bis-allylation can still take place.[98] In order to minimize the α-carboxylic acid esterification, the reaction was performed at low temperature (0-10 ºC). The amino group was then protected as *tert*-butoxycarbonyl (Boc) under standard conditions, to give *N*-(Boc)-aspartic acid β-allyl ester **45** (Scheme 1.3). On the other hand, the free OH group of the serine side-chain was not expected to react in the subsequent coupling reaction. Hence, only the α-carboxylic acid group was protected as methyl ester: serine methyl ester hydrochloride **46** was obtained by esterification of the corresponding free amino acid in refluxing methanol, in the presence of acetyl chloride (as a source of HCl). The hydrochloride salt **46** was then treated with benzaldehyde in methanol, in the presence of *i*Pr_2NEt to obtain the corresponding imine, that was subsequently reduced with sodium borohydride (Scheme 1.3) affording *N*-benzylserine methyl ester **47**. In order to minimize racemization during this reductive alkylation step, special attention should be given to both temperature (-10°C during addition of reagents) and reaction time.[99]

Scheme 1.3. Synthesis of precursors[a]

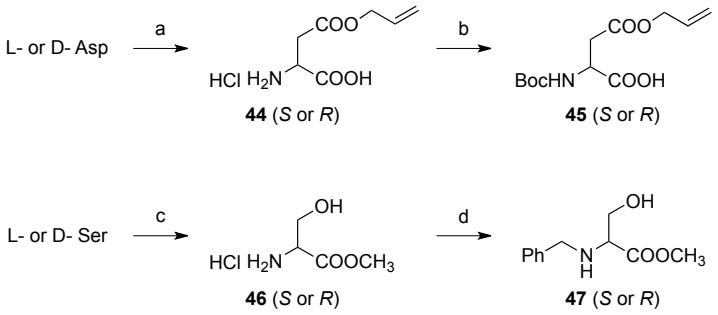

[a]Reagents and conditions: (a) CH_3COCl, CH_2=$CHCH_2OH$, 80%; (b) Et_3N, Boc_2O, 1:1 H_2O/THF, 96%; (c) CH_3COCl, CH_3OH, 100%; (d) Et_3N, PhCHO, CH_3OH, then $NaBH_4$, 93%.

It was then attempted to couple protected aspartic acid **45** with *N*-benzylserine **47**. This reaction was reported using Carpino's reagent HATU, and the formation of dipeptides **48** was reported to occur in good yield (70%).[94] After Boc-deprotection with TFA in dichloromethane, and subsequent basic activation in a biphasic medium (aqueous 1M $NaHCO_3$ solution, AcOEt), diketopiperazines **43** were expected to be formed through an intramolecular 6-*exo* ring closing (Scheme 1.4).

Scheme 1.4. Synthetic route to diketopiperazine **43**, as reported in the literature[a]

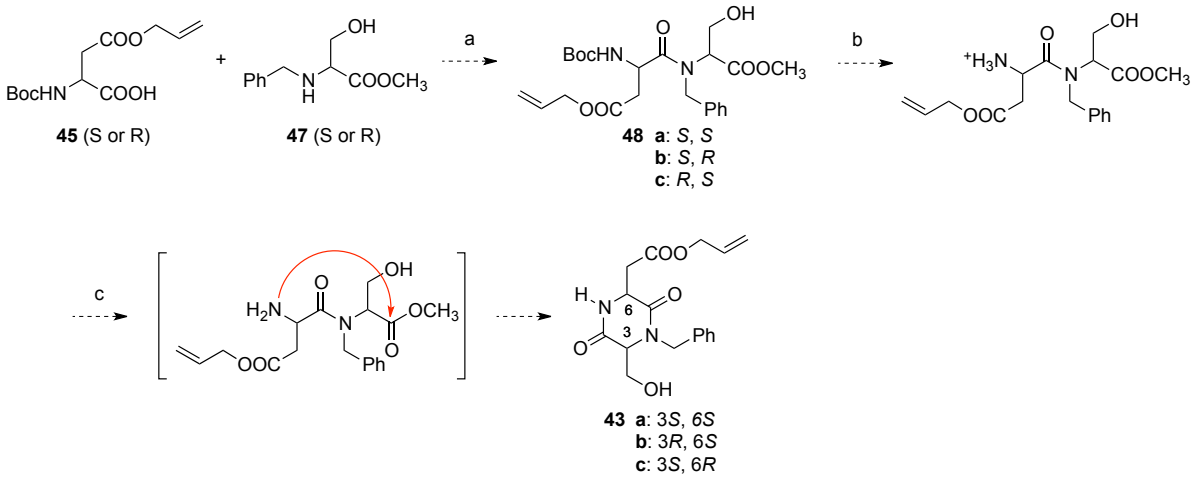

[a]Reagents and conditions: (a) HATU, HOAt, *i*Pr_2EtN, DMF, 72%; (b) CF_3COOH/CH_2Cl_2 1:1; (c) $NaHCO_{3\ aq.}$ 1M, AcOEt, 77% over two steps.

Diketopiperazines **43** were actually obtained in good yields with these synthetic steps. The structure of the *cis* compound **DKP1** (Figure 1.31) was also confirmed by X-ray.[94]

Being sure of having obtained compounds of structure **43**, we decided to investigate more carefully the reaction between aspartic acid derivatives **45** and the serin derivatives **47**. Direct coupling of these fragments (with HATU, iPr$_2$NEt or with EDC, DMAP) led to the isopeptides **49** in high yield, instead of forming the expected dipeptides **48** (Scheme 1.5).[100]

Scheme 1.5. Formation of an isopeptide by direct coupling of compounds **45** and **47**[a]

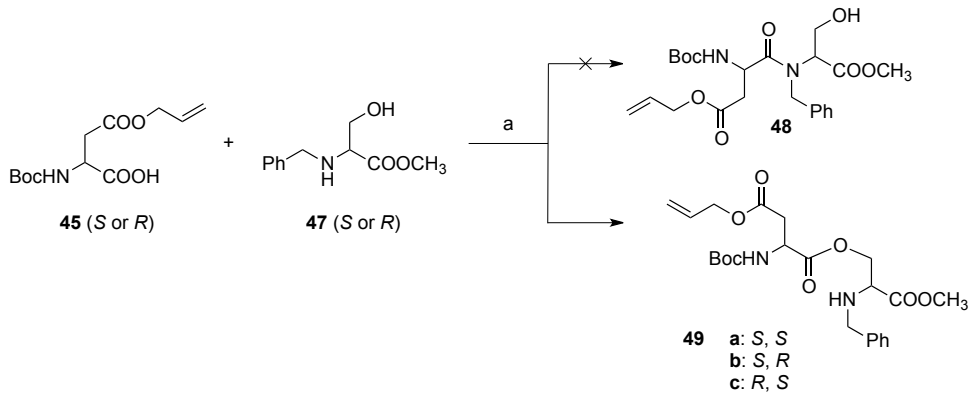

[a]Reagents and conditions: (a) HATU, HOAt, iPr$_2$NEt, DMF, 72%.

The spectroscopic properties of the intermediates were more closely inspected, revealing the the selective acylation of the unprotected β-hydroxy group of either (*S*)- or (*R*)-*N*-benzylserine, with no evidence peptide formation. Diagnostic of this outcome were the NMR spectra, studied in particolar for compounds **49a** and **49b**: (i) in the ^{1}H NMR spectrum, the O-CH$_2$ protons of serine were rather deshielded [**49a**: δ 4.32-4.48, m, 2H ($CDCl_3$); **49b**: δ 4.30, dd, 1H and δ 4.39, dd, 1H (CD_2Cl_2)]; (ii) in the HMBC (Heteronuclear Multiple Bond Coherence) spectrum of both compounds, a long-range coupling (through three bonds) was clearly evident between the O-CH$_2$ protons of serine and the α-carbonyl carbon of aspartic acid residue (Figure 1.35). Had we been in presence of dipeptide **48**, we would have expected other long range couplings, in particular between the the α-carbonyl carbon of Asp and both the CH$_2$-Ph and the C$_\alpha$-H of Ser.

Figure 1.35. HMBC spectra analysis of isopeptides **49a** and **49b**[a]

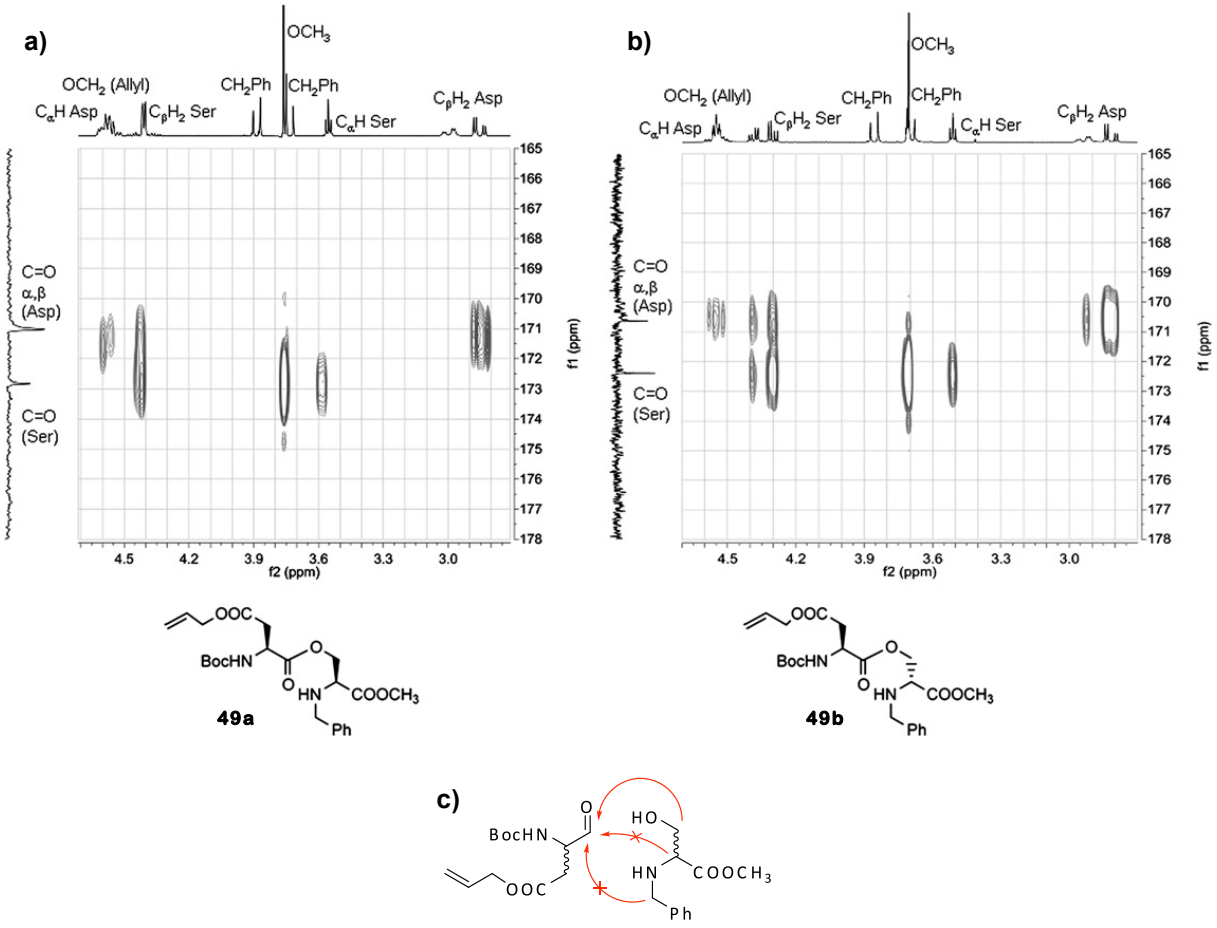

[a] HMBC spectra of a) **49a** ($CDCl_3$) and b) **49b** (CD_2Cl_2), highlighting the long range coupling (through three bonds) between the O-CH_2 protons of Ser and the α-carbonyl carbon of Asp; c) scheme representing the long range couplings highlighted from the HMBC spectra.

In order to further prove our hypothesis, an extra experiment was conducted on compound **49b**. Capping compound **49b** with acetic anhydride provided isopeptide **50** (Scheme 1.6).

Scheme 1.6. Acetylation of isopeptide **49b**[a]

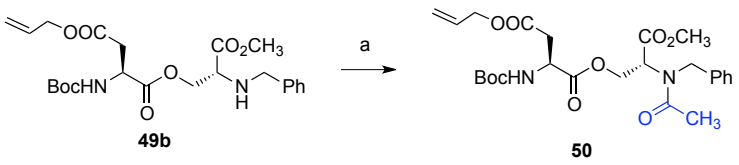

[a]Reagents and conditions: (a) Ac_2O, pyridine, 3h, quant.

In this case, a long range coupling (through three bonds) between the benzylic CH_2 protons of benzylserine and the acetyl carbonyl carbon was detected, confirming that acetylation had occurred on

the secondary amine group of serine, which was therefore not involved in an amide bond with the aspartic fragment (Figure 1.36).

Figure 1.36. HMBC spectrum of **50** in CD_2Cl_2

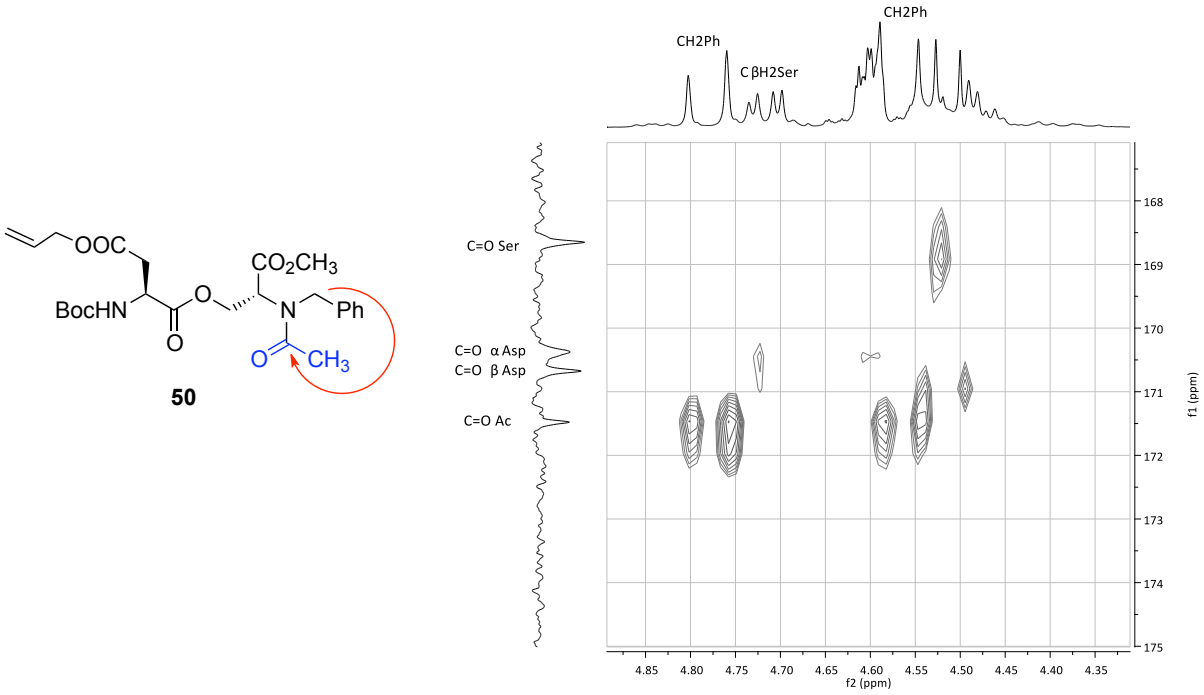

Thus, given that compound **43** was obtained quantitatively after Boc deprotection of compounds **49** with TFA and subsequent treatment with four equivalents of Et_3N or iPr_2NEt in methanol, it was clear that the deprotected isopeptide intermediate had to procede through an *O,N*-acyl transfer while forming the diketopiperazine ring. Puzzled by this behavior, we decided to investigate the conditions promoting *O,N*-acyl transfer/cyclization reactions, and the relevant mechanism that leads to diketopiperazine **43b** from isopeptide **49b**. Despite the presence of a nucleophilic nitrogen, isopeptide **59b** was stable both in solid state and in solution (dichloromethane). Instead, a complete degradation of the product was observed in methanol after 72 h, which could be attributed (as revealed from ^{1}H-NMR spectra) to the transesterification of the aspartate β-allyl ester and to the cleavage of the isopeptidic bond, giving rise to *N*-(*tert*-butoxycarbonyl)-aspartic acid dimethylester and *N*-benzylserine methyl ester. In any case, isomerisation to dipeptide **48b** was not observed.

Afterwards, the Boc group of isopeptide **49b** was cleaved by reaction with TFA to give the bis-TFA salt **51**, which was fully characterized (Scheme 1.7).

Scheme 1.7. Cleavage of the Boc group on **49b**[a]

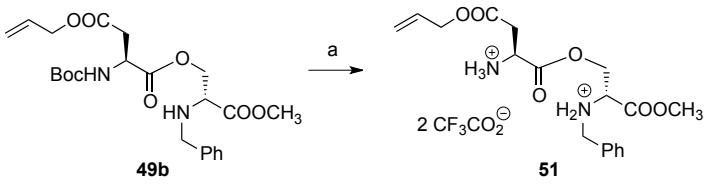

[a]Reagents and conditions: (a) CF_3CO_2H/CH_2Cl_2, 1:1, 2h, quantitative.

Also in this case, the HMBC spectrum of **51** confirmed that no *O*,*N*-acyl shift had occurred: no long-range couplings were detected between the α-carbonyl carbon of Asp and either the CH_2-Ph or the C_α-H of Ser. Only a long-range coupling between the O-CH_2 of Ser and the α-carbonyl carbon of Asp was highlighted in the spectrum (Figure 1.37).

Figure 1.37. HMBC spectrum of isopeptide bis trifluoroacetate salt **51**[a]

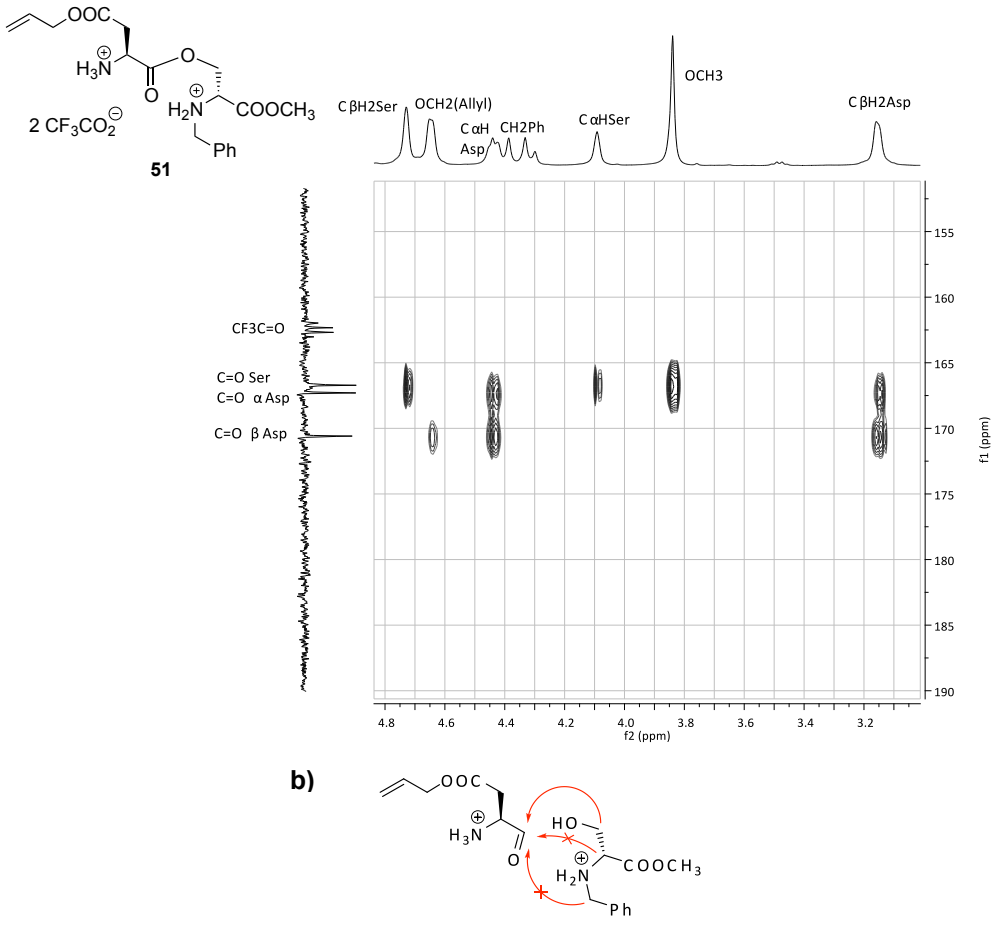

[a] a) HMBC spectrum of isopeptide bis trifluoroacetate salt **51** ($CDCl_3$), highlighting the long range coupling (through three bonds) between the O-CH_2 protons of Ser and the α-carbonyl carbon of Asp; b) scheme representing the long range couplings highlighted from the HMBC spectrum.

The reactivity of bis-TFA salt **51** was then investigated. *O*,*N*-Acyl migration was not observed after 48 h, monitoring a dichloromethane solution of compound **51** by ^{1}H-NMR; conversely, when dissolved in methanol, complete methanolysis of isopeptide bis-TFA salt was detected in 6 h, giving rise to (2*S*)-aspartic acid β-allyl ester α-methylester and *N*-benzylserine methyl ester. Even in this case isomerization to the dipeptide was not observed. Upon addition of 4 equivalents of a base (Et_3N or *i*Pr_2NEt) to a solution of bis-TFA salt **51** in methanol, ring closure occurred rapidly and was virtually complete after 2 h. However, monitoring the reaction by ^{1}H-NMR spectroscopy (CD_3OD / 4 eq. Et_3N), the dipeptide **48b** resulting from the *O*,*N*-acyl shift was never detected, and only signals concerning the starting bis-TFA salt **51** and the resulting diketopiperazine **43b** were identified.

As can be clearly seen in Figure 1.38, the two dd at δ 4.32 and δ 4.45, belonging to the O-CH_2 protons of benzylserine in the isopeptide bis-TFA salt **51**, decreased in intensity with time, while the dd at δ 3.93 and δ 4.02, corresponding to the same O-CH_2 protons in **43b**, proportionally increased.

Figure 1.38. ^{1}H-NMR monitoring of the transformation of isopeptide bis-TFA salt **51** into the diketopiperazine **43b** (CD_3OD / 4 eq. Et_3N).

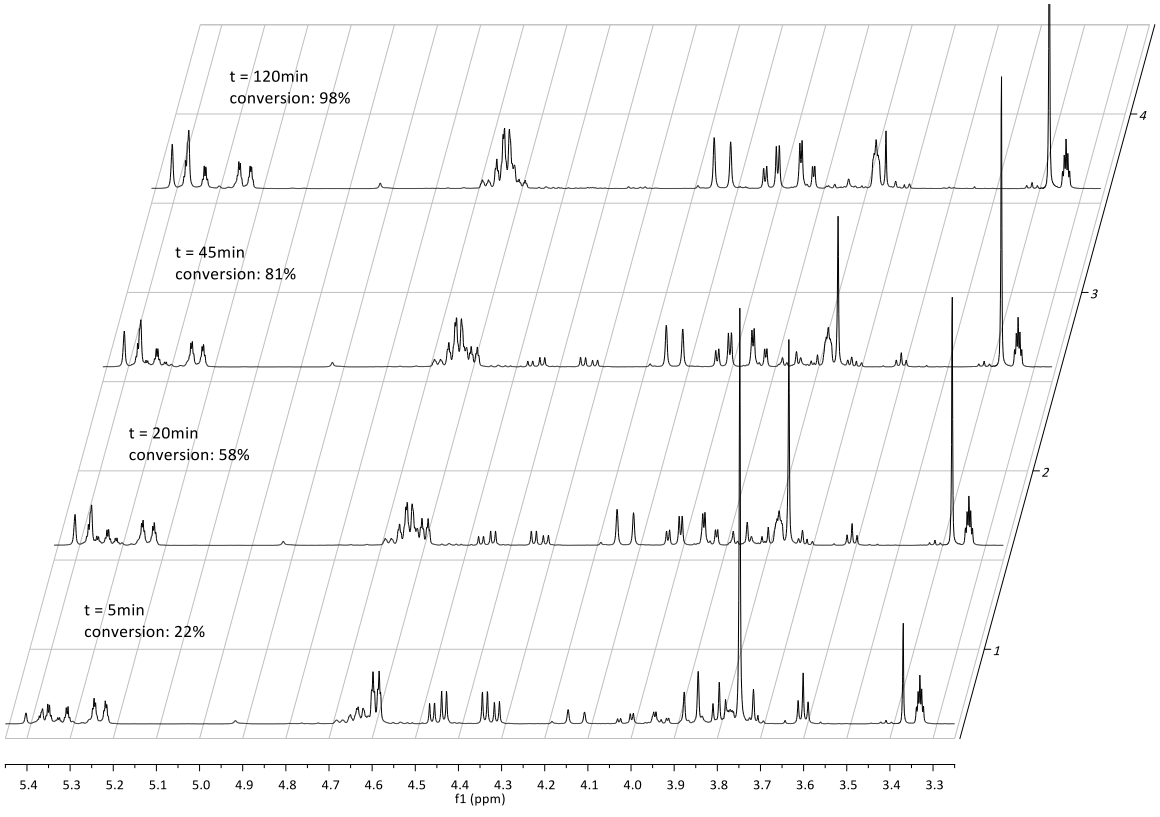

The same holds for the two doublet of the benzylic CH_2 protons, which in the isopeptide salt **51** resonate at δ 3.73 and δ 3.87, while in **43b** shift to δ 4.12 and δ 5.38, and for the serine C_α-H which moves from δ 3.6 to δ 3.77. The same transformation (bis-TFA salt **51** to **43b**) was followed by ^{1}H-NMR in an aprotic solvent (CD_2Cl_2 containing 4 eq. of Et_3N). In this case too, despite the much reduced reaction rate (only 32% conversion was observed after 15 h), no *O,N*-acyl shift product was ever detected (Figure 1.39).

Figure 1.39 - ^{1}H-NMR monitoring of the transformation of isopeptide bis-TFA salt **51** into the diketopiperazine **43b** (CD_2Cl_2 / 4 eq. Et_3N).

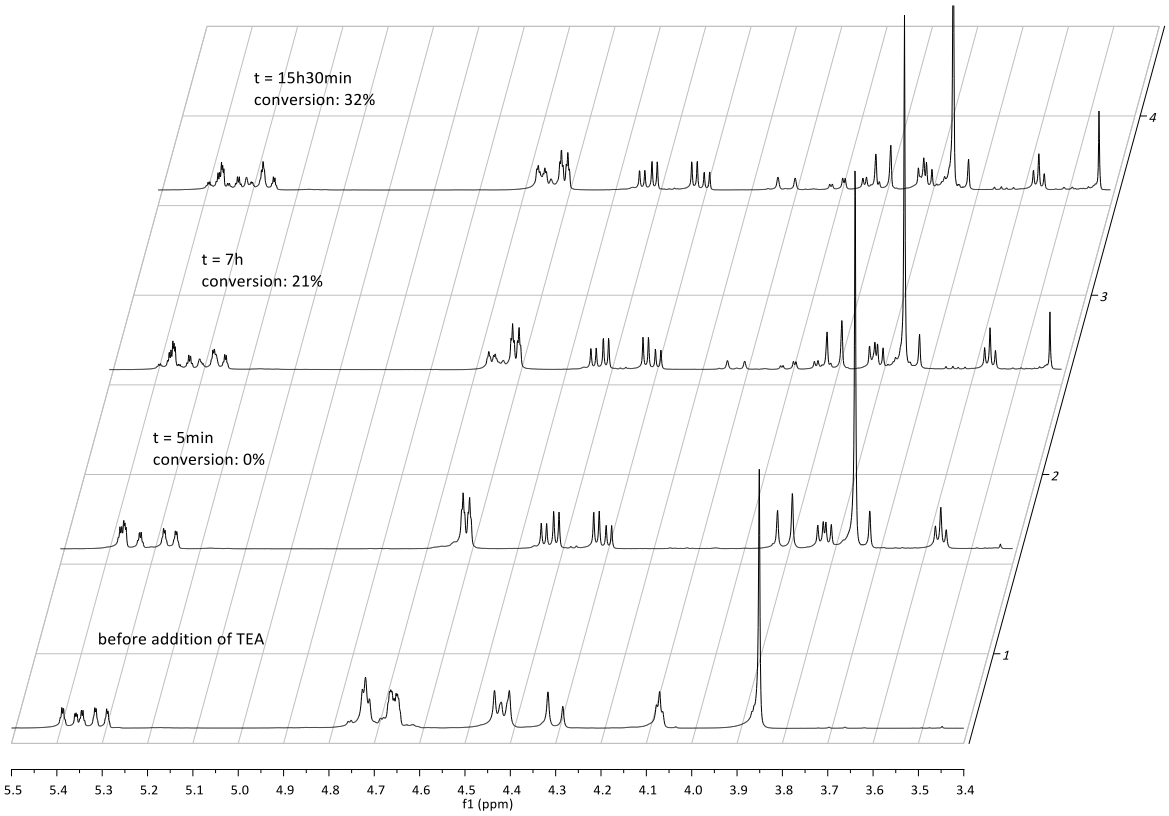

Based on these experimental observations, a reasonable mechanistic explanation involves a rate limiting *O,N*-acyl transfer with simultaneous ring closure to DKP, so that no dipeptide intermediate can be detected (Scheme 1.8). On a preparative scale, the synthesis of diketopiperazine **43b** from bis-TFA salt **51** was more efficiently performed (94% isolated yield) with *i*Pr_2NEt (4 eq.) in *i*PrOH instead of MeOH, that in the long run leads to transesterification of aspartic allyl ester.[100] Analogous results were also observed while synthesizing both diketopiperazines **43a** (*cis*) and **43c** (*trans*).

Scheme 1.8. Proposed diketopiperazine mechanism of formation[a]

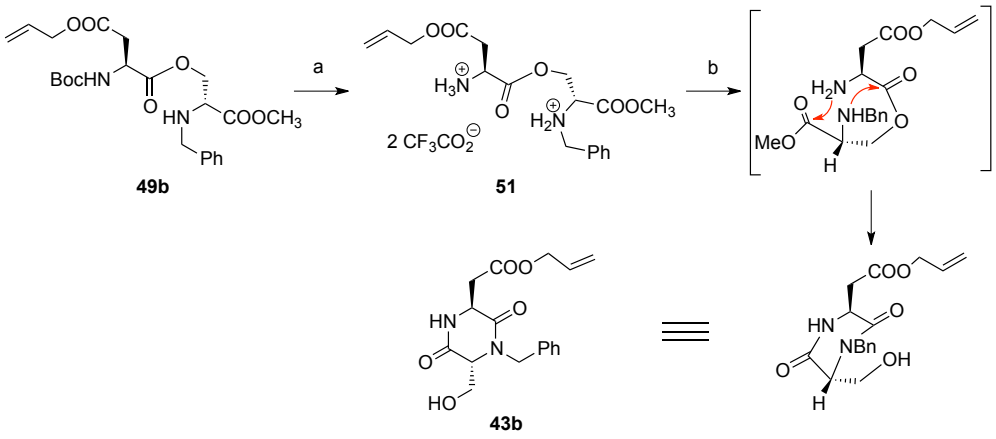

[a]Reagents and conditions: (a) CF_3CO_2H/CH_2Cl_2, 1:1; (b) 4 equiv. base (Et_3N or iPr_2EtN), MeOH.

In vision of scaling up the synthesis of isopeptide **49**, these studies gave us enough information on how to improve the coupling reaction between the two aminoacid derivatives **45** and **47**. Since an ester bond is formed instead of an amide bond, the more appropriate coupling reagent EDC (1-ethyl-3-(3-dimethylaminopropyl) carbodiimide) in presence of a catalytic amount of DMAP (4-dimethylaminopyridine) provided the best results (Scheme 1.9). Carpino's reagents (HATU, HOAt) are very useful to avoid epimerization on the α proton during aminoacid coupling, but also this methodology, monitoring temperature and reaction time, gives no epimerization on the α proton, as confirmed by ^{13}C-NMR. Furthermore, the yields we got were higher than those obtained with Carpino's reagent.

Scheme 1.9. Coupling reaction using EDC

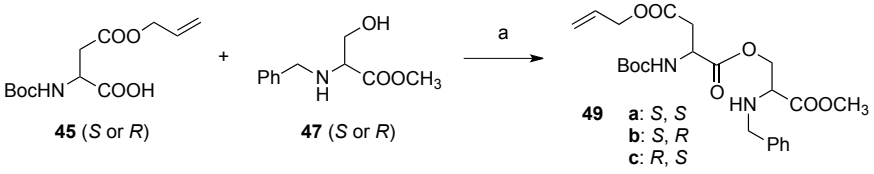

[a]Reagents and conditions: (a) EDC, $DMAP_{cat.}$, CH_2Cl_2, 94%

Once the coupling reaction and the subsequent diketopiperazine ring closure were improved, we focused on the transformation of the hydroxy moiety of **43** into the Boc-protected amino moiety present in **DKP1-DKP3**. Functional group interconversion was accomplished by a Mitsunobu type reaction,[101] followed by Staudinger reduction of the obtained azides **52** and *in situ* Boc-protection to

afford derivatives **53**. Deprotection of the allyl ester on compounds **53** was succesfully accomplished via a Pd^0 catalyzed Tsuji-Trost reaction, which proceeds quantitatively obtaining the final scaffolds **DKP1**-**DKP3** (Scheme 1.10).

Scheme 1.10. Synthesis of **DKP1-3**[a]

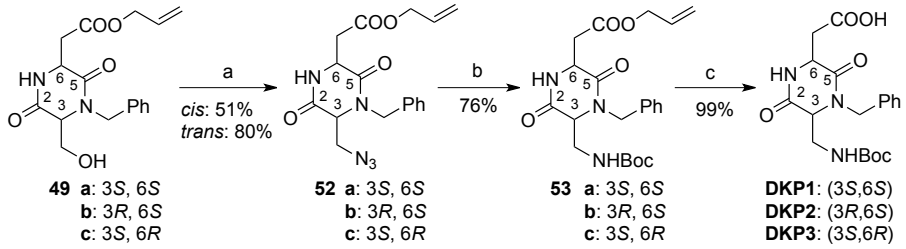

[a]Reagents and conditions: (a) PPh_3, DIAD, H_3N.tol, DCM/toluene, -20°C; (b) Me_3P, Boc-ON, THF, -20°C to room temp.; (c) $[Pd(PPh_3)_4]$, PPh_3, pyrrolidine, DCM, 0°C.

Mitsunobu transformation on substrates **43** is a quite sensitive reaction, since the activated hydroxy group can β eliminate before reacting with the hydrazoic acid (HN_3). The C(6) proton can be in fact easily abstracted due to its acidity, providing a diketopiperazine with an exocyclic double bond (**54**, Scheme 1.11).

Scheme 1.11. β-Elimination competing with the Mitsunobu reaction[a]

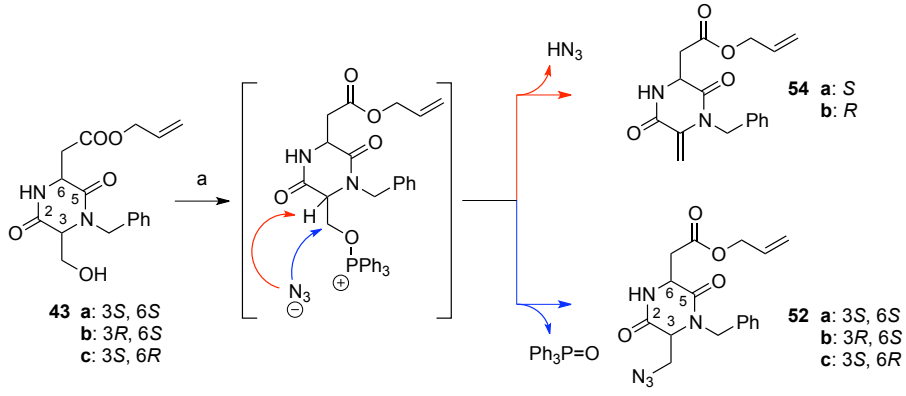

[a]Reagents and conditions: (a) PPh_3, DIAD, H_3N.tol, DCM/toluene, -20°C.

Monitoring temperature (which should not exceed -20°C), reaction time and order of reagent addition, we were able to drastically reduce the amount of **54** formed, reducing the ratio **52a**:**54a** to 3:1, **52b**:**54a** and **52c**:**54b** to 8:1. The reaction was carried out in a 2:1 toluene/dichloromethane mixture,

since toluene was not sufficient to solubilize diketopiperazines **43** at -20°C. β-Elimination side reaction proved to be particularly competitive in the case of the *cis* substrate **43a**. Purification from the by-product revealed even more difficult, as product **52a** showed almost the same elution time of the corresponding byproduct **54a**, with various eluents. These are the main reasons why yields are far lower for the *cis* product. NMR evidence of the formation of azide **52b**, namely the shift of C_α-H and C_β-H_2 derived from serine, is reported in Figure 1.40.

Figure 1.40. ^{1}H-NMR comparison of compounds **43b** and **52b**

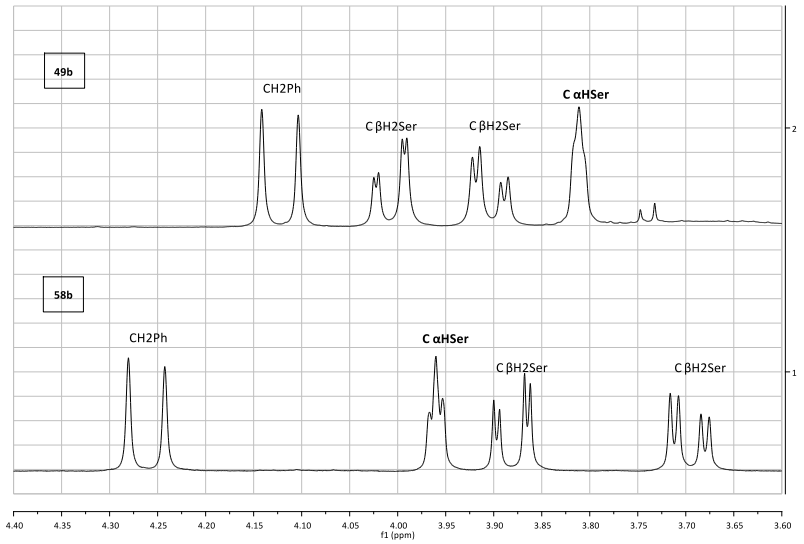

The next step involved a one-pot Staudinger reaction – Boc protection. The Staudinger reaction, a very mild azide reduction, involves the reaction of the azide with a phosphine to generate a phosphazide, which loses N_2 to form an iminophosphorane. Hydrolysis of this intermediate leads to the amine and the very stable phosphine oxide. In our case the intermediate iminophosphorane reacted directly with 2-(*t*-butoxycarbonyloxyimino)-2-phenylacetonitrile (Boc-ON),[102] present in the reaction medium, affording the desired Boc-protected amine in very good yield. The mechanism is reported in Scheme 1.12.

Scheme 1.12. Staudinger reaction, mechanism.

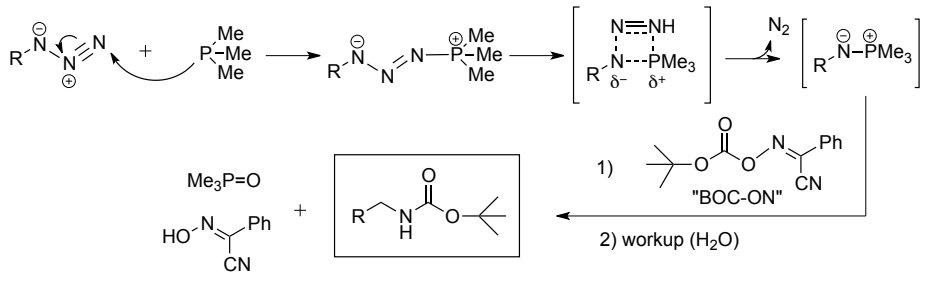

Finally the DKP scaffold allyl esters **53** (Scheme 1.10), were de-allylated in the presence of a catalytic amount of tetrakis(triphenylphosphine) palladium(0) [$Pd(PPh_3)_4$] and pyrrolidine, *i.e.* a nucleophile acting as an allyl scavenger to give the amino acid derivatives **DKP1-DKP3** in quantitative yield. Such methodology is of special interest for peptide synthesis because the deprotection conditions are usually mild enough to be compatible with the presence of acid labile *t*-Bu and Boc protective groups.[103]

A comprehensive scheme of the whole synthetic route to **DKP1-DKP3** is reported below (Scheme 1.13).

Scheme 1.13. A summary scheme of the whole synthetic route to **DKP1-DKP3**[a]

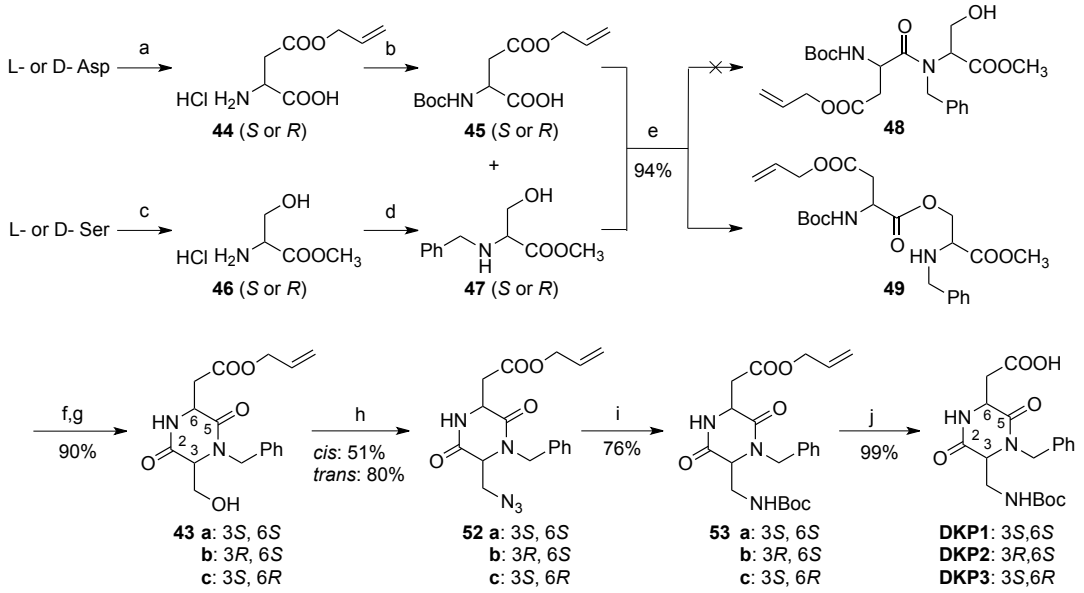

[a]Reagents and conditions: (a) CH_3COCl, CH_2=$CHCH_2OH$; (b) Et_3N, Boc_2O, 1:1 H_2O/THF; (c) CH_3COCl, CH_3OH; (d) Et_3N, PhCHO, CH_3OH, then $NaBH_4$; (e) EDC, $DMAP_{cat.}$, DCM; (f) TFA/DCM, 1:1; (g) *i*Pr_2EtN, *i*PrOH; (h) PPh_3, DIAD, H_3N.tol, DCM/toluene, -20°C; (i) Me_3P, Boc-ON, THF, -20°C -> r.t; (j) $[Pd(PPh_3)_4]$, PPh_3, pyrrolidine, DCM, 0°C.

2.3.2 - *Synthesis of **DKP4** and **DKP6***

A retrosynthetic analysis of scaffolds **DKP4** and **DKP6** (bearing a benzyl group at nitrogen N-1) suggested that, even in this case, the diketopiperazine ring **55** could be obtained from suitably protected aspartic acid and serine in the correct relative configuration (Scheme 1.14). We started investigating the synthesis of scaffold **DKP4**. As regards the aspartic acid derived fragment, both carboxylic acid moieties were protected as methyl esters and nitrogen was subsequently reductively alkylated to give derivative **56** (Scheme 1.15).

Scheme 1.14. Retrosynthetic analysis of scaffolds **DKP4** and **DKP6**

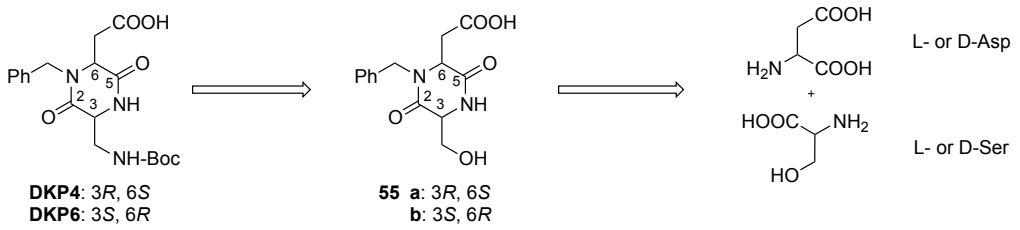

Protection of the Ser hydroxy group was necessary to avoid self-condensation: we initially decided to non-orthogonally protect the hydroxyl (as *t*Bu ether) and the amino functionalities (as Boc), which can be simultaneously deprotected in an acidic medium (*e.g*. TFA solution) before diketopiperazine ring closure; Boc-Ser(O*t*Bu)OH **57**, was commercially available (Fluorochem™).

Scheme 1.15. Synthesis of protected dipeptide Ser-Asp[a]

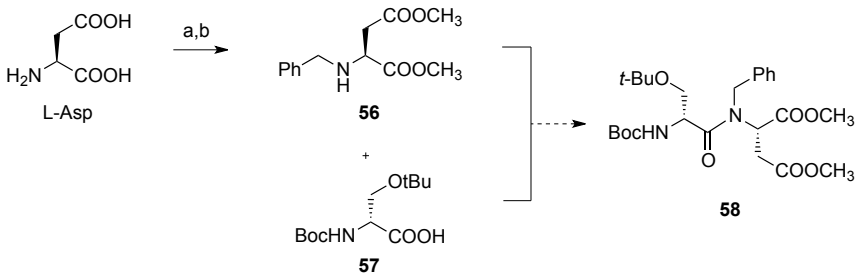

[a]Reagents and conditions: (a) CH_3COCl, CH_3OH: 99%; (b) $NaBH_3CN$, PhCHO, CH_3OH: 67%.

Coupling the two aminoacid fragments **56** and **57** proved to be very challenging: the secondary nitrogen of Asp (that should act as the nucleophile) is very hindered and, moreover, serine carboxylic group is hindered as well, due to the two surrounding *t*Bu groups. The use of classical aminoacid coupling agents, such as HATU, DPPA, PyBrOP (reported to be very useful in the coupling of *N*-methyl aminoacids),[104] was attempted first, but the desired dipeptide **65** could not be obtained (Scheme 1.16). Curiously, reaction with PyBrOP provided a pyrrolidine serine derivative in good yield. Other methods envisaging carboxyl activation *via N*-carboxyl anhydride (NCAs) derivatives were employed.[105] Original procedures prompted the treatment of an aminoacid with phosgene. Milder reactants, such as diphosgene ($ClCO_2CCl_3$) or chlorosilanes (such as Cl_2SiMe_2) were later developed to generate an NCA derivative (these compounds generate silylated NCA derivatives).

Scheme 1.16. Coupling attempts between compounds **56** and **57** with "traditional" methodologies.

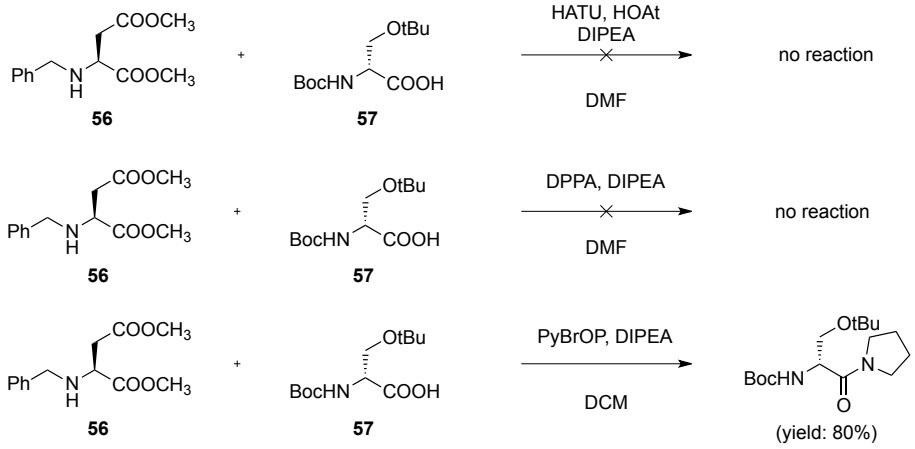

We attempted to use both of these mild methodologies to generate NCA-activated derivatives of H-D-Ser(*t*Bu)-OH (Fluorochem™). Unfortunately, only reaction with dimethylchlorosilane led to the NCA-like compound. Also this activation did not prove anyway strong enough to induce dipeptide formation when reacted with nucleophile **56** (Scheme 1.17).

Scheme 1.17. Coupling attempts between compounds **56** and **57** exploiting NCA derivatives

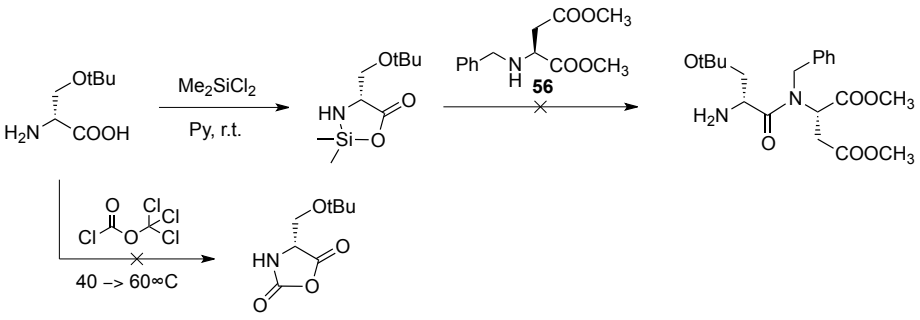

During the 1990s, Carpino *et al*. reported the use of aminoacid fluorides as active species for coupling.[106] The pK_a value of hydrogen fluoride, which is generated as a byproduct during the coupling reaction, is far higher than those of hydrogen chloride or bromide, thus allowing this procedure to be compatible with acid labile protective groups (*e.g*. Boc). The acyl fluoride derivative of **57** was prepared in crystalline form using cyanuric fluoride and was subjected to reaction with compound **56**, without previous purification: the isolated yield of dipeptide **58** after workup and chromatography purification was extremely low (10%, Scheme 1.18).

Scheme 1.18. Attempted activation of compound **57** as acyl floride

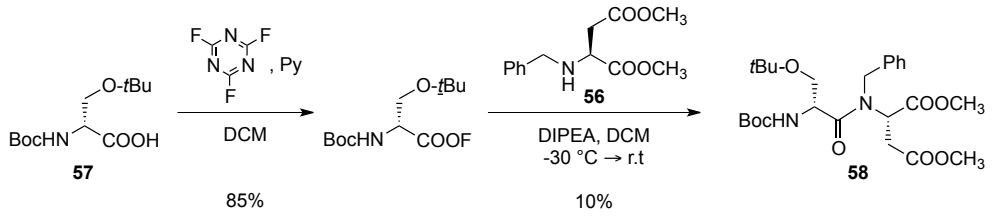

Further attempts were made activating Ser as its mixed and symmetric anhydrides.[107] The mixed anhydride of compound **57**, obtained after reaction with isobutylchloroformate (IBCF), was reacted in a one-pot procedure with aspartic derivative **56**. The nucleophile preferentially attacked on the wrong carbonyl of the mixed anhydride (probably due to steric factors), leading to a useless carbamate (Scheme 1.19).

Scheme 1.19. Mixed anhydride attempt

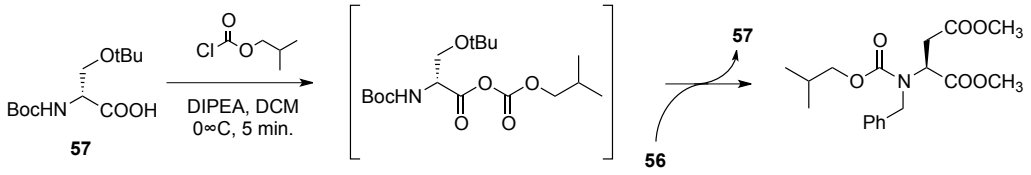

Finally, to our delight, pre-formation of the symmetric Boc-Ser(O*t*Bu) anhydride (with DCC) and coupling to *N*-Bn-Asp dimethyl ester **56** afforded the corresponding dipeptide **58** in a satisfactory 75% yield (Scheme 1.20). The symmetric anhydride was separated by filtration from the unsoluble dicylohexyl urea (DCU, formed as DCC byproduct), in order to prevent the undesidered condensation between DCU and the symmetric anhydride (Scheme 1.20). Furthermore, the unreacted serine derivative **57**, resulting from the breakdown of the symmetric anhydride, was recovered in the workup (Scheme 1.20). Treatment of dipeptide **58** with trifluoroacetic acid (to deprotect both *N*-Boc and *O*-*t*Bu) and subsequent ring closing reaction in methanol afforded diketopiperazine **55a** in good yield (Scheme 1.21). Planning to transform hydroxy group of **55a** in a protected amino group, we performed the Mitsunobu reaction under the same conditions used for the synthesis of scaffolds **DKP1-DKP3** (toluene/DCM, -20 °C), but we recovered only the starting material. Hence, we tried increasing temperature gradually, from -20 °C to 0 °C, without any results.

Scheme 1.20. Formation of dipeptide **58** *via* symmetric anhydride

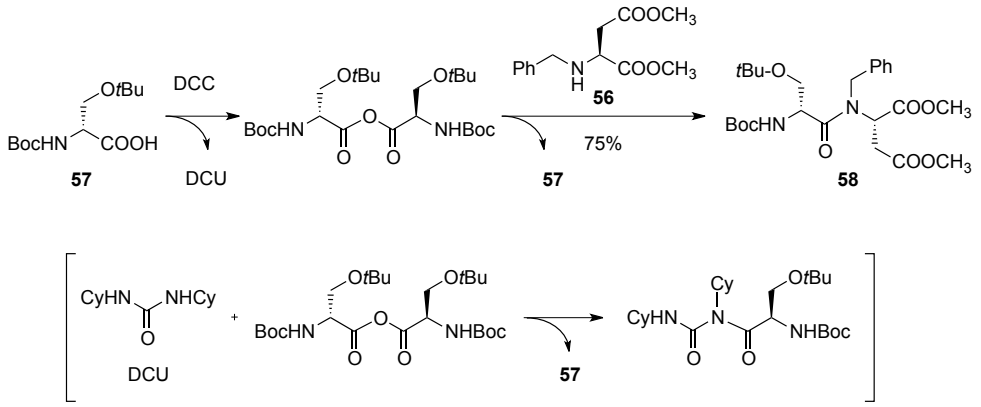

Scheme 1.21. Formation of DKP **55a**

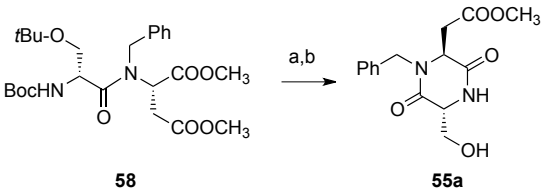

[a]Reagents and conditions: (a) TFA/DCM; (b) MeOH, DIPEA, 85% (over two steps).

The Mitsunobu reaction performed at room temperature afforded the azide **59**, although the major product was the olefin derivative **60** (ratio **59**/**60** = 2:3, Scheme 1.22).

Scheme 1.22. Mitsunobu reaction on compound **55a**

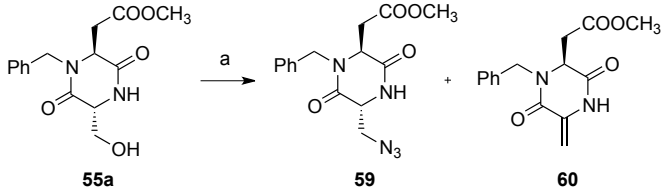

[a]Reagents and conditions: a) PPh_3, DIAD, HN_3·Tol, toluene/DCM, r.t.

The separation of this two-product mixture (i.e. compounds **59** and **60**) was not trivial, and we decided to change our synthetic strategy.

In order to circumvent the problem of β-elimination, simplify the synthetic sequence and avoid the use of an additional protecting group (*t*Bu), the hydroxy group of Boc-Ser-OMe **61** (either L or D) was directly transformed into the corresponding azide under Mitsunobu conditions in 78% yield (Scheme 1.23). The obtained compound **62** was then saponified with LiOH. Treatment of freshly prepared acid **63** with DCC afforded the symmetric anhydride **64** in a quantitative yield, which was isolated by filtering off DCU and evaporating the solvent, and immediately used in the next synthetic step without further purification (Scheme 1.23).

Scheme 1.23. Synthesis of symmetric anhydrides **64**[a]

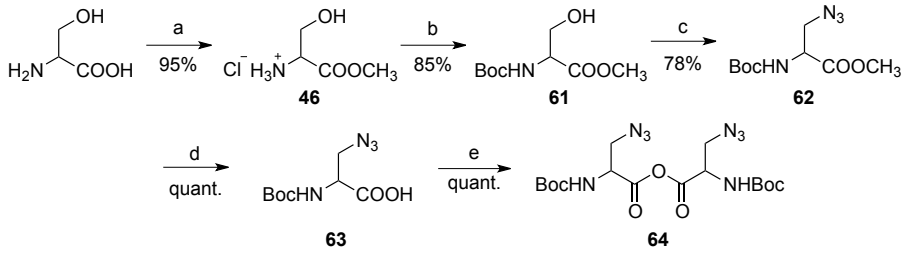

[a]Reagents and conditions: a) CH_3COCl, CH_3OH; b) Boc_2O, THF/H_2O 1:1; c) HN_3, DIAD, PPh_3, THF; d) LiOH, THF/H_2O 1:1; e) DCC, DCM.

The coupling of 3-azido-2-*N*-*tert*-butoxycarbonylaminopropionic anhydride **64** to either (*S*)- or (*R*)-*N*-benzyl-aspartic acid dimethylester **56** occurred in 80% yield, whereas the subsequent Boc cleavage and cyclization to diketopiperazines **59** were nearly quantitative (Scheme 1.24).

Scheme 1.24. Synthesis of diketopiperazines **59**[a]

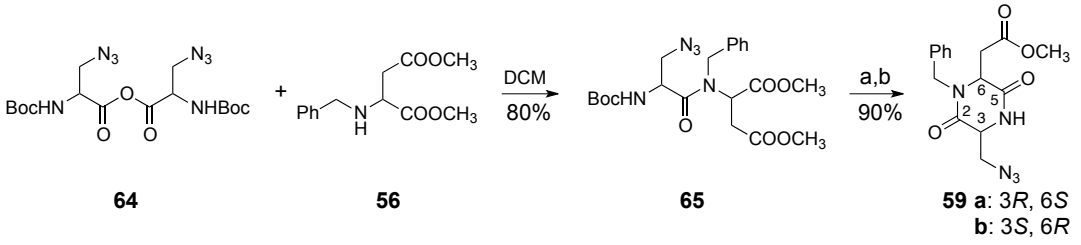

[a]Reagents and conditions: a) TFA/DCM 1:2; b) DIPEA, *i*PrOH.

The Staudinger-type reaction used for the synthesis of **DKP1-DKP3** (see § 2.3.1, in this chapter) could be employed to reduce azides **59**, but in this case, the absence of an allyl ester allowed us to use the more reliable catalytic hydrogenation, which provides amine **66**. Boc-protection and final

hydrolysis of the methyl ester provided diketopiperazines **DKP4** and **DKP6** in 90% yield over three steps (Scheme 1.25).

Scheme 1.25. Synthesis of **DKP4** and **DKP6**[a]

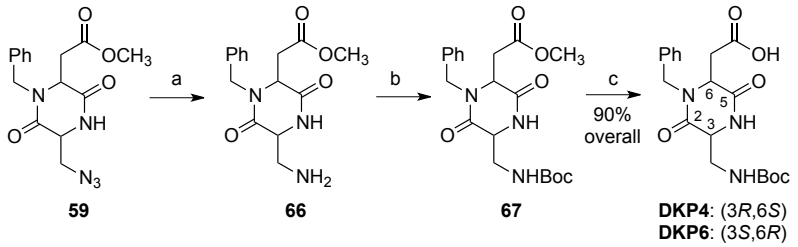

[a]Reagents and conditions: (a) H_2, Pd-C, THF; (b) Boc_2O, THF; (c) LiOH, THF/H_2O 1:1.

2.3.3 - *Synthesis of **DKP5** and **DKP7***

The synthesis of scaffolds **DKP5** and **DKP7** can in principle be achieved through the benzylation of the second diketopiperazine nitrogen of an advanced intermediate in the synthesis of either **DKP2** and **DKP4**, or **DKP3** and **DKP6**, respectively (Figure 1.41). With the aim to minimize the use of protecting groups, a suitable substrate for the nitrogen alkylation was identified in the azide derivative. The diketopiperazine intermediates bearing a free hydroxy group or a Boc-protected amino functionality could give over-alkylated by-products. The azido group was used as a protecting group here, being stable under the alkylation reaction conditions.

Figure 1.41. **DKP5** and **DKP7** retrosynthetical analysis

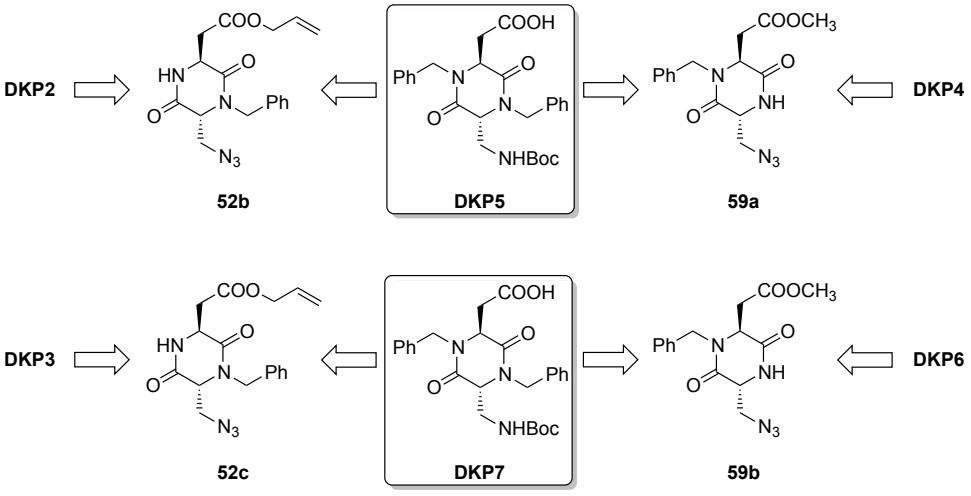

We initially investigated the *N*-benzylation on available intermediates **52b-c**. The alkylation of nitrogen N-4 was attempted using sodium hydride and benzyl bromide in dimethylformamide. This procedure generally provides good yields for amide benzylation, but in our case the major product was the diketopiperazine with an exocyclic double bond (compounds **54a-b**, Scheme 1.11), formed from the elimination of the azido gruop in presence of a strong non-hindered base (*i.e.* NaH). Better results were obtained using the more hindered base KHMDS (potassium bis(trimethylsilyl)amide) in presence of benzyl bromide at a temperature between -70 °C and -40 °C. Azides **68** were converted into **DKP5** and **DKP7** following the same protocols used for the synthesis of **DKP2** and **DKP3**: a Staudinger reduction provided *N*-Boc protected amine **69**, which was then subjected to a Tsuji-Trost-like ester deallylation (Scheme 1.26).

Scheme 1.26. Synthesis of **DKP5** and **DKP7**, starting from intermediates **58b** and **58c**, respectively[a]

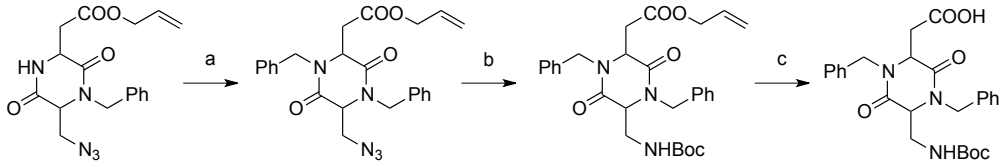

52 **b**: 3*S*, 6*R*
c: 3*R*, 6*S*

68 **a**: 3*R*, 6*S*
b: 3*S*, 6*R*

69 **a**: 3*R*, 6*S*
b: 3*S*, 6*R*

DKP5: 3*R*, 6*S*
DKP7: 3*S*, 6*R*

[a]Reagents and conditions: (a) KHMDS, BnBr, THF/DMF 7:3, 76%; (b) Me_3P, BocON, toluene, 65%; (c) pyrrolidine, PPh_3, [$Pd(PPh_3)_4$], DCM.

Intermediates **59a-b** resulted less prone to β-elimination under *N*-alkylation conditions. Azides **70** are catalytically hydrogenated to the corresponding amines, which could be easily Boc-protected to yield derivatives **71**. Methyl ester hydrolysis finally afforded the desired **DKP5** and **DKP7** (Scheme 1.27). This last approach seems to be slightly better than the previous one, even if both methods can considered comparably reliable.

Scheme 1.27. Synthesis of **DKP5** and **DKP7**, starting from intermediates **59a** and **59b**, respectively[a]

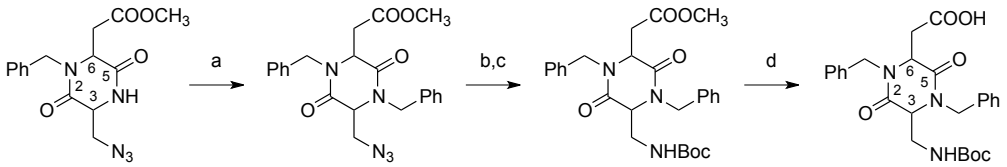

59 **a**: 3*R*, 6*S*
b: 3*S*, 6*R*

70 **a**: 3*R*, 6*S*
b: 3*S*, 6*R*

71 **a**: 3*R*, 6*S*
b: 3*S*, 6*R*

DKP5: 3*R*, 6*S*
DKP7: 3*S*, 6*R*

[a]Reagents and conditions: (a) KHMDS, BnBr, THF/DMF 7:3; (b) H_2, Pd-C, THF; (c) Boc_2O, THF (d) LiOH, THF/H_2O 1:1; 75% over four steps.

2.3.4 - *Synthesis of **DKP8***

Scaffold **DKP-8**, bearing a carboxyethyl side chain, was obtained through a synthetic strategy similar to the one adopted in the case of compounds **DKP1-DKP3** (see § 2.3.1, in this Chapter), starting from (*S*)-*N*-benzylserine methyl ester **47** (see Scheme 1.3) and (*R*)-*N*-(*tert*-butoxycarbonyl)glutamic acid γ-methyl ester **72**.[108] Also in this case, direct coupling of these fragments afforded isopeptide **73**, which was deprotected and cyclized to diketopiperazine **74**. Azidation of the -CH_2OH group through a Mitsunobu reaction, reduction by catalytic hydrogenation, protection with Boc_2O and final hydrolysis of the methylester afforded **DKP8** (Scheme 1.28).

Scheme 1.28. Synthesis of DKP8[a]

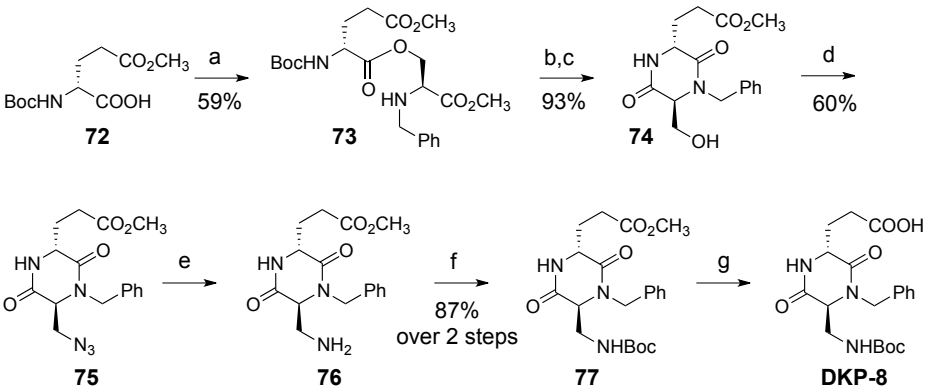

[a]Reagents and conditions: (a) **47**, HATU, HOAt, DIPEA, DMF; (b) TFA/CH_2Cl_2 1:2; (c) DIPEA, *i*PrOH; (d) HN_3, DIAD, PPh_3, CH_2Cl_2/toluene/DMF; (e) H_2, Pd-C, THF; (f) Boc_2O, THF; (g) LiOH, THF/30% H_2O_2 1:1.

The latest step was at first performed in the conditions already described for the synthesis of **DKP4-DKP7**, treating **77** with LiOH in a 1:1 mixture of THF and water. In this case the reaction did not procede as previously observed: it resulted considerably slower and severe racemization problems were detected. Hence, a milder and more selective procedure involving the *in situ* formation of LiOOH was adopted, with which enantiomerically pure **DKP8** was quantitatively obtained.

2.4 - *Synthesis of DKP-RGD peptidomimetics*

A solution-phase synthetic strategy was adopted for the synthesis of the cyclic RGD compounds (reported in Figure 1.15), by using Boc-Arg(Mtr), Gly-OBn and Cbz-Asp(O*t*Bu)-OH. The dipeptide Boc-Arg(Mtr)-Gly-OBn was Boc-deprotected and coupled to the acid of the appropriate diketopiperazine scaffold. Subsequent Boc deprotection of the DKP amino group and coupling of the

aspartic derivative Cbz-Asp(O*t*Bu)-OH afforded the linear peptidomimetic Cbz-Asp(O*t*Bu)-DKPArg(Mtr)-Gly-OBn (Scheme 1.29).

Scheme 1.29. Synthesis of cyclic RGD peptidomimetics **18-23** containing scaffolds **DKP3-DKP8**

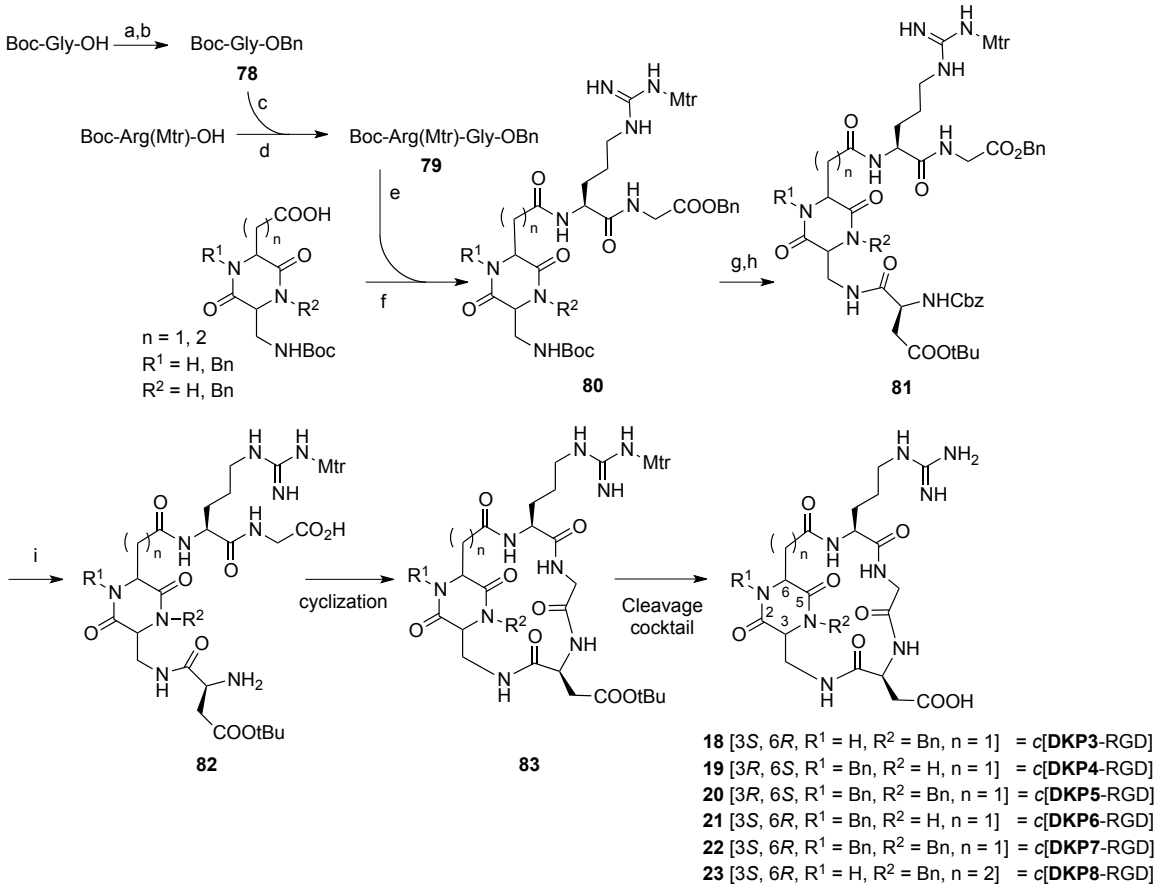

[a]Reagents and conditions: (a) Cs_2CO_3, MeOH; (b) BnBr, DMF: 95%; (c) TFA/DCM 1:2; (d) HBTU, HOBt, DIPEA, DMF: 90%; (e) TFA/DCM 1:2; (f) HATU, HOAt, *i*Pr_2EtN, DMF: 67%; (g) TFA/DCM 1:2; (h) Cbz-Asp(O*t*Bu)-OH, HATU, HOAt, *i*Pr_2EtN, DMF; (i) H_2, Pd/C, THF/H_2O 1:1.

Linear precursors were deprotected was deprotected by hydrogenolysis (Cbz and Bn), in presence of a catalytic amount of palladium on charcoal in methanol, under an H_2 atmosphere. A methylated by-product was formed under this reaction conditions, and the recovery of the desired product by preparative HPLC was not trivial. Thus, we tried different solvents and we found that the hydrogenolysis in THF/water mixture (1:1) proceeded quantitatively without any formation of methylated by-products. The macrocyclization step was optimized on **DKP3** containing compound **82** (3*S*, 6*R*, R^1 = H, R^2 = Bn, n = 1), by screening several synthetic procedures and reactants (Table 1.2). The best results were obtained when using DPPA or FDPP (75% and 73% respectively). DPPA was chosen, as FDPP left some impurities (visible from HPLC-MS profiles) that could not be removed with a flash chromatographic column.

Table 1.2. Optimization of macrolactamization conditions, on compound NH_2-D-**DKP3**-RG-OH (**82**).

Reagents and conditions	Purification	Yield
DPPA, DIPEA, 1.4 mM in DMF, 48 h	Flash silica gel column cromatography	75%
PyBrOP, DIPEA, 1.4 mM in DMF, 48 h	Flash silica gel column cromatography	28%
FDPP, DIPEA, 1.4 mM in DMF, 48 h	Flash silica gel column cromatography	73%
HATU, HOAt, collidine, 2 mM in DMF, 48 h	Flash silica gel column cromatography	40%

Anyway, in order to avoid purification problems, all the other linear intermediates **82** (containing **DKP4-8**) were efficiently macrolactamized using the more conventional HATU, in presence of HOAt and *i*Pr_2NEt. The final cleavage of the side chain protecting groups (Mtr and *t*Bu) was accomplished treating cyclized products **83** with a strongly acidic "cleavage cocktail". A first receipe envisaged a mixture TFA/triethylsilane/1,2-ethandithiol/phenol/thioanisole/H_2O 80:2.5:5:5:5:2.5. Far better results and cleaner crudes were obtained with the mixture TFA/thioanisole/ethanedithiol/anisole 90:5:3:2.

The *N*-dibenzyl derivatives **20** and **22** can exist as two different separable conformers (diastereomers) due to hindered rotation of one ring around the other, in a way reminiscent of the *ansa*-cyclopeptides[109] (*i.e.*, the DKP *N*-benzyl group cannot pass inside the macrolactam ring). In the case of **20**, we were able to isolate only one diastereomer (either because it was formed exclusively or because it was formed predominantly) and the minor one was not detected.

The two diastereomers of **22** (A and B), formed in the macrolactamization step, were isolated in a 2:1 ratio (Scheme 1.30). Although two sets of peaks (2:1 ratio) were visible in the ^{1}H NMR spectrum, the two diastereomers could not be separated by HPLC because they had the same elution time. However, after side-chain deprotection, the two diastereomers could be separated, analyzed and subjected to the binding assays (vide infra).

Scheme 1.30. Non-interconverting diastereoisomers **22 A** and **B**

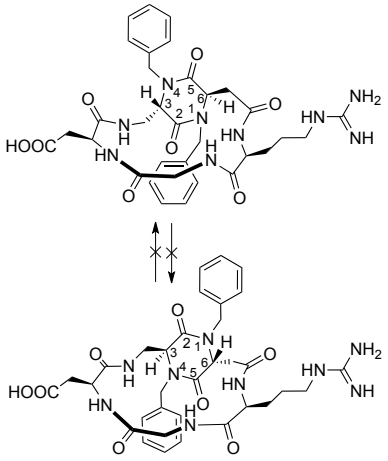

2.5 - *Biological evaluation* [110]

The cyclic RGD peptidomimetics were examined *in vitro* for their ability to inhibit biotinylated vitronectin binding to the purified $\alpha_v\beta_3$ and $\alpha_v\beta_5$ receptors (Table 1.3).

Table 1.3. Inhibition of biotinylated vitronectin binding to $\alpha_v\beta_3$ and $\alpha_v\beta_5$ receptors

Compound	Structure	$\alpha_V\beta_3$ IC_{50} [nM][a]	$\alpha_V\beta_5$ IC_{50} [nM][a]
16	*Cyclo*[**DKP1**-RGD] (*cis*)	3898 ± 418	$> 10^4$
17	*Cyclo*[**DKP2**-RGD] (*trans*)	3.2 ± 2.7	114 ± 99
18	*Cyclo*[**DKP3**-RGD] (*trans*)	4.5 ± 1.1	149 ± 25
19	*Cyclo*[**DKP4**-RGD] (*trans*)	7.6 ± 4.3	216 ± 5
20	*Cyclo*[**DKP5**-RGD] (*trans*)	12.2 ± 5.0	131 ± 29
21	*Cyclo*[**DKP6**-RGD] (*trans*)	2.1 ± 0.6	79 ± 3
22 A	*Cyclo*[**DKP7**-RGD] (A-major)	220.2 ± 82.3	$> 10^4$
22 B	*Cyclo*[**DKP7**-RGD] (B-minor)	0.2 ± 0.09	109 ± 15
23	*Cyclo*[**DKP8**-RGD] (*trans*)	7.5 ± 0.6	$> 10^3$
ref 1	c(RGDfV)	3.2 ± 1.3	7.5 ± 4.8
ref 2	ST1646	1.0 ± 0.5	1.4 ± 0.8

[a]IC_{50} values were calculated as the concentration of compound required for 50% inhibition of biotinylated vitronectin binding as estimated by GraphPad Prism software; all values are the arithmetic mean ± SD of triplicate determinations.

Screening assays were performed by incubating the immobilized integrin receptors with various concentrations (10^{-10} – 10^{-5} M) of the RGD ligands **16**-**23** in the presence of biotinylated vitronectin (1 μg/mL), and measuring the concentration of bound vitronectin in the presence of the competitive ligands. The ability of the new compounds to inhibit the binding of vitronectin to the isolated $\alpha_v\beta_3$ and $\alpha_v\beta_5$ receptors was compared with that of the reference compounds *c*(RGDfV)[111] (**4**, Figure 1.11) and ST1646[69] (**7**, Figure 1.12).

Low nanomolar values were obtained with all the ligands except *cyclo*[**DKP1**-RGD] **16**, which incorporates a *cis*-DKP and ligand **22 A**. The behavior of this last ligand is peculiar, considering that the diastereomeric compound **22 B** (see above for the definition of the two diastereomers) is the most potent ligand of this series, as it effectively inhibits the binding of vitronectin to the isolated $\alpha_v\beta_3$ receptor in subnanomolar concentration. Interestingly, unlike reference compounds *c*(RGDfV) and

ST1646, the RGD-peptidomimetics **16**-**22** were ca. 10-1000-fold more selective for the $\alpha_v\beta_3$ integrin with respect to the $\alpha_v\beta_5$, in this kind of assay.

2.6 - *NMR spectroscopy characterization and conformational studies* [112]

The structure and connectivity of ligands **16**-**22** and of their fully protected precursors were unambiguously assigned by means of mono- and bidimensional ^{1}H- and ^{13}C-NMR spectra.

The preferred conformations of the cyclic RGD peptidomimetics **16**-**22** in aqueous solution were then investigated, with the aim of rationalizing the affinity of these compounds for the $\alpha_v\beta_3$ receptor at a molecular level. In fact, as already mentioned, the high activity and selectivity of Cilengitide **3** has been attributed to an extended conformation of the RGD motif displaying a distance of ca. 9 Å between the C_β atoms of Asp and Arg. In such extended conformations, the carboxylate and guanidinium groups are properly positioned to effectively exert their function of electrostatic clamp. Monodimensional ^{1}H-NMR experiments were conducted to detect intramolecular hydrogen bonds, by measuring the chemical shift of the N–H protons and their temperature coefficients ($\Delta\delta/\Delta T$). NOESY spectra were recorded to investigate both sequential and long-range NOEs that provide evidence of preferred conformations. The relevant NMR data are summarized in Table 1.4, while the graphic in Figure 1.42 displays the temperature coefficients.

As already reported in the literature,[78] ligand **16** exists as an equilibrium of two different preferred conformations. The NOESY spectrum shows two mutually exclusive long-range NOE contacts. The cross peak between DKP-NH_{10} and NH_{Asp} (strong) is indicative of a β-turn conformation at Gly-Asp stabilized by a hydrogen bond between DKP-NH_{10} and Arg-C=O (referred to as type I H-bonding pattern, Figure 1.43 A). The chemical shift value (δ = 7.46 ppm) and the $\Delta\delta/\Delta$T value (-2 ppb K^{-1}) of the amide proton DKP-NH_{10} indicate that this proton is strongly locked in an intramolecularly H-bonded state. The cross peak between NH_{Gly} and NH_{Asp} (medium) is indicative of an alternative β-turn conformation at Arg-Gly, stabilized by a hydrogen bond between Asp-NH and C(8)=O (referred as type II H-bonding pattern, Figure 1.43 B).

Table 1.4. ^{1}H-NMR and NOE data of cyclic RGD-peptidomimetics **16-23** in water

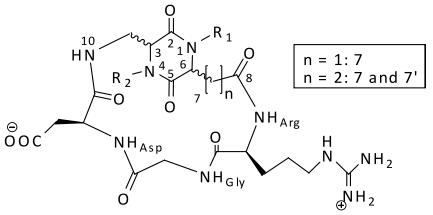

		NH_1	NH_4	NH_{10}	NH_{Arg}	NH_{Gly}	NH_{Asp}	Significant NOE contacts
16 *c*[**DKP1**-RGD]	***δ*** (ppm)	8,35	-	7,46	8,40	8,75	8,10	NH_{Asp}-NH_{10}; NH_{Asp}-NH_{Gly}
	Δ*δ*/ΔT (ppb/K)	-7.3	-	-2.0	-7.0	-8.0	-3.7	
17 *c*[**DKP2**-RGD]	***δ*** (ppm)	8.35	-	8.78	8.57	8.18	8.29	NH_{Arg}-NH_{Gly}
	Δ*δ*/ΔT (ppb/K)	-8.7	-	-10.7	-7.0	-5.7	-7.7	
18 *c*[**DKP3**-RGD]	***δ*** (ppm)	8.10	-	8.28	8.80	8.00	7.85	NH_{Arg}-NH_{Gly}
	Δδ/ΔT (ppb/K)	-5.7	-	-8.5	-6.0	-4.5	-3.5	
19 *c*[**DKP4**-RGD]	***δ*** (ppm)	-	8.17	7.59	8.29	8.27	8.88	--
	Δ*δ*/ΔT (ppb/K)	-	-9.1	-0.7	-9.3	-8.2	-9.3	
20 *c*[**DKP5**-RGD]	***δ*** (ppm)	-	-	8.58	8.48	8.23	8.42	NH_{Arg}-NH_{Gly}
	Δ*δ*/ΔT (ppb/K)	-	-	-11.0	-7.5	-4.7	-8.2	
21 *c*[**DKP6**-RGD]	***δ*** (ppm)	-	8.07	7.90	8.32	8.35	8.80	NH_{Asp}-NH_{10}; NH_4-NH_{10};
	Δ*δ*/ΔT (ppb/K)	-	-4.9	-5.1	-7.6	-6.7	-8.0	
22 A *c*[**DKP7**-RGD]-A	***δ*** (ppm)	-	-	8.04	8.66	7.93	7.76	NH_{Arg}-NH_{Gly}; NH_{Asp}-NH_{Gly}
	Δ*δ*/ΔT (ppb/K)	-	-	-7.5	-5.0	-3.0	-1.0	
22 B *c*[**DKP7**-RGD]-B	***δ*** (ppm)	-	-	7.72	8.34	8.45	8.55	NH_{Asp}-NH_{10}
	Δ*δ*/ΔT (ppb/K)	-	-	-4.0	-7.0	-7.0	-5.0	
23 *c*[**DKP8**-RGD]	***δ*** (ppm)	7.82	-	7.43	8.64	8.04	7.90	-
	Δ*δ*/ΔT (ppb/K)	-8.0	-	-6.0	-6.8	-4.4	-5.2	

Figure 1.42. Graphical illustration of temperature coefficients (Δδ/ΔT) for compounds **16-23** in H_2O/D_2O 9:1 between 290 K and 320 K

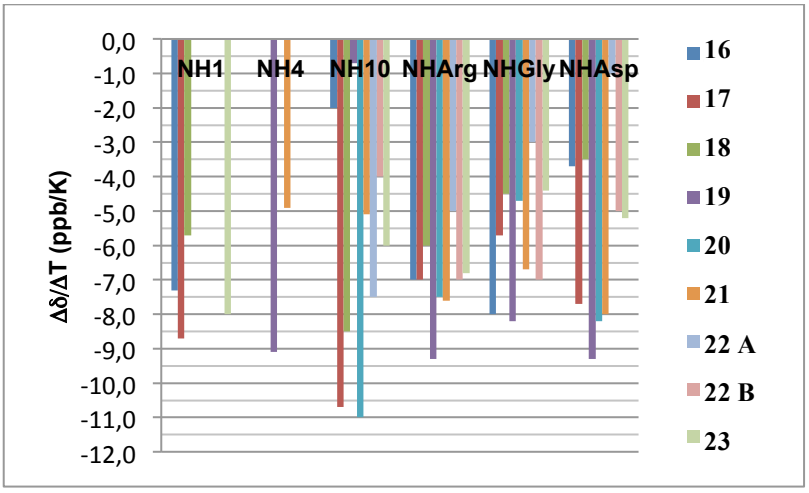

Figure 1.43. Preferred intramolecular hydrogen-bonding pattern proposed for compound **16** on the basis of spectroscopic data[a]

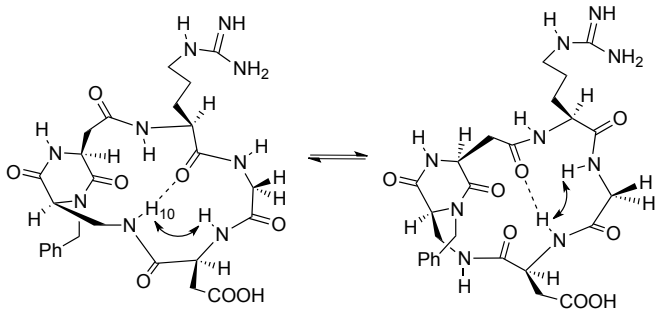

[a]The arrows indicate significant NOE contacts. A) Type I H-bonding pattern, Gly-Asp β-turn motif. B) Type II H- H-bonding pattern, Arg-Gly β-turn motif.

High affinity ligands **17** and **18** are apparently characterized by a high conformational mobility, as suggested by the values of chemical shifts and $\Delta\delta/\Delta T$ reported in Table 1.4. The only exception is proton NH-Asp of **18** (δ = 7.85 ppm, $\Delta\delta/\Delta T$ = -3,5 ppb K^{-1}), which might be involved in a Type II H-bonding pattern (Figure 1.43 B). On the other hand, the presence in both cases of a NOE contact between NH_{Gly} and NH_{Arg} suggests the formation of a β-turn motif at DKP-Arg, stabilized by a hydrogen bond between NH_{Gly} and C(5)=O (referred to as type III H-bonding pattern, Figure 1.44). The presence of this hydrogen bond is also supported by the rather upfield chemical shift value of NH_{Gly} in these two ligands (8.18 and 8.00 ppm for **17** and **18**, respectively) and the relatively low temperature dependence (δ = -5.7 ppm and $\Delta\delta/\Delta T$ = -4.5 ppb K^{-1}, respectively). The similarity of the NMR spectroscopy data and, hence, of the conformation of these two ligands is quite surprising, considering the opposite configuration of the diketopiperazine scaffold [**DKP2** (3*R*,6*S*) in **17**; **DKP3** (3*S*,6*R*) in **18**], which should impart a different stereochemical orientation to the two side arms of the diketopiperazine. This conformational similarity can be interpreted in terms of a quasi-enantiomeric structure of the two ligands (not considering the configuration of the remote RD amino acid side chains, Figure 1.44).

High affinity ligands **19** and **21**, featuring the diketopiperazine scaffolds **DKP4** (3*R*,6*S*) and **DKP6** (3*S*,6*R*) respectively (with the benzyl substitution at the endocyclic nitrogen N1, instead of N4), show a different NMR pattern.

Figure 1.44. Preferred intramolecular hydrogen-bonding pattern proposed for compound **17** and **18** on the basis of spectroscopic data[a]

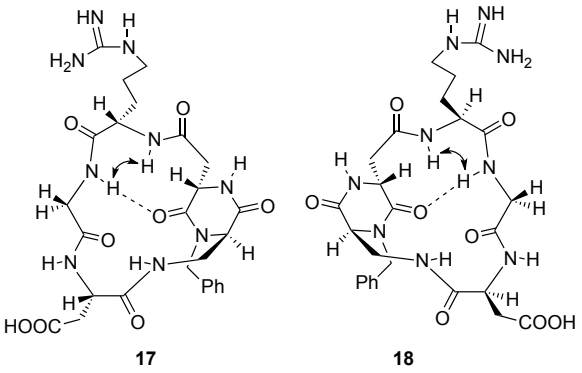

[a]The arrows indicate significant NOE contacts. The DKP-Arg β-turn motif is referred as Type III H-bonding pattern.

In particular, ligand **21** is characterized by a rather strong NOE contact between NH_{Asp} and NH_{10} and a moderate/weak one involving NH_4 and NH_{10}. These two contacts are mutually exclusive and are hence indicative of an equilibrium between two different conformations, respectively Type I and Type IV H-bonding patterns (Figure 1.45 A and B).

Figure 1.45. Preferred intramolecular hydrogen-bonded pattern proposed for compound **21** on the basis of spectroscopic data[a]

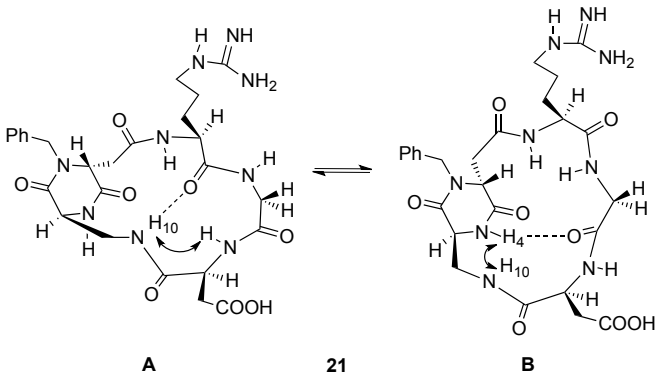

[a]The arrows indicate significant NOE contacts. A) Type I H-bonding pattern is characterized by a β-turn motif at Gly-Asp stabilized by a hydrogen bond between NH_{10} and Arg-C=O. B) Type IV H-bonding pattern which is characterized by a pseudo β-turn at Asp-DKP stabilized by a hydrogen bond between NH_4 and Gly-C=O.

The hydrogen bonded status of the two amide protons NH_4 and NH_{10}, as indicated by their rather low temperature dependence (-5.7 and -5.1 ppb K^{-1}, respectively) and by the quite upfield chemical shift

values (δ = 8.07 and δ = 7.90 ppm, respectively), corroborate this assumption. The Type IV H-bonding pattern could feature a pseudo β-turn at Asp-DKP stabilized by a hydrogen bond between NH_4 and Gly-C=O (NOE contact between NH_4 and NH_{10}).

Ligand **19**, on the other hand, is characterized by the absence of relevant NOE contacts, a very low temperature dependence (-0.7 ppb K^{-1}) and a quite upfield chemical shift value (δ = 7.59 ppm) for proton NH_{10}. These two features suggest a Type I H-bonding pattern, notwithstanding the apparent lack of NOE contact between NH_{Asp} and NH_{10}.

The dibenzylated diketopiperazine-containing peptidomimetics **20** and **22** were eventually studied. Ligand **22** shows NMR spectroscopy features similar to ligand **17** (Type III H-bonding pattern): a NOE contact between NH_{Gly} and NH_{Arg} and a rather shielded NH_{Gly} (δ = 8.23 ppm) with a relatively low temperature coefficient (-4.7 ppb K^{-1}). As discussed above, ligand *cyclo*[**DKP7**-RGD] was obtained as a mixture of two diastereomers **22 A** and **22 B**, the solution conformations of which were studied separately. In particular, the low affinity ligand **22 A** displays two mutually exclusive NOE contacts between NH_{Arg} and NH_{Gly} and between NH_{Asp} and NH_{Gly}. These three protons, on the other hand, show also a rather strong hydrogen bonded status, as indicated by their low temperature dependence and, at least for NH_{Asp} and NH_{Gly}, their upfield chemical shift (Table 1.4). These data indicate an equilibrium between two different conformations: one displaying a Type III H-bonding pattern and a second one showing a Type II H-bonding pattern (β-turn at Arg-Gly), like the low-affinity ligand **16**, *i.e. cyclo*[**DKP1**-RGD]. Finally, high affinity ligand **22 B** shows a single NOE contact between NH_{Asp} and NH_{10} and a hydrogen bonded status for NH_{10} (δ = 7.72 ppm and $\Delta\delta/\Delta T$ = -4 ppb K^{-1}, Table 1.4). These values are indicative of a Type I H-bonding pattern.

No NOE contacts were identified for compound **23**, containing the superior homolog of **DKP3** (*i.e.* **DKP8**). Moreover, also temperature coefficients of the amide protons are not relevant for the identification of H-bonds. Compound **23**, containing the carboxyethyl diketopiperazine scaffold **DKP8**, is characterized by temperature coefficients of amide protons (Table 1.4) greater than 5 ppb K^{-1}; this suggests the presence of an equilibrium between different conformations. The NOESY spectrum of this ligand shows a strong long-range NOE contact that involves DKP-NH_1 and NH_{Arg}. This contact is indicative of a conformation stabilized by a hydrogen bond between NH_1 and Arg-C=O (referred to as type V H-bonding pattern, Figure 1.46). The involvement of NH_1 in a hydrogen bond is also confirmed by its relatively low chemical shift value (δ = 7.75 ppm).

Figure 1.46. Preferred intramolecular hydrogen-bonded pattern (Type V H-bonding pattern) proposed for compound **23** on the basis of spectroscopic data[a]

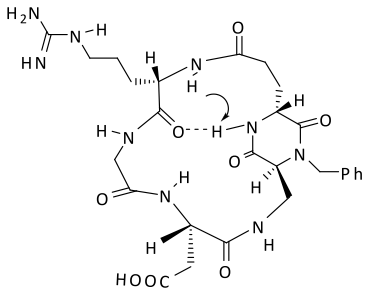

[a]The arrows indicate significant NOE contacts.

2.6.1 - *Conformational analysis*.

Conformational studies of the cyclic RGD-peptidomimetics were performed by mixed-mode Metropolis Monte Carlo/Stochastic Dynamics (MC/SD) simulations, using the implicit water GB/SA solvation model[2] and the OPLS_2001 force field.[113,114]

As outlined in the paragraph 1.6.1, a key parameter for the RGD fitting into the active site of the $\alpha_V\beta_3$ integrin is the distance of *ca*. 9 Å between the C_β atoms of Asp and Arg, imparted by an extended conformation of the Arg-Gly-Asp sequence. In such an extended conformation, the carboxylate and guanidinium groups are properly positioned to effectively exert their function of electrostatic clamp (*vide infra* for the relevant docking studies).

As mentioned in our preliminary studies,[78] three-dimensional structures satisfying long-range NOE contacts were generated for RGD peptidomimetic **16** performing two 10 ns restrained MC/SD simulations and applying the DKP-NH_{10}/NH_{Asp} or the NH_{Asp}/NH_{Gly} distance restraint derived from NOESY spectra. More than 90% of the conformations sampled during the first simulation adopted a non-extended arrangement of the RGD sequence characterized by a β-turn at Gly-Asp and by the presence of the corresponding hydrogen bond between DKP-NH_{10} and Arg-C=O. In addition, the formation of a γ-turn at Gly stabilized by the hydrogen bond between NH_{Asp} and Arg-C=O was observed for 40% of the conformers obtained in the simulation. A Cβ(Arg)–Cβ(Asp) average distance of 7.4 Å was obtained during this MC/SD calculation. A representative energy-minimized conformation selected by cluster analysis and featuring both H-bonds is shown in Figure 1.47 A (Type I-*cis* H-bonding pattern). Approximately 60% of the conformations sampled during the simulation of **16** featuring the NH_{Asp}/NH_{Gly} distance restraint, adopted a non-extended arrangement of the RGD sequence characterized by a β-turn at Arg-Gly and the corresponding hydrogen bond between NH_{Asp} and C(8)=O. In addition, the formation of a γ-turn at Arg stabilized by the hydrogen bond between NH_{Gly} and C(8)=O was observed for 40% of the simulation. The Cβ(Arg)–Cβ(Asp) average distance

in this MC/SD calculation was 6.8 Å. A representative energy minimized conformation selected by cluster analysis and featuring both H-bonds is shown in Figure 1.47 B (Type II H-bonding pattern).

Figure 1.47. Structures of **16** as obtained by restrained MC/SD simulations based on experimental distance information, after energy minimization[a]

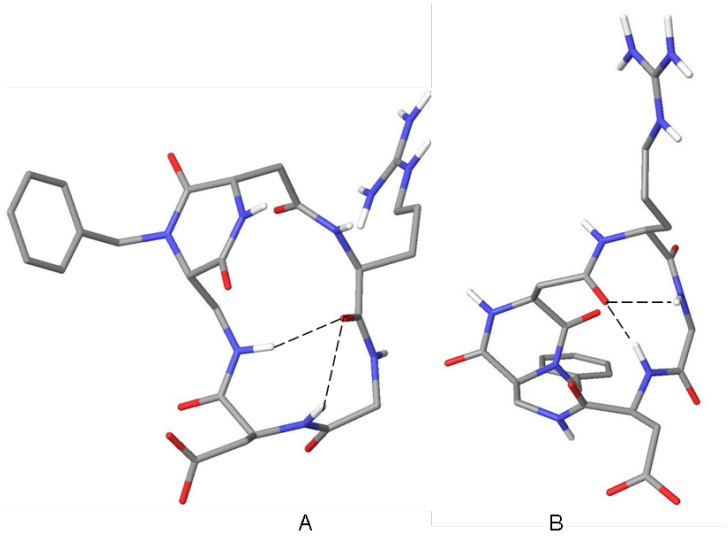

[a]A) Type I-*cis* H-bonding pattern, γ-turn at Gly and βII'-turn at Gly-Asp [CβArg)–Cβ(Asp)=7.9 Å]. B) Type II H-bonding pattern, γ-turn at Arg and βII'-turn at Arg-Gly [Cβ(Arg)–Cβ(Asp)=6.6 Å].

The NOESY spectra of high affinity ligands **17** (containing *N*-4-benzylated **DKP2**, 3*R*,6*S*), **18** (containing *N*-4-benzylated **DKP3**, 3*S*,6*R*) and **20** (containing *N*-dibenzylated **DKP5** 3*R*,6*S*) showed only one relevant long-range interaction between NH_{Gly} and NH_{Arg}: this NOE is indicative of a β-turn motif at DKP-Arg stabilized by a hydrogen bond between NH_{Gly} and C(5)=O (Figure 1.44, Type III H-bonding pattern). The distance restraint corresponding to the NOE contact between NH_{Gly} and NH_{Arg} was applied in the 10 ns MC/SD simulations of compounds **17**, **18** and **20**. More than 90% of the conformations sampled during each of these simulations adopted an extended arrangement of the RGD sequence characterized by a pseudo β-turn at DKP-Arg and the formation of the corresponding hydrogen bond between the NH_{Gly} and C(5)=O. Interestingly, only for compound **18**, the additional formation of a β-turn at Arg-Gly stabilized by the hydrogen bond between NH_{Asp} and C(8)=O was observed for 15% of the simulation. These results and the NMR data (showing δ=7.85 ppm and $\Delta\delta/\Delta T$=-3.5 ppb K^{-1} for NH_{Asp} of **18**) suggest the contribution of a Type II/Type III H-bonding pattern to the conformational equilibrium of **18** (mainly populated by a Type III H-bonding pattern).

Cβ(Arg)-Cβ(Asp) average distances of 9.3, 8.8, and 9.1 Å were obtained during the MC/SD calculations of **17**, **18** and **20**, respectively. A representative energy minimized conformation selected

by cluster analysis and featuring the H-bond between the Gly-NH and C(5)=O (Type III H-bonding pattern) is shown in Figure 1.48 for RGD peptidomimetic **17**.

Figure 1.48. Structure of **17** as obtained by restrained MC/SD simulations based on experimental distance information, after energy minimization[a]

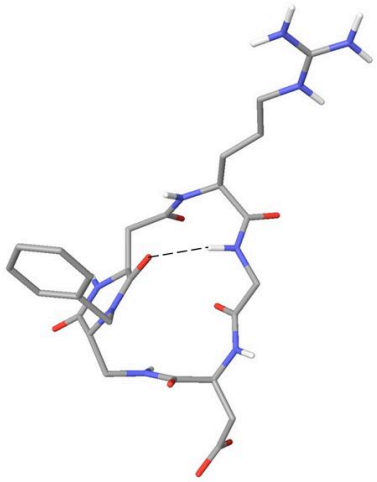

[a]Type III H-bonding pattern, distorted inverse γ-turn at Asp and pseudo β-turn at DKP-Arg, Cβ(Arg)–Cβ(Asp)=9.4 Å.

Due to the absence of relevant long-range NOE contacts, several 10 ns runs of unconstrained MC/SD simulations were performed for RGD peptidomimetic **19** (containing *N*-1-benzylated **DKP4**, 3*R*,6*S*) starting from different 3D structures. Most of the conformations sampled during these simulations adopted an extended arrangement of the RGD sequence [Cβ(Arg)-Cβ(Asp) average distance of 8.8 Å] and approximately 40% of them are characterized by a β-turn at Gly-Asp and the presence of the corresponding hydrogen bond between DKP-NH_{10} and Arg-C=O. These results provide a structural model compatible with NMR data showing a low temperature dependence ($\Delta\delta/\Delta T$ = -0.7 ppb K^{-1}) and an upfield chemical shift value (δ = 7.59 ppm) for proton NH_{10}.

A representative energy minimized conformation selected by cluster analysis and featuring the H-bond between DKP-NH_{10} and Arg-C=O (Type I-*trans* H-bonding pattern) is shown in Figure 1.49 for RGD peptidomimetic **19**. It is worth noting how the combination of the *trans* **DKP4** scaffold with the Gly-Asp β-turn occurs by generating an extended RGD arrangement, while the combination of the *cis* **DKP1** scaffold with the same secondary motif resulted in a non-extended RGD disposition (see above, Figure 1.47 A). Accordingly, two Type I H-bonding patterns have been defined, depending on the *cis* or *trans* relative stereochemistry of the diketopiperazine scaffold.

Three-dimensional structures satisfying long-range NOE contacts were generated for RGD peptidomimetic **21** (containing *N*-1-benzylated **DKP6**, 3*S*,6*R*) performing two 10 ns restrained

MC/SD simulations and applying the DKP-NH_{10}/NH_{Asp} or the NH_4/NH_{10} distance restraint derived from NOESY spectra (Table 1.4, Figure 1.42). Most of the conformations sampled during the first simulation adopted an extended arrangement of the RGD sequence (Cβ(Arg)-Cβ(Asp) average distance of 9.0 Å) and approximately 40% of them are characterized by a β-turn at Gly-Asp and the corresponding hydrogen bond between DKP-NH_{10} and Arg-C=O. A representative energy-minimized conformation selected by cluster analysis and featuring this H-bond is shown in Figure 1.49 A (Type I-*trans* H-bonding pattern). Approximately 70% of the conformations sampled during the simulation of **21** featuring the NH_4/NH_{10} distance restraint, adopted an extended arrangement of the RGD sequence [Cβ(Arg)-Cβ(Asp) average distance of 8.8 Å] characterized by a pseudo β-turn at Asp-DKP and the corresponding hydrogen bond between NH_4 and Gly-C=O. In addition, the formation of a γ-turn at Asp stabilized by the hydrogen bond between NH_{10} and Gly-C=O was observed for 50% of the conformers. A representative energy-minimized conformation selected by cluster analysis and featuring these H-bonds is shown in Figure 1.49 B (Type IV H-bonding pattern).

Figure 1.49. Structures of **21** as obtained by restrained MC/SD simulations based on experimental distance information, after energy minimization[a]

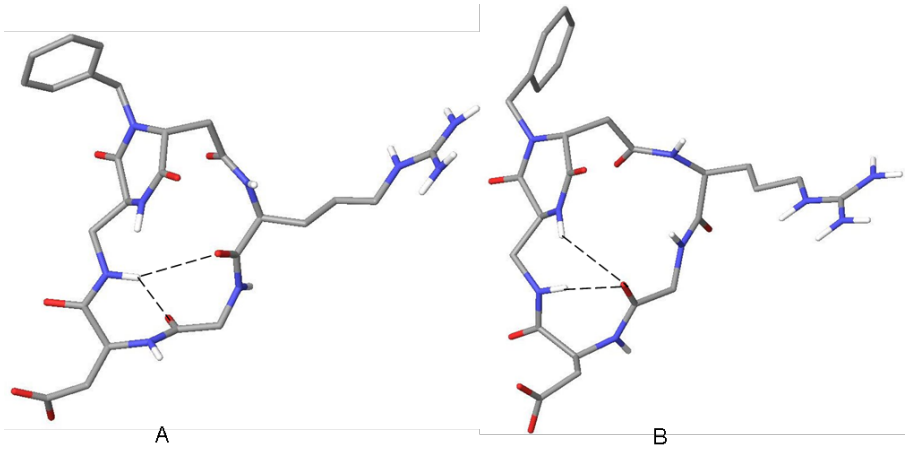

[a]A) Type I-*trans* H-bonding pattern, inverse γ-turn at Asp and distorted βII'-turn at Gly-Asp [Cβ(Arg)–Cβ(Asp)=9.0 Å]. B) Type IV H-bonding pattern, inverse γ-turn at Asp and pseudo β-turn at Asp-DKP [Cβ(Arg)–Cβ(Asp)=8.8 Å].

Three-dimensional structures fulfilling long-range NOE contacts were generated for RGD peptidomimetic **22** (containing *N*-dibenzylated **DKP7** 3*S*,6*R*) performing three 10 ns restrained MC/SD simulations and applying the distance restraints derived from NOESY spectra of diastereoisomers **22A** and **22B** (Table 1.4): in the first simulation NH_{Arg}/NH_{Gly} relevant in **22A**, in the second simulation NH_{Asp}/NH_{Gly} also relevant in **22A**, and in the third simulation DKP-NH_{10}/NH_{Asp} relevant in **22B**.

All the conformations sampled during the first two simulations adopted a non-extended arrangement of the RGD sequence [Cβ(Arg)-Cβ(Asp) average distance of 6.6 Å] characterized by the simultaneous presence of different turn motifs (pseudo β-turn at DKP-Arg, γ-turn at Gly and pseudo β-turn centered at the DKP unit). The structural models provided by these restrained MC/SD simulations differ from the conformations hypothesized on the basis of NMR data of **22A** [equilibrium between Type III (pseudo β-turn at DKP-Arg) and Type II (β-turn at Arg-Gly) H-bonding patterns, see the NMR spectroscopy section]. However, also the calculated structures are able to provide an explanation for the NOE contacts and the NMR temperature coefficients observed for **22A**.

The distance restraint corresponding to the NOE contact between DKP-NH_{10} and NH_{Asp} (observed in the NOESY spectrum of **22B**) was applied in the third 10 ns MC/SD simulation of compound **22**. Most of the conformations sampled during this simulation adopted an extended arrangement of the RGD sequence (Cβ(Arg)-Cβ(Asp) average distance of 9.0 Å) and approximately 50% of them are characterized by a β-turn at Gly-Asp and the corresponding hydrogen bond between DKP-NH_{10} and Arg-C=O. A representative energy-minimized conformation selected by cluster analysis and featuring this H-bond is shown in Figure 1.50 (Type I-*trans* H-bonding pattern).

Contrary to what observed for the other cyclic RGD peptidomimetics containing DKP scaffolds, rotation of the DKP ring can not be observed during the simulations performed on compound **22**: this confirms **22A** and **22B** as two different separable conformers (diastereomers) due to hindered rotation of one ring around the other.

Figure 1.50. Structure of **22B** as obtained by restrained MC/SD simulations based on experimental distance information, after energy minimization[a]

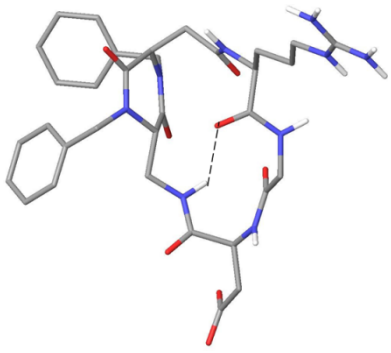

[a]Type I-*trans* H-bonding pattern, distorted inverse γ-turn at Asp and βII'-turn at Gly-Asp, Cβ(Arg)–Cβ(Asp)=9.2 Å).

The distance restraint corresponding to the NOE contact between NH_1 and NH_{Arg} was applied in the 10 ns MC/SD simulation of RGD peptidomimetic **23** (containing *N*-4-benzylated **DKP8**, 3*S*,6*R*). Approximately 60% of the conformations sampled during this simulation adopted an extended

arrangement of the RGD sequence characterized by the formation of the hydrogen bond between NH_1 and Arg-C=O (Figure 1.43, Type V H-bonding pattern). In addition, the formation of the hydrogen bond between NH_{Asp} and C(2)=O (Type Va H-bonding pattern) or the presence of a β-turn at Gly-Asp stabilized by the hydrogen bond between DKP-NH_{10} and Arg-C=O (Type Vb H-bonding pattern) were observed for 35% and 25% of the simulation, respectively. Representative energy-minimized conformations selected by cluster analysis and featuring the Type Va and Vb H-bonding patterns are shown in Figure 1.51 for RGD peptidomimetic **23**.

Figure 1.51. Structure of **23** as obtained by MC/SD simulations, after energy minimization (Cβ(Arg)–Cβ(Asp)=9.5 Å).

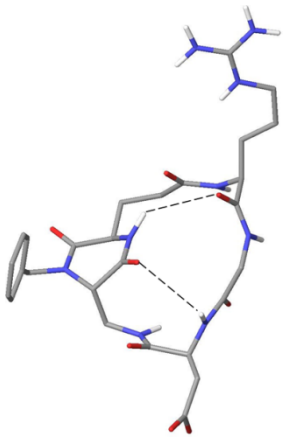

2.6.2 - *Molecular docking*

In order to rationalize, on a molecular basis, the affinity of cyclic RGD peptidomimetics for the $\alpha_v\beta_3$ receptor, docking studies were performed starting from the representative conformations obtained from the MC/SD simulations. The crystal structure of the extracellular segment of integrin $\alpha_v\beta_3$ complexed with the cyclic pentapeptide Cilengitide (1L5G, pdb code) was taken as a reference model for the interpretation of the docking results in terms of ligand-protein interactions. In the X-ray complex, Cilengitide binds to the interface of the α and β units forming specific electrostatic interactions. The acid and basic pharmacophoric groups and their orientation are essential for binding to the $\alpha_v\beta_3$ because they act like an electrostatic clamp, interacting with charged regions of the receptor binding site.

Docking calculations starting from geometries featuring the Type I-*cis* and Type II H-bonding patterns produced top-ranked poses conserving optimal interactions only with the α subunit of the $\alpha_v\beta_3$

receptor. Probably, the short Cβ(Arg)-Cβ(Asp) distances (values less than 8 Å) of these geometries prevent the guanidine and carboxylic groups from achieving the required separation for binding to the $\alpha_v\beta_3$ integrin. On the other hand, docking calculations starting from the RGD extended conformations featuring the Type I-*trans*, Type III and Type IV H-bonding patterns, produced top-ranked binding modes conserving all the important interactions of the X-ray complex. As examples, the best poses obtained for the compounds **18** and the highest affinity ligand **22B** are shown in Figure 1.52.

Figure 1.52. Docking best pose of compounds **18** and **22B**[a]

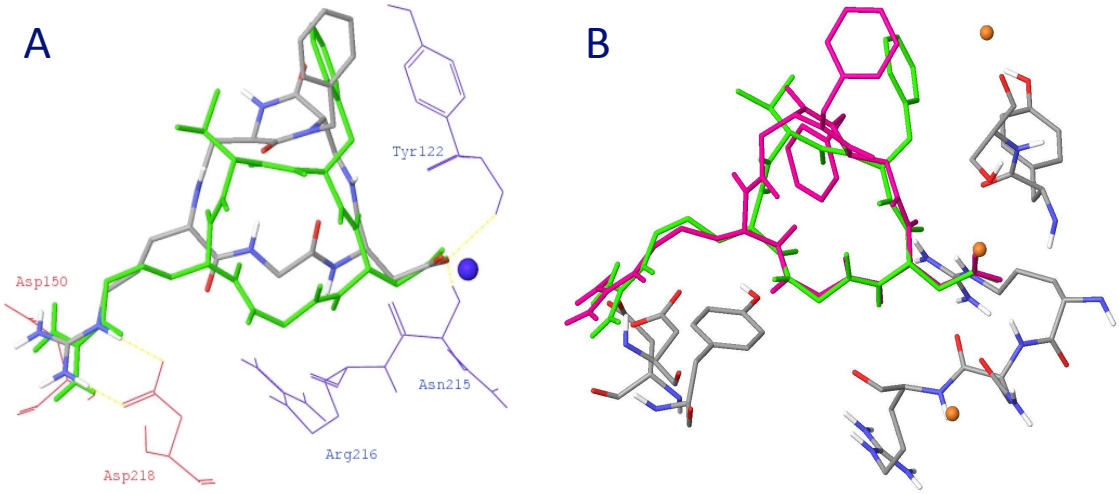

[a]Docking best pose of compounds A) ***cyclo*[DKP3-RGD] (18)** and B) ***cyclo*[DKP7-RGD] (22 B)** into the crystal structure of the extracellular domain of $\alpha_v\beta_3$ integrin overlaid on the bound conformation of Cilengitide (green).

The positively charged Arg guanidinium group of the ligand interacts with the negatively charged side chains of Asp218 and Asp150 in the α unit, one carboxylate oxygen of the ligand Asp side chain is coordinated to the metal cation in the metal-ion-dependent adhesion site (MIDAS) region of the β unit, while the second carboxylate oxygen forms hydrogen bonds with the backbone amides of Asn215 and Tyr122 in the β unit. A further stabilizing interaction involves the formation of a hydrogen bond between the ligand backbone NH of the Asp residue and the backbone carbonyl group of Arg216 in the β unit.

In light of all these considerations, the micromolar affinity of RGD peptidomimetics **16** and **22A** (3.9 and 0.2 μM, respectively) for $\alpha_v\beta_3$ (Table 1.3) can be explained in terms of their low pre-organization for binding. In fact, as determined by the computational and NMR studies, these compounds in solution mainly feature non-extended RGD conformations which, according to the docking results, are not able to properly fit into the $\alpha_v\beta_3$ receptor. On the contrary, the nanomolar affinity of RGD peptidomimetics **17-21**, **22B** and **23** for $\alpha_v\beta_3$ can be attributed to their high structural pre-organization.

In fact, as determined by the computational and NMR studies, these compounds in solution mainly feature extended RGD conformations (principally determined by Type I-*trans*, Type III and Type IV H-bonding patterns) similar to the RGD-bound conformation of Cilengitide.

References:

[1] R. O. Hynes, *Cell* **1987**, *48*, 549-554.

[2] M. Millard, S. Odde, N. Neamati, Theranostics 2011, 1, 154-188.

[3] a) M. Shimaoka, T. A. Springer. *Nature Rev. Drug Discov.* **2003**, *2*, 703-716; b) K.-E. Gottschalk, H. Kessler, *Angew. Chem. Int. Ed.* **2002**, *41*, 3767-3774; W. H. Miller, R. M. Keenan, R. N. Willette, M. W. Lark. *Drug Discovery Today* **2000**, *5*, 397-408; d) I. Ojima, *Bioorg. Med. Chem.* **1995**, *3*, 337-360.

[4] E. Ruoslahti. *Matrix Biol.* **2003**, *22*, 459-465; b) E. Ruoslahti. *Annu. Rev. Cell Dev. Biol.* **1996**, *12*, 967-715.

[5] a) J. P. Xiong, T. Stehle, B. Diefenbach, R. Zhang, R. Dunker, D. L. Scott, A. Joachimiak, S. L. Goodman, M. A. Arnaout. *Science* **2001**, *294*, 339-345; b) J. P. Xiong, T. Stehle, R. Zhang, A. Joachimiak, M. Frech, S. L. Goodman, M. A. Arnaout. *Science* **2002**, *296*, 151-155.

[6] a) W. Chen, C. Chang, M. K. Gilson. *J. Am. Chem. Soc.* **2006**, *128*, 4675-4684; b) L. Marinelli, A. Meyer, D. Heckmann, A. Lavecchia, E. Novellino, H. Kessler. *J. Med. Chem.* **2005**, *48*, 4204-4207; c) L. Marinelli, K.-E. Gottschalk, A. Meyer, E. Novellino, H. Kessler. *J. Med. Chem.* **2004**, *47*, 4166-4177; d) T. Xiao, J. Takagi, B. S. Coller, J.-H. Wang, T. A. Springer. *Nature* **2004**, *432*, 59-67; e) T. A. Springer, J. Zhu, T. Xiao. *J. Cell Biol.* **2008**, *182*, 791-800; f) T. J. You, D. S. Maxwell, T. P. Kogan, Q. Chen, J. Li, J. Kassir, G. W. Holland, R. A. F. Dixon. *Biophys. J.* **2002**, *82*, 447-457.

[7] R. O. Hynes. *Cell* **2002**, *110*, 673-687.

[8] T. A. Springer. *Proc. Natl. Acad. Sci. USA* **1997**, *94*, 65–72.

[9] M. J. Humphries. *Biochem. Soc. Trans.* **2000**, *28*, 311–339.

[10] M. Shimaoka, J. Takagi, T. A. Springer. *Annu. Rev. Biophys. Biomol. Struct.* **2002**, *31*, 485–516.

[11] S. C. Fagerholm, T. J. Hilden, C. G. Gahmberg. *Trends Biochem. Sci.* **2004**, *29*, 504–512.

[12] J. Ylanne. *Front. Biosci.* **1998**, *3*, 877–886.

[13] a) J. C. Loftus, J. W. Smith, M. H. Ginsberg. *J. Biol. Chem.* **1994**, *269*, 25235–25238; b) E. F. Plow, T. A. Haas, L. Zhang, J. C. Loftus, J. W. Smith. *J. Biol. Chem.* **2000**, *275*, 21785–21788; b) A. van der Flier, A. Sonnenberg, *Cell Tissue Res.* **2001**, *305*, 285–298.

[14] a) J. W. Smith, R. S. Piotrowicz, D. Mathis. *J. Biol. Chem.* **1994**, *269*, 960–967; b) A. P. Mould, S. K. Akiyama, M. J. Humphries. *J. Biol. Chem.* **1995**, *270*, 26270–26277.

[15] H. Jin, J. Varner. *Br. J. Cancer* **2004**, *90*, 561–565.

[16] B. A. Teicher, L. M. Ellis. Eds. *Antiangiogenic Agents in Cancer Therapy*, Humana Press, **2008**, *Chapter 3*, 49-71.

[17] M. Moser, K. R. Legate, R. Zent, R. Fässler. *Science* **2009**, *324*, 895-899.

[18] M. A. Arnaout, B. Mahalingam, and J.-P. Xiong. *Annu. Rev. Cell Dev. Biol.* **2005**, *21*, 381-410.

[19] K. Legate, S. Wickström, R. Fässler. *Genes Dev.* **2009**, *23*, 397-418.

[20] J. Desgrosellier, D. Cheresh. *Nat Rev Cancer*. **2010**, *10*, 9-22.

[21] P. Carmeliet. *Nat. Med.* **2003**, *9*, 653–660.

[22] N. Ferrara, R. S. Kerbel. *Nature* **2005**, *438*, 967–974.

[23] S. Kim, K. Bell, S. A.Mousa, J. A.Varner. *Am. J. Pathol.* **2000**, *156*, 1345–1362.

[24] N. Laurens, M. a Engelse, C. Jungerius, C. W. Löwik, V. W. M. van Hinsbergh, P. Koolwijk. *Angiogenesis* **2009**, *12*, 275-285.

[25] D. Phillips, I. Charo, R. Scarborough. *Cell* **1991**, *65*, 359-362.

[26] a) J. Zhu, B. H. Luo, T. Xiao, C. Zhang, N. Nishida, T. A. Springer. *Mol. Cell* **2008**, *32*, 849-861; b) T. A. Springer, J. Zhu, T. Xiao. *J. Cell Biol.* **2008**, *182*, 791-800.

[27] T. Kamata, K. K. Tieu, T. A. Springer, Y. Takada. *J. Biol. Chem.* **2001**, *276*, 44275-44283.

[28] a) M. Hoefling, H. Kessler, K.-E. Gottschalk. *Angew. Chem. Int. Ed.* **2009**, *48*, 6590-6593; b) T. Xiao, J. Takagi, B. S. Coller, J.-H. Wang, T. A. Springer. *Nature*, **2004**, *432*, 59-67.

[29] P. C. Brooks, R. A. Clark, D. A. Cheresh. *Science* **1994**, *264*, 569–571.

[30] P. C. Brooks, A. M. Montgomery, M. Rosenfeld, R. A. Reisfeld, T. Hu, G. Klier, D. A. Cheresh. *Cell* **1994**, *79*, 1157–1164.

[31] M. Friedlander, P. C. Brooks, R. W. Shaffer, C. M. Kincaid, J. A. Varner, D. A.Cheresh. *Science* **1995**, *270,* 1500–1502.

[32] L. E. Reynolds, L. Wyder, J. C. Lively, D. Taverna, S. D. Robinson, X. Huang, D. Sheppard, R. O. Hynes, K. M. Hodivala-Dilke. *Nat. Med.* **2002**, *8*, 27–34.

[33] D. G. Stupack, X. S. Puente, S. Boutsaboualoy, C. M. Storgard, D. A. Cheresh, *J. Cell Biol.* **2001**, *155*, 459–470.

[34] J.-P. Xiong, B. Mahalingham, J. L. Alonso, L. A. Borrelli, X. Rui, S. Anand, B. T. Hyman, T. Rysiok, D. Müller-Pompalla, S. L. Goodman, M. A Arnaout. *J. Cell Biol.* **2009**, *186*, 589-600.

[35] a) A. Meyer, J. Auernheimer, A. Modlinger, H. Kessler, *Curr. Pharm. Des.* **2006**, *12*, 2723-2747; b) L. Marinelli, K.-E. Gottschalk, A. Meyer, E. Novellino, H. Kessler. *J. Med. Chem.* **2004**, *47*, 4166-4177.

[36] S. Kim, M. Bakre, H. Yin, J. A. Varner. *J. Clin. Invest.* **2002**, *110*, 933–941.

[37] S. Kim, M. Harris, J. A. Varner. *J. Biol. Chem.* **2000**, *275*, 33920–33928.

[38] J. Takagi, K. Strokovich, T. A. Springer, T. Walz. *EMBO J.* **2003**, *22*, 4607-4615.

[39] L. Marinelli, A. Meyer, D. Heckmann, A. Laveccia, E. Novellino, H. Kessler. *J. Med. Chem.* **2005**, *48*, 4204-4207.

[40] A. Hillisch, L. F. Pineda, R. Hilgenfeld. *Drug Discov. Today* **2004**, *9*, 659-569.

[41] M. Nagae, S. Re, E. Mihara, T. Nogi, Y. Sugita, J. Takagi. *J. Cell Biol.* **2012**, *197*, 131-140.

[42] B. Furie. *Hematology* **2009**, 255–258.

[43] M. P. Bonaca, P. G. Steg, L. J. Feldman, J. F. Canales, J. J. Ferguson, L. Wallentin, R. M. Califf, R. A. Harrington, R. P. Giugliano. *J. Am. Coll. Cardiol.* **2009**, *54*, 969-984.

[44] D. Chua, A. Ignaszewski, *BMJ* **2009**, *338*, b1180.

[45] D. Cox, *Curr. Pharm. Des.* **2004**, *10*, 1587-1596.

[46] R. Evans, I. Patzak, L. Svensson, K. De Filippo, K. Jones, A. McDowall, N. Hogg. *J. Cell Sci.* **2009**, *122*, 215-225.

[47] A. Etzioni. *Clin. Rev. Allergy Immunol.* **2010**, *38*, 54-60.

[48] T. A. Yednock, C. Cannon, L. C. Fritz, F. Sanchez-Madrid, L. Steinman, N. Karin. *Nature* **1992**, *356*, 63-66.

[49] a) G. P. A. Rice, H. P. Hartung, P. A. Calabresi. *Neurology* **2005**, *64*, 1336-1342; b) S. R. Targan, B. G. Feagan, R. N. Fedorak. *Gastroenterology* **2007**, *132*, 1672-1683.

[50] E. Havrdova, S. Galetta, M. Hutchinson, D. Stefoski, D. Bates, C. H. Polman, P. W. O'Connor, G. Giovannoni, T. Phillips, F. D. Lublin, A. Pace, R. Kim, R. Hyde. *Lancet Neurol.* **2009**, *8*, 254-260.

[51] C. Warnke, T. Menge, H. P. Hartung, M. K. Racke P. D. Cravens, J. L. Bennett, E. M. Frohman, B. M. Greenberg, S. S. Zamvil, R. Gold, B. Hemmer, B. C. Kieseier, O. Stüve. *Arch. Neurol*, **2010**, *67*, 923-930.

[52] H. -J. Lee , S. -Y. Kim , J. -M. Koh, J. Bok, K. -J, Kim, K. -S. Kim, M. -H. Park, H. -D. Shin, B. L. Park, T. -H. Kim, J. M. Hong, E. K. Park, D. J. Kim, B. Oh, K. Kimm, G. S. Kim, J. -Y. Lee. *Bone* **2007**, *41*, 979-986.

[53] C. L. Tofteng, P. Bach-Mortensen, S. E. Bojesen, A. Tybjaerg-Hansen, L. Hyldstrup, B. G. Nordestgaard. *Pharmacogenet. Genomics* **2007**, *17*, 85-91.

[54] M. G. Murphy, K. Cerchio, S. A. Stoch, K. Gottesdiener, M. Wu. *J. Clin. Endocrinol. Metab.* **2005**, *90*, 2022-2028.

[55] M. D. Pierschbacher, E. Ruoslahti. *Nature* **1984**, *309*, 30-33.

[56] a) S. Swenson, S. Ramu, F.S. Markland. *Curr. Pharm. Des.* **2007**, *13*, 2860-2871; b) J. J. Calvete, C. Marcinkiewicz, D. Monleón, V. Esteve, B. Celda, P. Juárez, L. Sanz. *Toxicon* **2005**, *45*, 1063-1074; c) Y. Fujii, D. Okuda, Z.

Fujimoto. *J. Mol. Biol*. **2003**, *332*, 1115-1122; d) R. J. Gould, M. A. Polokoff, P. A. Friedman, T. F. Huang, J. C. Holt, J. J. Cook, S. Niewiarowski. *Proc. Soc. Exp. Biol. Med*. **1990**, *195*, 168-171.

[57] a) D. Simon, H. Xu, S. Ortlepp, C. Rogers, N. Rao. *Arterioscler. Thromb. Vasc. Biol*. **1997**, *17*, 528-535; b) M. Dennis, W. Henzel, R. Pitti, M. Lipari, M. Napier, T. Deisher, et al. *Proc. Natl. Acad. Sci. U. S. A*. **1990**, *87*, 2471-2475; c) I. Ojima, S. Chakravarty, Q. Dong, *Bioorg. Med. Chem*. **1995**, *3*, 337-360.

[58] a) T. Doi, S. Kamioka, S. Shimazu, T. Takahashi. *Org. Lett*. **2008**, *10*, 817-819; b) M. Ishikawa, M. Tsushima, D. Kubota, Y. Yanagisawa, Y. Hiraiwa, Y. Kojima, K. Ajito, N. Anzai. *Org. Proc. Res. Dev*. **2008,** *12,* 596-602; c) D. Heckmann, A. Meyer, L. Marinelli, G. Zahn, R. Stragies, H. Kessler. *Angew. Chem. Int. Ed*. **2007**, *46*, 3571-3574; d) D. Heckmann, A. Meyer, B. Laufer, G. Zahn, R. Stragies, H. Kessler. *ChemBioChem* **2008**, *9*, 1397-1407; e) S. Urman, K. Gaus, Y. Yang, U. Strijowski, N. Sewald, S. De Pol, O. Reiser. *Angew. Chem. Int. Ed*. **2007**, *46*, 3976-3978; f) R. Stupp, C. Rüegg. *J. Clin. Oncol*. **2007**, *25*, 1637-1638; g) A. Del Gatto, L. Zaccaro, P. Grieco, E. Novellino, A. Zannetti, S. Del Vecchio, F. Iommelli, M. Salvatore, C. Pedone, M. Saviano, *J. Med. Chem*. **2006**, *49*, 3416-3420; h) D. Neri, R. Bicknell. *Nature Rev*. **2005**, *5*, 436-446; i) P. Vianello, P. Cozzi, A. Galvani, M. Meroni, M. Varasi, D. Volpi, T. Bandiera, *Bioorg. Med. Chem. Lett*. **2004**, *14*, 657-661; j) Schaffner, P.; Dard, M.M., *Cell. Mol. Life Sci*. **2003**, *60*, 119-132; k) E. Lohof, E. Planker, C. Mang, F. Burkhart, M. A. Dechantsreiter, R. Haubner, H.-J. Wester, M. Schwaiger, G. Hölzemann, S. L. Goodman, H. Kessler. *Angew. Chem. Int. Ed*. **2000**, *39*, 2761-2764; l) M. A. Dechantsreiter, E. Planker, B. Mathä, E. Lohof, G. Hölzemann, A. Jonczyk, S. L. Goodman, H. Kessler. *J. Med. Chem*. **1999**, *42*, 3033-3040; m) J. Wermuth, S. L. Goodman, A. Jonczyk, H. Kessler. *J. Am. Chem. Soc*. **1997**, *119*, 1328-1335; n) M. A. Russo, M. Serra, L. Colombo, S. Schinelli, *Mini-Rev. Med. Chem*. **2009**, *9*, 1439-1446; o) Z. Liu, F. Wang, X. Chen, *Drug Dev. Res*. **2008**, *69*, 329-339.

[59] T. A. Springer, J. Zhu, T. Xiao, *J. Cell. Biol*. **2008**, *182*, 791-800.

[60] F. Curnis, A. Sacchi, A. Gasparri, R. Longhi, A. Bachi, C. Doglioni, C. Bordignon, C. Traversari, G.-P. Rizzardi, A. Corti. *Cancer Res*. **2008**, *68*, 7073-7082.

[61] A. Spitaleri, S. Mari, F. Curnis, C. Traversari, R. Longhi, C. Bordignon, A. Corti, G.-P. Rizzardi, G. Musco. *J. Biol. Chem*. **2008**, *283*, 19757-19768.

[62] F. Curnis, A. Cattaneo, R. Longhi, A. Sacchi, A. M. Gasparri, F. Pastorino, P. Di Matteo, C. Traversari, A. Bachi, M. Ponzoni, G.-P. Rizzardi, A. Corti. *J. Biol. Chem*. **2010**, *285*, 9114-9123.

[63] A. Corti, F. Curnis. *J. Cell Sci.* **2011**, *124*, 515-522.

[64] M. Ghitti, A. Spitaleri, B. Valentinis, S. Mari, C. Asperti, C. Traversari, G. P. Rizzardi, G. Musco. *Angew. Chem. Int. Ed.* **2012**, *51*, 7702-7705.

[65] M. Aumailley, M. Gurrath, G. Müller, J. Calvete, R. Timpl, H. Kessler. *FEBS Lett*. **1991**, *291*, 50-54.

[66] L. Auzzas, F. Zanardi, L. Battistini, P. Burreddu, P. Carta, G. Rassu, C. Curti, G. Casiraghi. *Curr. Med. Chem*. **2010**, *17*, 1255-1299.

[67] a) S. Hanessian, L. Auzzas. *Acc. Chem. Res*. **2008**, *41*, 1241-1251; b) A. Trabocchi, D. Scarpi, A. Guarna. *Amino Acids* **2008**, *34*, 1-24; c) S. M. Cowell, Y. S. Lee, J. P. Cain, V. J. Hruby. *Curr. Med. Chem*. **2004**, *11*, 2785-98.

[68] Haubner, R.; Schmitt, W.; Hölzemann, G.; Goodman, S.L.; Jonczyk, A.; Kessler, H. *J. Am. Chem. Soc*. **1996**, *118*, 7881-91.

[69] a) L. Belvisi, A. Bernardi, M. Colombo, L. Manzoni, D. Potenza, C. Scolastico, G. Giannini, M. Marcellini, T. Riccioni, M. Castorina, P. LoGiudice C. Pisano. *Bioorg. Med. Chem*. **2006**, *14*, 169-180; b) L. Manzoni, L. Belvisi, D. Arosio, M. Civera, M. Pilkington-Miksa, D. Potenza, A. Caprini, E. M. V. Araldi, E. Monferrini, M. Mancino, F. Podestà, C. Scolastico. *ChemMedChem* **2009**, *4*, 615 –632.

[70] L. Belvisi, T. Riccioni, M. Marcellini, L. Vesci, I. Chiarucci, D. Efrati, D. Potenza, C. Scolastico, L. Manzoni, K. Lombardo, M. A. Stasi, A. Orlandi, A. Ciucci, B. Nico, D. Ribatti, G. Giannini, M. Presta, P. Carminati, C. Pisano. *Mol. Cancer Ther.* **2005**, *4*, 1670-1680.

[71] D. Arosio, L. Belvisi, L. Colombo, M. Colombo, D. Invernizzi, L. Manzoni, D. Potenza, M. Serra, M. Castorina, C. Pisano, C. Scolastico. *ChemMedChem* **2008**, *3*, 1589-1603.

[72] R. Haubner, W. Schmitt, G. Hölzemann, S. L. Goodman, A. Jonczyk, H. Kessler. *J. Am. Chem. Soc.* **1996**, *118*, 7881-7891.

[73] F. Sladojevich, A. Trabocchi, A. Guarna. *J. Org. Chem.* **2007**, *72*, 4254-4257.

[74] a) R. M. Van Well, L. Marinelli, C. Altona, K. Erkelens, G. Siegal, M. van Raaij, A. L. Llamas-Saiz, H. Kessler, E. Novellino, A. Lavecchia, J. H. van Boom, M. Overhand. *J. Am. Chem. Soc.* **2003**, *125*, 10822-10829; b) R. M. Van Well, H. S. Overkleeft, G. A. van der Marel, D. Bruss, G. Thibault, P. G. de Groot, J. H. van Boom, M. Overhand. *Bioorg.Med. Chem. Lett.* **2003**, *13*, 331-334.

[75] G. Casiraghi, G. Rassu, L. Auzzas, P. Burreddu, E. Gaetani, L. Battistini, F. Zanardi, C. Curti, G. Nicastro, L. Belvisi, I. Motto, M. Castorina, G. Giannini, C. Pisano. *J. Med. Chem.* **2005**, *48*, 7675-7687.

[76] F. Zanardi, P. Burreddu, G. Rassu, L. Auzzas, L. Battistini, C. Curti, A. Sartori, G. Nicastro, G. Menchi, N. Cini, A. Bottoncetti, S. Raspanti, G. Casiraghi. *J. Med. Chem.* **2008**, *51*, 1771-82.

[77] a) M. Weller, D. Reardon, B. Nabors, R. Stupp. *Nat. Med.* **2009**, *15*, 726; b) A. R. Reynolds, K. M. Hodivala-Dilke. *Nat. Med.* **2009**, *15*, 727.

[78] A. S. M. da Ressurreição, A. Vidu, M. Civera, L. Belvisi, D. Potenza, L. Manzoni, S. Ongeri, C. Gennari, U. Piarulli. *Chem. Eur. J.* **2009**, *15*, 12184-8.

[79] A. S. M. Ressurreição, R. Delatouche, C. Gennari, U. Piarulli. *Eur. J. Org. Chem.* **2011**, 217-228.

[80] K. Burgess. *Acc. Chem. Res.* **2001**, *34*, 826-835.

[81] A. Golebiowski, S. R. Klopfenstein, J. J. Chen, X. Shao. *Tetrahedron Lett.* **2000**, *41*, 4841-4844.

[82] A. Golebiowski, S. R. Klopfenstein, X. Shao, J. J. Chen, A. O. Colson, A. L. Grieb, A. F. Russell. *Org. Lett.* **2000**, 2, 2615-2617.

[83] A. Golebiowski, J. Jozwik, S. R. Klopfenstein, A. O. Colson, A. L. Grieb, A. F. Russell, V. L. Rastogi, C. F. Diven, D. E. Portlock, J. J. Chen. *J. Comb. Chem.* **2002**, *4*, 584-590.

[84] H.-O. Kim, H. Nakanishi, M. S. Lee, M. Kahn. *Org. Lett.* **2000**, *2*, 301-302.

[85] J. Liu, F. Brahimi, H. U. Saragovi, K. Burgess. *J. Med. Chem.* **2010**, *53*, 5044-5048.

[86] J. A. Robinson, *Acc. Chem. Res.* **2008**, *41*, 1278-1288.

[87] G. Gellerman, E. Hazan, T. Brider, T. Traube, A. Albeck, S. Shatzmiler. *Int. J. Pept. Res. Ther.* **2008**, *14*, 183-192.

[88] G. Gellerman, E. Hazana, M. Kovaliov, A. Albeck, S. Shatuniler. *Tetrahedron* **2009**, *65*, 1389-1396.

[89] J. S. Davies, M. Stelmach-Diddams, R. Fromentin, A. Howells, R. Cotton. *J. Chem. Soc., Perkin Trans. 1* **2000**, 239-243.

[90] C. Bisang, C. Weber, J. A. Robinson. *Helv. Chim. Acta* **1996**, *79*, 1825–1842.

[91] M. Royo, W. Van den Nest, M. del Fresno, A. Frieden, D. Yahalom, M. Rosenblatt, M. Chorev, F. Albericio. *Tetrahedron Lett.* **2001**, *42*, 7387–7391.

[92] C. E. Schafmeister, Z. Z. Brown, S. Gupta. *Acc. Chem. Res.* **2008**, *41*, 1387-1398.

[93] C. G. Levins, C. E. Schafmeister. *J. Am. Chem. Soc.* **2003**, *125*, 4702-4703.

[94] A. S. M. Ressurreicao, A. Bordessa, M. Civera, L. Belvisi, C. Gennari, U. Piarulli. *J. Org. Chem.* **2008**, *73*, 652-660.

[95] The superscripted number after β specifies the position of the side chain on the corresponding β-amino acid, see: T. Hintermann, D. Seebach. *Synlett* **1997**, 437-438.

[96] R. Delatouche, M. Durini, M. Civera, L. Belvisi, U. Piarulli. *Tetrahedron Lett.* **2010**, *51*, 4278-4280.

[97] A. S. M. Ressurreicao, A. Vidu, M. Civera, L. Belvisi, D. Potenza, L. Manzoni, S. Ongeri, C. Gennari, U. Piarulli. *Chem.-Eur. J.* **2009**, *15*, 12184–12188.

[98] K. L. Webster, A. B. Maude, M. E. O'Donnell, A. P. Mehrotra, D. Gani. *J. Chem. Soc., Perkin Trans. 1* **2001**, 1673-1695.

[99] C. M. Thompson, J. A. Frick, D. L. C. Green. *J. Org. Chem.* **1990**, *55*, 111-116.

[100] M. Marchini, M. Mingozzi, R. Colombo, C. Gennari, M. Durini, U. Piarulli. *Tetrahedron* **2010**, *51*, 4278–4280.

[101] O. Mitsunobu, Y. Yamada. *Bull. Chem. Soc. Japan* **1967**, *40*, 2380-2382.

[102] X. Ariza, F. Urpí, C. Viladomat, J. Vilarrasa. *Tetrahedron Lett.* **1998**, *39*, 9101-9102.

[103] C. David, L. Bischoff, H. Meudal, A. Mothé, N. De Mota, S. DaNascimento, C. Llorens-Cortes, M.-C. Fournié-Zaluski, B. P. Roques. *J. Med. Chem.* **1999**, *42*, 5197-5211.

[104] J. Coste, E. Frerot, P. Jouin. *J. Org. Chem.* **1994**, *59*, 2437-2446.

[105] J. A. Fehrentz, C. G. Dellac, M. Amblard, F. Winternitz, A. Loffet, J. Martinez. *J. Pept. Sci.* **1995**, *1*, 124–131.

[106] L. A. Carpino, E.-S. M. E. Mansour, D. Sadat-Aalaee. *J. Org. Chem.* **1991**, *56*, 2611-2614.

[107] a) R. G. Denkewalter. *J.Am.Chem.Soc.* **1966**, *88*, 3163-3164; b) K. Jensen, J. Alsina, M. F. Songster, J. Vagner, F. Albericio, G. Barany. *J.Am.Chem.Soc.* **1998**, *120*, 5441 5452.

[108] V. Bavetsias, A. L. Jackman, R. Kimbell, W. Gibson, F. T. Boyle, G. M. F. Bisset, *J. Med. Chem.* **1996**, *39*, 73-85.

[109] M. De Greef, S. Abeln, K. Belkhasmi, A. D.mling, R. V. A. Orru, L. A. Wessjohann. *Synthesis* **2006**, 3997-4004.

[110] The biological studies reported in this section were carried out by Dr. Daniela Arosio from CNR-ISTM, Milan, whom I sincerely acknowledge for the kind collaboration.

[111] a) G. Müller, M. Gurrath, H. Kessler. *J. Comput.-Aided Mol. Des.* **1994**, *8*, 709-730; b) R. Haubner, R. Gratias, B. Diefenbach, S. L. Goodman, A. Jonczyk, H. Kessler. *J. Am. Chem. Soc.* **1996**, *118*, 7461-7472; c) M. Aumailley, M. Gurrath, G. Müller, J. Calvete, R. Timpl, H. Kessler. *FEBS Lett.* **1991**, *291*, 50-54.

[112] The NMR characterization and computational studies reported in this section were carried out by Dr. Laura Belvisi, Dr. Donatella Potenza, Dr. Monica Civera, Dr. Francesca Vasile, M.Sc. Ileana Guzzetti from the University of Milan, whom I sincerely acknowledge for the kind collaboration.

[113] W. L. Jorgensen, D. S. Maxwell, J. Tirado-Rives. *J. Am. Chem. Soc.* **1996**, *118*, 11225-11236.

[114] The OPLS_2001 force field, among several commonly used force fields, provided the highest correlation between calculated and experimental conformational preferences within the series of cyclic RGD-peptidomimetics containing diketopiperazine scaffolds with different stereochemistry and substitution at the piperazinic nitrogens.

CHAPTER 2

SYNTHESIS AND BIOLOGICAL EVALUATION (IN VITRO AND IN VIVO) OF CYCLIC RGD PEPTIDOMIMETIC - PACLITAXEL CONJUGATES TARGETING INTEGRIN $\alpha_V\beta_3$

1 - Chemotherapy

Chemotherapy has been one of the main approaches for the treatment of cancer for more than half a century and is based on the administration of drugs which often interfere with fundamental cellular functions (*e.g.*, DNA replication, cell division). The antitumor efficacy of anticancer drugs is thus limited by their nonspecific toxicity to normal cells, especially to rapidly growing cells such as blood, bone marrow and mucous membrane cells, resulting in a low therapeutic index and serious side-effects. The efficacy of chemotherapy is further limited by the occurrence or development of drug resistance: tumor cells can be regarded as a rapidly changing target because of their genetic instability, heterogeneity, and high rate of mutation, leading to selection and overgrowth of a drug-resistant tumor cell population.[1] In principle, the efficiency of the treatment can be improved by increasing the doses, but this approach commonly results in severe toxicity. Therefore, selective tumor targeting of chemotherapeutic agents represents a major goal, and various drug delivery systems have been recently developed,[2] including the use of liposomes, microspheres, micelles, polymers, protein- or antibody-drug conjugates, and pro-drugs (Figure 2.1).[3]

Considerable efforts are currently being made in this domain to such an extent that leaders of major pharmaceutical companies foresee that >60% of all existing drugs will be targeted in less than two decades.[4] In this field, an attractive avenue for selective tumor targeting are hybrid molecules designed to bind to specific over-expressed receptors on cancer cells.[5] Clearly, the success of this approach is heavily dependent on the rational selection of appropriate biological objectives.

Figure 2.1. Pharmaceutical nano-carriers for drug targeting[a]

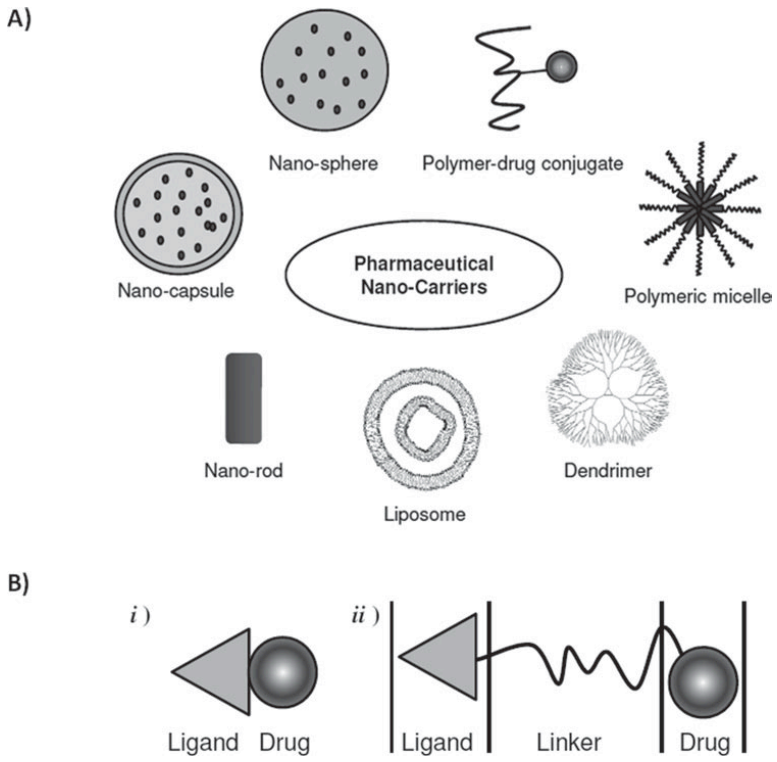

[a] A): Structural design of a ligand-targeted drug conjugate B): *i*) ligand-drug conjugate obtained by a direct linkage between the ligand and the drug or *ii*) connected through a linker.

Integrins are ideal pharmacological targets based on their key role in angiogenesis and tumor development and on their easy accessibility as cell surface receptors interacting with extracellular ligands.[6] They are also involved in tissue integrity and cell trafficking, growth, differentiation, proliferation and migration (see relevant discussion in Chapter 1).[7] As a consequence of their role in so many fundamental processes, integrin malfunction is connected to a large variety of diseases such as thrombosis, osteoporosis, inflammation, and cancer.[8] The tripeptide sequence arginine-glycine-aspartate (RGD) has been identified as the common motif used by several endogenous ligands to recognize and bind a group of integrins, including $\alpha_V\beta_3$, $\alpha_V\beta_5$, $\alpha_5\beta_1$, which are crucial in angiogenesis, tumor progression and metastasis, and $\alpha_{IIb}\beta_3$, which is involved in platelet aggregation.[9]

As mentioned in Chapter 1, the potent $\alpha_V\beta_3$ integrin ligand, *cyclo*[Arg-Gly-Asp-D-Phe-*N*(Me)-Val] (Cilengitide) developed by Kessler and co-workers (Figure 2.2),[10,11] is currently in phase III clinical trials as an angiogenesis inhibitor for patients with *glioblastoma multiforme*.[12] The high activity and selectivity of this derivative has been attributed to an extended conformation of the RGD motif displaying a distance of about 9 Å between the C_β atoms of Asp and Arg.[11,13] These observations prompted many other research groups to investigate the use of conformationally constrained cyclic

RGD peptidomimetics as active and selective integrin antagonists. A selection of these ligands, encompassing a wide variety of rigid scaffolds and featuring 13-, 14-, 15- and 16-membered rings, is shown in 2.2.[14]

Figure 2.2. Potent $\alpha_V\beta_3$ integrin ligands

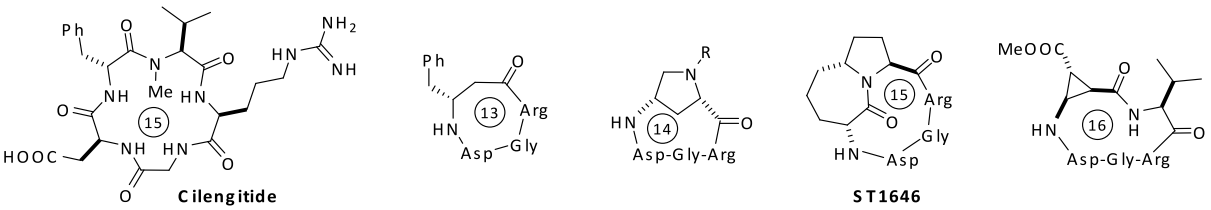

We have recently contributed to this field with a new class of cyclic RGD-peptidomimetics, containing bifunctional diketopiperazine (DKP) scaffolds and featuring 17-membered rings (Figure 2.3).[15] The *cis*-derivative *cyclo*[DKP-1-RGD] (**16**) inhibited biotinylated vitronectin binding to the purified $\alpha_V\beta_3$ receptor at a micromolar concentration (3.9 ± 0.4 μM), while *trans*-derivatives **17-22** ranged from submicro- to subnanomolar concentrations (220 - 0.2 nM).

Figure 2.3. Library of *cyclo*[DKP-RGD] integrin ligands

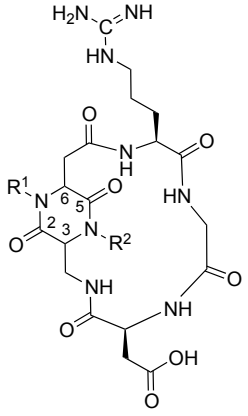

16 = *cyclo*[DKP-1-RGD] = 3*S*, 6*S*, R^1=H, R^2=Bn
17 = *cyclo*[DKP-2-RGD] = 3*R*, 6*S*, R^1=H, R^2=Bn
18 = *cyclo*[DKP-3-RGD] = 3*S*, 6*R*, R^1=H, R^2=Bn
19 = *cyclo*[DKP-4-RGD] = 3*R*, 6*S*, R^1=Bn, R^2=H
20 = *cyclo*[DKP-5-RGD] = 3*R*, 6*S*, R^1=Bn, R^2=Bn
21 = *cyclo*[DKP-6-RGD] = 3*S*, 6*R*, R^1=Bn, R^2=H
22a = *cyclo*[DKP-7-RGD][a] = 3*S*, 6*R*, R^1=Bn, R^2=Bn
22b = *cyclo*[DKP-7-RGD][a] = 3*S*, 6*R*, R^1=Bn, R^2=Bn

[a]*N,N'*-dibenzyl *cyclo*[DKP-7-RGD] was isolated as two different separable conformers (diastereomers, **22a** and **22b**) due to hindered rotation of one ring around the other, *i.e.*, the DKP *N*-benzyl group cannot pass inside the macrolactam ring, see Chapter 1

1.1 - *RGD ligand - cytotoxic conjugates*

It is currently emerging that antiangiogenic therapy alone is not sufficient to fight and eradicate tumors: recent pre-clinical findings of a paradoxical pro-angiogenic activity of RGD-mimetic agents (like Cilengitide) at low concentrations have stimulated the debate on the use of antiangiogenetics as single drugs.[16] After 25 years of research on integrins as pharmacological targets, only four drugs are currently on the market (see Table 2.1 and Figure 2.4).

Table 2.1. Integrin inhibitors in late-stage (Market, Phase III or Phase II) clinical studies[a]

Clinical phase	Indication[b]	Target	Drug	Synonyms	Drug class	Status
Approved	MS	a4bx[c]	Natalizumab	Tysabri, Antegren, AN-100226, BG-00002	Hu-mAb	L
	Thrombosis	gpIIbIIIa	Abciximab	ReoPro, Clotinab, CentoRx	Chi-mAb-Fab	L
	Thrombosis	gpIIbIIIa	Tirofiban	L-700462, MK-383, Aggrastat	SM	L
	Thrombosis	gpIIbIIIa	Intrifiban	Eptifibatide, SB-1, Sch-60936, Integrelin	cPep	L
Phase III	IBD, UC, Crohn's	a4bx	AJM-300		oSM	A
	UC, Crohn's	a4b7	Vedolizumab	MLN-02, LDP-02	Chi-mAb	A
	Dry eye, conjunctivitis	aLb2	SAR-1118		SM	A
	Immunosuppression	aLb2	Odulimomab		Chi-mAb	ndr
	Stroke, ischemia	aLb2	Rovelizumab	23F2G, LeukArrest	Chi-mAb	ndr
	Thrombosis	gpIIbIIIa	Alnidofibatide	RPR-109891, Klerval	Pep-der	A
	Thrombosis	gpIIbIIIa	Orbofiban	SC-57099B, CS-511	SM	A
	Diagnostics	gpIIbIIIa	DMP-444 (Tc99m)	RP-444	Diag	ndr
	Thrombosis	gpIIbIIIa	Lefradafiban	BIBU-104	SM	ndr
	Cancer	avb3, avb5	Cilengitide	EMD 121974, EMD 85189, NSC-707544	cPep	A
Phase II	Arthritis	a4b1	MDL-819767	HMR-1031	SM	A
	Crohn's	a4bx	TRK-170		oSM	A
	IBD, MS, RA, asthma, Crohn's	a4bx	firategrast	SB-683699, T-0047	oSM	A
	Arthritis, asthma	a4bx	RO-27-0608	Valategrast, R411	SM	A
	Ulcerative colitis	a4b7, aEb7	Etrolizumab	Pro-145223, RG-7413	hu-Mab	A
	Asthma, rhinitis	a4b1	RBx-7796	RBx-4638, clafrinast	SM	ndr
	HIV infection	aLb2	Cytolin		hu-mAb	A
	IS, psoriasis	aLb2	BMS-587101		oSM	ndr
	Thrombosis	gpIIbIIIa	MK-0852	L-367073	cPep	A
	AP, stroke, thrombosis	gpIIbIIIa	Cromafiban	CT-50352	SM	ndr
	Restenosis, thrombosis	gpIIbIIIa	FK-633	FR-144633	SM	ndr
	Thrombosis	gpIIbIIIa	Elarofiban	RWJ-53308	SM	ndr
	Thrombosis	gpIIbIIIa	SR-121787		SM	ndr
	Cancer, Crohn's	a5b1	ATN-161		Pep	A
	Cancer, AMD	a5b1	Volociximab	M-200, EOS-200-4	mAb	A
	Arthritis, cancer, osteoporosis, psoriasis, restenosis, RA	avb3	Etaracizumab	MED-522, hLM609, Vitaxin-2, Abegrin	mAb	A
	Cancer	avbx	Intetumumab	CNTO-95	mAb	A
	Cancer: diagnostics	avb3, avb5	Fluciclatide (^{18}F)	GE-135, [^{18}F]-AH-111585	Diag	A
	Cancer: diagnostics	avb3	^{99}mTc-Maraciclatide	NC100692	Diag	A
	Kidney TR, PF	avb6	STX-100	3G9	hu-mAb	A
	Cancer	avbx	EMD-525797	DI17E6	hu-mAb	A
	Osteoporosis	avb3	MRL-123		SM	ndr
	AMD, diabetic retinopathy	avbx, a5b1	AGR-1001		cPep	A

[a] Cut-off: November 2012.

[b] Abbreviations: A, trials active; AP, angina pectoris; cPep, cyclic peptide; Chi-mAb-Fab, chimeric monoclonal antibody, Fab' fragment; Diag, diagnostic reagent; HIV, human immunodeficiency virus; Hu-mAb, humanized monoclonal antibody; IS, ischemic stroke; L, launched/drug approved for clinical use; mAb, monoclonal antibody; MS, multiple sclerosi, ndr, no development reported, drug not discontinued, but trials not apparently active; oSM, orally available small molecule; Pep-der, peptide derivative; PF, pulmonary fibrosis; RA, rheumatoid arthritis; SM, small molecule; TR, transplant rejection; UC, ulcerative colitis.

[c] βx indicates that all associated β chains are targeted.

Although it initially appeared a promising strategy, successful therapeutic inhibition of integrins has proven to be elusive, despite the discovery of highly potent inhibitors. This is due to a number of reasons, including redundancy among the integrins, the importance of integrins in key physiological systems and antagonists that had less than optimal properties.[17]

Figure 2.4. Integrin inhibitors in clinical trials or on the market.

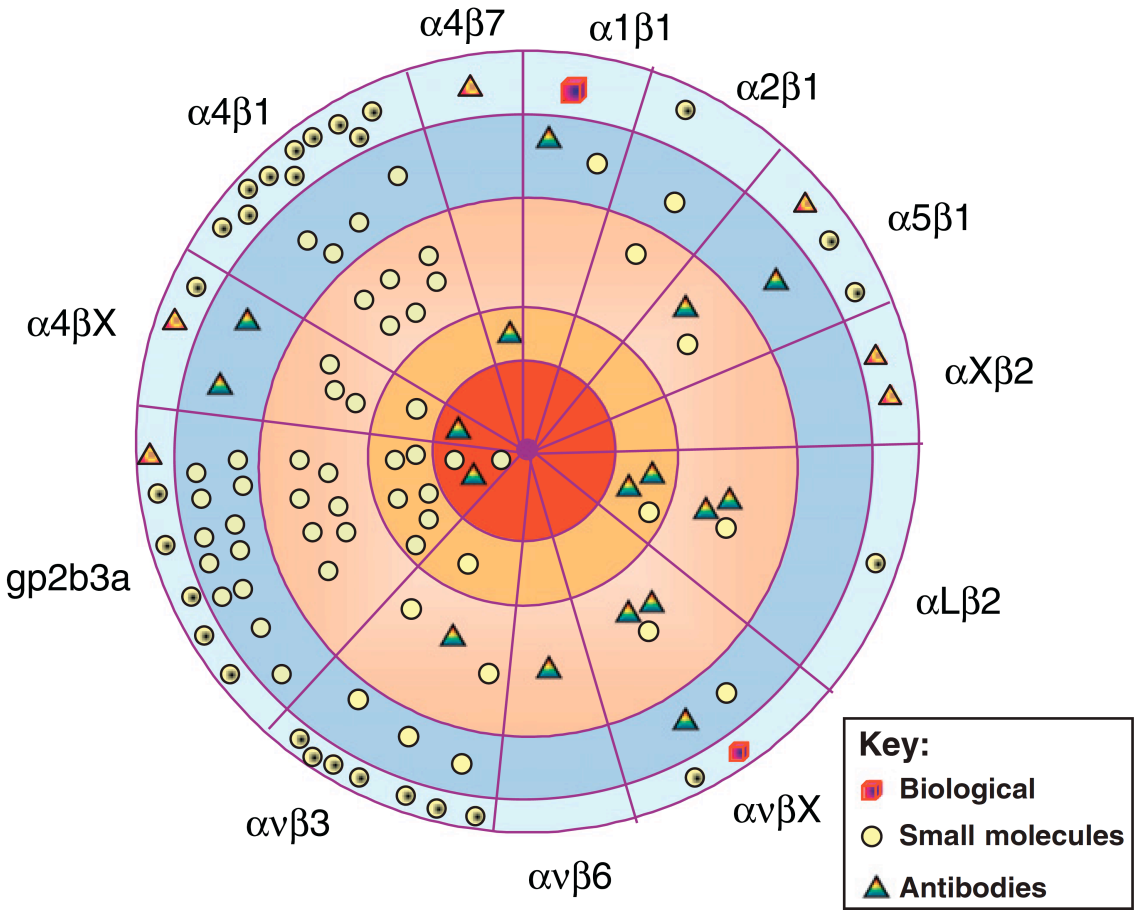

[a] The current distribution of integrins as therapeutic targets and the stages of related clinical trials. If targeting affects all α chains ('αx') or all β chains ('βx') the trial is classified accordingly (e.g., intetumumab affects all αv integrins independently of associated β chains – and is classed under αvβx). Trials discontinued (light blue); at Phase I (dark blue); at Phase II (pale orange); at Phase III (mid orange); or approved drugs (red). Symbols: small molecules and peptides (circles yellow); antibodies (triangles); biologicals (cubes). Symbols with black centers represent discontinued trials.

Since α_V integrins, which can be internalized by cells, are involved in tumor angiogenesis and are overexpressed on the surface of cancer cells, integrin ligands can be usefully employed as tumor-homing peptidomimetics for site-directed delivery of cytotoxic drugs.[18] During the past fifteen years, a number of RGD-cytotoxic drug conjugates have been developed.

In a pioneering work Arap and co-workers used a phage display library to isolate peptides that home specifically to tumor blood vessels.[19a] Recovery of phage from tumors led to identification of RGD-4C as best candidates. To determinate if this RGD-compound could be used to improve the therapeutic index of cancer chemotherapeutics, they coupled the RGD-4C ligand to doxorubicin (a well known anticancer agent). The RGD-4C-doxorubicin conjugate (see Figure 2.5) was used to treat mice bearing tumors derived from human MDA-MB-435 breast carcinoma cells. An enhanced efficacy and reduced toxicity of the drug against the human breast cancer xenografts in nude mice were observed. These results demonstrated the utilities of targeted chemotherapy strategies based on selective expression of receptors in tumor vasculature. The same conjugate (RGD-4C-doxorubicin) was evaluated by Lee and Kim in an orthotopic murine hepatoma model. When given intravenously to mice the construct suppressed the growth of hepatoma more effectively than free doxorubicin, confirming the previously reported results on a different tumor model.[19b]

Figure 2.5. RGD-4C-doxorubicin conjugate

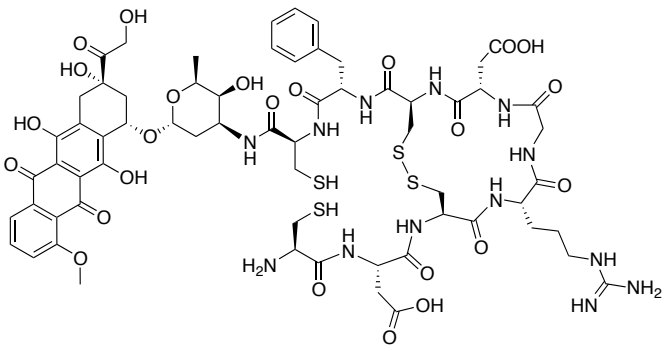

RGD-4C - doxorubicin

Ryppa and co-workers also developed doxorubicin conjugates with a divalent RGD peptidomimetic E[*cyclo*(RGDfK)]$_2$.[20] In particular, they prepared a 6-maleimidocaproyl amide derivative of doxorubicin, which was conjugated with E[*cyclo*(RGDfK)]$_2$ elongated by introducing a thiol group (2-iminothiolane, Traut's reagent) at the α position of the glutamic acid moiety (Figure 2.6).

In vivo studies in an OVCAR-3 xenograft model, the doxorubicin conjugate showed unconvincing antitumor efficacy: the construct resulted inactive compared to free doxorubicin, being also toxic with a mortality of 50%.

Figure 2.6. E[*cyclo*(RGDfK)]$_2$-doxorubicin conjugate

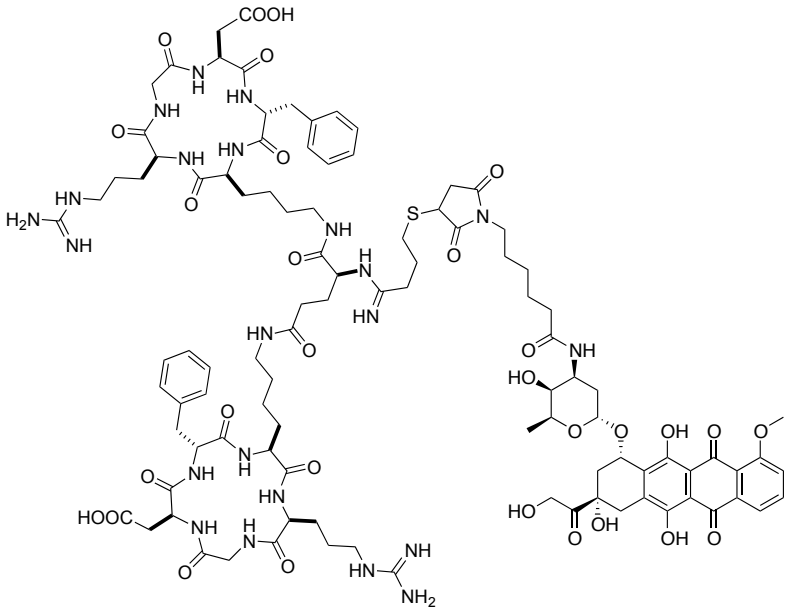

E[*c*(RGDfK)$_2$]-DOXO

Koch and co-workers synthesized two conjugates of the doxorubicin pro-drug (doxsaliform) with either the acyclic form of RGD-4C peptide or *cyclo*[(*N*-Me)VRGDf-NH] (Figure 2.7).[21] A hydroxylamine ether tether was used to attach 5'-formyldoxsaliform to the RGD ligands *via* an oxime functional group. Although the two conjugates showed promising results *in vitro* (cytotoxicity and integrin binding assays), no *in vivo* data are reported. For this reason, the real efficacy of these constructs could be speculated but not demonstrated.

Figure 2.7. RGD ligands-doxsaliform conjugates

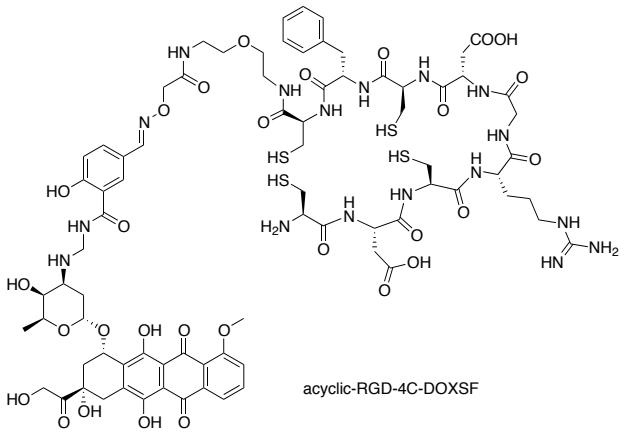

acyclic-RGD-4C-DOXSF

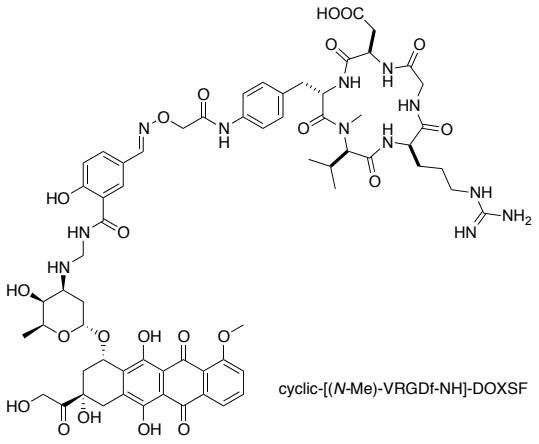

cyclic-[(*N*-Me)-VRGDf-NH]-DOXSF

In 2008, Lippard and co-workers reported the synthesis of a few functionalized platinum(IV) complexes conjugated to linear or cyclic RGD peptides, as tumor homing devices to target tumor endothelial cell selectivity over healthy cells (Figure 2.8).[22]

Figure 2.8. RGD ligands-doxsaliform conjugates

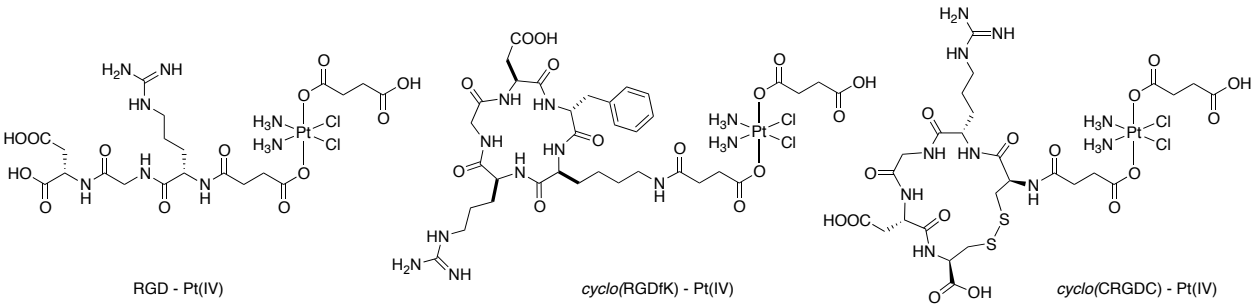

The Pt(IV)-RGD conjugates were highly and specifically cytotoxic to cell containing overexpressed levels of $\alpha_V\beta_3$ and $\alpha_V\beta_5$ integrins. In contrast, Pt(IV)-AGR complexes (used as negative control) were significantly less active than Pt(IV)-RGD compounds.

Five RGD peptide-camptothecin constructs were designed and synthesized by Dal Pozzo, Pisano, and co-workers with the purpose of improving the therapeutic index of the drug.[23] They used cyclic peptide analogs of *cyclo*[RGDfV], replacing valine with a functionalized non-proteogenic aminoacid for the attachment of cytotoxic drugs. The conjugation to the drug was achieved through either a stable amide/oxime or an acid-labile amide/hydrazone linkers (see compounds **84**, **85** and **86** in Figure 2.9). Conjugates **84** and **85** showed lower *in vitro* and *in vivo* activity than the parent drug, probably due to the excessive stability of the linker even inside the tumor cells. On the contrary, the hydrazone bond-containing conjugates exhibited high *in vitro* cytotoxicity, but their stability at pH 7.4 was much lower than expected; as a consequence, their activity has been mostly attributed to a prematurely delivery of the drug. Moreover, their poor solubility hampered *in vivo* experiments. To overcome these drawbacks, Dal Pozzo, Pisano and co-workers developed dimeric RGD ligands conjugated to a camptothecin derivative through PEGilated linkers containing protease-sensitive peptides suitable for releasing the drug by enzymatic hydrolysis inside the tumor cells. These constructs increased the affinity for integrin receptors together with appreciable stability and solubility. Evaluation of the best candidates in preclinical animal model were programmed but, up to date, no *in vivo* data are reported.

The same group very recently reported the synthesis of four camptothecins conjugated to a RGD mimics, using a piperazine carbamate linker (to prevent a rapid hydrolysis). The best candidate (compound **87**, Figure 2.9) revealed a potent affinity to integrin receptors, high cytotoxic activity on A2780 cancer cells (which present a high level of integrin receptors) and a superior stability in plasma ($t_{1/2}$ = 13 h for compound **87** vs. $t_{1/2}$ = 45 min for the unconjugated camptothecin parent). *In vivo*

experiments showed a reduced metastatic area and inhibition of tumor growth comparable to those observed with the parent drug, without a real improvement.

Figure 2.9. Camptothecin derivatives conjugated to RGD peptides or peptidomimetic.

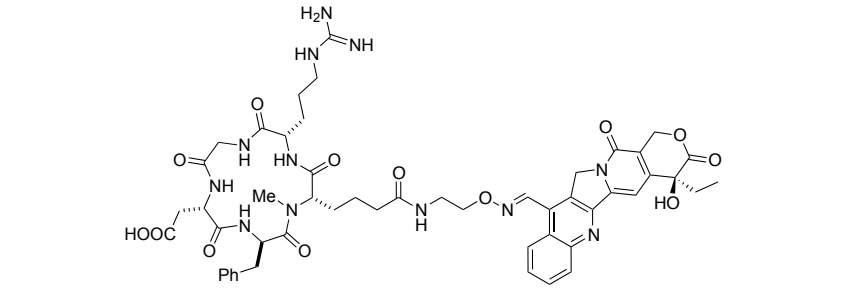

cyclo[RGDf-Aad]-campthotecin **84**

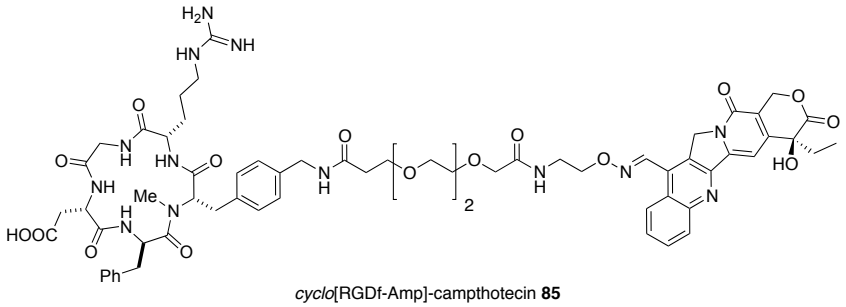

cyclo[RGDf-Amp]-campthotecin **85**

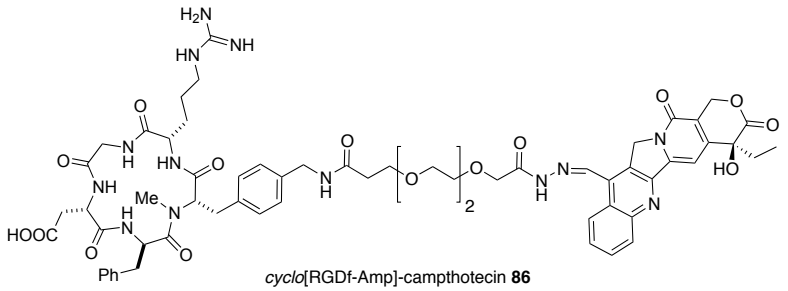

cyclo[RGDf-Amp]-campthotecin **86**

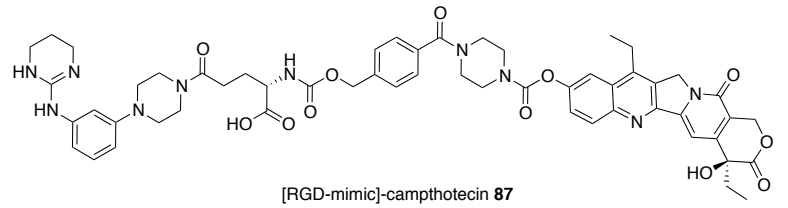

[RGD-mimic]-campthotecin **87**

Summarizing, a few cyclic RGD integrin ligands (*e.g.*, RGD-4C[19], *cyclo*[(*N*-Me)VRGDf-NH],[22] *cyclo*[RGDfK],[21,22] *cyclo*[CRGDC],[22] *cyclo*[RGDf-Aad],[23a] *cyclo*[RGDf-Amp][23a]) were conjugated to a cytotoxic drug (*e.g.*, doxorubicin,[19,20] doxsaliform,[19] camptothecin,[23a,b] cisplatin[22]) through different linkers, such as amides,[19,22,23a] oximes,[19,23a] maleimides,[20] carbamates,[23b] and hydrazones.[23a]

Notably, Chen and co-workers prepared the RGD ligand - Paclitaxel conjugate **88** (Figure 2.10), which was covalently assembled by joining the microtubule-stabilizing anticancer agent to the dimeric RGD peptide E[*cyclo*(RGDyK)]$_2$ via a cleavable succinyl ester linker, and evaluated its antitumor activity on the metastatic breast cancer cell line MDA-MB-435.[24] In mice, conjugate **89** showed a moderately improved antitumor effect over Paclitaxel, but no tumor regression could be observed. The stability of the succinyl linker was not assessed and a premature release of Paclitaxel can be suspected.

Figure 2.10. Dimeric RGD ligand-Paclitaxel conjugates

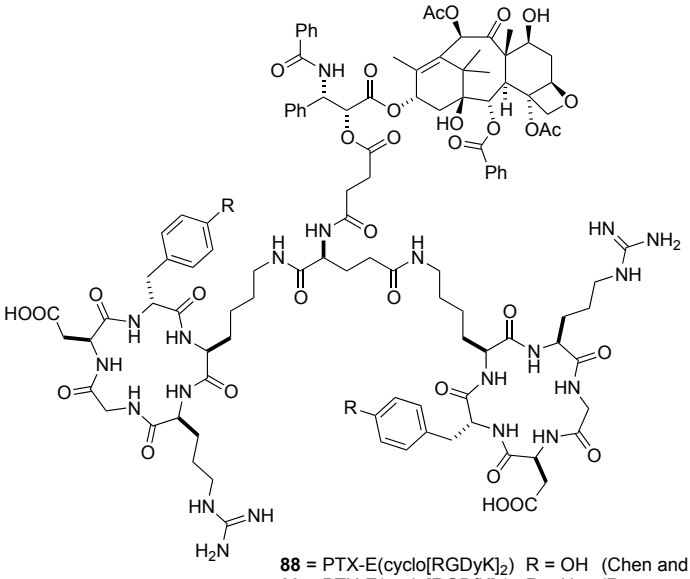

88 = PTX-E(cyclo[RGDyK]$_2$) R = OH (Chen and co-workers)
89 = PTX-E(cyclo[RGDfK]$_2$) R = H (Ryppa and co-workers)

A very similar conjugate (*i.e.*, compound **89** reported in Figure 2.10) was extensively evaluated in a recent study by Ryppa and co-workers on an ovarian carcinoma xenograft model (OVCAR-3).[25] Although the construct provided promising results *in vitro*, unfortunately it did not show any antitumor effect *in vivo*. The stability of conjugate **89** in a glucose phosphate buffer solution at pH=7 was studied over 24 h, yielding a half-life of only ~2 h at 37 °C. Half-life in the bloodstream is expected to be much shorter, and the inefficacy of this conjugate was attributed to hydrolysis of the ester bond at the 2' position of Paclitaxel, which causes premature release of the cytotoxic agent and loss of the tumor-homing effect.

The full account of our investigations on this topic reporting is presented in this Chapter,[26] including: (i) the synthesis of new *cyclo*[DKP-RGD] integrin ligands, bearing a free amino group suitable for conjugation to a cytotoxic drug; (ii) the conjugation of these ligands to Paclitaxel *via* a succinyl linker to give *cyclo*[DKP-RGD]-Paclitaxel conjugates **10**-**13** (Figure 2.11); (iii) the stability of a *cyclo*[DKP-RGD]-Paclitaxel construct in a physiological solution and in both human and murine plasma, which

turned out to be far better than that of previously reported Paclitaxel conjugates;[25] (iv) the ability of the *cyclo*[DKP-RGD]-Paclitaxel conjugates to compete with biotinylated vitronectin for binding to the purified $\alpha_V\beta_3$ and $\alpha_V\beta_5$ receptors; (v) the *in vitro* cytotoxic activity of the *cyclo*[DKP-RGD]-Paclitaxel conjugates against a panel of human cancer cell lines; (vi) the *in vivo* tumor-targeting efficacy against the IGROV-1/Pt1 human ovarian carcinoma xenotransplanted in nude mice; (vii) the effects of tumor treatment, analyzed using immunohistochemistry.

Figure 2.11. Structure of *cyclo*[DKP-RGD]-Paclitaxel conjugates **90**-**93**

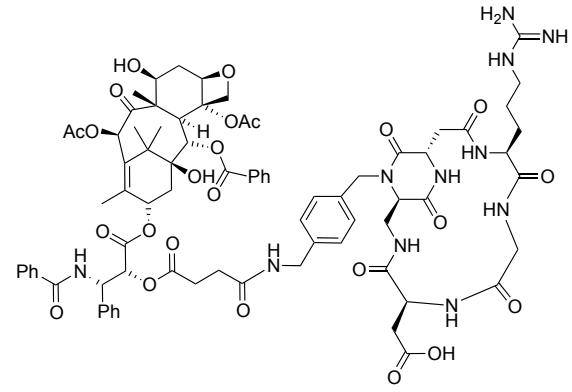

90 = *cyclo*[DKP-*f*2-RGD]-PTX

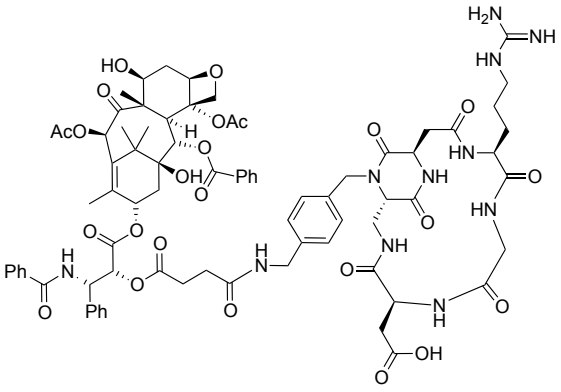

91 = *cyclo*[DKP-*f*3-RGD]-PTX

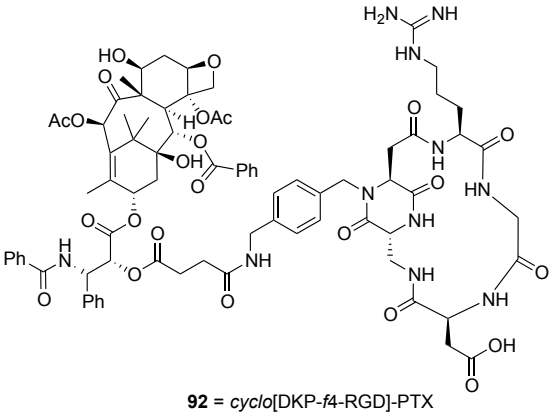

92 = *cyclo*[DKP-*f*4-RGD]-PTX

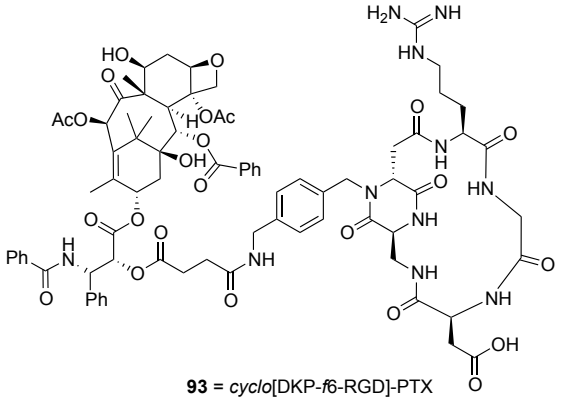

93 = *cyclo*[DKP-*f*6-RGD]-PTX

2 - Synthesis and biological evaluation of *cyclo*[DKP-RGD]-PTX Conjugates

2.1 - *Synthesis*

In order to prepare cyclic RGD-peptidomimetics covalently linked to Paclitaxel (compounds **90-93**, Figure 2.11), four functionalized (*f*) *trans* diketopiperazines (*i.e.*, DKP-*f*2, DKP-*f*3, DKP-*f*4, DKP-*f*6)

were synthesized, varying the position of the *p*-aminomethylbenzyl *N*-substituent (*N*-1 or *N*-4) and the absolute stereochemistry at C-3 and C-6 (Schemes 2.1-2.3). These DKPs were used for the synthesis of *cyclo*[DKP-RGD] integrin ligands (Scheme 2.4), which were conjugated to 2'-succinyl Paclitaxel (Scheme 2.5).

For the preparation of the functionalized *trans* diketopiperazines DKP-*f*2, DKP-*f*3, DKP-*f*4, and DKP-*f*6, it was selected a linker bearing both an aldehyde (for successive reductive alkylation) and an amino group (for the final conjugation to Paclitaxel). Thus, linker **94** was synthesized in three steps from 4-aminomethyl benzoic acid via $LiAlH_4$ reduction, primary amine protection as 4-methoxy-2,3,6-trimethylbenzenesulphonamide (Mtr) and benzylic alcohol oxidation using activated MnO_2 (Scheme 2.1). The Mtr protecting group was chosen because of its stability and orthogonality with the methyl, benzyl, allyl, *t*Bu, Boc, and Cbz protecting groups.

Scheme 2.1. Synthesis of aldehyde **94**[a]

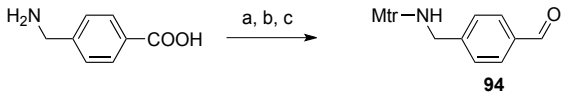

[a]Reagents and conditions: (a) $LiAlH_4$, THF, 8 h, reflux, 70%; (b) Mtr-Cl, *i*-Pr_2NEt, THF, 6 h, room temp., 85%; (c) MnO_2, THF, overnight, room temp., quant..

Trans scaffolds DKP-*f*2, DKP-*f*3 (Scheme 2.2) and DKP-*f*4, DKP-*f*6 (Scheme 2.3) were synthesized starting from commercially available (*R*)- or (*S*)-aspartic acid and (*R*)- or (*S*)-serine. Two different synthetic strategies were developed depending on the nitrogen substitution. In particular, the synthesis of DKP-*f*2 and DKP-*f*3 (bearing the linker on DKP nitrogen *N*-4, former serine nitrogen) was realized making use of a serine ligation strategy,[27] as described in Scheme 2.2. (*R*)- and (*S*)-Aspartic acid were initially protected as allyl ester on the side chain and as *N*-Boc to give the enantiomeric derivatives (*S*)**-95** and (*R*)-**96**. (*R*)- and (*S*)-Serine were protected as methyl ester and reductively alkylated with aldehyde **94** and sodium triacetoxyborohydride to afford the enantiomeric compounds (*R*)**-97** and (*S*)-**98**. Direct coupling (HATU, *i*Pr_2NEt) of protected aspartic acid (*S*)**-15** with functionalized serine (*R*)-**97**, or of the enantiomers (*R*)-**96** with (*S*)-**98**, led to the isopeptides (*S*,*R*)-**99** and (*R*,*S*)-**100** in high yield (86%), rather than forming the expected dipeptides. The *O*,*N*-acyl migration[27] was then triggered by cleavage of the Boc protecting group and treatment with a base (*i*Pr_2NEt) in a protic solvent (*i*PrOH), which also promoted the simultaneous cyclization to the *trans* diketopiperazines **101** and **102** (93% overall yield). The hydroxyl group of **101** and **102** was converted into azides **103** and **104** via a Mitsunobu reaction in good yield (86%), using HN_3·Tol in a toluene / dichloromethane solution. Finally, a one-pot Staudinger reduction - Boc protection, followed by allyl deprotection yielded the

trans scaffolds DKP-*f*2 (**107**; 3*R*,6*S*) and DKP-*f*3 (**108**; 3*S*,6*R*) in 88% yield. This synthetic route involves a high overall yield (60%) and only a few chromatographic purifications, which allows easy preparation on a multi-gram scale.

Scheme 2.2. Synthesis of DKP-*f*2 and DKP-*f*3[a,b]

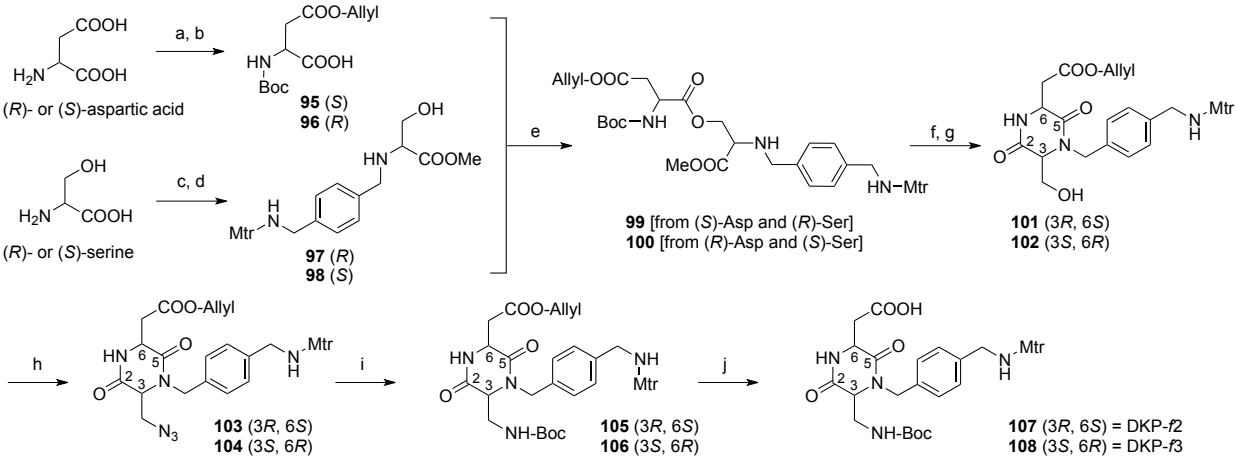

[a]Reagents and conditions: (a) allyl alcohol, AcCl; (b) Boc_2O, TEA, Dioxane, water, 95% over two steps; (c) MeOH, AcCl, quant.; (d) aldehyde **94**, $NaBH(OAc)_3$, THF, 3 h, room temp., quant.; (e) HATU, HOAT, iPr_2NEt, DMF, 3 h, 0 °C to room temp., 86%; (f) TFA/DCM 1:2, 3 h, 0 °C to room temp.; (g) iPr_2NEt, *i*PrOH, 6 h, room temp., 93% over two steps; (h) HN_3·Tol, DIAD, Ph_3P, DCM/Tol 1:2, 7 h, -20 °C, 86%; (i) Me_3P, BOC-ON, THF, 6 h, -20 °C to room temp., 88%; (j) pyrrolidine, PPh_3, $[Pd(PPh_3)_4]$, DCM, 4 h, room temp., quant.. [b]Yields reported are the average of six experiments, including different reaction batches with the two enantiomeric products.

For the synthesis of *trans* scaffolds DKP-*f*4 and DKP-*f*6 (Scheme 2.3), (*R*)- and (*S*)-aspartic acid were protected as dimethyl ester and reductively alkylated with aldehyde **94** to obtain the enantiomeric derivatives (*S*)-**109** and (*R*)-**110**. The hydroxyl group of (*R*)- or (*S*)-Boc-Ser-OMe was first transformed into the corresponding azide under Mitsunobu conditions in 78% yield and then the methyl ester was saponified. The resulting enantiomeric acids (*R*)-**111** and (*S*)-**112**, stable only for a few hours, were immediately self-condensed with DCC in DCM to give the symmetric anhydrides (*R*,*R*)-**113** and (*S*,*S*)-**114**, which were isolated by filtering off the *N*,*N*′-dicyclohexylurea (DCU) and immediately reacted with the functionalized aspartic acid dimethylester (*S*)-**109** or (*R*)-**110** to obtain the enantiomeric dipeptides (*S*,*R*)-**115** and (*R*,*S*)-**116** in moderate yield (40%). Yield optimization was pursued by extensively varying the reaction conditions (equivalents, solvents, temperature, time) but all the attempts were not successful, and markedly differed from the analogous reaction run on *N*-benzyl-aspartic acid dimethylester (*i.e.* **109** or **110** missing the Mtr-NH-CH_2- side chain) where the yield was uniformly higher (80%, see Scheme 1.24 of Chapter 1).[15b] All other coupling reagents tested (HATU, PyBrOP, DPPA, etc.) were ineffective for this reaction; although no coupling product of the

dehydroalanine derivative was ever detected, the beta-elimination possibly caused by excess *i*Pr_2NEt in the HATU, PyBrOP and DPPA tentative couplings might be an additional reason for this failure, combined with the poor reactivity of the sterically hindered secondary amine of the aspartic derivative. After Boc deprotection, the six-membered cyclization occurred spontaneously with 4 equiv of *i*Pr_2NEt in *i*PrOH, to give diketopiperazines (3*R*,6*S*)-**117** and (3*S*,6*R*)-**118** in 92% yield. *Trans* scaffolds DKP-*f*4 (**121**; 3*R*,6*S*) and DKP-*f*6 (**122**; 3*S*,6*R*) were finally obtained by catalytic hydrogenation of the azide, Boc protection of the primary amine and hydrolysis of the methyl ester (96% overall yield).

Scheme 2.3. Synthesis of DKP-*f*4 and DKP-*f*6[a,b]

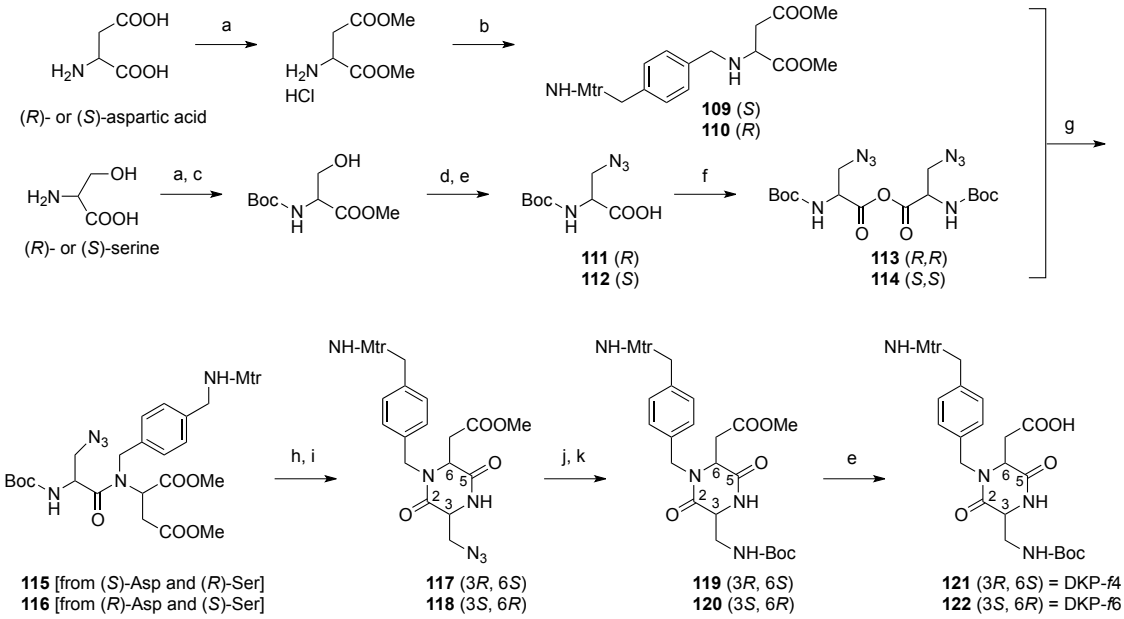

[a]Reagents and conditions: (a) MeOH, AcCl, quant.; (b) aldehyde **94**, $NaBH_3(CN)$, MeOH, 4 h, room temp., 66%; (c) Boc_2O, TEA, dioxane-water, 95%; (d) HN_3·Tol, DIAD, Ph_3P, THF, 7 h, -20 °C, 78%; (e) LiOH, H_2O/THF 1:1, 1 h, 0 °C, quant.; (f) DCC, DCM, 1 h, room temp., quant.; (g) DCM, overnight, room temp., 40%; (h) TFA, Et_3SiH, DCM, 3 h, room temp., quant.; (i) *i*Pr_2NEt, *i*PrOH, 6 h, room temp., 92%; (j) H_2, 10% Pd/C, THF, 4 h, room temp., quant.; (k) Boc_2O, *i*Pr_2NEt, DCM, 6 h, room temp., 96%. [b]Yields reported are the average of six experiments, including different reaction batches with the two enantiomeric products.

Trans diketopiperazines DKP-*f*2, DKP-*f*3, DKP-*f*4 and DKP-*f*6 were used as scaffolds for the synthesis of functionalized *cyclo*[DKP-RGD] integrin ligands **143**-**146**, following a solution-phase strategy (Scheme 2.4). Dipeptide Boc-Arg(Mtr)-Gly-OBn, prepared on a multigram scale following our reported procedure,[15b] was Boc-deprotected and coupled to the chosen diketopiperazine scaffold to give compounds **123**-**126** in good yields (83-85%). The Boc protecting group of compounds **123**-**126** was then removed and the resulting free amines **127**-**130** were coupled to Cbz-Asp(O*t*Bu)-OH to obtain the linear Cbz-Asp(OtBu)-DKP-Arg(Mtr)-Gly-OBn peptidomimetics **131-134** in high yields

(86-88%). After carboxybenzyl and benzyl groups simultaneous deprotection by catalytic hydrogenolysis to give **135-138** quantitatively, the synthesis of protected *cyclo*(DKP-RGD) **139-142** was accomplished in good yield (60-81%) by 17-membered macrolactamization in a highly diluted DMF solution (1.4 mM) utilizing HATU, HAOT, *i*-Pr_2NEt (4:4:6 equiv). The final step was the non trivial removal of the side chain protecting groups.

Scheme 2.4. Synthesis of functionalized *cyclo*[DKP-RGD] integrin ligands **143**-**146**[a]

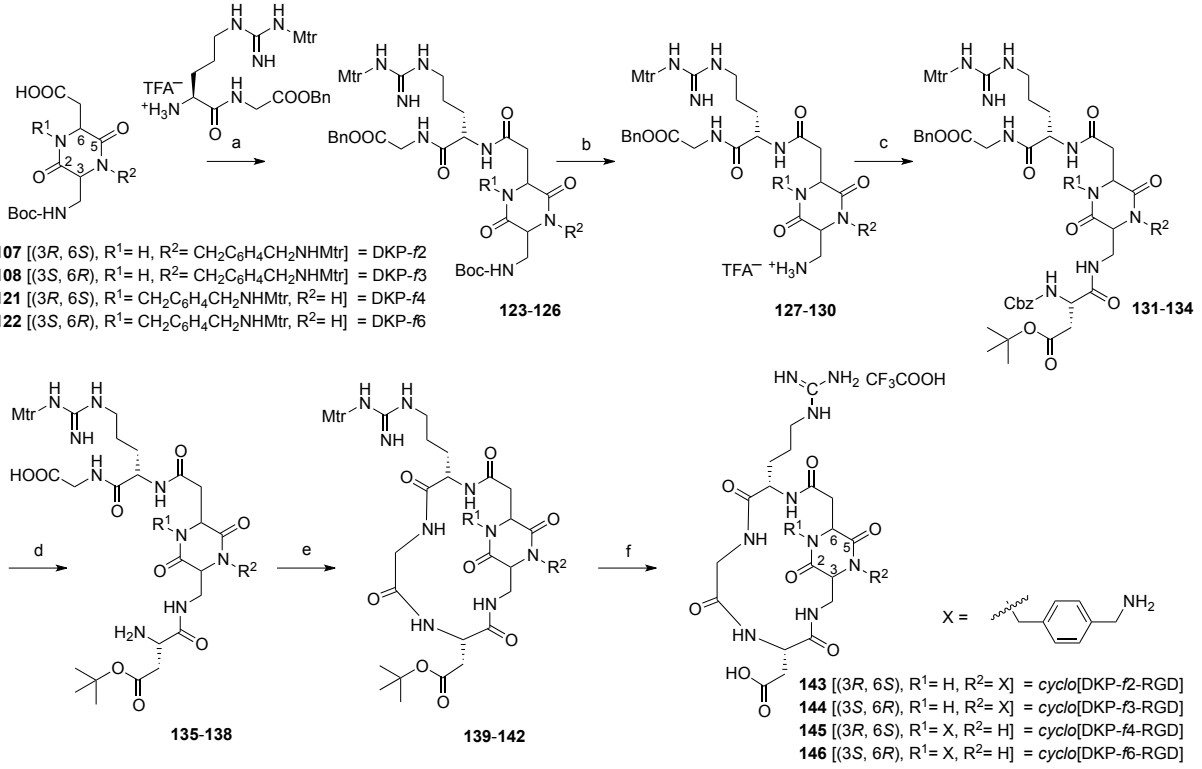

[a]Reagents and conditions: (a) HATU, HOAT, *i*Pr_2NEt, DMF, overnight, room temp., 83-85%; (b) TFA/DCM 1:2, 3 h, room temp., quant.; (c) Cbz-Asp(OtBu)-OH, HATU, HOAT, *i*Pr_2NEt, DMF, overnight, room temp., 86-88%; (d) H_2, 10% Pd/C, THF/H_2O 1:1, overnight, room temp., quant.; (e) HATU, HOAT, *i*Pr_2NEt, 1.4 mM in DMF, overnight, room temp., 60-81%; (f) TFA/TMSBr/thioanisol/EDT/phenol 70:14:10:5:1, 2 h, room temp., 70-85%.

The O*t*Bu and the Mtr on the arginine were easily deprotected while the Mtr on the benzylic amine was very stable. Several cleavage cocktails were screened and the more classic[28] ["Reagent K" (TFA/phenol/water/TIPS, 88/5/5/2), "Reagent R" (TFA/thioanisole/EDT/anisole, 90/5/3/2) and "Reagent P+" (TFA/phenol/methanesulfonic acid, 95/2.5/2.5)] failed, giving the mono-protected compound as main product (the Mtr on the amine was still present), with a low yield (5-20%) of the desired totally deprotected product, even after 48 h. Finally, with the use of

TFA/TMSBr/thioanisole/EDT/phenol (70/14/10/5/1) cleavage cocktail at room temperature for 2 h, fully deprotected compounds **143**-**146** were obtained in 70-85% isolated yield.

Thus, we were ready to conjugate Paclitaxel to our ligands: the 2'-hydroxyl function of Paclitaxel was derivatized with succinic anhydride, following a reported procedure.[29] The resulting Paclitaxel hemisuccinate ester **147**[29] was activated using diisopropylcarbodiimide (DIC) and *N*-hydroxysulfosuccinimide sodium salt (sulfo-NHS), followed by coupling with *cyclo*[DKP-RGD] ligands **143**-**146** (Scheme 2.5).

Scheme 2.5. Synthesis of *cyclo*[DKP-RGD] - PTX conjugates **90**-**93**[a]

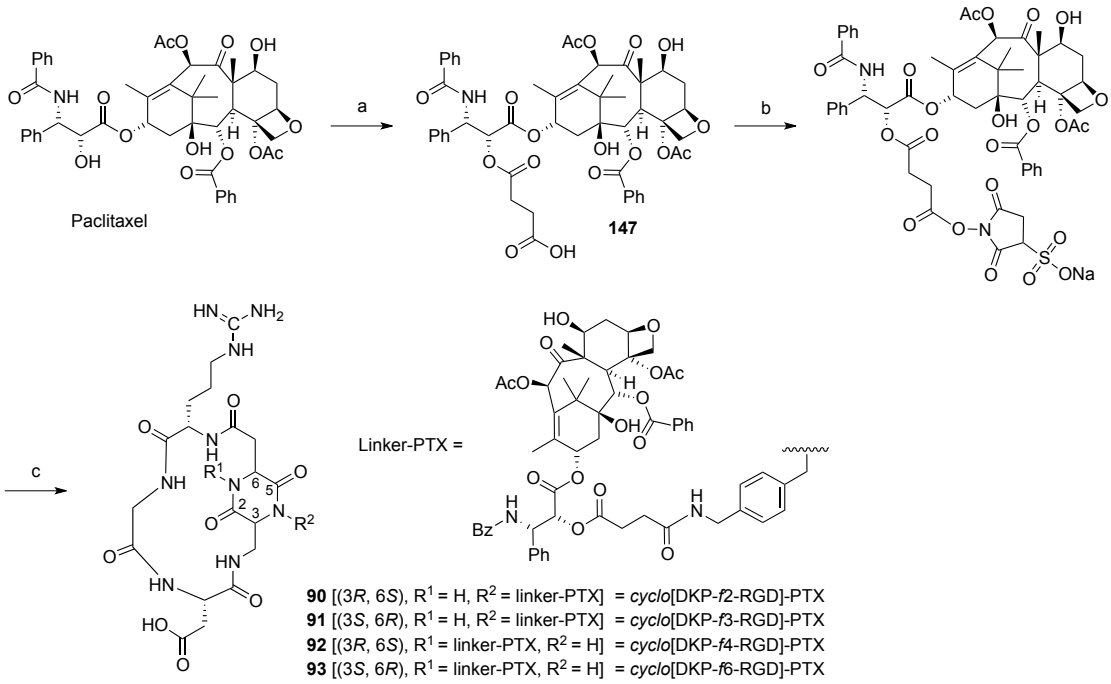

[a]Reagents and conditions: (a) succinic anhydride, py, DCM, overnight, 0 °C to room temp., 94%; (b) *N*-hydroxysulfosuccinimide sodium salt, DIC, DMF, overnight, room temp.; (c) *cyclo*(DKP-RGD) **143, 144**, **145** or **146**, CH_3CN, aq. phosphate buffer, pH = 7.3, 10 h at 0 °C then 8 h at room temp., 60-70%.

The conjugation yield was strongly pH-dependent: at pH < 7.0 the reaction did not proceed, whereas at pH > 7.5 the hydrolysis of the sulfo-NHS ester substantially competed with the primary amine reaction. The synthesis of conjugates **90-93** was finally achieved in good yield (60-70%) by adding a 0.1 M aqueous NaOH solution when required throughout the reaction, for maintaining the pH value at 7.3.

We also prepared the hemisuccinamide **148**, which is theoretically formed if the hydrolysis of the *cyclo*[DKP-*f*3-RGD] **91** takes place at the Paclitaxel-2' position. The synthesis was carried out derivatizing the amine of *cyclo*[DKP-*f*3-RGD] with the *tert*-butyl hemisuccinate (see Scheme 2.6).

The final deprotection of the *t*Bu protecting group afforded the hemisuccinamide **148** in 54% overall yield.

Scheme 2.6. Synthesis of *cyclo*[DKP-*f*3-RGD]-hemisuccinamide **148**[a]

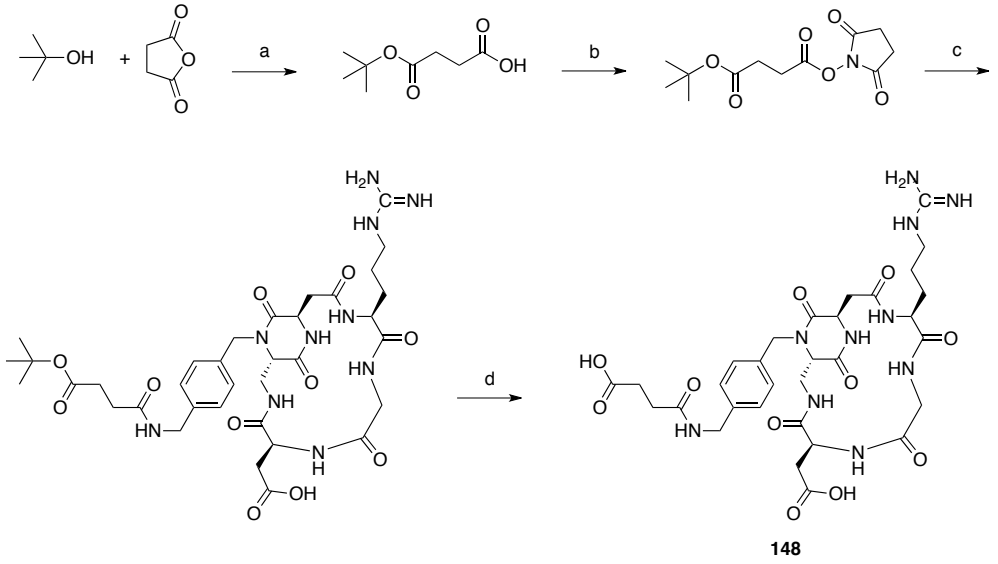

[a]Reagents and conditions: (a) *N*-hydroxysuccinimide, Et_3N, DMAP, Toluene, DCM, 48 h, reflux, 80%; (b) *N*-hydroxysuccinimide, DIC, DCM, 4 h, room temp., quant.; (c) *cyclo*(DKP-*f*3-RGD) **64**, CH_3CN, aq. phosphate buffer, pH = 7.3, 10 h at 0 °C then 8 h at room temp., 68%; (d) TFA/DCM 1:2, TES, 3 h, 0 °C to room temp., quant.

2.2 - *Biological results*

2.2.1 - *Solubility and stability in a physiological solution*

The solubility of conjugate *cyclo*[DKP-*f*3-RGD]-PTX **91** was investigated in a physiological solution (0.9% NaCl in H_2O)/Cremophor EL/ethanol (90:5:5 v/v) by quantitative HPLC. A 1.92 mM clear solution turned out to be oversaturated and slowly flocculated to reach a concentration of 1.28 mM in 2 days (Figure 2.12, left diagram). The precipitate was the conjugate **91** itself, with a purity > 99.5%. Compound **91** (1.28 μmol) dissolved in 0.1 mL of Cremophor EL/ethanol (1:1 v/v) and diluted with 0.9 mL of physiological solution, was perfectly stable for one week, with a purity > 99.5%. The 1.28 mM solution did not undergo any precipitation or decomposition (Figure 2.12, right diagram).

Figure 2.12. Solubility and stability of *cyclo*[DKP-*f*3-RGD]-PTX **91** in a physiological solution[a]

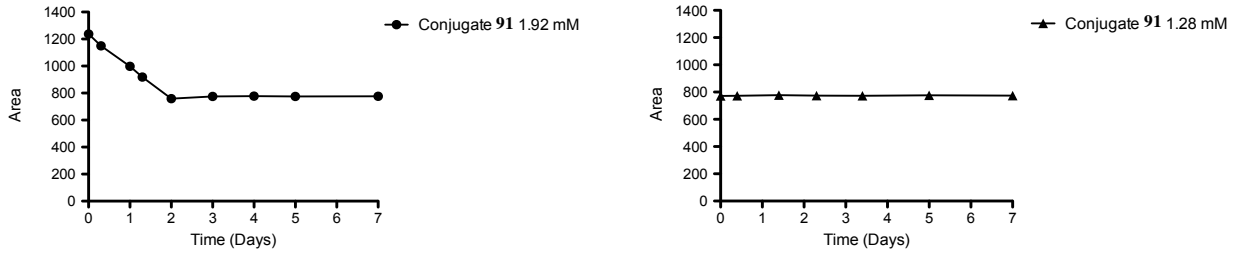

[a]Quantitative HPLC determination of solubility and stability of compound **91** in a physiological solution (0.9% NaCl in H_2O)/Cremophor EL/ethanol (90:5:5 v/v). A 1.92 mM clear solution of **91** turned out to be oversaturated and slowly flocculated to reach a concentration of 1.28 mM in 2 days (left diagram). The 1.28 mM solution did not undergo any precipitation or decomposition over seven days (right diagram).

2.2.2 - *Plasma stability assays*

Paclitaxel conjugate **91** (1.28 μmol) was dissolved in DMSO (128 μL) and then diluted with pH 7.5 phosphate buffer (PBS) to give a 200 μM stock solution. Murine plasma was spiked with the stock solution to obtain a final 10 μM concentration and incubated at 37 °C. At time points varying from 1 min to 330 min, aliquots of 50 μL were taken and quenched with 200 μL of ice-cold acetonitrile (containing Verapamil as internal standard, see Chapter 4 for details). Samples were centrifuged at 3000 rpm for 20 min and the supernatant was analyzed by RP-HPLC UV-MS/MS.

The data were fitted using a signal phase exponential decay and the calculated half-life was = 165 ± 2 min (Figure 2.12, left diagram). The same procedure was adopted for a pooled human plasma stability assay and in this case the calculated half-life was = 143 ± 3 min (Figure 2.12, right diagram). Free Paclitaxel accumulated during the assays as a result of hydrolysis of the succinyl ester bond at the PTX-2' position. These results were very encouraging and showed that *cyclo*[DKP-*f*3-RGD]-PTX **91** is sufficiently stable to undergo animal testing with murine models. In fact, similar RGD ligands showed significant (maximum) tumor uptakes *in mice* after 10,[30] 20,[31] 30,[32] and 60 min.[33]

Summarizing, we have investigated the stability of compound **91** to hydrolysis both in a physiological solution and in murine and human plasma. As a matter of fact, *cyclo*[DKP-*f*3-RGD]-PTX **91** turned out to be far more stable than PTX-E[*cyclo*(RGDfK)]$_2$ **89**[25] (see Figure 2.10, and the relevant discussion therein). The rather high stability of **91** can possibly be attributed to a more lipophilic structure, where the ester linkage is less accessible in the protic medium than in Ryppa's compound **89**.

Figure 2.13. Stability of *cyclo*[DKP-*f*3-RGD]-PTX **91** in murine and human plasma[a]

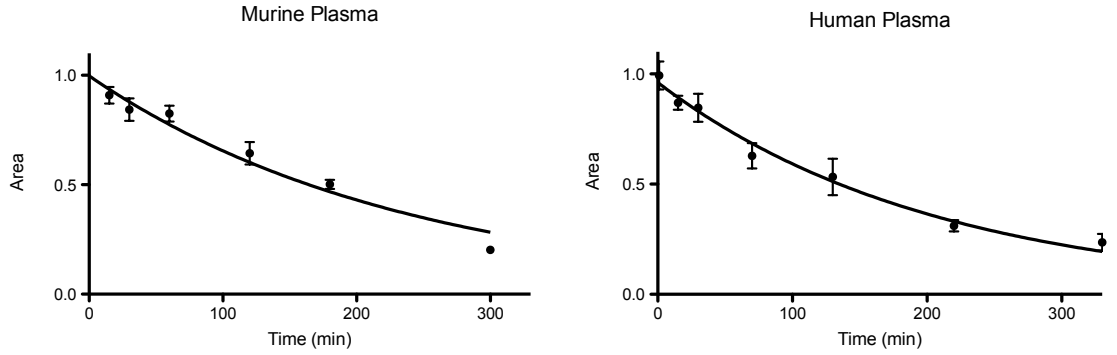

[a] Quantitative HPLC determination of stability of compound **91** (10 μM) in murine plasma (left diagram) and in human plasma (right diagram) at 37 °C.

2.2.3 - *Integrin receptors competitive binding assays*[34]

Cyclo[DKP-RGD] - PTX conjugates **90-93** were examined *in vitro* for their ability to inhibit biotinylated vitronectin binding to the purified $\alpha_v\beta_3$ and $\alpha_v\beta_5$ receptors and compared to their unfunctionalized analogs **17**, **18**, **19** and **21**, to the unconjugated ligands **144** and **148**, and to the reference compounds *cyclo*[RGDfV][35] and ST1646.[36] The results are collected in Table 2.2. Screening assays were performed incubating the immobilized integrin receptors with various concentrations (10^{-12} - 10^{-5} M) of the RGD ligands in the presence of biotinylated vitronectin (1 μg/mL), and measuring the concentration of bound vitronectin in the presence of the competitive ligands. Low nanomolar values were obtained with all the Paclitaxel-RGD constructs (**90**-**93**), comparable to the unfunctionalized ligands (**17**, **18**, **19** and **21**). These data reassured us that the enormous increase of steric hindrance in the *cyclo*[DKP-RGD] - PTX conjugates, due to presence of the linker bearing Paclitaxel through the succinate tether, did not influence the high affinity for integrin receptors $\alpha_v\beta_3$ and $\alpha_v\beta_5$. Notably, for inhibition of vitronectin binding to the $\alpha_v\beta_3$ receptor, unconjugated ligand **144** required a 5-fold higher concentration than both its unfunctionalized and conjugated analogs (compounds **18** and **91**, respectively). This reduced affinity may result from perturbation of the electrostatic clamp (*i.e.* the binding interactions of the carboxylate and guanidinium groups with the charged regions of the receptor),[13] induced by the free amine present in **144**.

Table 2.2. Inhibition of biotinylated vitronectin binding to $\alpha_v\beta_3$ and $\alpha_v\beta_5$ receptors

Compound	Structure	$\alpha_v\beta_3$ IC_{50} [nM][a]	$\alpha_v\beta_5$ IC_{50} [nM][a]
90	*cyclo*[DKP-*f*2-RGD]-PTX[b]	8.5 ± 0.8	518 ± 10
91	*cyclo*[DKP-*f*3-RGD]-PTX[b]	5.2 ± 2.3	219 ± 124
92	*cyclo*[DKP-*f*4-RGD]-PTX[b]	0.9 ± 0.6	76 ± 32
93	*cyclo*[DKP-*f*6-RGD]-PTX[b]	1.1 ± 0.1	22 ± 3
144	*cyclo*[DKP-*f*3-RGD][c]	26.4 ± 3.7	$> 5 \cdot 10^3$
148	*cyclo*[DKP-*f*3-RGD]-hemisuccinamide[d]	4.1 ± 0.6	75 ± 1
17	*cyclo*[DKP-2-RGD][e]	3.2 ± 2.7	114 ± 99
18	*cyclo*[DKP-3-RGD][e]	4.5 ± 1.1	149 ± 25
19	*cyclo*[DKP-4-RGD][e]	7.6 ± 4.3	216 ± 5
21	*cyclo*[DKP-6-RGD][e]	2.1 ± 0.6	79 ± 3
cyclo[RGDfV][f]	*cyclo*[RGDfV]	3.2 ± 1.3	7.5 ± 4.8
ST1646[f]	ST1646[g]	1.0 ± 0.5	1.4 ± 0.8

[a]IC_{50} values were calculated as the concentration of compound required for 50% inhibition of biotinylated vitronectin binding as estimated by GraphPad Prism software; all values are the arithmetic mean ± SD of triplicate determinations. [b]See Figure 2.11. [c]See Scheme 2.4. [d]see Scheme 2.6. [e]See Figure 2.3. [f]Reference compound. [g]See Figure 2.2.

Derivatization of the amine with succinic anhydride gave the hemisuccinamide **148** and restored the high binding affinity for the $\alpha_v\beta_3$ receptor. Interestingly, unlike reference compounds *cyclo*(RGDfV) and ST1646, the *cyclo*[DKP-RGD] peptidomimetics were ca. 20-200 fold more selective for the $\alpha_v\beta_3$ integrin with respect to the $\alpha_v\beta_5$ in this kind of assay.

2.2.4 - *Sensitivity of tumor cell lines treated with cyclo[DKP-RGD] - PTX conjugates **90-93***[37]

Cyclo[DKP-RGD] - PTX conjugates **90-93** were tested *in vitro* for their cytotoxic activity in comparison with Paclitaxel, against a panel of human tumor cell lines. The cell sensitivity assays (Table 2.3) clearly indicated that the functionalized *cyclo*[DKP-*f*3-RGD] integrin ligand **144** was not cytotoxic, while the *cyclo*[DKP-RGD]-PTX conjugates displayed a cytotoxic activity similar to that of Paclitaxel (same order of magnitude). These data imply that free Paclitaxel is released at some stage, possibly after the conjugates have been internalized into the cells, because it is well known that the free 2'-OH group is necessary for Paclitaxel to exert its cytotoxic and microtubule-stabilizing activities.[38] Compounds **90-93**, **144** and Paclitaxel were also tested *in vitro* on normal HDFC fibroblasts. When cells started to proliferate and were exposed to different concentrations of these

compounds (range of concentrations tested = 64-1000 nM), a marginal inhibition of cell growth was observed. The effect was not concentration-dependent, suggesting that the compounds were not cytotoxic but were at best cytostatic in these cells. The data reported in Table 2.3 did not identify undoubtedly a lead compound for evaluation of antitumor activity with *in vivo* models. Therefore, we chose *cyclo*[DKP-*f*3-RGD]-PTX **91** as our lead conjugate mainly because of its straightforward synthetic accessibility on a multi-gram scale.

Flow cytometry was used to detect the expression of $\alpha_V\beta_3$ and $\alpha_V\beta_5$ integrins on the surface of the different cancer cell lines (Table 2.4). Among these, the cisplatin-resistant IGROV-1/Pt1 cells expressed very high levels of integrin $\alpha_V\beta_3$, making them attractive to be tested in murine models with *cyclo*[DKP-RGD]-PTX construct **91** (*vide infra* the *in vivo* experiments).

Table 2.3. Cell sensitivity of different tumor cell lines to compounds **90-93** and **144**[a]

Compd	Structure	IC_{50} (nM)					
		IGROV-1	IGROV-1 /Pt1	U2-OS	SKOV3	PANC-1	MIA-PaCa2
90	*Cyclo*[DKP-*f*2-RGD]-PTX	17.7 ± 6.0	18.7 ± 6.0	2.2 ± 0.5	1.6 ± 1.0	5.8 ± 4.0	2.0 ± 0.7
91	*Cyclo*[DKP-*f*3-RGD]-PTX	61.3 ± 19.1	4.9 ± 2.0	12.8 ± 0.1	1.2 ± 0.1	2.4 ± 0.8	2.3 ± 0.4
92	*Cyclo*[DKP-*f*4-RGD]-PTX	34.4 ± 29.0	3.7 ± 2.0	6.8 ± 4.6	2.4 ± 0.9	3.2 ± 0.7	1.8 ± 0.6
93	*Cyclo*[DKP-*f*6-RGD]-PTX	48.2 ± 2.2	2.4 ± 1.9	5.7 ± 4.4	2.4 ± 1.1	3.5 ± 0.1	2.5 ± 0.6
144	*Cyclo*[DKP-*f*3-RGD]	> 1200	> 18000	> 6300	> 11600	> 11600	> 11600
PTX	Paclitaxel	23.0 ± 0.8	2.2 ± 0.8	3.4 ± 0.4	2.7 ± 1.1	5.2 ± 1.9	7.2 ± 3.8

[a]Cell sensitivity was evaluated by growth inhibition assays based on cell counting. Cells were seeded and 24 h later they were exposed to the compounds for 72 h. At the end of treatment, cells were counted using a cell counter.

Table 2.4. Integrin expression of tumor cell lines of different tumor types[a]

Integrin	Mean fluorescence intensity					
	IGROV-1	IGROV-1 /Pt1	U2-OS	SKOV3	PANC-1	MIA-PaCa2
$\alpha_V\beta_3$	4.8 ± 1.9	23.3 ± 5.0	1.8 ± 0.6	6.4 ± 0.05	7.9 ± 2.8	1.2 ± 0.1
$\alpha_V\beta_5$	3.4 ± 0.9	3.3 ± 0.5	27.4 ± 0.1	4.4 ± 0.5	25.7 ± 6.5	5.6 ± 0.9

[a]Integrin expression levels were examined by immunofluorescence using a flow cytometer. The ratios between the mean fluorescence intensity of cells incubated with primary antibody and isotypic control are shown.

Comparing the data presented in Tables 2.3 and 2.4, it is quite clear that there is no correlation between the phenotypic integrin expression levels and efficacy of *cyclo*[DKP-RGD]-PTX conjugates, in *in vitro* assays. The cell sensitivity studies were carried out to determine whether Paclitaxel was released from the conjugate; in these *in vitro* assays, no tumor homing effect can be expected and therefore the different response can be attributed only to a higher or lower sensitivity of the different cell lines to the particular compound tested, independently of the integrin receptor expression. On the other hand, the evaluation of integrin expression was important for the choice of the best *in vivo* model for efficacy studies (i.e., the choice of cisplatin-resistant IGROV-1/Pt1, a cell line where the expression of integrin $\alpha_v\beta_3$ is particularly relevant).

2.2.5 - *Adhesion studies*[37]

Adhesion assay experiments performed on a panel of human cancer cell lines show that 50% inhibition of cell adhesion to vitronectin-coated plates can be obtained using *cyclo*[DKP-3-RGD] **18** at 2-15 μM concentration (cell adhesion IC_{50}, unpublished results from our group). Following the referee's recommendation, the capability of IGROV-1/Pt1 cells to adhere to vitronectin-coated plates was evaluated. When cells were pretreated with *cyclo*[DKP-*f*3-RGD] **144** at a suboptimal 0.064 μM concentration, only 13% inhibition was observed (Figure 2.14). When cells were pretreated with *cyclo*[DKP-*f*3-RGD]-PTX **91** at 0.064 μM concentration (corresponding to the compound **91** cell sensitivity IC_{80}), a more pronounced inhibition (36%) was observed.

Figure 2.14. IGROV-1/Pt1 cell adhesion assays to vitronectin-coated plates[a]

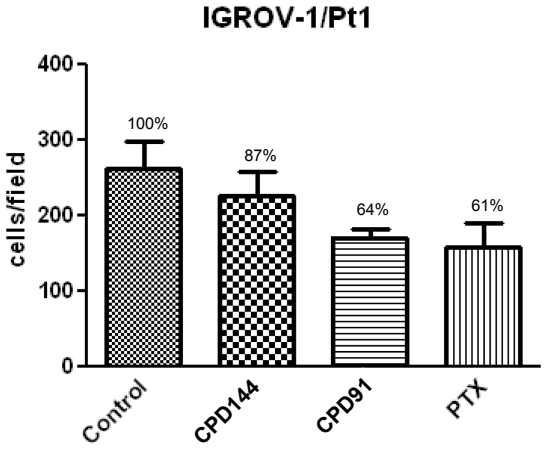

[a]Cells were pretreated with compound **144** (CPD144, 0.064 μM), compound **91** (CPD11, 0.064 μM), or Paclitaxel (PTX, 0.10 μM) for 24 h.

However, when cells were pretreated with an equitoxic concentration of Paclitaxel (PTX, Paclitaxel cell sensitivity IC_{80} = 0.10 μM), a similar inhibition (39%) was observed, which is probably due to its direct toxicity to the cells. It has been demonstrated that the inability of the cytoskeleton to rearrange by depolymerization, caused by Paclitaxel, results in a 35-40% reduction in cell adhesion.[39] Under the experimental conditions used, the assay is inconclusive and does not allow to distinguish between RGD-promoted and toxicity-promoted adhesion inhibition.

2.2.6 - *Evaluation of in vivo antitumor activity*[40]

Antitumor activity of our lead conjugate *cyclo*[DKP-*f*3-RGD]-PTX **91,** delivered i.v. and administered every 4 days for 4 times (q4dx4), was examined on the $\alpha_V\beta_3$-rich IGROV-1/Pt1 carcinoma grown in athymic mice as subcutaneous (s.c.) tumor. A significant, dose-related antitumor effect was observed following administration of two dose levels of compound **91** (15 mg/kg and 30 mg/kg). Moreover, when compound **91** (30 mg/kg, *i.e.* 19.1 μmol/kg) was compared to Paclitaxel (30 mg/kg, *i.e.* 35.1 μmol/kg) administered with the same weight dosage and schedule, it displayed better effects in terms of tumor volume inhibition (TVI, 85 vs 76%), despite the lower (ca. half) molar dosage used (Figure 2.15).

Figure 2.15. *In vivo* antitumor activity studies of *cyclo*[DKP-*f*3-RGD]-PTX **91** compared to Paclitaxel on IGROV-1/Pt1 ovarian carcinoma[a]

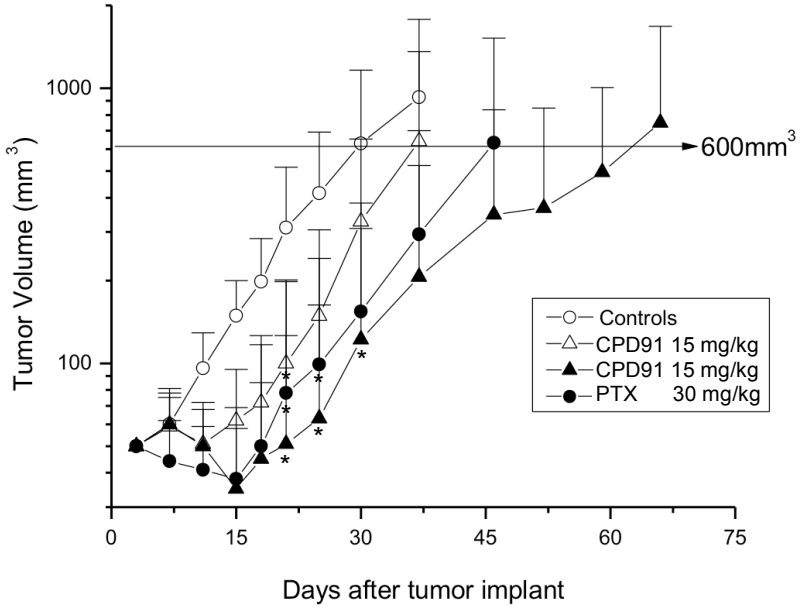

[a]Efficacy of compound **91** (CPD11) and Paclitaxel (PTX) administered intravenously every fourth day for four times on the ovarian carcinoma IGROV-1/Pt1 xenografted subcutaneously in athymic nude mice. The solvent was injected for the control group (○). Each point represents the mean tumor volume from 8 tumors. Bars represent S.D. *, $P < 0.05$ by Student's t test on tumor volumes over control mice.

Furthermore, 2 out of 8 tumors in animals receiving conjugate **91** disappeared without any evidence of disease until the end of the experiment. Thus, an improved and more persistent effect against the growth of treated tumors was achieved, as indicated also by the higher Log_{10} Cell Kill value (LCK, 1.4 vs 0.7, Table 2.5). Treatment was well tolerated, as no deaths or significant weight losses were observed among the treated animals.[41]

Table 2.5. *In vivo* antitumor activity and toxicity profile of *cyclo*[DKP-*f*3-RGD]-PTX **91** and Paclitaxel against human ovarian cancer xenografts (IGROV-1/Pt1) in mice, as a function of dose.

Treatment	Dose (mg/kg)	Dose (μmol/kg)	TVI%[a]	CR[b]	NED[c]	LCK[d]	BWL%[e]	D/T[f]
Paclitaxel	30	35.1	76	3/8	0/8	0.7	4	0/4
Cyclo [DKP-*f*3-RGD]-PTX **91**	15	9.6	64	0/8	-	0.3	0	0/4
Cyclo [DKP-*f*3-RGD]-PTX **91**	30	19.1	85	2/8	2/8	1.4	3	0/4

[a]TVI%: Tumor Volume Inhibition percent in treated over control mice, calculated 10 d after the end of treatments.
[b]CR: Complete Response: disappearance of tumors lasting at least 10 days.
[c]NED: No Evidence of Disease at the end of experiment (at day 66).
[d]LCK: Gross Log_{10} Cell Kill to reach 600 mm^3 of tumor volume (see Figure 2.15).
[e]BWL%: Body Weight Loss percentage induced by drug treatment.
[f]D/T: Dead/Treated mice.

2.2.7 - *Immunohistochemistry of treatment effects*[42]

To investigate the mechanism underlying the improved antitumor activity of *cyclo*[DKP-*f*3-RGD]-PTX **11** over paclitaxel, histopathological and Western blot analyses were carried out in tumors from untreated mice and from mice treated with *cyclo*[DKP-*f*3-RGD]-PTX **91**, compound **144**, and Paclitaxel (Figure 2.16). The comparison between Paclitaxel and *cyclo*[DKP-*f*3-RGD]-PTX **91** was carried out administering 30 mg/kg for both compounds, amounts which correspond to 35.1 μmol/kg for Paclitaxel and to 19.1 μmol/kg for *cyclo*[DKP-*f*3-RGD]-PTX **91**. Histological analysis indicated the presence of a high number of mitotic cells in the group treated with *cyclo*[DKP-*f*3-RGD]-PTX **91**, compared to the other groups (Figure 2.16). In addition, the majority of the mitoses observed in the groups treated with either *cyclo*[DKP-*f*3-RGD]-PTX **91** or Paclitaxel were aberrant, an observation consistent with the mechanism of action of spindle poisons.[43] High levels of aberrant mitoses were observed with *cyclo*[DKP-*f*3-RGD]-PTX **91**, already 24 h after the second treatment and persisted after the fourth treatment. On the contrary, the amount of aberrant mitotic cells observed after mice treatment with Paclitaxel decreased over time.

Figure 2.16. Histopathological analysis of IGROV-1/Pt1 xenograft, after treatment with *cyclo*[DKP-*f*3-RGD]-PTX **91**[a]

A

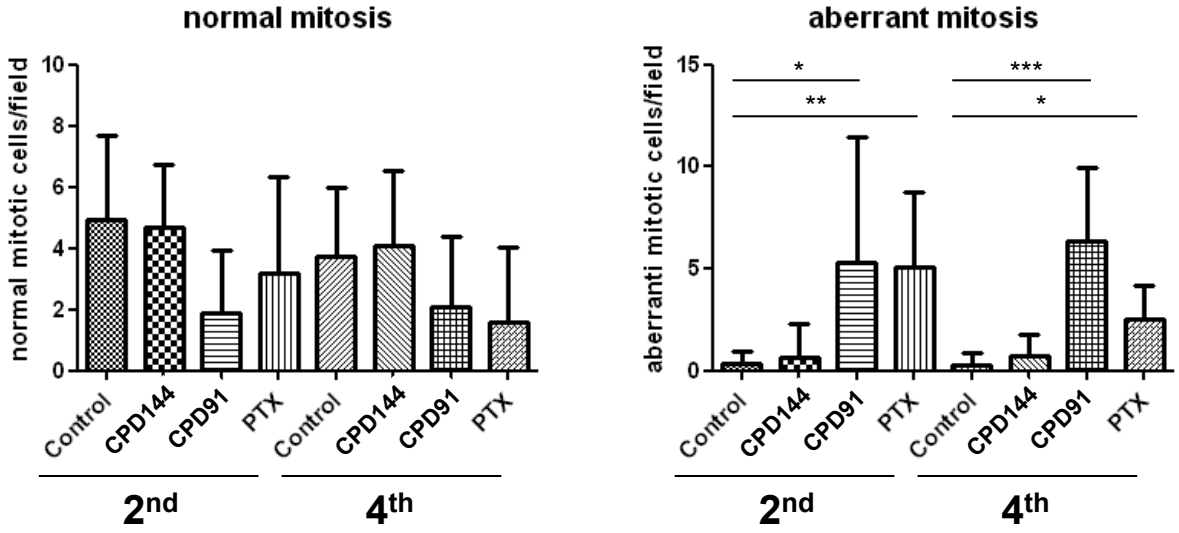

B

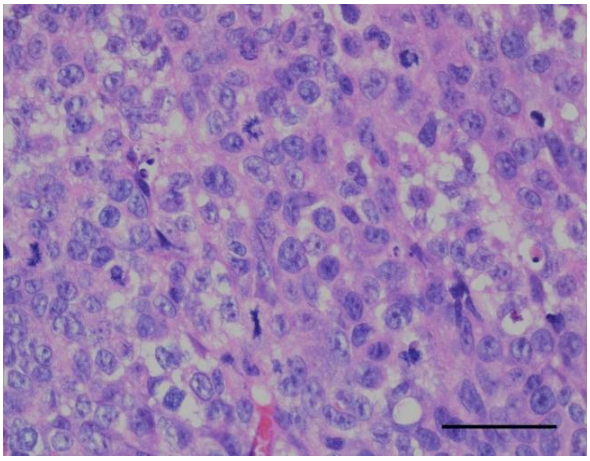

C

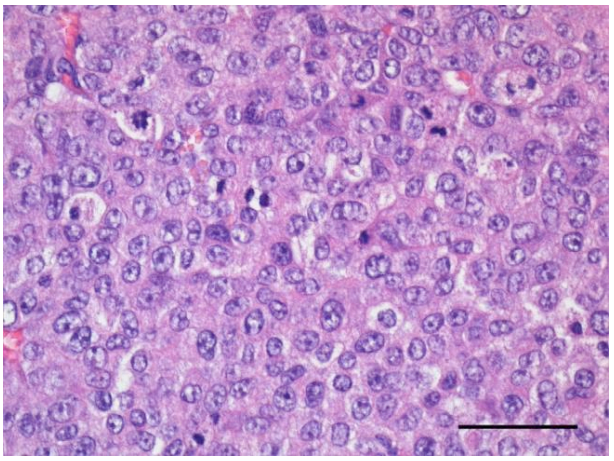

D

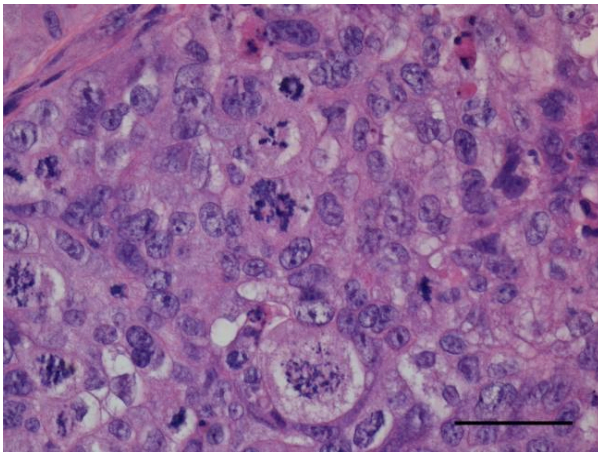

E

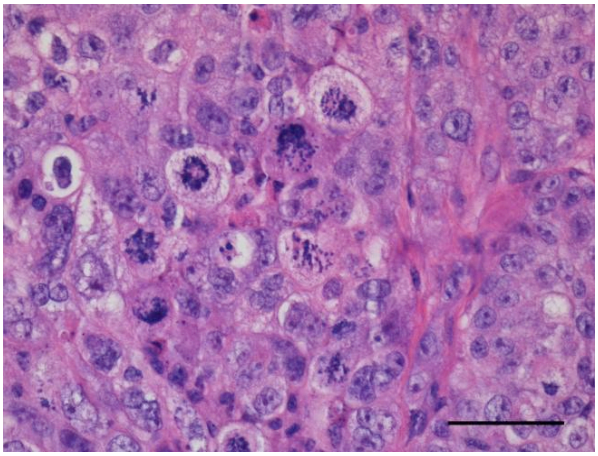

[a]A. Quantitative analysis of mitoses. Mitoses were evaluated in 3 randomly selected 400x fields using quadruplicate samples. The reported numbers correspond to the mean number of normal/aberrant mitoses in analyzed groups: control groups (control); groups treated with compound **144** (CPD144); group treated with compound **91** (CPD91); groups treated with Paclitaxel (PTX). Note that tumors were obtained from mice sacrificed 24 h after the second or the fourth treatment. B. Randomly selected high power field (hpf) within the bulk of the tumor from a control group sample, characterized by normal mitoses (hematoxyilin and eosin; Bar, 50 μm). C. Randomly selected hpf within the bulk of the tumor from a sample treated with compound 64. Hyperchromatic nuclei with condensed chromatin are evident (hematoxylin and eosin; Bar, 50μm). D. Randomly selected hpf within the bulk of the tumor from a sample treated with compound 11. Note markedly aberrant mitoses, with formation of nuclear envelops around individual clusters of missegregated chromosomes (mitotic catastrophe) (hematoxylin and eosin; Bar, 50μm). E. Randomly selected hpf within the bulk of the tumor from a sample treated with Paclitaxel. Note markedly aberrant mitoses, with formation of nuclear envelops around individual clusters of missegregated chromosomes (mitotic catastrophe) (hematoxylin and eosin; Bar, 50μm).

Since tumors from mice treated with *cyclo*[DKP-*f*3-RGD]-PTX **91** had the highest number of mitoses and the major part of them were atypical, it is likely that tumor cells treated with compound **91** entered mitosis, but failed to replicate and incurred in mitotic arrest.

References:

[1] H. J. Broxterman, J. Lankelma, K. Hoekman. *Drug Resist. Updates*. **2003**, *6*, 111-127.

[2] J. Siepmann, R. A. Siegel, M. J. Rathbone. Fundamentals and applications of controlled release drug delivery. Springer: New York, **2012**; pp 493-516.

[3] (a) T. Lammers, F. Kiessling, W. E. Hennink G. Storm. *J. Controlled Release* **2012**, *161*, 175-187. (b) F. Kratz, I. A. Müller, C. Ryppa, A. Warnecke. *ChemMedChem*. **2008**, *3*, 20–53.

[4] (a) P. S. Low. *Mol. Pharmacol*. **2007**, *4*, 629-630. (b) O. H. Aina, R. W. Liu; J. L. Sutcliffe, J. Marik, C. X. Pan, K. S. Lam. *Mol. Pharmacol*. **2007**, *4*, 631-651.

[5] (a) E. Ruoslahti, S. N. Bhatia, M. J. Sailor. *J. Cell Biol*. **2010**, *188*, 759–768. (b) R. Mahato, W. Tai, K. Cheng. *Adv. Drug Delivery. Rev*. **2011**, *63*, 659-670.

[6] X. Lu, D. Lu, M. Scully, V. Kakkar. *Perspect. Med. Chem*. **2008**, *2*, 57-73.

[7] R. O. Hynes. *Cell* **2002**, *110*, 673-687.

[8] (a) M. Shimaoka, T. A. Springer. *Nature Rev. Drug Discov*. **2003**, *2*, 703-716. (b) R. Rathinam, S. K. Alahari. *Cancer Metastasis Rev*. **2010**, *29*, 223–237.

[9] E. F. Plow, T. A. Haas, L. Zhang, J. Loftus, J. W. Smith. *J. Biol. Chem*. **2000**, *275*, 21785-21788.

[10] M. A. Dechantsreiter, E. Planker, B. Mathä, E. Lohof, G. Hölzemann, A. Jonczyk, S. L. Goodman, H. Kessler. *J. Med. Chem*. **1999**, *42*, 3033-3040.

[11] E. K. Gottschalk, H. Kessler. *Angew. Chem. Int. Ed*. **2002**, *41*, 3967-3774.

[12] C. Mas-Moruno, F. Rechenmacher, H. Kessler. *Anti-Cancer Agents Med. Chem*. **2010**, *10*, 753-768.

[13] J.-P. Xiong, T. Stehle, R. Zhang, A. Joachimiak, M. Frech, S. L. Goodman, M.A. Arnaout. *Science* **2002**, *296*, 151-155.

[14] L. Auzzas, F. Zanardi, L. Battistini, P. Burreddu, P. Carta, G. Rassu, C. Curti, G. Casiraghi. *Curr. Med. Chem*. **2010**, *17*, 1255-1299.

[15] (a) A. S. M. Ressurreicao, A. Vidu, M. Civera, L. Belvisi, D. Potenza, L. Manzoni, S. Ongeri, C. Gennari, U. Piarulli. *Chem.-Eur. J*. **2009**, *15*, 12184–12188. (b) M. Marchini, M. Mingozzi, R. Colombo, I. Guzzetti, L. Belvisi, F. Vasile, D. Potenza, U. Piarulli, D. Arosio, C. Gennari. *Chem.-Eur. J*. **2012**, *18*, 6195-6207.

[16] (a) A. R. Reynolds, I. R. Hart, A. R. Watson, J. C. Welti, R. G. Silva, S. D. Robinson, G. Da Violante, M. Gourlaouen, M. Salih, M. C. Jones, D. T. Jones, G. Saunders, V. Kostourou, F. Perron-Sierra, J. C. Norman, J. C. Tucker, K. M. Hodivala-Dilke. *Nat. Med*. **2009**, 15, 392-400. (b) S. M. Weis, D. G. Stupack, D. A. Cheresh. *Cancer Cell* **2009**, *15*, 359-361. (c) S. H. Shabbir, J. L. Eisenberg, M. Mrksich. *Angew. Chem. Int. Ed*. **2010**, *49*, 7706-7709. (d) S. D. Robinson, K. M. Hodivala-Dilke. *Curr. Opin. Cell Biol*. **2011**, *23*, 630-637.

[17] D. Cox, M. Brennan, N. Moran. *Nat. Rev. Drug Discov*. 2010, 9, 804–820

[18] K. Chen, X. Chen. *Theranostics* **2011**, *1*, 189-200.

[19] (a) W. Arap, R. Pasqualini, E. Ruoslahti. *Science* **1998**, *279*, 377–80. (b) J. W. Kim, H. S. Lee. *Int. J. Mol. Med*. **2004**,*14*, 529-535.

[20] C. Ryppa, H. Mann-Steinberg, I. Fichtner, H. Weber, R. Satchi-Fainaro, M. L. Biniossek, F. Kratz. *Bioconjugate Chem*. **2008**, *19*, 1414-22.

[21] D. J. Burkhart, B. T. Kalet, M. P. Coleman, G. C. Post, T. H. Koch. *Mol. Cancer Ther*. **2004**, *3*, 1593-604.

[22] S. Mukhopadhyay, C. M. Barnés, A. Haskel, S. M. Short, K. R. Barnes, S. J. Lippard. *Bioconjugate Chem*. **2008**, *19*, 39-49.

[23] (a) A. Dal Pozzo, M. H. Ni, E. Esposito, S. Dallavalle, L. Musso, A. Bargiotti, C. Pisano, L. Vesci, F. Bucci, M. Castorina, R. Fodera, G. Giannini, C. Aulicino, S. Penco. *Bioorg. Med. Chem. Lett.* **2010**, *18*, 64-72. (b) D. Alloatti, G. Giannini, G.; Vesci, L.; Castorina, M.; Pisano, C.; Badaloni, E.; Cabri, W. *Bioorg. Med. Chem. Lett.* **2012**, *22*, 6509**–**6512.

[24] (a) X. Chen, C. Plasencia, Y. Hou, N. Neamati. *J. Med. Chem.* **2005**, *48*, 1098-106 (corrigendum *J. Med. Chem*, **2005**, *48*, 5874). (b) Q. Cao, Z.-B. Li, K. Chen, Z. Wu, L. He, N. Neamati, X. Chen. *Eur. J. Nucl. Med. Mol. Imaging*. **2008**, *35*, 1489-98.

[25] C. Ryppa, H. Mann-Steinberg, M. L. Biniossek, R. Satchi-Fainaro, F. Kratz. *Int. J. Pharm*. **2009**, *368*, 89-97.

[26] (a) Nuovi Composti Antitumorali, C. Gennari, L. Belvisi, D. Potenza, R. Colombo, M. Mingozzi, M. Marchini, L. Manzoni, D. Arosio, P. Perego, N. Zaffaroni, M. De Cesare, U, Piarulli. *Italian Patent* - Application 31 January **2012**, N. MI2012A000121; (b) R. Colombo, M. Mingozzi, L. Belvisi, D. Arosio, U. Piarulli, N. Carenini, P. Perego, N. Zaffaroni, M. De Cesare, V. Castiglioni, E. Scanziani C. Gennari. *J. Med. Chem*. **2012**, *55*, 10460-10474.

[27] M. Marchini, M. Mingozzi, R. Colombo, C. Gennari, M. Durini, U. Piarulli. *Tetrahedron* **2010**, *66*, 9528-9531.

[28] H. Choi, J. V. Aldrich. *Int. J. Pept. Protein Res*. **1993**, *42*, 58-63.

[29] H. M. Deutsch, J. A. Glinski, M. Hernandez, R. D. Haugwitz, V. L. Narayanan, M. Suffness, L. H. Zalkow. *J. Med. Chem*. **1989**, *32*, 788-792.

[30] (a) F. Buchegger, M. Kosinski, D. Viertl, C. Poitry-Yamate, S. Baechler, J. Prior. *J. Nucl. Med. Meeting Abstracts* **2011**, *52*, 1487. (b) Y. Ye, L. Zhu, Y. Ma, G. Niu, X. Chen. *Bioorg. Med. Chem. Lett*. **2011**, *21*, 1146–1150.

[31] S. Liu, Z. Liu, K. Chen, Y. Yan, P. Watzlowik, H. J. Wester, F. T. Chin, X. Chen. *Mol. Imaging Biol*. **2010**, *12*, 530-538.

[32] (a) M. Fani, D. Psimadas, C. Zikos, S. Xanthopoulos, G. K. Loudos, P. Bouziotis, A. D. Varvarigou. *Anticancer Res*. **2006**, *26*, 431-434. (b) L. Lang, W. Li, N. Guo, Y. Ma, D. O. Kiesewetter, G. Niu, X. Chen. *Bioconjugate Chem*. **2011**, *22*, 2415–2422. (c) W. Li, L. Lang, G. Niu, N. Guo, Y. Ma, D. O. Kiesewetter, B. Shen, X. Chen. *Amino Acids* **2012**, *43*, 1349-1357.

[33] (a) M. L. Janssen, W. J. Oyen, I. Dijkgraaf, L. F. Massuger, C. Frielink, D. S. Edwards, M. Rajopadhye, H. Boonstra, F. H. Corstens, O. C. Boerman. *Cancer Res*. **2002**, *62*, 6146-6151. (b) S. Lanzardo, L. Conti, C. Brioschi, M. P. Bartolomeo, D. Arosio, L. Belvisi, L. Manzoni, A. Maiocchi, F. Maisano, G. Forni. *Contrast Media Mol. Imaging* **2011**, *6*, 449–458.

[34] The studies reported in this section were carried out by D. Arosio from the CNR-ISTM, whom I sincerely acknowledge for the kind collaboration.

[35] R. Haubner, W. Schmitt, G. Hö1lzemann, S. L. Goodman, A. Jonczyk, H. Kessler. *J. Am. Chem. Soc*. **1996**, *118*, 7881-7891.

[36] L. Manzoni, L. Belvisi, D. Arosio, M. Civera, M. Pilkington-Miksa, D. Potenza, A. Caprini, E. M. V. Araldi, E. Monferrini, M. Mancino, F. Podestà, C. Scolastico. *ChemMedChem* **2009**, *4*, 615-632, and references cited therein.

[37] The studies reported in this section were carried out by P. Perego, N. Carenini, and N. Zaffaroni from Fondazione IRCCS Istituto Nazionale Tumori, whom I sincerely acknowledge for the kind collaboration.

[38] Y. Fu, S. Li, Y. Zu, G. Yang, Z. Yang, M. Luo, S. Jiang, M. Wink, T. Efferth. *Curr. Med. Chem*. **2009**, *16*, 3966-3985.

[39] (a) A. Eldar-Boock, K. Miller, J. Sanchis, R. Lupu, M. J. Vicent, R. Satchi-Fainaro. *Biomaterials* **2011**, *32*, 3862-3874. (b) D. Shearer. The effects of membrane and cytoskeletal mechanics on cell adhesiveness. Ph.D. Dissertation, Massachusetts Institute of Technology, Cambridge, MA, **2004**, http://dspace.mit.edu/handle/1721.1/32785.

[40] The studies reported in this section were carried out by M. De Cesare from Fondazione IRCCS Istituto Nazionale Tumori, whom I sincerely acknowledge for the kind collaboration.

[41] Recently, a azabicycloalkane-RGD bound to Paclitaxel via a cleavable diglycolyl ester linker at C2' was reported to provide promising *in vitro* and *in vivo* antitumor activity, see: M. Pilkington-Miksa, D. Arosio, L. Battistini, L. Belvisi, M. De Matteo, F. Vasile, P. Burreddu, P. Carta, G. Rassu, P. Perego, N. Carenini, F. Zunino, M. De Cesare, V. Castiglioni, E. Scanziani, C. Scolastico, C. Casiraghi, F. Zanardi, L. Manzoni. *Bioconjugate Chem*. **2012**, *23*, 1610-1622.

[42] The studies reported in this section were carried out by P. Perego, N. Carenini, and N. Zaffaroni from Fondazione IRCCS Istituto Nazionale Tumori and by V. Castiglioni and E. Scanziani from Dipartimento di Scienze Veterinarie e Sanita Pubblica, Universita degli Studi di Milano, whom I sincerely acknowledge for the kind collaboration.

[43] (a) D. R. Matson, P. T. Stukenberg. *Molecular interventions* **2011**, *11*, 141-150. (b) J. Portugal, S. Mandilla, M. Bataller. *Current Pharmaceutical Design* **2010**, *16*, 69-78; (c) I. B. Roninson, E. V. Broude, B. D. Chang. *Drug Resistance Updates* **2001**, *4*, 303-313.

CHAPTER 3

CONLCUSIONS

Integrins are transmembrane heterodimeric cell adhesion receptors, consisting of an α- and a β-subunit, involved in many fundamental processes, such as cell growth, cell division, cell survival, cellular differentiation, apoptosis. As a consequence, integrin malfunctions are connected to a large variety of diseases (*e.g.* thrombosis, cancer, osteoporosis, inflammation), and integrins themselves represent attractive targets for pharmacological research. Of the 24 different heterodimers known, the RGD-binding integrins $\alpha_V\beta_3$, $\alpha_V\beta_5$, $\alpha_5\beta_1$ are key-factors of angiogenesis, *i.e.* the formation and maturation of new blood vessels. A small localized tumor releases angiogenic growth factors, promoting the generation of abnormal blood vessels which can feed the tumor. Hence, angiogenesis plays a pivotal role in tumor growth and metastatic spreading.

Particular integrins are able to selectively bind different spatial presentations of a single binding motif (RGD) in multiple ECM proteins. Therefore, synthetic RGD-ligands can bind and inhibit endogenous-ligand-binding to integrins with an RGD-recognition specificity ($\alpha_V\beta_3$, $\alpha_V\beta_5$, $\alpha_5\beta_1$), thus significantly inhibiting angiogenesis, tumor growth and metastasis.

An efficient synthesis in solution of constrained peptides (**16-23**) containing the **Arg-Gly-Asp** (RGD) motif and diketopiperazine scaffolds **DKP1-DKP8** was developed and optimized.

All the bifunctional 2,5-diketopiperazine scaffolds (**DKP1-DKP8**) derive from L- or D-Ser and either L- or D-Asp (**DKP1-DKP7**) or D-Glu (**DKP8**) and feature a carboxylic acid functionality and an amino moiety protected as Boc, which can be locked in a *cis*- (**DKP1**) or *trans*-relationship (**DKP2-DKP8**) as a consequence of the absolute configurations of the two α-amino acids. Moreover, the DKP scaffolds differ each from the other for the substitution at the diketopiperazine nitrogens (N-1, N-4), as they are either mono (**DKP1-DKP4**, **DKP6**, **DKP8**,) or bis-benzylated (**DKP5**, **DKP7**). While being derived from α-amino acids, they can be seen as a constrained dipeptide formed by two β- or a β- and a γ-amino acid. Ligands **16-23** were tested for their ability to inhibit biotinylated vitronectin binding to $\alpha_v\beta_3$ and $\alpha_v\beta_5$ receptors. All the ligands, except for the one containing a *cis*-scaffold, displayed low nanomolar affinity for both $\alpha_V\beta_3$ and $\alpha_V\beta_5$ integrins, with a slight selectivity towards the former receptor. Notably, two different separable conformers (diastereomers) were isolated for compound **22**, containing bis-benzylated scaffold **DKP7**, due to hindered rotation of one ring around the other. Interestingly, the two diastereomeric compounds showing atropoisomerism (**22 A**, **22 B**) are the most and the least selective and potent of the series.

Our ligands were fully characterized by NMR spectroscopy, detecting both H-bondings and long-range NOE contacts. Moreover, three-dimensional structures satisfying long-range NOE contacts were generated by restrained simulations. Five different H-bonding patterns were observed for our ligands on the basis of the conformational analysis, each one featuring at least a β-turn motif. A Cβ (Asp)-Cβ (Arg) distance of around 9 Å was detected from the structures obtained by restrained MC/SD simulations for the ligands displaying good affinity towards $\alpha_V\beta_3$ and $\alpha_V\beta_5$ integrins, while shorter distances were observed for the *cis* compound (**16**). In order to rationalize, on a molecular basis, the affinity of cyclic RGD peptidomimetics for the $\alpha_v\beta_3$ receptor, docking studies were performed starting from the representative conformations obtained from the MC/SD simulations. The crystal structure of the extracellular segment of integrin $\alpha_v\beta_3$ complexed with the cyclic pentapeptide Cilengitide (1L5G, pdb code) was taken as a reference model for the interpretation of the docking results in terms of ligand-protein interactions. In most of the cases the electrostatic clamp interactions of the pharmacophoric groups were maintained; moreover, further stabilizing interactions were observed in the case of higher affinity compounds.

Since α_v integrins, which can be internalized by cells, are involved in tumor angiogenesis and are overexpressed on the surface of cancer cells, integrin ligands can be usefully employed as tumor-homing peptidomimetics for site-directed delivery of cytotoxic drugs. A small library of integrin ligand - Paclitaxel conjugates **90**-**93** was synthesized with the aim of using *cyclo*[DKP-RGD] peptidomimetics as recognition motif for "tumor homing drug delivery".

In order to prepare cyclic RGD-peptidomimetics covalently linked to Paclitaxel, four functionalized (*f*) *trans* diketopiperazines (*i.e.*, **DKP-*f*2**, **DKP-*f*3**, **DKP-*f*4**, **DKP-*f*6**) were synthesized, varying the position of the *p*-aminomethylbenzyl *N*-substituent (*N*-1 or *N*-4) and the absolute stereochemistry at C-3 and C-6. These DKPs were used for the synthesis of *cyclo*[DKP-RGD] integrin ligands, which were finally conjugated to 2'-succinyl Paclitaxel.

All the Paclitaxel-RGD constructs **90**-**93** inhibited biotinylated vitronectin binding to the purified $\alpha_V\beta_3$ receptor at low nanomolar concentration, showing that the enormous increase of steric hindrance in the conjugates, due to presence of the linker bearing Paclitaxel through the succinate tether, did not influence the high affinity for the integrin receptors. *Cyclo*[DKP-RGD]-PTX conjugates **90-93** showed *in vitro* cytotoxic activity against a panel of human tumor cell lines similar to that of Paclitaxel. Among the cell lines, the cisplatin-resistant IGROV-1/Pt1 cells expressed high levels of integrin $\alpha_V\beta_3$, making them attractive to be tested in *in vivo* models. *Cyclo*[DKP-*f*3-RGD]-PTX **91** displayed sufficient stability in physiological solution and in both human and murine plasma to be a good candidate for *in vivo* testing. In tumor-targeting experiments against the IGROV-1/Pt1 human ovarian carcinoma xenotransplanted in nude mice, compound **91** exhibited better effects than Paclitaxel in terms of tumor volume inhibition and Log_{10} Cell Kill, despite the lower (ca. half) molar dosage used. Moreover, 2 out of 8 tumors in animals receiving conjugate **91** disappeared without any evidence of

disease until the end of experiment, suggesting an improved and more persistent antitumor effect. Treatment was well tolerated, as no deaths or significant weight losses were observed among the treated animals. Comparison of the *in vitro* data (where conjugate **91** is apparently two-fold less cytotoxic than Paclitaxel with respect to the IGROV-1/Pt-1 cancer cell line) with the *in vivo* data (where conjugate **91** shows a superior antitumor effect compared to Paclitaxel against the IGROV-1/Pt1 human ovarian carcinoma xenotransplanted in nude mice) is not contradictory but rather reinforces the tumor homing effect claimed for compound **91**. In fact, *in vivo* the conjugate is targeted to the tumor, whereas *in vitro* it acts through release of Paclitaxel. The histological examination of tumor specimens supports this view, because the induction of aberrant mitosis observed after treatment with conjugate **91** was more frequent, pronounced and persistent than that observed with Paclitaxel, consistent with a successful drug delivery to the target. The superior *in vivo* activity of *cyclo*[DKP-*f*3-RGD]-PTX **91** as compared to Paclitaxel supports the view that integrin ligands are promising tools to improve delivery of cytotoxic drugs.

CHAPTER 4

EXPERIMENTAL SECTION - CHEMISTRY

1 - General remarks and procedures

MATERIALS AND METHODS: All manipulations requiring anhydrous conditions were carried out in flame-dried glassware, with magnetic stirring and under a nitrogen atmosphere. All commercially available reagents were used as received. Anhydrous solvents were purchased from commercial sources and withdrawn from the container by syringe, under a slight positive pressure of nitrogen. (*S*)-and-(*R*)-serine methyl ester hydrochloride,[1] (*S*)- and (*R*)-serine methyl ester hydrochloride,[2] (2*R*)- and (2*S*)-aspartic acid β-allyl ester hydrochloride,[3] *N*-(*tert*-butoxycarbonyl)-(2*R*)-aspartic acid β-allyl ester,3 (*S*)- and (*R*)-*N*-Boc-serine methyl ester,[4] (*S*)- and (*R*)-methyl 3-azido-2-(tert-butoxycarbonylamino)propanoate,[5] (*S*)- and (*R*)-3-azido-2-(tert-butoxycarbonylamino) propanoic acid,5 (*S*)- and (*R*)-dimethyl aspartate hydrochloride,[6] (*S*)- and (*R*)-*N*-benzyl-dimethyl aspartate,[7] γ-methyl glutamate hydrochloride[8] and *N*-Boc-glycine benzyl ester[9] were prepared according to literature procedures and their analytical data were in agreement with those already published. Reactions were monitored by analytical thin layer chromatography using 0.25 mm pre-coated silica gel glass plates (DURASIL-25 UV254) and compounds visualized using UV fluorescence, aqueous potassium permanganate or ninhydrin. Flash column chromatography was performed according to the method of Still and co-workers[10] using Chromagel 60 ACC (40-63 μm) silica gel. Melting points were obtained in an open capillary apparatus and are uncorrected. ^{1}H-NMR spectra were recorded on a spectrometer operating at 400.16 MHz. Proton chemical shifts are reported in ppm (δ) with the solvent reference relative to tetramethylsilane (TMS) employed as the internal standard. The following abbreviations are used to describe spin multiplicity: s = singlet, d = doublet, t = triplet, q = quartet, m = multiplet, br = broad signal, dd = doublet of doublet. ^{13}C-NMR spectra were recorded on a spectrometer operating at 100.63 MHz, with complete proton decoupling. Carbon chemical shifts are reported in ppm (δ) relative to TMS with the respective solvent resonance as the internal standard. Infrared spectra were recorded on a standard FT-IR and peaks are reported in cm^{-}. Optical rotation values were measured on an automatic polarimeter with a 1 dm cell at the sodium D line and are given in units of 10^{-1} deg cm^2 g^{-1}. High resolution mass spectra (HRMS) were performed on a Fourier Transform Ion Cyclotron Resonance (FT-ICR) Mass Spectrometer APEX II & Xmass software

(Bruker Daltonics) – 4.7 T Magnet (Magnex) equipped with ESI source, available at CIGA (Centro Interdipartimentale Grandi Apparecchiature) c/o Università degli Studi di Milano. Low resolution mass spectra (MS) were measured on a Waters Acquity UPLC-MS (ESI ion source). All described compounds showed a purity > 98%, as determined by HPLC (UV and MS detectors). LC-UV/MS data were collected with an Agilent 1100 HPLC connected to a Bruker Esquire 3000+ ion trap mass spectrometer through an ES interface.

I really thank Indena S.p.A. for a generous gift of Paclitaxel

GENERAL PROCEDURES:

GENERAL PROCEDURE FOR Boc-DEPROTECTION REACTIONS:

GP1: To a solution of the *N*-Boc-protected amino acid or peptide in CH_2Cl_2 (0.13 M) was added half volume of TFA. The reaction mixture was stirred at for 2 h r.t. and then concentrated at reduced pressure. The excess TFA was azeotropically removed from the residue with toluene. Diethyl ether was added to the residue and the resulting suspension was evaporated under reduced pressure to afford the corresponding TFA salt.

GENERAL PROCEDURE FOR COUPLING REACTIONS:

GP2: To a solution of the *N*-protected amino acid in DMF, under nitrogen atmosphere and at 0 ºC, HATU (1.2 eq.), HOAt (1.2 eq.) and DIPEA (4 eq.) were added successively. After 30 min, a solution of the *N*-deprotected TFA salt of the peptide in DMF was added and the reaction mixture was stirred at 0 ºC for 1 h and at r.t. overnight. The mixture was afterwards diluted with EtOAc and consecutively washed with 1 M $KHSO_4$ (2×), aqueous $NaHCO_3$ (2×) and brine (2×), and dried over Na_2SO_4. Volatiles were evaporated under reduced pressure to afford the crude product.

GENERAL PROCEDURE FOR Cbz AND OBn HYDROGENOLYTIC CLEAVAGE:

GP3: protected compound (1 eq.) was dissolved in a mixture of THF/H_2O (1:1) and Pd/C 10% (0.1 eq.) was added. The reaction mixtures were subjected to three vacuum/hydrogen cycles and then left stirring overnight at room temperature under 1 bar of hydrogen. The mixture was filtered through Celite, and the cake thus obtained was washed thoroughly with THF/H_2O (1:1). The filtrate was concentrated and dried to give the crude product as white solid (100%).

GENERAL PROCEDURE FOR MACROLACTAMIZATION:

GP4: to a 1.4 mM solution of deprotected linear compound (1 eq.) in DMF, under nitrogen atmosphere and at 0 ºC, HATU (4 eq.), HOAt (4 eq.) and DIPEA (6 eq.) were added successively.

After stirring the reaction mixture at 0 ºC for 1 h, it was allowed to reach r.t., and stirred overnight. DMF was then removed under reduced pressure and the residue was purified by flash chromatography on silica gel to afford the product as white foam (31-74%).

GENERAL PROCEDURE FOR Mtr AND O*t*Bu ESTER REMOVAL:

GP5: protected macrolactams was treated with TFA (0.01 M solution), in the presence of ion scavengers: thioanisole (5%), ethanedithiol (3%), anisole (2%). After TFA removal, under reduced pressure, the residue was dissolved in a 1:1 mixture of diisopropyl ether/water. Phases were separated and the aqueous layer was washed several times with diisopropyl ether. The aqueous phase was concentrated under reduced pressure to give the crude product, which was purified by HPLC to give the desired compound as white solid (60-80%).

Preparation of hydrazoic acid

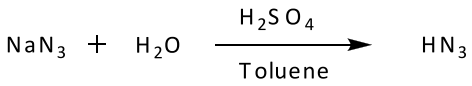

In a three-necked flask, NaN_3 (3 g) was dissolved in H_2O (3 mL). Once completely dissolved, toluene (20 mL) was added and the reaction mixture was cooled to 0 °C under vigorous stirring. Concentrated H_2SO_4 (1.2 mL) was added extremely slowly, so that the solution temperature did not exceed 10 °C. The reaction was stirred for one hour at 0 °C and then filtered on cotton wool. The residue was washed twice with toluene. The toluene solution was titrated by diluting 1 mL in distilled water (50 mL), and addition of NaOH (0.1 M) with phenolphthalein as indicator.

2 - Synthesis of diketopiperazine scaffolds DKP1-DKP8

2.1 - *DKP1-DKP3*

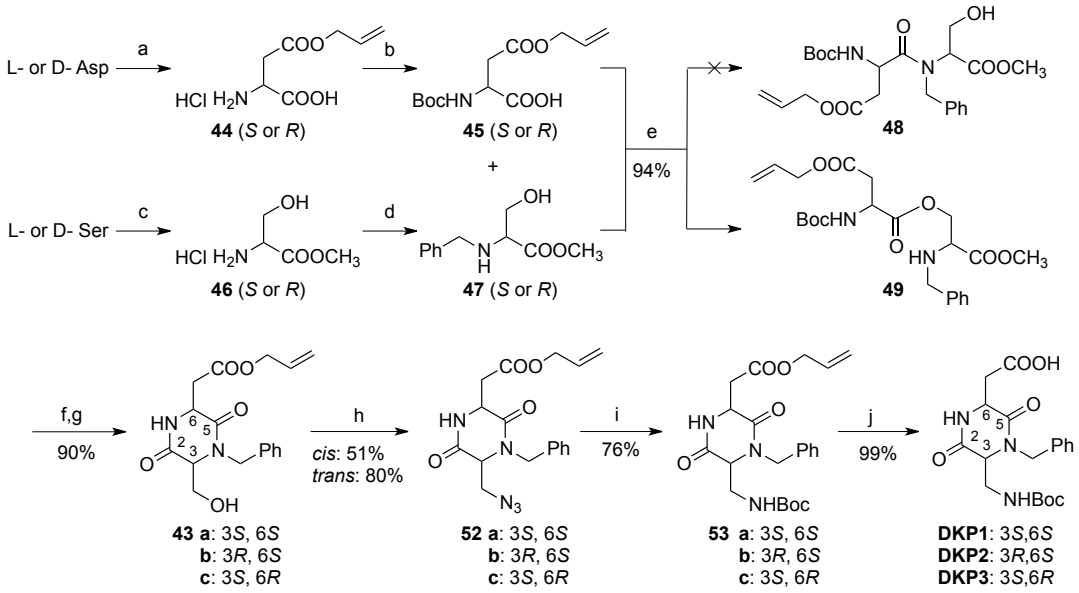

Reagents and conditions: (a) CH_3COCl, CH_2=$CHCH_2OH$; (b) Et_3N, Boc_2O, 1:1 H_2O/THF; (c) CH_3COCl, CH_3OH; (d) Et_3N, PhCHO, CH_3OH, then $NaBH_4$; (e) EDC, $DMAP_{cat.}$, DCM; (f) TFA/DCM, 1:1; (g) *i*Pr_2EtN, *i*PrOH; (h) PPh_3, DIAD, H_3N.tol, DCM/toluene, -20°C; (i) Me_3P, Boc-ON, THF, -20°C -> r.t; (j) [$Pd(PPh_3)_4$], PPh_3, pyrrolidine, DCM, 0°C.

(*R*)- and (*S*)-β-allyl aspartic acid hydrochloride 44

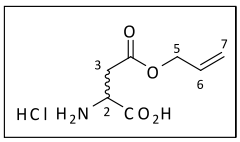

In a round bottom flask cooled at 0 °C were diluted 5 g (37.57 mmol) of L- or D- aspartic acid in 45 mL of allylic alcohol. Acetyl chloride (10.4 mL, 146.5 mmol, 3.9 eq.) was then slowly added dropwise with a dropping funnel into the reaction mixture. Once the addition was finished, the reaction flask was removed from the ice bath and let react at room temperature for 18 h. The reaction mixture was diluted in Et_2O making the product precipitate entirely. The salt was filtered through a glass filter and washed twice with more Et_2O. The salt was recovered and dried under vacuum affording 5.94 g (80%) of the monoallylated aspartic acid hydrochloride white solide.

$[\alpha]_D^{20}$=+22.7 (*S*-; MeOH, *c*=1.00); mp: 181 - 183 °C. litt. = 184 - 185 °C; ^{1}H NMR (400 MHz, D_2O) δ 5.96-5.86 (m, 1H, H_6), 5.33-5.23 (m, 2H, H_7), 4.64 (d, *J*=5.74 Hz, 2H, H_5), 4.37-4.34 (m, 1H, H_2), 3.14-3.08 (dd, *J1*=4.8 Hz, *J2*=18.4 Hz, 2H, H_3); ^{13}C NMR (101 MHz, D_2O) δ 171.5 (C=O), 171.2 (C=O), 131.8 (C_6), 119.3 (C_7), 67.1 (C_5), 49.7 (C_2), 34.4 (C_3); IR (cm^{-1}): 3437, 2913, 1742, 1726, 1505, 1227, 1206.

(*R*)- and (*S*)-*N*-Boc-β-allyl aspartic acid 45

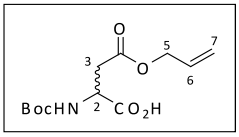

In a round bottom flask were solved 5.9 g (28.14 mmol) of either (*R*)- or (S)- allyl aspartic acid hydrochloride **44** in 120 mL of THF/water 1:1 solution. The reaction flask was lowered into an ice bath and 11.77 mL (84.42 mmol, 3 eq.) of triethylamine were added. Then, 7.37 g (33.77 mmol, 1.2 eq.) of Boc_2O were added and the reaction was stirred at room temperature for 24 h. The reaction mixture was then diluted with 200 mL of EtOAc and washed with aqueous $KHSO_4$ 1M until pH = 3 and brine. The organic phase was dried over Na_2SO_4, filtered and concentrated under reduced pressure. The product was then dried under high vacuum for a few hours affording 7.38 g (96%) of the pure expected product as viscous transparent oil.

R_f=0.1 (EtOAc 100%); $[\alpha]_D^{20}$=+33.3 ($CHCl_3$, *c*=1.00) for (*S*)-*N*-Boc-β-allyl aspartic acid; ^{1}H NMR (400 MHz, $CDCl_3$) δ 9,90 (bs, 1H, OH), 5.94-5.86 (m, 1H, H_6), 5.57 (d, *J*=8.4, 1H, NH), 5.19-5.32 (m, 2H, H_7), 4.52- 4.60 (m, 3H, H_2, H_5), 3.07 (dd, *J*1=4.2 Hz, *J2*=17.2 Hz, 1H, H_{3a}), 2.89 (dd, *J*1=4.8Hz, *J*2=17.1 Hz, 1H, H_{3b}), 1.46 (s, 9H, *t*Bu); ^{13}C NMR (101 MHz, $CDCl_3$) δ 176.0 (C=O), 171.2 (C=O), 156.0 (C=O), 132.0 (C_6), 119.1 (C_7), 80.9 ($\underline{C}(CH_3)_3$), 66.2 (C_5), 50.2 (C_2), 36.9 (C_3), 28.7 ($C(\underline{C}H_3)_3$); IR (cm^{-1}): 3331, 2980, 1732, 1504, 1385, 1163.

(*S*)- and (*R*)-serine methyl ester hydrochloride 46

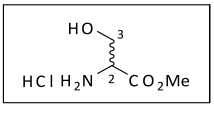

In a round bottom flask at 0°C were dissolved 6 g (57.09 mmol) of L- or D-serine in 45mL MeOH. Acetyl chloride (16.2 mL, 228 mmol, 4 eq.) was added dropwise in the reaction mixture. Once the addition was finished, the reaction flask was equipped with a condenser and the mixture was heated to reflux. After 2.5 h reflux was then stopped and the flask was cooled to room temperature. 200 mL of Et_2O were added provoking the precipitation of the resulting salt which was filtered on a glass funnel and dried under high vacuum affording 8.79 g (99%) of serine methyl ester hydrochloride as a white solid.

mp: 162-164 °C; $[\alpha]_D^{20}$=+3.98 (MeOH, *c*=1.00) for (*S*)-serine methyl ester hydrochloride; ^{1}H NMR (400 MHz, D_2O) δ 4.25 (t, *J*=3.8 Hz, 1H, H_2), 4.08 (dd, *J1*=4.3 Hz, *J2*=12.6 Hz, 1H, H_{3a}), 3.98 (dd, *J1*=3.4 Hz, *J2*=12.6 Hz, 1H, H_{3b}), 3.83 (s, 3H, OCH_3); ^{13}C NMR (101 MHz, D_2O) δ 169.3 (C=O), 59.6 (C_3), 55.1 (C_2), 54.1 (OCH_3); IR (cm^{-1}): 3358, 2928, 1750, 1595, 1510, 1260, 1095, 1040

(*S*)- and (*R*)-*N*-benzyl-serine methyl ester 47

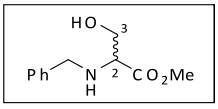

6 g (38.6 mmol) of (*S*)- or (*R*)-serine methylester hydrochloride **46** were dissolved in 90 mL MeOH, and the mixture was cooled to -10°C. 9.4 mL of *i*Pr_2EtN (54.0 mmol, 1.4 eq.) and 0,79 mL (7.71 mmol, 1eq.) of freshly distilled benzaldehyde were successively added dropwise. The reaction was stirred for 4 hours at r.t.. The temperature was then lowered again to -10°C and 2.9 g (76.6 mmol, 2eq.) of $NaBH_4$ were added portionwise over 30 min. The reaction mixture was again let react for half an hour, then, reaction was quenched by adding at low temperature HCl 4 M until no more gas formation was observed. The mixture was washed 3 times with Et_2O. The organic phases were combined and extracted with HCl 4 M twice. The aqueous phases were then combined and neutralized by careful addition of saturated $NaHCO_3$ solution until a pH=8 was reached. The aqueous phase was then extracted 4 times with Et_2O. The organic phase was separated and dried over Na_2SO_4, filtered, concentrated under reduced pressure and dried under vacuum affording 7.35 g (91%) of benzyl serine methyl ester as transparent oil.

R_f=0.2 (EtOAc/ hexane 1:1); $[\alpha]_D^{20}$=+39.4 (*R*-; $CHCl_3$, *c*=1.00); ^{1}H NMR (400 MHz, $CDCl_3$) δ 7.38 – 7.26 (m, 5H, C_6H_5), 3.91 (d, *J* = 13.0, 1H, CH_2Ph), 3.82 (dd, *J* = 4.4, 10.9, 1H, H_3), 3.77 (m, 4H, CH_2Ph, OCH_3), 3.66 (dd, *J* = 6.2, 10.8, 1H, H_3), 3.46 (dd, *J* = 4.5, 6.1, 1H, H_2), 2.78 (s, 1H, OH); ^{13}C NMR (101 MHz, $CDCl_3$) δ 173.6 (C=O), 139.3 (C_6H_5 quat), 129.0 (C_6H_5), 128.8 (C_6H_5), 127.8(C_6H_5), 62.8 (C_3), 62.2 (C_2), 52.6 (OCH_3), 52.4 (CH_2Ph); IR (cm^{-1}): 3320, 2951, 1736, 1454, 1202, 1142, 1057

4-allyl 1-[2-(benzylamino)-3-methoxy-3-oxopropyl] *N*-(*tert*-butoxycarbonyl)-aspartate (49a-c)

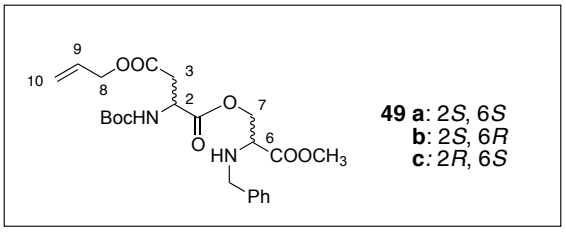

To a solution of either (*R*)- or (*S*)-*N*-benzylserine methyl ester **47** (734 mg, 3.51 mmol, 1 eq.) and EDC·HCl (3.4 g, 17.6 mmol, 5 eq.) in dry CH_2Cl_2 (20 ml) at 0°C under a N_2 atmosphere, β-allyl (2*R*)- or (2*S*)-*N*-(tert-butoxycarbonyl) aspartate ester **45** (1.92 g, 7.01 mmol, 2 eq.) was added as a solution in CH_2Cl_2. After 30 min, DMAP (214 mg, 1.76 mmol, 0.5 eq.) was added in one portion. The mixture was stirred at 0°C for 2 h and for additional 4 h at r.t.. The resulting mixture was diluted with EtOAc (70 ml) and washed with $KHSO_4$ 1M aqueous solution (2x40 ml), aqueous $NaHCO_3$ (2x40 ml) and brine (2x40 ml), dried over Na_2SO_4, and volatiles were removed under reduced pressure. The residue was purified by flash chromatography on silica gel (Hexane/EtOAc, 7:3) to afford the desired product as a transparent oil (1.54 g, 94%).

R_f=0.30 (Hexane/EtOAc 6:4);

a) $[\alpha]_D^{20}$=-2.65 (c=1.00, $CHCl_3$); ^{1}H NMR (400 MHz, $CDCl_3$) δ 7.24-7.34 (m, 5H, C_6H_5), 5.83-5.93 (m, 1H, H_9), 5.48 (d, *J* = 8.5 Hz, 1H, NHBoc), 5.30 (d, *J* = 17.2 Hz, 1H, H_{10a}), 5.23 (d, *J* = 10.4 Hz, 1H, H_{10b}), 4.51-4.61 (m, 3H, H_2, H_8), 4.32-4.48 (m, 2H, H_7), 3.88 (d, *J* = 13.1 Hz, 1H, C$\underline{H_2}$Ph), 3.75 (s, 3H, OCH_3), 3.73 (d, *J* = 13.1 Hz, 1H, C$\underline{H_2}$Ph), 3.55 (t, *J* = 4.7 Hz, 1H, H_6), 2.99 (dd, J_1 = 17.0 Hz, J_2=4.3 Hz, 1H, H_{3a}), 2.85 (dd, J_1=17.0 Hz, J_2=4.7 Hz, 1H, H_{3b}), 2.21 (bs, 1H, OH), 1.45 (s, 9H, $C(CH_3)_3$); ^{13}C NMR (101 MHz, $CDCl_3$) δ 172.8 (C=O), 171.0 (2C=O), 155.7 (COBoc), 139.6 (C_6H_5 - quat), 132.1 (C_9), 128.9 (C_6H_5), 128.7 (C_6H_5), 127.6 (C_6H_5), 119.1 (C_{10}), 80.6 ($\underline{C}(CH_3)_3$), 66.2 (C_8), 66.1 (C_7), 59.5 (C_6), 52.7 (C_2), 52.2 (CH_2Ph), 50.3 (OCH_3), 37.1 (C_3), 28.7 ($C(\underline{C}H_3)_3$); IR (cm^{-1}): 3358, 2928, 1738, 1500, 1454, 1385, 1163, 1053.

b) $[\alpha]_D^{20}$=+11 (c=1.00 in $CHCl_3$); ^{1}H NMR (400 MHz, $CDCl_3$) δ 7.26-7.34 (m, 5H, C_6H_5), 5.83-5.93 (m, 1H, H_9), 5.47 (d, *J* = 8.4, 1H, NHBoc), 5.32 (d, *J* = 17.2, 1H, H_{10a}), 5.25 (d, *J* = 10.5, 1H, H_{10b}), 4.66 – 4.52 (m, 3H, H_2, H_8), 4.46 (dd, *J* = 4.6, 11.0, 1H, H_{7a}), 4.35 (dd, *J* = 4.8, 11.0, 1H, H_{7b}), 3.89 (d, *J* = 13.1, 1H, C$\underline{H_2}$Ph), 3.80 – 3.68 (m, 4H, OCH_3, C$\underline{H_2}$Ph), 3.55 (t, *J* = 4.7, 1H, H_6), 3.01 (dd, *J* = 4.3, 17.0, 1H, H_{3a}), 2.86 (dd, *J* = 4.7, 17.1, 1H, H_{3b}), 1.96 (s, 1H, OH), 1.45 (s, 9H, $C(CH_3)_3$); IR (cm^{-1}): 3362, 2978, 1740, 1500, 1455, 1368, 1167, 1053.

c) ^{1}H NMR (400 MHz, CD_2Cl_2) δ 7.37-7.20 (m, 5H), 5.95-5.82 (m, 1H), 5.41 (br d, 1H, *J* = 7.9 Hz), 5.34-5.18 (m, 2H), 4.61-4.48 (m, 3H), 4.39 (dd, 1H, *J* = 10.9, 4.6 Hz), 4.30 (dd, 1H, *J* = 10.9, 4.9 Hz), 3.86 (d, 1H, *J* = 13.1 Hz), 3.71 (s, 3H), 3.70 (d, 1H, *J* = 13.1 Hz), 3.51 (t, 1H, *J* = 4.7 Hz),

2.94 (dd, 1H, *J* = 17.2, 4.7 Hz), 2.82 (dd, 1H, *J* = 17.0, 4.8 Hz), 1.42 (s, 9H); ^{13}C NMR (101 MHz, CD_2Cl_2) δ 172.4, 170.6, 139.7, 131.9, 128.3, 128.2, 127.1, 118.1, 65.9, 65.6, 59.1, 52.0, 51.8, 50.0, 36.7, 28.0; HRMS (ESI) *m/z* calcd for $[C_{23}H_{33}N_2O_8]^+$: 465.22314 $[M+H]^+$; found: 465.22267.

OH-DKP1-CO_2Allyl (43 a);

OH-DKP2-CO_2Allyl (43 b);

OH-DKP3-CO_2Allyl (43 c)

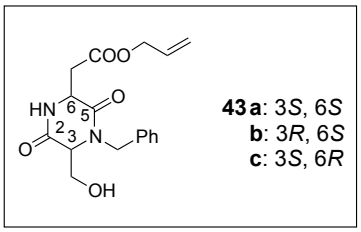

Compound **49** (1.08 g, 1.82 mmol, 1 eq.) was deprotected according to general procedure **GP1**. The corresponding trifluoroacetate salt **51** was dissolved in *i*PrOH (20 ml) and *i*Pr_2EtN (0.9 ml, 5.6 mmol, 4 eq.) was added at r.t.. The reaction was stirred for 18 h at r.t., monitoring the formation of DKP by TLC (EtOAc/Hexane: 8/2). The solution was then concentrated under reduced pressure and the residue was purified by flash chromatography on silica gel (Hexane/EtOAc, 75:25) to afford the desired product as a white foam (543.8 mg, 90%).

43 a) R_f=0.25 (EtOAc/Hexane: 8/2); $[\alpha]_D^{20}$=-72.1 (*c*= 1.00 in $CHCl_3$); ^{1}H NMR (300 MHz, $CDCl_3$) δ 7.41 – 7.19 (m, 5H), 7.02 (d, *J* = 2.1 Hz, 1H), 5.96 – 5.78 (m, *J* = 17.1, 10.4, 5.8 Hz, 1H), 5.38 – 5.19 (m, 3H), 4.67 – 4.53 (m, 2H), 4.53 – 4.43 (m, 1H), 4.06 (d, *J* = 15.0 Hz, 1H), 4.00 – 3.91 (m, *J* = 6.7 Hz, 1H), 3.91 – 3.80 (m, *J* = 3.1 Hz, 2H), 3.20 (dd, *J* = 17.6, 3.5 Hz, 1H), 3.11 (dd, *J* = 17.6, 10.1 Hz, 1H); ^{13}C NMR (101 MHz, $CDCl_3$) δ 171.8, 166.8, 166.2, 135.6, 131.9, 129.5, 128.6, 128.6, 119.5, 66.4, 61.2, 60.6, 52.8, 47.8, 40.7; IR (cm^{-1}): 3427, 2928, 1740, 1653, 1452, 1383, 1339, 1275, 1184, 1128.

43 b) R_f=0.10 (EtOAc/Hexane 8:2); $[\alpha]_D^{20}$=-35.3 (*c*=1.00 in $CHCl_3$); ^{1}H NMR (400 MHz, CD_2Cl_2) δ 7.43 - 7.25 (m, 5H), 7.20 (br s, 1H), 6.02 - 5.83 (m, 1H), 5.39 - 5.20 (m, 3H), 4.70 - 4.55 (m, 3H), 4.12 (d, 1H, *J* = 15.2 Hz), 4.01 (dd, 1H, *J* = 11.8, 1.9 Hz), 3.90 (dd, 1H, *J* = 11.8, 3.1 Hz), 3.81 (bs, 1H,), 3.21 (dd, 1H, *J* = 17.4, 4.0 Hz), 2.86 (dd, 1H, *J* = 17.4, 8.0 Hz); ^{13}C NMR (101 MHz, CD_2Cl_2) δ 170.8, 168.2, 166.6, 135.9, 131.8, 128.8, 127.9, 127.9, 127.8, 118.3, 117.9, 65.7, 61.9, 61.6, 51.1, 47.3, 37.1; IR (neat): ν_{max} 3364, 3032, 2942, 1738, 1651, 1452, 1383, 1329, 1273, 1183, 1129; HRMS (ESI) *m/z* calcd for $[C_{17}H_{20}N_2NaO_5]^+$: 355.12644 $[M+Na]^+$; found: 355.12590.

N_3-DKP1-CO_2Allyl (52 a);

N_3-DKP2-CO_2Allyl (52 b);

N_3-DKP3-CO_2Allyl (52 c)

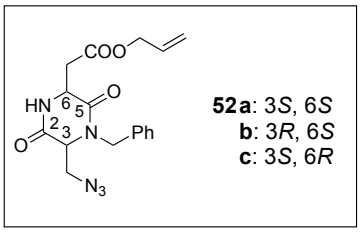

To a solution of diketopiperazine **43** (559 mg, 1.7 mmol, 1 eq.) in CH_2Cl_2/toluene (6.6 ml/12.2 ml), under a nitrogen atmosphere and at -20 ºC, PPh_3 (535 mg, 2.0 mmol, 1.2 eq.) was added and the mixture was stirred until a solution was obtained. Addition of hydrazoic acid (0.45 M in toluene, 7.5 ml, 3.4 mmol, 2 eq.) was followed by dropwise addition of DIAD (0.42 ml, 2.0 mmol, 1.2 eq.) and the reaction was stirred at -20ºC during 3.5 h. The reaction mixture was loaded onto a silica gel column (Hexane/EtOAc, 6:4) thus removing the hydrazo-derivative. The resulting crude residue was further purified by flash chromatography (CH_2Cl_2/MeOH, 99:1) to afford the desired product as a white foam (**a:** 309 mg, 51%; **b**-**c:** 486 mg, 80%).

In the case of the *cis* isomer, an almost unseparable mixture of compounds **52a** and **54a** was obtained in a 3:1 ratio.

a) R_f=0.25 (EtOAc/Hexane: 8/2); $[\alpha]_D^{20}$=-72.1 (*c*= 1.00 in $CHCl_3$) ^{1}H NMR (400 MHz, $CDCl_3$) δ 7.39 – 7.21 (m, 5H), 6.77 (s, 1H), 5.84-5.91 (m, 1H), 5.41 – 5.27 (m, 2H), 5.25 (d, *J* = 15.0, 1H), 4.70 – 4.57 (m, 2H), 4.52 (dt, *J* = 2.7, 10.7, 1H), 4.17 (d, *J*=15.0 Hz, 1H), 4.03 (q, *J* = 3.5, 1H), 3.92 – 3.85 (m, 2H, H2), 3.24 (dd, *J* = 2.7, 17.7, 1H), 3.16 (br s, 1H); 3.11 (dd, *J* = 10.9, 17.7, 1H); ^{13}C NMR (101 MHz, $CDCl_3$) δ 171.8, 166.8, 166.2, 135.6, 131.9, 129.5, 128.6, 128.6, 119.5, 66.4, 61.2, 60.6, 52.8, 47.8, 40.7; IR (cm^{-1}): 3427, 2928, 1740, 1653, 1452, 1383, 1339, 1275, 1184, 1128.

c) R_f=0.13 (Hexane/EtOAc 6:4); $[\alpha]_D^{20}$=+55.9 (*c*=1.00 in $CHCl_3$); ^{1}H NMR (400 MHz, CD_2Cl_2) δ 7.39 – 7.26 (m, 5H), 7.09 (d, 1H, *J* = 11.3 Hz), 6.00 – 5.83 (m, 1H), 5.35 (dq, 1H, *J* = 1.5, 17.2 Hz), 5.28 (dq, 1H, *J* = 1.3, 10.4 Hz), 5.16 (d, 1H, *J* = 15.1 Hz), 4.69 – 4.60 (m, 3H), 4.26 (d, 1H, *J* = 15.1 Hz), 3.95 (t, 1H, *J* = 2.9 Hz), 3.89 (dd, 1H, *J* = 2.3, 12.7 Hz), 3.65 (dt, 1H, *J* = 6.6, 13.2 Hz), 3.29 (dd, 1H, *J* = 3.6, 17.5 Hz), 2.84 (dd, 1H, *J* = 8.9, 17.5 Hz); ^{13}C NMR (101 MHz, CD_2Cl_2) δ 171.0, 166.8, 166.4, 135.61, 131.9, 129.5, 128.7, 128.5, 119.4, 66.3, 59.5, 52.1, 51.5, 51.4, 48.3, 37.6; IR (cm^{-1}): ν_{max} 3250, 2937, 2118, 1732, 1694, 1447, 1329, 1277, 1184; MS (ESI) *m/z* calcd for $[C_{17}H_{20}N_5O_4]^+$: 380.13 $[M+H]^+$; found: 380.2.

***N*-Boc-DKP1- CO_2Allyl (53 a);**

***N*-Boc-DKP2- CO_2Allyl (53 b);**

***N*-Boc-DKP3- CO_2Allyl (53 c)**

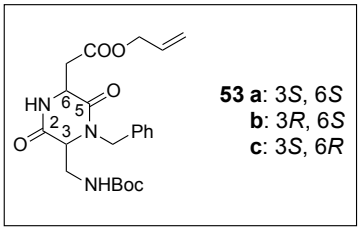

53 a: 3*S*, 6*S*
b: 3*R*, 6*S*
c: 3*S*, 6*R*

To a solution of azide **52** (268 mg, 0.75 mmol, 1 eq.) in THF (2.5 ml), under a nitrogen atmosphere and at -20 ºC, Me_3P (0.83 ml of 1 M solution in THF, 0.83 mmol, 1.1 eq.) and 2-(*t*-butoxycarbonyloxyimino)-2-phenylacetonitrile (Boc-ON, 206 mg, 0.83 mmol, 1.1 eq.) were added successively. After stirring for 5 h at r.t., the solution was diluted with CH_2Cl_2 (60 ml) and washed with H_2O (3x30 ml) and brine. The organic phase was dried over Na_2SO_4 and volatiles were removed under reduced pressure. The residue was purified by flash chromatography on silica gel (CH_2Cl_2/MeOH, 99:1) to afford the desired product as a white foam (**a**: 308 mg, 95%; **b**: 246 mg, 76%).

a) R_f=0.2 (CH_2Cl_2/MeOH 97:3); $[\alpha]_D^{20}$=-123.7 (*c*=1.00 in $CHCl_3$); ^{1}H NMR (400 MHz, $CDCl_3$) δ 7.33 (m, 5H), 6.99 (s, 1H), 5.92 (m, 1H), 5.56 (d, *J* = 15.1, 1H), 5.35 (dd, *J* = 1.3, 17.2, 1H), 5.28 (dd, *J* = 0.9, 10.4, 1H), 5.20 (t, *J* = 6.4, 1H), 4.65 (d, *J* = 5.7, 2H), 4.50 (dt, *J* = 2.6, 11.2, 1H), 4.09 (d, *J* = 15.1, 1H), 3.90 – 3.76 (m, 2H), 3.49 (m, 1H), 3.28 (dd, *J* = 2.4, 17.6, 1H), 2.84 (dd, *J* = 11.2, 17.6, 1H), 1.46 (s, 9H); ^{13}C NMR (101 MHz, $CDCl_3$) δ 171.5, 166.7, 164.9, 156.2, 135.6, 131.8, 129.4, 128.9, 128.5, 119.3, 80.8, 66.4, 59.2, 52.4, 47.2, 40.8, 40.6, 28.7; IR (cm^{-1}): 3389, 2928, 1663, 1524, 1453, 1339, 1271, 1169.

b) R_f=0.14 (DCM/MeOH 97:3); $[\alpha]_D^{20}$=+16.9 (*c*=1.00 in $CHCl_3$); ^{1}H NMR (400 MHz, $CDCl_3$) δ 7.41 – 7.21 (m, 5H), 6.94 (s, 1H), 5.91 (m, 1H), 5.51 (d, 1H, *J* = 15.1 Hz), 5.39 – 5.23 (m, 2H), 5.05 (br s, 1H), 4.64 (d, 2H, *J* = 5.6 Hz), 4.49 (dd, 1H, *J* = 2.8, 9.3 Hz), 4.09 (d, 1H, *J* = 15.1 Hz), 3.83 – 3.76 (m, 2H), 3.61 – 3.47 (m, 1H), 3.35 (dd, 1H, *J* = 3.3, 17.6 Hz), 2.79 (dd, 1H, *J* = 9.4, 17.6 Hz), 1.45 (s, 9H); ^{13}C NMR (101 MHz, $CDCl_3$) δ 171.3, 167.6, 165.3, 156.3, 135.8, 131.8, 129.4, 128.8, 128.5, 119.4, 80.8, 66.4, 59.7, 51.3, 47.6, 41.1, 38.3, 28.7; IR (cm^{-1}): ν_{max} 3328, 2980, 1692, 1524, 1453, 1329, 1273, 1171; MS (ESI) *m/z* calcd for $[C_{22}H_{30}N_3O_6]^+$: 432.21 $[M+H]^+$; found: 432.3.

***N*-Boc-DKP-COOH (DKP1-DKP3)**

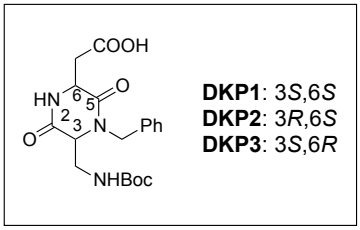

DKP1: 3*S*,6*S*
DKP2: 3*R*,6*S*
DKP3: 3*S*,6*R*

Allyl ester **53** (363 mg, 0.84 mmol, 1 eq.) was dissolved in CH_2Cl_2 (6.0 ml) under a nitrogen atmosphere. After cooling the solution at 0 ºC, pyrrolidine (83 µl, 1.01 mmol, 1.2 eq), PPh_3 (40 mg, 0.15 mmol, 0.18 eq) and $[Pd(PPh_3)_4]$ (39 mg, 0.034 mmol, 0.04 eq) were added successively. After stirring for 1 h at 0°C, the mixture was diluted with EtOAc (25 ml) and extracted with aqueous $NaHCO_3$ (4x10 ml). The combined aqueous phases were acidified to pH 2 with a 1 M $KHSO_4$ solution and then extracted with CH_2Cl_2. The resulting organic phase was dried over Na_2SO_4 and the solvent was evaporated to afford the desired product as a fluffy white solid (327 mg, 99%) that was used without further purification.

2.2 - *DKP4-DKP6*

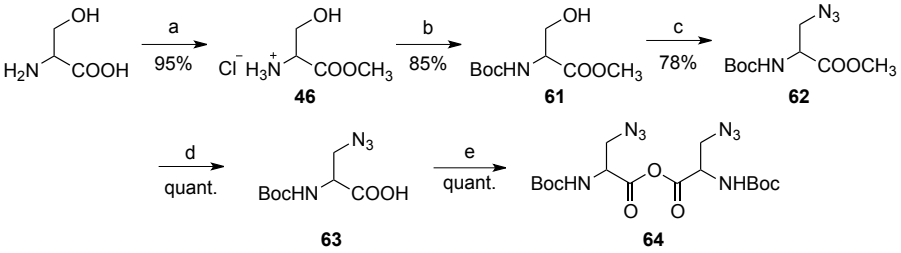

Reagents and conditions: a) CH_3COCl, CH_3OH; b) Boc_2O, THF/H_2O 1:1; c) HN_3, DIAD, PPh_3, THF; d) LiOH, THF/H_2O 1:1; e) DCC, DCM.

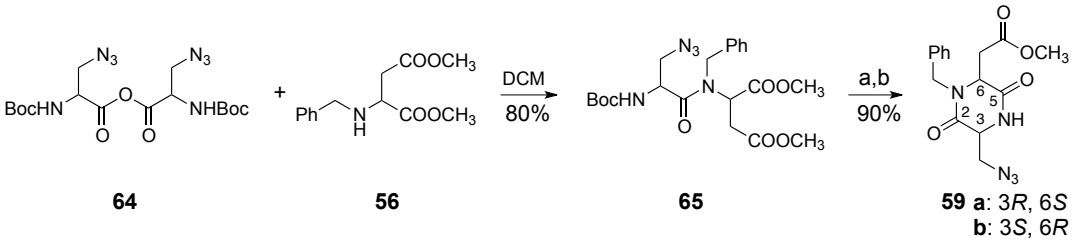

Reagents and conditions: a) TFA/DCM 1:2; b) DIPEA, *i*PrOH

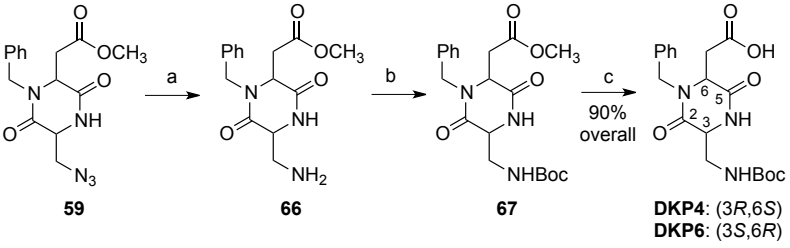

Reagents and conditions: (a) H_2, Pd-C, THF; (b) Boc_2O, THF; (c) LiOH, THF/H_2O 1:1.

N-benzyl-dimethyl aspartate (56) [6,7]

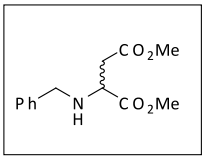

At 0 °C to 50 ml of anhydrous methanol, 3.75 ml (47.5 mmol) of thinly chloride was added dropwise. The solution was stirred at 0 °C for 30 min and then 6.332 g (47.5 mmol) of Asp was added. The reaction mixture was stirred at r.t. for 24 h and TLC (CH_3Cl/CH_3OH, 9:1) indicated complete disappearance of Asp. The reaction mixture was evaporated under reduced pressure and the residue

was triturated with petroleum ether repeatedly to provide 7.495 mg (98%) of HCl•Asp-$(OCH_3)_2$ as a colorless which was directly used for the next reaction.

To a vigorously stirred solution of 500 mg (2.54 mmol) of dimethyl aspartate hydrochloride and 160 mg (2.54 mmol) of sodium cyanoborohydride in 12 mL of methanol at rt was added 265 mg (2.54 mmol) of benzaldehyde in one portion. After being stirred for 4 h, the mixture was cooled in an ice bath, and the pH was lowered to ca. 1 with concd HCl. The mixture was then allowed to warm to r.t. for 2 h, and the methanol was removed under reduced pressure at r.t.. The white residue was dissolved into a minimum volume of water, and the pH was raised to ca. 10 with saturated aqueous Na_2CO_3. After three ethyl acetate extractions, combined organic portions were washed with brine, dried over Na_2CO_3, and evaporated to give a pale yellow oil.

Methyl 3-azido-2-(tert-butoxycarbonylamino)propanoate (62)

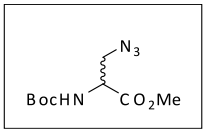

In a round bottom flask were solved (10.0 g, 64.3 mmol, 1 eq.) of serine methyl ester hydrochloride in 232 mL of THF/water 1:1 solution. The reaction flask was lowered into an ice bath and 27 ml (193 mmol, 3 eq.) of triethylamine were added. Then, 16.8 g (77.1 mmol, 1.2 eq.) of Boc_2O were added and the reaction was stirred at room temperature for 24 h. The reaction mixture was then diluted with 200 mL of EtOAc and washed with aqueous $KHSO_4$ 1M until pH = 3 and brine. The organic phase was dried over Na_2SO_4, filtered and concentrated under reduced pressure. The product was then dried under high vacuum for a few hours affording 12.3 g (90 %) of pure Boc-Ser-OMe **61** as viscous transparent oil, which was used in the next step without purification.

To triphenyl phosphine (1.45 g, 5.54 mmol, 1.2 eq.) in THF (11 mL) at -78 °C was added DIAD (1 ml, 5.54 mmol, 1.2 eq.) in THF (10 mL) followed by the HN_3 solution (1.8 M in toluene, 3.1 ml, 5.54mmol, 1.2 eq.) and Boc-serine methyl ester **61** (1.00 g, 4.62 mmol) in THF (10 mL). After the mixture stirred at -78 °C for 30 min and then allowed to slowly reach 0°C (within 3 h). The solvent was evaporated and the residue was chromatographed with hexane/EtOAc 9:1 to provide 839 mg (74%) of the azide as a mobile oil which crystallizes upon standing in the refrigerator.

3-azido-2-(tert-butoxycarbonylamino)propanoic acid (63)

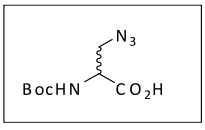

Compound **62** (350.0 mg, 1.433 mmol) in THF (6 mL) at 0 °C was treated with LiOH monohydrate (84.0 mg, 2.00 mmol) in water (4 mL). After 1 h, the mixture was concentrated, diluted with water, washed with ether, acidified with 1 M $KHSO_4$, and extracted into DCM which was dried and evaporated to provide 329.2 mg (quant.) of a colorless oil.

(*R*)-dimethyl-2-((*S*)-3-azido-*N*-benzyl-2-(*tert*-butoxycarbonylamino)propanamido)succinate (65a);
(*S*)-dimethyl-2-((*R*)-3-azido-*N*-benzyl-2-(*tert*-butoxycarbonylamino)propanamido)succinate (65b)

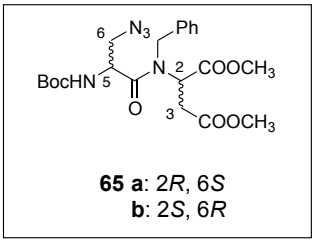

65 a: 2*R*, 6*S*
b: 2*S*, 6*R*

DCC (1.77 g, 8.56 mmol, 1 eq.) was added to a solution of *N*-Boc-Ser(N_3)-OH (**62**) (3.94g, 17.11 mmol, 2 eq.) 60 ml of CH_2Cl_2, in one portion. A white precipitate (DCU) formed and stirring continued for 1h at r.t.. The mixture was then filtered on a cotton wool to remove DCU. The white DCU residue was washed twice with cold CH_2Cl_2. The filtrate was concentrated under reduced pressure at r.t., and dried under high vacuum to afford symmetric anhydride **64a** or **64b** as a pale yellow foam, which was used without further purification. *N*-benzyl-aspartic acid dimethylester **56** (1.51 g, 6.01 mmol, 0.7 eq.) was dissolved in CH_2Cl_2 (50 ml) and the mixture was cooled to 0°C. A solution of symmetric anhydride in 50 ml of CH_2Cl_2 was then added dropwise, very slowly. The reaction mixture was let to reach r.t. and stirred overnight. The solvent was afterwards removed under reduced pressure and the residue was purified by flash chromatography on silica gel (Hexane/EtOAc, 8:2) to afford the desired product as a viscous transparent oil (2.22 g, 80%).

R_f=0.37 (Hexane/EtOAc, 7:3); $[\alpha]_D^{20}$=-38.6 (**65 a**, *c*=1.0 in $CHCl_3$); ^{1}H NMR (400 MHz, CD_2Cl_2) (rotamers ratio in CD_2Cl_2 A/B = 4:1) δ 7.51 – 7.11 (m, 5H), 5.61 – 5.50 (m, $1H_B$), 5.40 – 5.28 (m, $1H_B$, overlapping with solvent signal), 5.17 (t, $1H_B$, *J* = 7.1 Hz), 5.07 – 4.99 (m, $1H_B$), 4.86 – 4.69 (m, $3H_A$, $1H_B$), 4.54 – 4.38 (m, $1H_A$, $1H_B$), 3.74 (dd, $1H_B$, *J* = 12.3, 5.4 Hz), 3.69 – 3.65 (m, $3H_A$, $1H_B$), 3.63 (s, $3H_A$), 3.52 (dd, $1H_A$, *J* = 12.4, 6.3 Hz), 3.41 (dd, $1H_A$, *J* = 12.3, 6.0 Hz), 3.28 (dd, $1H_A$, *J* = 16.9, 7.4 Hz), 3.05 (dd, $1H_B$, *J* = 17.1, 7.0 Hz), 2.71 (dd, $1H_B$, *J* = 17.2, 7.3 Hz), 2.55 (dd, $1H_A$, *J* = 16.1, 6.1 Hz), 1.45 (s, 9H); ^{13}C NMR (101 MHz, CD_2Cl_2) δ 171.9, 171.3, 170.4, 155.5, 136.3, 129.5, 129.3,

129.2, 129.1, 129.0, 128.8, 128.2, 128.0, 127.9, 80.9, 58.0, 56.9, 56.6, 53.4, 53.1, 53.0, 52.6, 52.4, 51.4, 48.1, 35.3, 34.9, 28.6; IR (neat): ν_{max} 3343, 2979, 2953, 2106, 1739, 1712, 1651, 1497, 1438, 1367, 1289, 1250, 1166; MS (ESI) *m/z* calcd for $[C_{21}H_{29}N_5NaO_7]^+$: 486.20 $[M+Na]^+$; found: 486.3.

N_3-DKP4-CO_2Me (59 a);
N_3-DKP6-CO_2Me (59 b)

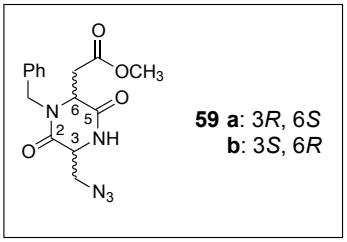

Dipeptide **65** (1.44 g, 3.11 mmol, 1 eq.) was deprotected according to general procedure **GP1**, with the addition of Et_3SiH (1.24 ml, 7.78 mmol, 2.5 eq.) as an ion scavenger. The corresponding trifluoroacetate salt was dissolved in *i*PrOH (40 ml) and *i*Pr_2EtN (2.13 ml, 12.44 mmol, 4 eq.) was added at r.t.. The reaction was stirred for 5 h at r.t., then the solution was concentrated under reduced pressure and the residue was purified by flash chromatography on silica gel (EtOAc/Hexane, 8:2) to afford the desired product as a white foam (927.4 mg, 90%).

R_f=0.33 (Hexane/EtOAc 2:8); $[\alpha]_D^{20}$=+32.2 (**59 a**, *c*=1 in $CHCl_3$); ^{1}H NMR (400 MHz, CD_2Cl_2) δ 7.45 – 7.24 (m, 5H), 6.83 (s, 1H), 5.13 (d, 1H, *J* = 15.3 Hz), 4.53 – 4.47 (m, 1H), 4.24 (d, 1H, *J* = 15.3 Hz), 4.12 (t, 1H, *J* = 4.7 Hz), 3.91 (dd, 1H, *J* = 12.5, 5.8 Hz), 3.85 (dd, 1H, *J* = 12.5, 3.6 Hz), 3.65 (s, 3H), 3.07 (dd, 1H, *J* = 17.5, 3.3 Hz), 2.88 (dd, 1H, *J* = 17.5, 5.0 Hz); ^{13}C NMR (101 MHz, CD_2Cl_2) δ 170.4, 167.6, 164.5, 135.6, 128.9, 127.9, 127.8, 56.0, 54.3, 52.0, 47.4, 34.6; IR (neat): ν_{max} 3249, 3066, 3030, 3007, 2953, 2924, 2852, 2362, 2342, 2117, 1736, 1558, 1496, 1449, 1372, 1332, 1281, 1204, 1180, 1138; MS (ESI) *m/z* calcd for $[C_{15}H_{18}N_5O_4]^+$: 332.14 $[M+H]^+$; found: 332.3.

NH_2-DKP4-CO_2Me (66 a);
NH_2-DKP6-CO_2Me (66 b)

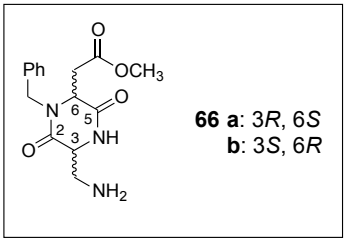

Compound **59** (737 mg, 2.22 mmol, 1 eq.) was dissolved in THF (45 ml) and Pd/C (237 mg, 0.22 mmol, 0.1 eq.) was added. The flask was thoroughly purged with H_2, and the system was closed. The reaction mixture was stirred at r.t. for 4 h, and then filtered through a Celite pad. The cake thus obtained was washed thoroughly with THF. The filtrate was concentrated and dried to give the crude product as a transparent paste (643.9 mg, 95%) which was used without further purification.

R_f=0.13 (CH_2Cl_2/MeOH 95:5); $[\alpha]_D^{20}$=+83.2 (**66 a**, *c*=1 in $CHCl_3$); ^{1}H NMR (400 MHz, CD_2Cl_2) δ 7.30 – 7.09 (m, 5H), 6.75 (br s, 1H), 4.99 (d, 1H, *J* = 15.3 Hz), 4.15 – 4.04 (m, 2H), 4.00 (br s, 1H), 3.53 (s, 3H), 3.18 (dd, 1H, *J* = 13.1, 3.6 Hz), 2.99 – 2.84 (m, 2H), 2.73 (dd, 1H, *J* = 17.0, 5.1 Hz), 1.33 (s, 2H); ^{13}C NMR (101 MHz, CD_2Cl_2) δ 170.3, 167.4, 166.2, 136.1, 128.8, 127.7, 56.3, 55.9, 51.9, 47.2, 44.2, 35.0; IR (neat): ν_{max} 1736, 1685, 1659, 1496, 1449, 1371, 1318, 1254, 1203, 1179, 1109; MS (ESI) *m/z* calcd for $[C_{15}H_{20}N_3O_4]^+$: 306.14 $[M+H]^+$; found: 306.3.

NHBoc-DKP4-CO_2Me (67 a); NHBoc-DKP6-CO_2Me (67 b)

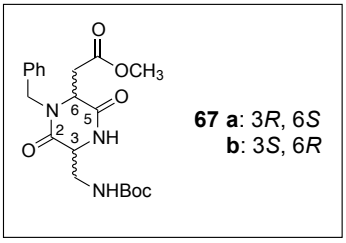

To a solution of **66** (586 mg, 1.92 mmol, 1 eq.) in THF (35 ml), Boc_2O (461 mg, 2.11 mmol, 1.1 eq.) was added in one portion. After stirring the mixture at r. t. overnight, EtOAc (60 ml) was added. The solution was washed with 1 M $KHSO_4$ (4x) and brine (1x). The organic phase was dried over Na_2SO_4 and volatiles were removed under reduced pressure, to afford the desired product as a white foam (739.5 mg, 95%), which was used without further purification.

R_f=0.23 (EtOAc/Hex 7:3); $[\alpha]_D^{20}$=+82.2 (**67 a**, *c*=1 in $CHCl_3$); ^{1}H NMR (400 MHz, CD_2Cl_2) δ 7.33 – 7.06 (m, 5H), 6.69 (br s, 1H), 5.12 (br s, 1H), 4.96 (d, 1H, *J* = 15.2 Hz), 4.26 (s, 1H), 4.14 (d, 1H, *J* = 15.3 Hz), 4.00 (s, 1H), 3.68 – 3.57 (m, 3H), 3.56 – 3.45 (m, 4H), 2.86 (d, 1H, *J* = 16.9 Hz), 2.72 (dd, 1H, *J* = 17.1, 4.9 Hz), 1.35 (s, 9H); ^{13}C NMR (101 MHz, CD_2Cl_2) δ 170.3, 167.3, 166.0, 146.7, 135.9, 128.8, 127.8, 127.6, 79.9, 56.6, 55.9, 51.9, 47.7, 42.2, 35.1, 28.0; IR (neat): ν_{max} 3328, 3004, 2979, 2953, 2934, 1809, 1737, 1690, 1586, 1508, 1497, 1450, 1393, 1368, 1333, 1250, 1208, 1168, 1119; MS (ESI) *m/z* calcd for $[C_{20}H_{28}N_3O_6]^+$: 406.20 $[M+H]^+$; found: 406.3.

NHBoc-DKP4-COOH (DKP4);
NHBoc-DKP6-COOH (DKP6)

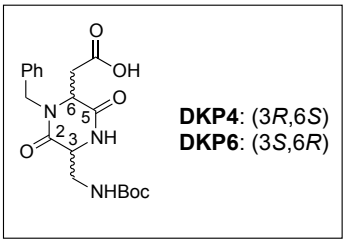

Compound **67** (710 mg, 1.75 mmol, 1 eq.) was dissolved in THF (60 ml) and the mixture was cooled to 0 °C. A solution of $LiOH \cdot H_2O$ (183.7 mg, 4.38 mmol, 2.5 eq.) in H_2O (30 ml) was added dropwise. The resulting solution was let reacting for 1 h at 0 °C. Then, maintaining the temperature at 0 °C, the mixture was acidified with HCl 1M to pH = 1-2, and extracted with CH_2Cl_2 (4x). The collected organic phases were dried over Na_2SO_4 and volatiles removed under reduced pressure. Either **DKP4** or **DKP6** were afforded as a white foam (685 mg, 100%), which was used in subsequent steps without further purification.

2.3 - *DKP5-DKP7*

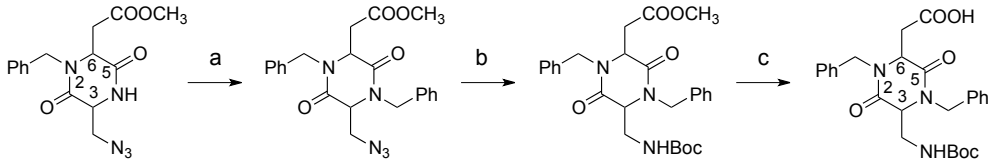

59 a: 3*R*, 6*S* **b**: 3*S*, 6*R*
70 a: 3*R*, 6*S* **b**: 3*S*, 6*R*
71 a: 3*R*, 6*S* **b**: 3*S*, 6*R*
DKP5: 3*R*, 6*S* **DKP7**: 3*S*, 6*R*

Reagents and conditions: (a) KHMDS, BnBr, THF/DMF 7:3; (b) Me_3P, Boc-ON, THF, -20°C -> r.t; (c) LiOH, THF/H_2O 1:1; 75% over three steps.

N_3-DKP5-CO_2Me (70 a);

N_3-DKP7-CO_2Me (70 b)

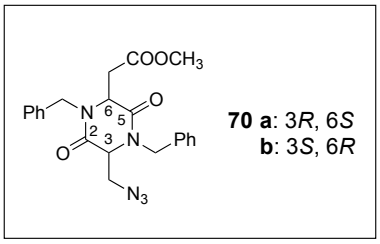

70 a: 3*R*, 6*S*
b: 3*S*, 6*R*

A flame-dried flask under N_2 was charged with a solution of **59** (640 mg, 1.93 mmol, 1 eq.) in dry THF (32 ml). The temperature was lowered to -78°C and KHMDS (4.25 ml of a 0.5 M solution in toluene, 2.12 mmol, 1.1 eq.) was added dropwise. After 30 min benzyl bromide (1.18 ml, 9.65 mmol, 5 eq.) was added, and a final solvent ratio THF/DMF 7:3 was reached by adding DMF (13.6 ml). The mixture was allowed to reach -40°C and stirred for 3 h. Then aqueous NH_4Cl was slowly added and the mixture was extracted with EtOAc (3x). Organic phases were washed with brine and dried over Na_2SO_4. Volatiles were removed under reduced pressure and the residue was purified by flash chromatography on silica gel (Hex/EtOAc, 7:3) to afford the desired product as a viscous transparent oil (761 mg, 86%).

R_f=0.20 (Hexane/EtOAc 6:4); $[\alpha]_D^{20}$=+14.8 (**70 b**, *c*=1 in $CHCl_3$); ^{1}H NMR (400 MHz, CD_2Cl_2) δ 7.46 – 7.27 (m, 10H), 5.42 – 5.34 (m, 1H, overlapping with solvent signal), 5.29 (d, 1H, *J* = 15.5 Hz), 4.31 – 4.25 (m, 1H), 4.23 – 4.14 (m, 3H), 4.11 (dd, 1H, *J* = 12.9, 2.0 Hz), 3.82 (dd, 1H, *J* = 12.8, 3.2 Hz), 3.61 (s, 3H), 3.26 (dd, 1H, *J* = 17.5, 2.9 Hz), 2.93 (dd, 1H, *J* = 17.5, 5.1 Hz); ^{13}C NMR (101 MHz, CD_2Cl_2) δ 170.9, 166.7, 165.6, 136.0, 129.5, 128.8, 128.4, 127.3, 104.3, 59.0, 55.7, 52.5, 52.1, 47.8, 47.6, 35.4; IR (neat): ν_{max} 2117, 1735, 1660, 1449, 1439, 1362, 1329, 1267, 1216, 1174; MS (ESI) *m/z* calcd for $[C_{22}H_{24}N_5O_4]^+$: 422.18 $[M+H]^+$; found: 422.3.

NHBoc-DKP5-CO_2Me (71 a); NHBoc-DKP7-CO_2Me (71 b)

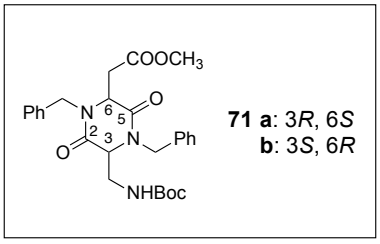

71 a: 3*R*, 6*S*
b: 3*S*, 6*R*

To a solution of azide **70** (751 mg, 1.78 mmol, 1 eq.) in THF (48 ml), under a nitrogen atmosphere and at -20 ºC, 2-(*t*-butoxycarbonyloxyimino)-2-phenylacetonitrile (Boc-ON, 964 mg, 3.92 mmol, 2.2 eq.) and Me_3P (3.57 ml of 1 M solution in toluene, 3.56 mmol, 2 equiv) were added successively. After stirring for 6 h at r.t., the solution was diluted with CH_2Cl_2 and washed with H_2O (3x) and brine. The organic phase was dried over Na_2SO_4 and volatiles were removed under reduced pressure. The residue was purified by flash chromatography on silica gel (CH_2Cl_2/EtOAc, 8:2) to afford the desired product as a white foam (716 mg, 87%).

R_f=0.39 (CH_2Cl_2/EtOAc, 9:1); [*a*]D20=-103.6 (**71 b**, *c*=1.5 in $CHCl_3$); ^{1}H NMR (400 MHz, CD_2Cl_2) δ 7.48 – 7.24 (m, 10H), 5.56 (d, 1H, *J* = 15.3 Hz), 5.12 (d, 1H, *J* = 15.1 Hz), 4.98 (br s, 1H), 4.36 – 4.18 (m, 3H), 4.05 (s, 1H), 3.87 – 3.63 (m, 2H), 3.57 (s, 3H), 3.23 (dd, 1H, *J* = 17.3, 2.7 Hz), 2.92 (dd, 1H, *J* = 17.3, 4.9 Hz), 1.47 (s, 9H); ^{13}C NMR (101 MHz, CD_2Cl_2) δ 170.8, 166.7, 166.4, 156.5, 136.5, 136.3, 129.6, 129.4, 129.2, 128.5, 128.4, 80.3, 59.4, 56.0, 52.5, 48.0, 47.1, 41.5, 35.7, 28.8; IR (neat): ν_{max} 3323, 2978, 1738, 1714, 1658, 1497, 1450, 1366, 1330, 1252, 1202, 1168; MS (ESI) *m/z* calcd for $[C_{27}H_{34}N_3O_6]^+$: 496.24 $[M+H]^+$; found: 496.3.

NHBoc-DKP5-CO_2H (DKP5); NHBoc-DKP7-CO_2H (DKP7)

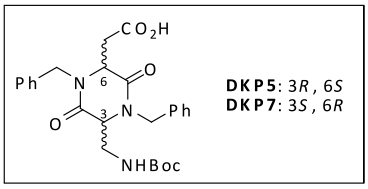

Compound **78** (370 mg, 0.75 mmol, 1 eq.) was dissolved in THF (30 ml) and the mixture was cooled to 0 °C. A solution of LiOH·H_2O (78.3 mg, 1.86 mmol, 2.5 eq.) in H_2O (15 ml) was added dropwise. The resulting solution was let reacting for 1 h at 0 °C. Then, maintaining the temperature at 0 °C, the mixture was acidified with HCl 1M to pH = 1-2, and extracted with CH_2Cl_2 (4x). The collected organic phases were dried over Na_2SO_4 and volatiles removed under reduced pressure. Either **DKP5** or **DKP7** were afforded as a white foam (361 mg, 100%), which was used in subsequent steps without further purification.

2.4 - *DKP8*

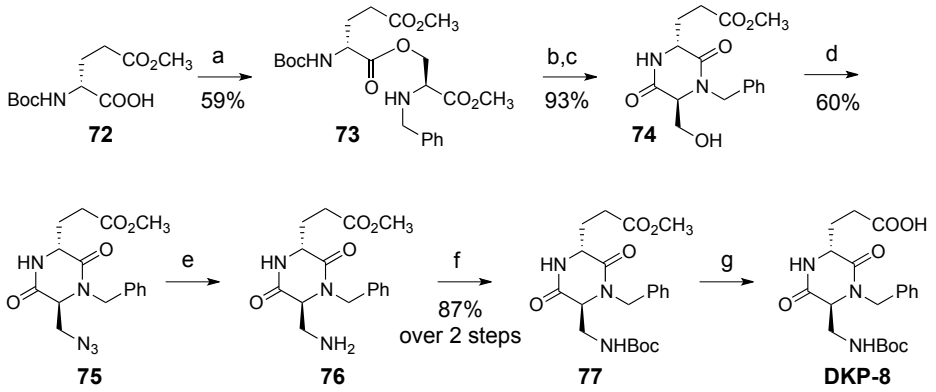

Reagents and conditions: (a) **46**, HATU, HOAt, DIPEA, DMF; (b) TFA/CH_2Cl_2 1:2; (c) DIPEA, *i*PrOH; (d) HN_3, DIAD, PPh_3, CH_2Cl_2/toluene/DMF; (e) H_2, Pd-C, THF; (f) Boc_2O, THF; (g) LiOH, THF/30% H_2O_2 1:1.

(*R*)-*N*-(tert-butoxycarbonyl)glutamic acid γ-methyl ester (72)

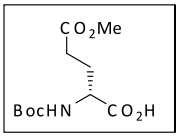

To a flask containing MeOH (4,6 ml) and cooled to -14 °C was slowly added Acetyl chloride (1.3ml, 18.4 mmol, 2.7 eq) followed by D-glutamic acid (1g, 6.8 mmol, 1eq). Cooling bath was removed, and the solution was stirred for 30 min at r.t. and then poured into Et2O (330 mL). The precipitate was filtered off and washed well with Et_2O (50 mL) to give (*R*)- glutamic acid γ-methyl ester hydrochloride (1.25 g, 93%) as a white solid, which was used without further purification.

In a round bottom flask was solved 1 g (5.06 mmol, 1 eq) of (*R*)- glutamic acid γ-methyl ester hydrochloride in 20 mL of THF/water 1:1 solution. The reaction flask was lowered into an ice bath, and triethylamine (2.12 ml, 15.2 mmol, 3 eq.) and Boc_2O (1.21 g, 5.56 mmol, 1.1 eq) were added. After stirring at r.t. for 24 h. The reaction mixture was diluted with 60 mL of EtOAc and washed with aqueous $KHSO_4$ 1M until pH = 3 and brine. The organic phase was dried over Na_2SO_4, filtered and concentrated under reduced pressure. The product was then dried under high vacuum for a few hours affording 1.3 g (98%) of the pure expected product as viscous transparent oil.

(*R*)-1-((*S*)-2-(benzylamino)-3-methoxy-3-oxopropyl)5-methyl2-(tert-butoxycarbonylamino)pentanedioate (73)

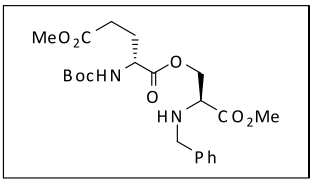

(*R*)-*N*-(tert-butoxycarbonyl)glutamic acid γ-methyl ester **72** (1.0 g, 3.8 mmol, 1.3 eq.) was coupled with (*S*)-*N*-benzylserine methyl ester **47** (607 mg, 2.9 mmol, 1 eq.) according to general procedure **GP2**. The crude product was purified by flash chromatography on silica gel (Hexane/EtOAc, 7:3) to afford the desired product as a transparent oil (774 mg, 59%).

R_f=0.35 (Hexane/EtOAc 7:3); $[\alpha]_D^{20}$=-4 (*c*=1.00 in $CHCl_3$); ^{1}H NMR (400 MHz, $CDCl_3$) δ 7.31 (m,5H), 5.12 (m, 1H), 4.47 (dd, *J* = 11.0, 4.9 Hz, 1H), 4.30 (dd, *J* = 11.0, 4.9 Hz, 1H), 3.90 (d, *J* = 13.1 Hz, 1H), 3.79 – 3.74 (m, 4H), 3.71 (d, *J* = 10.3 Hz, 1H), 3.68 (s, 3H), 3.56 (t, *J* = 4.9 Hz, 1H), 2.49 – 2.34 (m, 2H), 2.17 (dt, *J* = 13.3, 7.4 Hz, 1H), 1.95 (dt, *J* = 14.8, 7.9 Hz, 1H), 1.45 (s, 9H); ^{13}C NMR (101 MHz, CD_2Cl_2) δ 173.7, 173.1, 172.5, 155.8, 140.3, 129.0, 128.8, 127.7, 80.3, 66.2, 59.8, 53.5, 52.7, 52.4, 52.2, 30.5, 28.6, 28.2; IR (neat): ν_{max} 3368, 2976, 2953, 1739, 1716, 1509, 1454, 1367, 1249, 1201, 1166, 1051; MS (ESI) *m/z* calcd for $[C_{22}H_{33}N_2O_8]^+$: 453,22 $[M+H]^+$; found: 453.6.

HO-DKP8-CO_2Me (74)

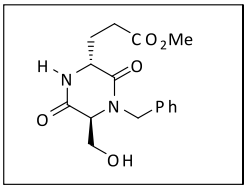

Isopeptide **73** (440 mg, 0.97 mmol, 1 eq.) was deprotected according to general procedure **GP1**. The corresponding trifluoroacetate salt was dissolved in *i*PrOH (12 ml) and *i*Pr_2EtN (0.7 ml, 3.9 mmol, 4 eq.) was added at r.t. The reaction was stirred for 18 h at r.t., monitoring the formation of DKP by TLC (EtOAc). The solution was then concentrated under reduced pressure and the residue was purified by flash chromatography on silica gel (EtOAc) to afford the desired product as a white foam (289 mg, 93%).

R_f=0.12 (EtOAc); $[\alpha]_D^{20}$=+29.5 (*c*=1.00 in $CHCl_3$); ^{1}H NMR (400 MHz, $CDCl_3$) *δ* 7.41 – 7.25 (m, 5H), 5.32 (d, *J* = 15.1 Hz, 1H), 4.43 (t, *J* = 4.4 Hz, 1H), 4.13 (d, *J* = 15.1 Hz, 1H), 3.95 (dd, *J* = 11.7, 2.4

Hz, 2H), 3.80 (t, *J* = 2.1 Hz, 1H), 3.67 (s, 3H), 2.53 – 2.26 (m, 3H), 2.23 – 2.10 (m, 1H); ^{13}C NMR (101 MHz, CD_3OD) δ 174.35, 169.95, 168.69, 136.75, 129.19, 128.77, 128.25, 128.17, 62.82, 61.46, 53.77, 51.51, 47.41, 29.05, 27.25; IR (neat): ν_{max} 3420, 2952, 1732, 1682, 1653, 1496, 1449, 1328, 1259, 1175, 1122, 1070; MS (ESI) *m/z* calcd for $[C_{16}H_{21}N_2O_5]^+$: 321,14 $[M+H]^+$; found: 321.4.

N_3-DKP8-CO_2Me (75)

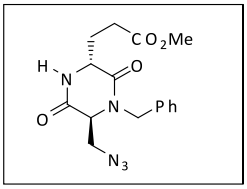

To a solution of diketopiperazine **74** (104 mg, 0.32 mmol, 1 eq.) in CH_2Cl_2/toluene/DMF (3 ml / 2.5 ml / 1 ml), under nitrogen atmosphere and at -20 ºC, PPh_3 (128 mg, 0.49 mmol, 1.5 eq.) was added and the mixture was stirred until a solution was obtained. Hydrazoic acid (1.9 M in toluene, 0.51 ml, 0.97 mmol, 3 eq.) was added followed by dropwise addition of DIAD (0.096 ml, 0.49 mmol, 1.5 eq.) and the reaction was stirred at -20ºC overnight. The reaction mixture was loaded onto a silica gel column (EtOAc/Hexane 8:2) to afford the desired product as a white foam (72 mg, 65%).

R_f=0.52 (EtOAc); $[\alpha]_D^{20}$=+57.9 (*c*=1.00 in $CHCl_3$); ^{1}H NMR (400 MHz, $CDCl_3$) δ 7.44 – 7.30 (m, 3H), 7.30 – 7.23 (m, 2H), 5.15 (d, *J* = 15.0 Hz, 1H), 4.43 (t, *J* = 4.7 Hz, 1H), 4.25 (d, *J* = 15.0 Hz, 1H), 3.94 (d, *J* = 2.7 Hz, 1H), 3.88 (dd, *J* = 12.8, 2.4 Hz, 1H), 3.71 (s, 3H), 3.64 (dd, *J* = 12.7, 3.4 Hz, 1H), 2.61 – 2.46 (m, 2H), 2.34 (dd, *J* = 9.1, 3.7 Hz, 2H); ^{13}C NMR (101 MHz, $CDCl_3$) δ 174.58, 167.72, 167.37, 136.06, 129.82, 128.97, 128.71, 78.02, 77.70, 59.99, 54.39, 52.71, 52.42, 48.51, 30.24, 27.73; IR (neat): ν_{max} 2116, 1733, 1686, 1654, 1437, 1327, 1289, 1258, 1174; MS (ESI) *m/z* calcd for $[C_{16}H_{20}N_5O_4]^+$: 346,15 $[M+H]^+$; found: 346.3.

NHBoc-DKP8-CO_2Me (77)

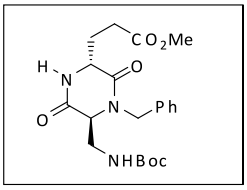

Azide **75** (192 mg, 0.55 mmol, 1 eq.) was dissolved in 12 ml of THF. After addition of 59 mg of Pd/C 10% (0.05 mmol, 0.1 eq.), the mixture was hydrogenated under vigorous stirring over 3 h. Pd/C was then filtered off on a celite pad, which was thoroughly washed with THF. The filtrate was concentrated to dryness, obtaining amine **83** as a white solid, which was dissolved in THF. The mixture was cooled to 0°C before adding Boc anhydride (132 mg, 0.6 mmol, 1.1 eq.) and *i*Pr_2EtN (0.19 ml, 1.1 mmol, 2 eq.). The mixture was afterwards let to reach r.t. and stirred for 18 h. Volatiles were then removed under reduced pressure, and the residue was purified by flash chromatography on silica gel (EtOAc/Hexane, 1:1) to afford the desired product as a white foam (201 mg, 87%).
R_f=0.34 (EtOAc); [*a*]D20=-4.4 (*c*=1.00 in $CHCl_3$); ^{1}H NMR (400 MHz, $CDCl_3$) δ 7.44 (d, *J* = 9.9 Hz, 1H), 7.39 – 7.14 (m, 5H), 5.48 (d, *J* = 15.1 Hz, 1H), 5.29 (s, 1H), 4.25 (t, *J* = 4.4 Hz, 1H), 4.06 (d, *J* = 15.0 Hz, 1H), 3.80 (s, 1H), 3.77 – 3.57 (m, 4H), 3.57 – 3.43 (m, 1H), 2.60 – 2.42 (m, 2H), 2.38 – 2.19 (m, *J* = 6.1 Hz, 2H), 1.43 (s, 9H); ^{13}C NMR (101 MHz, $CDCl_3$) δ 174.56, 168.93, 166.59, 156.62, 136.35, 129.64, 128.92, 128.66, 80.80, 60.21, 53.98, 52.59, 47.78, 41.22, 29.96, 28.96, 28.28; IR (neat): ν_{max} 3298, 2978, 2952, 1689, 1523, 1448, 1393, 1366, 1329, 1253, 1169, 1059; MS (ESI) *m/z* calcd for $[C_{21}H_{30}N_3O_6]^+$: 420.21 $[M+H]^+$; found: 420.3.

NHBoc-DKP8-CO_2H (DKP8)

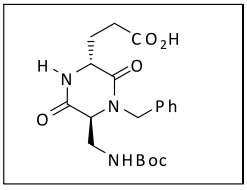

Compound **84** (117 mg, 0.28 mmol, 1 eq.) was dissolved in THF (7 ml). The mixture was cooled to 0°C and a 2.7M solution of LiOOH in H_2O_2 (453 mg of LiOH in 7 ml of H_2O_2 35%) was added dropwise. The mixture was stirred for additional 30 min at 0°C, then warmed up to r.t. and stirred for 7h. After the addition of Na_2SO_3 (30.6 mg, 0.24 mmol, 6 eq.) the reaction mixture was diluted with 8 ml of THF/H_2O 1:1. $KHSO_4$ 1M was added to reach pH = 1-2, and the mixture was extracted with DCM (4x). The collected organic phases were dried over Na_2SO_4 and volatiles removed under reduced pressure, to afford crude **DKP8** as a yellowish solid. Crude product was dissolved in EtOAc and extracted with $NaHCO_3$ sat.; collected aqueous layers were acidified with $KHSO_4$ 1M to reach pH 1-2, and extracted with DCM (4x). Collected organic phases were dried over Na_2SO_4 and volatiles removed under reduced pressure, to afford **DKP8** as a white foam (100 mg, 90%), which was used without further purification.

3 - Synthesis of *cyclic*[DKP-RGD] compounds 18-23

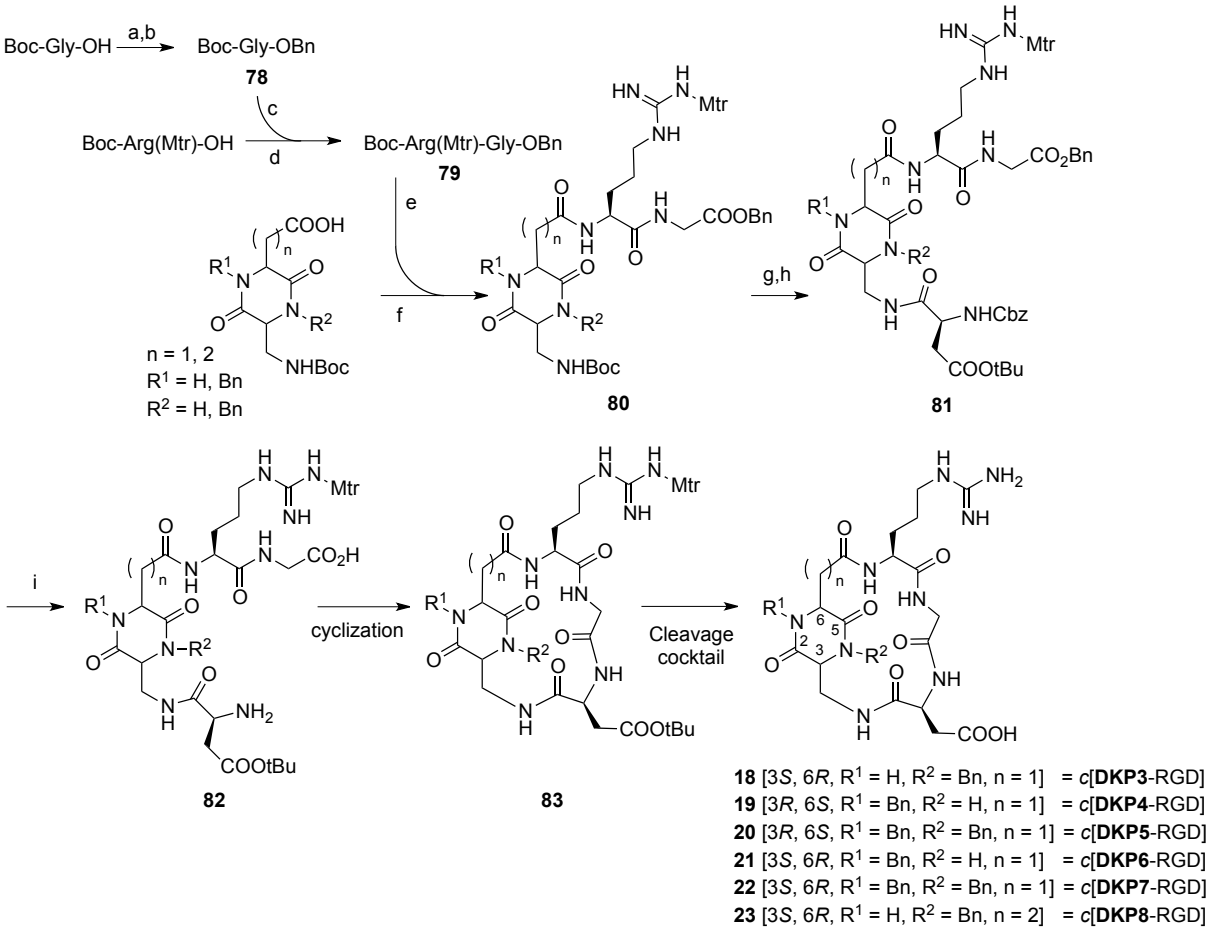

Reagents and conditions: (a) Cs_2CO_3, MeOH; (b) BnBr, DMF: 95%; (c) TFA/DCM 1:2; (d) HBTU, HOBt, DIPEA, DMF: 90%; (e) TFA/DCM 1:2; (f) HATU, HOAt, *i*Pr_2EtN, DMF: 67%; (g) TFA/DCM 1:2; (h) Cbz-Asp(O*t*Bu)-OH, HATU, HOAt, *i*Pr_2EtN, DMF; (i) H_2, Pd/C, THF/H_2O 1:1.

Boc-Arg(Mtr)-Gly-OBn (79)

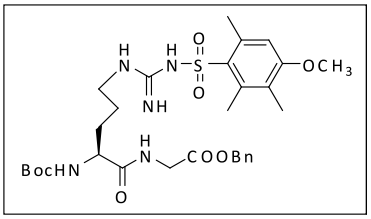

N-Boc glycine benzylester **78** (1.6 mg, 6 mmol, 1.2 eq.) was deprotected according to general procedure **GP1**. The corresponding trifluoroacetate salt was then coupled with Boc-Arg(Mtr)-OH (2.5g, 5.14 mmol, 1 eq.) according to general procedure **GP2**. The residue was purified by flash

chromatography on silica gel (CH_2Cl_2/MeOH; 97:3) to afford the desired product as white foam (2.9 g, 90%).

R_f=0.21 (CH_2Cl_2/MeOH 97:3); $[\alpha]_D^{20}$=-6.0 (*c*=0.5 in $CHCl_3$); ^{1}H NMR (400 MHz, CD_2Cl_2) δ 7.40 - 7.31 (m, 5H), 7.27 (br, 1H), 6.58 (s, 1H), 6.19 (s, 2H), 6.00 (br, 1H), 5.50 (d, 1H, *J* = 6.6), 5.15 (s, 2H), 4.24 (m, 1H), 4.09 (dd, 1H, *J* = 17.5, 6.4), 3.99 (dd, 1H, *J* = 17.9, 5.7), 3.84 (s, 3H), 3.25 (m, 2H), 2.67 (s, 3H), 2.60 (s, 3H), 2.14 (s, 3H), 1.84 (m, 2H), 1.61 (m, 2H), 1.43 (s, 9H); ^{13}C NMR (101 MHz, CD_2Cl_2) δ 172.9, 170.0, 158.5, 156.5, 156.0, 138.4, 136.5, 135.4, 133.4, 128.5, 128.4, 128.2, 124.8, 111.7, 80.1, 67.1, 55.4, 50.5, 41.2, 40.4, 30.0, 28.0, 25.1, 23.8, 18.1, 11.6; IR (neat): ν_{max} 3343, 2937, 1669, 1621, 1555, 1455, 1366, 1307, 1251, 1171, 1120; MS (ESI) *m/z* calcd for $[C_{30}H_{44}N_5O_8S]^+$: 634.29 $[M+H]^+$; found: 634.3.

N-Boc-DKP-Arg(Mtr)-Gly-OBn 80

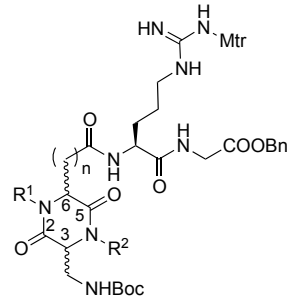

80 **a** [3*S*, 6*R*, R^1 = H, R^2 = Bn, n = 1]
b [3*R*, 6*S*, R^1 = Bn, R^2 = H, n = 1]
c [3*R*, 6*S*, R^1 = Bn, R^2 = Bn, n = 1]
d [3*S*, 6*R*, R^1 = Bn, R^2 = H, n = 1]
e [3*S*, 6*R*, R^1 = Bn, R^2 = Bn, n = 1]
f [3*S*, 6*R*, R^1 = H, R^2 = Bn, n = 2]

a) *N*-Boc-DKP3-Arg(Mtr)-Gly-OBn

Compound **79** (973.5 mg, 1.54 mmol, 1.2 eq.) was deprotected according to general procedure **GP1**. The corresponding trifluoroacetate salt was then coupled with **DKP3** (500 mg, 1.28 mmol, 1 eq.) according to general procedure **GP2**. The residue was purified by flash chromatography on silica gel (CH_2Cl_2/MeOH, 93:7) to afford the desired product as white foam (811 mg, 70%).

R_f=0.34 (CH_2Cl_2/MeOH 9:1); $[\alpha]_D^{20}$=-1.8 (*c*=0.2 in $CHCl_3$); ^{1}H NMR (400 MHz, CD_2Cl_2) δ 7.85 (br, 1H), 7.69 (br, 1H), 7.53 – 7.28 (m, 11H), 6.56 (s, 1H), 6.35 – 6.03 (br, 3H), 5.64 (br, 1H), 5.35 (m, 1H), 5.12 (d, 2H, *J* = 8.3), 4.60 (m, 1H), 4.50 (m, 1H), 4.09 – 4.97 (m, 3H), 3.84 – 3.80 (m, 4H), 3.66 – 3.45 (m, 2H), 3.30 – 2.79 (m, 4H), 2.65 (s, 3H), 2.59 (s, 3H), 2.12 (s, 3H), 1.95 – 1.50 (m, 4H), 1.39 (s, 9H); ^{13}C NMR (101 MHz, CD_2Cl_2) δ 172.5, 170.6, 170.4, 169.9, 167.7, 166.4, 158.5, 156.6, 156.1, 138.4, 136.5, 135.8, 135.4, 133.3, 128.8, 128.5, 128.4, 128.2, 127.9, 124.8, 111.7, 79.8, 67.2, 67.1, 60.0, 55.4, 52.7, 51.5, 47.4, 41.2, 40.8, 39.7, 38.1, 31.6, 29.7, 28.0, 25.1, 23.8, 22.6, 18.1, 13.8, 11.7; IR (neat): ν_{max} 3335, 2937, 1651, 1557, 1455, 1307, 1251; MS (ESI) *m/z* calcd for $[C_{44}H_{59}N_8O_{11}S]^+$: 907.40 $[M+H]^+$; found: 907.6.

b) *N*-Boc-DKP4-Arg(Mtr)-Gly-OBn

Compound **79** (973.5 mg, 1.54 mmol, 1.2 eq.) was deprotected according to general procedure **GP1**. The corresponding trifluoroacetate salt was then coupled with **DKP4** (500 mg, 1.28 mmol, 1 eq.) according to general procedure **GP2**. The residue was purified by flash chromatography on silica gel (CH_2Cl_2/MeOH, 93:7) to afford the desired product as white foam (811 mg, 70%).

R_f=0.36 (CH_2Cl_2/MeOH 9:1); $[\alpha]_D^{20}$=+21.7 (*c*=1 in $CHCl_3$); ^{1}H NMR (400 MHz, Acetone-d_6) δ 7.85 (t, 1H, *J* = 5.8 Hz), 7.61 (d, 1H, *J* = 7.7 Hz), 7.44 – 7.23 (m, 10H), 6.69 (s, 1H), 6.54 (br s, 2H), 6.19 (br s, 1H), 5.24 (d, 1H, *J* = 15.2 Hz), 5.17 (s, 2H), 4.56 – 4.47 (m, 1H, *J* = 8.1 Hz), 4.35 (t, 1H, *J* = 4.8 Hz), 4.17 (d, 1H, *J* = 15.2 Hz), 4.10 (t, 1H, *J* = 5.4 Hz,), 4.00 (d, 2H, *J* = 5.9 Hz), 3.85 (s, 3H), 3.77 – 3.68 (m, 1H), 3.62 – 3.50 (m, 1H), 3.34 – 3.11 (m, 2H), 2.92 (d, 2H, *J* = 5.4 Hz), 2.69 (s, 3H), 2.64 (s, 3H), 2.12 (s, 3H), 1.97 – 1.79 (m, 1H), 1.69 – 1.49 (m, 3H), 1.43 (s, 9H); ^{13}C NMR (101 MHz, Acetone-d_6) δ 138.9, 137.4, 136.9, 135.6, 129.3, 129.1, 128.7, 128.5, 128.2, 124.6, 112.3, 79.3, 66.8, 57.6, 55.9, 55.6, 53.1, 47.4, 42.9, 41.5, 40.8, 37.3, 28.4, 26.1, 24.0, 18.5, 11.9; IR (neat): ν_{max} 3331, 2936, 1681, 1555, 1454, 1392, 1366, 1333, 1306, 1249, 1172, 1120; MS (ESI) *m/z* calcd for $[C_{44}H_{59}N_8O_{11}S]^+$: 907.40 $[M+H]^+$; found: 907.5.

c) *N*-Boc-DKP5-Arg(Mtr)-Gly-OBn

Compound **79** (410 mg, 0.65 mmol, 1.2 eq.) was deprotected according to general procedure **GP1**. The corresponding trifluoroacetate salt was then coupled with **DKP5** (260 mg, 0.54 mmol, 1 eq.) according to general procedure **GP2**. The residue was purified by flash chromatography on silica gel (CH_2Cl_2/MeOH, 97:3) to afford the desired product as white foam (323 mg, 60% yield).

R_f=0.44 (CH_2Cl_2/MeOH, 9:1); $[\alpha]_D^{20}$=-51.2 (*c*=0.6 in $CHCl_3$); ^{1}H NMR (400 MHz, CD_2Cl_2) δ 7.69 (br s, 1H), 7.41 (br s, 1H), 7.38 – 7.22 (m, 15H), 6.57 (s, 1H), 6.26 (br s, 2H), 5.33 (d, 1H, *J* = 15.6 Hz), 5.24 (d, 1H, *J* = 15.3 Hz), 5.12 (s, 2H), 4.77 (br s, 1H), 4.51 – 4.41 (m, 1H), 4.36 (br s, 1H), 4.28 (d, 1H, *J* = 15.5 Hz), 4.17 (d, 1H, *J* = 15.4 Hz), 4.08 – 3.95 (m, 3H), 3.84 (s, 3H), 3.76 – 3.65 (m, 1H), 3.64 – 3.53 (m, 1H), 3.34 – 3.13 (m, 2H), 3.07 (d, 1H, *J* = 13.3 Hz), 2.93 (dd, 1H, *J* = 15.8, 6.6 Hz), 2.66 (s, 3H), 2.58 (s, 3H), 2.11 (s, 3H), 2.01 – 1.88 (m, 1H), 1.75 – 1.48 (m, 3H), 1.42 (s, 9H); ^{13}C NMR (101 MHz, CD_2Cl_2) δ 172.9, 170.6, 170.3, 167.8, 166.7, 159.1, 157.1, 139.1, 137.1, 136.5, 136.1, 134.0, 129.6, 129.5, 129.2, 128.9, 128.9, 128.6, 128.5, 128.4, 125.4, 112.4, 67.7, 59.8, 56.3, 56.1, 47.6, 41.9, 41.6, 41.1, 37.2, 30.3, 29.5, 28.7, 26.2, 24.5, 18.8, 12.3; IR (neat): ν_{max} 3329, 2938, 2357, 2341, 1750, 1719, 1660, 1652, 1557, 1455, 1369, 1301, 1257, 1176, 1121; MS (ESI) *m/z* calcd for $[C_{51}H_{65}N_8O_{11}S]^+$: 997.45 $[M+H]^+$; found: 997.5.

d) *N*-Boc-DKP-6-Arg(Mtr)-Gly-OBn

Compound **79** (973 mg, 1.54 mmol, 1.2 eq.) was deprotected according to general procedure **GP1**. The corresponding trifluoroacetate salt was then coupled with **DKP6** (500 mg, 1.28 mmol, 1 eq.) according to general procedure **GP2**. The residue was purified by flash chromatography on silica gel (CH_2Cl_2/MeOH, 93:7) to afford the desired product as white foam (811 mg, 70%).

R_f=0.38 (CH_2Cl_2/MeOH 9:1); $[\alpha]_D^{20}$=+23.4 (*c*=1 in $CHCl_3$); ^{1}H NMR (400 MHz, Acetone-d_6) δ 7.93 (t, 1H, *J* = 5.8 Hz), 7.73 (d, 1H, *J* = 8.1 Hz,), 7.45 – 7.24 (m, 10H), 6.69 (s, 1H), 6.59 (br s, 2H), 6.24 (br s, 1H), 5.34 (d, 1H, *J* = 15.2 Hz,), 5.16 (s, 2H), 4.68 – 4.58 (m, 1H), 4.34 (t, 1H, *J* = 4.6 Hz), 4.17 (d, 1H, *J* = 15.1 Hz), 4.11 – 3.93 (m, 3H), 3.85 (s, 3H), 3.75 – 3.65 (m, 1H), 3.65 – 3.54 (m, 1H), 3.32 – 3.11 (m, 2H), 3.07 (dd, 1H, *J* = 15.2, 5.8 Hz), 2.97 – 2.85 (m, 1H, overlapping with water signal), 2.70 (s, 3H), 2.65 (s, 3H), 2.11 (s, 3H), 1.92 – 1.80 (m, 1H), 1.67 – 1.47 (m, 3H), 1.42 (s, 9H); ^{13}C NMR (101 MHz, Acetone-d_6) δ 172.5, 170.2, 169.7, 168.7, 167.2, 158.7, 157.4, 157.3, 138.9, 137.1, 136.9, 136.8, 135.6, 129.4, 129.1, 128.8, 128.6, 128.2, 124.6, 112.3, 79.3, 66.9, 57.3, 56.1, 55.7, 52.7, 47.0, 43.1, 41.5, 40.8, 37.1, 30.5, 28.4, 25.7, 24.1, 18.5, 11.9; ; IR (neat): ν_{max} 3329, 2932, 1687, 1560, 1451, 1387, 1361, 1338, 1310, 1243, 1177, 1121; MS (ESI) *m/z* calcd for $[C_{44}H_{59}N_8O_{11}S]^+$: 907.40 $[M+H]^+$; found: 907.5.

e) *N*-Boc-DKP7-Arg(Mtr)-Gly-OBn

Compound **79** (327 mg, 0.52 mmol, 1.1 eq.) was deprotected according to general procedure **GP1**. The corresponding trifluoroacetate salt was then coupled with DKP-7 (227 mg, 0.47 mmol, 1 eq.) according to general procedure **GP2**. The residue was purified by flash chromatography on silica gel (CH_2Cl_2/MeOH, 95:5) to afford the desired product as white foam (286 mg, 61%).

R_f=0.45 (CH_2Cl_2/MeOH 9:1); $[\alpha]_D^{20}$=-55.6 (*c*=0.7 in $CHCl_3$); ^{1}H NMR (400 MHz, Acetone-d_6) δ 7.85 (t, 1H, *J* = 5.7 Hz), 7.55 (d, 1H, *J* = 8.2 Hz), 7.51 – 7.22 (m, 15H), 6.68 (s, 1H), 6.54 (br s, 2H), 6.26 (br s, 1H), 5.92 (br s, 1H), 5.50 (d, 1H, *J* = 15.6 Hz), 5.29 (d, 1H, *J* = 15.3 Hz), 5.16 (s, 2H), 4.68 – 4.56 (m, 1H), 4.32 (d, 2H, *J* = 15.2 Hz), 4.26 – 4.20 (m, 1H), 4.06 (t, 1H, *J* = 3.3 Hz), 4.03 – 3.92 (m, 2H), 3.84 (s, 3H), 3.79 – 3.65 (m, 2H), 3.40 – 3.22 (m, 1H), 3.22 – 2.99 (m, 3H), 2.69 (s, 3H), 2.64 (s, 3H), 2.10 (s, 3H), 1.96 – 1.79 (m, 1H), 1.68 – 1.48 (m, 3H), 1.43 (s, 9H); ^{13}C NMR (101 MHz, Acetone-d_6) δ 171.7, 169.4, 169.1, 166.8, 166.4, 158.0, 156.7, 155.9, 138.3, 136.3, 128.7, 128.5, 128.3, 128.1, 127.6, 127.3, 123.9, 111.6, 78.5, 66.1, 58.9, 55.5, 54.9, 51.8, 46.5, 46.2, 40.8, 40.5, 39.9, 36.1, 27.7, 25.1, 23.4, 17.8, 11.2; IR (neat): ν_{max} 3326, 2936, 2361, 2343, 1748, 1714, 1659, 1650, 1555, 1453, 1366, 1306, 1253, 1172, 1120; MS (ESI) *m/z* calcd for $[C_{51}H_{65}N_8O_{11}S]^+$: 997.45 $[M+H]^+$; found: 997.6.

f) *N*-Boc-DKP8-Arg(Mtr)-Gly-OBn

Compound **79** (200 mg, 0.31 mmol, 1.1 eq.) was deprotected according to general procedure **GP1**. The corresponding trifluoroacetate salt was then coupled with **DKP-8** (116 mg, 0.29 mmol, 1 eq.) according to general procedure **GP2**. The residue was purified by flash chromatography on silica gel (CH_2Cl_2/MeOH, 95:5) to afford the desired product as white foam (163 mg, 61%).

R_f=0.4 (CH_2Cl_2/MeOH 9:1); $[\alpha]_D^{20}$=-2.0 (*c*=0.2 in $CHCl_3$); ^{1}H NMR (400 MHz, CD_3OD) δ 7.42 – 7.26 (m, 10H), 6.67 (s, 1H), 5.39 (d, 1H, *J* = 15.3 Hz), 5.16 (s, 2H), 4.43 – 4.36 (m, 1H), 4.30 (t, 1H, *J* = 3.7 Hz), 4.09 – 4.00 (m, 2H), 3.93 (d, 1H, *J* = 17.6 Hz), 3.84 (s, 3H), 3.82 – 3.73 (m, 2H), 3.45 (d, 1H, *J* = 13.2 Hz), 3.25 – 3.09 (m, 2H), 2.69 (s, 3H), 2.63 (s, 3H), 2.46 – 2.22 (m, 3H), 2.22 – 2.16 (m, 1H), 2.14 (s, 3H), 1.87 – 1.76 (m, 1H), 1.68 – 1.52 (m, 3H), 1.44 (s, 9H); ^{13}C NMR (101 MHz, CD_2Cl_2) δ 173.7, 173.1, 170.3, 168.8, 167.0, 158.8, 157.0, 156.5, 138.8, 136.8, 136.5, 135.8, 133.9, 129.2, 128.9, 128.7, 128.5, 128.3, 125.1, 112.1, 80.0, 67.4, 60.6, 55.8, 53.9, 53.0, 48.0, 41.6, 41.1, 40.8, 31.6, 30.3, 28.4, 28.0, 25.6, 24.2, 18.5, 12.1; IR (neat): ν_{max} 3328, 3066, 3007, 2974, 2937, 1747, 1660, 1550, 1455, 1392, 1366, 1306, 1254, 1173, 1120; MS (ESI) *m/z* calcd for $[C_{45}H_{61}N_8O_{11}S]^+$: 921.42 $[M+H]^+$; found: 921.7.

Cbz-Asp(O*t*Bu)-DKP-Arg(Mtr)-Gly-OBn 81

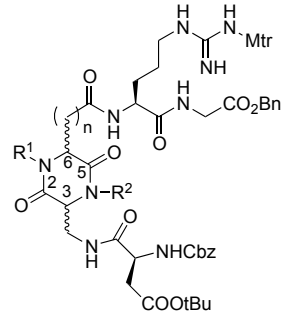

81 **a** [3*S*, 6*R*, R^1 = H, R^2 = Bn, n = 1]
b [3*R*, 6*S*, R^1 = Bn, R^2 = H, n = 1]
c [3*R*, 6*S*, R^1 = Bn, R^2 = Bn, n = 1]
d [3*S*, 6*R*, R^1 = Bn, R^2 = H, n = 1]
e [3*S*, 6*R*, R^1 = Bn, R^2 = Bn, n = 1]
f [3*S*, 6*R*, R^1 = H, R^2 = Bn, n = 2]

a) Cbz-Asp(O*t*Bu)-DKP3-Arg(Mtr)-Gly-OBn

Compound **80 a** (290 mg, 0.32 mmol, 1 eq.) was deprotected according to general procedure **GP1**. The corresponding trifluoroacetate salt was then coupled with Cbz-L-Asp(O*t*Bu)-OH (155 mg, 0.48 mmol, 1.5 eq.) according to general procedure **GP2**. The residue was purified by flash chromatography on silica gel (CH_2Cl_2/MeOH, 9:1) to afford the desired product as white foam (320 mg, 90%).

R_f=0.25 (CH_2Cl_2/MeOH 9:1); $[\alpha]_D^{20}$=-7.0 (*c*=1 in $CHCl_3$); ^{1}H NMR (400 MHz, CD_2Cl_2) δ 7.85 – 7.55 (m, 3H), 7.41 – 7.16 (m, 16H), 6.55 (s, 1H), 6.36 – 6.00 (br, 3H), 5.24 (d, 1H, *J* = 13.9 Hz),

5.17 – 5.03 (m, 3H), 4.92 (d, 1H, *J* = 12.3 Hz), 4.70 – 4.39 (m, 3H), 4.17 (d, 1H, *J* = 14.7 Hz), 4.01 – 3.71 (m, 7H), 3.68 – 3.53 (m, 1H), 3.31 – 2.48 (m, 12H), 2.11 (s, 3H), 2.02 – 1.48 (m, 4H), 1.42 (s, 9H); ^{13}C NMR (101 MHz, CD_2Cl_2) δ 172.5, 172.0, 171.4, 170.6, 170.4, 170.0, 167.5, 166.6, 165.9, 165.7, 158.5, 156.6, 138.4, 136.5, 136.2, 135.8, 135.4, 133.5, 128.8, 128.5, 128.3, 127.9, 127.8, 124.8, 111.7, 81.6, 67.1, 59.5, 55.4, 52.4, 51.7, 51.2, 47.5, 41.2, 40.5, 39.6, 38.6, 37.3, 31.6, 29.7, 27.7, 25.1, 23.8, 22.6, 18.1, 13.8, 11.7; IR (neat): ν_{max} 3327, 2938, 1730, 1651, 1549, 1455, 1367, 1306, 1254, 1158, 1120; MS (ESI) *m/z* calcd for $[C_{55}H_{70}N_9O_{14}S]^+$: 1112.48 $[M+H]^+$; found: 1112.6.

b) Cbz-Asp(O*t*Bu)-DKP4-Arg(Mtr)-Gly-OBn

Compound **80 b** (290 mg, 0.32 mmol, 1 eq.) was deprotected according to general procedure **GP1**. The corresponding trifluoroacetate salt was then coupled with Cbz-L-Asp(O*t*Bu)-OH (124 mg, 0.38 mmol, 1.2 eq.) according to general procedure **GP2**. The residue was purified by flash chromatography on silica gel (CH_2Cl_2/MeOH, 9:1) to afford the desired product as white foam (327 mg, 92%).

R_f=0.45 (CH_2Cl_2/MeOH 9:1); $[\alpha]_D^{20}$=+22.1 (*c*=1 in $CHCl_3$); ^{1}H NMR (400 MHz, Acetone-d_6) δ 7.84 (t, 1H, *J* = 5.8 Hz), 7.77 (t, 1H, *J* = 5.9 Hz), 7.60 (d, 1H, *J* = 8.0 Hz), 7.46 – 7.21 (m, 16H), 6.77 (d, 1H, *J* = 8.2 Hz), 6.69 (s, 1H), 6.54 (br s, 2H), 6.43 – 6.17 (br, 1H), 5.23 (d, 1H, *J* = 15.2 Hz), 5.19 – 5.10 (m, 3H), 5.06 (d, 1H, *J* = 12.5 Hz), 4.58 (td, 1H, *J* = 7.8, 5.6 Hz), 4.53 – 4.46 (m, 1H), 4.43 (t, 1H, *J* = 5.3 Hz), 4.18 (d, 1H, *J* = 15.2 Hz), 4.12 (t, 1H, *J* = 5.3 Hz), 4.06 – 3.93 (m, 2H), 3.93 – 3.81 (m, 4H), 3.70 – 3.59 (m, 1H), 3.31 – 3.11 (m, 2H), 2.97 – 2.89 (m, 2H), 2.87 – 2.77 (m, 1H, overlapping with water signal), 2.76 – 2.58 (m, 7H), 2.12 (s, 3H), 1.97 – 1.77 (m, 1H), 1.70 – 1.48 (m, 3H), 1.42 (s, 9H).; ^{13}C NMR (101 MHz, Acetone-d_6) δ 172.3, 172.0, 170.2, 169.8, 169.4, 168.5, 166.4, 158.4, 157.1, 156.5, 138.7, 137.4, 137.1, 136.6, 135.4, 129.1, 128.8, 128.7, 128.4, 128.2, 127.9, 124.3, 112.0, 80.9, 66.7, 66.6, 57.4, 55.4, 54.7, 47.1, 41.7, 41.3, 40.6, 37.9, 36.9, 29.9, 29.7, 29.6, 29.4, 29.2, 29.0, 28.8, 27.7, 25.8, 23.8, 18.2, 11.6; IR (neat): ν_{max} 3317, 2937, 1726, 1667, 1548, 1454, 1367, 1306, 1254, 1190, 1156, 1120; MS (ESI) *m/z* calcd for $[C_{55}H_{70}N_9O_{14}S]^+$: 1112.48 $[M+H]^+$; found: 1112.5.

c) Cbz-Asp(O*t*Bu)-DKP5-Arg(Mtr)-Gly-OBn

Compound **80 c** (147 mg, 0.15 mmol, 1 eq.) was deprotected according to general procedure **GP1**. The corresponding trifluoroacetate salt was then coupled with Cbz-L-Asp(O*t*Bu)-OH (58 mg, 0.18 mmol, 1.2 eq.) according to general procedure **GP2**. The residue was purified by flash chromatography on silica gel (CH_2Cl_2/MeOH, 95:5) to afford the desired product as white foam (172 mg, 96%).

R_f=0.43 (CH_2Cl_2/MeOH 95:5); $[\alpha]_D^{20}$=-23.6 (*c*=0.7 in $CHCl_3$); ^{1}H NMR (400 MHz, Acetone-d_6) δ 7.89 (t, 1H, *J* = 5.9 Hz), 7.51 – 7.19 (m, 20H), 6.75 – 6.65 (m, 2H), 6.55 (br s, 2H), 6.33 (br s, 1H), 5.39 (d, 1H, *J* = 15.4 Hz), 5.16 (s, 2H), 5.10 (d, 1H, *J* = 13.8 Hz), 5.04 (d, 1H, *J* = 15.5 Hz), 4.59 – 4.49 (m, 3H), 4.46 (d, 1H, *J* = 15.6 Hz), 4.28 (d, 1H, *J* = 15.5 Hz), 4.20 – 4.15 (m, 1H), 4.08 – 3.91 (m, 3H), 3.84 (s, 3H), 3.81 – 3.73 (m, 1H), 3.39 – 3.24 (m, 1H), 3.22 – 3.11 (m, 1H), 3.08 (dd, 1H, *J* = 15.9, 3.5 Hz), 2.92 (dd, 1H, *J* = 15.9, 6.4 Hz), 2.87 – 2.77 (m, 4H), 2.73 – 2.60 (m, 4H), 2.08 (s, 3H, overlapping with solvent signal), 1.95 – 1.81 (m, 1H), 1.69 – 1.50 (m, 3H), 1.42 (s, 9H); ^{13}C NMR (101 MHz, Acetone-d_6) δ 171.7, 171.2, 169.8, 169.4, 166.1, 162.8, 158.0, 156.7, 147.4, 136.9, 136.5, 128.7, 128.6, 128.3, 128.1, 128.0, 127.8, 127.6, 127.3, 111.6, 80.4, 66.3, 66.1, 58.5, 55.9, 54.9, 52.2, 52.0, 46.8, 46.6, 40.9, 40.1, 39.3, 37.2, 35.9, 27.3, 25.6, 23.4, 17.8, 11.2; IR (neat): ν_{max} 3324, 2938, 1731, 1660, 1654, 1546, 1451, 1368, 1310, 1253, 1160, 1122; MS (ESI) *m/z* calcd for $[C_{62}H_{76}N_9O_{14}S]^+$: 1202.52 $[M+H]^+$; found: 1202.5.

d) Cbz-Asp(O*t*Bu)-DKP6-Arg(Mtr)-Gly-OBn

Compound **80 d** (400 mg, 0.44 mmol, 1 eq.) was deprotected according to general procedure **GP1**. The corresponding trifluoroacetate salt was then coupled with Cbz-L-Asp(O*t*Bu)-OH (171 mg, 0.52 mmol, 1.2 eq.) according to general procedure **GP2**. The residue was purified by flash chromatography on silica gel (CH_2Cl_2/MeOH, 9:1) to afford the desired product as white foam (451 mg, 92%).

R_f=0.46 (CH_2Cl_2/MeOH 9:1); $[\alpha]_D^{20}$=+25.1 (*c*=1 in $CHCl_3$); ^{1}H NMR (400 MHz, Acetone-d_6) δ 7.92 (br s, 1H), 7.82 (br s, 1H), 7.70 (br s, 1H), 7.43 – 7.22 (m, 15H), 6.81 (d, 1H, *J* = 8.1 Hz), 6.68 (s, 1H), 6.58 (br s, 2H), 5.31 (d, 1H, *J* = 15.1 Hz), 5.19 – 5.10 (m, 3H), 5.05 (d, 1H, *J* = 12.6 Hz), 4.60 (m, 2H), 4.41 (t, 1H, *J* = 5.1 Hz), 4.17 (d, 1H, *J* = 15.1 Hz), 4.10 – 3.91 (m, 3H), 3.89 – 3.80 (m, 4H), 3.80 – 3.68 (m, 1H), 3.31 – 3.11 (m, 2H), 3.04 (dd, 1H, *J* = 15.3, 5.7 Hz), 2.98 – 2.86 (m, 1H, overlapping with water signal), 2.82 (dd, 1H, *J* = 16.2, 5.4 Hz), 2.70 (s, 3H), 2.65 (s, 3H), 2.11 (s, 3H), 1.92 – 1.79 (m, 1H), 1.70 – 1.46 (m, 3H), 1.41 (s, 9H); ^{13}C NMR (101 MHz, Acetone-d_6) δ 172.7, 172.5, 170.4, 170.2, 169.7, 168.7, 167.0, 158.7, 157.4, 156.9, 138.9, 137.7, 137.1, 136.9, 136.8, 135.6, 129.4, 129.3, 129.1, 129.0, 128.8, 128.7, 128.5, 128.2, 124.6, 112.3, 81.1, 66.9, 57.3, 55.7, 55.3, 52.8, 52.7, 47.1, 44.0, 43.7, 41.9, 41.5, 40.8, 38.6, 38.3, 37.0, 30.5, 28.0, 25.8, 24.1, 18.5, 11.9; IR (neat): ν_{max} 3312, 2943, 1729, 1672, 1553, 1453, 1369, 1309, 1259, 1186, 1161, 1124; MS (ESI) *m/z* calcd for $[C_{55}H_{70}N_9O_{14}S]^+$: 1112.48 $[M+H]^+$; found: 1112.5.

e) Cbz-Asp(O*t*Bu)-DKP7-Arg(Mtr)-Gly-OBn

Compound **80 e** (210 mg, 0.21 mmol, 1 eq.) was deprotected according to general procedure **GP1**. The corresponding trifluoroacetate salt was then coupled with Cbz-L-Asp(O*t*Bu)-OH (82 mg, 0.25 mmol, 1.2 eq.) according to general procedure **GP2**. The residue was purified by flash

chromatography on silica gel (CH_2Cl_2/MeOH, 97:3) to afford the desired product as white foam (226 mg, 90%).

R_f=0.45 (CH_2Cl_2/MeOH 95:5); $[\alpha]_D^{20}$=-28.9 (c=0.8 in $CHCl_3$); ^{1}H NMR (400 MHz, Acetone-d_6) δ 7.85 (t, 1H, J = 5.8 Hz), 7.53 (d, 1H, J = 8.1 Hz), 7.50 – 7.21 (m, 21H), 6.71 (d, 1H, J = 8.3 Hz), 6.67 (s, 1H), 6.53 (br s, 2H), 6.24 (br s, 1H), 5.44 (d, 1H, J = 15.5 Hz), 5.24 (d, 1H, J = 15.2 Hz), 5.18 – 5.10 (m, 3H), 5.07 (d, 1H, J = 12.6 Hz), 4.64 – 4.50 (m, 2H), 4.39 – 4.30 (m, 2H), 4.27 (s, 1H), 4.14 (t, 1H, J = 3.5 Hz), 4.06 – 3.94 (m, 2H), 3.94 – 3.77 (m, 5H), 3.38 – 3.22 (m, 1H), 3.20 – 3.01 (m, 3H), 2.84 – 2.78 (m, 1H, overlapping with water signal), 2.69 (s, 3H), 2.66 – 2.56 (m, 4H), 2.09 (s, 3H), 1.94 – 1.78 (m, 1H), 1.66 – 1.45 (m, 3H), 1.41 (s, 9H); ^{13}C NMR (101 MHz, Acetone-d_6) δ 172.1, 171.5, 170.0, 169.8, 169.5, 167.5, 166.7, 158.4, 157.1, 138.6, 136.7, 136.6, 129.2, 128.9, 128.8, 128.7, 128.6, 128.5, 128.4, 128.2, 127.9, 127.6, 124.3, 111.9, 80.7, 66.6, 66.5, 58.7, 55.9, 55.4, 52.3, 52.2, 47.0, 46.6, 41.2, 40.3, 39.5, 37.7, 36.4, 30.2, 27.7, 25.6, 23.8, 18.2, 11.6; IR (neat): ν_{max} 3322, 2936, 1729, 1659, 1651, 1549, 1454, 1367, 1306, 1256, 1161, 1120; MS (ESI) m/z calcd for $[C_{62}H_{76}N_9O_{14}S]^+$: 1202.52 $[M+H]^+$; found: 1202.5.

f) Cbz-Asp(O*t*Bu)-DKP8-Arg(Mtr)-Gly-OBn

Compound **80 f** (143 mg, 0.16 mmol, 1 eq.) was deprotected according to general procedure **GP1**. The corresponding trifluoroacetate salt was then coupled with Cbz-L-Asp(O*t*Bu)-OH (62 mg, 0.19 mmol, 1.2 eq.) according to general procedure **GP2**. The residue was purified by flash chromatography on silica gel (CH_2Cl_2/EtOH, 95:5) to afford the desired product as white foam (155 mg, 86%).

R_f=0.5 (CH_2Cl_2/MeOH 9:1); $[\alpha]_D^{20}$=-3.0 (c=0.35 in $CHCl_3$); ^{1}H NMR (400 MHz, Acetone-d_6) δ 8.02 (s, 1H), 7.97 – 7.89 (m, 2H), 7.58 (d, 1H, J = 7.9 Hz), 7.39 – 7.21 (m, 15H), 6.87 (d, 1H, J = 8.6 Hz), 6.66 (s, 1H), 6.54 (br s, 2H), 5.31 (d, 1H, J = 15.2 Hz), 5.16 – 5.09 (m, 3H), 5.01 (d, 1H, J = 12.5 Hz), 4.61 – 4.52 (m, 2H), 4.41 (br s, 1H), 4.14 (d, 1H, J = 15.2 Hz), 4.04 (dd, 1H, J = 17.6, 6.0 Hz), 3.95 (dd, 1H, J = 17.6, 5.8 Hz), 3.90 – 3.86 (m, 1H), 3.85 – 3.76 (m, 4H), 3.76 – 3.66 (m, 1H), 3.28 – 3.10 (m, 2H), 2.81 (dd, 1H, J = 16.3, 5.3 Hz), 2.70 – 2.59 (m, 7H), 2.56 – 2.40 (m, 2H), 2.36 – 2.24 (m, 1H), 2.23 – 2.11 (m, 1H), 2.08 (s, 3H), 1.89 – 1.78 (m, 1H), 1.70 – 1.49 (m, 3H), 1.38 (s, 9H); ^{13}C NMR (101 MHz, Acetone-d_6) δ 174.0, 173.2, 172.7, 170.7, 170.5, 168.5, 167.6, 158.9, 157.6, 157.2, 139.1, 137.8, 137.1, 137.0, 135.8, 129.6, 129.3, 129.2, 129.0, 128.8, 128.7, 128.4, 124.9, 112.5, 81.3, 67.3, 67.2, 60.6, 55.9, 54.2, 53.3, 53.0, 48.0, 41.8, 41.1, 40.4, 38.3, 31.9, 30.5, 28.2, 28.0, 26.3, 24.3, 18.7, 12.1; IR (neat): ν_{max} 3309, 2932, 2359, 1731, 1652, 1541, 1455, 1258, 1120; MS (ESI) m/z calcd for $[C_{56}H_{72}N_9O_{14}S]^+$: 1126.49 $[M+H]^+$; found: 1126.7.

H-Asp(O*t*Bu)-DKP-Arg(Mtr)-Gly-OH 82

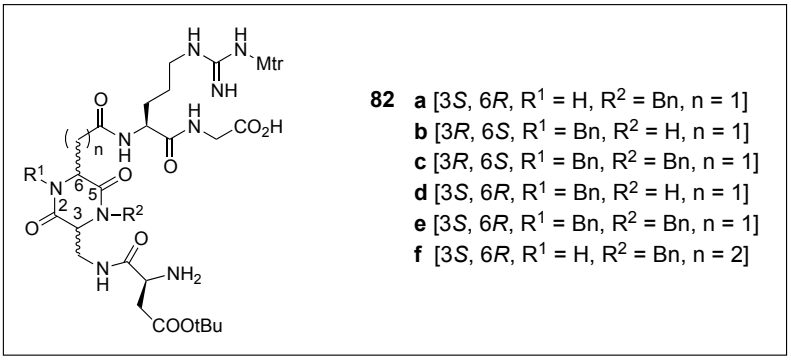

82 **a** [3*S*, 6*R*, R^1 = H, R^2 = Bn, n = 1]
b [3*R*, 6*S*, R^1 = Bn, R^2 = H, n = 1]
c [3*R*, 6*S*, R^1 = Bn, R^2 = Bn, n = 1]
d [3*S*, 6*R*, R^1 = Bn, R^2 = H, n = 1]
e [3*S*, 6*R*, R^1 = Bn, R^2 = Bn, n = 1]
f [3*S*, 6*R*, R^1 = H, R^2 = Bn, n = 2]

a) H-Asp(O*t*Bu)-DKP3-Arg(Mtr)-Gly-OH

Compound **81 a** (307 mg, 0.28 mmol, 1 eq.) was treated with Pd/C 10% (29.3 mg, 0.03 mmol, 0.1 eq.) in the conditions described in general procedure **GP3**. The crude product was obtained as white solid (248 mg, 100%) that was used without further purification.

b) H-Asp(O*t*Bu)-DKP4-Arg(Mtr)-Gly-OH

Compound **81 b** (307 mg, 0.28 mmol, 1 eq.) was treated with Pd/C 10% (29.3 mg, 0.03 mmol, 0.1 eq.) in the conditions described in general procedure **GP3**. The crude product was obtaine as white solid (248 mg, 100%) that was used without further purification.

c) H-Asp(OtBu)-DKP5-Arg(Mtr)-Gly-OH

Compound **81 c** (170 mg, 0.14 mmol, 1 eq.) was treated with Pd/C 10% (14.9 mg, 0.014 mmol, 0.1 eq.) in the conditions described in general procedure **GP3**. The crude product was obtained as white solid (137 mg, 100%) that was used without further purification.

d) H-Asp(O*t*Bu)-DKP6-Arg(Mtr)-Gly-OH

Compound **81 d** (400 mg, 0.36 mmol, 1 eq.) was treated with Pd/C 10% (38.1 mg, 0.04 mmol, 0.1 eq.) in the conditions described in general procedure **GP3**. The crude product was obtained as white solid (322 mg, 100%) that was used without further purification.

e) H-Asp(O*t*Bu)-DKP7-Arg(Mtr)-Gly-OH

Compound **81 e** (218 mg, 0.18 mmol, 1 eq.) was treated with Pd/C 10% (19.3 mg, 0.018 mmol, 0.1 eq.) in the conditions described in general procedure **GP3**. The crude product was obtained as white solid (176 mg, 100%) that was used without further purification.

f) H-Asp(O*t*Bu)-DKP8-Arg(Mtr)-Gly-OH

Compound **81 f** (148 mg, 0.13 mmol, 1 eq.) was treated with Pd/C 10% (13.8 mg, 0.013 mmol, 0.1 eq.) in the conditions described in general procedure **GP3**. The crude product was obtained as white solid (124 mg, 100%) that was used without further purification.

***Cyclo*[Arg(Mtr)-Gly-Asp(O*t*Bu)-DKP] 83**

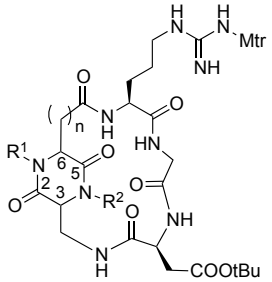

83 **a** [3*S*, 6*R*, R^1 = H, R^2 = Bn, n = 1]
b [3*R*, 6*S*, R^1 = Bn, R^2 = H, n = 1]
c [3*R*, 6*S*, R^1 = Bn, R^2 = Bn, n = 1]
d [3*S*, 6*R*, R^1 = Bn, R^2 = H, n = 1]
e [3*S*, 6*R*, R^1 = Bn, R^2 = Bn, n = 1]
f [3*S*, 6*R*, R^1 = H, R^2 = Bn, n = 2]

a) *Cyclo*[Arg(Mtr)-Gly-Asp(O*t*Bu)-DKP3]

To a solution of **82 a** (80 mg, 0.09 mmol, 1 eq.) in DMF (64 ml), under nitrogen atmosphere and at 0 ºC, DIPEA (92 µl, 0.54 mmol, 6 eq.) and DPPA (58 µl, 0.27 mmol, 3 eq.) were added successively. After stirring the reaction mixture at 0 ºC for 5 h, it was allowed to reach r.t., and stirred for 2 days. DMF was then removed under reduced pressure and the residue was purified by flash chromatography on silica gel (CH_2Cl_2/MeOH, 95:5) to afford the desired product as white foam (58.7 mg, 75%).

R_f=0.34 (CH_2Cl_2/MeOH, 9:1); ^{1}H NMR (400 MHz, CD_3OD) δ 7.33 – 7.14 (m, 5H), 6.57 (s, 1H), 5.06 (d, 1H, *J* = 15.1 Hz), 4.87 – 4.79 (m, 1H), 4.49 – 4.40 (m, 1H), 4.33 (d, 1H, *J* = 17.2 Hz), 3.92 – 3.80 (m, 3H), 3.74 (s, 3H), 3.69 (dd, 1H, *J* = 10.2, 4.6 Hz), 3.45 – 3.34 (m, 2H), 3.10 (t, 2H, *J* = 6.6 Hz), 2.78 (dd, 1H, *J* = 16.4, 8.5 Hz), 2.64 (dd, 1H, *J* = 13.4, 10.1 Hz), 2.58 (s, 3H), 2.51 (s, 3H), 2.46 – 2.33 (m, 2H), 2.03 (s, 3H), 2.01 – 1.76 (m, 2H), 1.58 – 1.37 (m, 2H), 1.32 (s, 9H); ^{13}C NMR (101 MHz, CD_3OD) δ 173.8, 173.3, 172.3, 171.7, 171.2, 159.8, 158.2, 139.5, 137.9, 136.9, 134.9, 130.1, 129.1, 125.7, 114.2, 112.9, 82.4, 60.3, 56.0, 53.2, 50.4, 48.4, 43.6, 39.6, 38.5, 37.1, 28.3, 27.5, 27.0, 24.2, 18.8, 12.1**;** MS (ESI) *m/z* calcd for $[C_{40}H_{56}N_9O_{11}S]^+$: 870.38 $[M+H]^+$; found: 870.8.

b) *Cyclo*[Arg(Mtr)-Gly-Asp(O*t*Bu)-DKP4]

Compound **82 b** (224 mg, 0.25 mmol, 1 eq.) was cyclized in the conditions described in general procedure **GP4**, in presence of HATU (380.2 mg, 1 mmol, 4 eq.), HOAt (136.1 mg, 1 mmol, 4 eq.) and DIPEA (0.26 ml, 1.5 mmol, 6 eq). The crude product was purified by flash chromatography on silica gel (CH_2Cl_2/MeOH, 95:5) to afford yellowish solid that was further purified by Biotage (gradient: 95% H_2O / 5% acetonitrile to 5% H_2O / 95% acetonitrile), to obtain the product as white foam (133 mg, 61%).

R_f=0.45 (CH_2Cl_2/MeOH 9:1); ^{1}H NMR (400 MHz, CD_3OD) δ 7.41 – 7.21 (m, 5H), 6.68 (s, 1H), 5.36 (br s, 1H), 4.53 – 4.41 (m, 1H), 4.39 – 4.28 (m, 1H), 4.24 – 3.89 (m, 3H), 3.85 (s, 1H), 3.78 (d, 1H, *J* = 10.6 Hz,), 3.68 – 3.48 (m, 1H), 3.31 – 3.26 (m, 1H) 3.20 (t, 2H, *J* = 5.7 Hz), 2.98 – 2.86 (m, 1H), 2.83 – 2.72 (m, 2H), 2.72 – 2.56 (m, 7H), 2.14 (s, 3H), 1.89 – 1.75 (m, 1H), 1.74 – 1.52 (m, 3H), 1.49 (s, 9H); ^{13}C NMR (101 MHz, CD_3OD) δ 172.3, 172.1, 169.9, 169.4, 168.4, 166.9, 158.5, 138.1, 136.5, 128.6, 127.5, 124.3, 111.4, 81.3, 56.8, 54.6, 53.2, 41.9, 40.7, 40.1, 35.8, 30.7, 27.8, 26.9, 22.8, 17.3, 10.7; MS (ESI) *m/z* calcd for $[C_{40}H_{56}N_9O_{11}S]^+$: 870.38 $[M+H]^+$; found: 870.4.

c) *Cyclo*[Arg(Mtr)-Gly-Asp(O*t*Bu)-DKP5]

Compound **82 c** (224 mg, 0.25 mmol, 1 eq.) was cyclized in the conditions described in general procedure **GP4**, in presence of HATU (103.4 mg, 0.27 mmol, 4 eq.), HOAt (37.3 mg, 0.27 mmol, 4 eq.) and DIPEA (54 µl, 0.41 mmol, 6 eq). The crude product was purified by flash chromatography on silica gel (CH_2Cl_2/MeOH, 95:5) to afford yellowish solid that was further purified by Biotage (gradient: 95% H_2O / 5% acetonitrile to 5% H_2O / 95% acetonitrile), to obtain the product as white foam (20 mg, 31%).

R_f=0.33 (CH_2Cl_2/MeOH 9:1); ^{1}H NMR (400 MHz, Acetone-d_6) δ 8.00 (d, 1H, *J* = 6.9 Hz), 7.84 (d, 1H, *J* = 6.7 Hz), 7.79 – 7.70 (m, 1H), 7.58 (d, 1H, *J* = 7.7 Hz), 7.48 – 7.17 (m, 10H), 6.69 – 6.62 (m, 2H), 6.52 (br s, 2H), 6.38 (br s, 2H), 5.30 (d, 1H, *J* = 15.4 Hz), 5.24 (d, 1H, *J* = 16.0 Hz), 5.02 (d, 1H, *J* = 8.2 Hz), 4.65 – 4.38 (m, 2H), 4.38 – 3.89 (m, 5H), 3.82 (s, 3H), 3.52 (dd, 1H, *J* = 15.6, 2.3 Hz), 3.42 (dd, 1H, *J* = 13.9, 4.4 Hz), 3.28 – 3.13 (m, 2H), 2.87 (dd, 1H, *J* = 16.2, 8.2 Hz), 2.72 – 2.54 (m, 9H), 2.08 (s, 3H), 1.91 – 1.78 (m, 1H), 1.73 – 1.48 (m, 3H), 1.40 (s, 9H); ^{13}C NMR (101 MHz, Acetone-d_6) δ 172.1, 171.7, 171.6, 169.4, 169.1, 166.9, 158.0, 156.6, 138.5, 138.2, 136.3, 136.1, 128.9, 128.5, 127.9, 127.7, 127.0, 123.9, 111.6, 80.4, 58.9, 58.7, 54.9, 50.8, 49.3, 46.7, 41.9, 40.3, 39.4, 39.2, 36.8, 27.7, 27.3, 26.2, 23.3, 17.7, 11.2; MS (ESI) *m/z* calcd for $[C_{47}H_{62}N_9O_{11}S]^+$: 960.43 $[M+H]^+$; found: 960.7.

d) *Cyclo*[Arg(Mtr)-Gly-Asp(O*t*Bu)-DKP6]

Compound **82 d** (322 mg, 0.36 mmol, 1 eq.) was cyclized in the conditions described in general procedure **GP4**, in presence of HATU (547.2 mg, 1.44 mmol, 4 eq.), HOAt (195.8 mg, 1.44 mmol, 4 eq.) and DIPEA (0.37 ml, 2.2 mmol, 6 eq). The crude product was purified by flash chromatography on silica gel (CH_2Cl_2/MeOH, 95:5) to afford yellowish solid that was further purified by Biotage (gradient: 95% H_2O / 5% acetonitrile to 5% H_2O / 95% acetonitrile), to obtain the product as white foam (180 mg, 58%).

R_f=0.47 (CH_2Cl_2/MeOH 9:1); ^{1}H NMR (400 MHz, DMSO-d_6) δ 9.08 – 8.95 (m, 1H), 8.37 (d, 1H, *J* = 8.2 Hz), 7.95 (br s, 1H), 7.71 – 7.61 (m, 1H), 7.46 (br s, 1H, *J* = 7.6 Hz), 7.39 – 7.22 (m, 5H), 6.88 – 6.64 (m, 2H), 6.55 – 6.25 (m, 1H), 5.14 (d, 1H, *J* = 14.9 Hz), 4.21 (br s, 2H), 4.05 (d, 1H, *J* = 16.0 Hz), 3.99 – 3.92 (m, 1H), 3.90 – 3.75 (m, 5H), 3.63 – 3.43 (m, 3H), 3.01 (m, 2H), 2.88 (dd,

1H, *J* = 16.2, 7.4 Hz), 2.78 – 2.48 (m, 8H, overlapping with solvent signal), 2.44 (dd, 1H, *J* = 16.3, 7.0 Hz), 2.06 (s, 3H), 1.74 – 1.58 (m, 1H), 1.56 – 1.26 (m, 12H); ^{13}C NMR (101 MHz, DMSO-d_6) δ 172.3, 171.6, 170.9, 169.8, 167.4, 166.7, 158.6, 157.2, 138.8, 137.8, 136.7, 135.7, 129.8, 128.8, 128.5, 124.7, 112.9, 81.2, 58.5, 56.6, 55.6, 53.4, 51.5, 47.2, 43.6, 42.1, 36.6, 35.5, 32.4, 29.9, 28.8, 26.8, 24.7, 19.1, 12.9; MS (ESI) *m/z* calcd for $[C_{40}H_{56}N_9O_{11}S]^+$: 870.38 $[M+H]^+$; found: 870.4.

e) *Cyclo*[Arg(Mtr)-Gly-Asp(O*t*Bu)-DKP7]

Compound **82 e** (167 mg, 0.17 mmol, 1 eq.) was cyclized in the conditions described in general procedure **GP4**, in presence of HATU (259.7 mg, 0.68 mmol, 4 eq.), HOAt (93 mg, 0.68 mmol, 4 eq.) and DIPEA (0.17 ml, 1.02 mmol, 6 eq). The crude product was purified by flash chromatography on silica gel (CH_2Cl_2/MeOH, 95:5) to afford yellowish solid that was further purified by Biotage (gradient: 95% H_2O / 5% acetonitrile to 5% H_2O / 95% acetonitrile), to obtain the product (75 mg, 46%) as a 2:1 mixture of two inseparable diastereomers.

R_f=0.32 (CH_2Cl_2/MeOH 9:1); ^{1}H NMR (400 MHz, CD_3OD) δ (two diastereomers A and B; A/B = 2:1) 7.47 – 7.19 (m, $10H_A$+ $10H_B$), 6.70 – 6.65 (m, $1H_A$ + $1H_B$), 5.40 (d, $1H_B$, *J* = 15.2 Hz), 5.35 (d, $1H_B$, *J* = 16.6 Hz), 5.19 (d, $1H_A$, *J* = 14.9 Hz), 5.05 – 4.94 (m, $2H_A$), 4.78 (dd, $1H_A$, *J* = 11.5, 2.1 Hz), 4.57 (t, $1H_B$, *J* = 6.7 Hz), 4.52 (d, $1H_B$, *J* = 16.7 Hz), 4.46 (d, $1H_A$, *J* = 17.4 Hz), 4.43 – 4.39 (m, $1H_B$), 4.34 (d, $1H_B$, *J* = 16.5 Hz), 4.29 – 4.19 (m, $1H_A$ + $2H_B$), 4.13 (d, $1H_A$, *J* = 15.1 Hz), 4.08 – 3.96 (m, $2H_A$), 3.91 (d, $1H_B$, *J* = 15.3 Hz), 3.88 – 3.78 (m, $3H_A$ + $4H_B$), 3.70 (dd, $1H_A$, *J* = 10.4, 4.1 Hz), 3.66 – 3.56 (m, $1H_A$ + $1H_B$), 3.53 – 3.42 (m, $1H_A$ + $1H_B$), 3.28 – 3.09 (m, $2H_A$ + $2H_B$), 3.03 – 2.80 (m, $2H_A$ + $1H_B$), 2.78 – 2.65 (m, $4H_A$ + $4H_B$), 2.63 (s, $3H_B$), 2.60 (s, $3H_A$), 2.58 – 2.43 (m, $1H_A$ + $2H_B$), 2.15 (s, $3H_B$), 2.13 (s, $3H_A$), 2.11 – 2.00 (m, $1H_A$), 1.94 – 1.81 (m, $1H_A$ + $1H_B$), 1.80 – 1.70 (m, $1H_B$), 1.66 – 1.52 (m, $2H_A$ + $2H_B$), 1.49 – 1.44 (m, $9H_A$ + $9H_B$); ^{13}C NMR (101 MHz, CD_3OD) δ (two rotamers) 173.2, 172.2, 171.7, 171.1, 170.7, 170.4, 169.8, 168.5, 167.5, 158.5, 156.7, 138.1, 136.9, 136.5, 135.8, 135.5, 133.5, 128.7, 128.6, 128.5, 128.3, 127.9, 127.8, 127.0, 126.9, 126.1, 124.3, 111.4, 80.9, 59.7, 58.4, 56.9, 56.8, 54.6, 53.8, 50.2, 48.7, 43.2, 42.2, 39.7, 38.2, 35.9, 35.6, 35.1, 28.3, 26.9, 26.0, 25.5, 22.9, 17.4, 13.0, 10.7; MS (ESI) *m/z* calcd for $[C_{47}H_{62}N_9O_{11}S]^+$: 960.43 $[M+H]^+$; found: 960.5.

f) *Cyclo*[DKP-8-Arg(Mtr)-Gly-Asp(O*t*Bu)]

Compound **82 f** (124 mg, 0.13 mmol, 1 eq.) was cyclized in the conditions described in general procedure **GP4**, in presence of HATU (197 mg, 0.52 mmol, 4 eq.), HOAt (70 mg, 0.52 mmol, 4 eq.), and DIPEA (137 µl, 0.8 mmol, 6 eq.). The crude product was purified by flash chromatography on silica gel (CH_2Cl_2/MeOH, 93:7) to afford the desired product as white foam (85 mg, 74%).

R_f=0.4 (CH_2Cl_2/MeOH, 9:1); ^{1}H NMR (400 MHz, CD_3OD) δ 7.41 – 7.22 (m, 5H), 6.66 (s, 1H), 5.31 (d, 1H, *J* = 15.3 Hz), 4.47 (dd, 1H, *J* = 8.4, 4.9 Hz), 4.27 (dd, 1H, *J* = 8.7, 5.8 Hz), 4.18 – 4.08

(m, 2H), 4.05 (d, 1H, *J* = 15.3 Hz), 3.97 (d, 1H, *J* = 16.8 Hz), 3.88 – 3.79 (m, 4H), 3.67 (d, 1H, *J* = 16.8 Hz), 3.55 (d, 1H, *J* = 13.7 Hz), 3.26 – 3.14 (m, 2H), 2.91 (dd, 1H, *J* = 16.6, 4.9 Hz), 2.76 (dd, 1H, *J* = 16.6, 8.4 Hz), 2.71 – 2.56 (m, 7H), 2.56 – 2.42 (m, 2H), 2.12 (s, 3H), 1.86 – 1.52 (m, 5H), 1.44 (s, 9H); ^{13}C NMR (101 MHz, CD_3OD) δ 176.4, 175.9, 175.0, 173.9, 171.6, 171.6, 169.6, 169.5, 159.9, 158.2, 139.5, 138.0, 137.4, 134.8, 130.0, 129.0, 125.7, 112.8, 82.4, 60.4, 56.0, 54.9, 53.0, 52.4, 48.2, 44.0, 41.1, 40.2, 37.5, 31.8, 30.7, 29.0, 28.3, 27.4, 24.4, 18.9, 12.1**;** MS (ESI) *m/z* calcd for $[C_{41}H_{58}N_9O_{11}S]^+$: 884.40 $[M+H]^+$; found: 884.46.

***Cyclo*[Arg-Gly-Asp-DKP]**

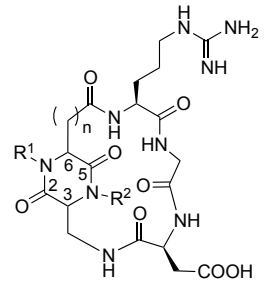

18 [3*S*, 6*R*, R^1 = H, R^2 = Bn, n = 1] = *c*[**DKP3**-RGD]
19 [3*R*, 6*S*, R^1 = Bn, R^2 = H, n = 1] = *c*[**DKP4**-RGD]
20 [3*R*, 6*S*, R^1 = Bn, R^2 = Bn, n = 1] = *c*[**DKP5**-RGD]
21 [3*S*, 6*R*, R^1 = Bn, R^2 = H, n = 1] = *c*[**DKP6**-RGD]
22 [3*S*, 6*R*, R^1 = Bn, R^2 = Bn, n = 1] = *c*[**DKP7**-RGD]
23 [3*S*, 6*R*, R^1 = H, R^2 = Bn, n = 2] = *c*[**DKP8**-RGD]

***Cyclo*[Arg-Gly-Asp-DKP3] 18**

Compound **83 a** (50 mg, 0.06 mmol) was fully deprotected in the conditions described in general procedure **GP5**. The crude product was purified by HPLC (Water's Atlantis 21 mm x 10 cm column, gradient: 90% H_2O / 10% acetonitrile to 70% H_2O / 30% acetonitrile) to give the desired compound (as trifluoroacetate salt) as white solid (34 mg, 80%).

^{1}H NMR (600 MHz, H_2O/D_2O 9:1, T= 298K) δ 8.76 (d, 1H, *J* = 8.2 Hz, Arg-NH), 8.28 (t, 1H, *J* = 6.7 Hz, DKP-NH10), 8.06 (s, 1H, DKP-NH1), 8.02 – 7.95 (m, 1H, Gly-NH), 7.85 (d, 1H, *J* = 8.6 Hz, Asp-NH), 7.37 – 7.18 (m, 5H, H-Ar), 7.10 (t, 1H, *J* = 5.9 Hz, NH-guan), 5.01 (m, 1H, $\underline{CH_2}$-Ph), 4.76 (m, 1H, αH-Asp), 4.48 (m, 1H, DKP-H6), 4.21 (dd, 1H, *J* = 17.7, 8.2 Hz, αH-Gly), 4.16 – 4.00 (m, 3H, DKP-H3 + $\underline{CH_2}$-Ph + αH-Arg), 3.90 (dd, 1H, *J* = 15.8, 7.1 Hz, DKP-H9), 3.63 – 3.47 (m, 2H, DKP-H9 + αH-Gly), 3.13 (dd, 2H, *J* = 13.2, 6.8 Hz, δH-Arg), 2.86 – 2.76 (m, 2H, DKP-H7, βH-Asp), 2.68 (dd, 1H, *J* = 17.1, 7.0 Hz, DKP-H7), 2.56 (dd, 1H, *J* = 14.4, 5.3 Hz, βH-Asp), 1.95 – 1.84 (m, 1H, βH-Arg), 1.77 – 1.66 (m, 1H, βH-Arg), 1.63 – 1.46 (m, 2H, γH-Arg); ^{13}C NMR (151 MHz, D_2O, T= 298K) δ 174.2, 173.9, 173.0, 172.9, 171.0, 170.2, 168.6, 135.1, 128.7, 127.6, 127.5, 59.3, 53.8, 51.9, 49.3, 47.7, 42.4, 40.5, 39.1, 37.8, 34.7, 25.5, 24.4; HRMS (ESI) m/z calcd for $[C_{26}H_{35}N_9O_8Na]^+$: 624.25008 $[M+Na]^+$; found: 624.24928.

***Cyclo*[Arg-Gly-Asp-DKP4] 19**

Compound **83 b** (93.7 mg, 0.11 mmol) was fully deprotected in the conditions described in general procedure **GP5**. The crude product was purified by HPLC (Water's Atlantis 21 mm x 10 cm column, gradient: 90% H_2O / 10% acetonitrile to 70% H_2O / 30% acetonitrile) to give the desired compound as white solid (62 mg, 80%).

^{1}H NMR (400 MHz, H_2O/D_2O 9:1, T= 298K) δ 8.88 (br s, 1H, Asp-NH), 8.37 – 8.23 (m, 2H, Arg-NH + Gly-NH), 8.20 (m, 1H, DKP-NH4), 7.59 (m, 1H, DKP-NH10), 7.35 – 7.19 (m, 5H, H-Ar), 7.11 (t, 1H, J = 6.1 Hz, NH-guan), 5.08 (m, 1H, $\underline{CH_2}$-Ph), 4.35 (m, 1H, αH-Asp), 4.29 – 4.14 (m, 2H, αH-Arg + DKP-H6), 4.01 – 3.82 (m, 2H, αH-Gly + DKP-H3), 3.77 – 3.58 (m, 2H, αH-Gly + DKP-H9), 3.34 (m, 1H, DKP-H9), 3.12 (m, 2H, δH-Arg), 3.01 – 2.67 (m, 4H, DKP-H7 + βH-Asp), 1.85 – 1.43 (m, 4H, βH-Arg + γH-Arg); ^{13}C NMR (101 MHz, D_2O, T= 298K) δ 173.8, 172.8, 170.8, 168.5, 156.8, 135.3, 128.7, 127.6, 57.5, 53.5, 53.3, 52.0, 47.3, 42.3, 40.7, 40.6, 35.7, 34.3, 28.0, 24.4; HRMS (ESI) *m/z* calcd for $[C_{26}H_{35}N_9O_8Na]^+$: 624.25008 $[M+Na]^+$; found: 624.24942.

***Cyclo*[Arg-Gly-Asp-DKP5] 20**

Compound **83 c** (20 mg, 0.02 mmol) was fully deprotected in the conditions described in general procedure **GP5**. The crude product was purified by HPLC (Water's Atlantis 21 mm x 10 cm column, gradient: 90% H_2O / 10% acetonitrile to 30% H_2O / 70% acetonitrile) to give the desired compound (as trifluoroacetate salt) as white solid (9.5 mg, 60%).

^{1}H NMR (400 MHz, H_2O/D_2O 9:1, T= 298K) δ 8.61 – 8.53 (m, 1H, DKP-NH10), 8.48 (d, 1H, J = 6.6 Hz, Arg-NH), 8.42 (d, 1H, J = 8.3 Hz, Asp-NH), 8.23 (d, 1H, J = 9.6 Hz, Gly-NH), 7.44 – 7.19 (m, 10H, H-Ar), 7.11 – 7.03 (m, 1H, NH-guan), 5.10 (m, 1H, $\underline{CH_2}$-Ph), 5.00 (m, 1H, $\underline{CH_2}$-Ph), 4.62 (m, 1H, αH-Asp), 4.41 (m, 1H, DKP-H6), 4.37 (m, 1H, $\underline{CH_2}$-Ph), 4.33 (m, 1H, DKP-H3), 4.32 (m, 1H, DKP-H9), 4.23 (m, 1H, αH-Gly), 4.15 (d, 1H, J = 15.4 Hz, $\underline{CH_2}$-Ph), 4.11 (m, 1H, αH-Arg), 3.42 (d, 1H, J = 17.3 Hz, αH-Gly), 3.34 (m, 1H, DKP-H9), 3.10 (dd, 2H, J = 12.6, 6.6 Hz, δH-Arg), 2.86 (dd, 1H, J = 16.8, 7.8 Hz, βH-Asp), 2.70 (dd, 1H, J = 17.0, 7.2 Hz, βH-Asp), 2.55 (m, 2H, DKP-H7), 1.82 – 1.50 (m, 4H, βH-Arg + γH-Arg); ^{13}C NMR (101 MHz, D_2O, T= 298K) δ 175.0, 174.8, 174.4, 173.7, 173.3, 169.7, 167.8, 136.5, 135.5, 129.1, 129.0, 128.7, 128.5, 127.6, 126.2, 59.5, 55.1, 51.5, 50.1, 48.3, 48.1, 41.9, 40.3, 39.7, 39.4, 38.6, 26.8, 24.3; HRMS (ESI) *m/z* calcd for $[C_{33}H_{41}N_9O_8Na]^+$: 714.29703 $[M+Na]^+$; found: 714.29588.

***Cyclo*[Arg-Gly-Asp-DKP6] 21**

Compound **83 d** (80.2 mg, 0.09 mmol) was fully deprotected in the conditions described in general procedure **GP5**. The crude product was purified by (Water's Atlantis 21 mm x 10 cm column, gradient: 90% H_2O / 10% acetonitrile to 70% H_2O / 30% acetonitrile) to give the desired compound (as trifluoroacetate salt) as white solid (54 mg, 82%).

^{1}H NMR (400 MHz, H_2O/D_2O 9:1, T= 298K) δ 8.80 (d, 1H, *J* = 6.4 Hz, Asp-NH), 8.40 – 8.26 (m, 2H, Gly-NH + Arg-NH), 8.07 (s, 1H, DKP-NH4), 7.89 (t, 1H, *J* = 6.1 Hz, DKP-NH10), 7.40 – 7.22 (m, 5H, H-Ar), 7.10 (t, 1H, *J* = 5.7 Hz, NH-guan), 5.06 (d, 1H, *J* = 17.9 Hz, $\underline{CH_2}$-Ph), 4.35 (m, 1H, αH-Asp), 4.29 (m, 1H, αH-Arg), 4.26 – 4.19 (m, 2H, DKP-H6 + $\underline{CH_2}$-Ph), 3.96 – 3.89 (m, 1H, DKP-H3), 3.90 – 3.75 (m, 2H, αH-Gly + DKP-H9), 3.67 (dd, 1H, *J* = 15.6, 6.1 Hz, αH-Gly), 3.58 – 3.43 (m, 1H, DKP-H9), 3.13 (dd, 2H, *J* = 12.9, 6.9 Hz, δH-Arg), 2.81 – 2.67 (m, 3H, DKP-H7 + βH-Asp), 2.56 (dd, 1H, *J* = 16.1, 8.3 Hz, βH-Asp), 1.84 – 1.48 (m, 4H, βH-Arg + γH-Arg); ^{13}C NMR (101 MHz, D_2O, T= 298K) δ 174.6, 173.3, 172.7, 171.9, 171.0, 168.3, 166.7, 135.3, 129.1, 128.6, 127.6, 57.6, 54.9, 53.1, 51.3, 47.7, 47.1, 42.8, 40.4, 35.4, 35.0, 27.8, 24.2; HRMS (ESI) *m/z* calcd for $[C_{26}H_{35}N_9O_8Na]^+$: 624.25008 $[M+Na]^+$; found: 624.24929.

***Cyclo*[Arg-Gly-Asp-DKP7] 22**

Compound **83 e** (65 mg, 0.068 mmol) was fully deprotected in the conditions described in general procedure **GP5**. The crude product was purified by HPLC (Water's Atlantis 21 mm x 10 cm column, gradient: 90% H_2O / 10% acetonitrile to 40% H_2O / 60% acetonitrile) to give **22A** (as trifluoroacetate salt) (21.3 mg) and **22B** (as trifluoroacetate salt) (10.6 mg) as white solids (60% overall).

22A: ^{1}H NMR (400 MHz, H_2O/D_2O 9:1, T= 298K) δ 8.66 (d, 1H, *J* = 7.7 Hz, Arg-NH), 8.04 (t, 1H, *J* = 6.6 Hz, DKP-NH10), 7.95 – 7.89 (m, 1H, Gly-NH), 7.77 – 7.70 (m, 1H, Asp-NH), 7.44 – 7.16 (m, 10H, H-Ar), 7.10 – 7.04 (m, 1H, NH-guan), 5.06 – 4.99 (m, 1H, $\underline{CH_2}$-Ph), 4.89 (m, 1H, αH-Asp), 4.80 (m, 1H, $\underline{CH_2}$-Ph), 4.69 (m, 1H, DKP-H6), 4.57 (m, 1H, $\underline{CH_2}$-Ph), 4.39 – 4.33 (m, 2H, αH-Gly, DKP-H3), 4.14 – 4.07 (m, 1H, αH-Arg), 4.04 (d, 1H, *J* = 14.8 Hz, $\underline{CH_2}$-Ph), 3.91 (dd, 1H, *J* = 15.4, 7.1 Hz, DKP-H9), 3.71 – 3.61 (m, 1H, DKP-H9), 3.60 – 3.52 (m, 1H, αH-Gly), 3.10 (dd, 2H, *J* = 12.9, 6.9 Hz, δH-Arg), 2.90 – 2.76 (m, 2H, DKP-H7, βH-Asp), 2.62 (dd, 1H, *J* = 17.1, 6.3 Hz, βH-Asp), 2.58 – 2.49 (m, 1H, DKP-H7), 2.01 – 1.87 (m, 1H, βH-Arg), 1.73 – 1.58 (m, 1H, βH-Arg), 1.55 – 1.42 (m, 2H, γH-Arg); ^{13}C NMR (101 MHz, D_2O, T= 298K) δ 174.3, 173.4, 173.0, 172.4, 171.2, 170.6, 169.4, 156.8, 129.3, 129.1, 128.5, 127.8, 126.5, 58.7, 56.9, 53.7, 48.9, 48.3, 47.6, 43.2, 40.9, 39.7, 37.7, 36.9, 25.4, 24.4; HRMS (ESI) *m/z* calcd for $[C_{33}H_{41}N_9O_8Na]^+$: 714.29703 $[M+Na]^+$; found: 714.29618.

22B: ^{1}H NMR (400 MHz, H_2O/D_2O 9:1, T= 298K) δ 8.55 (d, 1H, *J* = 8.1 Hz, Asp-NH), 8.45 (t, 1H, *J* = 5.8 Hz, Gly-NH), 8.34 (d, 1H, *J* = 5.9 Hz, Arg-NH), 7.73 (d, 1H, *J* = 8.4 Hz, DKP-NH10), 7.46 – 7.16 (m, 10H, H-Ar), 7.16 – 7.10 (m, 1H, NH-guan), 5.27 – 5.15 (m, 2H, $\underline{CH_2}$-Ph), 4.52 (m, 1H, αH-Asp), 4.44 (m, 1H, DKP-H6), 4.36 – 4.29 (m, 1H, $\underline{CH_2}$-Ph), 4.20 (d, 1H, *J* = 14.8 Hz, $\underline{CH_2}$-Ph), 4.16 – 4.07 (m, 2H, αH-Arg, DKP-H3), 3.80 (dd, 1H, *J* = 15.2, 4.1 Hz, αH-Gly), 3.76 – 3.63 (m, 2H, αH-Gly, DKP-H9), 3.38 – 3.28 (m, 1H, DKP-H9), 3.16 (dd, 2H, *J* = 13.6, 7.1 Hz, δH-Arg), 2.94 (dd, 1H, *J* = 14.9, 6.1 Hz, DKP-H7), 2.87 – 2.72 (m, 2H, DKP-H7,

βH-Asp), 2.60 (dd, 1H, *J* = 16.6, 7.2 Hz, βH-Asp), 1.77 (dd, 2H, *J* = 15.6, 8.3 Hz, βH-Arg), 1.69 – 1.52 (m, 2H, γH-Arg);^{13}C NMR (101 MHz, D_2O, T= 298K) *δ* 174.5, 174.1, 171.9, 171.6, 170.8, 169.0, 168.3, 136.8, 135.4, 129.2, 129.0, 128.3, 127.8, 127.6, 125.9, 60.7, 56.8, 53.6, 51.4, 49.6, 47.5, 43.5, 40.6, 39.3, 36.7, 35.6, 27.8, 24.7; HRMS (ESI) *m/z* calcd for $[C_{33}H_{41}N_9O_8Na]^+$: 714.29703 $[M+Na]^+$; found: 714.29676.

***Cyclo*[Arg-Gly-Asp-DKP8] 23**

Compound **83 f** (50 mg, 0.06 mmol) was fully deprotected in the conditions described in general procedure **GP5**. The crude product was purified by HPLC HPLC (Water's Atlantis 21 mm x 10 cm column, gradient: 95% H_2O / 5% acetonitrile to 80% H_2O / 20% acetonitrile) to give the desired compound (as trifluoroacetate salt) as white solid (34 mg, 80%).

^{1}H NMR (600 MHz, H_2O/D_2O 9:1, T= 298K) *δ* 8.42 (d, 1H, *J* = 7.3 Hz, Arg-NH), 8.27 (t, 1H, *J* = 6.6 Hz, Gly-NH), 8.16 – 8.14 (m, 2H, Asp-NH, DKP-NH10), 7.75 (s, 1H, DKP-NH1), 7.26 – 7.14 (m, 5H, H-Ar), 7.05 (t, 1H, *J* = 5.9 Hz, NH-guan), 5.03 (d, 1H, *J* = 17.6 Hz, $\underline{CH_2}$-Ph), 4.42 (m, 1H, αH-Asp), 4.16 (q, 1H, *J* = 7.8 Hz, αH-Arg), 4.02 (d, 1H, *J* = 15.9, $\underline{CH_2}$-Ph), 4.05 – 3.96 (m, 2H, DKP-H3, DKP-H6), 3.90 – 3.75 (m, 3H, αH-Gly, DKP-H9), 3.65 (dd, 1H, *J* = 15.0, 6.2 Hz, DKP-H9), 3.10 (q, 2H, *J* = 7.1 Hz, δH-Arg), 2.76 – 2.71 (m, 2H, βH-Asp), 2.50 – 2.30 (m, 3H, DKP-H7, DKP-H8), 1.75 – 1.45 (m, 5H, DKP-H8, βH-Arg, γH-Arg); ^{13}C NMR (151 MHz, D_2O, T= 298K) *δ* 174.9, 174.5, 174.3, 173.8, 171.1, 168.6, 168.2, 157.1, 135.4, 129.1, 128.1, 127.6, 59.3, 53.6, 51.9, 50.9, 47.6, 42.3, 40.6, 39.4, 35.3, 30.3, 29.6, 27.1, 24.5; HRMS (ESI) *m/z* calcd for $[C_{27}H_{37}N_9O_8Na]^+$: 638.26573 $[M+Na]^+$; found: 638.26512.

4 - Synthesis of RGD ligand – Paclitaxel conjugates

4.1 - *Synthesis of aldehyde 14*[a]

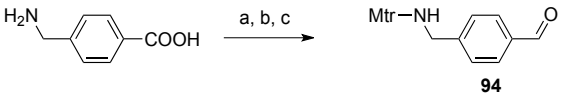

94

[a]Reagents and conditions: (a) $LiAlH_4$, THF, 8 h, reflux, 70%; (b) Mtr-Cl, *i*-Pr_2NEt, THF, 6 h, room temp., 85%; (c) MnO_2, THF, overnight, room temp., quant..

(4-(aminomethyl)phenyl)methanol

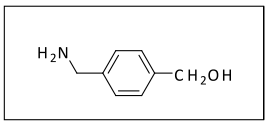

$LiAlH_4$ (2.01 g, 52.92 mmol, 4 equiv) was added in three portions to a stirred suspension of commercially available 4-(aminomethyl)benzoic acid (2 g, 13.23 mmol, 1 equiv) in THF (20 mL) kept at 0 °C. The mixture was heated to reflux and stirred overnight before cooling down again to 0 °C and quenching with H_2O (2 mL) / 15% NaOH (2 mL) / H2O (6 mL). After stirring for 10 min at rt the mixture was filtered on a pad of celite (washing with AcOEt). Evaporation of the filtrate gave (4-(aminomethyl)phenyl)methanol[11] as a white solid (1.27 g, 70% yield), which was used without purification.

4-((4-methoxy-2,3,6-trimethylphenylsulfonyl)aminomethyl)benzylic alcohol

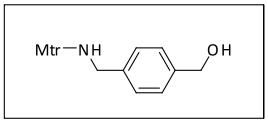

To a solution of (4-(aminomethyl)phenyl)methanol (1.3 g, 9.4 mmol, 1 equiv) and *i*-Pr_2NEt (3.3 mL, 1.88 mmol, 2 equiv) in dry THF (80 mL) at 0 °C under a N_2 atmosphere, 4-methoxy-2,3,6-trimethylbenzene-1-sulfonyl chloride (2.57 g, 10.3 mmol, 1.1 equiv) was added dropwise as a solution

in dry THF (20 mL). After stirring for 30 min, the mixture was warmed up to rt and stirred for 6 h. A white precipitate was formed. The solid was filtered off over a small pad of celite, and volatiles were removed under reduced pressure to obtain viscous pale yellow oil. Dry DCM (5 mL) was then added and this mixture was sonicated for a few minutes, until a white precipitate was formed. This precipitate was collected by filtration on a buchner funnel, washed with a minimum volume of cold DCM, a minimum volume of cold Et_2O and dried to obtain the pure desired 4-((4-methoxy-2,3,6-trimethylphenylsulfonyl)aminomethyl)benzylic alcohol as a white powder (2.79 g, 85% yield).

R_f=0.40 (Hexane/AcOEt 3:7); ^{1}H NMR (400 MHz, CD_3OD) δ 7.22-7.14 (AB system, 4H), 6.76 (s, 1H), 6.63 (t, 1H, J = 6.3 Hz), 4.57 (d, 2H, J = 5.1 Hz), 4.10 (t, 1H, J = 5.1 Hz), 4.05 (d, 2H, J = 6.3 Hz), 3.88 (s, 1H), 2.66 (s, 3H), 2.55 (s, 3H), 2.1 (s, 3H); ^{13}C NMR (101 MHz, acetone-d_6) δ 159.9, 142.4, 139.4, 139.3, 137.2, 131.2, 128.5, 127.2, 127.1, 125.4, 113.0, 64.3, 56.0, 46.8, 24.4, 18.1, 12.0; m.p.: 157-158 °C; IR (film) 3502, 2925, 1579, 1558, 1307, 1140 cm^{-1}; MS (ESI) *m/z* calcd for $[C_{18}H_{24}NO_4S]^+$: 350.14 $[M+H]^+$; found: 350.1.

4-((4-methoxy-2,3,6-trimethylphenylsulfonyl)aminomethyl)benzaldehyde 94

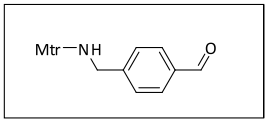

To a solution of alcohol 4-((4-methoxy-2,3,6-trimethylphenylsulfonyl)aminomethyl)benzylic alcohol (2.79 g, 8.0 mmol, 1 equiv) in dry THF (200 mL) at rt, was added activated MnO_2 (7.65 g, 88 mmol, 11 equiv). The mixture was stirred overnight, then filtered over a small pad of celite. The solvent was evaporated to obtain **94** as a white solid. (2.76 g, quantitative yield).

R_f=0.60 (Hexane/AcOEt 1:1); ^{1}H NMR (400 MHz, acetone-d_6) δ 9.97 (s, 1H), 7.76 (d, 2H, J = 8.2 Hz), 7.43 (d, 2H, J = 8.2 Hz), 6.89 (t, 1H, J = 6.5 Hz), 6.73 (s, 1H), 4.21 (d, 2H, J = 6.5 Hz), 3.86 (s, 3H), 2.64 (s, 3H), 2.55 (s, 3H).; ^{13}C NMR (101 MHz, acetone-d_6) δ 192.4, 160.0, 145.7, 139.4, 139.3, 136.6, 130.1, 129.1, 129.0, 125.5, 113.0, 56.0, 46.8, 24.4, 18.1, 12.0; m.p.: brown at 95 °C and melt with decomposition at 145 °C; IR (film) 3320, 2977, 2940, 2848, 1694, 1608, 1308, 1142, 843 cm^{-1}; MS (ESI) *m/z* calcd for $[C_{18}H_{22}NO_4S]^+$: 348.13 $[M+H]^+$; found: 348.2.

4.2 - *Synthesis of DKP-f2 and DKP-f3*[a,b]

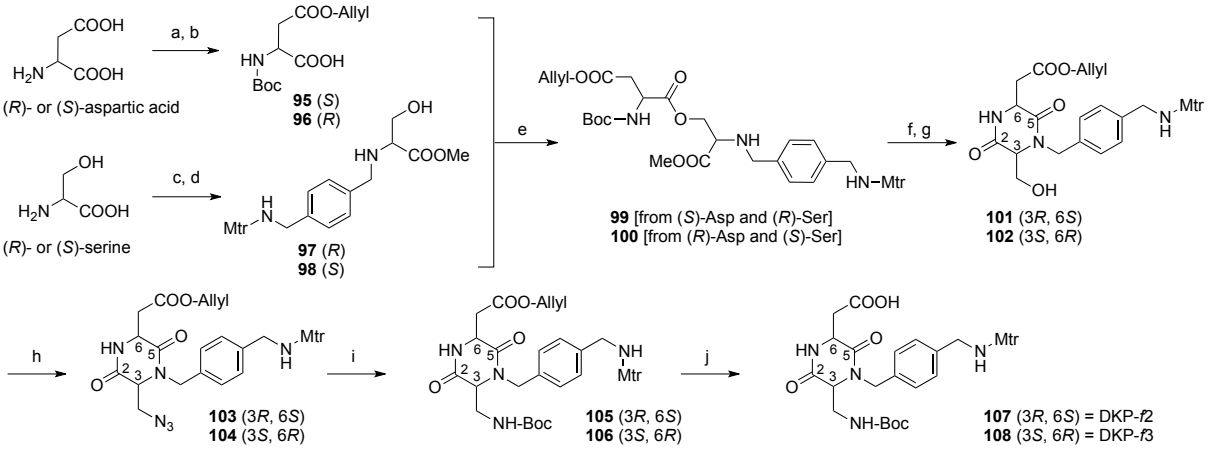

[a]Reagents and conditions: (a) allyl alcohol, AcCl; (b) Boc_2O, TEA, Dioxane, water, 95% over two steps; (c) MeOH, AcCl, quant.; (d) aldehyde **14**, $NaBH(OAc)_3$, THF, 3 h, room temp., quant.; (e) HATU, HOAT, *i*Pr_2NEt, DMF, 3 h, 0 °C to room temp., 86%; (f) TFA/DCM 1:2, 3 h, 0 °C to room temp.; (g) *i*Pr_2NEt, *i*PrOH, 6 h, room temp., 93% over two steps; (h) HN_3Tol, DIAD, Ph_3P, DCM/Tol 1:2, 7 h, -20 °C, 86%; (i) Me_3P, BOC-ON, THF, 6 h, -20 °C to room temp., 88%; (j) pyrrolidine, PPh_3, $[Pd(PPh_3)_4]$, DCM, 4 h, room temp., quant.. [b]Yields reported are the average of six experiments, including different reaction batches with the two enantiomeric products.

(*S*)-4-(allyloxy)-2-((*tert*-butoxycarbonyl)amino)-4-oxobutanoic acid 95

(*R*)-4-(allyloxy)-2-((*tert*-butoxycarbonyl)amino)-4-oxobutanoic acid 96

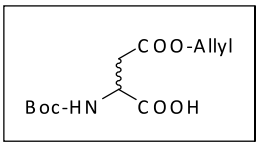

The compounds **95** or **96** were prepared starting from (*S*) or (*R*)-aspartic acid, according to procedures reported by Webster and co-workers.[3]

(*R*)-methyl 3-hydroxy-2-(4-((4-methoxy-2,3,6 trimethylphenylsulfonamido) methyl) benzylamino) propanoate 97

(*S*)-methyl 3-hydroxy-2-(4-((4-methoxy-2,3,6 trimethylphenylsulfonamido) methyl) benzylamino) propanoate 98

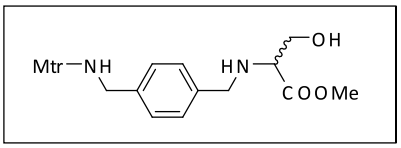

To a suspension of (*S*) or (*R*)-serine methyl ester hydrochloride (1.1 g, 7.0 mmol, 1.2 equiv), 4-((4-methoxy-2,3,6-trimethylphenylsulfonyl)aminomethyl)benzaldehyde **94** (2.0 g, 5.7 mmol, 1 equiv) and TEA (1.2 mL, 8.6 mmol, 1.5 equiv) in dry THF (100 mL) at 25 °C under a N_2 atmosphere, $NaBH(OAc)_3$ (3.6 g, 17.0 mmol, 3 equiv) was added in small portions. The mixture was stirred for 5 h. Then aqueous $NaHCO_3$ was added, and it was extracted with AcOEt (3x60 mL). The organic phases were combined, washed with brine, dried over Na_2SO_4, and volatiles were removed under reduced pressure to afford the desired pure products **97** or **98** as a white solid (2.6 g, 99% yield).

R_f=0.30 (AcOEt 100%); $[\alpha]_D^{20}$ = +19.0 (*c*=1.0 in CH_2Cl_2) for the (*R*)-enantiomer; ^{1}H NMR (400 MHz, CD_2Cl_2) δ 7.21 (d, 2H, *J* = 8.2 Hz), 7.10 (d, 2H, *J* = 8.2 Hz), 6.61 (s, 1H), 4.82 (t, 1H, *J* = 6.3 Hz), 4.01 (d, 2H, *J* = 6.3 Hz), 3.85 (s, 3H), 3.81 (d, 1H, *J* = 13.2 Hz), 3.73-3.70 (m, 4H), 3.65 (d, 1H, *J* = 13.2 Hz), 3.57 (dd, 1H, *J* = 6.3, 10.5 Hz), 3.57 (dd, 1H, *J* = 4.6, 6.3 Hz), 2.65 (s, 3H), 2.51 (s, 3H), 2.11 (s, 3H); ^{13}C NMR (101 MHz, CD_2Cl_2) δ 173.7, 159.8, 139.7, 139.3, 139.0, 136.1, 129.3, 128.7, 128.3, 125.7, 112.6, 62.8, 62.3, 55.9, 52.4, 51.9, 46.9, 24.4, 18.1, 12.1; m.p.: 105-106 °C; IR (film) 3316, 2940, 2848, 1735, 1585, 1562, 1308, 1141 cm^{-1}; MS (ESI) *m/z* calcd for $[C_{22}H_{31}N_2O_6S]^+$: 451.18 $[M+H]^+$; found: 451.2.

(*S*)-4-allyl 1-((*R*)-3-methoxy-2-(4-((4-methoxy-2,3,6-trimethylphenylsulfonamido)methyl)benzylamino)-3-oxopropyl) 2-(*tert*-butoxycarbonylamino)succinate 99

(*R*)-4-allyl 1-((*S*)-3-methoxy-2-(4-((4-methoxy-2,3,6-trimethylphenylsulfonamido)methyl)benzylamino)-3-oxopropyl) 2-(*tert*-butoxycarbonylamino)succinate 100

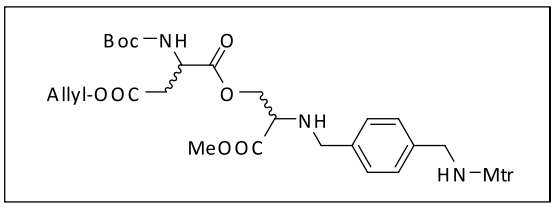

To a solution *N*-(*tert*-butoxycarbonyl)-aspartic acid β-allyl ester (1.9 g, 7.1 mmol, 1.3 equiv), in dry DMF (50 mL) at 0 °C under a N_2 atmosphere, HATU (2.7 g, 7.1 mmol, 1.3 equiv), HOAt (0.97 g, 7.1 mmol, 1.3 equiv) and *i*-Pr_2NEt (1.9 mL, 11.0 mmol, 2 equiv) were added. After stirring the mixture for

30 min, compound **97** or **98** (2.5 g, 5.5 mmol, 1 equiv) was added. The reaction mixture was stirred at 0 ºC for 1 h and at rt overnight. The mixture was diluted with AcOEt (250 mL) and consecutively washed with 1 M $KHSO_4$ (2×50), aqueous $NaHCO_3$ (2×50) and brine (2×50), dried over Na_2SO_4 and the solvent evaporated under reduced pressure to afford the crude product. The residue was purified by flash chromatography on silica gel (Hexane/AcOEt from 7:3 to 5:5, solid load) to afford the desired product **99** or **100** as a transparent oil (3.4 g, 86% yield).

R_f=0.30 (Hexane/AcOEt 6:4); $[\alpha]_D^{20}$=+11.4 (c=1.0 in CH_2Cl_2) for (*S*)-4-allyl 1-((*R*)-3-methoxy-2-(4-((4-methoxy-2,3,6-trimethylphenylsulfonamido)methyl)benzylamino)-3-oxopropyl) 2-(*tert*-butoxycarbonylamino)succinate; ^{1}H NMR (400 MHz, CD_2Cl_2) δ 7.21 (d, 2H, J = 8.1 Hz), 7.09 (d, 2H, J = 8.1 Hz), 6.61 (s, 1H), 5.88 (ddt, 1H, J = 5.7, 10.5, 17.2 Hz), 5.40 (d, 1H, J = 8.2 Hz), 5.28 (dq, 1H, J = 1.3, 17.2 Hz), 5.21 (dq, 1H, J = 1.3, 10.4 Hz), 4.87 (t, 1H, J = 6.2 Hz), 4.59-4.48 (m, 3H), 4.35 (dd, 1H, J = 4.7, 10.9 Hz), 4.28 (dd, 1H, J = 4.7, 10.9 Hz), 4.01 (d, 2H, J = 6.3 Hz), 3.85 (s, 3H), 3.81 (d, 1H, J = 13.3 Hz), 3.70 (s, 3H), 3.63 (d, 1H, J = 13.3 Hz), 3.46 (t, 1H, J = 4.7 Hz), 2.92 (dd, 1H, J = 4.7, 16.9 Hz), 2.80 (dd, 1H, J = 4.7, 16.9 Hz), 2.65 (s, 3H), 2.51 (s, 3H), 2.11 (s, 3H), 1.41 (s, 9H); ^{13}C NMR (101 MHz, CD_2Cl_2) δ 172.7, 171.0, 170.8, 159.8, 155.5, 139.7, 139.3, 139.0, 136.0, 132.3, 129.2, 128.7, 128.3, 125.6, 118.5, 112.5, 80.3, 66.2, 65.9, 59.5, 55.9, 52.4, 51.7, 50.3, 46.9, 37.0, 28.4, 24.4, 18.1, 12.1; IR (film) 3338, 2976, 2940, 1738, 1586, 1563, 1308, 1143 cm^{-1}; MS (ESI) m/z calcd for $[C_{34}H_{48}N_3O_{11}S]^+$: 706.30 $[M+H]^+$; found: 706.3.

HO-(3*R*,6*S*)-DKP-*f*2-COOAllyl 101
HO-(3*S*,6*R*)-DKP-*f*3-COOAllyl 102

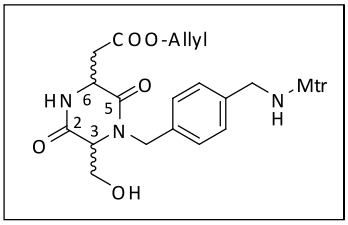

Boc-isopeptide **99** or **100** (3.0 g, 4.3 mmol, 1 equiv) was deprotected according to general procedure **GP1**. The corresponding trifluoroacetate salt was dissolved in *i*PrOH (70 mL) and *i*Pr$_2$EtN (3 mL, 2.28 mmol, 4 equiv) was added at rt. The reaction was stirred for 5 h at rt, then the solution was concentrated under reduced pressure and the residue was purified by flash chromatography on silica gel (AcOEt/Hexane, 8:2) to afford the desired product **101** or **102** as a white foam (2.3, 93% yield).

R_f=0.30 (AcOEt 100%); $[\alpha]_D^{20}$=+26.9 (c=1.0 in CH_2Cl_2) for HO-(3*R*,6*S*)-DKP-*f*2-COOAllyl; ^{1}H NMR (400 MHz, CD_2Cl_2) δ 7.15 (A_2 second order system, 4H), 6.99 (s, 1H), 6.62 (s, 1H), 5.90 (ddt, 1H, J =

5.7, 10.5, 17.2 Hz), 5.30 (dq, 1H, *J* = 1.3, 17.2 Hz), 5.22 (dq, 1H, *J* = 1.3, 10.5 Hz), 5.14-5.10 (m, 2H), 4.59 (dt, 2H, *J* = 1.3, 5.7 Hz), 4.56 (dd, 1H, *J* = 3.9, 8.0 Hz), 4.07 (d, 1H, *J* = 15.2 Hz), 3.99 (d, 2H, *J* = 6.3), 3.92 (1H, dd, *J* = 3.5, 10.5), 3.87-3.77 (m, 4H), 3.73 (br t, 1H), 3.39 (br t, 1H), 3.14 (dd, 1H, *J* = 3.9, 17.4), 2.79 (dd, 1H, *J* = 8.0, 17.4), 2.63 (s, 3H), 2.51 (s, 3H) , 2.12 (s, 3H); ^{13}C NMR (101 MHz, CD_2Cl_2) δ 171.1, 168.5, 166.9, 159.8, 139.3, 139.1, 137.0, 135.8, 132.2, 129.0, 128.7, 128.5, 125.6, 118.7, 112.5, 66.1, 62.3, 62.0, 55.9, 51.4, 47.5, 46.7, 37.3, 24.4, 18.1, 12.1; IR (film) 3346, 2940, 1734, 1675, 1585, 1559, 1458, 1308, 1141 cm^{-1}; MS (ESI) *m/z* calcd for $[C_{28}H_{36}N_3O_8S]^+$: 574.22 $[M+H]^+$; found: 574.2.

N_3-(3*R*,6*S*)-DKP-*f*2-COOAllyl 103

N_3-(3*S*,6*R*)-DKP-*f*3-COOAllyl 104

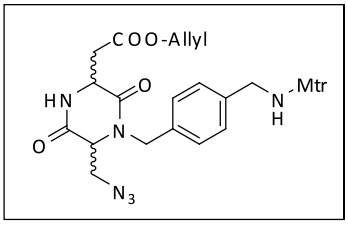

To a solution of diketopiperazine **101** or **102** (1.4 g, 2.44 mmol, 1 equiv) in CH_2Cl_2/toluene (48 mL, 4:6), under nitrogen atmosphere and at -20 ºC, PPh_3 (850 mg, 3.2 mmol, 1.33 equiv) was added and the mixture was stirred until a solution was obtained. Hydrazoic acid (1.5 M in toluene, 10 mL, 15 mmol, 6.25 equiv) was added followed by dropwise addition of DIAD (0.7 mL, 3.5 mmol, 1.4 equiv) and the reaction was stirred overnight at -25 ºC. The reaction mixture was loaded on silica gel without previous evaporation and purified by flash-chromatography (Hexane/AcOEt, from 5:5 to 4:6) to afford the desired product **103** or **104** as a white foam (1.25 g, 86% yield).

R_f=0.3 (Hexane/AcOEt 5:5); $[\alpha]_D^{20}$=-26.1 (*c*=1.0 in CH_2Cl_2) for N_3-(3*R*,6*S*)-DKP-*f*2-COOAllyl; ^{1}H NMR (400 MHz, CD_2Cl_2) δ 7.16 (A_2 second order system, 4H), 6.62 (br s, 2H), 5.92 (ddt, 1H, *J* = 5.7, 10.5, 17.2 Hz), 5.36-5.30 (m, 1H, overlapped with solvent signal), 5.25 (dq, 1H, *J* = 1.3, 10.5 Hz), 5.05 (d, 1H, *J* = 15.2 Hz), 4.86 (br t, 1H, *J* = 6.3 Hz), 4.62 (dt, 2H, *J* = 1.3, 5.7 Hz), 4.56 (dd, 1H, *J* = 3.4, 8.9 Hz), 4.16 (d, 1H, *J* = 15.2 Hz), 4.01 (d, 2H, *J* = 6.3), 3.88-3.82 (m, 5H), 3.64 (dd, 1H, *J* = 3.3, 12.7 Hz), 3.21 (dd, 1H, *J* = 3.6, 17.5 Hz), 2.79 (dd, 1H, *J* = 8.8, 17.5), 2.64 (s, 3H), 2.53 (s, 3H) , 2.12 (s, 3H); ^{13}C NMR (101 MHz, CD_2Cl_2) δ 170.9, 166.3, 166.2, 159.8, 139.3, 139.0, 137.2, 135.6, 132.1, 129.0, 128.7, 128.5, 125.7, 118.8, 112.5, 66.2, 59.7, 55.9, 52.2, 51.4, 47.7, 46.7, 37.5, 24.4, 18.1, 12.1; IR (film) 3269, 2938, 2116, 1735, 1690, 1670, 1585, 1560, 1308, 1141 cm^{-1}; MS (ESI) *m/z* calcd for $[C_{28}H_{35}N_5O_7S]^+$: 599.23 $[M+H]^+$; found: 598.3.

Boc-(3*R*,6*S*)-DKP-*f*2-COOAllyl 105

Boc-(3*S*,6*R*)-DKP-*f*3-COOAllyl 106

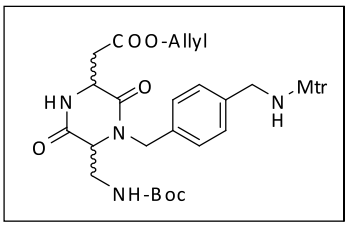

To a solution of azide **103** or **104** (1.2 g, 2 mmol, 1 equiv) in THF (50 mL), under nitrogen atmosphere and cooled to -20 ºC, Me_3P (5.0 mL of 1 M solution in THF, 5 mmol, 2.5 equiv) and 2-(*t*-butoxycarbonyloxyimino)-2-phenylacetonitrile (Boc-ON, 1.2 g, 0.83 mmol, 2.5 equiv) were added. After stirring for 5 h at rt, CH_2Cl_2 (200 mL) was added and the solution was washed with H_2O (3x50 mL) and brine. The organic phase was dried over Na_2SO_4 and volatiles were removed under reduced pressure. The residue was purified by flash chromatography on silica gel (CH_2Cl_2/MeOH, from 99:1 to 95:5) to afford the desired product **105** or **106** as a white foam (1.2 g, 88% yield).

R_f=0.25 (DCM/MeOH 97:3); $[\alpha]_D^{20}$=-26.1 (*c*=1.0 in CH_2Cl_2) for Boc-(3*R*,6*S*)-DKP-*f*2-COOAllyl; ^{1}H NMR (400 MHz, CD_2Cl_2) δ 7.14 (AB system, 4H), 6.82 (br s, 1H) 6.62 (br s, 1H), 5.90 (ddt, 1H, *J* = 5.7, 10.5, 17.2 Hz), 5.31 (dq, 1H, overlapped with solvent signal, *J* = 1.3, 17.2 Hz), 5.23 (dq, 1H, *J* = 1.3, 10.5 Hz), 5.1 (br s, 1H), 4.96 (t, 1H, *J* = 6.3 Hz), 4.60 (dt, 2H, *J* = 1.3, 5.7 Hz), 4.42 (dd, 1H, *J* = 3.6, 8.5 Hz), 4.03-3.99 (m, 3H), 3.85 (s, 3H), 3.73-3.62 (m, 2H), 3.47 (ddd, 1H, *J* = 2.5, 6.2, 14.4), 3.20 (dd, 1H, *J* = 3.6, 17.5 Hz), 2.80 (dd, 1H, *J* = 8.5, 17.5), 2.64 (s, 3H), 2.52 (s, 3H) , 2.11 (s, 3H); ^{13}C NMR (101 MHz, CD_2Cl_2) δ 171.0, 167.4, 165.5, 159.8, 156.2, 139.3, 139.0, 136.9, 135.8, 132.1, 129.0, 128.7, 125.6, 118.8, 112.5, 80.3, 66.1, 60.0, 55.9, 51.2, 47.2, 46.7, 41.1, 37.8, 28.3, 24.4, 18.1, 12.1; IR (film) 3345, 2970, 2939, 1740, 1680, 1652, 1585, 1555, 1455, 1308, 1141 cm^{-1}; MS (ESI) *m/z* calcd for $[C_{33}H_{45}N_4O_9S]^+$: 673.29 $[M+H]^+$; found: 673.3.

Boc-(3*R*,6*S*)-DKP-*f*2-COOH 107 (DKP-*f*2)

Boc-(3*S*,6*R*)-DKP-*f*3-COOH 108 (DKP-*f*3)

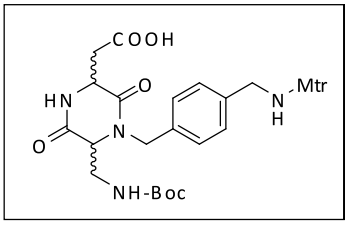

To a solution of allyl ester **105** or **106** (1.2 g, 1.78 mmol, 1 equiv) in CH_2Cl_2 (40 mL), under nitrogen atmosphere and at 0 ºC, pyrrolidine (0.28 mL, 3.56 mmol, 2 equiv), PPh_3 (220 mg, 0.89 mmol, 0.5 equiv) and then $[Pd(PPh_3)_4]$ (170 mg, 0.147 mmol, 0.08 equiv) were added. After stirring for 1 h at 0 ºC, AcOEt (200 mL) was added and the solution was acidified to pH 2 with aqueous $KHSO_4$ (1 M, 100 mL). The organic phase was separated and the aqueous phase was then extracted with AcOEt (2x50 mL). The organic phases were combined, dried over Na_2SO_4 and the solvents were evaporated to afford a white solid (desired product + Ph_3P). The crude was dissolved in DCM and loaded on a small pad of silica gel. Triphenylphosphine was removed washing the silica pad with DCM and then the desired product was eluted with DCM-MeOH 9:1. The acid (**107** or **108**), a white fluffy solid, (1.1 g, 99% yield) was used without further purification.

4.3 - *Synthesis of DKP-f4 and DKP-f6*[a,b]

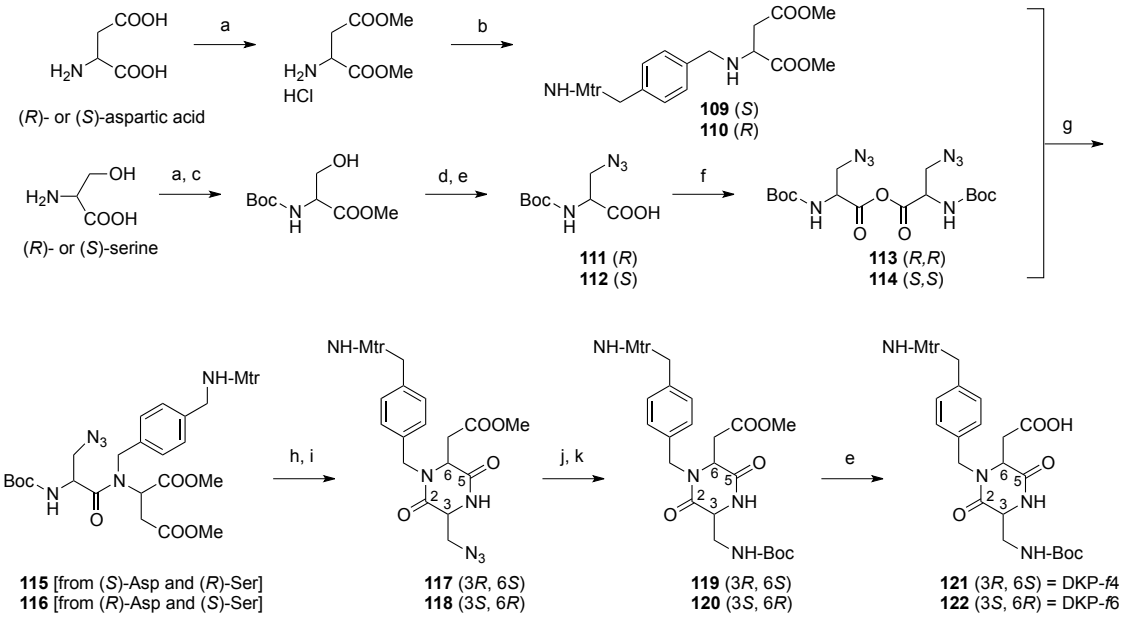

[a]Reagents and conditions: (a) MeOH, AcCl, quant.; (b) aldehyde **94**, $NaBH_3(CN)$, MeOH, 4 h, room temp., 66%; (c) Boc_2O, TEA, dioxane-water, 95%; (d) HN_3Tol, DIAD, Ph_3P, THF, 7 h, -20 °C, 78%; (e) LiOH, H_2O/THF 1:1, 1 h, 0 °C, quant.; (f) DCC, DCM, 1 h, room temp., quant.; (g) DCM, overnight, room temp., 40%; (h) TFA, Et_3SiH, DCM, 3 h, room temp., quant.; (i) *i*Pr_2NEt, *i*PrOH, 6 h, room temp., 92%; (j) H_2, 10% Pd/C, THF, 4 h, room temp., quant.; (k) Boc_2O, *i*Pr_2NEt, DCM, 6 h, room temp., 96%. [b]Yields reported are the average of six experiments, including different reaction batches with the two enantiomeric products.

(*S*)-dimethyl-2-(4-((4-methoxy-2,3,6-trimethylphenylsulfonamido)methyl)benzylamino) succinate 109

(*R*)-dimethyl-2-(4-((4-methoxy-2,3,6-trimethylphenylsulfonamido)methyl)benzylamino) succinate 110

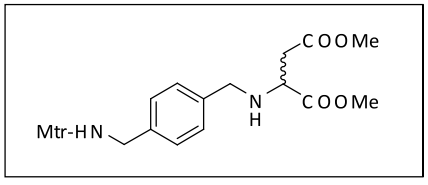

To a vigorously stirred solution of (*S*)- or (*R*)-dimethylaspartate hydrochloride (490 mg, 2.5 mmol, 1 equiv) and sodium cyanoborohydride (160 mg, 2.5 mmol, 1 equiv) in methanol (12 mL), *N*-(4-formylbenzyl)-4-methoxy-2,3,6-trimethylbenzenesulfonamide **94** (870 mg, 2.5 mmol, 1 equiv) was

added in one portion at rt under N_2. After being stirred for 4 h, the mixture was cooled to 0 °C and the pH was lowered to approximately 1 with a few drops of 37% aqueous HCl (v/v). The mixture was allowed to warm and stirred at rt for 2 h. The solvent was removed under reduced pressure at rt, the residue was suspended in a small volume of water and the pH was adjusted to 7 with an aqueous $NaHCO_3$ solution. AcOEt was added and the mixture was stirred for a few minutes. Then, the emulsion was filtered over a small pad of celite to afford a separable mixture. The aqueous phase was extracted 3 times with AcOEt and the organic phases were collected, dried with Na_2SO_4 and the solvent was evaporated to afford a clear oil.

This oil was dissolved in THF (50 mL) and treated with an excess of activated MnO_2: in this way, the small amount (ca. 10%) of benzyl-alcoholic byproduct [*i.e.* *N*-(4-(hydroxymethyl)benzyl)-4-methoxy-2,3,6-trimethylbenzenesulfonamide] was re-oxidized to aldehyde **94**, which is less polar with respect to the alcohol (which co-eluted with the desired product). The mixture was stirred for 4 h, filtered over a pad of celite and the solvent was evaporated under reduced pressure. The brown oil was purified by column chromatography on silica gel (Hexane/AcOEt, 1:1) to afford the desired product **109** or **110** as a viscous transparent oil (800 mg, 66% yield).

R_f=0.45 (Hexane/AcOEt, 1:1); $[\alpha]_D^{20}$=-20.5 (*c*=1.0 in CH_3OH) for the (*S*)-enantiomer; ^{1}H NMR (400 MHz, CD_2Cl_2) δ 7.18 (AB system, 4H), 6.66 (s, 1H), 4.88 (t, 1H, *J* = 5.6 Hz), 4.06 (d, 2H, *J* = 6.3 Hz), 3.90 (s, 3H), 3.85 (d, 1H, *J* = 13.9 Hz), 3.75 (s, 3H), 3.69-3.61 (m, 5H), 2.77-2.64 (m, 5H), 2.56 (s, 3H), 2.16 (s, 3H); ^{13}C NMR (101 MHz, CD_2Cl_2) δ 174.2, 171.5, 159.7, 139.9, 139.2, 139.0, 135.9, 129.2, 128.6, 128.2, 125.6, 112.5, 57.4, 55.9, 52.3, 52.0, 51.8, 46.9, 38.3, 24.4, 18.1, 12.1; IR (film) 3356, 2940, 2847, 1736, 1585, 1562, 1308, 1141 cm^{-1}; MS (ESI) *m/z* calcd for. $[C_{24}H_{33}N_2O_7S]^+$: 493.20 $[M+H]^+$; found: 493.2.

(*S*)-dimethyl-2-((*R*)-3-azido-2-(*tert*-butoxycarbonylamino)-*N*-(4-((4-methoxy-2,3,6-trimethylphenylsulfonamido)methyl)benzyl)propanamido)succinate 115
(*R*)-dimethyl-2-((*S*)-3-azido-2-(*tert*-butoxycarbonylamino)-*N*-(4-((4-methoxy-2,3,6-trimethylphenylsulfonamido)methyl)benzyl)propanamido)succinate 116

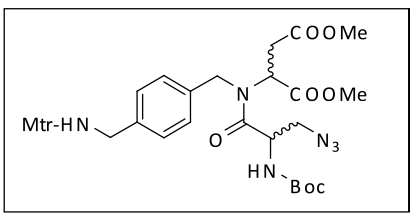

N-Boc-Ser(N_3)-OMe (1.96 g, 8.0 mmol, 5 equiv) was dissolved in THF (120 mL) and treated dropwise at 0 °C with a solution of $LiOH·H_2O$ (840 mg, 20 mmol, 12.5 equiv) in H_2O (60 mL). The resulting

solution was stirred for 1 h at 0 °C. The mixture was then acidified with 1M HCl to pH 1-2 at 0 °C and the resulting solution was extracted with AcOEt (4x100 mL). The collected organic phases were dried over Na_2SO_4 and volatiles were removed under reduced pressure, to afford the crude acid **111** or **112** as a viscously oil, which was used without further purification.

(*S*)- or (*R*)-3-azido-2-(*tert*-butoxycarbonylamino) propanoic acid **111** or **112** (1.84 g, 8.0 mmol, 5 equiv) was dissolved in CH_2Cl_2 (12 mL) and then DCC (826 g, 4 mmol, 2.5 equiv) was added in one portion. A white precipitate (DCU) was formed and stirring was continued for 1h at rt. The mixture was then filtered on cotton funnel to remove DCU, which was washed with cold CH_2Cl_2. The filtrate and the washings were concentrated under reduced pressure at rt, to afford symmetric anhydride **113** or **34** as a pale yellow foam, which was immediately used without further purification.

(*S*)- or (*R*)-*N*-(*N*-Mtr-aminomethylbenzyl)-Asp(OMe)-OMe **109** or **110** (780 mg, 1.59 mmol, 1 equiv) was dissolved in CH_2Cl_2 (12 mL) and cooled to 0 °C. A solution of symmetric anhydride in CH_2Cl_2 (8 mL) was added dropwise and very slowly. The reaction was warmed up to rt and stirred overnight. Then solvent was removed under reduced pressure and the residue was purified by flash chromatography on silica gel (Hexane/AcOEt, 6:4) to afford the desired product **115** or **116** as a viscous transparent oil (440 mg, 40% yield).

R_f=0.43 (Hex/AcOEt 1:1); $[\alpha]_D^{20}$=-31.6 (*c*=0.5 in CH_2Cl_2) for (*S*)-dimethyl-2-((*R*)-3-azido-2-(*tert*-butoxycarbonylamino)-*N*-(4-((4-methoxy-2,3,6-trimethylphenylsulfonamido)methyl)benzyl) propanamido) succinate; ^{1}H NMR (400 MHz, CD_2Cl_2) (rotamers ratio in CD_2Cl_2 A/B = 4:1) δ 7.34 – 7.17 (m, $4H_A$), 7.12 – 7.01 (m, $4H_B$), 6.66 – 6.60 (m, $1H_A$ + $1H_B$), 5.49 (d, $1H_B$, J = 8.2 Hz), 5.26 (d, $1H_A$, J = 8.5 Hz), 5.14 – 5.07 (m, $1H_B$), 4.99 – 4.92 (m, $1H_B$), 4.78 (t, $1H_A$, J = 6.3 Hz), 4.74 – 4.60 (m, $3H_A$ + $1H_B$), 4.36 (t, $1H_A$, J = 6.4 Hz), 4.29 (d, $1H_B$, J = 15.9 Hz), 4.05 – 3.96 (m, $2H_A$ + $2H_B$), 3.85 (s, $3H_A$ + $3H_B$), 3.71 – 3.53 (m, $6H_A$ + $8H_B$), 3.45 (dd, $1H_A$, J = 12.3, 6.3 Hz), 3.34 (dd, $1H_A$, J = 12.3, 6.1 Hz), 3.22 (dd, $1H_A$, J = 16.9, 7.3 Hz), 2.98 (dd, $1H_B$, J = 17.3, 7.0 Hz), 2.72 – 2.61 (m, $3H_A$ + $4H_B$), 2.60 – 2.45 (m, $4H_A$ + $3H_B$), 2.14 (s, $3H_A$ + $3H_B$), 1.50 – 1.35 (m, $9H_A$ + $9H_B$); ^{13}C NMR (101 MHz, CD_2Cl_2) δ 171.6, 171.0, 170.0, 159.8, 155.2, 139.3, 139.0, 137.3, 135.6, 129.4, 128.8, 128.2, 127.8, 125.7, 112.5, 80.7, 57.8, 56.7, 55.9, 53.1, 52.8, 52.4, 52.2, 51.1, 50.7, 47.5, 46.7, 35.0, 34.6, 28.3, 24.4, 18.1, 12.1; IR (film) 3301, 2933, 2112, 1736, 1691, 1670, 1585, 1561, 1307, 1140 cm^{-1}; MS (ESI) m/z calcd for $[C_{32}H_{45}N_6O_{10}S]^+$: 705.29 $[M+H]^+$; found: 705.4.

N_3-(3*R*,6*S*)-DKP-*f*4-COOMe 117

N_3-(3*S*,6*R*)-DKP-*f*6-COOMe 118

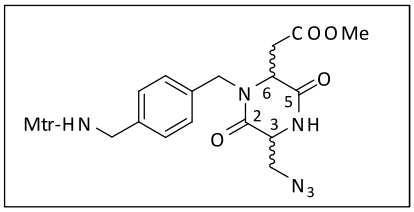

Dipeptide-N_3 **115** or **116** (400 mg, 0.57 mmol, 1 equiv) was deprotected according to general procedure **GP1**, with the addition of Et_3SiH (0.23 mL, 1.43 mmol, 2.5 equiv) as ion scavenger. The corresponding trifluoroacetate salt was dissolved in *i*PrOH (8 mL) and *i*Pr_2EtN (0.4 mL, 2.28 mmol, 4 equiv) was added at rt. The reaction was stirred for 5 h at rt, then the solution was concentrated under reduced pressure and the residue was purified by flash chromatography on silica gel (AcOEt/Hexane, 8:2) to afford the desired product **117** or **118** as a white foam (300 mg, 92% yield).

R_f=0.49 (AcOEt); $[\alpha]_D^{20}$=+15.6 (*c*=0.5 in CH_2Cl_2) for N_3-(3*R*,6*S*)-DKP-*f*4-COOMe; ^{1}H NMR (400 MHz, CD_2Cl_2) δ 7.17 – 7.10 (m, 4H), 6.62 (s, 1H), 6.59 (s, 1H), 5.08 (d, 1H, *J* = 15.3 Hz), 4.92 (t, 1H, *J* = 6.3 Hz), 4.46 – 4.40 (m, 1H), 4.08 (d, 1H, *J* = 15.3 Hz), 4.04 – 3.97 (m, 3H), 3.90 – 3.82 (m, 4H), 3.79 (dd, 1H, *J* = 12.6, 3.5 Hz), 3.60 (s, 3H), 3.00 (dd, 1H, *J* = 17.5, 3.4 Hz), 2.80 (dd, 1H, *J* = 17.5, 5.0 Hz), 2.64 (s, 3H), 2.52 (s, 3H), 2.12 (s, 3H); ^{13}C NMR (101 MHz, CD_2Cl_2) δ 170.7, 167.7, 164.9, 159.8, 139.3, 139.0, 137.1, 135.5, 128.8, 128.3, 125.7, 112.5, 56.2, 55.9, 54.6, 53.7, 52.4, 47.3, 46.7, 34.9, 24.4, 18.1, 12.1; IR (film) 3265, 2933, 2110, 1735, 1690, 1671, 1586, 1559, 1308, 1141 cm^{-1}; MS (ESI) m/z calcd for $[C_{26}H_{33}N_6O_7S]^+$: 573.21 $[M+H]^+$; found: 573.5.

Boc-(3*R*,6*S*)-DKP-*f*4-COOMe 119

Boc-(3*S*,6*R*)-DKP-*f*6-COOMe 120

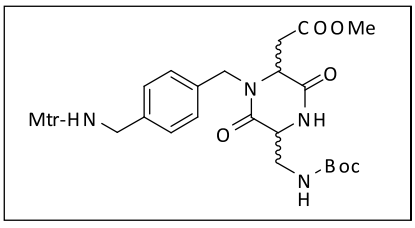

A solution of azide **117** or **118** (300 mg, 0.52 mmol, 1 equiv) in THF (45 mL) was treated with 10% Pd/C (56 mg, 0.052 mmol, 0.1 equiv), and the flask was purged three times with vacuum/H_2. The mixture was stirred at rt for 4 h under H_2 atmosphere, then filtered through a pad of Celite and the

Celite cake was washed thoroughly with THF. The solvent was removed under vacuum to give the crude amine as a white foam (280 mg, 99% yield), which was used without further purification.

To a solution of the crude amine (280 mg, 0.52 mmol, 1 equiv) in DCM (40 mL) at 0 °C, *i*-Pr_2NEt (0.17 mL, 1.0 mmol, 2 equiv) and Boc_2O (132 mg, 0.6 mmol, 1.2 equiv) were added. The mixture was stirred at rt for 6 h, the solvent was evaporated and the crude compound was purified over a small pad of silica gel with AcOEt as eluent, to afford the desired product **119** or **120** as a white foam (320 mg, 96% yield).

R_f=0.59 (AcOEt); $[\alpha]_D^{20}$=+60.0 (*c*=1.00 in CH_2Cl_2) for Boc-(3*R*,6*S*)-DKP-*f*4-COOMe; ^{1}H NMR (400 MHz, CD_2Cl_2) δ 7.17 – 7.06 (m, 5H), 6.62 (s, 1H), 5.39 (t, 1H, *J* = 6.0 Hz), 5.27 (t, 1H, *J* = 5.9 Hz), 4.97 (d, 1H, *J* = 15.3 Hz), 4.29 (t, 1H, *J* = 4.4 Hz), 4.14 (d, 1H, *J* = 15.3 Hz), 4.03 – 3.96 (m, 3H, *J* = 6.1 Hz), 3.85 (s, 3H), 3.66 (ddd, 1H, *J* = 14.2, 6.6, 4.3 Hz), 3.59 (s, 3H), 3.57 – 3.48 (m, 1H), 2.92 (dd, 1H, *J* = 17.1, 4.1 Hz), 2.76 (dd, 1H, *J* = 17.1, 5.1 Hz), 2.63 (s, 3H), 2.52 (s, 3H), 2.11 (s, 3H), 1.41 (s, 9H); ^{13}C NMR (101 MHz, CD_2Cl_2) δ 170.7, 167.8, 166.5, 159.7, 157.2, 139.3, 139.1, 137.1, 135.7, 128.7, 128.1, 125.6, 112.5, 80.1, 56.8, 56.0, 55.9, 52.4, 47.6, 46.6, 42.7, 35.3, 28.4, 24.4, 18.1, 12.1; IR (film) 3340, 2971, 2937, 1741, 1681, 1650, 1586, 1554, 1455, 1307, 1141 cm^{-1}; MS (ESI) m/z calcd for $[C_{31}H_{43}N_4O_9S]^+$: 647.27 $[M+H]^+$; found: 647.4

Boc-(3*R*,6*S*)-DKP-*f*4-COOH 121 (DKP-*f*4)

Boc-(3*S*,6*R*)-DKP-*f*6-COOH 122 (DKP-*f*6)

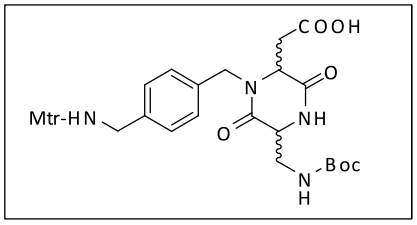

A solution of compound **119** or **120** (320 mg, 0.5 mmol, 1 equiv) in THF (20 mL) was cooled to 0 °C and treated dropwise with a solution of $LiOH·H_2O$ (52 mg, 1.24 mmol, 2.5 equiv) in H_2O (10 mL). The resulting solution was stirred for 1 h at 0 °C, then acidified with a 1M $KHSO_4$ solution to pH 1-2. The mixture was extracted with CH_2Cl_2 (4x), and the collected organic extracts were dried over Na_2SO_4 and evaporated under reduced pressure, to afford the acid (**109** or **110**) as a white foam (310 mg, 100% yield), which was used without further purification.

4.4 - *Synthesis of functionalized cyclo[DKP-RGD] integrin ligands 143-146*[a]

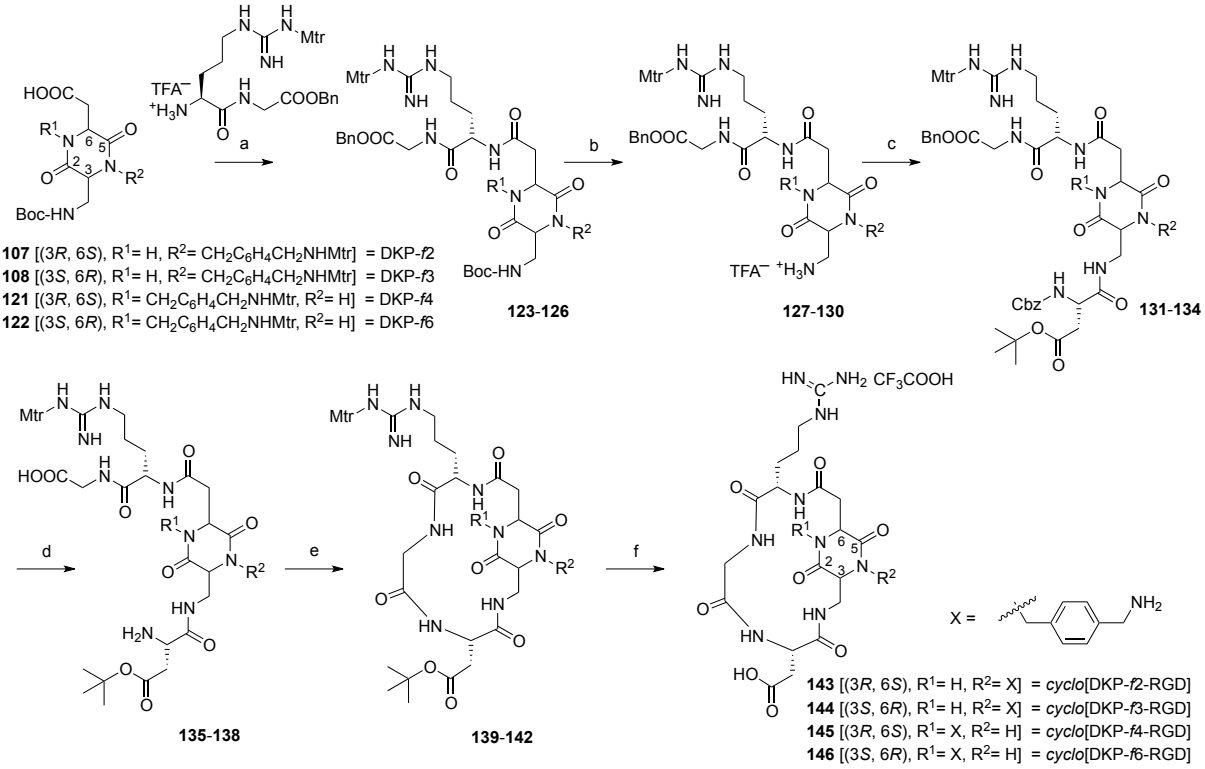

[a]Reagents and conditions: (a) HATU, HOAT, *i*Pr_2NEt, DMF, overnight, room temp., 83-85%; (b) TFA/DCM 1:2, 3 h, room temp., quant.; (c) Cbz-Asp(OtBu)-OH, HATU, HOAT, *i*Pr_2NEt, DMF, overnight, room temp., 86-88%; (d) H_2, 10% Pd/C, THF/H_2O 1:1, overnight, room temp., quant.; (e) HATU, HOAT, *i*Pr_2NEt, 1.4 mM in DMF, overnight, room temp., 60-81%; (f) TFA/TMSBr/thioanisol/EDT/phenol 70:14:10:5:1, 2 h, room temp., 70-85%.

Boc-DKP-*f*2-Arg(Mtr)-Gly-OBn 123 [(3*R*, 6*S*), R^1= H, R^2= $CH_2C_6H_4CH_2NHMtr$]

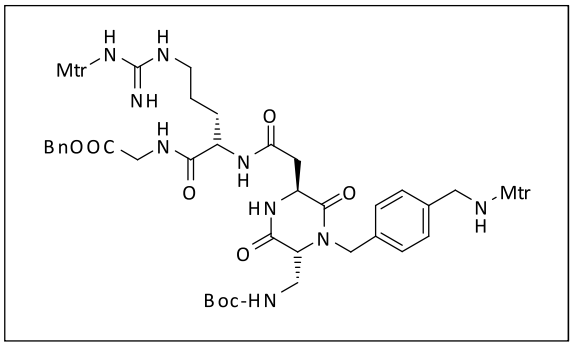

Dipeptide Boc-Arg(Mtr)-Gly-OBn (480 mg, 0.76 mmol, 1.2 equiv) was deprotected according to general procedure **GP1**. The corresponding trifluoroacetate salt was then coupled with DKP-*f*2 **107**

(400 mg, 0.63 mmol, 1 equiv), according to general procedure **GP2**. The residue was purified by flash chromatography on silica gel (CH_2Cl_2/MeOH, 93:7) to afford the desired product **123** as a white foam (613 mg, 85%).

R_f=0.4 (CH_2Cl_2/MeOH 9:1); $[\alpha]_D^{20}$=+34.7 (*c*=1.0 in CH_2Cl_2); ^{1}H NMR (400 MHz, CD_2Cl_2) δ 7.79 (br s, 2H), 7.39 (br s, 1H), 7.32-7.24 (m, 5H), 7.15 (AB system, 4H), 6.60 (s, 1H), 6.50 (s, 1H), 6.17-5.9 (m, 4H), 5.71 (br s, 1H), 5.28 (d overlapped to solvent signal, 1H, *J* = 14.3 Hz), 5.07 (s, 2H), 4.55 (br s, 1H), 4.42 (br s, 1H), 4.01-3.83 (m, 9H), 3.77 (s, 3H), 3.74-3.61 (m, 1H), 3.50-3.38 (m, 1H), 3.15-2.81 (m, 4H), 2.61 (s, 3H), 2.60 (s, 3H), 2.53 (s, 3H), 2.50 (s, 3H), 2.10 (s, 3H), 2.05 (s, 3H), 1.80-1.69 (m, 1H), 1.63-1.52 (m, 1H), 1.51-1.30 (m, 11H); ^{13}C NMR (101 MHz, CD_2Cl_2) δ 173.0, 170.9, 170.4, 168.1, 167.1, 159.7, 158.6, 156.8, 156.5, 139.1, 138.8, 137.5, 136.8, 135.8, 135.5, 134.0, 129.3, 128.9, 128.7, 128.6, 128.4, 125.6, 125.1, 112.5, 112.1, 80.1, 67.5, 60.5, 55.9, 55.8, 53.1 51.2, 47.5, 46.3, 41.7, 41.2, 40.8, 37.7 28.3, 24.5, 24.2, 18.5, 18.1, 12.1, 12.0; IR (film) 3344, 2971, 2938, 1741, 1682, 1650, 1585, 1558, 1456, 1308, 1141 cm^{-1}; MS (ESI) *m/z* calcd for $[C_{55}H_{74}N_9O_{14}S_2]^+$: 1148.48 $[M+H]^+$; found: 1148.6.

Boc-DKP-*f*3-Arg(Mtr)-Gly-OBn 124 [(3*S*, 6*R*), R^1= H, R^2= $CH_2C_6H_4CH_2NHMtr$]

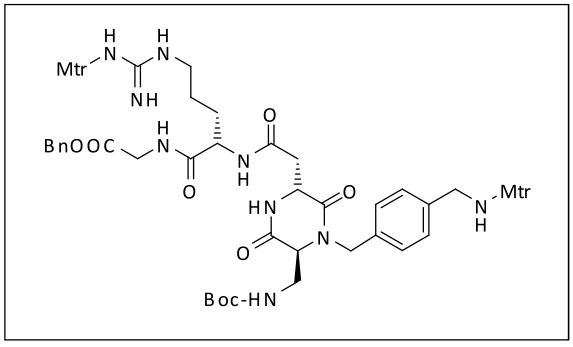

Dipeptide Boc-Arg(Mtr)-Gly-OBn (1.5 g, 2.37 mmol, 1.25 equiv) was deprotected according to general procedure **GP1**. The corresponding trifluoroacetate salt was then coupled with DKP-*f*3 **108** (1.2 g, 1.90 mmol, 1 equiv), according to general procedure **GP2**. The residue was purified by flash chromatography on silica gel (CH_2Cl_2/MeOH, 93:7) to afford the desired product **124** as a white foam (1.8 g, 84%).

R_f=0.4 (CH_2Cl_2/MeOH 9:1); $[\alpha]_D^{20}$=-29.0 (*c*=1.0 in CH_2Cl_2); ^{1}H NMR (400 MHz, acetone-d_6) δ 7.86 (t, 1H, *J* = 6.0 Hz), 7.61 (d, 2H, *J* = 11.0 Hz), 7.39-7.29 (m, 5H), 7.18 (AB system, 4H), 6.76 (s, 1H), 6.70-6.66 (m, 2H), 6.49-6.44 (m, 3H), 5.35 (d, 1H, *J* = 15.5 Hz), 5.14 (s, 2H), 4.60-4.50 (m, 2H), 4.04-3.91 (m, 5H), 3.88 (s, 3H), 3.82 (s, 3H), 3.76-3.70 (m, 2H), 3.55-3.45 (m, 1H), 3.24-3.11 (m, 2H), 3.07 (dd, 1H, *J* = 15.6, 4.6 Hz), 2.78 (dd, 1H, *J* = 15.6, 6.8 Hz), 2.67 (s, 3H), 2.64 (s, 3H), 2.62 (s, 3H), 2.55

(s, 3H), 2.10 (s, 3H), 2.08 (s, 3H) 1.92-1.83 (m, 1H), 1.66-1.58 (m, 3H), 1.40 (s, 9H); ^{13}C NMR (101 MHz, acetone-d_6) δ 173.0, 171.1, 170.4, 167.9, 167.4, 160.0, 159.0, 157.6, 156.9, 139.49, 139.31, 139.16, 138.2, 137.14, 137.03, 136.5, 135.8, 131.2, 129.3, 129.0, 128.7, 125.5, 124.9, 113.1, 112.5, 79.6, 67.2, 60.8, 56.1, 55.9, 53.3, 52.3, 47.5, 46.7, 41.8, 41.5, 41.1, 38.8, 30.3, 29.8, 28.7, 26.1, 24.42, 24.30, 18.7, 18.2, 12.15, 12.14; IR (film) 3349, 2972, 2939, 1740, 1680, 1654, 1585, 1555, 1455, 1307, 1143 cm^{-1}; MS (ESI) *m/z* calcd for $[C_{55}H_{74}N_9O_{14}S_2]^+$: 1148.48 $[M+H]^+$; found: 1148.5.

Boc-DKP-*f*4-Arg(Mtr)-Gly-OBn 125 [(3*R*, 6*S*), R^1= $CH_2C_6H_4CH_2NHMtr$, R^2= H]

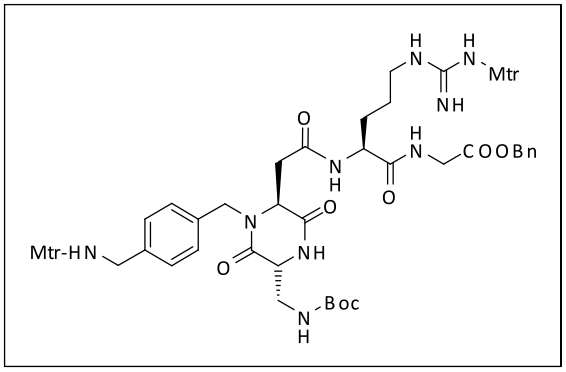

Dipeptide Boc-Arg(Mtr)-Gly-OBn (280 mg, 0.44 mmol, 1.2 equiv) was deprotected according to general procedure **GP1**. The corresponding trifluoroacetate salt was then coupled with DKP-*f*4 **121** (230 mg, 0.37 mmol, 1 equiv), according to general procedure **GP2**. The residue was purified by flash chromatography on silica gel (CH_2Cl_2/MeOH, 93:7) to afford the desired product **125** as a white foam (350 mg, 83%).

R_f=0.36 (CH_2Cl_2/MeOH 9:1); $[\alpha]_D^{20}$=+29.7 (*c*=1.0 in CH_2Cl_2); ^{1}H NMR (400 MHz, acetone-d_6) δ 7.84 (t, 1H, *J* = 5.9 Hz), 7.49 (d, 1H, *J* = 7.3 Hz), 7.40-7.32 (m, 5H), 7.19-7.15 (A2 system, 4H), 6.76 (s, 1H), 6.71-6.67 (m, 2H), 6.51 (br s, 2H), 6.16 (t, 1H, *J* = 4.7 Hz), 5.15 (s, 2H), 5.06 (d, 1H, *J* = 15.2 Hz), 4.52-4.47 (m, 1H), 4.33 (t, 1H, *J* = 4.9 Hz), 4.20 (d, 1H, *J* = 15.2 Hz), 4.07-4.02 (m, 3H), 4.00 (d, 2H, *J* = 6.8 Hz), 3.88 (s, 3H), 3.84 (s, 3H), 3.70 (ddd, 1H, *J* = 14.0, 5.9, 4.6 Hz), 3.57-3.51 (m, 1H), 3.27-3.11 (m, 2H), 2.92-2.82 (m overlapped with water signal, 2H), 2.67 (s, 3H), 2.63 (s, 3H), 2.62 (s 3H), 2.57 (s, 3H), 2.10 (s, 6H), 1.87-1.82 (m, 1H), 1.63-1.52 (m, 4H), 1.41 (s, 9H); ^{13}C NMR (101 MHz, acetone-d_6) δ 172.6, 170.3, 169.9, 169.1, 167.0, 160.0, 159.0, 157.57, 157.53, 139.51, 139.32, 139.17, 138.2, 137.12, 137.08, 136.7, 135.8, 131.2, 129.3, 129.12, 128.99, 128.97, 128.6, 125.5, 124.9, 113.0, 112.5, 79.6, 67.1, 58.0, 56.14, 56.10, 55.91, 53.3, 47.6, 46.8, 43.2, 41.8, 41.1, 37.5, 30.2, 28.6, 26.3, 24.42, 24.28, 18.7, 18.2, 12.1; IR (film) 3343, 2972, 2939, 1741, 1680, 1656, 1586, 1557, 1455, 1306, 1140 cm^{-1}; MS (ESI) *m/z* calcd for $[C_{55}H_{74}N_9O_{14}S_2]^+$: 1148.48 $[M+H]^+$; found: 1148.6.

Boc-DKP-*f*6-Arg(Mtr)-Gly-OBn 126 [(3*S*, 6*R*), R^1= $CH_2C_6H_4CH_2NHMtr$, R^2= H]

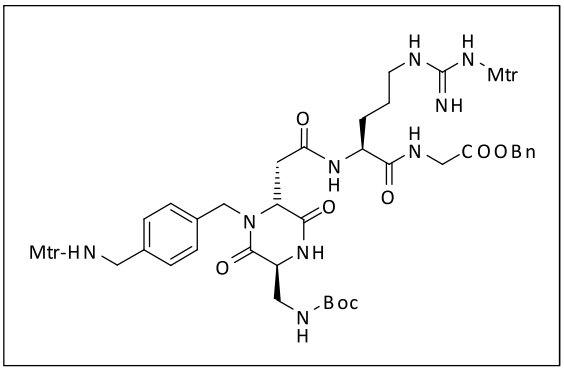

Dipeptide Boc-Arg(Mtr)-Gly-OBn (460 mg, 0.73 mmol, 1.1 equiv) was deprotected according to general procedure **GP1**. The corresponding trifluoroacetate salt was then coupled with DKP-*f*6 **122** (420 mg, 0.66 mmol, 1 equiv), according to general procedure **GP2**. The residue was purified by flash chromatography on silica gel (CH_2Cl_2/MeOH, 93:7) to afford the desired product **126** as a white foam (630 mg, 83%).

R_f=0.47 (DCM/MeOH 9:1); $[\alpha]_D^{20}$=-34.8 (*c*=1.0 in CH_2Cl_2); ^{1}H NMR (400 MHz, acetone-d_6) δ 7.97 (br s, 1H , *J* = 5.3 Hz), 7.73 (d, 1H, *J* = 7.4 Hz), 7.49 (s, 1H), 7.40 – 7.27 (m, 5H), 7.23 – 7.13 (m, 4H), 6.80 – 6.73 (m, 2H), 6.67 (s, 1H), 6.58 (br s, 2H), 6.25 (t, 1H, *J* = 5.0 Hz), 5.25 (d, 1H, *J* = 15.1 Hz), 5.13 (s, 2H), 4.68 – 4.58 (m, 1H, *J* = 4.4 Hz), 4.31 (br s, 1H, *J* = 3.8 Hz), 4.14 – 3.91 (m, 6H), 3.87 (s, 3H), 3.82 (s, 3H), 3.74 – 3.63 (m, 1H), 3.62 – 3.52 (m, 1H), 3.15 (m, 2H), 3.02 (dd, 2H), 2.89 (d, 1H, *J* = 12.7 Hz), 2.68 (s, 3H), 2.66 – 2.60 (m, 6H), 2.55 (s, 3H), 2.09 (s, 6H), 1.89 – 1.77 (m, 1H), 1.66 – 1.46 (m, 3H), 1.40 (s, 9H); ^{13}C NMR (101 MHz, acetone-d_6) δ 172.9, 170.4, 170.0, 169.0, 167.3, 159.9, 158.9, 157.6, 157.4, 139.4, 139.3, 139.2, 138.3, 137.1, 136.9, 136.1, 135.6, 131.0, 129.3, 129.1, 129.0, 128.8, 125.4, 124.9, 113.0, 112.5, 79.6, 67.2, 57.4, 56.2, 56.1, 55.9, 52.9, 46.9, 46.6, 43.3, 41.7, 40.9, 37.3, 30.7, 28.6, 25.9, 24.4, 24.3, 18.7, 18.2, 12.1; IR (film) 3340, 2971, 2937, 1740, 1684, 1660, 1584, 1558, 1456, 1307, 1141 cm^{-1}; MS (ESI) m/z calcd for $[C_{55}H_{74}N_9O_{14}S_2]^+$: 1148.48 $[M+H]^+$; found: 1148.7

Cbz-Asp(O*t*Bu)-DKP-*f*2-Arg(Mtr)-Gly-OBn 131 [(3*R*, 6*S*), R^1= H, R^2= $CH_2C_6H_4CH_2NHMtr$]

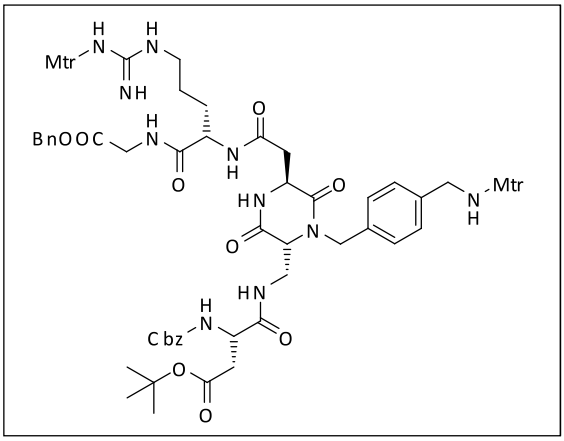

Boc-DKP-*f*2-Arg(Mtr)-Gly-OBn **123** (500 mg, 0.32 mmol, 1 equiv) was deprotected according to general procedure **GP1**. The corresponding trifluoroacetate salt **127** was then coupled with Cbz-L-Asp(O*t*Bu)-OH (155 mg, 0.48 mmol, 1.5 equiv), according to general procedure **GP2**. The residue was purified by flash chromatography on silica gel (CH_2Cl_2/MeOH, 9:1) to afford the desired product **131** as a white foam (385 mg, 88%).

R_f=0.35 (CH_2Cl_2/MeOH 9:1); $[\alpha]_D^{20}$=+8.0 (*c*=1.0 in CH_3OH); ^{1}H NMR (400 MHz, acetone-d_6) δ 8.00 (t, 1H, *J* = 6.2 Hz), 7.84 (t, 1H, *J* = 6.1 Hz), 7.65 (d, 1H, *J* = 7.8 Hz), 7.52 (s, 1H), 7.38-7.29 (m, 10H), 7.18 (AB system, 4H), 6.76-6.74 (m, 2H), 6.67-6.64 (m, 2H), 6.49 (br s, 2H), 6.25 (br s, 1H), 5.25 (d, 1H, *J* = 15.4 Hz), 5.14-5.05 (m, 4H), 4.67 (t, 1H, *J* = 5.8 Hz), 4.59-4.50 (m, 2H), 4.10 (d, 2H, *J* = 15.4 Hz), 4.04-3.93 (m, 4H), 3.88 (s, 3H), 3.85-3.82 (m, 4H), 3.59 (dt, 1H, *J* = 4.7, 13.9 Hz), 3.26-3.12 (m, 2H), 3.02 (dd, 1H, *J* = 15.4, 5.6 Hz), 2.84-2.72 (m overlapped with water signal, 2H), 2.67 (s, 3H), 2.64 (s, 3H), 2.63-2.57 (m, 4H), 2.55 (s, 3H), 2.10 (s, 3H), 2.08 (s, 3H), 1.96-1.86 (m, 1H), 1.69-1.52 (m, 3H), 1.39 (s, 9H); ^{13}C NMR (101 MHz, acetone-d_6) δ 172.8, 172.5, 171.3, 170.6, 170.5, 167.8, 167.7, 160.0, 159.0, 157.6, 157.5, 139.5, 139.4, 139.2, 138.2, 137.9, 137.1, 136.7, 136.0, 131.2, 129.34, 129.26, 129.03, 128.96, 128.95, 128.86, 128.82, 128.73, 125.5, 124.9, 113.1, 112.5, 81.3, 67.3, 67.1, 60.4, 56.1, 55.9, 53.4, 53.0, 52.1, 47.9, 46.8, 41.8, 41.1, 40.4, 38.36, 38.28, 28.3, 26.4, 24.4, 24.3, 18.7, 18.2, 12.16, 12.13; IR (film) 3340, 3298, 2927, 1718, 1684, 1653, 1558, 1456, 1307, 1144 cm^{-1}; MS (ESI) *m/z* calcd for $[C_{66}H_{85}N_{10}O_{17}S_2]^+$: 1353.56 $[M+H]^+$; found: 1353.6.

Cbz-Asp(O*t*Bu)-DKP-*f*3-Arg(Mtr)-Gly-OBn 132 [(3*S*, 6*R*), R^1= H, R^2= $CH_2C_6H_4CH_2NHMtr$]

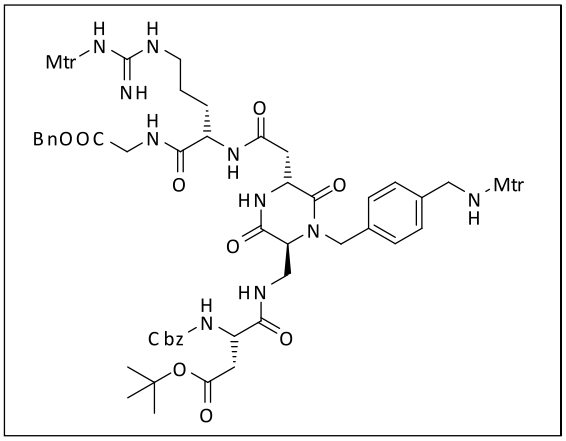

Boc-DKP-*f*3-Arg(Mtr)-Gly-OBn **124** (1.4 g, 1.22 mmol, 1 equiv) was deprotected according to general procedure **GP1**. The corresponding trifluoroacetate salt **128** was then coupled with Cbz-L-Asp(O*t*Bu)-OH (455 mg, 0.48 mmol, 1.2 equiv), according to general procedure GP2. The residue was purified by flash chromatography on silica gel (CH_2Cl_2/MeOH, 9:1) to afford the desired product **132** as a white foam (1.43 g, 87%).

R_f=0.31 (CH_2Cl_2/MeOH 9:1); $[\alpha]_D^{20}$=-15.5 (*c*=1.0 in CH_2Cl_2); ^{1}H NMR (400 MHz, acetone-d_6) δ 7.83 (t, J = 6.1 Hz, 1H), 7.79 (t, 1H, *J* = 6.2 Hz), 7.59 (m, 2H), 7.38-7.28 (m, 10H), 7.19 (AB system, 4H), 6.75 (m, 2H), 6.66 (d, 2H, *J* = 6.4 Hz), 6.48 (br s, 2H), 5.28 (d, 1H, *J* = 15.5 Hz), 5.14-5.00 (m, 4H), 4.63-4.51 (m, 3H), 4.09 (d, 1H, *J* = 15.5 Hz), 4.03 (d, 2H, *J* = 6.3 Hz), 3.97 (dd, 2H, *J* = 5.8, 3.5 Hz), 3.90-3.81 (m, 8H), 3.63 (ddd, 1H, *J* = 13.5, 5.8, 3.5 Hz), 3.17 (m, 2H), 3.05 (dd, 1H, *J* = 15.7, 4.7 Hz), 2.85-2.80 (m, 1H), 2.79-2.76 (m, 1H), 2.67 (s, 3H), 2.65 (m, 4H), 2.62 (s, 3H), 2.55 (s, 3H), 2.10 (s, 3H), 2.08 (s, 3H), 1.93-1.84 (m, 1H), 1.65-1.55 (m, 3H), 1.39 (s, 9H); ^{13}C NMR (101 MHz, acetone-d_6) δ 172.9, 172.5, 171.1, 170.7, 170.4, 167.63, 167.44, 160.0, 159.0, 157.5, 157.2, 139.51, 139.33, 139.17, 138.1, 137.9, 137.13, 137.06, 136.6, 135.9, 131.2, 129.33, 129.26, 129.02, 128.99, 128.75, 128.73, 125.5, 124.9, 113.1, 112.5, 81.3, 67.30, 67.15, 60.3, 56.1, 55.9, 53.2, 53.0, 52.2, 47.7, 46.8, 41.8, 41.1, 40.4, 38.6, 38.2, 30.4, 28.3, 26.2, 24.44, 24.31, 18.7, 18.2, 12.16, 12.14; IR (film) 3349, 3292, 2928, 1719, 1685, 1654, 1558, 1456, 1307, 1142 cm^{-1}; MS (ESI) *m/z* calcd for $[C_{66}H_{85}N_{10}O_{17}S_2]^+$: 1353.56 $[M+H]^+$; found: 1353.6.

Cbz-Asp(O*t*Bu)-DKP-*f*4-Arg(Mtr)-Gly-OBn 133 [(3*R*, 6*S*), R^1= $CH_2C_6H_4CH_2NHMtr$, R^2= H]

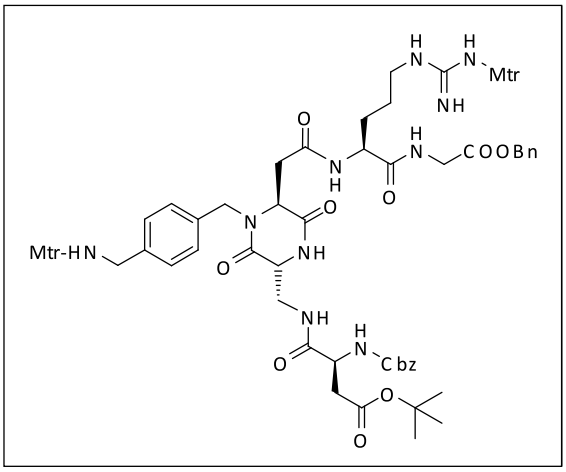

Boc-DKP-*f*4-Arg(Mtr)-Gly-OBn **125** (270 mg, 0.235 mmol, 1 equiv) was deprotected according to general procedure **GP1**. The corresponding trifluoroacetate salt **129** was then coupled with Cbz-L-Asp(O*t*Bu)-OH (91 mg, 0.28 mmol, 1.2 equiv), according to general procedure **GP2**. The residue was purified by flash chromatography on silica gel (CH_2Cl_2/MeOH, 9:1) to afford the desired product **133** as a white foam (280 mg, 88%).

R_f=0.45 (CH_2Cl_2/MeOH 9:1); $[\alpha]_D^{20}$=+22.1 (*c*=1.0 in CH_2Cl_2); ^{1}H NMR (400 MHz, acetone-d_6) δ 7.85 (t, 1H, *J* = 5.5 Hz), 7.74 (t, 1H, *J* = 5.8 Hz), 7.47 (d, 1H, *J* = 7.9 Hz), 7.40-7.28 (m, 10H), 7.17 (A2 system, 4H), 6.76 (m, 2H), 6.68 (m, 2H), 6.51 (br s, 2H), 5.14-5.01 (m, 5H), 4.54 (td, 1H, *J* = 7.8, 6.0 Hz), 4.47 (m, 1H), 4.41 (t, 1H, *J* = 5.4 Hz), 4.22 (d, 1H, *J* = 15.1 Hz), 4.06 (t, 1H, *J* = 5.3 Hz), 4.02 (d, 2H, *J* = 6.3), 3.99 (d, 2H, *J* = 6.6), 3.90-3.84 (m, 4H), 3.83 (s, 3H), 3.61 (dt, *J* = 14.0, 6.6 Hz, 1H), 3.25-3.12 (m, 2H), 2.91-2.85 (m, 2H), 2.81-2.79 (m overlapped with water signal, 1H), 2.69-2.65 (m, 4H), 2.64 (s, 3H), 2.62 (s, 3H), 2.55 (s, 3H), 2.10 (s, 6H), 1.87-1.81 (m, 1H), 1.62-1.51 (m, 3H), 1.40 (s, 9H); ^{13}C NMR (101 MHz, acetone-d_6) δ 172.8, 172.5, 170.7, 170.3, 169.8, 169.0, 166.9, 160.0, 158.9, 157.5, 157.0, 139.51, 139.34, 139.17, 138.07, 137.88, 137.12, 137.08, 136.8, 135.8, 129.32, 129.23, 129.14, 129.09, 128.99, 128.95, 128.7, 125.5, 124.8, 113.0, 112.5, 81.4, 67.21, 67.11, 58.1, 56.08, 55.88, 55.2, 53.3, 52.9, 47.6, 46.8, 42.3, 41.8, 38.4, 37.5, 30.3, 28.2, 26.2, 24.43, 24.29, 18.7, 18.2, 12.1; IR (film) 3343, 3291, 2927, 1718, 1685, 1655, 1554, 1456, 1308, 1141 cm^{-1}; MS (ESI) *m/z* calcd for $[C_{66}H_{85}N_{10}O_{17}S_2]^+$: 1353.56 $[M+H]^+$; found: 1353.6.

Cbz-Asp(O*t*Bu)-DKP-*f*6-Arg(Mtr)-Gly-OBn 134 [(3*S*, 6*R*), R^1= $CH_2C_6H_4CH_2NHMtr$, R^2= H]

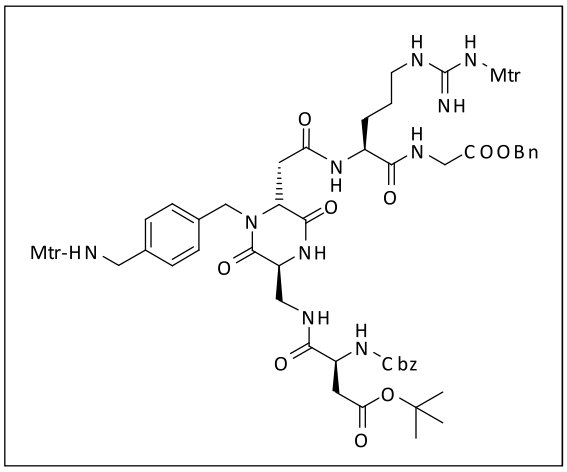

Boc-DKP-*f*6-Arg(Mtr)-Gly-OBn **126** (420 mg, 0.37 mmol, 1 equiv) was deprotected according to general procedure **GP1**. The corresponding trifluoroacetate salt **130** was then coupled with Cbz-L-Asp(O*t*Bu)-OH (141.6 mg, 0.44 mmol, 1.2 equiv), according to general procedure **GP2**. The residue was purified by flash chromatography on silica gel (CH_2Cl_2/MeOH, 9:1) to afford the desired product **134** as a white foam (428 mg, 86%).

R_f=0.49 (DCM/MeOH 9:1); $[\alpha]_D^{20}$=-27.6 (*c*=0.5 in MeOH); ^{1}H NMR (400 MHz, acetone-d_6) δ 7.97 (t, 1H, *J* = 5.5 Hz), 7.83 (br s, 1H), 7.70 (d, 1H, *J* = 6.8 Hz), 7.48 (s, 1H), 7.40 – 7.24 (m, 10H), 7.24 – 7.14 (m, 4H), 6.84 (d, 1H, *J* = 8.2 Hz), 6.79 – 6.71 (m, 2H), 6.66 (s, 1H), 6.58 (br s, 2H), 5.21 (d, 1H, *J* = 15.0 Hz), 5.16 – 5.06 (m, 3H), 5.00 (d, 1H, *J* = 12.5 Hz), 4.65 – 4.55 (m, 2H), 4.38 (t, 1H, *J* = 4.8 Hz), 4.17 – 3.92 (m, 6H), 3.90 – 3.77 (m, 7H), 3.75 – 3.65 (m, 1H), 3.28 – 3.09 (m, 2H), 3.04 – 2.95 (m, 1H), 2.94 – 2.86 (m, 1H), 2.85 – 2.76 (m, 1H), 2.75 – 2.59 (m, 10H), 2.55 (s, 3H), 2.17 – 2.05 (m, 6H), 1.88 – 1.76 (m, 1H), 1.66 – 1.46 (m, 3H), 1.38 (s, 9H); ^{13}C NMR (101 MHz, acetone-d_6) δ 172.9, 170.7, 170.4, 170.0, 168.9, 167.1, 159.9, 158.9, 157.6, 157.1, 139.3, 139.2, 138.2, 137.8, 137.1, 136.9, 136.2, 135.7, 131.0, 129.2, 129.0, 128.7, 125.4, 124.9, 113.0, 112.5, 81.4, 67.2, 57.5, 56.1, 55.9, 55.4, 53.0, 52.9, 47.1, 46.7, 42.3, 41.8, 41.0, 38.4, 37.3, 30.7, 28.2, 26.1, 24.4, 18.7, 18.2, 12.1; IR (film) 3342, 3299, 2927, 1718, 1683, 1658, 1557, 1453, 1307, 1141 cm^{-1}; MS (ESI) m/z calcd for $[C_{66}H_{85}N_{10}O_{17}S_2]^+$: 1353.55 $[M+H]^+$; found: 1353.8.

H-Asp(O*t*Bu)-DKP-*f*2-Arg(Mtr)-Gly-OH 135 [(3*R*, 6*S*), R^1= H, R^2= $CH_2C_6H_4CH_2NHMtr$]

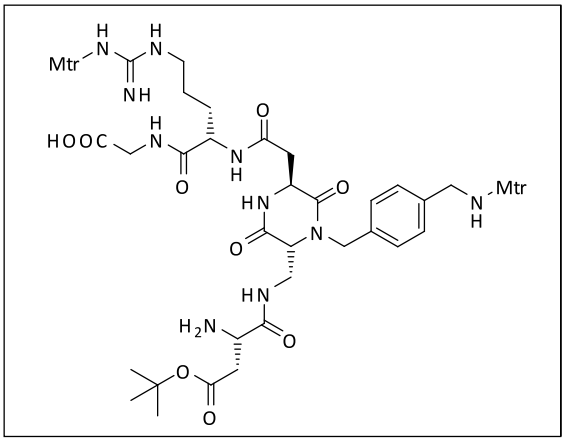

A solution of Cbz-Asp(O*t*Bu)-DKP-*f*2-Arg(Mtr)-Gly-OBn **131** (380 mg, 0.28 mmol, 1 equiv) in THF/H_2O 1:1 (100 mL) was treated with 10% Pd/C (30 mg, 0.028 mmol, 0.1 equiv), and the flask was purged three times with vacuum/H_2. The mixture was stirred at rt overnight under H_2 atmosphere, then filtered through a pad of Celite and the Celite cake was washed thoroughly with THF/H_2O 1:1. The solvents were removed under vacuum to give the crude product **135** as a white solid (320 mg, 100%), which was used without further purification.

H-Asp(O*t*Bu)-DKP-*f*3-Arg(Mtr)-Gly-OH 136 [(3*S*, 6*R*), R^1= H, R^2= $CH_2C_6H_4CH_2NHMtr$]

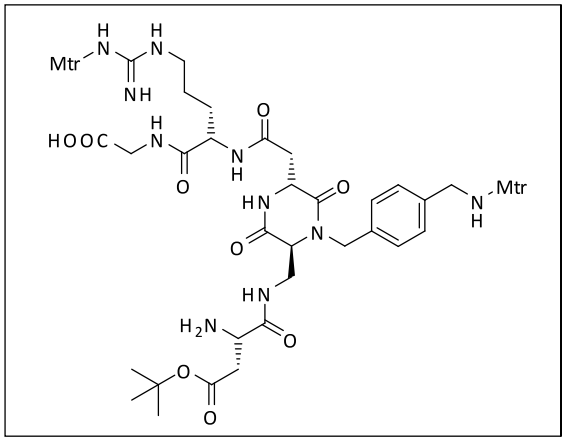

A solution of Cbz-Asp(O*t*Bu)-DKP-*f*3-Arg(Mtr)-Gly-OBn **132** (700 mg, 0.52 mmol, 1 equiv) in THF/H_2O 1:1 (200 mL) was treated with 10% Pd/C (100 mg, 0.10 mmol, 0.2 equiv), and the flask was purged three times with vacuum/H_2. The mixture was stirred at rt overnight under H_2 atmosphere, then filtered through a pad of Celite and the Celite cake was washed thoroughly with THF/H_2O 1:1. The

solvents were removed under vacuum to give the crude product **136** as a white solid (580 mg, 100%), which was used without further purification.

H-Asp(O*t*Bu)-DKP-*f*4-Arg(Mtr)-Gly-OH 137 [(3*R*, 6*S*), R^1= $CH_2C_6H_4CH_2NHMtr$, R^2= H]

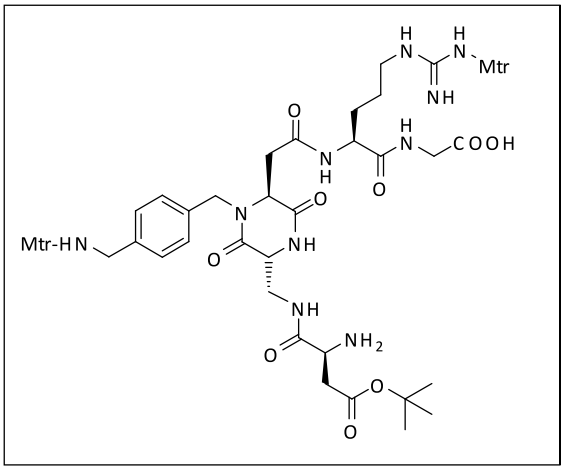

A solution of Cbz-Asp(O*t*Bu)-DKP-*f*4-Arg(Mtr)-Gly-OBn **133** (200 mg, 0.148 mmol, 1 equiv) in THF/H_2O 1:1 (50 mL) was treated with 10% Pd/C (16 mg, 0.015 mmol, 0.1 equiv), and the flask was purged three times with vacuum/H_2. The mixture was stirred at rt overnight under H_2 atmosphere, then filtered through a pad of Celite and the Celite cake was washed thoroughly with THF/H_2O 1:1. The solvents were removed under vacuum to give the crude product **137** as a white solid (166 mg, 100%), which was used without further purification.

H-Asp(O*t*Bu)-DKP-*f*6-Arg(Mtr)-Gly-OH 138 [(3*S*, 6*R*), R^1= $CH_2C_6H_4CH_2NHMtr$, R^2= H]

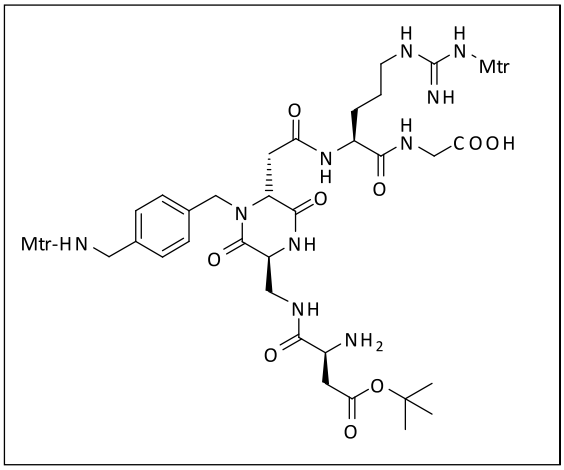

A solution of Cbz-Asp(O*t*Bu)-DKP-*f*6-Arg(Mtr)-Gly-OBn **134** (317 mg, 0.23 mmol, 1 equiv) in THF/H_2O 1:1 (80 mL) was treated with 10% Pd/C (25 mg, 0.023 mmol, 0.1 equiv), and the flask was purged three times with vacuum/H_2. The mixture was stirred at rt overnight under H_2 atmosphere, then filtered through a pad of Celite and the Celite cake was washed thoroughly with THF/H_2O 1:1. The solvents were removed under vacuum to give the crude product **138** as a white solid (260 mg, 100%), which was used without further purification.

***Cyclo*[DKP-*f*2-Arg(Mtr)-Gly-Asp(O*t*Bu)] 139** [(3*R*, 6*S*), R^1= H, R^2= $CH_2C_6H_4CH_2NHMtr$]

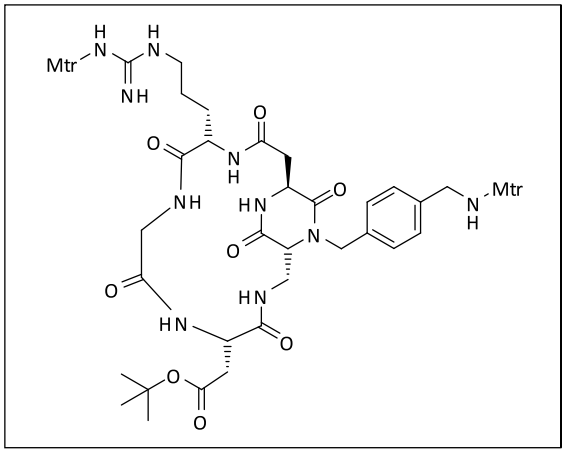

To a solution of H-Asp(O*t*Bu)-DKP-*f*2-Arg(Mtr)-Gly-OH **135** (200 mg, 0.18 mmol, 1 equiv) in DMF (130 mL), under nitrogen atmosphere and at 0 ºC, HATU (273 mg, 0.72 mmol, 4 equiv), HOAt (98 mg, 0.72 mmol, 4 equiv) and *i*-Pr_2NEt (0.180 mL, 1.06 mmol, 6 equiv) were added. The reaction was warmed up to rt and stirred overnight. DMF was then removed under reduced pressure and the residue was dissolved in AcOEt (200 mL). The resulting solution was washed with 1 M aqueous $KHSO_4$ (2×30 mL), saturated aqueous $NaHCO_3$ (2×30 mL) and brine (2×30 mL), dried over Na_2SO_4 and the solvent evaporated under reduced pressure to afford the crude product. The crude was purified by flash-chromatography on silica gel (CH_2Cl_2/MeOH, 9:1) to afford the desired product **139** as a fluffy solid (116 mg, 60%).

R_f=0.34 (CH_2Cl_2/MeOH, 9:1); $[\alpha]_D^{20}$=+7.5 (*c*=1.0 in CH_2Cl_2); ^{1}H NMR (400 MHz, DMSO-d_6) δ 8.59 (br s, 1H), 8.49 (d, 1H, J = 7.0 Hz), 8.13 (s, 1H), 8.05 (d, 1H, J = 8.0 Hz), 7.89-7.83 (m, 2H), 7.14 (AB system, 4H), 6.76 (s, 1H), 6.68 (s, 1H), 5.06 (d, 1H, *J* = 15.0 Hz), 4.53-4.45 (m, 2H), 4.28-4.17 (m, 1H), 4.00-3.84 (m, 5 H), 3.82 (s, 3H), 3.79 (s, 3H), 3.62 (d, 1H, *J* = 5.4 Hz), 3.49 (br d, 1H, *J* = 13.6 Hz), 3.09-3.0 (m, 2H), 2.76-2.67 (m, 2H), 2.60 (s, 3H), 2.56 (s, 3H), 2.52 (s, 3H), 2.45 (s, 3H), 2.27 (dd, 1H, *J* = 12.6, 3.0 Hz), 2.05 (s, 6H), 1.72-1.63 (m, 1H), 1.53-1.46 (m, 3H), 1.37 (s, 9H); ^{13}C NMR

(101 MHz, DMSO-d_6) δ 171.6, 171.1, 170.7, 169.0, 168.5, 168.2, 167.1, 158.4, 157.4, 156.1, 138.2, 137.73, 137.57, 137.4, 135.5, 135.1, 134.6, 130.0, 127.9, 127.4, 124.0, 123.5, 112.2, 111.7, 80.2, 58.6, 55.61, 55.43, 54.1, 51.4, 49.8, 45.9, 45.0, 41.6, 39.8, 39.0, 38.1, 37.0, 28.9, 27.6, 25.9, 23.73, 23.54, 17.9, 17.6, 11.71, 11.69; IR (film) 3437, 3304, 3060, 2928, 2855, 1720, 1674, 1654, 1584, 1559, 1458, 1307 cm^{-1}; MS (ESI) *m/z* calcd for $[C_{51}H_{71}N_{10}O_{14}S_2]^+$: 1111.46 $[M+H]^+$; found: 1111.7.

***Cyclo*[DKP-*f*3-Arg(Mtr)-Gly-Asp(O*t*Bu)] 140** [(3*S*, 6*R*), R^1= H, R^2= $CH_2C_6H_4CH_2NHMtr$]

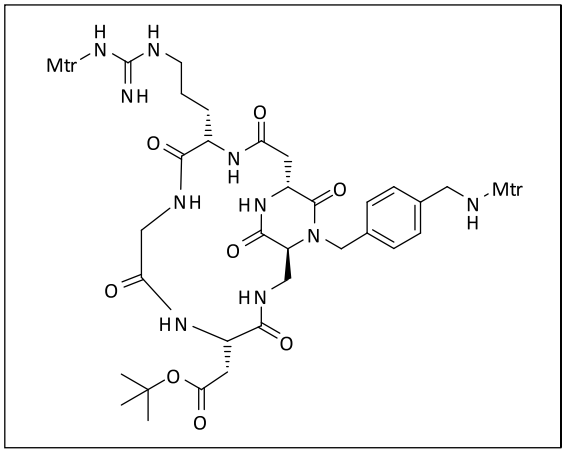

To a solution of H-Asp(O*t*Bu)-DKP-*f*3-Arg(Mtr)-Gly-OH **136** (580 mg, 0.52 mmol, 1 equiv) in DMF (440 mL), under nitrogen atmosphere and at 0 ºC, HATU (900 mg, 2.36 mmol, 4.5 equiv), HOAT (323 mg, 2.36 mmol, 4.5 equiv) and *i*-Pr_2NEt (0.630 mL, 3.70 mmol, 7 equiv) were added. The reaction was warmed up to rt and stirred overnight. DMF was then removed under reduced pressure to afford a yellowish solid. The solid was dissolved in AcOEt (200 mL) and the resulting solution was washed with 1 M aqueous $KHSO_4$ (2×30 mL), saturated aqueous $NaHCO_3$ (2×30 mL) and brine (2×30 mL), dried over Na_2SO_4 and the solvent evaporated under reduced pressure to afford the crude product. The crude was purified by flash-chromatography on silica gel (CH_2Cl_2/MeOH, 9:1) to afford the desired product **140** as a fluffy solid (470 mg, 81%).

R_f=0.34 (CH_2Cl_2/MeOH, 9:1); $[\alpha]_D^{20}$=-41.6 (*c*=1.0 in CH_3OH); ^{1}H NMR (400 MHz, acetone-d_6) δ 8.63 (d, 1H, *J* = 6.7 Hz), 8.01 (dd, 1H, *J* = 9.3, 2.4 Hz), 7.47 (d, 1H, *J* = 8.8 Hz), 7.22 (AB system, 4H), 6.92 (s, 1H), 6.76-6.73 (m, 2H), 6.68 (s, 1H), 6.53 (s, 2H), 5.06 (d, 1H, *J* = 14.9 Hz), 4.88 (td, 1H, *J* = 8.9, 6.3 Hz), 4.44 (td, 2H, *J* = 9.7, 7.4 Hz), 4.14 (d, 1H, *J* = 14.9 Hz), 4.08 (d, 2H, *J* = 6.3 Hz), 4.02 (dd, 1H, *J* = 13.9, 7.2 Hz), 3.90-3.80 (m, 8H), 3.50 (dt, 1H, *J* = 13.9, 6.8 Hz), 3.35 (dd, 1H, *J* = 16.9, 2.4 Hz), 3.25 (m, 2H), 2.91 (dd, 1H, *J* = 16.2, 9.0 Hz), 2.81-2.78 (m overlapped with water signal, 1H), 2.68 (s, 3H), 2.63 (s, 6H), 2.55-2.50 (m, 4H), 2.43 (dd, 1H, *J* = 16.2, 6.1 Hz), 2.20-2.10 (m, 7H), 1.99-1.93 (m, 1H), 1.72-1.51 (m, 2H), 1.41 (s, 9H); ^{13}C NMR (101 MHz, acetone-d_6) δ 173.1, 172.7,

171.47, 171.30, 171.10, 170.8, 170.3, 159.9, 158.9, 157.4, 139.46, 139.29, 139.12, 138.7, 137.0, 135.9, 131.2, 129.3, 129.0, 125.5, 124.8, 113.0, 112.5, 81.0, 60.3, 56.10, 56.02, 55.88, 52.8, 49.6, 47.8, 46.7, 43.2, 39.2, 38.6, 36.7, 28.2, 27.4, 26.9, 24.41, 24.26, 18.7, 18.2, 12.1; IR (film) 3300, 3062, 2927, 2856, 1719, 1672, 1655, 1584, 1559, 1458, 1308 cm^{-1}; MS (ESI) *m/z* calcd for $[C_{51}H_{71}N_{10}O_{14}S_2]^+$: 1111.46 $[M+H]^+$; found: 1111.6.

***Cyclo*[DKP-*f*4-Arg(Mtr)-Gly-Asp(O*t*Bu)] 141** [(3*R*, 6*S*), R^1= $CH_2C_6H_4CH_2NHMtr$, R^2= H]

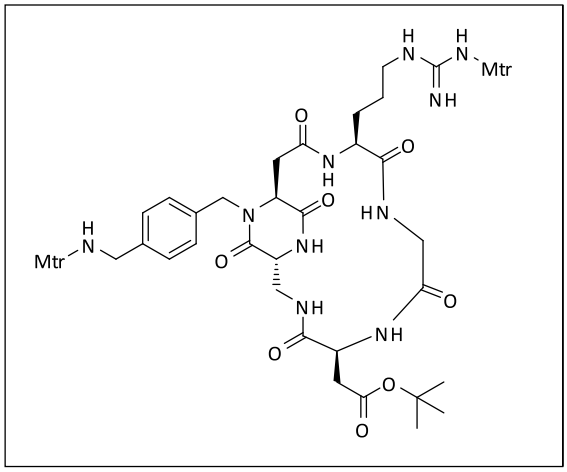

To a solution of H-Asp(O*t*Bu)-DKP-*f*4-Arg(Mtr)-Gly-OH **137** (166 mg, 0.148 mmol, 1 equiv) in DMF (110 mL), under nitrogen atmosphere and at 0 ºC, HATU (224 mg, 0.593 mmol, 4 equiv), HOAt (81 mg, 0.592 mmol, 4 equiv) and *i*-Pr_2NEt (0.160 mL, 0.89 mmol, 6 equiv) were added. The reaction was warmed up to rt and stirred overnight. DMF was then removed under reduced pressure to afford a yellowish solid. The solid was dissolved in AcOEt (150 mL) and the resulting solution was washed with 1 M aqueous $KHSO_4$ (2×20 mL), saturated aqueous $NaHCO_3$ (2×20 mL) and brine (2×32 mL), dried over Na_2SO_4 and the solvent evaporated under reduced pressure to afford the crude product. The crude was purified by flash-chromatography on silica gel (CH_2Cl_2/MeOH, 9:1) to afford the desired product **141** as a fluffy solid (110 mg, 67%).

R_f=0.4 (CH_2Cl_2/MeOH 9:1); $[\alpha]_D^{20}$=-42.0 (*c*=1.0 in DMSO); ^{1}H NMR (400 MHz, DMSO-d_6) δ 8.88 (br s, 1H), 8.25 (m, 2H), 8.03 (br s, 1H), 7.85 (t, 1H, *J* = 6.2 Hz), 7.41 (br s, 1H), 7.12 (AB system, 4H), 6.75 (s, 1H), 6.68 (s, 1H), 6.41 (br s, 1H), 5.18 (d, 1H, *J* = 14.1 Hz), 4.26-4.18 (m, 2H), 4.02-3.97 (m, 1H), 3.92-3.87 (m, 3H), 3.82 (s, 3H), 3.80-3.74 (m, 4H), 3.70-3.56 (m, 2H), 3.34 (m overlapped with water signal, 1H), 3.08-2.95 (m, 3H), 2.93-2.83 (m, 1H), 2.64-2.60 (m, 4H), 2.54 (m, 7H), 2.50 (m overlapped with solvent signal, 1H), 2.44 (s, 3H), 2.05 (s, 3H), 2.04 (s, 3H), 1.73-1.61 (m, 1H), 1.55-1.40 (m, 12H); ^{13}C NMR (101 MHz, DMSO-d_6) δ 171.2, 170.3, 169.8, 169.1, 168.4, 167.6, 158.5, 157.5, 156.1, 138.2, 137.79, 137.65, 137.3, 135.6, 135.0, 130.0, 128.0, 127.5, 124.0, 123.5, 112.2,

111.7, 80.5, 55.67, 55.50, 52.19, 52.05, 51.98, 45.10, 45.00, 42.1, 39.9, 39.7, 36.1, 35.6, 28.1, 27.7, 25.8, 23.81, 23.64, 18.0, 17.7, 11.8; IR (film) 3436, 3309, 3055, 2927, 2857, 1720, 1674, 1656, 1584, 1557, 1458, 1306 cm^{-1}; MS (ESI) *m/z* calcd for $[C_{51}H_{71}N_{10}O_{14}S_2]^+$: 1111.46 $[M+H]^+$; found: 1111.7.

***Cyclo*[DKP-*f*6-Arg(Mtr)-Gly-Asp(O*t*Bu)] 142** [(3*S*, 6*R*), R^1= $CH_2C_6H_4CH_2NHMtr$, R^2= H]

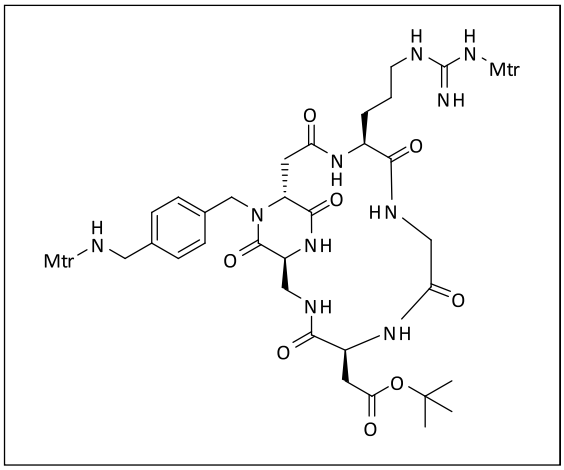

To a solution of H-Asp(O*t*Bu)-DKP-*f*6-Arg(Mtr)-Gly-OH **138** (260 mg, 0.23 mmol, 1 equiv) in DMF (165 mL), under nitrogen atmosphere and at 0 ºC, HATU (350 mg, 0.92 mmol, 4 equiv), HOAt (125 mg, 0. 92 mmol, 4 equiv) and *i*-Pr_2NEt (0.236 mL, 1.38 mmol, 6 equiv) were added. The reaction was warmed up to rt and stirred overnight. DMF was then removed under reduced pressure to afford a yellowish solid. The solid was dissolved in AcOEt (200 mL) and the resulting solution was washed with 1 M aqueous $KHSO_4$ (2×20 mL), saturated aqueous $NaHCO_3$ (2×20 mL) and brine (2×32 mL), dried over Na_2SO_4 and the solvent evaporated under reduced pressure to afford the crude product. The crude was purified by flash-chromatography on silica gel (CH_2Cl_2/MeOH, 9:1) to afford the desired product **142** as a fluffy solid (170 mg, 68%).

R_f=0.35 (DCM/MeOH 9:1); $[\alpha]_D^{20}$=-38.0 (*c*=0.5 in DMSO); ^{1}H NMR (400 MHz, CD_3OD) δ 7.19 – 7.06 (m, 4H), 6.67 (s, 1H), 6.65 (s, 1H), 5.18 (d, 1H, *J* = 14.7 Hz), 4.50 – 4.39 (m, 2H), 4.12 – 3.95 (m, 5H), 3.92 – 3.81 (m, 7H), 3.78 – 3.65 (m, 2H), 3.61 (dd, 1H, *J* = 13.7, 3.6 Hz), 3.29 – 3.08 (m, 2H), 2.99 (dd, 1H, *J* = 16.6, 7.0 Hz), 2.75 – 2.69 (m, 2H), 2.66 (s, 3H), 2.64 – 2.56 (m, 7H), 2.47 (s, 3H), 2.11 (s, 3H), 2.07 (s, 3H), 1.83 – 1.71 (m, 1H), 1.69 – 1.49 (m, 3H), 1.45 (s, 9H); ^{13}C NMR (101 MHz, CD_3OD) δ 174.2, 174.0, 173.1, 172.3, 171.8, 171.3, 160.7, 159.9, 158.2, 139.9, 139.5, 138.6, 137.9, 136.3, 134.7, 131.0, 129.5, 129.0, 126.1, 125.7, 113.2, 112.8, 82.3, 56.2, 56.0, 54.5, 52.2, 47.8, 46.9, 44.0, 42.5, 36.6, 36.1, 28.3, 24.5, 24.4, 18.9, 18.2, 12.1; IR (film) 3304, 3060, 2927, 2855, 1719, 1674, 1654, 1584, 1559, 1456, 1307 cm^{-1}; MS (ESI) m/z calcd for $[C_{51}H_{71}N_{10}O_{14}S_2]^+$: 1111.46 $[M+H]^+$; found: 1111.6

***Cyclo*[DKP-*f*2-Arg-Gly-Asp] 143** [(3*R*, 6*S*), R^1= H, R^2= $CH_2C_6H_4CH_2NH_2$]

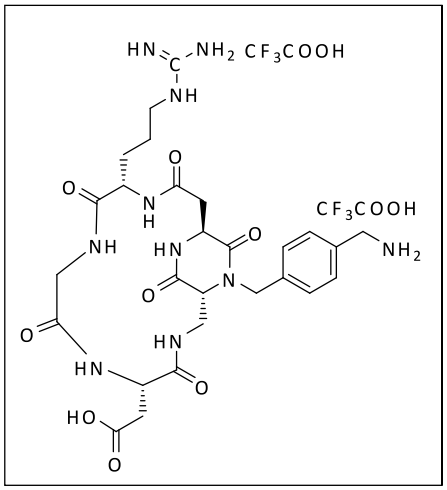

Cyclo[DKP-*f*2-Arg(Mtr)-Gly-Asp(O*t*Bu)] **139** (110 mg, 0.10 mmol) was treated with TFA (10 mL), in the presence of ion scavengers thioanisole (1.5 mL), ethanedithiol (0.75 mL) and phenol (150 mg). The mixture was cooled to 0 °C and flushed with N_2. Trimethylsilylbromide (2 mL) was then added, the flask was open and the mixture warmed up to rt and stirred for 2 h. All volatiles were then evaporated and the crude was dissolved in a mixture of water and diisopropyl ether 1:1 (30 mL). The aqueous phase was washed several time with diisopropyl ether and then concentrated under reduced pressure to give the crude compound, which was purified by semipreparative-HPLC (Water's Atlantis 21 mm x 10 cm column, gradient: 95% H_2O / 5% acetonitrile to 80% H_2O / 20% acetonitrile) to give the desired compound **143** (as trifluoroacetate salt) as a white solid (63 mg, 75% yield).

^{1}H NMR (400 MHz, D_2O) δ 7.47 (d, 2H, *J* = 8.1 Hz), 7.39 (d, 1H, *J* = 8.1 Hz), 5.13 (d, 1H, *J* = 15.6 Hz), 4.89 (t, 1H, *J* = 7.1 Hz), 4.61 (dd, 1H, *J* = 7.8, 5.8 Hz), 4.33 (d, 1H, *J* = 17.0 Hz), 4.26-4.18 (m, 5H), 4.02 (d, 1H, *J* = 14.9 Hz), 3.71-3.61 (m, 2H), 3.25 (t, 2H, *J* = 6.8 Hz), 2.99-2.90 (m, 2H), 2.81 (dd, 1H, *J* = 7.0, 17.0 Hz), 2.69 (dd, 1H, *J* = 5.4, 14.0 Hz), 1.83 (ddt, 1H, *J* = 14.3, 9.7, 4.7 Hz), 1.83 (ddt, 1H, *J* = 14.3, 9.7, 4.7 Hz), 1.74-1.61 (m, 2H); ^{13}C NMR (101 MHz, D_2O) δ 174.7, 174.5, 173.7, 173.5, 171.5, 170.7, 157.4, 136.6, 133.1, 130.1, 128.9, 60.1, 54.6, 52.8, 50.1, 48.3, 43.3, 43.2, 41.3, 39.9, 38.7, 35.3, 26.5, 25.3; IR (film) 3258, 3065, 2940, 1670, 1545, 1425, 1202, 1136 cm^{-1}; MS (ESI) *m/z* calcd for $[C_{27}H_{39}N_{10}O_8]^+$: 631.30 $[M+H]^+$; found: 631.4

***Cyclo*[DKP-*f*3-Arg-Gly-Asp] 144** [(3*S*, 6*R*), R^1= H, R^2= $CH_2C_6H_4CH_2NH_2$]

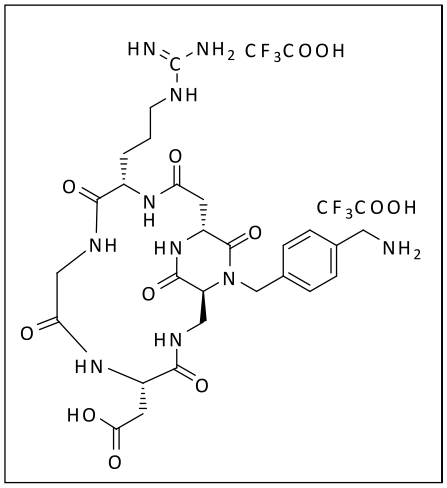

Cyclo[DKP-*f*3-Arg(Mtr)-Gly-Asp(O*t*Bu)] **140** (200 mg, 0.18 mmol) was treated with TFA (20 mL), in the presence of ion scavengers thioanisole (3 mL), ethanedithiol (1.5 mL) and phenol (300 mg). The mixture was cooled to 0 °C and flushed with N_2. Trimethylsilylbromide (4 mL) was then added, the flask was open and the mixture warmed up to rt and stirred for 2 h. All volatiles were then evaporated and the crude was dissolved in a mixture of water and diisopropyl ether 1:1 (50 mL). The aqueous phase was washed several time with diisopropyl ether and then concentrated under reduced pressure to give the crude compound, which was purified by semipreparative-HPLC (Water's Atlantis 21 mm x 10 cm column, gradient: 95% H_2O / 5% acetonitrile to 80% H_2O / 20% acetonitrile) to give the desired compound **144** (as trifluoroacetate salt) as a white solid (144 mg, 85% yield).

^{1}H NMR (400 MHz, D_2O) δ 7.43 (AB system, 4H), 5.12 (d, 1H, J = 15.6 Hz), 4.89 (t, 1H, J = 7.1 Hz), 4.61 (dd, 1H, J = 7.8, 5.8 Hz), 4.33 (d, 1H, J = 17.0 Hz), 4.26-4.19 (m, 5H), 4.02 (d, 1H, J = 14.9 Hz), 3.71-3.61 (m, 2H), 3.25 (t, 2H, J = 6.8 Hz), 2.99-2.90 (m, 2H), 2.81 (dd, 1H, J = 17.0, 7.0 Hz), 2.69 (dd, 1H, J = 14.0, 5.4 Hz), 2.02 (ddt, 1H, J = 14.2, 9.9, 4.9 Hz), 1.83 (ddt, 1H, J = 14.3, 9.7, 4.7 Hz), 1.75-1.59 (m, 2H); ^{13}C NMR (101 MHz, D_2O) δ 174.74, 174.55, 173.67, 173.51, 171.5, 170.7, 169.3, 157.4, 136.6, 133.1, 130.1, 128.9, 60.1, 54.6, 52.8, 50.1, 48.3, 43.34, 43.17, 41.3, 39.9, 38.7, 35.3, 26.5, 25.3; IR (film) 3265, 3060, 2936, 1672, 1545, 1428, 1201, 1135 cm^{-1} MS (ESI) *m/z* calcd for $[C_{27}H_{39}N_{10}O_8]^+$: 631.30 $[M+H]^+$; found: 631.4.

***Cyclo*[DKP-*f*4-Arg-Gly-Asp] 145** [(3*R*, 6*S*), R^1= $CH_2C_6H_4CH_2NH_2$, R^2= H]

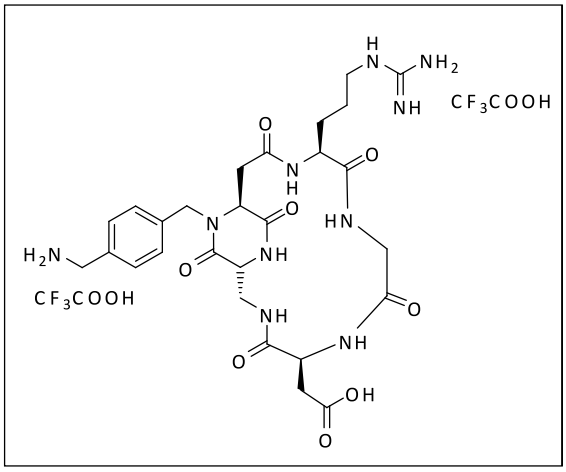

Cyclo[DKP-*f*4-Arg(Mtr)-Gly-Asp(O*t*Bu)] **141** (90 mg, 0.081 mmol) was treated with TFA (10 mL), in the presence of ion scavengers thioanisole (1.5 mL), ethanedithiol (0.75 mL) and phenol (150 mg). The mixture was cooled to 0 °C and flushed with N_2. Trimethylsilylbromide (2 mL) was then added, the flask was open and the mixture warmed up to rt and stirred for 2 h. All volatiles were then evaporated and the crude was dissolved in a mixture of water and diisopropyl ether 1:1 (30 mL). The aqueous phase was washed several time with diisopropyl ether and then concentrated under reduced pressure to give the crude compound, which was purified by semipreparative-HPLC (Water's Atlantis 21 mm x 10 cm column, gradient: 95% H_2O / 5% acetonitrile to 80% H_2O / 20% acetonitrile) to give the desired compound **145** (as trifluoroacetate salt) as a white solid (49 mg, 70% yield).

^{1}H NMR (400 MHz, D_2O) δ 7.40 (AB system, 4H), 5.35-5.18 (m, 1H), 4.44 (br s, 1H), 4.35 (dd, 1H, *J* = 9.1, 5.0 Hz), 4.28 (br s, 1H), 4.22-4.12 (m, 3H), 4.08-3.94 (m, 2H), 3.78-3.63 (m, 2H), 3.43 (br s, 1H), 3.22 (t, 2H, *J* = 6.6 Hz), 3.10-3.00 (m, 1H), 2.96-2.83 (m, 3H), 1.93-1.76 (m, 2H), 1.73-1.61 (m, 2H); ^{13}C NMR (101 MHz, D_2O,) δ 174.5, 173.9, 173.4, 171.3, 169.1, 157.4, 136.7, 132.9, 130.0, 128.6, 58.2, 54.2, 53.6, 53.0, 47.3, 43.3, 43.1, 41.05, 41.02, 36.9, 35.2, 28.3, 25.2; IR (film) 3258, 3063, 2942, 1671, 1545, 1425, 1202, 1133 cm^{-1} MS (ESI) *m/z* calcd for $[C_{27}H_{39}N_{10}O_8]^+$: 631.30 $[M+H]^+$; found: 631.4

***Cyclo*[DKP-*f*6-Arg-Gly-Asp] 146** [(3*S*, 6*R*), R^1= $CH_2C_6H_4CH_2NH_2$, R^2= H]

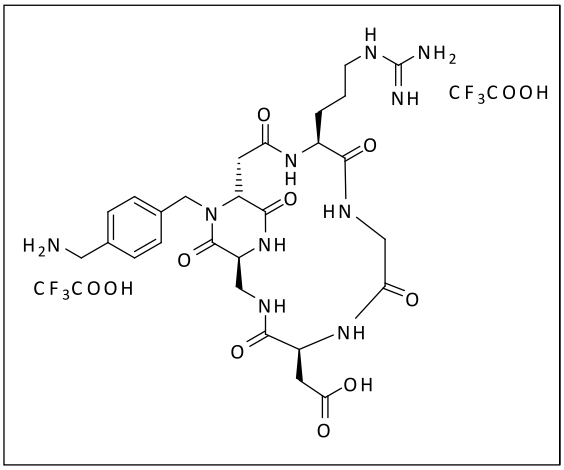

Cyclo[DKP-*f*6-Arg(Mtr)-Gly-Asp(O*t*Bu)] **142** (90 mg, 0.081 mmol) was treated with TFA (10 mL), in the presence of ion scavengers thioanisole (1.5 mL), ethanedithiol (0.75 mL) and phenol (150 mg). The mixture was cooled to 0 °C and flushed with N_2. Trimethylsilylbromide (2 mL) was then added, the flask was open and the mixture warmed up to rt and stirred for 2 h. All volatiles were then evaporated and the crude was dissolved in a mixture of water and diisopropyl ether 1:1 (30 mL). The aqueous phase was washed several time with diisopropyl ether and then concentrated under reduced pressure to give the crude compound, which was purified by semipreparative-HPLC (Water's Atlantis 21 mm x 10 cm column, gradient: 95% H_2O / 5% acetonitrile to 80% H_2O / 20% acetonitrile) to give the desired compound **146** (as trifluoroacetate salt) as a white solid (50 mg, 71% yield).

^{1}H NMR (400 MHz, D_2O) δ 8.06 (t, 1H, J = 6.1 Hz), 7.43 (AB system, 4H), 5.16 (d, 1H, J = 15.7 Hz), 4.53 (t, 1H, J = 7.1 Hz), 4.39 (dd, 1H, J = 9.3, 5.7 Hz), 4.36 – 4.29 (m, 2H), 4.20 (s, 2H), 4.05 (t, 1H, J = 6.2 Hz), 3.89 (d, 1H, J = 15.4 Hz), 3.82 (d, 1H, J = 15.4 Hz), 3.77 – 3.71 (m, 2H), 3.21 (t, 2H, J = 6.8 Hz), 3.11 (dd, 1H, J = 17.0, 6.8 Hz), 2.92 – 2.76 (m, 3H), 1.92 – 1.54 (m, 4H); ^{13}C NMR (101 MHz, D_2O) δ 175.2, 173.9, 173.3, 172.5, 171.6, 168.8, 167.4, 157.4, 136.9, 132.9, 130.0, 128.8, 58.9, 55.4, 54.2, 51.6, 48.3, 43.4, 43.4, 41.7, 41.0, 35.9, 34.4, 28.4, 25.1; IR (film) 3254, 3062, 2942, 1671, 1545, 1423, 1202, 1134 cm^{-1}; MS (ESI) m/z calcd for $[C_{27}H_{39}N_{10}O_8]^+$: 631.29 $[M+H]^+$; found: 631.5

4.5 - *Synthesis of cyclo[DKP-RGD] - PTX conjugates 90-93*[a]

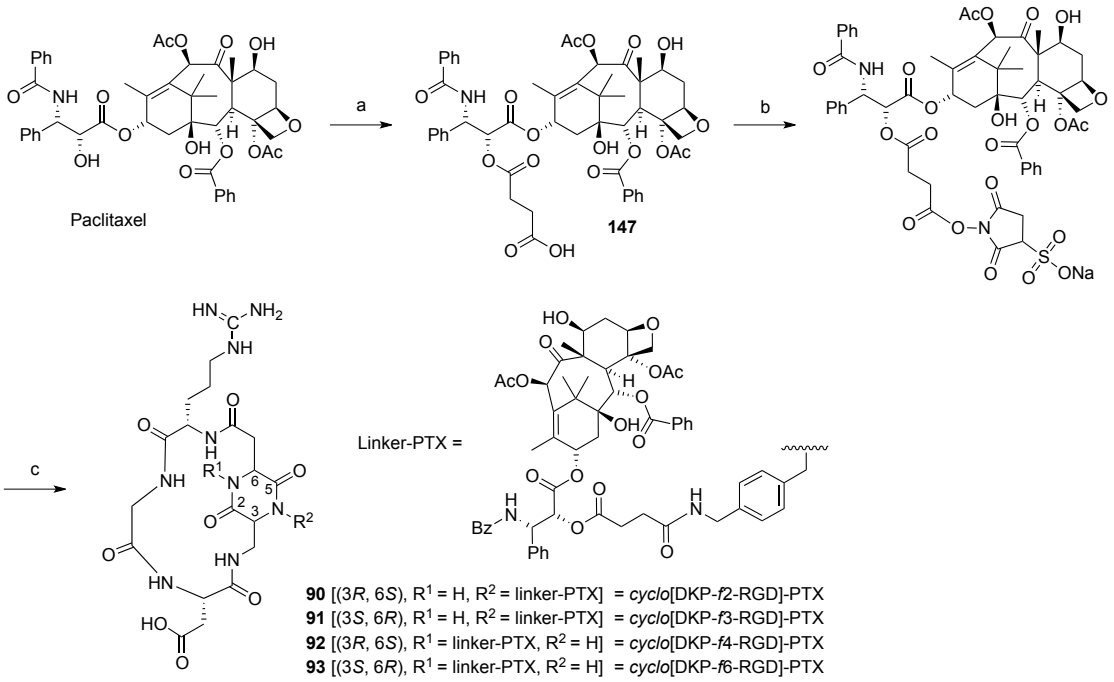

[a]Reagents and conditions: (a) succinic anhydride, py, DCM, overnight, 0 °C to room temp., 94%; (b) *N*-hydroxysulfosuccinimide sodium salt, DIC, DMF, overnight, room temp.; (c) *cyclo*(DKP-RGD) **143, 144**, **145** or **146**, CH_3CN, aq. phosphate buffer, pH = 7.3, 10 h at 0 °C then 8 h at room temp., 60-70%.

2′-Succinyl-Paclitaxel 147

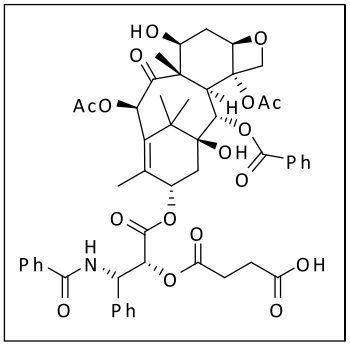

A solution of Paclitaxel (200 mg, 0.234 mmol) and succinic anhydride (28.0 mg, 0.281 mmol, 1.2 equiv) in dry dichloromethane (1.0 mL), under argon at 0 °C, was treated with pyridine (1.90 mL, 23.4 mmol, 100 equiv). The resulting mixture was stirred for 3 hours at 0 °C, then warmed up to room

temperature and stirred for further 20 h. The reaction mixture was then concentrated *in vacuo*, the resulting solid was dissolved in water/acetonitrile/acetic acid (2 mL, 1:1:1) and purified by medium pressure reverse phase chromatography (Reveleris Grace) eluting with water and acetonitrile to give compound 67 as a white solid (200 mg, 94% yield). The analytical and spectroscopic data were in agreement with those already published.

^{1}H NMR (400 MHz, CD_3OD): δ 8.14 (d, 2H, J = 7.2 Hz), 7.85 (d, 2H, J = 7.2 Hz), 7.42-7.72 (m, 10H), 7.30 (t, 1H, J = 7.5 Hz), 6.47 (s, 1H), 6.10 (m, 1H), 5.86 (d, 1H, J = 6.4 Hz), 5.66 (d, 1H, J = 6.4 Hz), 5.50 (d, 1H, J = 6.4 Hz), 5.02 (d, 1H, J = 9.2 Hz), 4.36 (m, 1H), 4.21 (s, 2H), 3.84 (d, 1H, J = 6.8 Hz), 2.64-2.74 (m, 4H), 2.49 (m, 1H), 2.42 (s, 3H), 2.15-2.30 (m, 4H), 1.94 (s, 3H), 1.86 (m, 1H), 1.81 (m, 1H), 1.68 (s, 3H), 1.16 (s, 6H; ^{13}C NMR (101 MHz, CD_3OD): δ 206.1, 177.0, 174.4, 172.5, 172.2, 171.5, 171.3, 168.6, 143.4, 139.3, 136.5, 135.7, 135.5, 133.7, 132.3, 132.1, 130.9, 130.6, 130.4, 129.5, 86.8, 83.1, 79.9, 78.3, 77.7, 77.1, 76.8, 73.8, 73.1, 60.1, 56.1, 48.8, 45.4, 38.4, 37.3, 30.3, 27.8, 24.1, 23.2, 21.6, 15.8, 11.2; MS (ESI) *m/z* calcd. for $[C_{51}H_{56}NO_{17}]^+$ 954.36 $[M+H]^+$; found: 954.2

***Cyclo*[DKP-*f*2-RGD]-PTX 90**

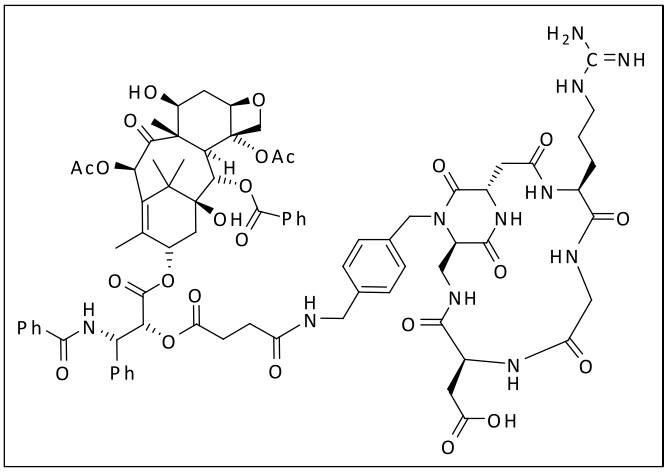

Diisopropylcarbodiimide (11.93 μL, 9.72 mg, 0.077 mmol, 1.9 equiv) was added to a solution of 2′-succinyl-Paclitaxel **144** (49 mg, 0.0513 mmol, 1.25 equiv) and *N*-hydroxysulfosuccinimide sodium salt (13.94 mg, 0.0642 mmol, 1.55 equiv) in dry dimethylformamide (2.0 mL). The resulting solution was stirred under argon at room temperature for 24 h. Volatiles were then removed *in vacuo* to give an off-white solid, which was re-dissolved in acetonitrile (2 mL). A solution of *cyclo*[DKP-*f*2-RGD] **143** (35 mg, 0.0414 mmol) in pH 7.0 phosphate buffer (0.5 M, 1.0 mL) was then added to the acetonitrile solution, and the pH was adjusted to 7.3 with NaOH (0.2 M, a few drops). The resulting solution was rapidly cooled to 0 °C and stirred for 10 hours, warmed to room temperature and stirred for further 18 h. During the entire period the pH value was kept near 7.3 adding 0.1 M aqueous NaOH, when

required. Dioxane/water (1:1, 10 mL) was then added to the reaction mixture and the resulting solution was freeze-dried. The solid recovered from freeze-drying was purified by semipreparative-HPLC [Water's Atlantis 21 mm x 10 cm column, gradient: 90% (H_2O + 0.1% HCOOH) / 10% (CH_3CN + 0.1% HCOOH) to 30% (H_2O + 0.1% HCOOH) / 70% (CH_3CN + 0.1% HCOOH)]. The purified product was then freeze dried to give the desired compound **90** as a white solid (40 mg, 60% yield).
^{1}H NMR (400 MHz, CD_3OD) δ 8.09 (dd, 2H, J = 8.4, 1.2 Hz), 7.84 (dd, 2H, J = 7.1, 1.6 Hz), 7.74 (tt, 1H, J = 6.8, 1.6 Hz), 7.64 (t, 2H, J = 7.6 Hz), 7.59-7.54 (m, 1H), 7.49-7.44 (m, 6H), 7.28-7.25 (m, 4H), 7.22 (tt, 1H, J = 5.8, 2.8 Hz), 6.43 (s, 1H), 5.98 (t, 1H, J = 9.1 Hz), 5.69 (d, 1H, J = 7.9 Hz), 5.61 (d, 1H, J = 7.0 Hz), 5.45 (d, 1H, J = 7.9 Hz), 5.24 (d, 1H, J = 15.1 Hz), 5.10 (dd, 1H, J = 9.7, 1.6 Hz), 4.77 (m overlapped with water signal, 1H), 4.65 (m overlapped with water signal, 1H), 4.40-4.30 (m, 4H), 4.21 (m, 3H), 4.08 (d, 2H, J = 15.7 Hz), 3.85 (d, 1H, J = 4.6 Hz), 3.78 (d, 1H, J = 7.0 Hz), 3.64 (d, 1H, J = 16.3 Hz), 3.28 (m overlapped with solvent signal, 1H), 3.22 (t, 2H, J = 6.7 Hz), 2.98 (dd, 1H, J = 13.2, 7.4 Hz), 2.84-2.75 (m, 2H), 2.71-2.68 (m, 2H), 2.64-2.50 (m, 3H), 2.37-2.34 (m, 4H), 2.18 (s, 3H), 2.01 (m, 1H), 1.89-1.79 (m, 5H), 1.75-1.59 (m, 7H), 1.14 (s, 3H), 1.11 (s, 3H); ^{13}C NMR (101 MHz, CD_3OD) δ 205.7, 175.8, 175.0, 174.5, 174.17, 174.02, 173.7, 172.09, 171.96, 171.1, 170.74, 170.54, 169.8, 168.0, 158.3, 142.3, 139.6, 137.9, 135.5, 135.04, 134.95, 134.7, 133.2, 131.1, 130.8, 130.2, 129.94, 129.82, 129.71, 129.3, 129.0, 128.64, 128.46, 85.9, 82.0, 79.1, 77.5, 76.7, 76.14, 76.06, 72.9, 72.1, 60.3, 59.1, 55.8, 55.4, 53.2, 51.3, 48.1, 47.8, 44.3, 43.7, 43.0, 40.7, 39.9, 37.32, 37.21, 36.0, 31.0, 29.9, 28.2, 26.8, 26.2, 23.4, 22.3, 20.9, 15.0, 10.6; IR (film) 3361, 3075, 2940, 1730, 1715, 1698, 1667, 1538, 1422, 1243, 1135, 1072 cm^{-1}; MS (ESI) m/z calcd. for $[C_{78}H_{92}N_{11}O_{24}]^+$: 1566.63 $[M+H]^+$; found: 1566.6.

Cyclo[DKP-*f*3-RGD]-PTX 91

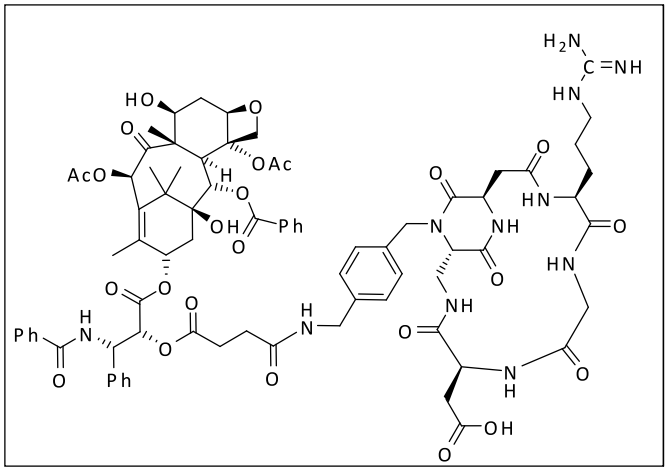

Diisopropylcarbodiimide (11.93 μL, 9.72 mg, 0.077 mmol, 1.9 equiv) was added to a solution of 2′-succinyl-Paclitaxel **147** (49 mg, 0.0513 mmol, 1.25 equiv) and *N*-hydroxysulfosuccinimide sodium salt (13.94 mg, 0.0642 mmol, 1.55 equiv) in dry dimethylformamide (2.0 mL). The resulting solution was stirred under argon at room temperature for 24 h. Volatiles were then removed *in vacuo* to give an off-white solid, which was re-dissolved in acetonitrile (2 mL). A solution of *cyclo*[DKP-*f*3-RGD] **144** (35 mg, 0.0414 mmol) in pH 7.0 phosphate buffer (0.5 M, 1.0 mL) was then added to the acetonitrile solution, and the pH was adjusted to 7.3 with NaOH (0.2 M, a few drops). The resulting solution was rapidly cooled to 0 °C and stirred for 10 hours, warmed to room temperature and stirred for further 18 h. During the entire period the pH value was kept near 7.3 adding 0.1 M aqueous NaOH, when required. Dioxane/water (1:1, 10 mL) was then added to the reaction mixture and the resulting solution was freeze-dried. The solid recovered from freeze-drying was purified by semipreparative-HPLC [Water's Atlantis 21 mm x 10 cm column, gradient: 90% (H_2O + 0.1% HCOOH) / 10% (CH_3CN + 0.1% HCOOH) to 30% (H_2O + 0.1% HCOOH) / 70% (CH_3CN + 0.1% HCOOH)]. The purified product was then freeze dried to give the desired compound **91** as a white solid (47 mg, 70% yield).
^{1}H NMR (400 MHz, CD_3OD) δ 8.12 (dd, 2H, *J* = 8.5, 1.4 Hz), 7.83 (dd, 2H, *J* = 8.5, 1.4 Hz), 7.71-7.66 (m, 1H), 7.60 (t, 2H, *J* = 7.5 Hz), 7.56-7.52 (m, 1H), 7.50-7.42 (m, 6H), 7.30 (s, 4H), 7.25 (tt, 1H, *J* = 7.1, 1.6 Hz), 6.45 (s, 1H), 6.05 (td, 1H, *J* = 9.1, 1.0 Hz), 5.79 (d, 1H, *J* = 6.5 Hz), 5.64 (d, 1H, *J* = 7.2 Hz), 5.44 (d, 1H, *J* = 6.5 Hz), 5.13 (d, 1H, *J* = 14.9 Hz), 5.03 (dd, 1H, *J* = 9.4, 1.6 Hz), 4.91-3.86 (m, 1H), 4.75 (dd, 1H, *J* = 6.5, 4.7 Hz), 4.44-4.36 (m, 3H), 4.30-4.22 (m, 2H), 4.20 (br s, 2H, *J* = 4.2 Hz), 4.16 (ddd, 1H, *J* = 12.0, 8.7, 3.6 Hz), 4.09-4.08 (m, 2H), 3.90 (d, 1H, *J* = 6.0 Hz), 3.82 (d, 1H, *J* = 7.1 Hz), 3.74-3.68 (m, 2H), 3.61 (d, 1H, *J* = 17.2 Hz), 3.54 (dt, 1H, *J* = 11.7, 2.8 Hz), 3.42 (dd, 1H, *J* = 14.6, 6.4), 3.27-3.16 (m, 2H), 2.80-2.75 (m, 2H), 2.72-2.51 (m, 7H), 2.37 (s, 3H), 2.18-2.12 (m, 4H), 2.09-2.01 (m, 1H), 1.92 (s, 3H), 1.86-1.76 (m, 3H), 1.68-1.63 (m, 5H), 1.14 (s, 3H), 1.13 (s, 3H); ^{13}C NMR (101 MHz, CD_3OD) δ 205.5, 174.0, 173.60, 173.46, 173.0, 171.63, 171.54, 171.46, 171.2, 170.5, 167.7, 142.4, 140.2, 138.4, 135.5, 134.80, 134.63, 132.9, 131.39, 131.22, 130.1, 129.72, 129.60, 129.56, 129.3, 128.6, 100.0, 85.9, 82.3, 79.0, 77.5, 76.9, 76.2, 75.9, 72.9, 72.4, 61.6, 60.6, 59.2, 55.4, 54.4, 53.2, 50.5, 48.0, 44.6, 43.76, 43.69, 42.2, 39.9, 37.6, 36.49, 36.36, 31.1, 29.8, 27.7, 26.9, 26.5, 25.1, 23.3, 22.3, 20.8, 15.1, 10.5; IR (film) 3360, 3075, 2940, 1729, 1714, 1693, 1665, 1537, 1421, 1241, 1135, 1071 cm^{-1}; MS (ESI) *m/z* calcd. for $[C_{78}H_{92}N_{11}O_{24}]^+$: 1566.63 $[M+H]^+$; found: 1566.6. $[M+H]^{+1}$; HRMS (QTOF) *m/z* calcd. for $[C_{78}H_{92}N_{11}O_{24}]^+$: 1566.6238 $[M+H]^+$; found: 1566.6283 (error: 3.2 ppm) $[M+H]^{+1}$.

HRMS of *Cyclo*[DKP-*f*3-RGD]-PTX **91**:

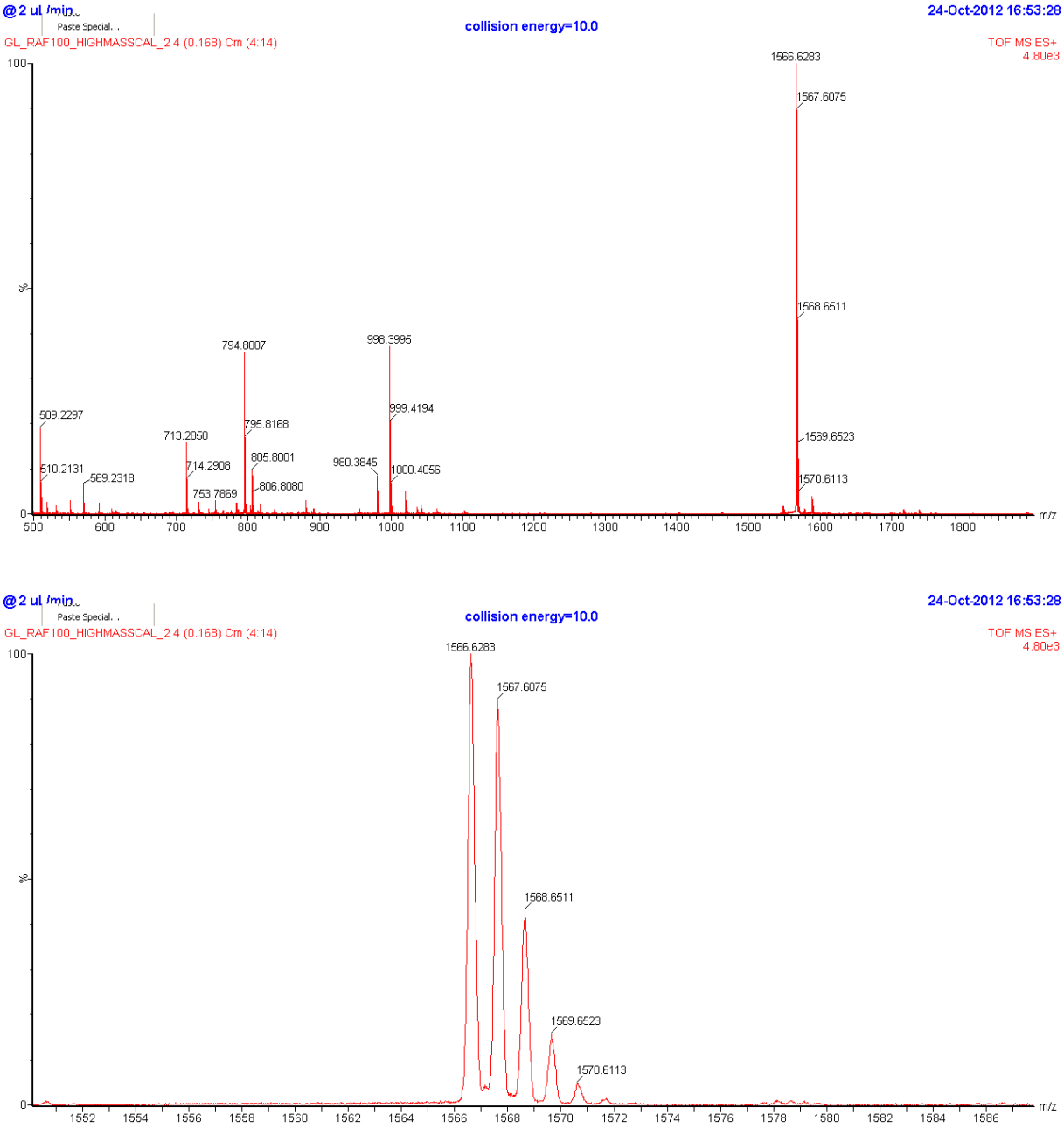

***Cyclo*[DKP-*f*4-RGD]-PTX 92**

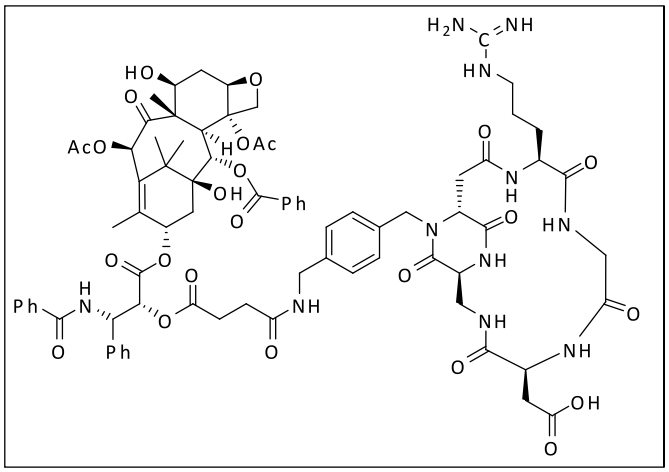

Diisopropylcarbodiimide (11.93 μL, 9.72 mg, 0.077 mmol, 1.9 equiv) was added to a solution of 2′-succinyl-Paclitaxel **147** (49 mg, 0.0513 mmol, 1.25 equiv) and *N*-hydroxysulfosuccinimide sodium salt (13.94 mg, 0.0642 mmol, 1.55 equiv) in dry dimethylformamide (2.0 mL). The resulting solution was stirred under argon at room temperature for 24 h. Volatiles were then removed *in vacuo* to give an off-white solid, which was re-dissolved in acetonitrile (2 mL). A solution of *cyclo*[DKP-*f*4-RGD] **145** (35 mg, 0.0414 mmol) in pH 7.0 phosphate buffer (0.5 M, 1.0 mL) was then added to the acetonitrile solution, and the pH was adjusted to 7.3 with NaOH (0.2 M, a few drops). The resulting solution was rapidly cooled to 0 °C and stirred for 10 hours, warmed to room temperature and stirred for further 18 h. During the entire period the pH value was kept near 7.3 adding 0.1 M aqueous NaOH, when required. Dioxane/water (1:1, 10 mL) was then added to the reaction mixture and the resulting solution was freeze-dried. The solid recovered from freeze-drying was purified by semipreparative-HPLC [Water's Atlantis 21 mm x 10 cm column, gradient: 90% (H_2O + 0.1% HCOOH) / 10% (CH_3CN + 0.1% HCOOH) to 30% (H_2O + 0.1% HCOOH) / 70% (CH_3CN + 0.1% HCOOH)]. The purified product was then freeze dried to give the desired compound **92** as a white solid (42 mg, 63% yield).
^{1}H NMR (400 MHz, DMSO-d_6) δ 9.22 (d, 1H, J = 8.5 Hz), 8.95 (s, 1H), 8.79 (s, 1H), 8.44-8.40 (m, 1H), 8.35 (t, 1H, J = 5.7 Hz), 8.20 (s, 1H), 7.98 (dd, 2H, J = 7.1, 1.3 Hz), 7.86 (dd, 2H, J = 7.2, 1.3 Hz), 7.76-7.69 (m, 1H, J = 1.5 Hz), 7.69-7.63 (m, 2H), 7.59-7.53 (m, 1H), 7.49 (d, 1H, J = 7.6 Hz), 7.46-7.42 (m, 5H), 7.23-7.17 (m, 5H), 6.30 (s, 1H), 5.83 (t, 1H, J = 8.9 Hz), 5.54 (t, 1H, J = 8.7 Hz), 5.42 (d, 1H, J = 7.1 Hz), 5.36 (d, 1H, J = 8.9 Hz), 5.21 (d, 1H, J = 14.4 Hz), 4.92 (d, 2H, J = 10.6 Hz), 4.62 (s, 1H), 4.27-4.07 (m, 5H), 4.04-3.99 (m, 3H), 3.94-3.87 (m, 1H), 3.83-3.79 (m, 1H), 3.70 (br s, 2H), 3.58 (d, 1H, J = 7.1 Hz), 3.43-3.26 (m overlapped with water signal, 2H), 3.07 (br s, 2H), 2.89 (br s, 2H), 2.69-2.56 (m, 3H), 2.45 (t, 2H, J = 6.8 Hz), 2.38-2.30 (m, 2H), 2.24-2.20 (m, 4H), 2.10 (s, 3H), 1.84-1.76 (m, 5H), 1.64 (t, 1H, J = 12.4 Hz), 1.54-1.41 (m, 7H), 1.02 (s, 3H), 1.00 (s, 3H); ^{13}C NMR (101 MHz, DMSO-d_6) δ 202.3, 173.9, 172.13, 171.94, 170.8, 170.2, 169.63, 169.50, 169.1, 168.84,

168.74, 168.3, 167.9, 166.4, 165.2, 157.3, 139.4, 138.7, 137.3, 134.8, 134.3, 133.45, 133.33, 132.7, 131.4, 129.95, 129.93, 129.56, 129.54, 128.73, 128.65, 128.55, 128.29, 128.14, 127.83, 127.71, 127.65, 127.4, 83.6, 80.2, 76.7, 75.3, 74.68, 74.54, 74.50, 72.5, 70.7, 70.4, 57.4, 56.1, 53.98, 53.86, 52.17, 52.13, 46.1, 44.9, 42.9, 42.1, 41.9, 40.1, 39.9, 38.2, 36.5, 35.7, 34.4, 29.5, 28.7, 27.6, 26.3, 25.3, 22.5, 21.4, 20.63, 20.52, 13.9, 9.7; IR (film) 3370, 3071, 2941, 1731, 1714, 1699, 1667, 1538, 1421, 1243, 1135, 1071 cm^{-1}; MS (ESI) *m/z* calcd. for $[C_{78}H_{92}N_{11}O_{24}]^+$: 1566.63 $[M+H]^+$; found: 1566.6

***Cyclo*[DKP-*f*6-RGD]-PTX 93**

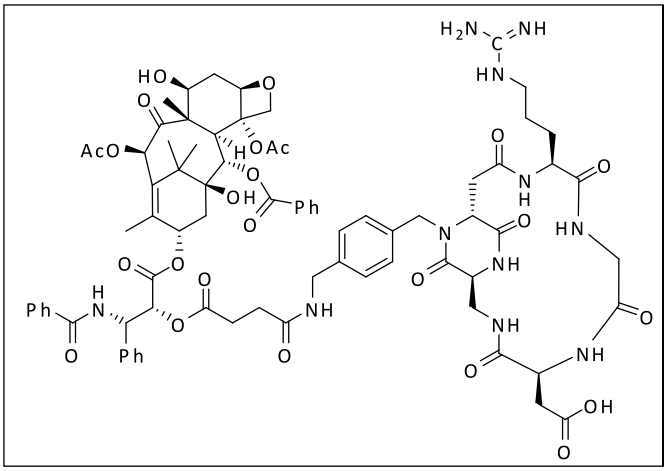

Diisopropylcarbodiimide (11.93 μL, 9.72 mg, 0.077 mmol, 1.9 equiv) was added to a solution of 2′-succinyl-Paclitaxel **147** (49 mg, 0.0513 mmol, 1.25 equiv) and *N*-hydroxysulfosuccinimide sodium salt (13.94 mg, 0.0642 mmol, 1.55 equiv) in dry dimethylformamide (2.0 mL). The resulting solution was stirred under argon at room temperature for 24 h. Volatiles were then removed *in vacuo* to give an off-white solid, which was re-dissolved in acetonitrile (2 mL). A solution of *cyclo*[DKP-*f*6-RGD] **146** (35 mg, 0.0414 mmol) in pH 7.0 phosphate buffer (0.5 M, 1.0 mL) was then added to the acetonitrile solution, and the pH was adjusted to 7.3 with NaOH (0.2 M, a few drops). The resulting solution was rapidly cooled to 0 °C and stirred for 10 hours, warmed to room temperature and stirred for further 18 h. During the entire period the pH value was kept near 7.3 adding 0.1 M aqueous NaOH, when required. Dioxane/water (1:1, 10 mL) was then added to the reaction mixture and the resulting solution was freeze-dried. The solid recovered from freeze-drying was purified by semipreparative-HPLC [Water's Atlantis 21 mm x 10 cm column, gradient: 90% (H_2O + 0.1% HCOOH) / 10% (CH_3CN + 0.1% HCOOH) to 30% (H_2O + 0.1% HCOOH) / 70% (CH_3CN + 0.1% HCOOH)]. The purified product was then freeze dried to give the desired compound **93** as a white solid (43 mg, 65% yield).

^{1}H NMR (400 MHz, DMSO-d_6) δ 9.42 (s, 1H), 9.25 (d, 1H, J = 8.5 Hz), 8.74 (s, 1H), 8.62 (s, 1H), 8.45 (s, 1H), 8.37 (t, 1H, J = 5.7 Hz), 7.99-7.97 (m, 2H), 7.87-7.84 (m, 3H), 7.73 (t, 1H, J = 7.3 Hz), 7.66 (t, 2H, J = 7.4 Hz), 7.56 (tt, 1H, J = 7.3, 2.0 Hz), 7.50-7.44 (m, 7H), 7.25-7.15 (m, 5H), 6.30 (s, 1H), 5.83 (t, 1H, J = 8.8 Hz), 5.53 (t, 1H, J = 8.7 Hz), 5.41 (d, 1H, J = 7.2 Hz), 5.35 (d, 1H, J = 9.0 Hz), 5.11 (d, 1H, J = 14.9 Hz), 4.98-4.90 (t, 2H), 4.64 (s, 1H), 4.29-4.20 (m, 3H), 4.17-4.08 (m, 2H), 4.04-3.95 (m, 3H), 3.93-3.79 (m, 3H), 3.74-3.64 (m, 1H), 3.59 (d, 1H, J = 6.8 Hz), 3.53-3.43 (m, 1H), 3.26-3.19 (m, 1H), 3.07 (br s, 1H), 2.97 (br s, 1H), 2.72-2.58 (m, 4H), 2.56-2.52 (m, 1H), 2.45 (t, 2H, J = 6.8 Hz), 2.40-2.28 (m, 2H), 2.23 (s, 3H), 2.10 (s, 3H), 1.82-1.60 (m, 7H), 1.52-1.46 (m, 6H), 1.02 (s, 3H), 1.00 (s, 3H); ^{13}C NMR (101 MHz, DMSO-d_6) δ 202.7, 172.0, 171.8, 170.3, 169.72, 169.57, 169.2, 168.79, 168.72, 166.8, 166.4, 165.2, 157.3, 139.5, 137.4, 135.2, 134.3, 133.5, 133.32, 133.28, 132.7, 131.5, 129.9, 129.6, 128.7, 128.38, 128.21, 128.0, 127.7, 127.5, 83.6, 80.3, 76.7, 75.3, 74.69, 74.62, 74.49, 70.7, 70.4, 57.2, 54.4, 54.1, 51.98, 51.92, 46.10, 45.97, 43.0, 41.9, 40.9, 39.7, 37.8, 36.6, 34.4, 29.5, 28.7, 28.0, 26.4, 24.4, 22.6, 21.4, 20.7, 14.0, 9.8; IR (film) 3365, 3071, 2940, 1732, 1716, 1699, 1665, 1537, 1421, 1243, 1135, 1071 cm^{-1}; MS (ESI) m/z calcd. for $[C_{78}H_{92}N_{11}O_{24}]^{+}$: 1566.63 $[M+H]^{+}$; found: 1566.6.

4.6 - *Synthesis of cyclo[DKP-f3-RGD]-hemisuccinamide 148*[a]

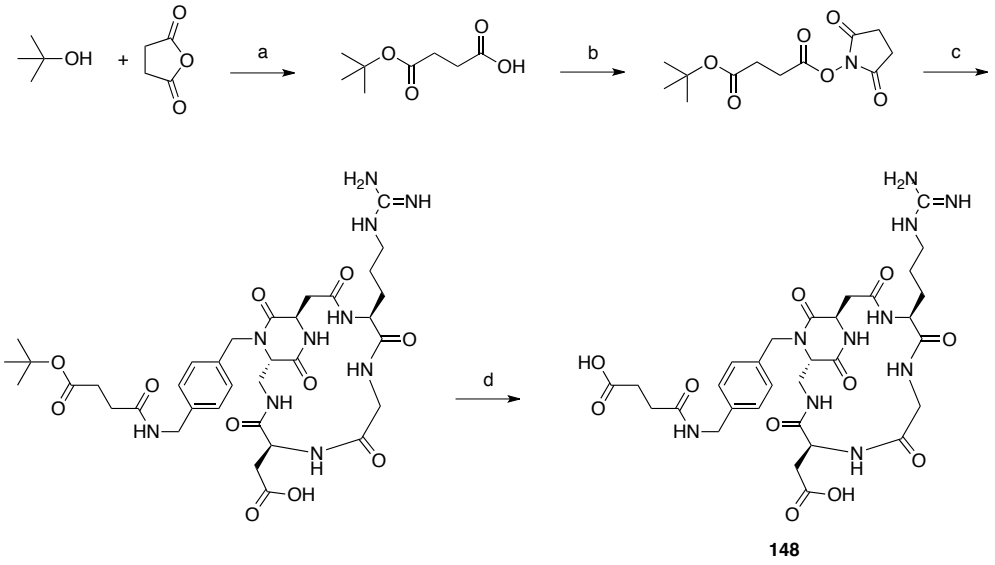

[a]Reagents and conditions: (a) *N*-hydroxysuccinimide, Et_3N, DMAP, Toluene, DCM, 48 h, reflux, 80%; (b) *N*-hydroxysuccinimide, DIC, DCM, 4 h, room temp., quant.; (c) *cyclo*(DKP-*f*3-RGD) **144**, CH_3CN, aq. phosphate buffer, pH = 7.3, 10 h at 0 °C then 8 h at room temp., 68%; (d) TFA/DCM 1:2, TES, 3 h, 0 °C to room temp., quant.

Tert-butyl hemisuccinate

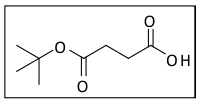

To a mixture of succinic anhydride (1.5 g, 15 mmol), *N*-hydroxysuccinimide (0.5 g, 4.5 mmol) and DMAP (0.18 g, 1.45 mmol) in toluene (25 mL), triethylamine (0.63 mL, 4.5 mmol) and *tert*-butyl alchohol (2.5 mL) were added. The brownish solution was refluxed for 24 h, cooled to room temperature, diluted with ethyl acetate (30 mL), washed with 10% citric acid (2 x 30 mL) and brine, and dried over Na_2SO_4. Volatiles were removed under vacuum to give a brown oil, which was recrystallized from Et_2O / *n*-hexane 1/3 to afford the pure *tert*-butyl hemisuccinate as a white solid (2.08 g, 80% yield).

^{1}H NMR (400 MHz, $CDCl_3$) δ 11.56 (s, 1H), 2.62 (m, 2H), 2.55 (m 2H), 1.39 (s, 9H); ^{13}C NMR (100 MHz, $CDCl_3$) δ 176.91, 171.46, 81.05, 30.08, 28.92, 28.00; MS (ESI) *m/z* calcd. for $[C_8H_{15}O_4]^+$: 175.10 $[M+H]^+$; found: 175.2

Cyclo[DKP-*f*3-RGD]-hemisuccinamide 148

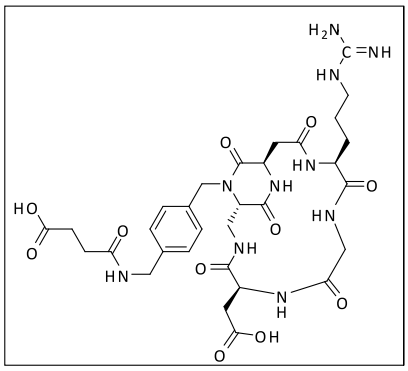

Diisopropylcarbodiimide (11.9 μL, 9.72 mg, 0.077 mmol, 3.3 equiv) was added to a solution of *tert*-butyl hemisuccinate (7 mg, 0.0401 mmol, 1.7 equiv) and *N*-hydroxysuccinimide (5.4 mg, 0.0466 mmol, 2 equiv) in dry DCM (2.0 mL). The resulting solution was stirred under argon at room temperature for 2 h. Volatiles were then removed *in vacuo* to give an off-white solid, which was re-dissolved in acetonitrile (2 mL). A solution of *cyclo*[DKP-*f*3-RGD] **144** (20 mg, 0.0233 mmol) in pH 7.5 phosphate buffer (0.5 M, 1.0 mL) was then added to the acetonitrile solution, and the pH was adjusted to 7.3 with NaOH (0.2 M, a few drops). The resulting solution was rapidly cooled to 0 °C and stirred for 10 hours, warmed to room temperature and stirred for further 18 h. During the entire period the pH value was kept near 7.3 adding 0.1 M aqueous NaOH, when required. Volatiles were removed under vacuum, the residue was dissolved in DMC/TFA/Et_3SiH (2:1:0.1, 2 mL) and stirred for 2 h. The solution was concentrated to dryness and the residue was purified by semipreparative-HPLC [Water's Atlantis 21 mm x 10 cm column, gradient: 95% (H_2O + 0.1% TFA) / 5% (CH_3CN + 0.1% TFA) to 30% (H_2O + 0.1% TFA) / 70% (CH_3CN + 0.1% TFA)] to afford the desired compound **148** as a white solid (12 mg, 68% yield).

^{1}H NMR (400 MHz, DMSO-d_6): δ 12.18 (s, 1H), 9.08 (d, 1H, J = 6.7 Hz), 8.33 (t, 1H, J = 5.8 Hz), 8.14 (s, 1H), 7.98 (t, 1H, J = 6.2 Hz), 7.81 (dd, 1H, J = 8.9, 2.7 Hz), 7.59-7.45 (m, 1H), 7.21 (AB-system, 4H), 5.00 (d, 1H, J = 15.1 Hz), 4.84-4.78 (m, 1H), 4.38 (dd, 1H, J = 9.5, 3.8 Hz), 4.27-4.20 (m, 3H), 3.89 (d, 1H, J = 15.0 Hz), 3.79-3.72 (m, 3H), 3.53-3.44 (m, 1H), 3.38 (m, 1H), 3.15 (m, 2H), 2.80 (dd, 1H, J = 16.5, 9.3 Hz), 2.60 (dd, 1H, J = 13.4, 10.1 Hz), 2.48-2.42 (m, 3H), 2.40 (m, 3H), 2.04 (m, 1H), 1.77-1.67 (m, 1H), 1.54-1.41 (m, 2H).; ^{13}C NMR (100 MHz, $CDCl_3$) δ 173.7, 171.4, 171.2, 170.98, 170.90, 170.7, 169.3, 169.1, 168.6, 156.6, 139.0, 134.5, 127.7, 127.5, 58.6, 53.7, 51.0, 48.2, 46.3, 41.76, 41.64, 40.45, 40.33, 37.4, 35.2, 30.0, 29.1, 26.0, 25.8; MS (ESI) *m/z* calcd. for $[C_{31}H_{43}N_{10}O_{11}]^+$: 731.31 $[M+H]^+$; found: 731.3

References:

[1] Y. Huang, D. R. Dalton, P. J. Carroll, *J. Org. Chem.* **1997**, *62*, 372-376.

[2] C. M. Thompson, J. A. Frick, D. L. Green, *J. Org. Chem.* **1990**, *55*, 111-116.

[3] K. L.Webster, A. B.Maude, M. E. O'Donnell, A. P. Mehrotra, D. J. Gani, *Chem. Soc. Perkin Trans. 1* **2001**, 1673-1695.

[4] M.C. Pirrung, S.W. Shuey, *J. Org. Chem.* **1994**, *59*, 3890-3897.

[5] S H. Rosenberg, K. P. Spina, K. W. Woods, J. Polakowski, D. L. Martin, Z. Yao, H. H. Stein, J. Cohen, J. L. Barlow, D. A. Egan, K. A. Tricarico, W. R. Baker, H. D. Kleinert, *J. Med. Chem.* **1993**, *36*, 449-459.

[6] K. Gu, L. Bi, M. Zhao, C. Wang, J. Juc, S. Peng, *Bioorg. Med. Chem.* **2007**, *15*, 6273-6290.

[7] J. M. Humphrey, R. J. Bridges, J. A. Hart, A. R. Chamberlin, *J. Org. Chem.* **1994**, *59*, 2467-2472.

[8] V. Bavetsias, A. L. Jackman, R. Kimbell, W. Gibson, F. T. Boyle, G. M. F. Bisset, *J. Med. Chem.* **1996**, *39*, 73-85.

[9] Y. Narukawa, K. N. Juneau, D. Snustad, D. B. Miller, L. S. Hegedus, *J. Org. Chem.* **1992**, *57*, 5453-5462.

[10] W. C. Still, M. Kahn, A. Mitra. *J. Org. Chem.* **1978**, *43*, 2923-2925.

[11] Z. Dogan, R. Paulini, J. A. Rojas Stutz, S. Narayanan, C. Richert. *J. Am. Chem. Soc.* **2004**, *126*, 4762-4763.

CHAPTER 5

EXPERIMENTAL SECTION – NMR, COMPUTATIONAL AND BIOLOGICAL PROCEDURES

1 - NMR studies

NMR experiments were performed at a temperature of 298 K on Bruker Avance 400 and 600 MHz spectrometers. All proton and carbon chemical shifts were assigned unambiguously. The NMR experiments were carried out in a D_2O/H_2O 1:9 mixture in order to observe amide protons. Two-dimensional experiments (TOCSY, NOESY, and HSQC) were carried out on samples of cyclic RGD-peptidomimetics **16-23** at a concentration in the range 3-6 mM. NOESY experiments were performed at 0.7 or 0.8 s. The water resonance was saturated with the excitation sculpting sequence from the Bruker library. The conformations of the cyclic pentapeptides were analyzed with respect to hydrogen bonding of amide protons (VT-NMR spectroscopy) and NOE contacts.

2 - Computational procedures

All calculations were run using the Schrödinger suite of programs (http://www.schrodinger.com) through the Maestro graphical interface. *Conformational analysis*. Conformational preferences of the RGD-peptidomimetics were investigated by Monte Carlo/stochastic dynamics (MC/SD) hybrid simulations using the NMR restraints derived from the experimental NOE contacts (for distance restraints used for each calculation, see the Supporting Information). All the NOE restraints have been set to a distance value of 2±0.5Å with a force constant of 100 kJ/mol·Å^2. MC/SD simulations were performed at 300K within the framework of MacroModel version 9.5 employing the OPLS_2001 force field and the implicit water GB/SA solvation model RGD side-chain dihedral angles were defined as internal coordinate degrees of freedom in the Monte Carlo part of the algorithm. A time step of 1 fs was used for the stochastic dynamics (SD) part of the algorithm for 10 ns of simulation time. Samples were taken at 2 ps intervals during each simulation, yielding 5000 conformations for analysis. The percentages of H-bonds discussed in the paper have been calculated as percentages of

conformations sampled during the simulation in which donor H - acceptor O distance < 2.5 Å (γ-turn) or < 4 Å (β-turn).

2.1 - *Molecular docking*

The recently solved crystal structure of the extracellular domain of the integrin $\alpha_v\beta_3$ receptor in complex with Cilengitide and in the presence of the proadhesive ion Mn2+ (PDB entry code 1L5G) was used for docking studies. Docking was performed only on the globular head of the integrin because the headgroup of integrin has been identified in the X-ray structure as the ligand-binding region. The protein structure was setup for docking as follows; the protein was truncated to residue sequences 41-342 for chain α and 114-347 for chain β. Due to a lack of parameters, the Mn2+ ions in the experimental protein structure were modelled by replacing them with Ca2+ ions. The resulting structure was prepared using the Protein Preparation Wizard of the graphical user interface Maestro and the OPLSAA force field. The automated docking calculations were performed using Glide (Grid-based Ligand Docking with Energetics). The grid generation step started from the extracellular fragment of X-ray structure of $\alpha_v\beta_3$ complex with Cilengitide, as described in the protein setup section. The center of the grid enclosing box was defined by the center of the bound ligand, as described in the original PDB entry. The enclosing box dimensions, which are automatically deduced from the ligand size, fit the entire active site. For the docking step, the size of the bounding box for placing the ligand center was set to 12 Å. No further modifications were applied to the default settings. The GlideScore function was used to select 20 poses for each ligand. The Glide program was initially tested for its ability to reproduce the crystallized binding geometry of cilengitide. The program was successful in reproducing the experimentally determined binding mode of this compound, as it corresponds to the best-scored pose.

3 - Biological procedures

3.1 - *Plasma stability assays*

A 10 mM stock solution of *cyclo*[DKP-*f*3-RGD]-PTX **11** (MW 1566.62) was obtained by dissolving 2 mg of compound in 127.66 μL of DMSO. A further dilution 1:50 in pH 7.5 phosphate buffer (PBS) was performed (10 μL of stock solution into 490 μL PBS) to obtain a 200 μM solution; from this last solution, 25 μL were spiked into 475 μL of plasma (murine or human) to obtain the final concentration of 10 μM. Standards (lidocaine and 2-Piperidinoethyl-4-amino-5-chloro-2-methoxybenzoate) were

tested at 2.5 μM final concentration starting from a 500 μM stock solution in DMSO, further diluted 1:10 into PBS and 1:20 into plasma.

Aliquots of 50 μL volume were taken at 0, 15, 30, 60, 120, 180 and 300 minutes of incubation at 37 °C and immediately quenched with 200 μL of a solution of Verapamil 250 ng/mL (internal standard) in acetonitrile. Samples were centrifuged for 20 min at 3000 rpm and supernatants analyzed by UPLC (Waters) interfaced with a Premiere XE Triple Quadrupole (Waters). Eluents were Phase A: 95% H_2O, 5% CH_3CN + 0.1% HCOOH and Phase B: 5% H_2O, 95% CH_3CN + 0.1% HCOOH. Waters UPLC: flow 0.6 mL/min, column BEH C18, 50x2.1mm 1.7 μm at 50 °C, vol inj. 5 μL. Samples were analyzed in MRM conditions: ESI Positive, Desolvation Temperature 450 °C, Desolvation Gas 900 L/h, Cone Gas 90 L/h, Collision Gas 0.2 L/h. Results are presented as Mean ± S.D., n=2 for standards, n=3 for *cyclo*[DKP-*f*3-RGD]-PTX **91**.

3.2 - *Solid-phase receptor-binding assay*

Purified $\alpha_v\beta_3$ and $\alpha_v\beta_5$ receptors (Chemicon International, Inc., Temecula, CA, USA) were diluted to 0.5 μg/mL in coating buffer containing 20 mM Tris-HCl (pH 7.4), 150 mM NaCl, 1 mM $MnCl_2$, 2 mM $CaCl_2$ and 1 mM $MgCl_2$. An aliquot of diluted receptors (100 μL/well) was added to 96-well microtiter plates (NUNC MW 96F MEDISORP STRAIGHT) and incubated overnight at 4 °C. The plates were then incubated with blocking solution (coating buffer plus 1% bovine serum albumin) for additional 2 hours at room temperature to block nonspecific binding followed by 3-hour incubation at room temperature with various concentrations (10^{-12}–10^{-5} M) of test compounds in the presence of 1 μg/mL biotinylated vitronectine. Biotinylation was performed using EZ-Link Sulfo-NHS-Biotinylation kit (Pierce, Rockford, IL). After washing, the plates were incubated for 1 hour at room temperature with streptavidin-biotinylated peroxidase complex (Amersham Biosciences, Uppsala, Sweden) followed by 30 minutes incubation with 100 μL Substrate Reagent Solution (R&D Systems, Minneapolis, MN) before stopping the reaction by addition of 50 μL of 2 N H_2SO_4. Absorbance at 415 nm was read in a Synergy™ HT Multi-Detection Microplate Reader (BioTek Instruments, Inc.). Each data point is the result of the average of triplicate wells and was analyzed by nonlinear regression analysis with Prism GraphPad program.

3.3 - *Cell sensitivity studies*

The human ovarian carcinoma IGROV-1 cell line, the cisplatin-resistant IGROV-1/Pt1 subline the human ovarian carcinoma cell line SKOV3, the human pancreatic carcinoma cell lines PANC-1 and MIA-PaCa2 were cultured in DMEM medium; the human osteosarcoma U2-OS cell line was grown in Mc Coy's 5A medium; HDFC cells were cultured in DMEM-F12 medium. In all cases, the medium was supplemented with 10% fetal calf serum. The cell sensitivity to drugs was measured by using the growth-inhibition assay based on cell counting. Cells were seeded in duplicates into 6-well plates and exposed to drug 24 h later. Paclitaxel and the studied compounds were dissolved in dimethylsulfoxide (DMSO) and then added to culture medium. DMSO concentration in medium never exceeded 0.25%. After 72 h of drug incubation, cells were harvested for counting with a cell counter (Z1 Beckman Coulter counter). IC_{50} is defined as the drug concentration producing 50% decrease of cell growth. At least five independent experiments were performed.

3.4 - *Analysis of integrin levels*

The expression of integrins was measured by flow cytometry, following optimization of antibody concentration. Exponentially growing cells were harvested and incubated fro 30 min at 4 °C with anti human $\alpha_v\beta_3$ or $\alpha_v\beta_5$ antibodies or isotypic controls (Millipore, Temecula, CA; Chemicon International). Cells were than washed and samples were immediately used for flow cytometric analysis (FACScan, Becton-Dickinson). Expression of integrins was expressed as ratio between the mean fluorescence intensity obtained in cells incubated with anti-integrin antibodies divided by that of cells incubated with isotypic control.

3.5 - *In vivo antitumor activity studies*

All experiments of were carried out using female athymic Swiss nude mice, 8-10 weeks-old (Charles River, Calco, Italy). Mice were maintained in laminar flow rooms keeping temperature and humidity constant. Mice had free access to food and water. Experiments were approved by the Ethics Committee for Animal Experimentation of the Istituto Nazionale Tumori of Milan according to institutional guidelines. The IGROV-1/Pt1 human tumor xenograft, derived from cultures of the corresponding ovarian carcinoma cell line, was used. Exponentially growing cells (10^7/mouse) were s.c. injected into the right flank of athymic nude mice and the tumor line was achieved by serial s.c. passages of fragments of re-growing tumors into healthy mice. Groups of four mice bearing bilateral

s.c. tumors were employed. Tumor fragments were implanted on day 0 and tumor growth was followed by biweekly measurements of tumor diameters with a Vernier caliper. Tumor volume (TV) was calculated according to the formula: TV (mm^3) = $d^2xD/2$ where d and D are the shortest and the longest diameter, respectively. Compounds were delivered i.v. and administered every 4 days for 4 times (q4dx4). Treatment started three days after tumor implant, when tumors were just palpable. The efficacy of the drug treatment was assessed as: 1) Tumor volume inhibition percentage (TVI %) in treated versus control mice, calculated as: TVI% = 100-(mean TV treated/mean TV control x 100); 2) Log_{10} cell kill (LCK) calculated by the formula: LCK = (T-C)/3.32xDT where T and C are the mean times (days) required for treated (T) and control (C) tumors, respectively, to reach an established TV and DT is the doubling time of control tumors, obtained from semilog best-fit curves of mean tumor volumes plotted against time; 3) Complete regression (CR), i.e. disappearance of the tumor lasting at least 10 days after the end of treatments. Tumors not re-grown at the end of experiment were considered no evidence of disease (NED). The toxicity of the drug treatment was determined as body weight loss (BWL) and lethal toxicity (D/T, dead/treated mice). The highest body weight loss percentage induced by treatments is reported in the Tables. Deaths occurring in treated mice before the death of the first control mouse were ascribed to toxic effects. Two-sided Student's t test was used for statistical comparison of tumor volumes in control over treated mice. For *in vivo* studies PTX was dissolved in a mixture of ethanol and cremophor ELP (50+50%) and kept at 4 °C. At treatment the drug was diluted in 90% of cold saline after magnetic stirring and administered i.v.. *Cyclo*[DKP-*f3*-RGD]-PTX **11** was dissolved and administered like Paclitaxel at room temperature.

3.6 - *Immunohistochemistry*

Tumor xenografts and adjacent tissues were excised and formalin fixed and paraffin embedded. Four μm sections from each tumor xenograft were routinely stained with Hematoxylin-Eosin (HE) and evaluated under a light microscope. Mitoses were evaluated in 3 randomly selected 400x fields within the bulk of the xenograft, avoiding areas of necrosis and hemorrhage. The total number of mitoses and the mean value for each sample were evaluated. Furthermore, mitoses were classified as "normal" and "aberrant", considering in this latter class both small condensed hyperchromatic nuclei and large cells composed by nuclear envelope around individual clusters of missegregated chromosomes (mitotic catastrophe), and the ratio between these two classes was evaluated. The analysis of mitoses was performed in a blind fashion. Statistical analysis of the obtained data was carried out with Kruskal Wallis test followed by Dunn's multiple comparison test using GraphPad Prism (GraphPad Software, Inc.).

APPENDIX OF NMR DATA

β-allyl aspartic acid hydrochloride 44

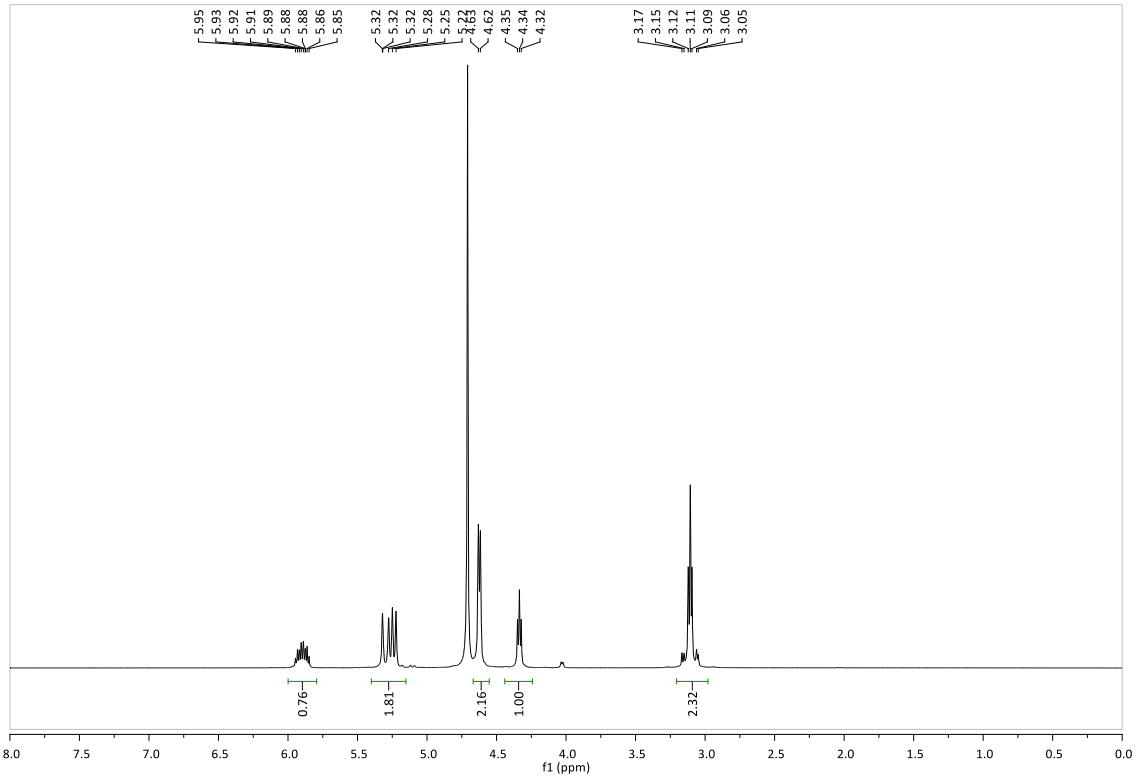

N-Boc-β-allyl aspartic acid 45

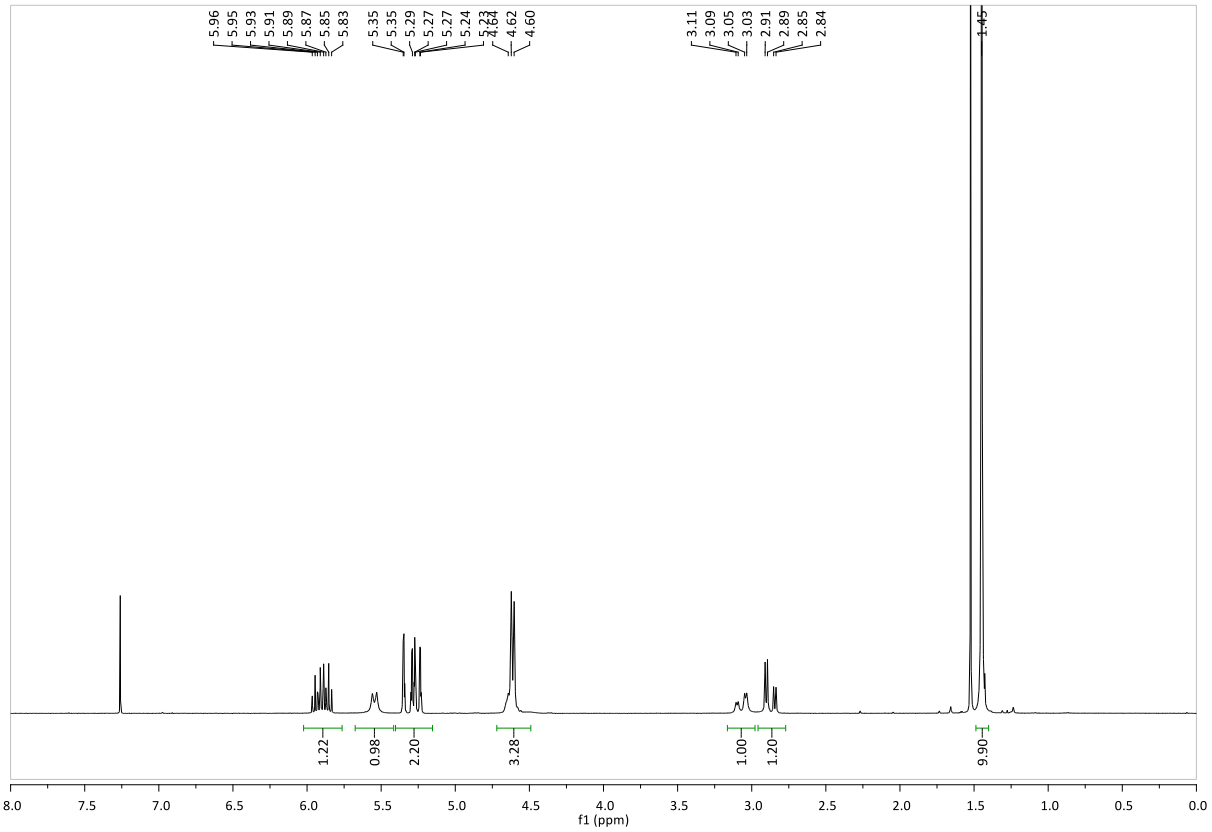

serine methylester hydrochloride 46

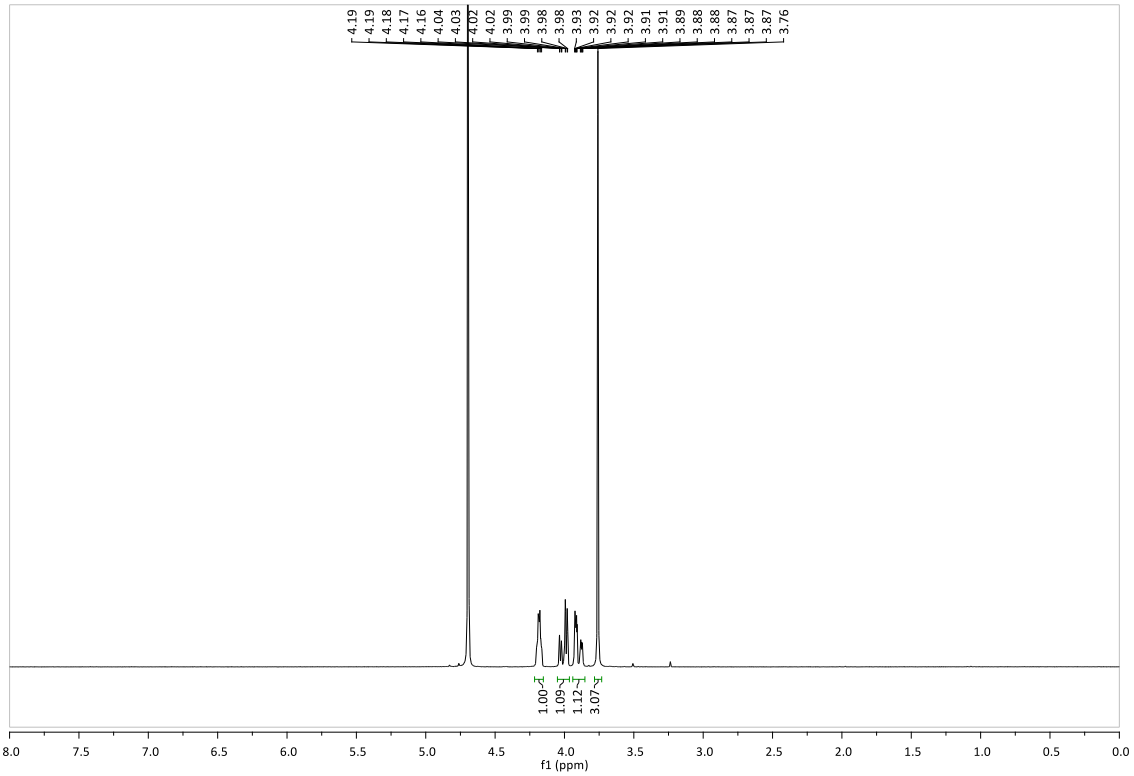

***N*-Bn-Ser-OMe 47**

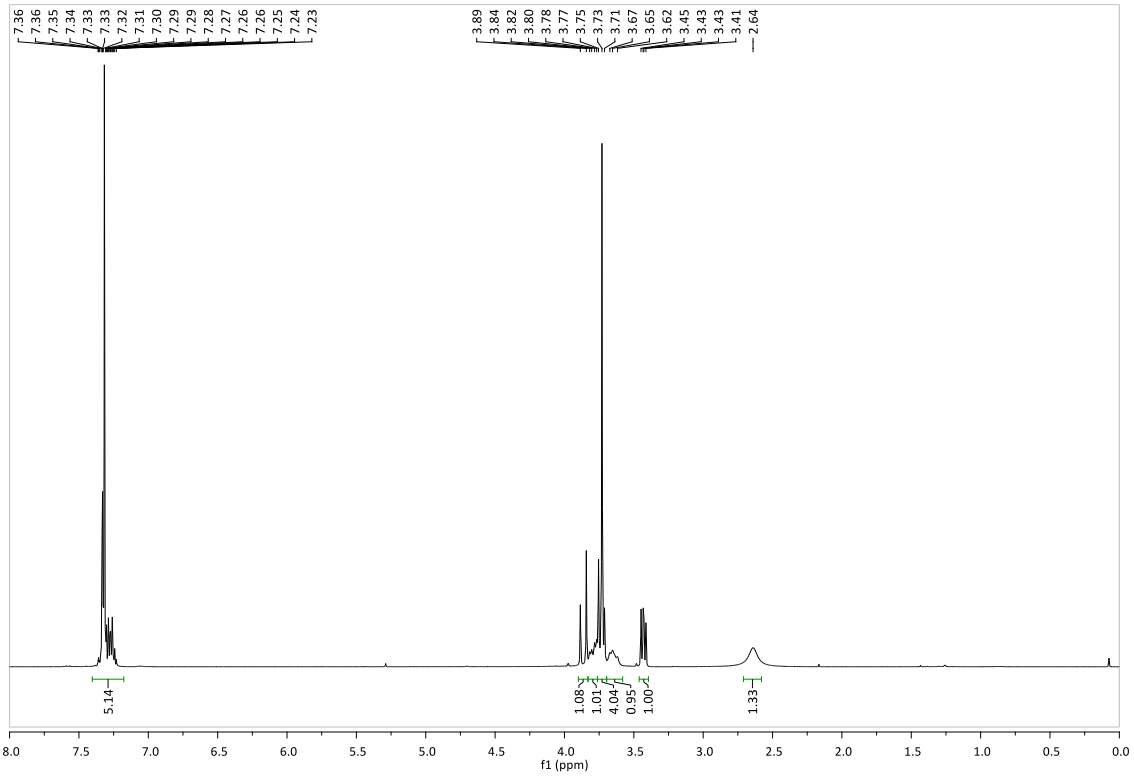

N-Bn-Ser(O-(*S*)-*N*-Boc-Asp(OAll))-OMe 55 a + b

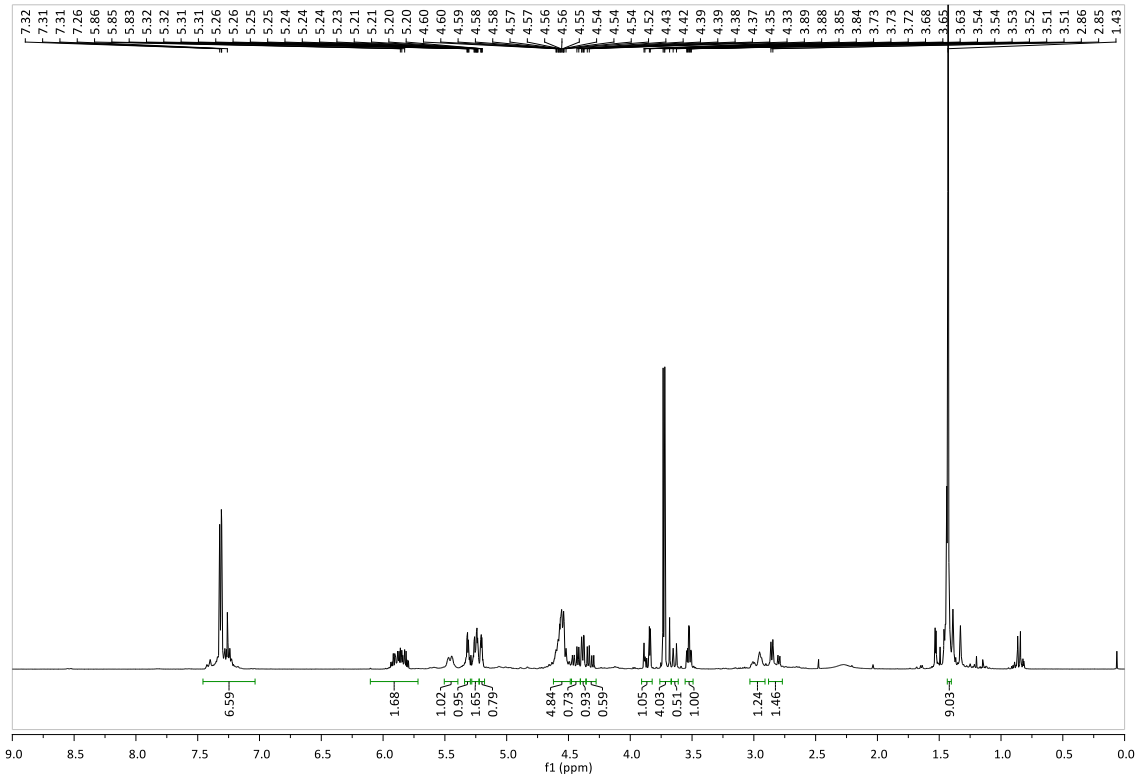

(*S*)-*N*-Bn-Ser(O-(*R*)-*N*-Boc-Asp(OAll))-OMe 49c

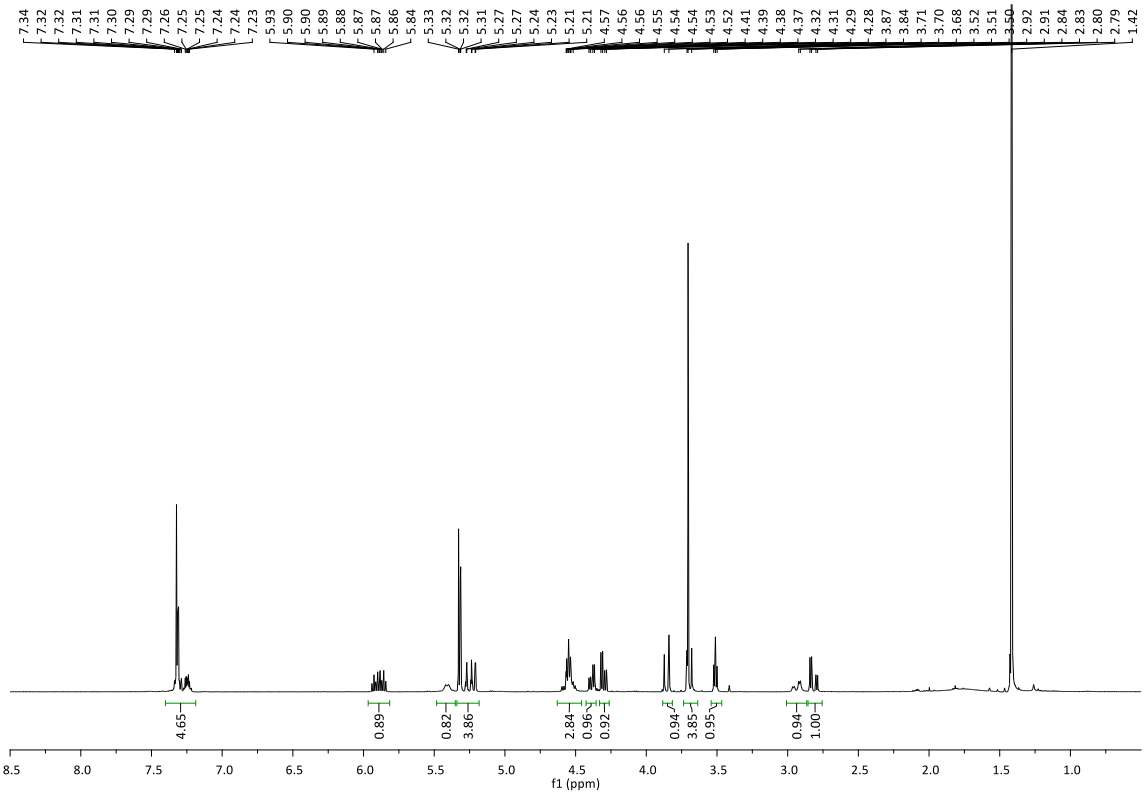

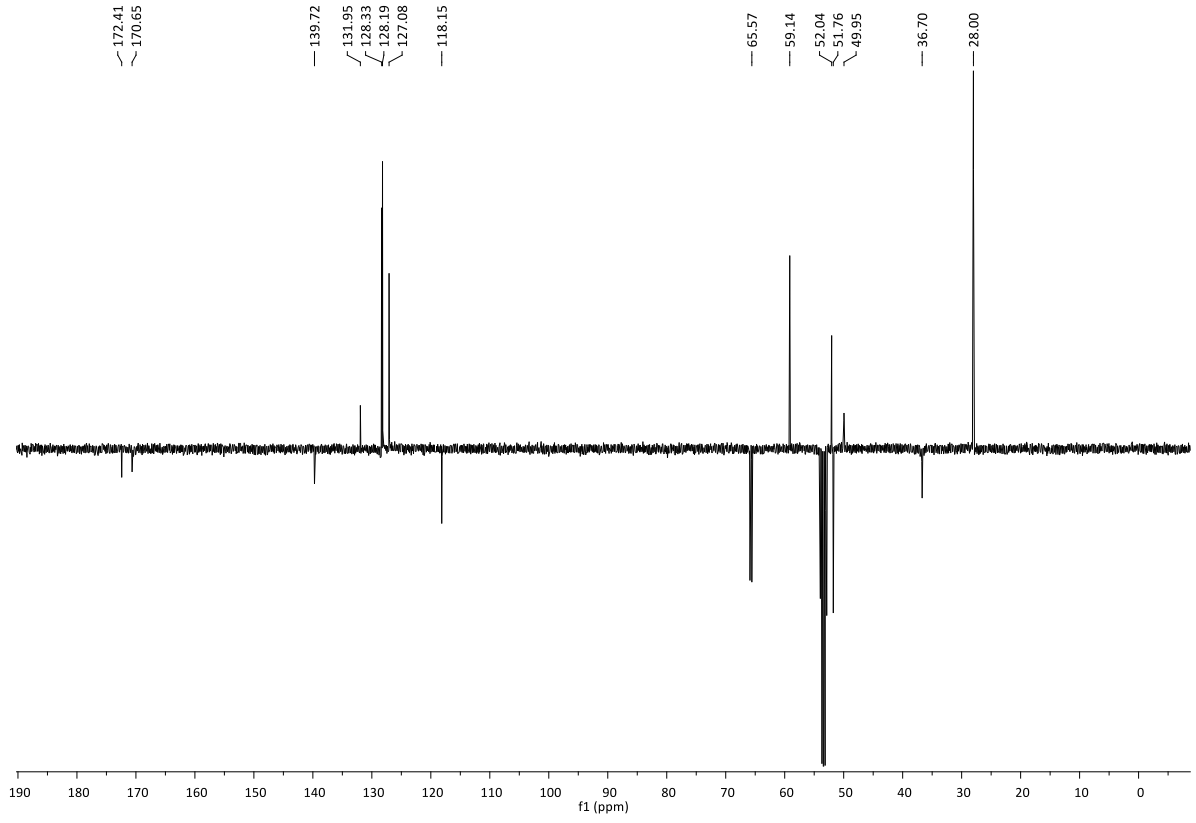

(*S*)-*N*-Bn-Ser(O-(*R*)-Asp(OAll))-OMe bis-trifluoroacetate 51c:

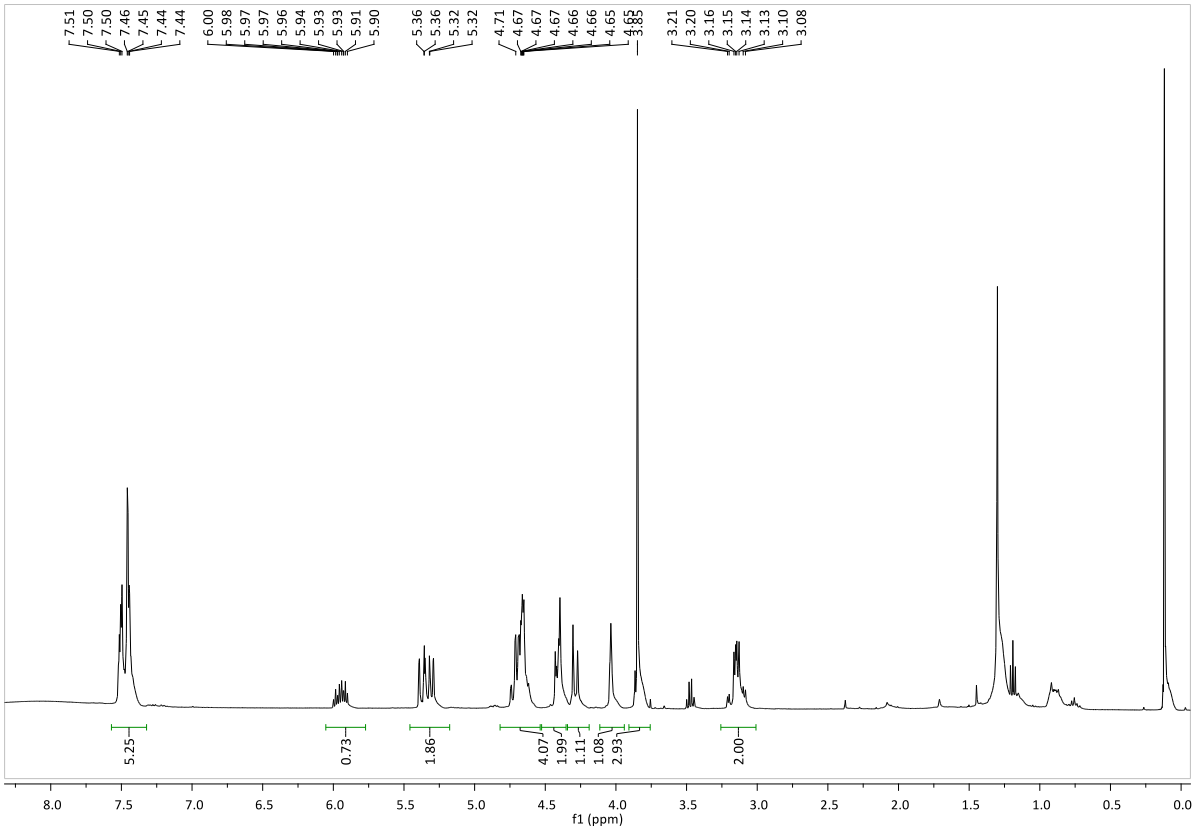

OH-DKP1-OAll 49a:

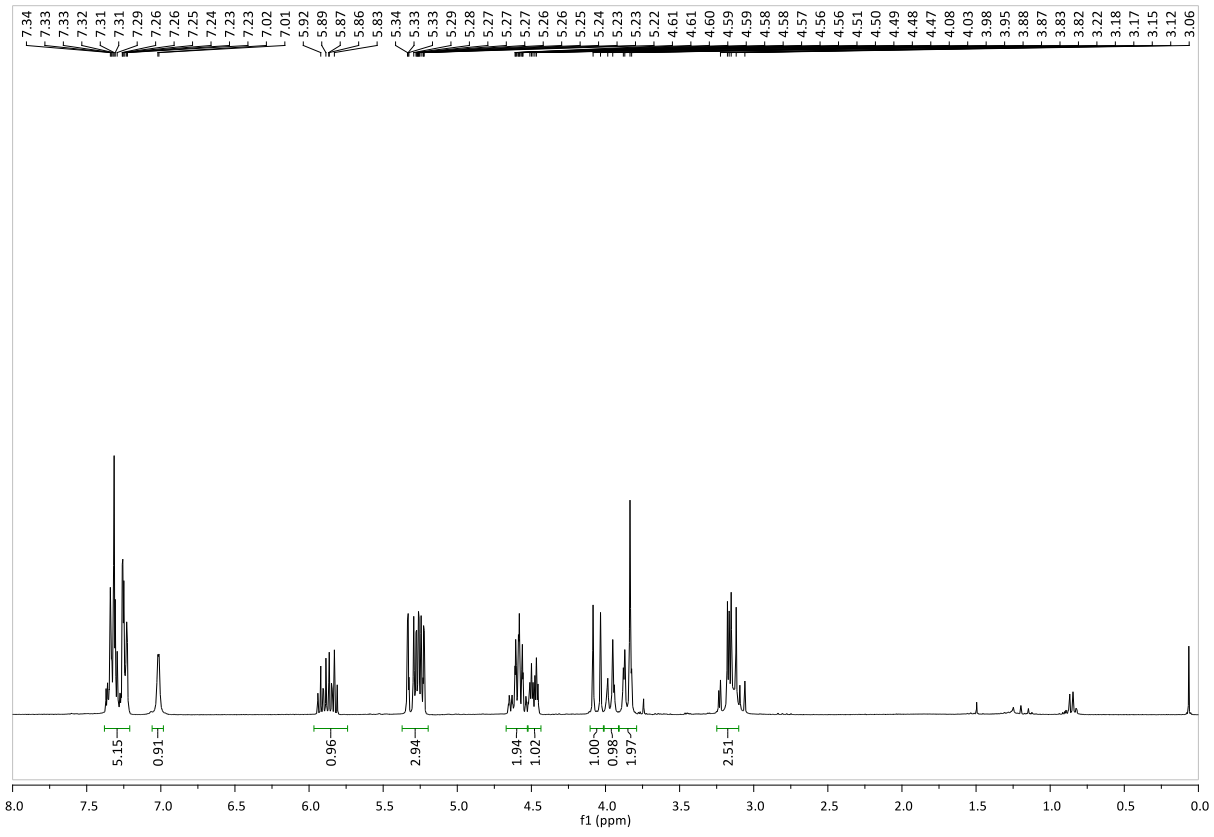

Enantiomeric compounds (3*R*,6*S*)-**OH-DKP2-OAll 43b** and (3*S*,6*R*)-**OH-DKP3-OAll 43c**

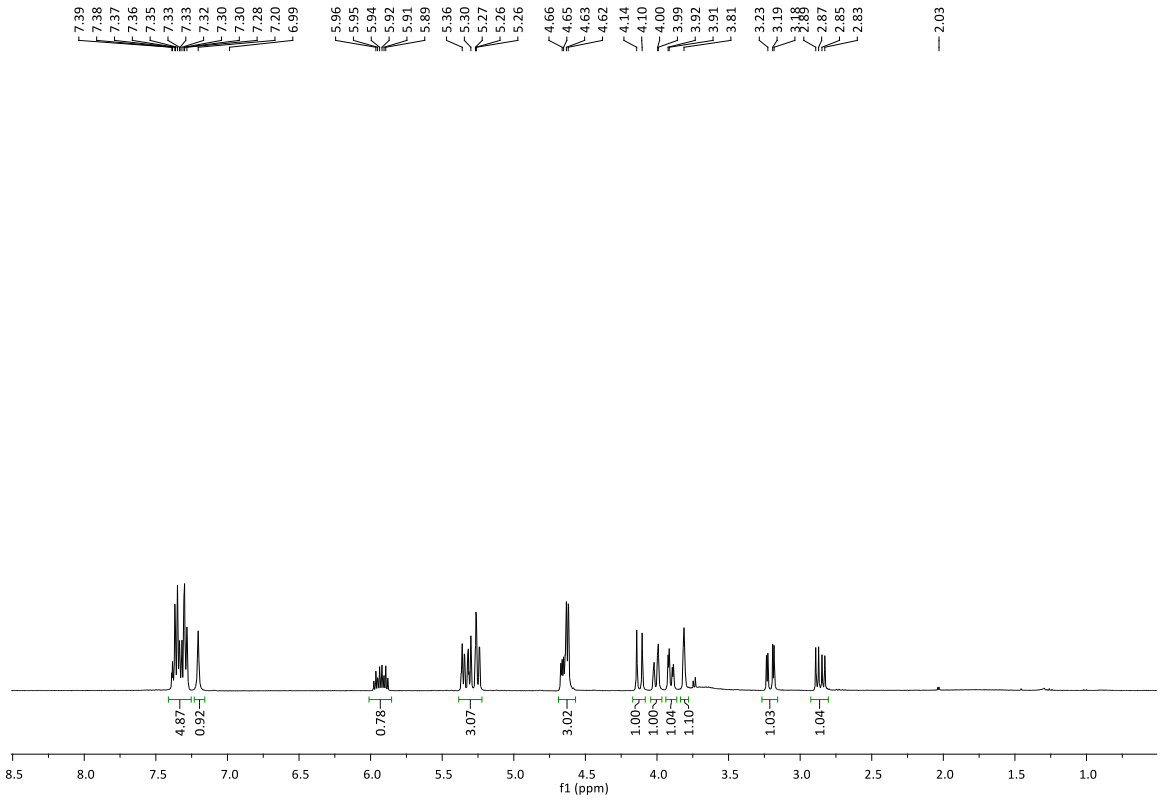

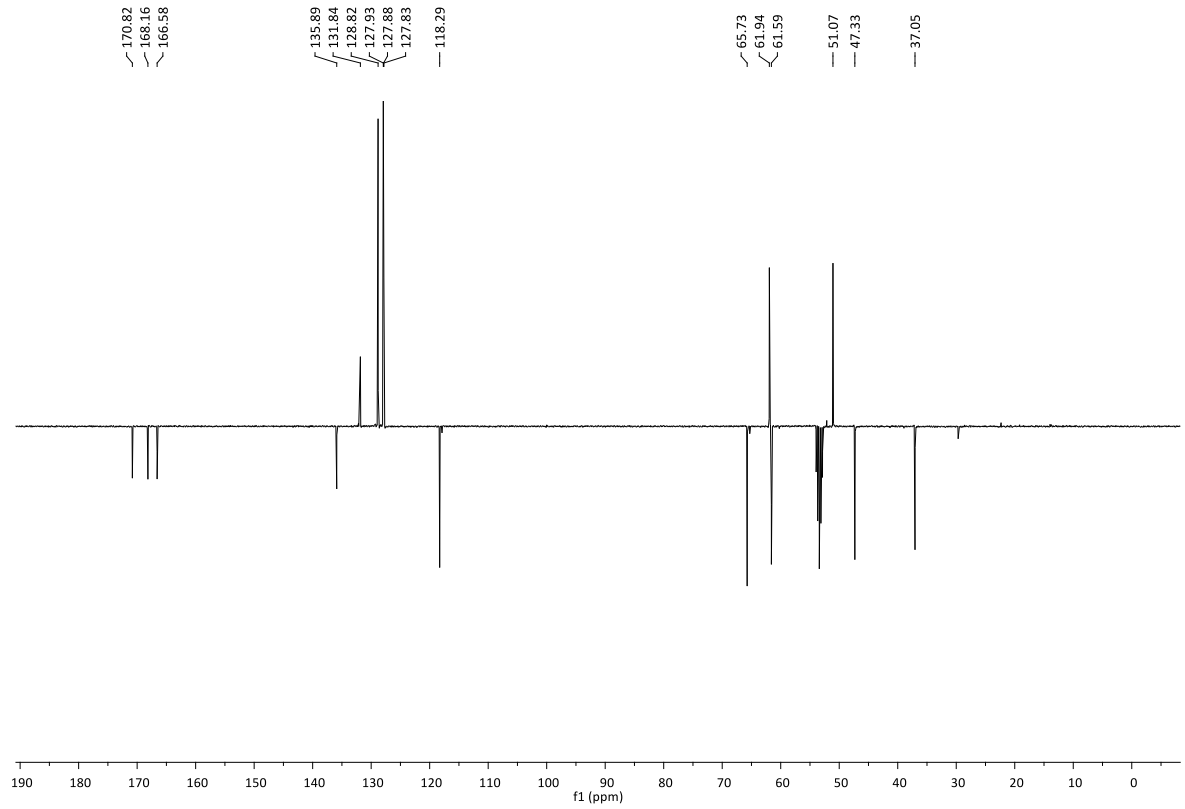

N_3-DKP1-CO_2Allyl 52a (+ H_2C=DKP-CO_2Allyl 54a)

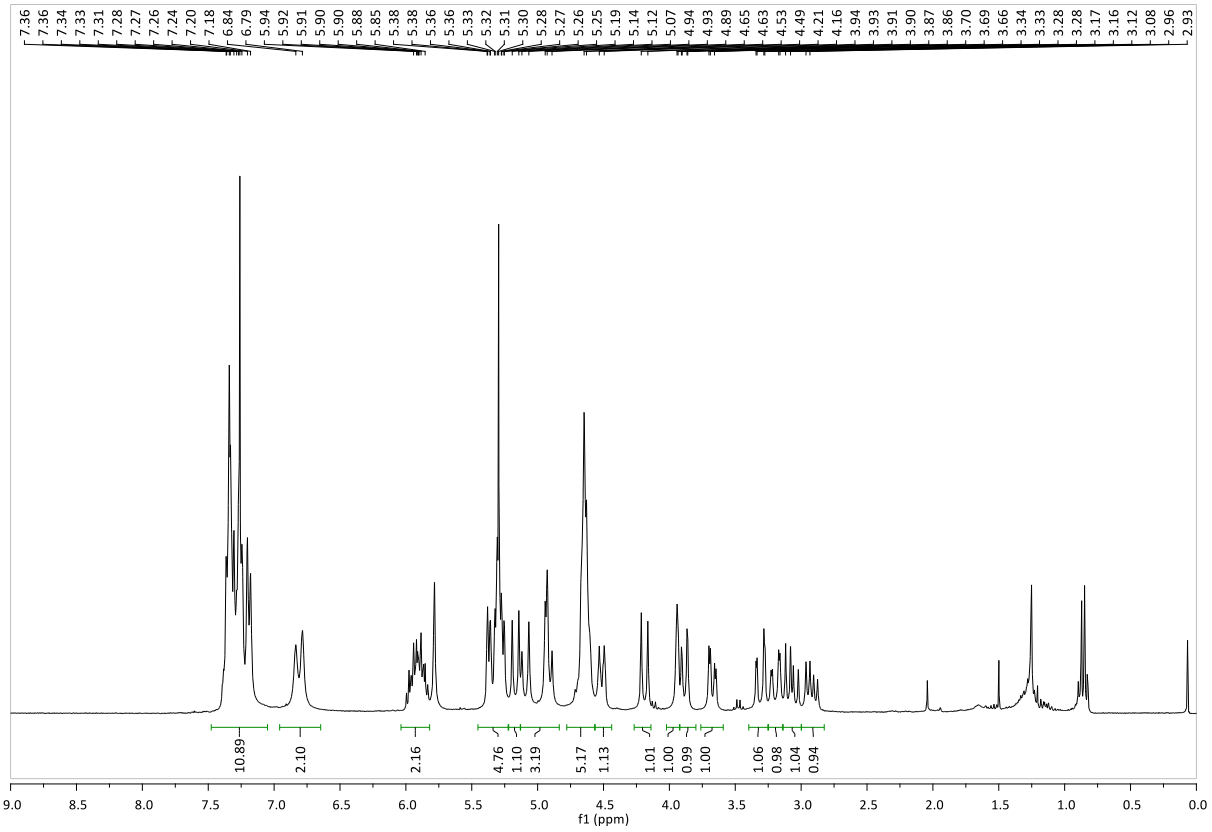

Enantiomeric compounds (3*R*,6*S*)-**N_3-DKP2-OAll 52b** and (3*S*,6*R*)-**N_3-DKP3-OAll 52c**

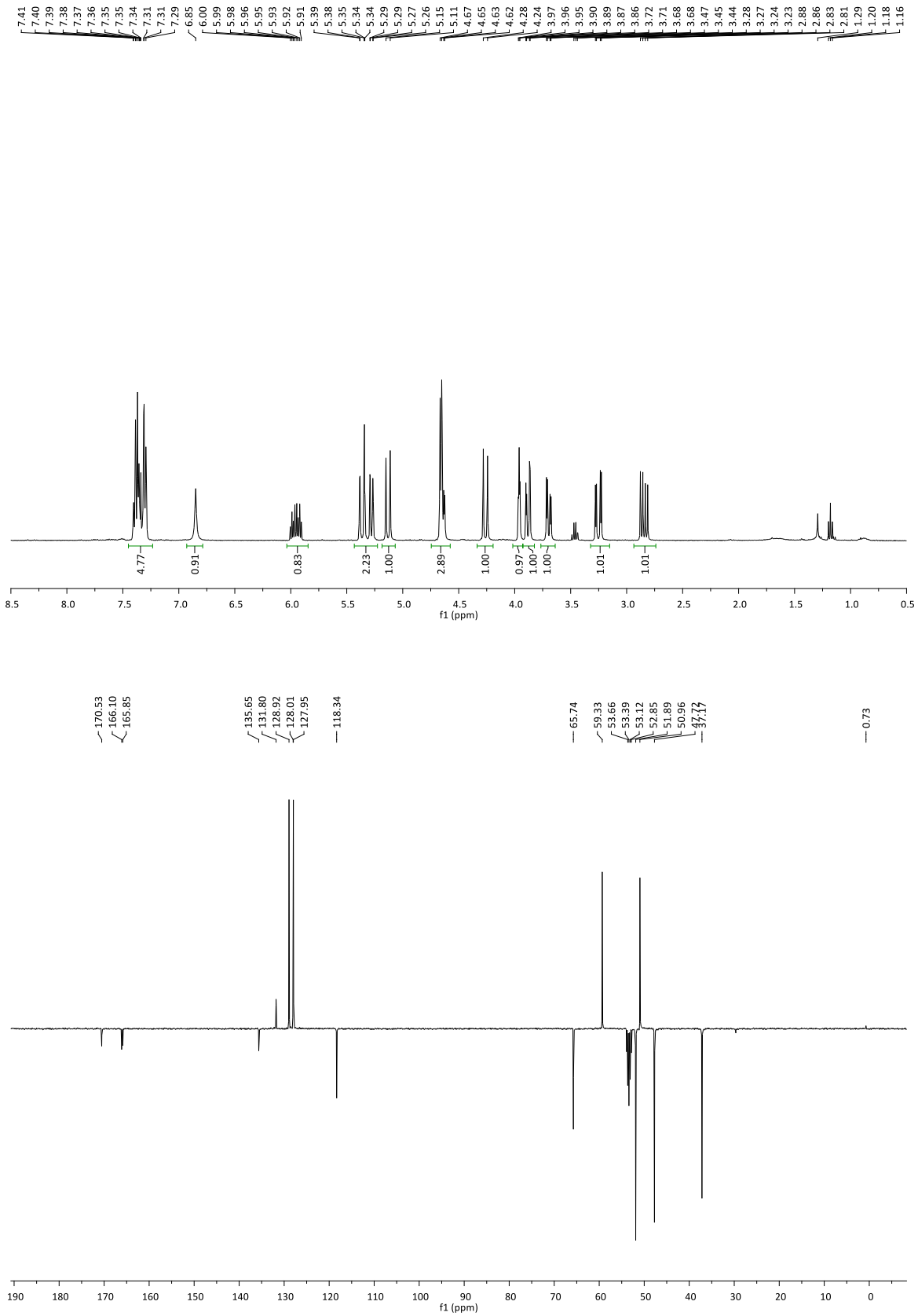

Enantiomeric compounds (3*R,*6*S*)-***N*-Boc-DKP2-OAll 53b** and (3*S,*6*R*)-***N*-Boc-DKP3-OAll 53c**

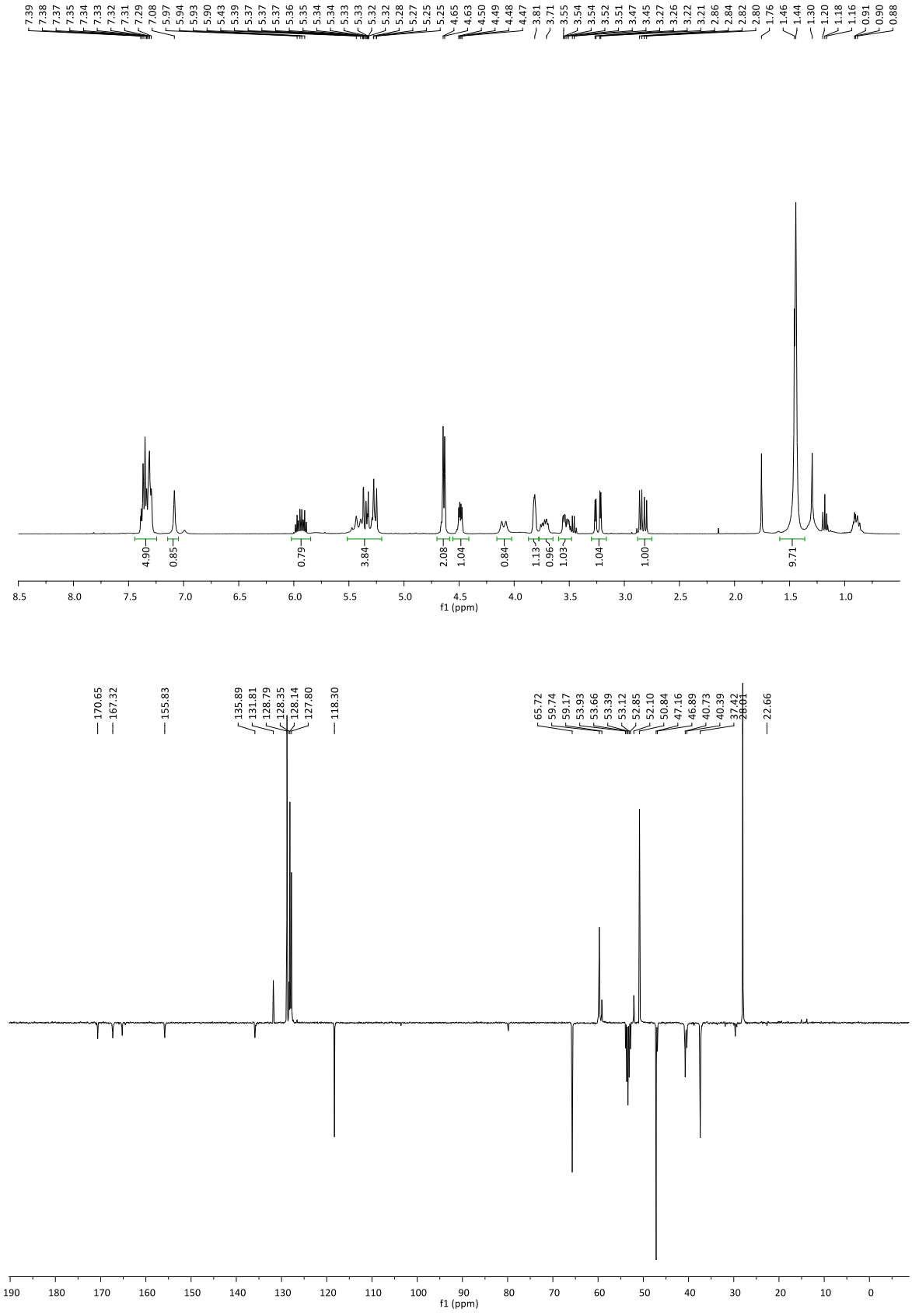

Enantiomeric compounds ***N*-Boc-(*R*)-Ser(N_3)-*N*-Bn-(*S*)-Asp(OMe)-OMe 65a** and ***N*-Boc-(*S*)-Ser(N_3)-*N*-Bn-(*R*)-Asp(OMe)-OMe 65b**

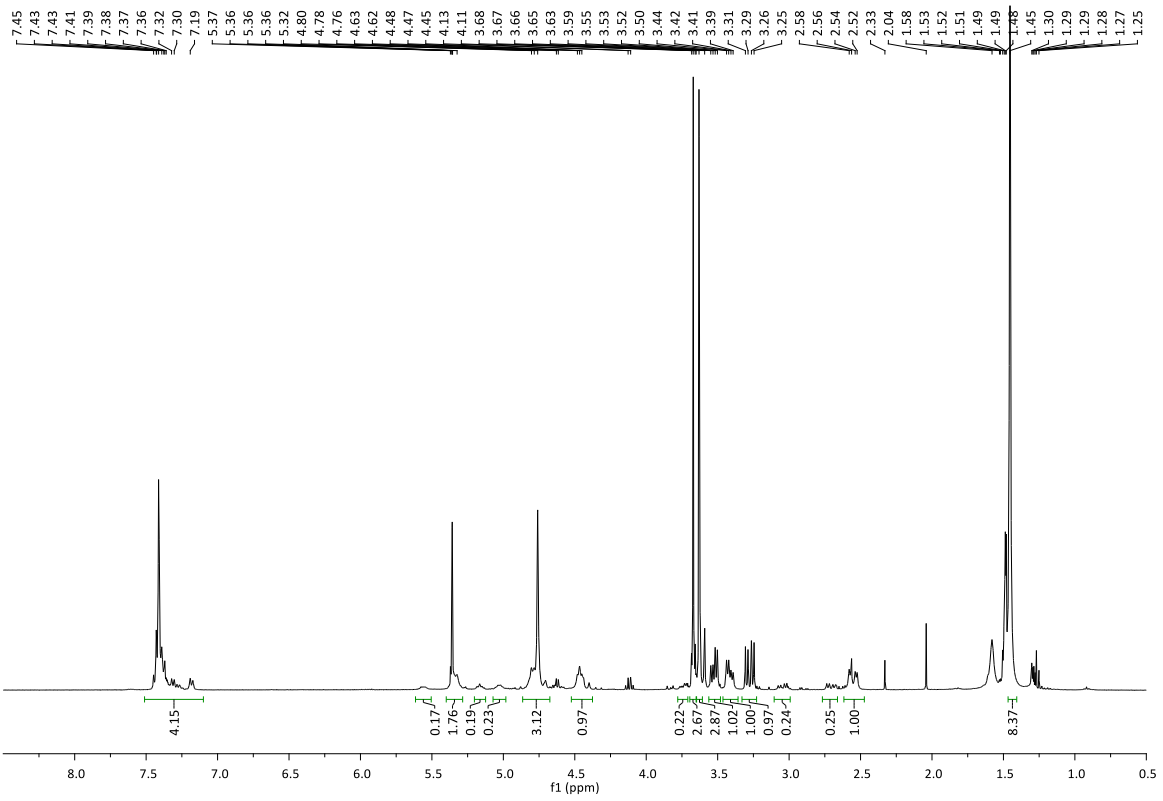

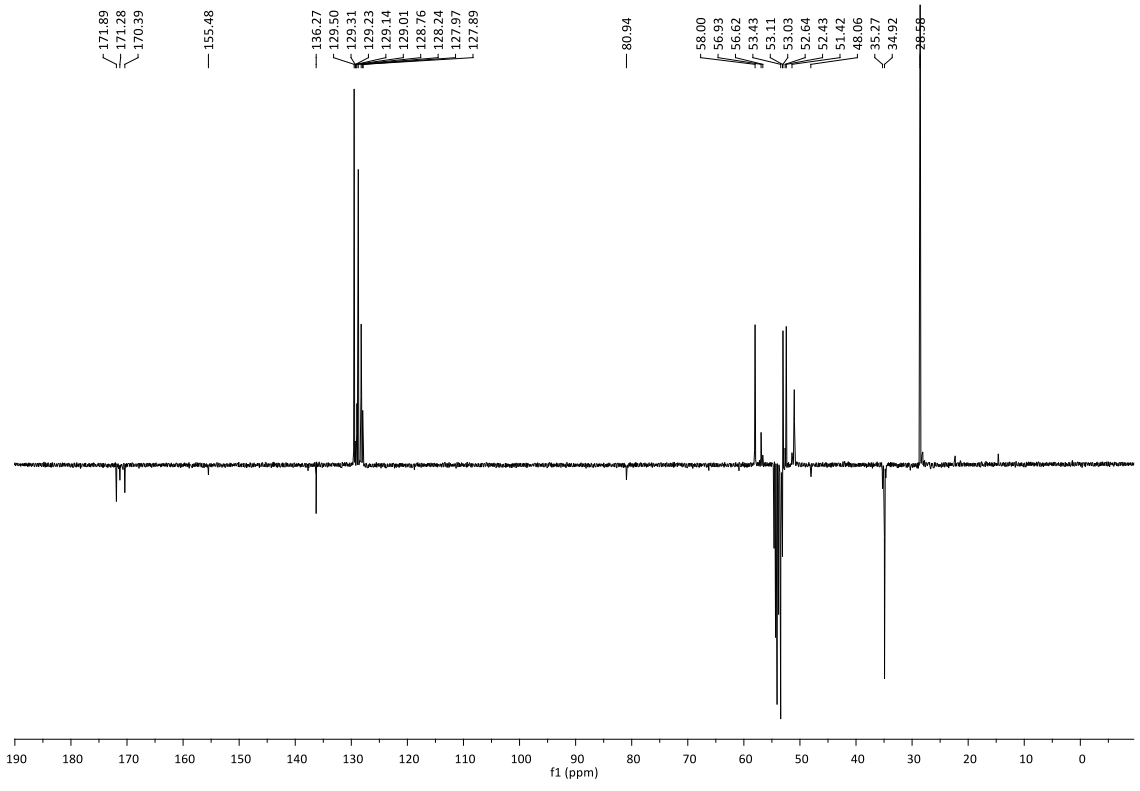

Enantiomeric compounds (3*R*,6*S*)-**N_3-DKP4-CO_2Me 59a** and (3*S*,6*R*)-**N_3-DKP6-CO_2Me 59b**

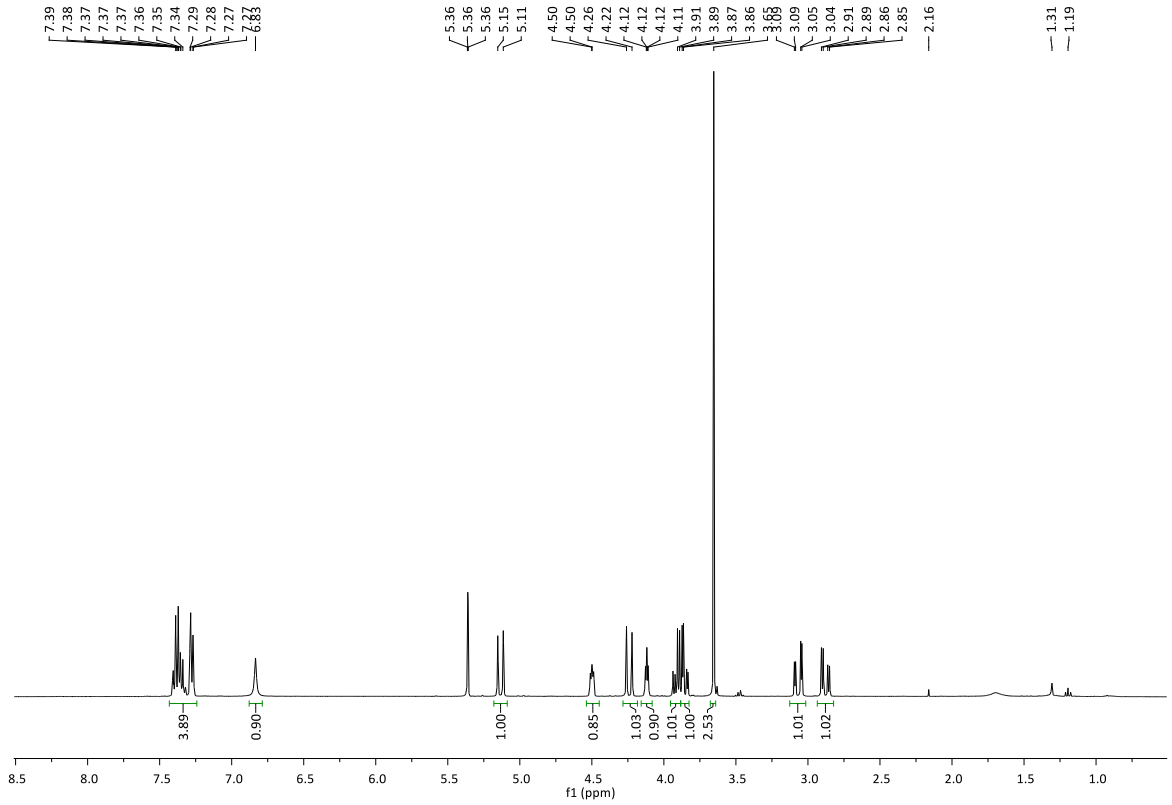

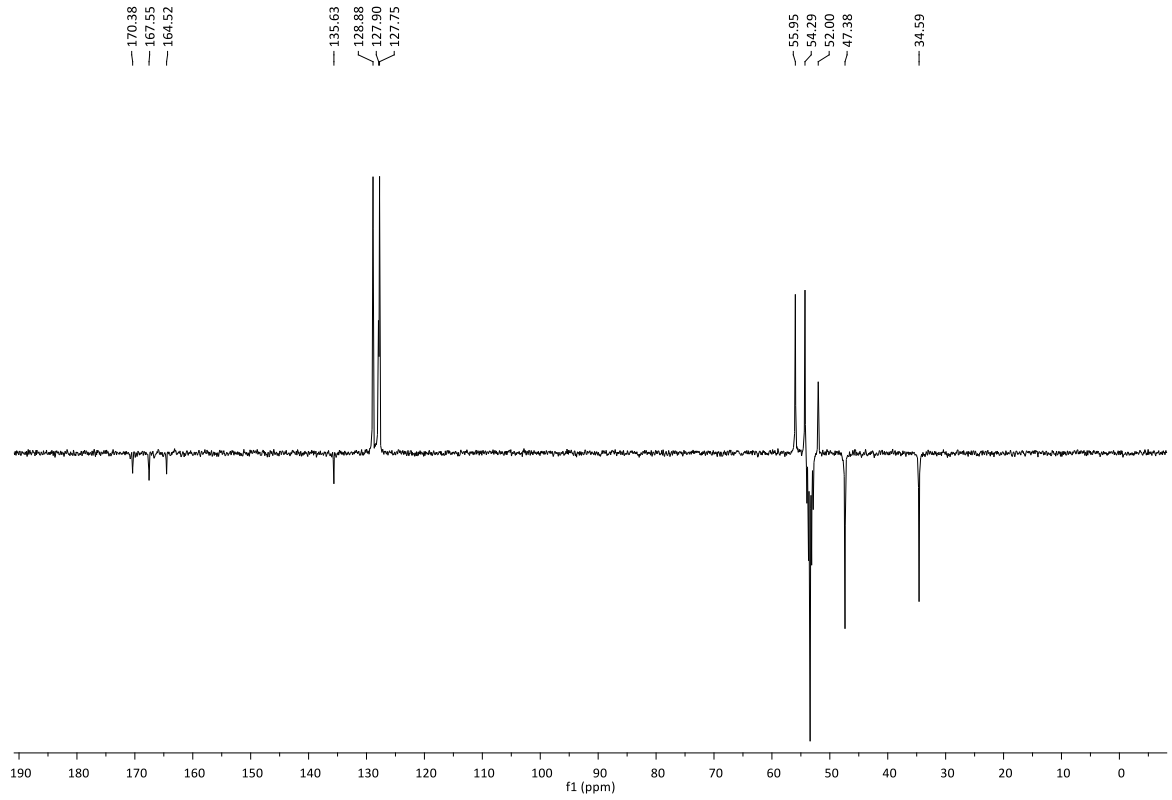

Enantiomeric compounds (3*R*,6*S*)-**NH_2-DKP4-CO_2Me 66a** and (3*S*,6*R*)-**NH_2-DKP6-CO_2Me 66b**

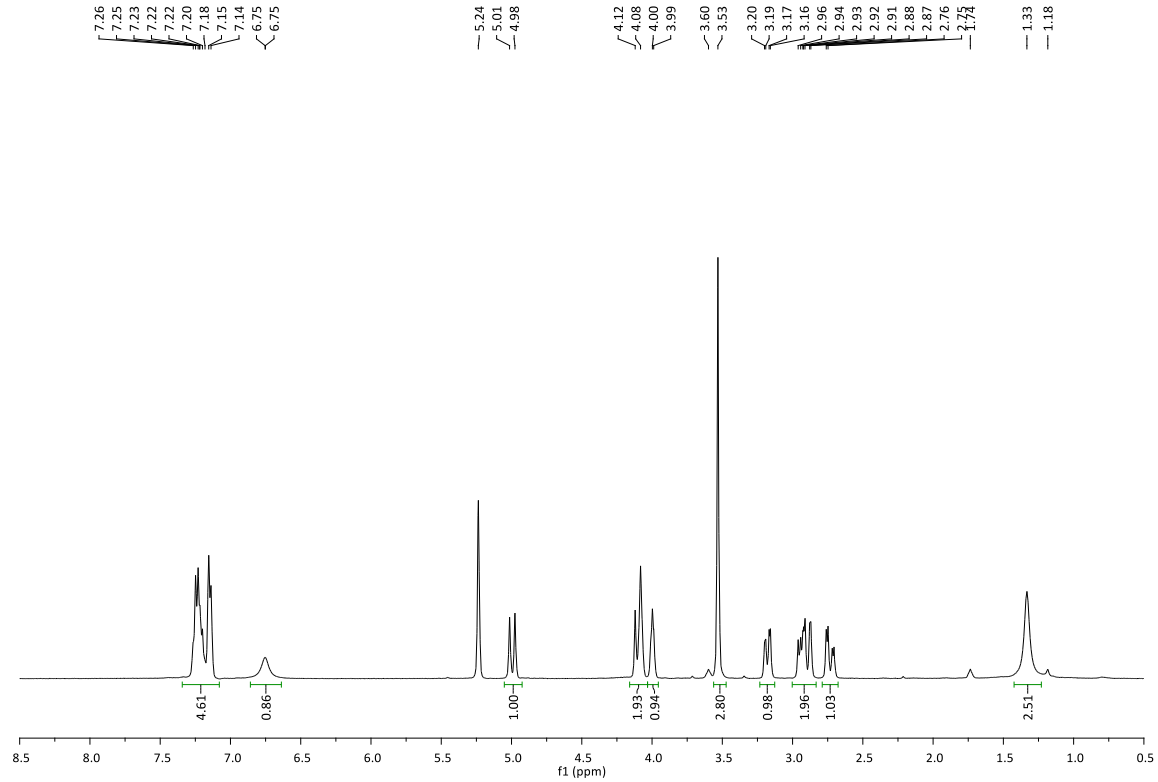

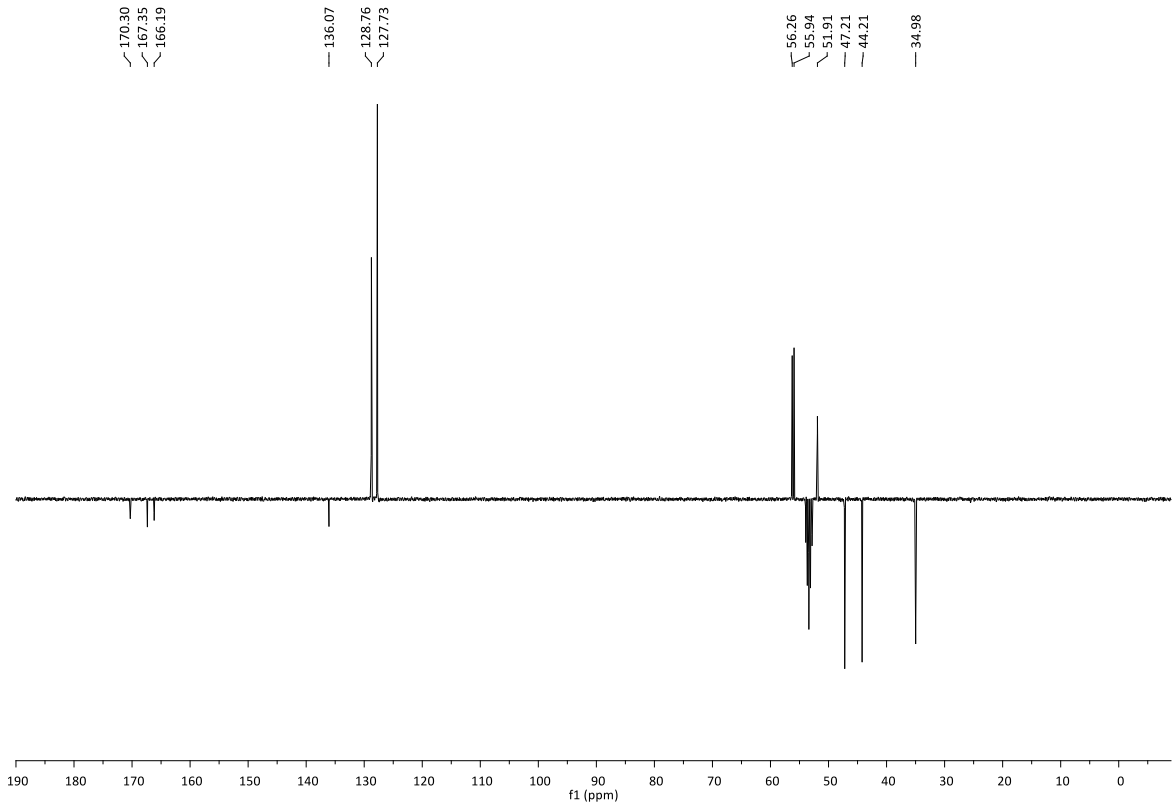

Enantiomeric compounds (3*R*,6*S*)-**NHBoc-DKP4-CO_2Me 67a** and (3*S*,6*R*)-**NHBoc-DKP6-CO_2Me 67b**

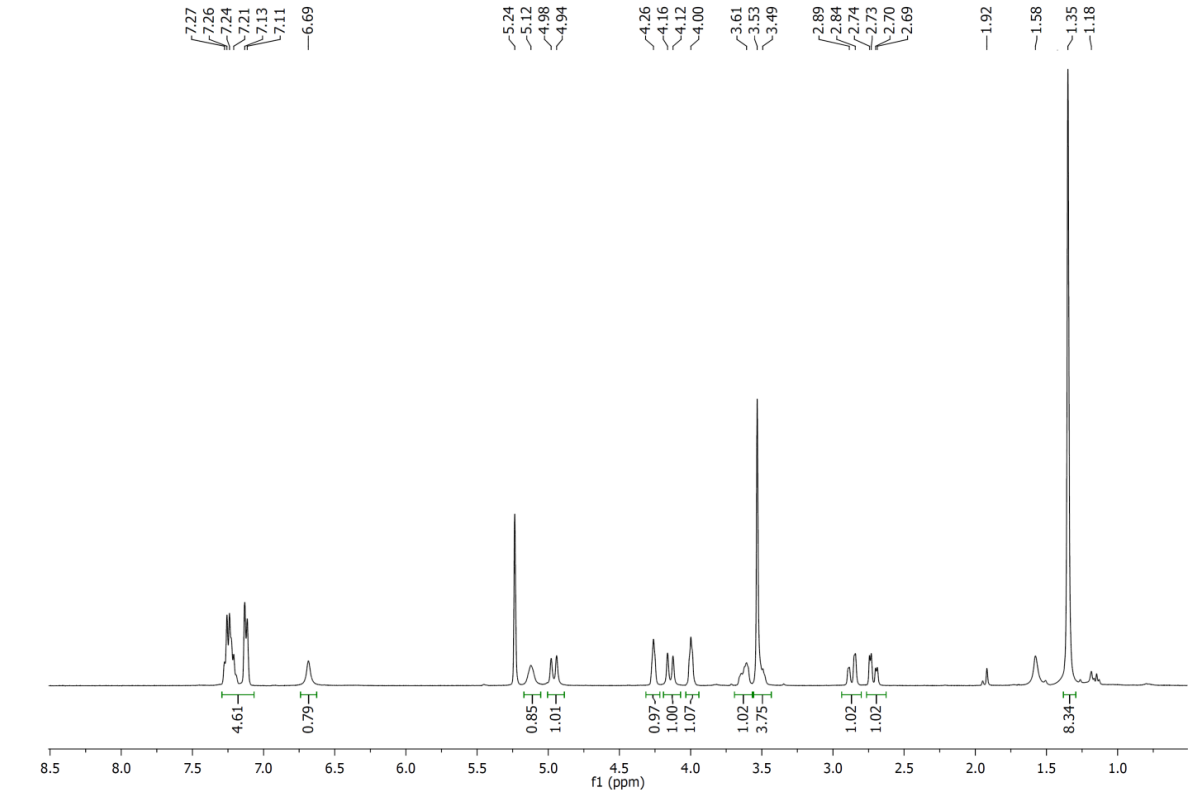

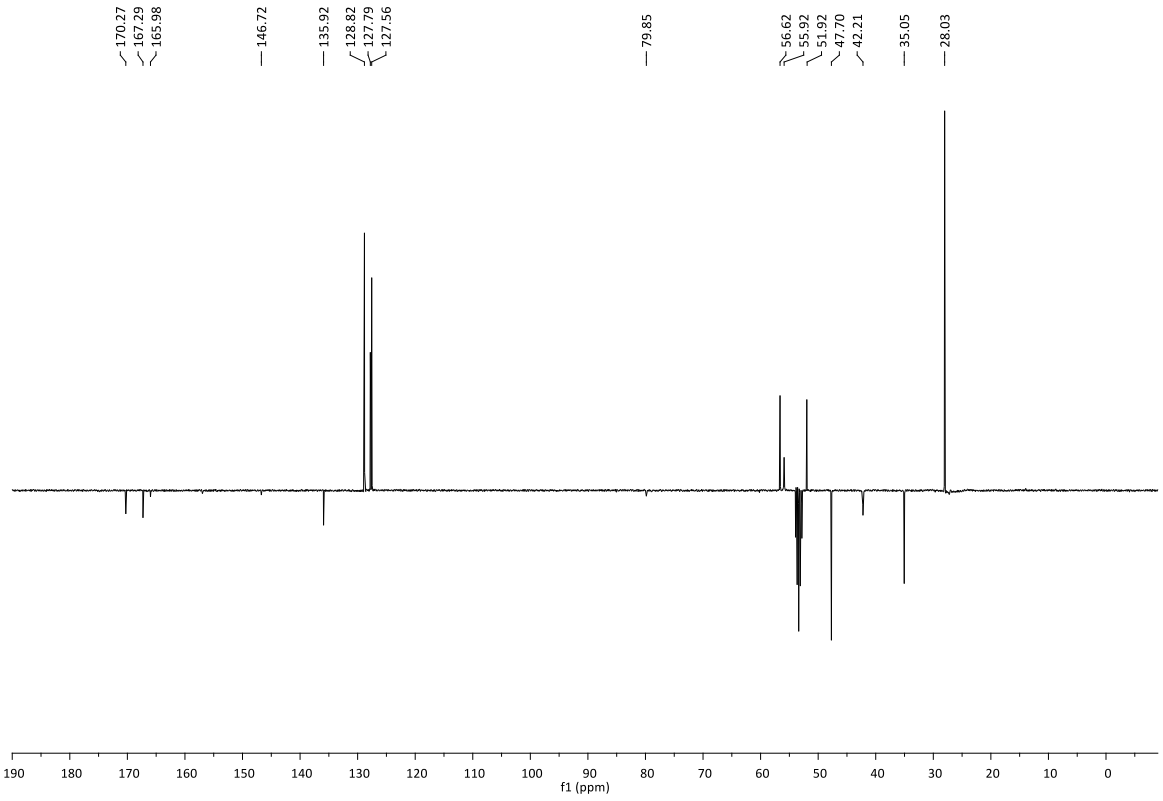

Enantiomeric compounds (3*R*,6*S*)-**N_3-DKP5-CO_2Me 70a** and (3*S*,6*R*)-**N_3-DKP7-CO_2Me 70b**

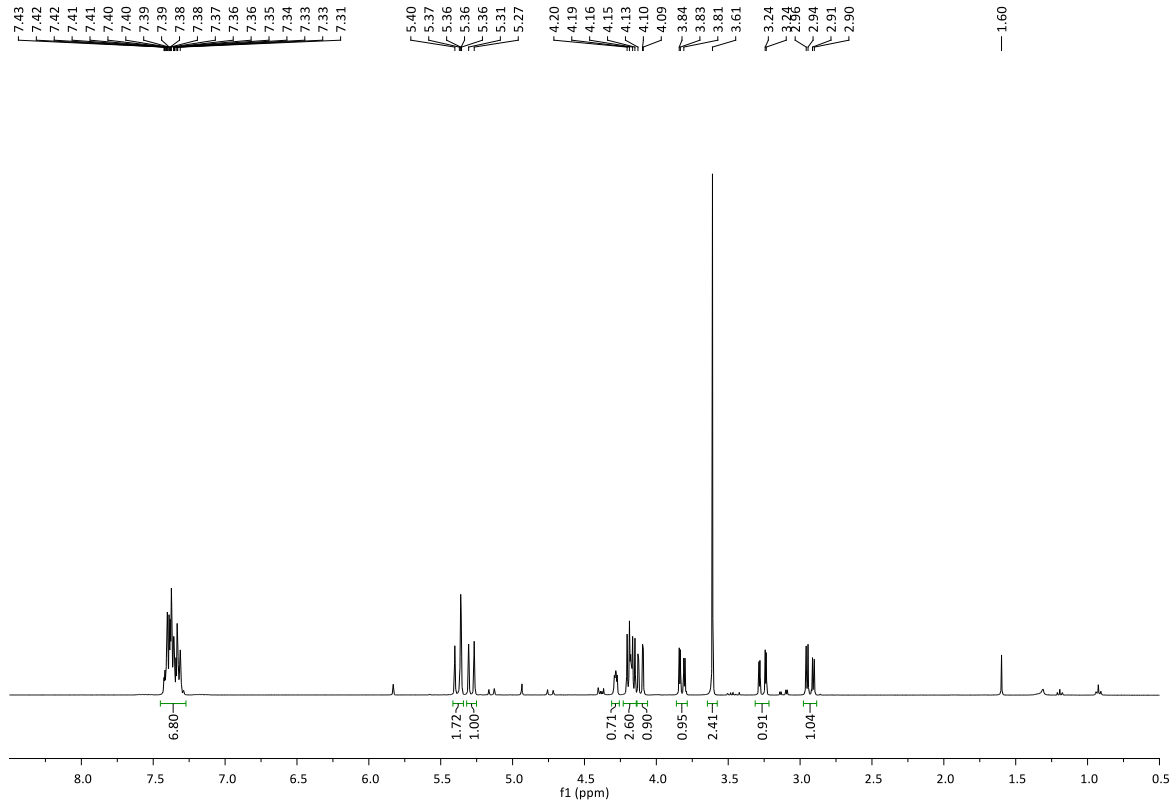

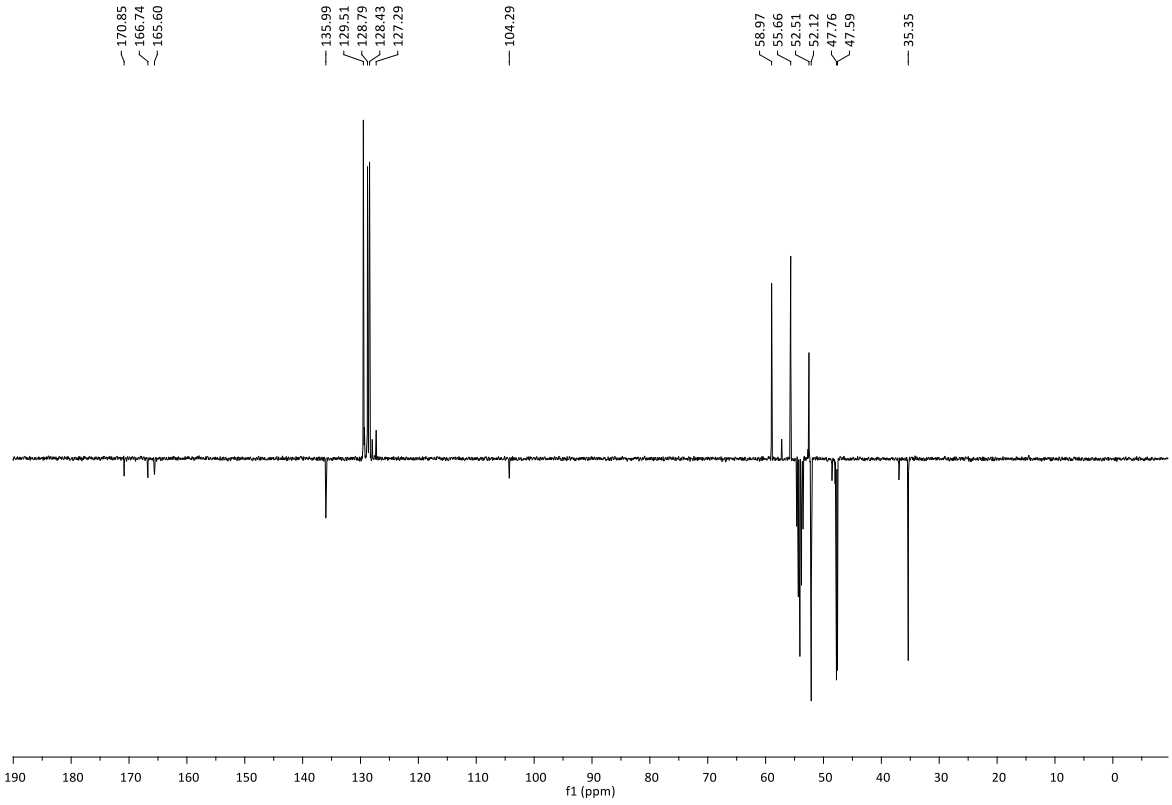

Enantiomeric compounds (3*R*,6*S*)-**NHBoc-DKP5-CO_2Me 71a** and (3*S*,6*R*)-**NHBoc-DKP7-CO_2Me 71b**

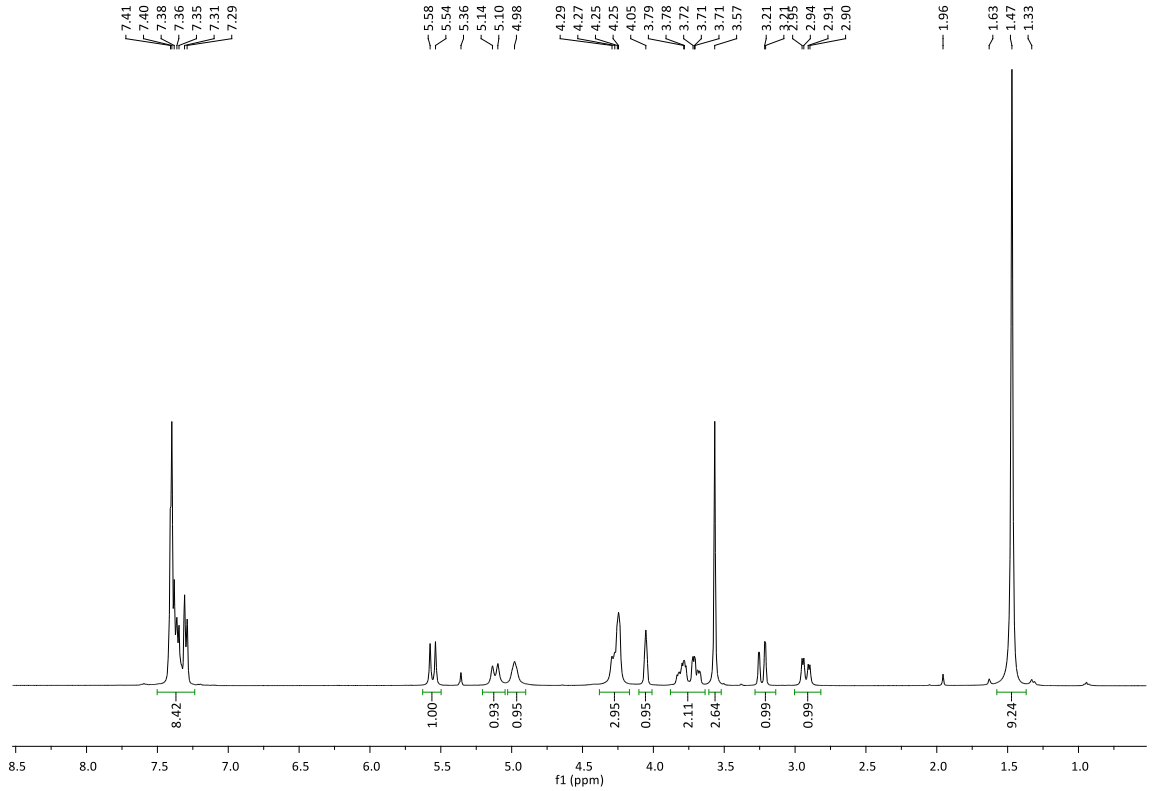

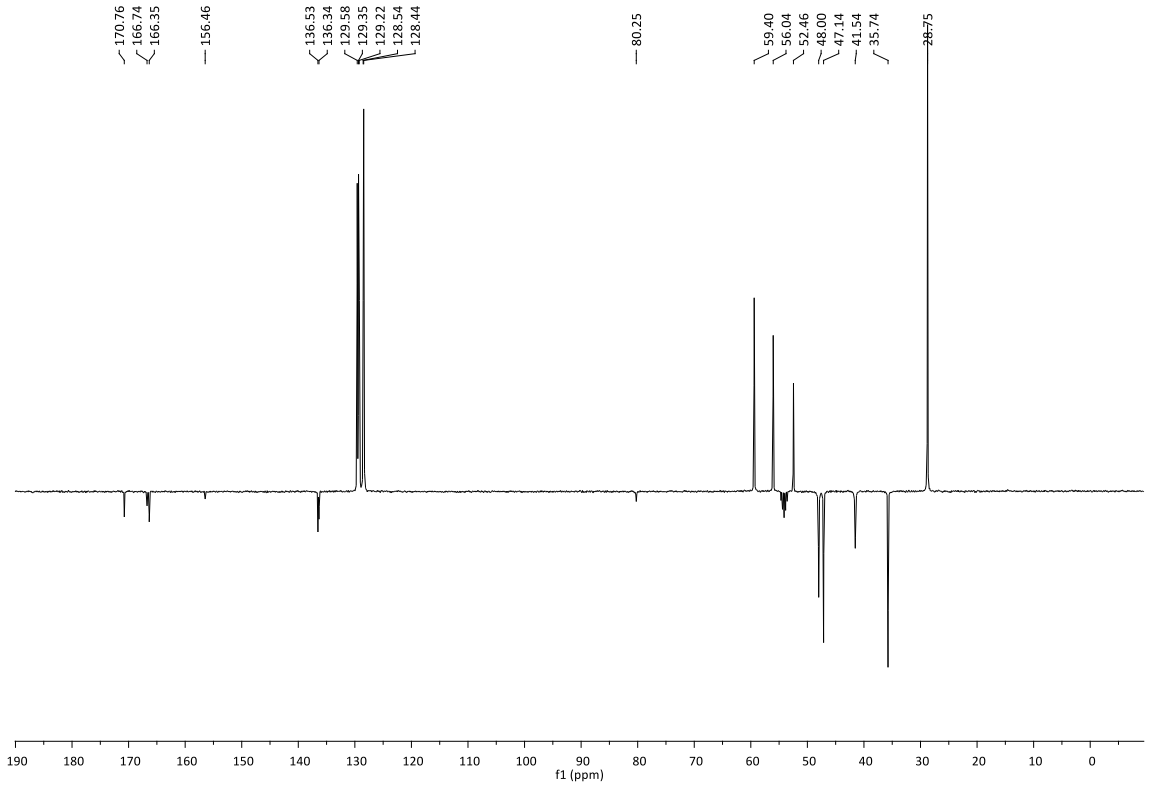

(*S*)-*N*-Bn-Ser(O-(*R*)-*N*-Boc-Glu(OMe))-OMe 73

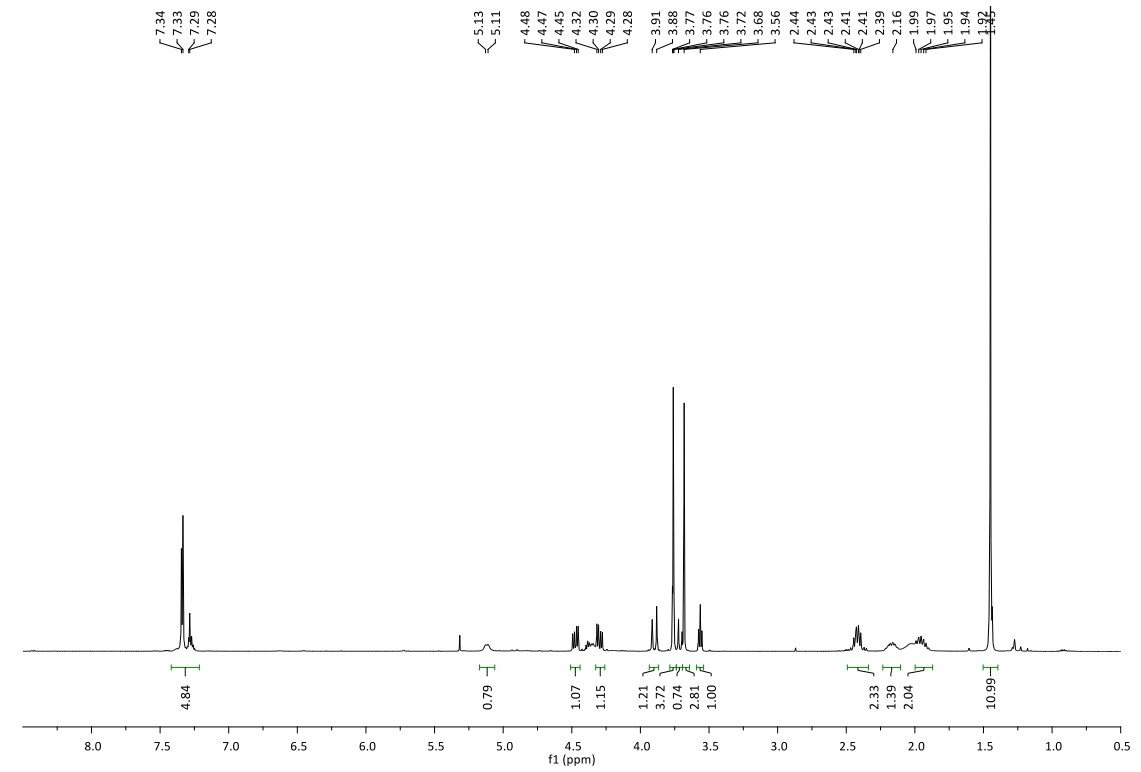

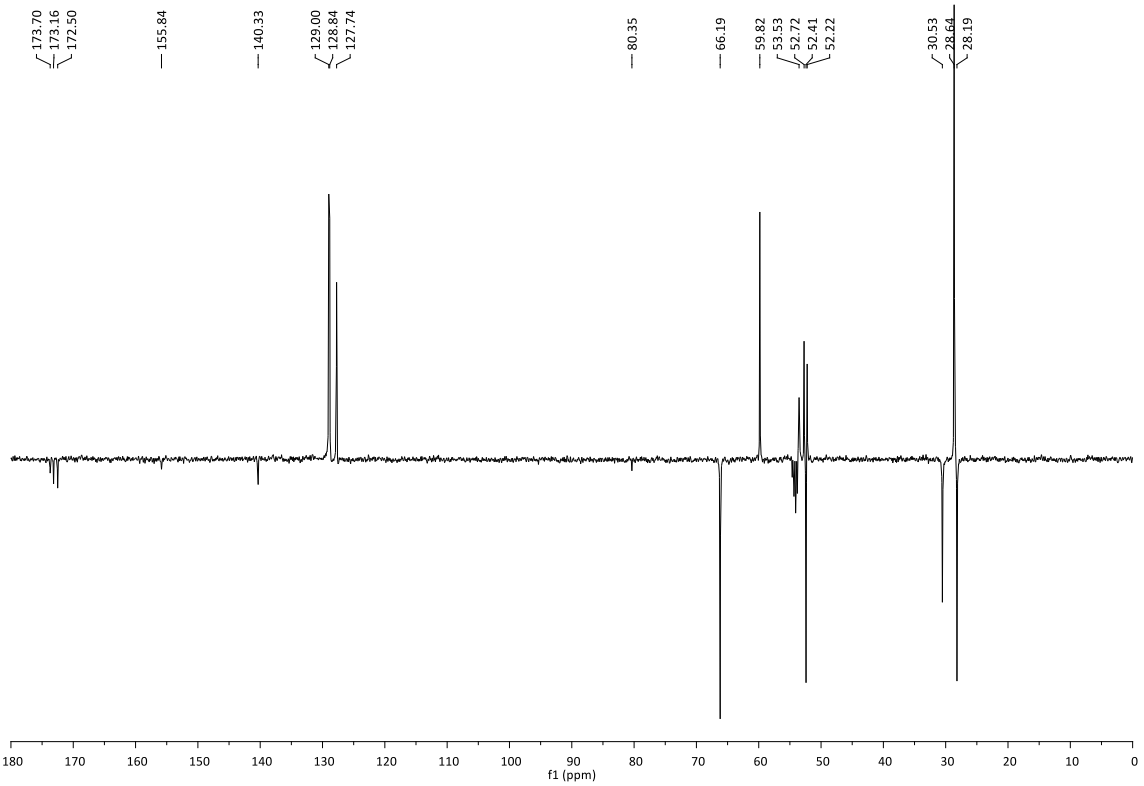

HO-DKP8-CO_2Me 74

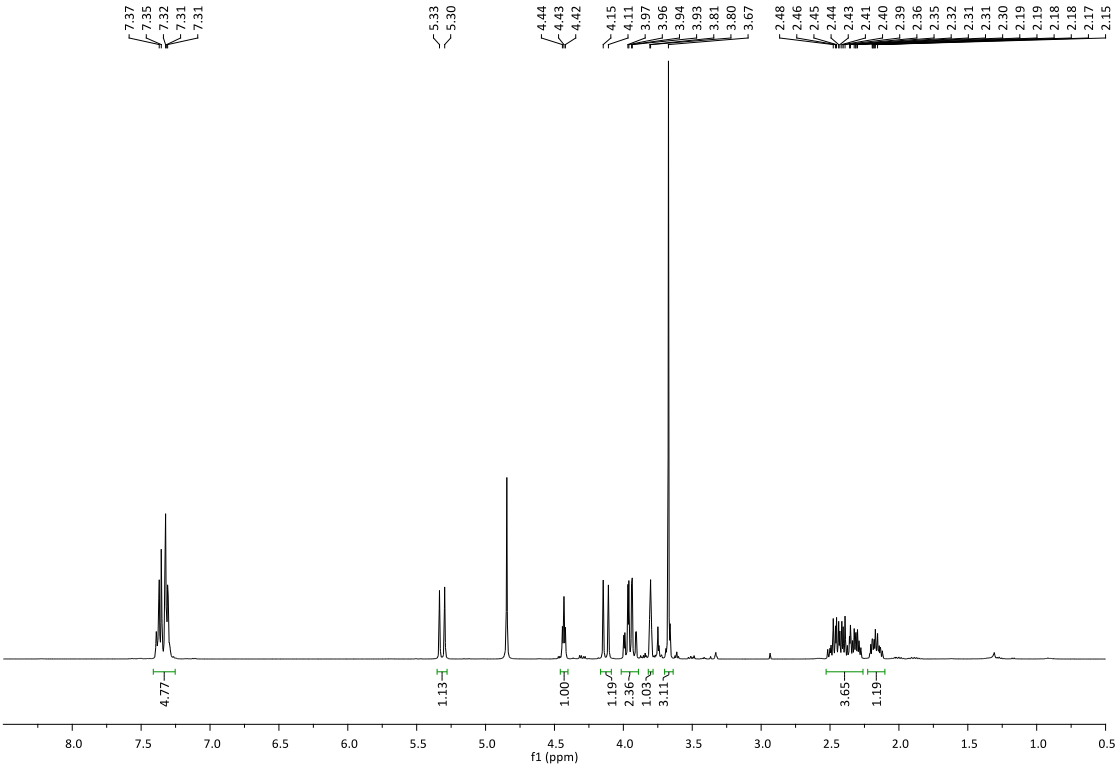

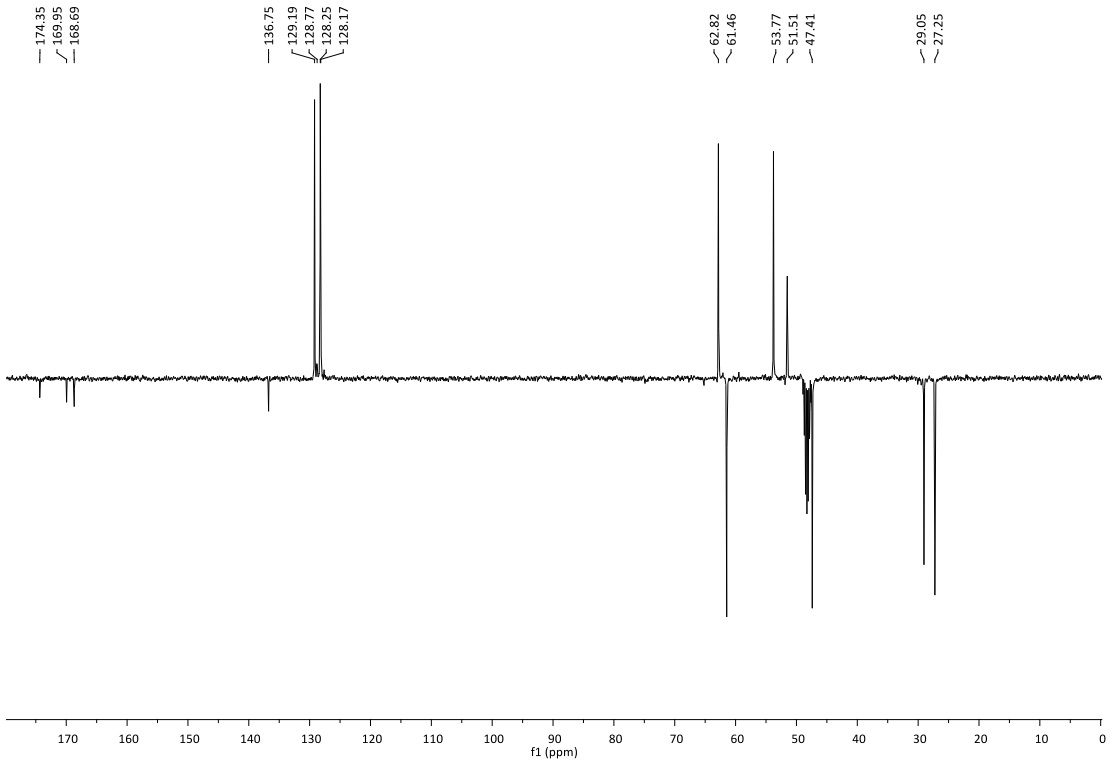

N_3-DKP8-CO_2Me 75

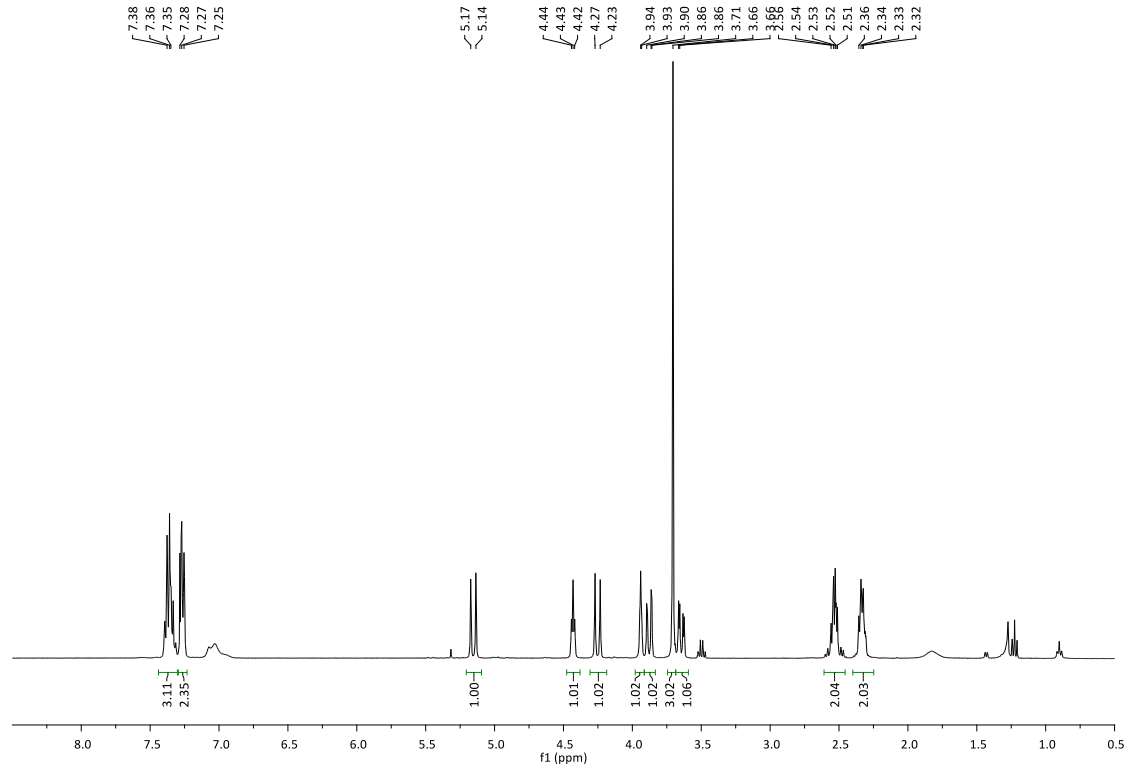

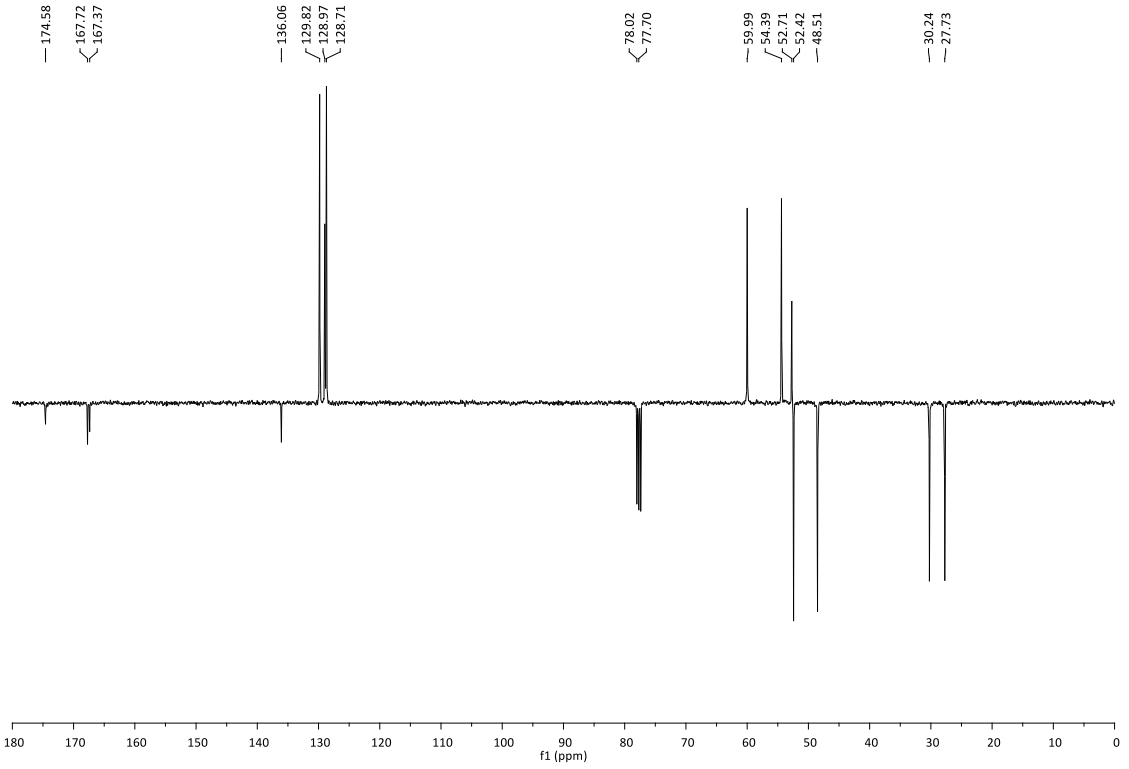

NHBoc-DKP8-CO_2Me 77

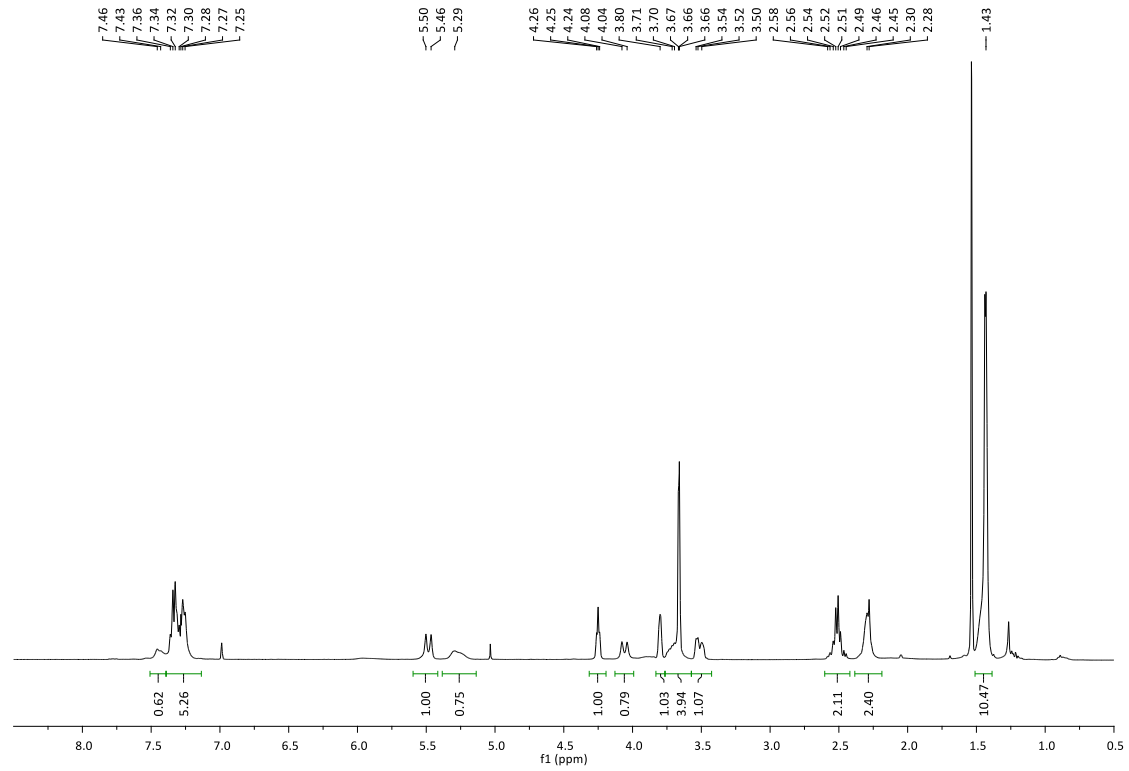

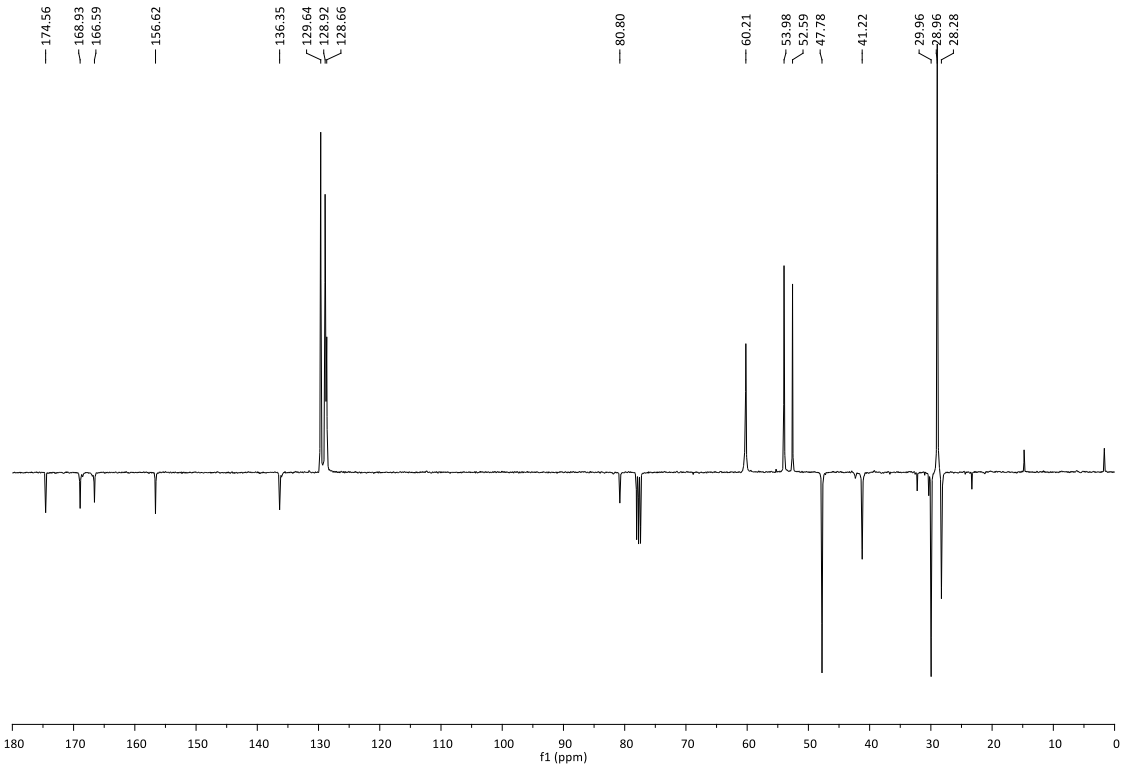

N-Boc-Arg(Mtr)-Gly-OBn 79

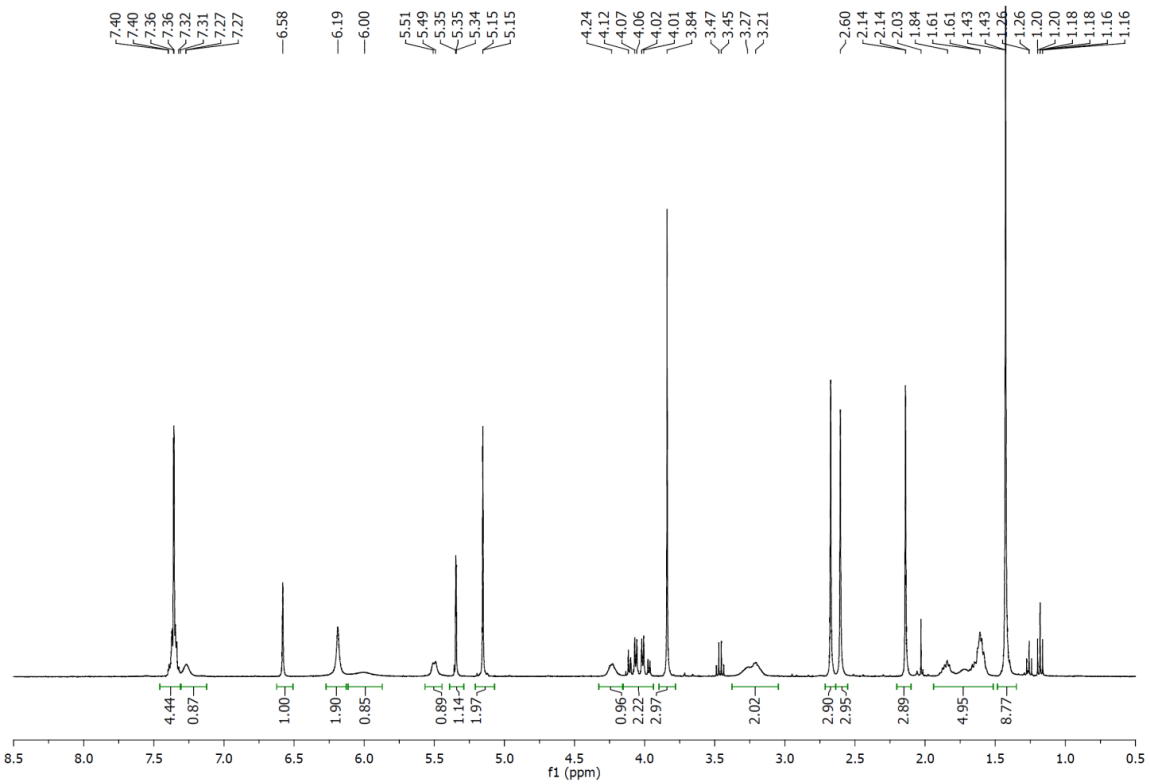

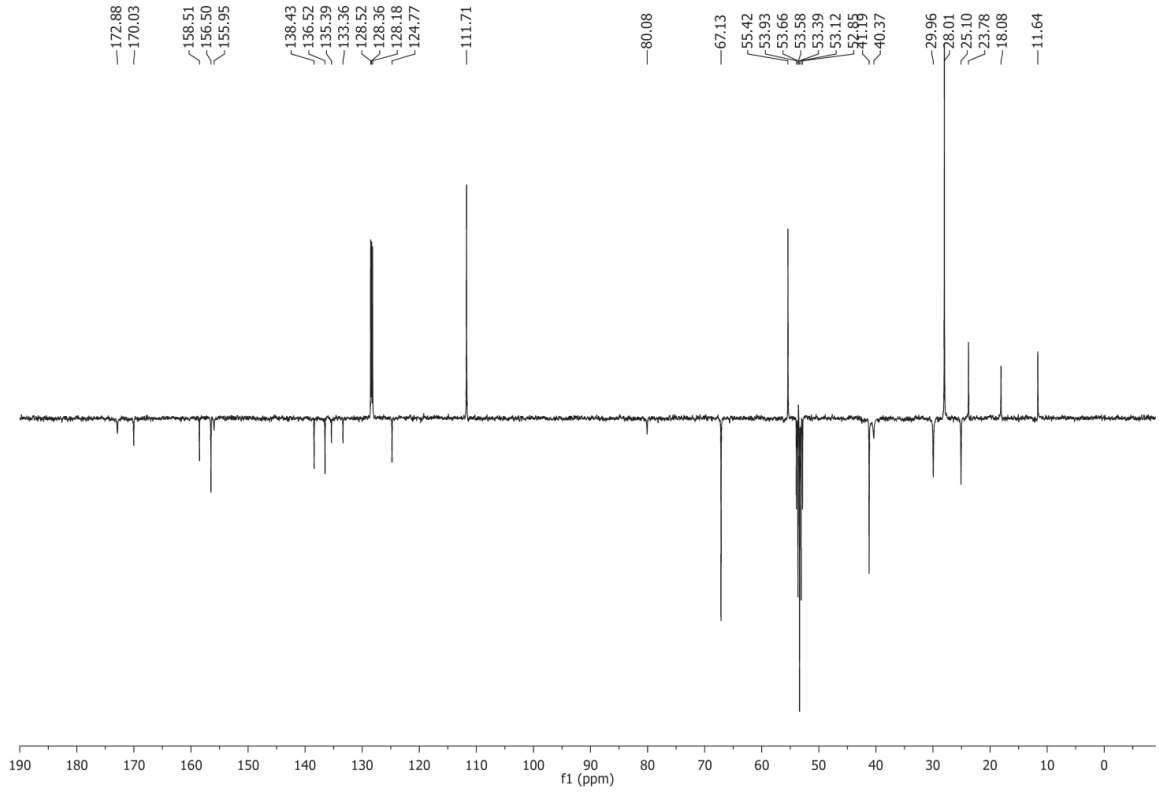

N-Boc-DKP3-Arg(Mtr)-Gly-OBn 80a

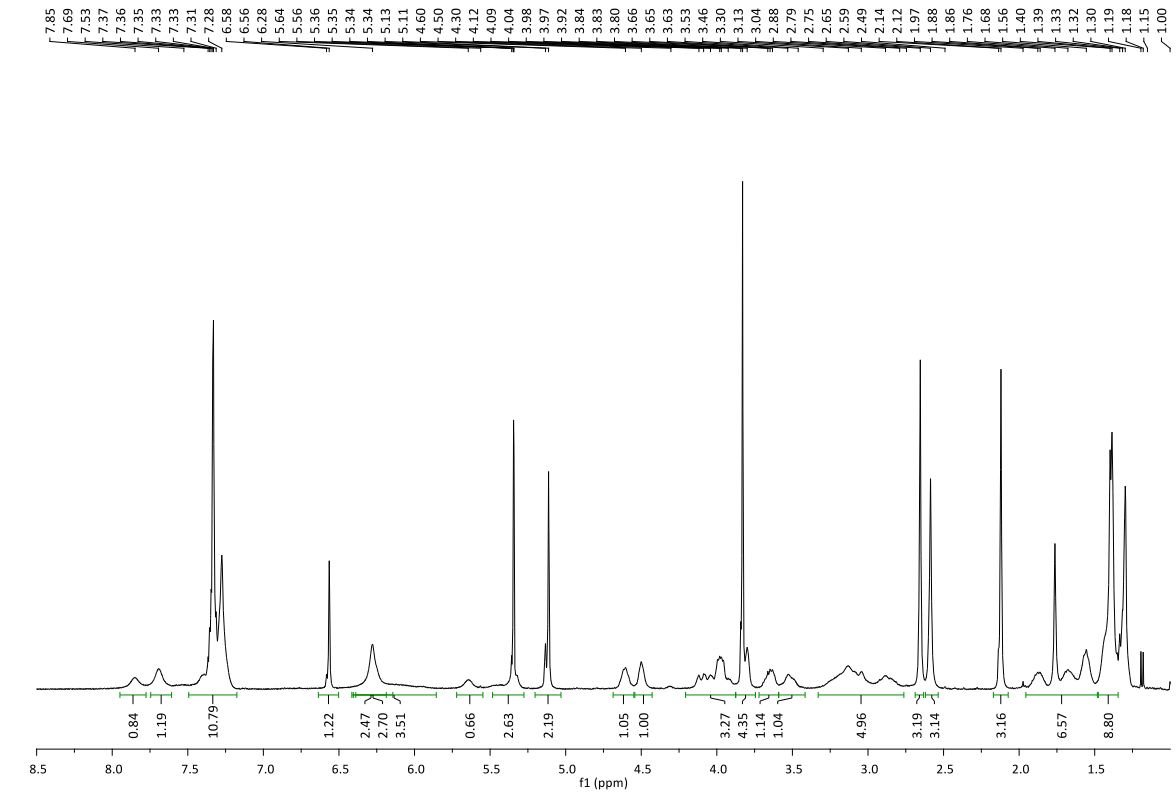

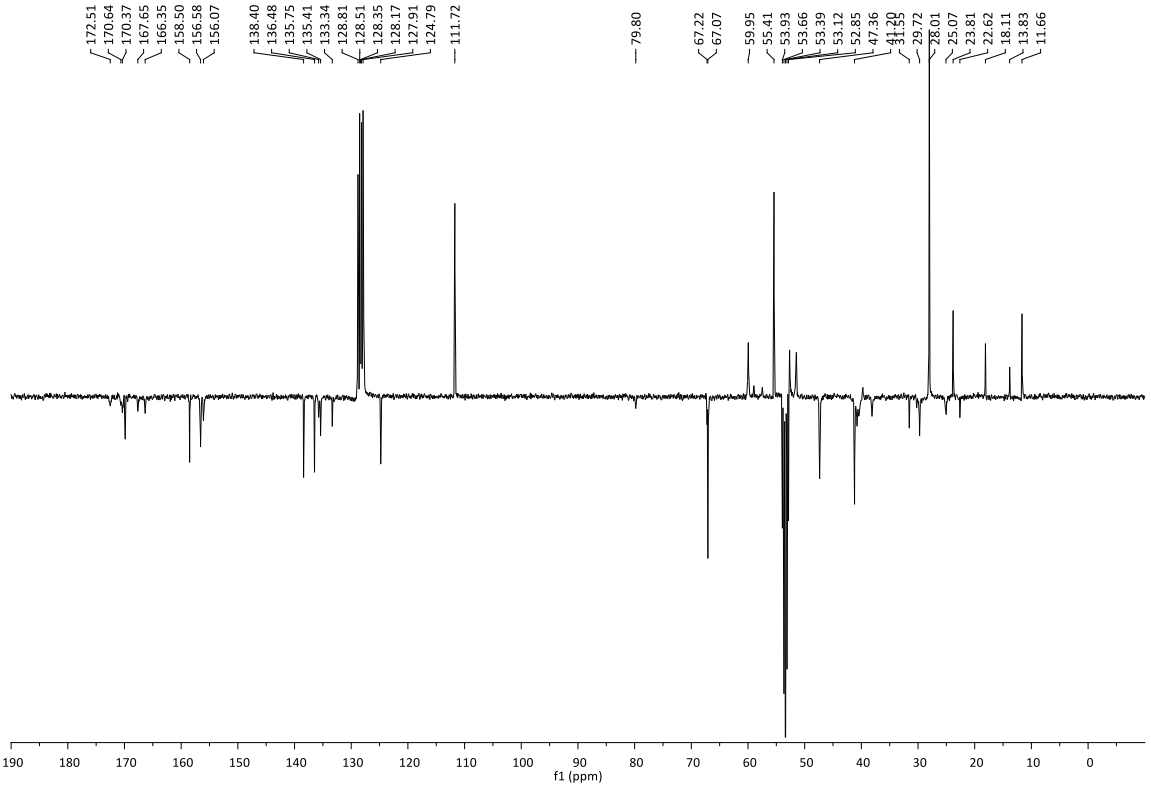

N-Boc-DKP4-Arg(Mtr)-Gly-OBn 80b

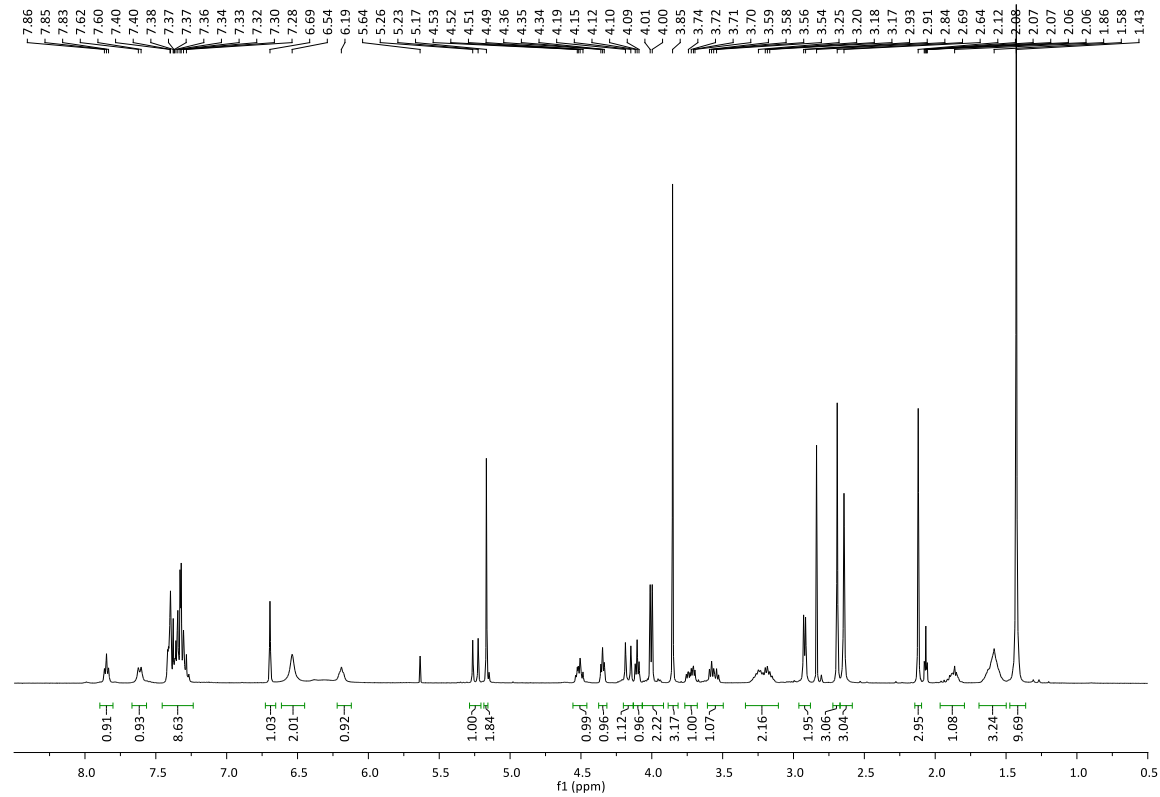

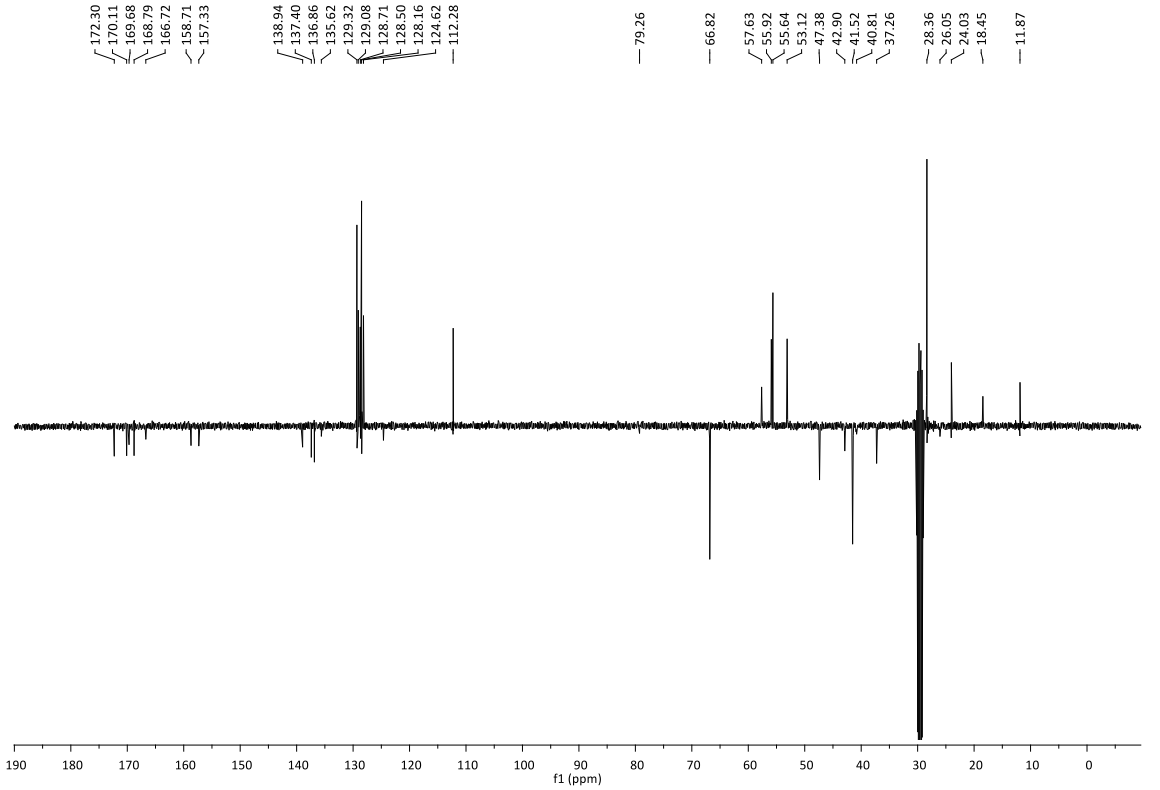

N-Boc-DKP5-Arg(Mtr)-Gly-OBn 80c

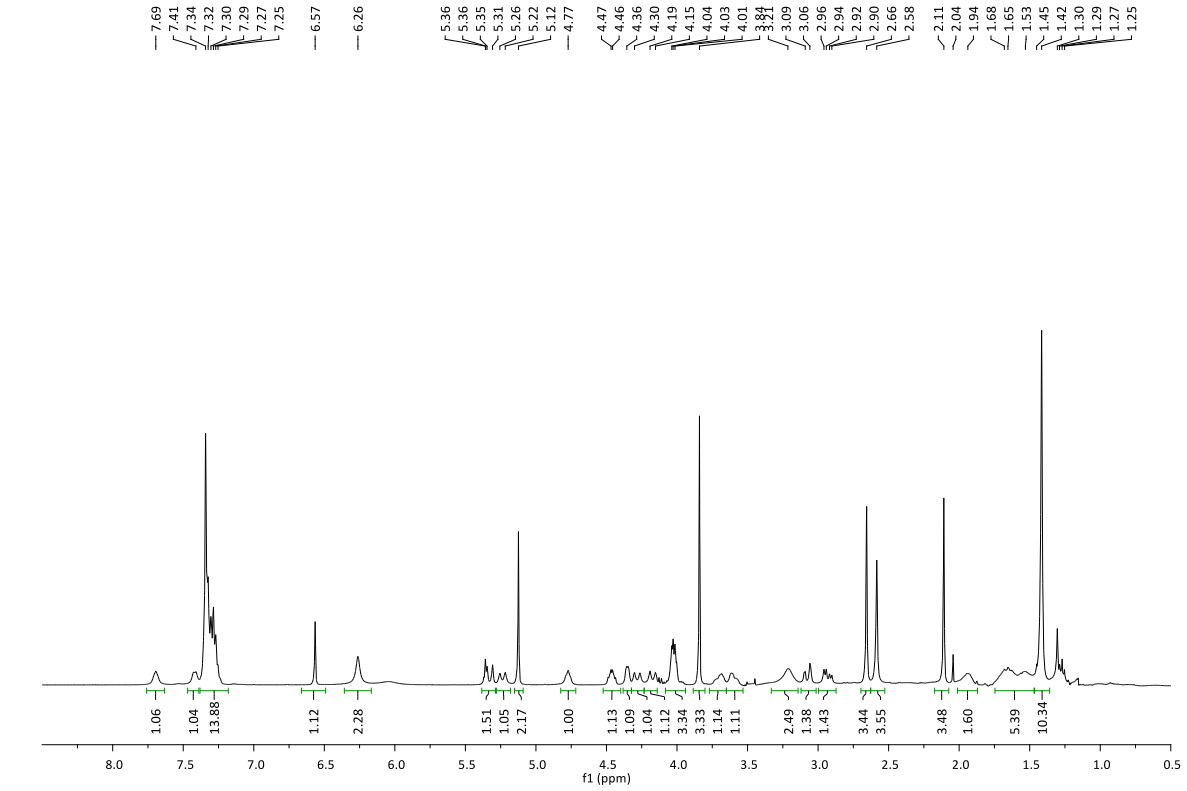

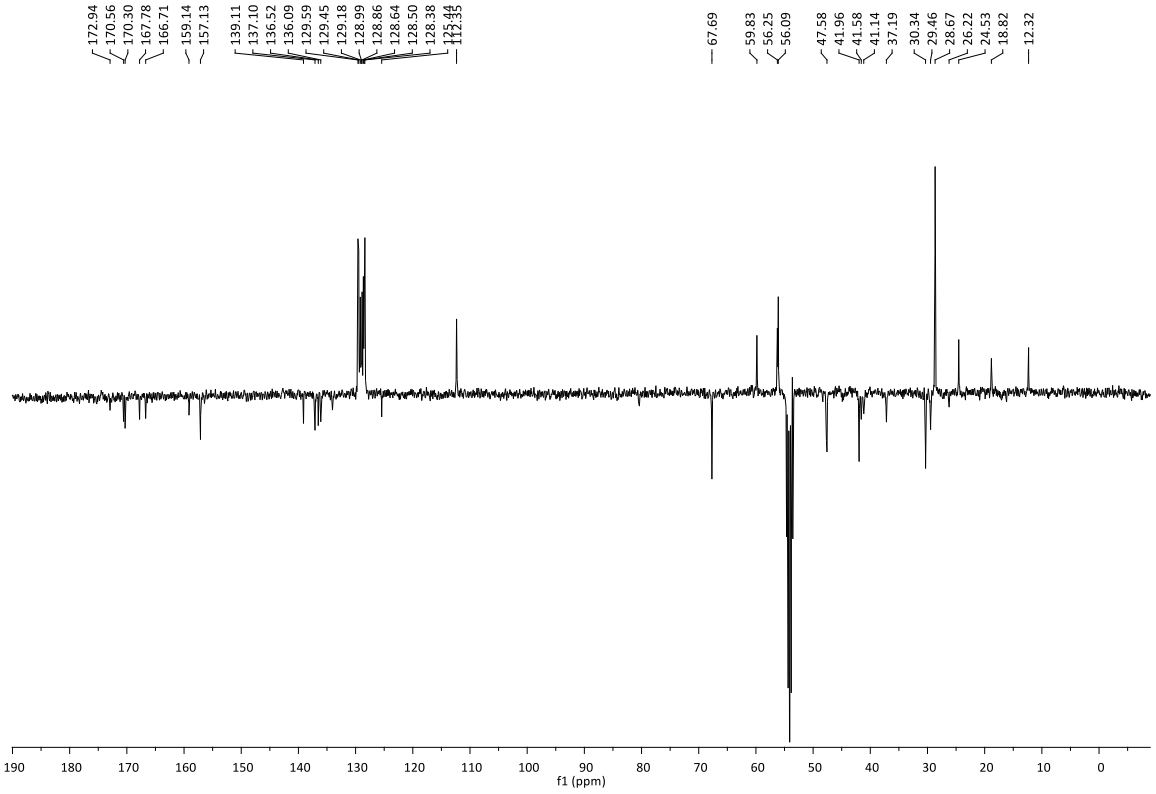

N-Boc-DKP6-Arg(Mtr)-Gly-OBn 80d

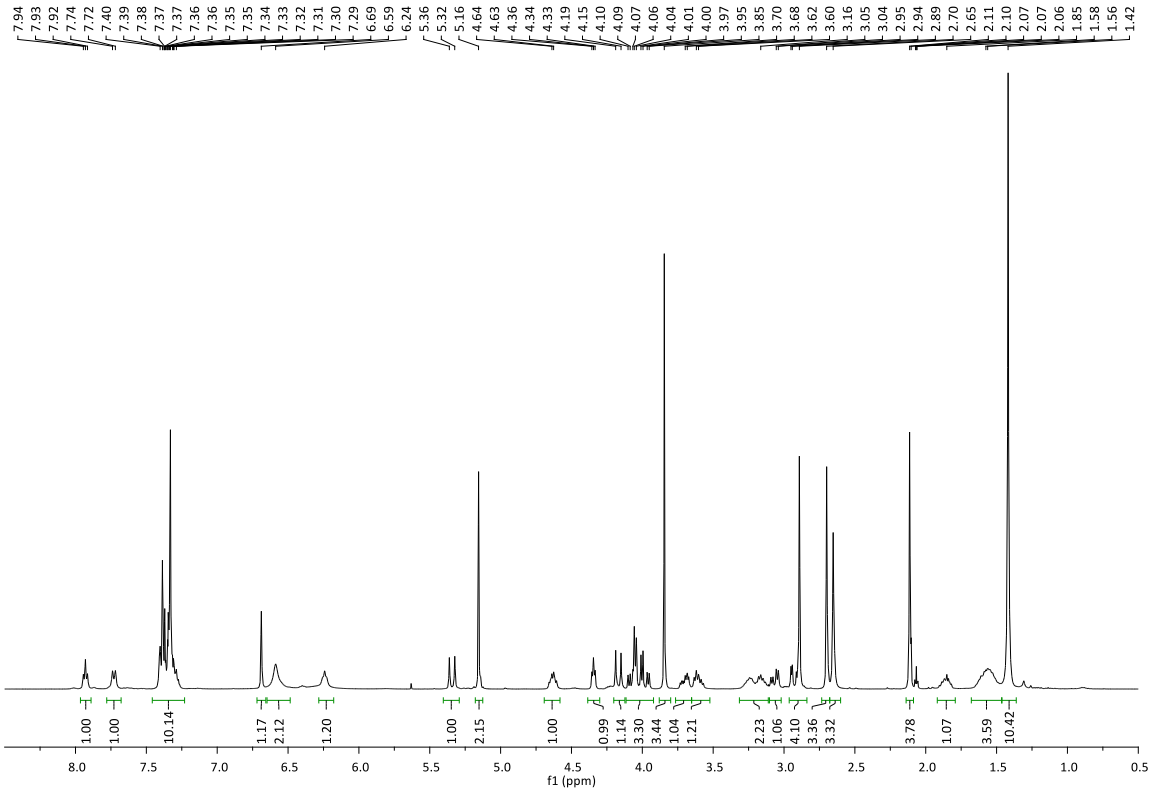

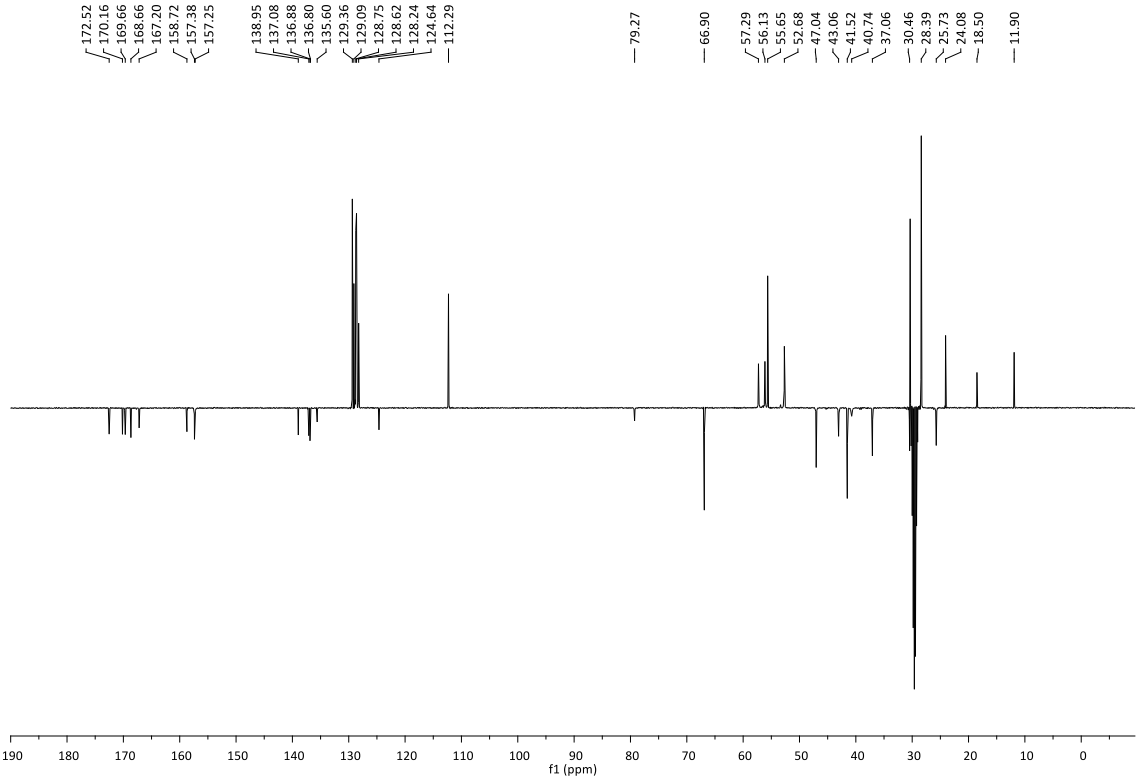

N-Boc-DKP7-Arg(Mtr)-Gly-OBn 80e

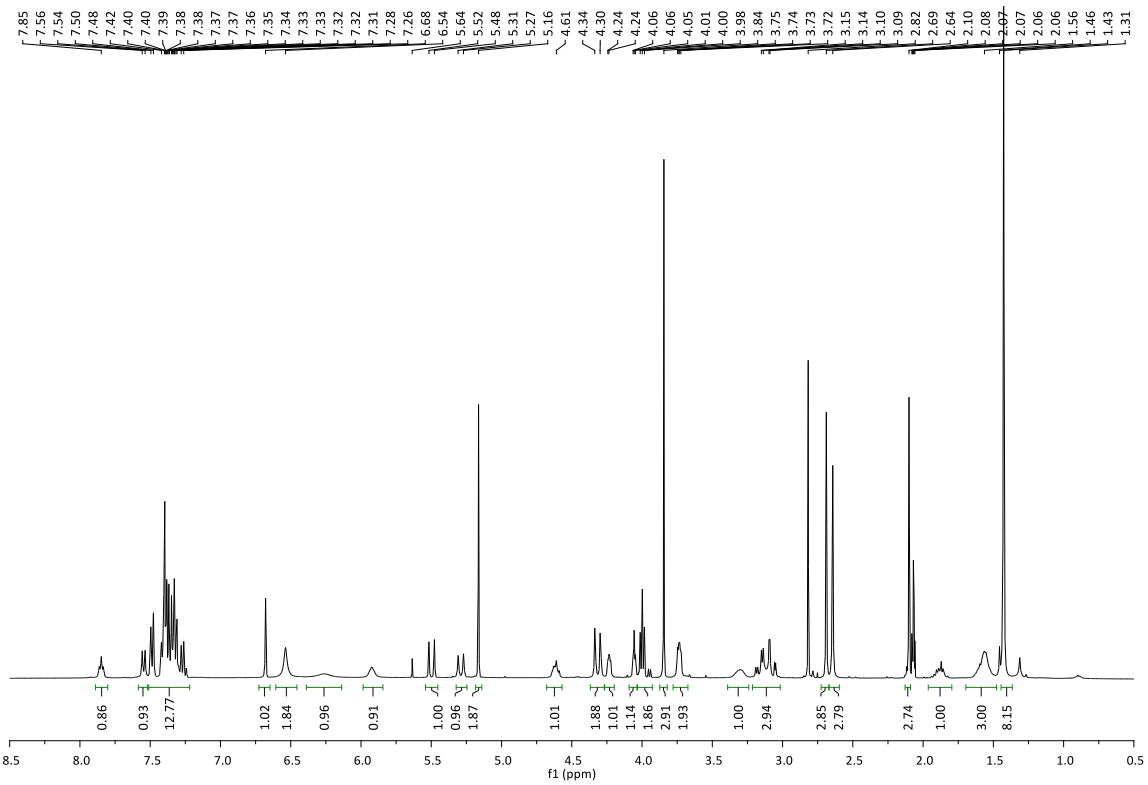

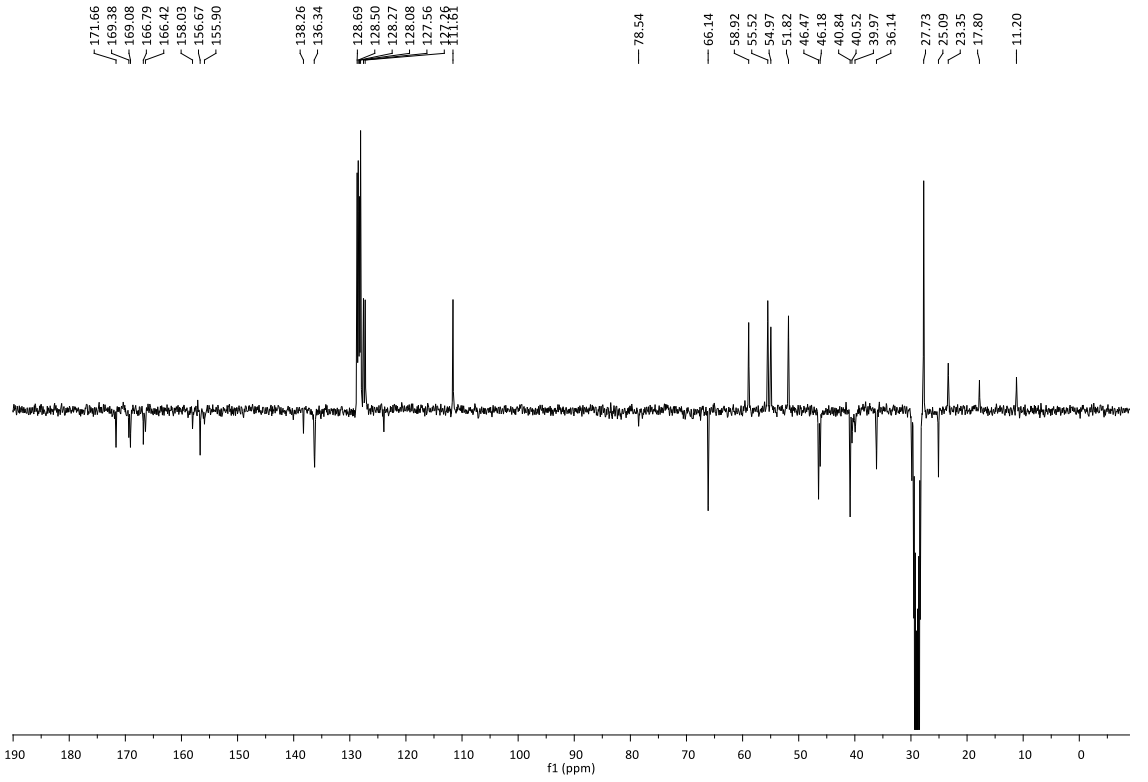

N-Boc-DKP8-Arg(Mtr)-Gly-OBn 80f

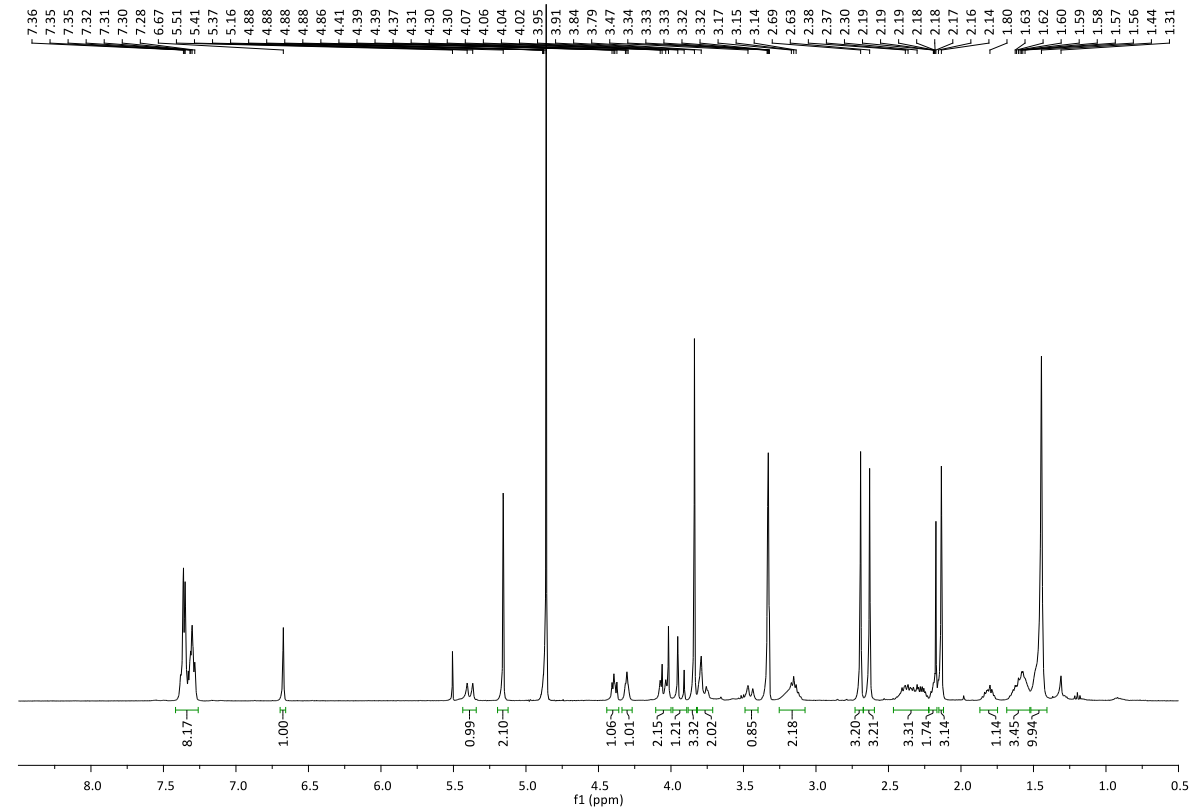

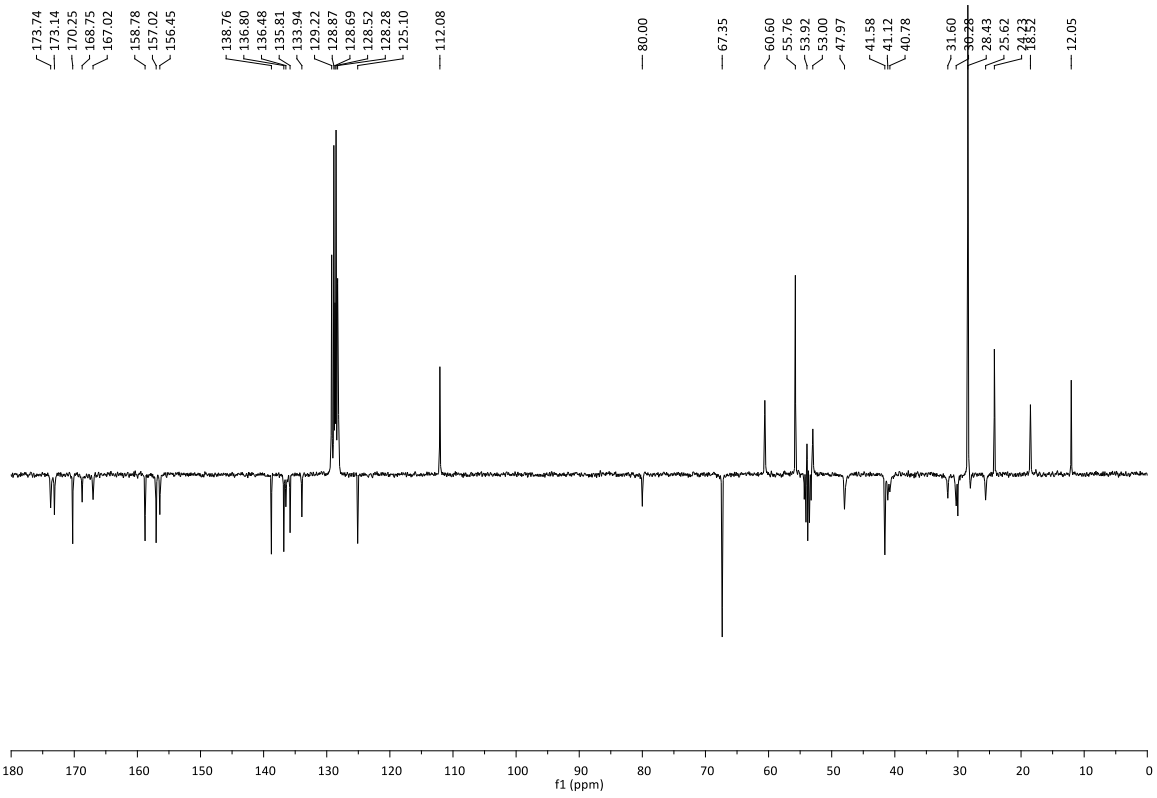

Cbz-Asp(O*t*Bu)-DKP3-Arg(Mtr)-Gly-OBn 81a

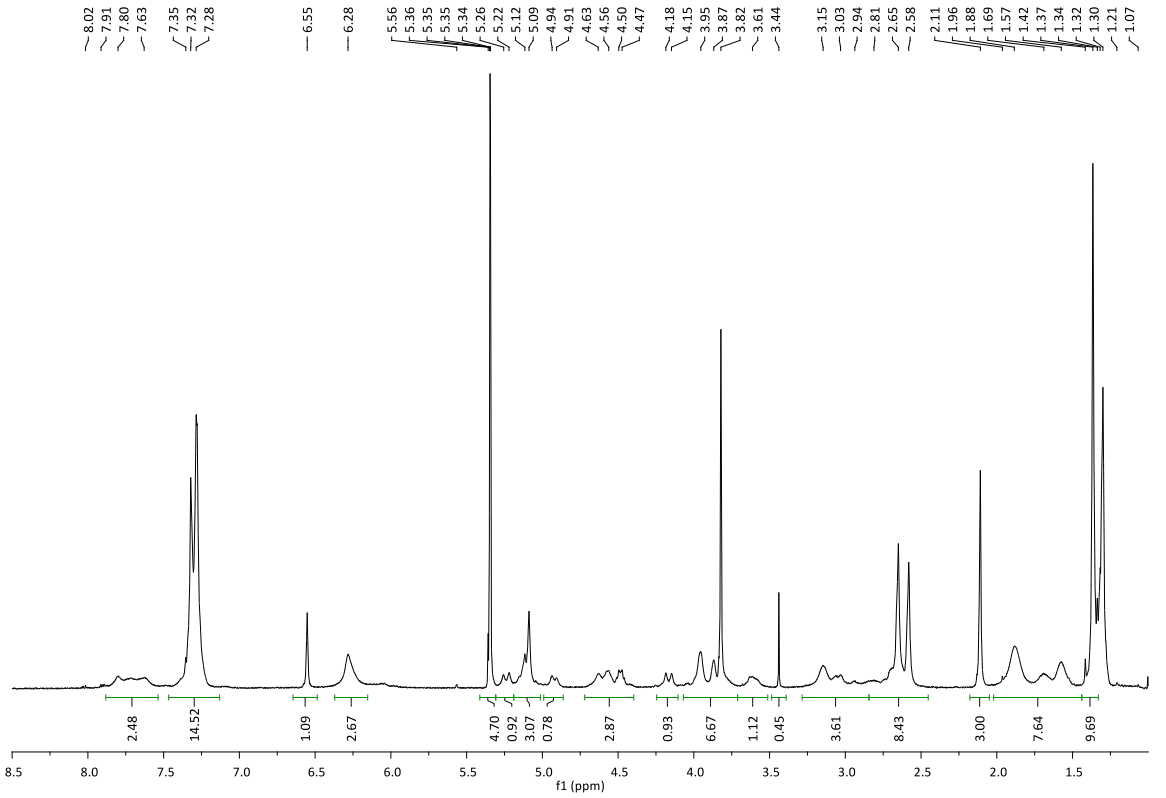

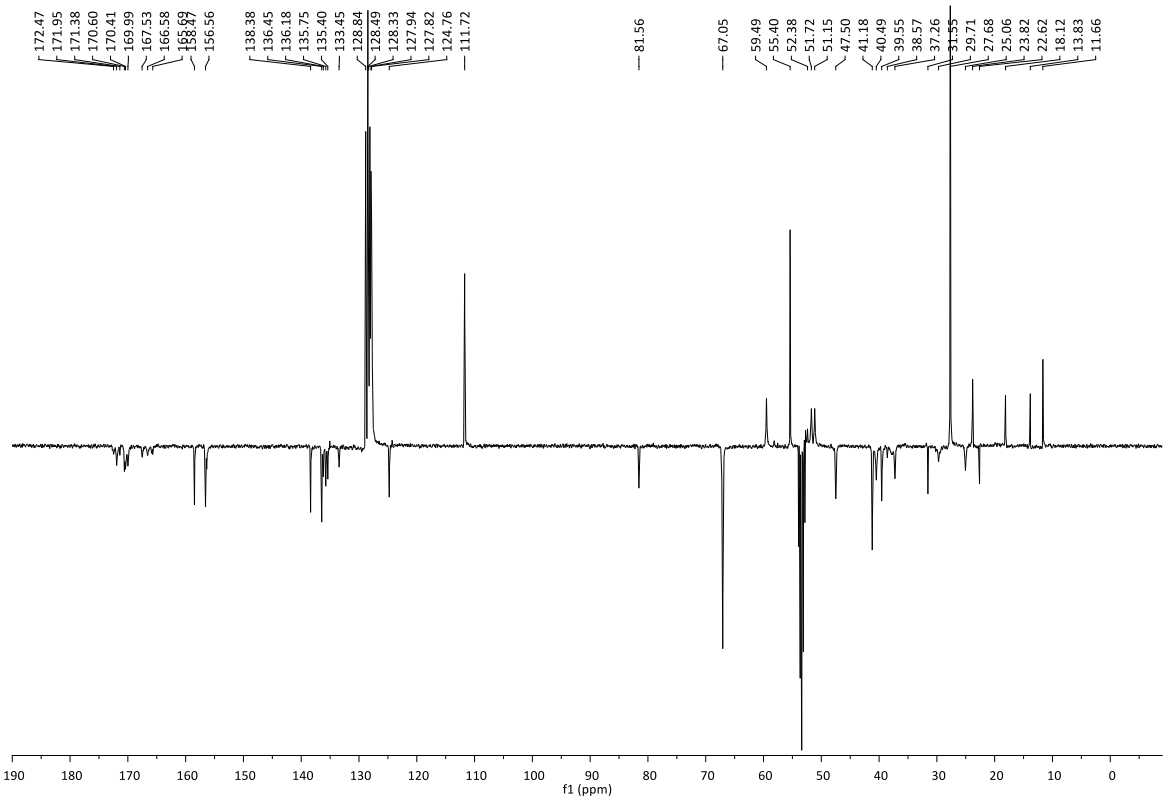

Cbz-Asp(O*t*Bu)-DKP4-Arg(Mtr)-Gly-OBn 81b

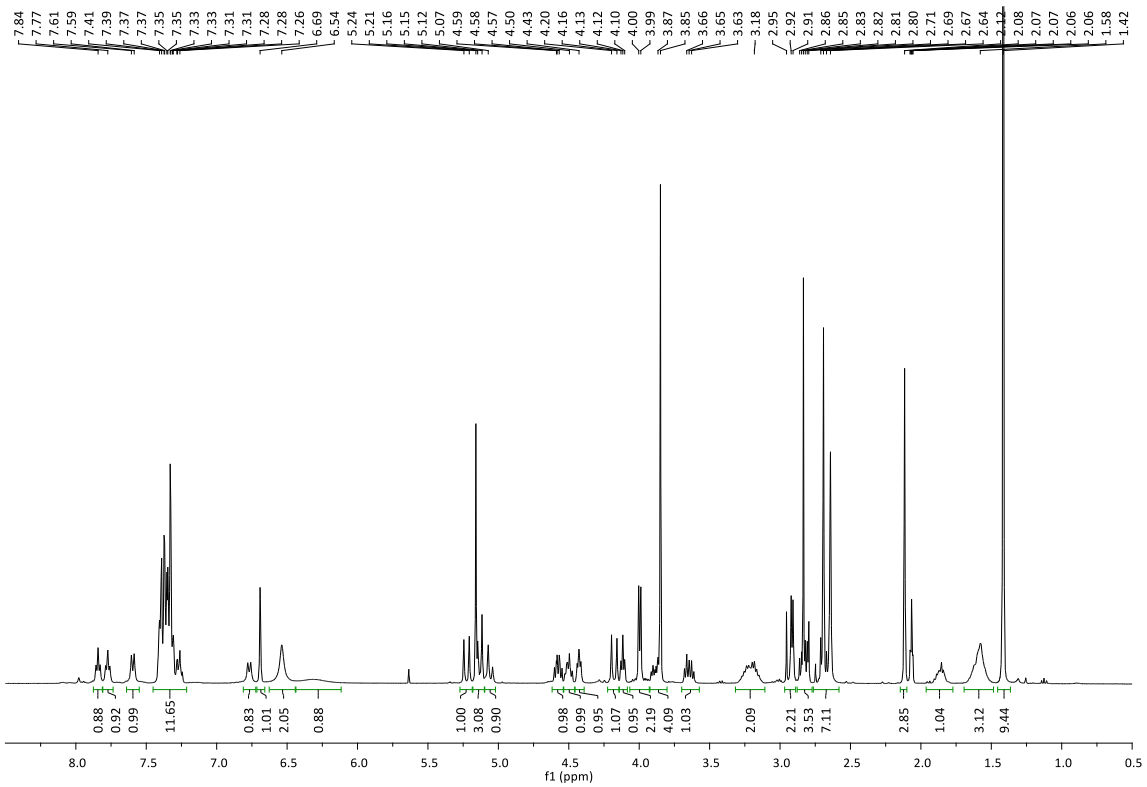

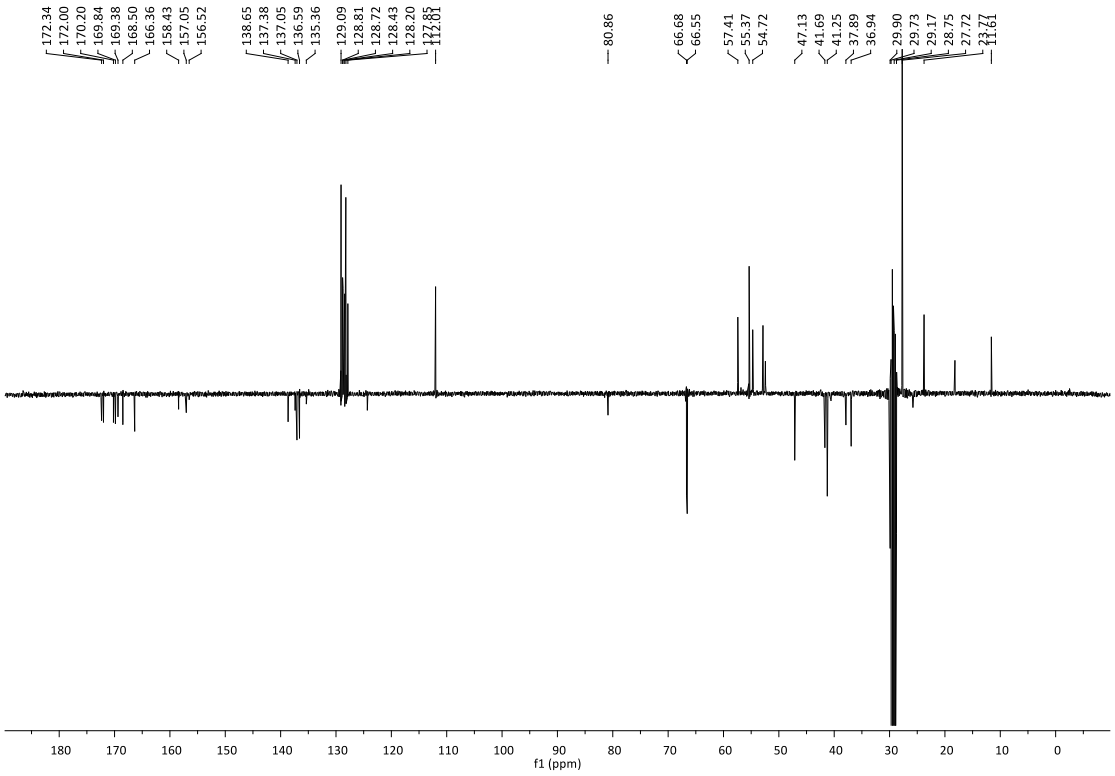

Cbz-Asp(O*t*Bu)-DKP5-Arg(Mtr)-Gly-OBn 81c

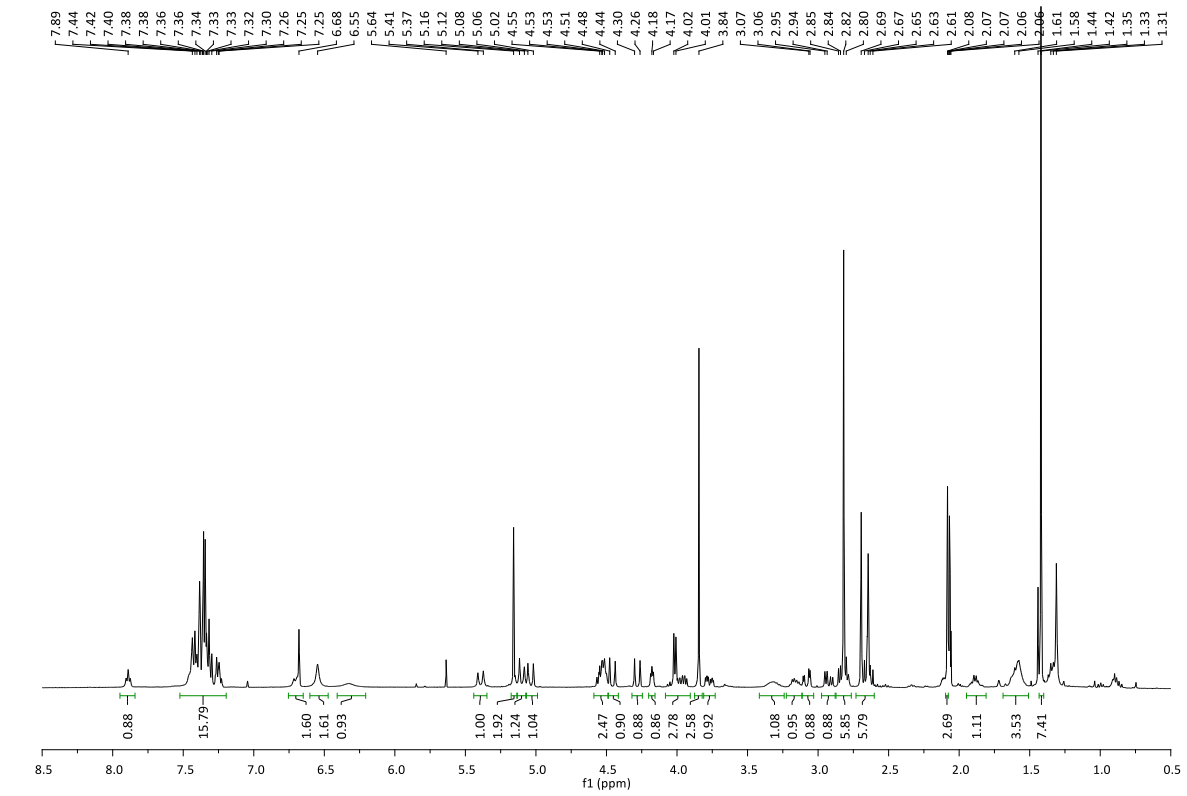

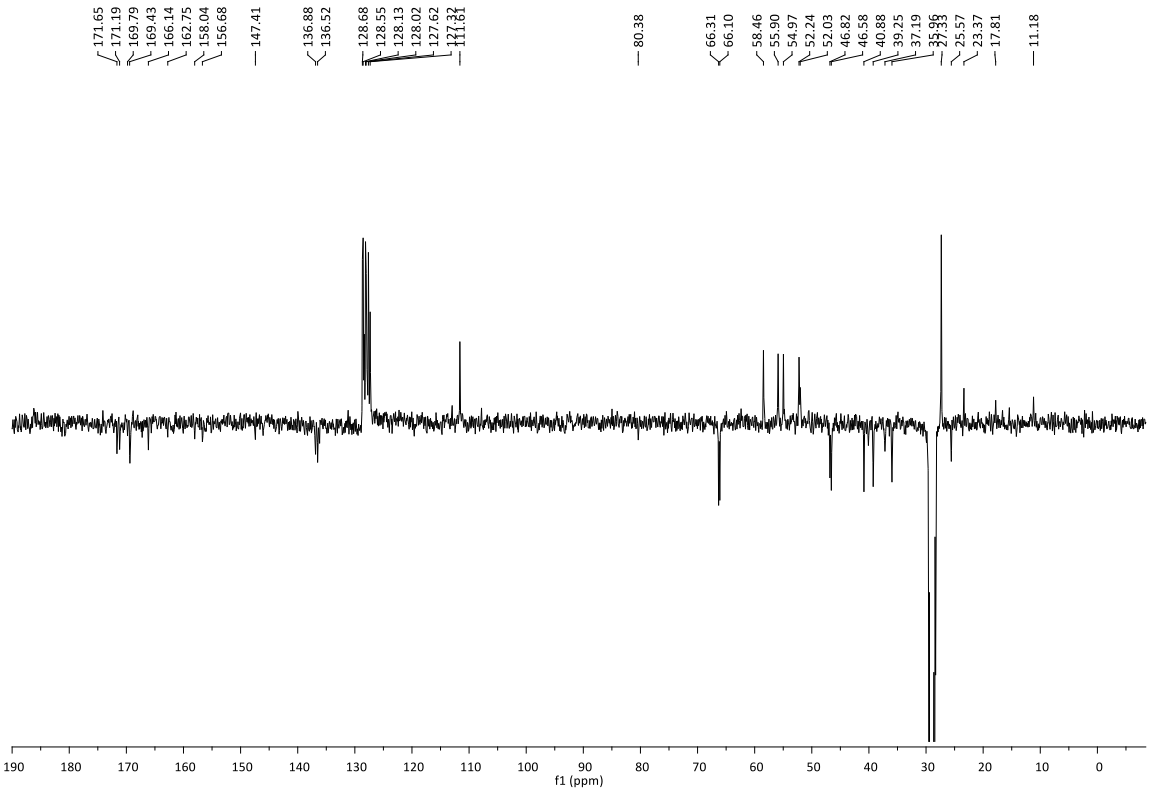

Cbz-Asp(O*t*Bu)-DKP6-Arg(Mtr)-Gly-OBn 81d

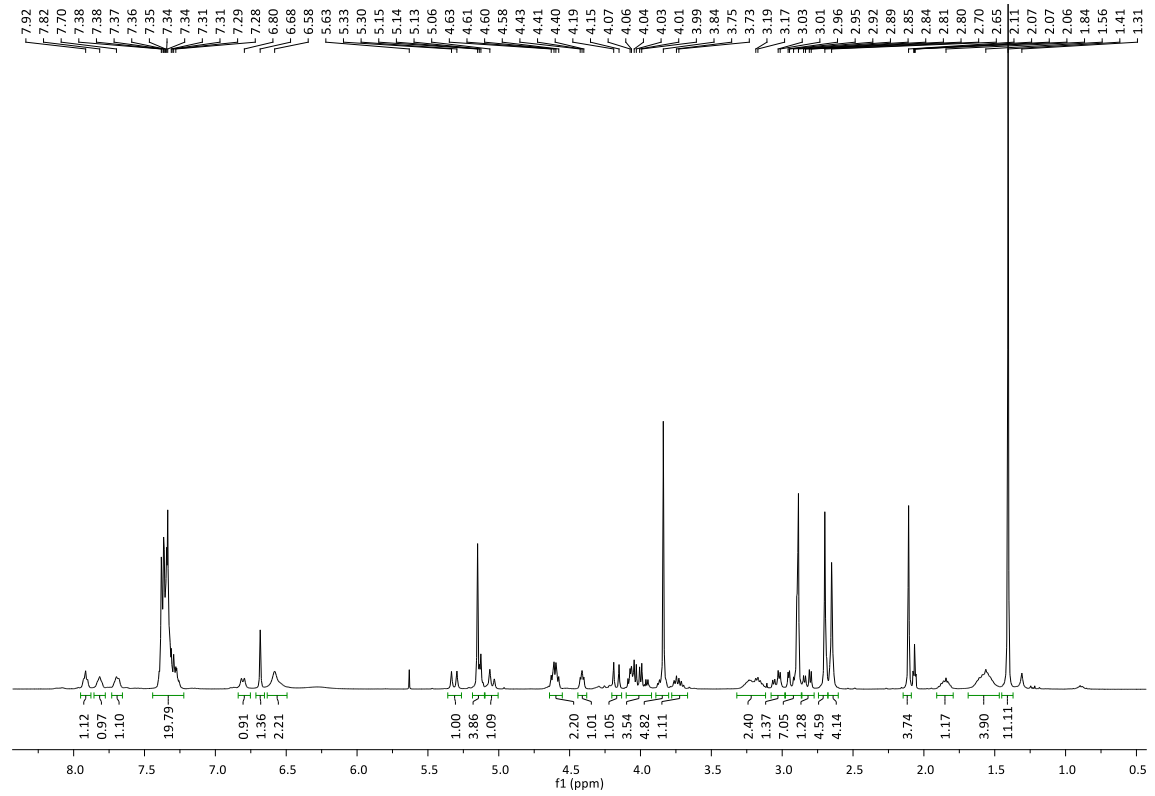

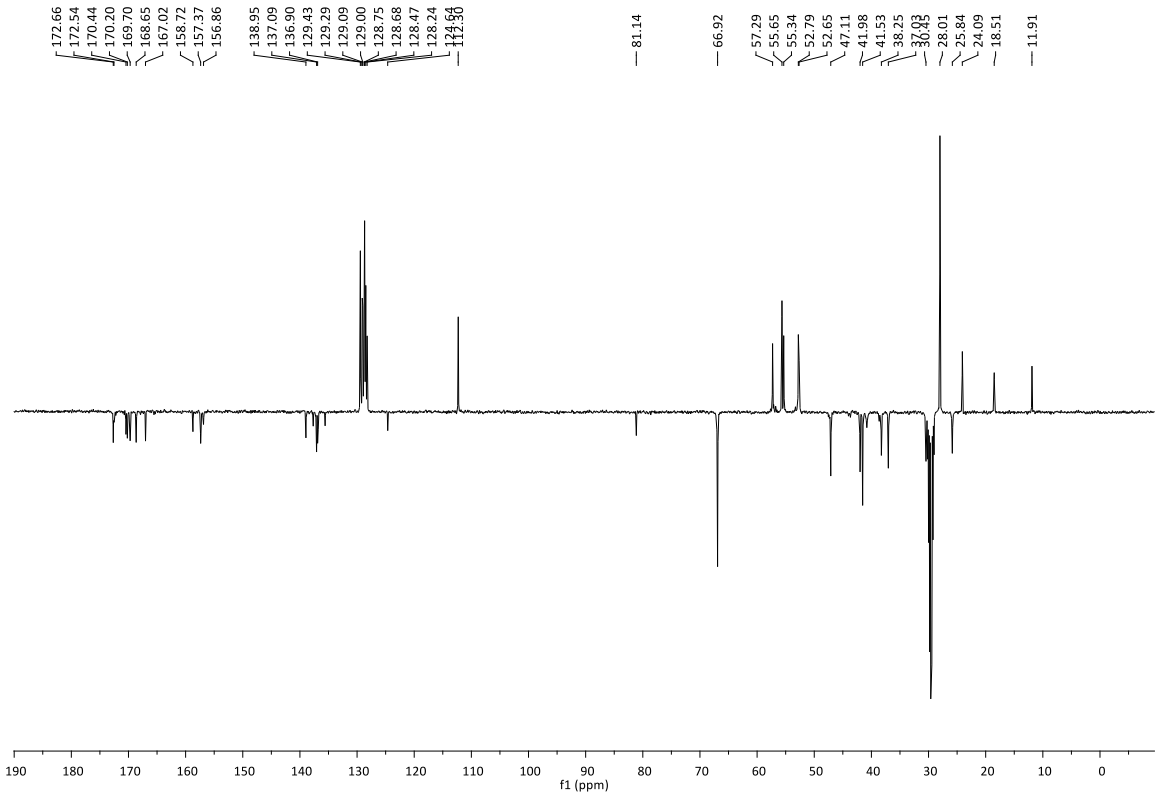

Cbz-Asp(O*t*Bu)-DKP7-Arg(Mtr)-Gly-OBn 81e

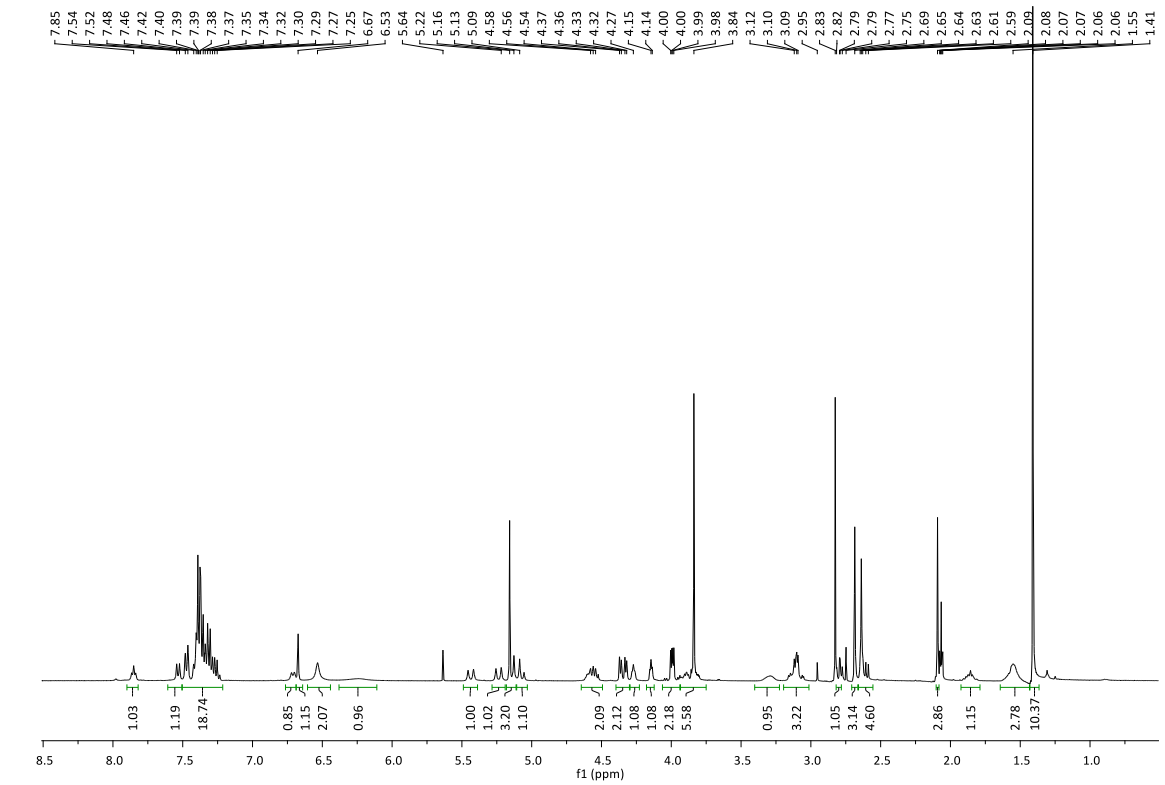

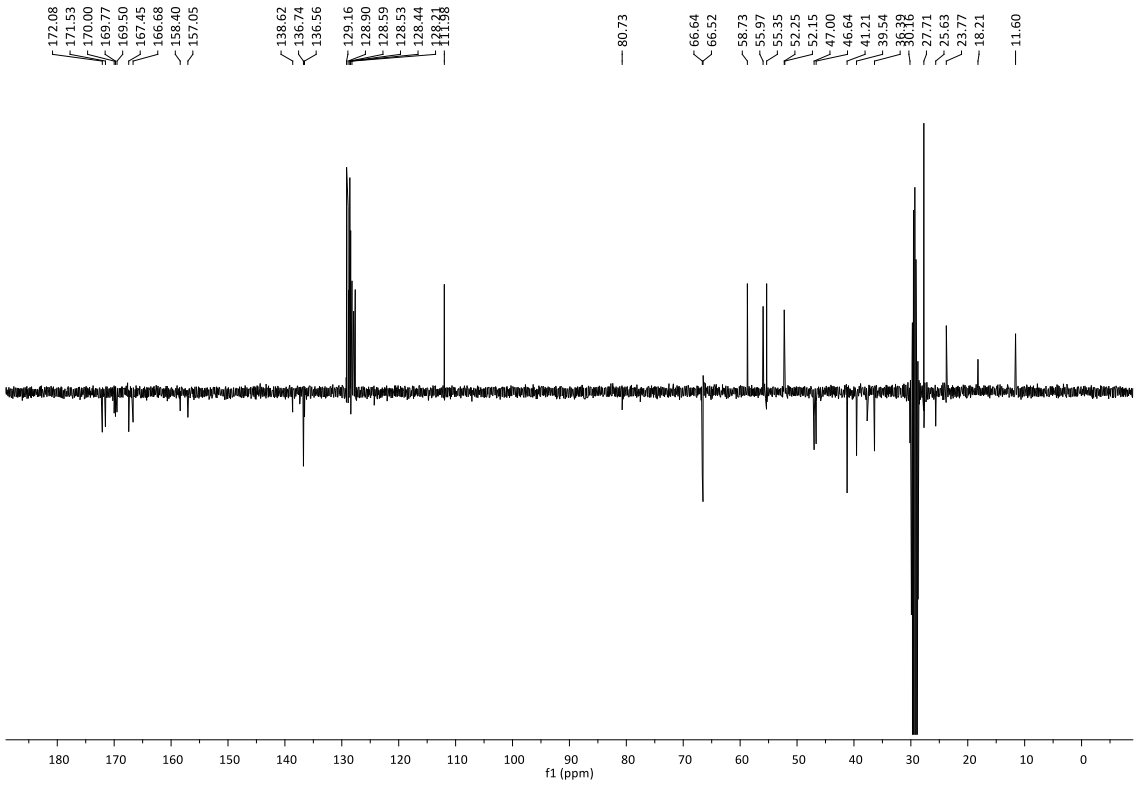

Cbz-Asp(O*t*Bu)-DKP8-Arg(Mtr)-Gly-OBn 81f

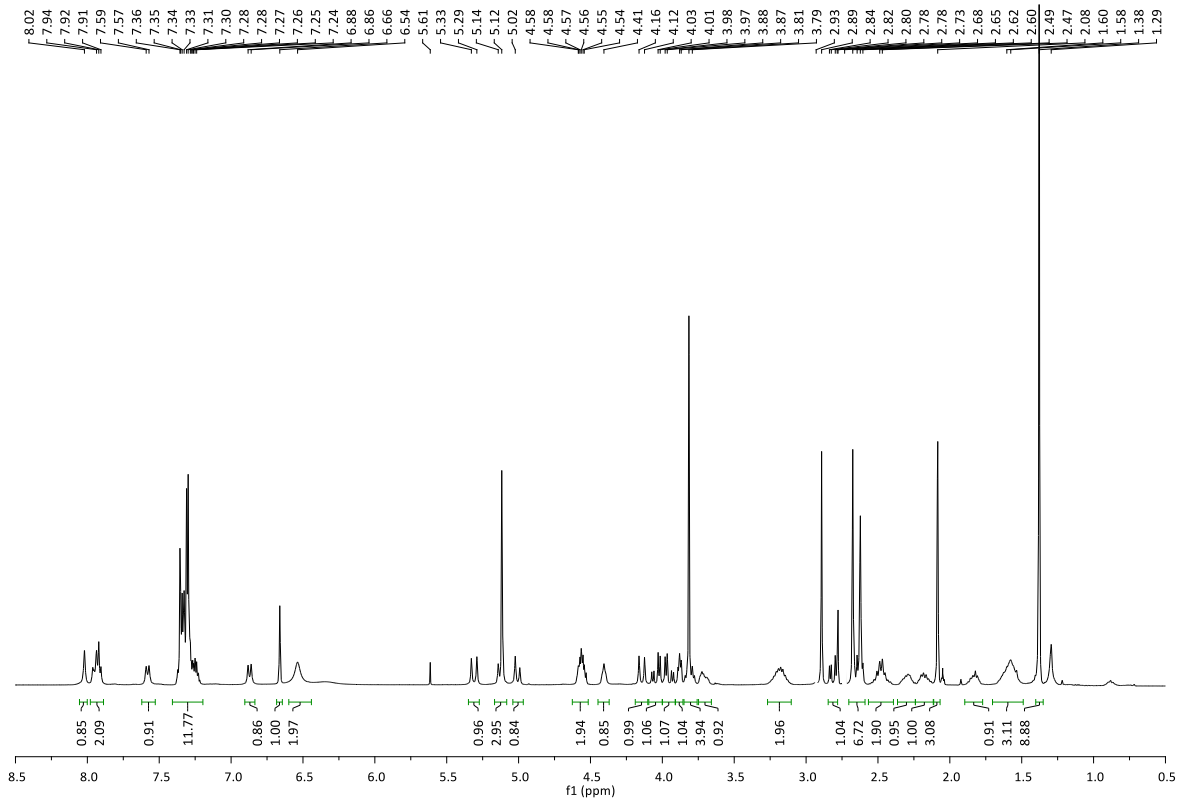

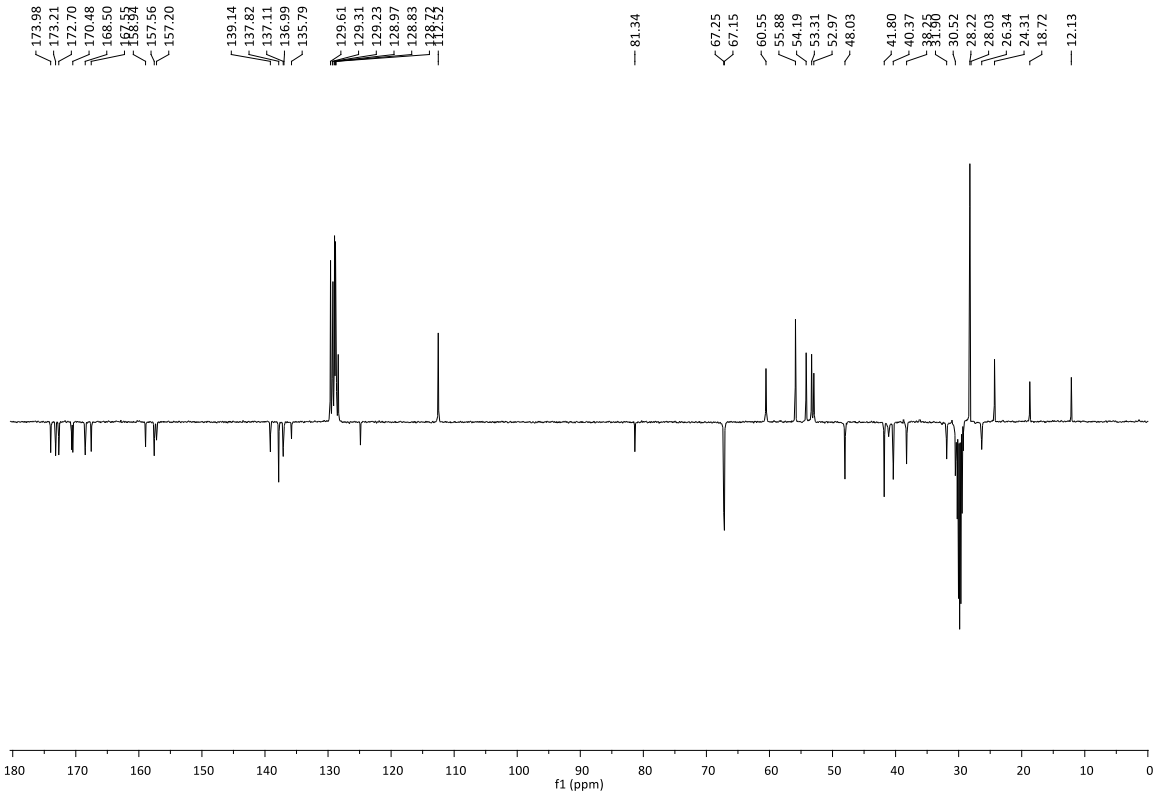

Cyclo[Arg(Mtr)-Gly-Asp(O*t*Bu)-DKP3] 83a

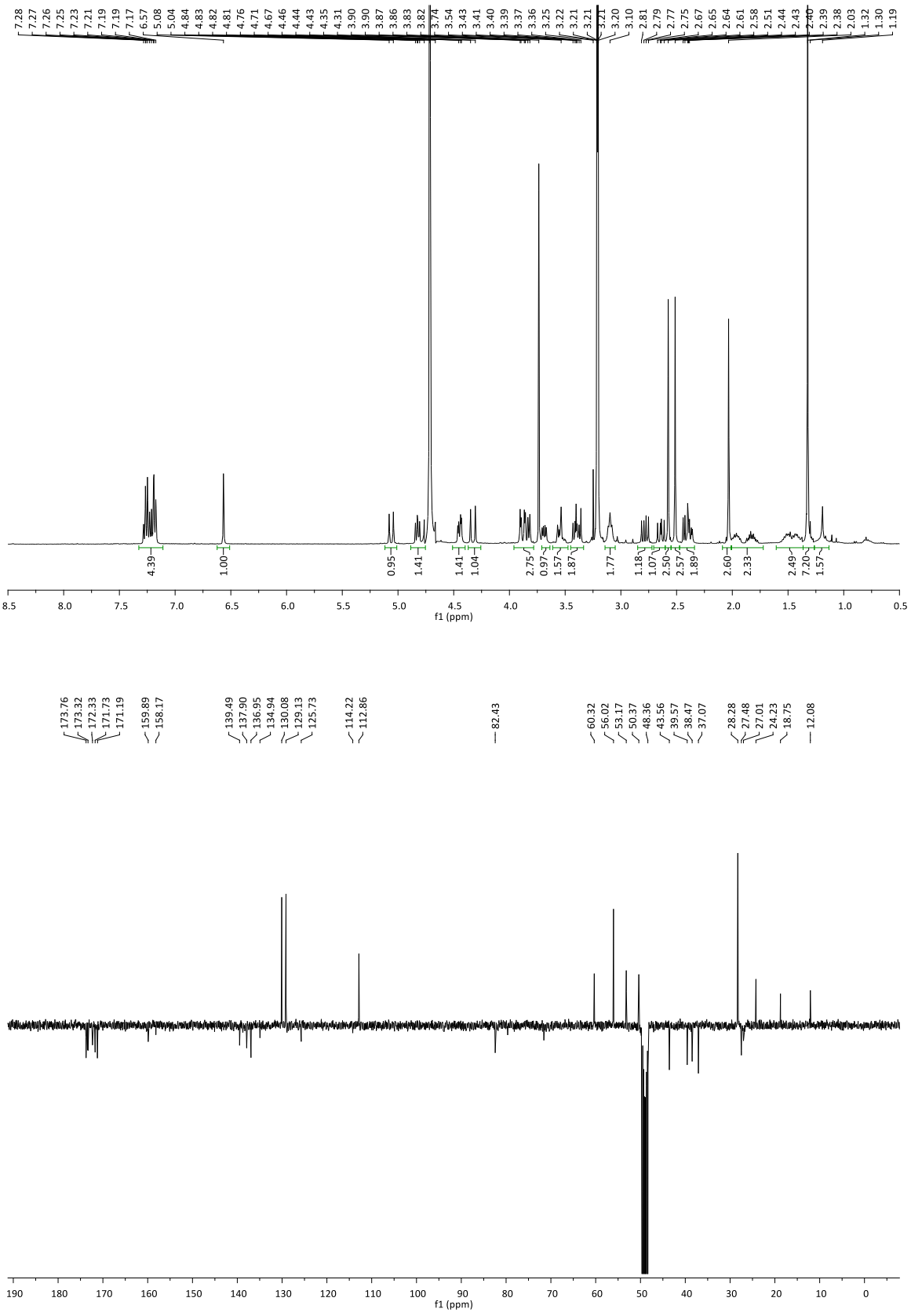

Cyclo[Arg(Mtr)-Gly-Asp(O*t*Bu)-DKP4] 83b

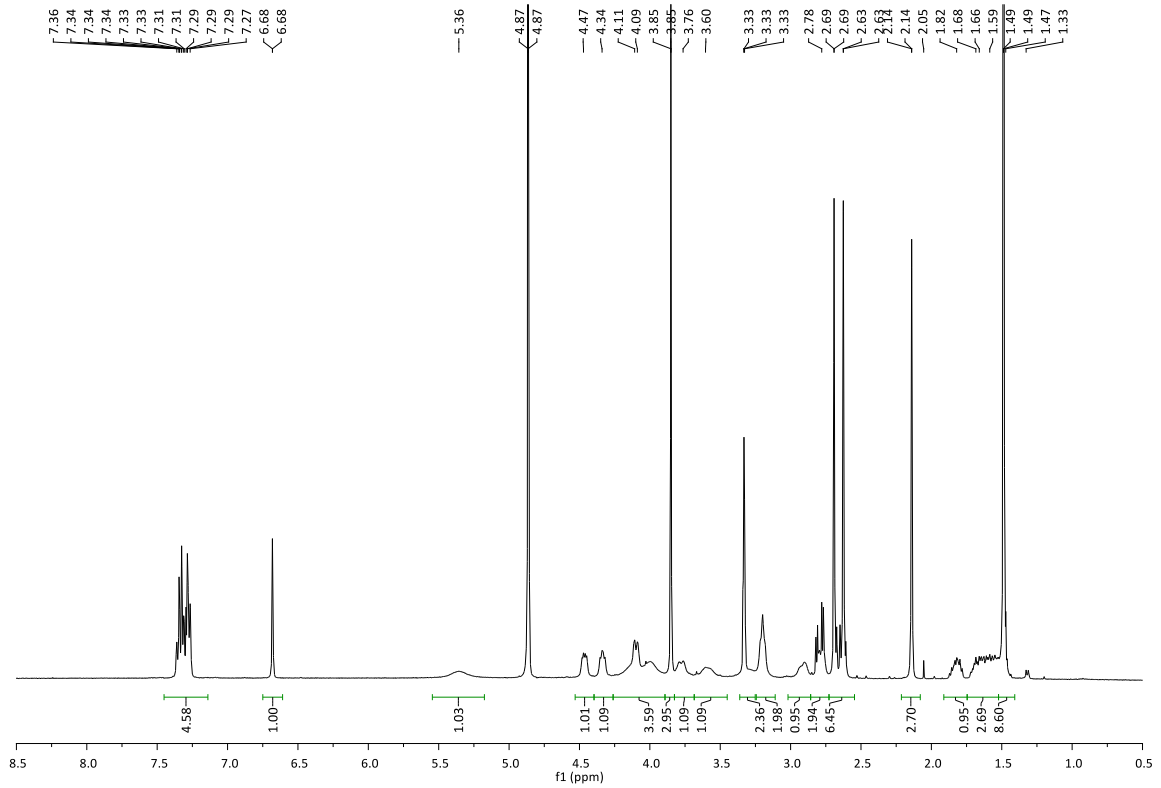

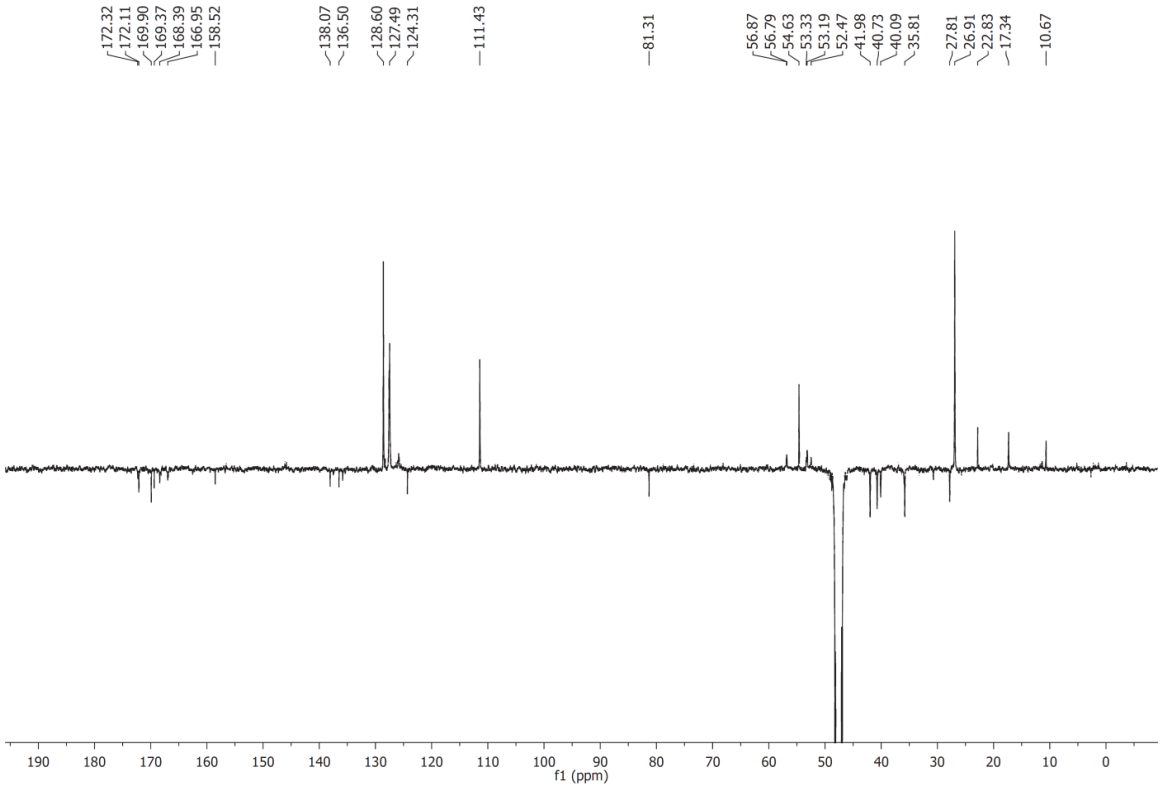

Cyclo[Arg(Mtr)-Gly-Asp(O*t*Bu)-DKP5] 83c

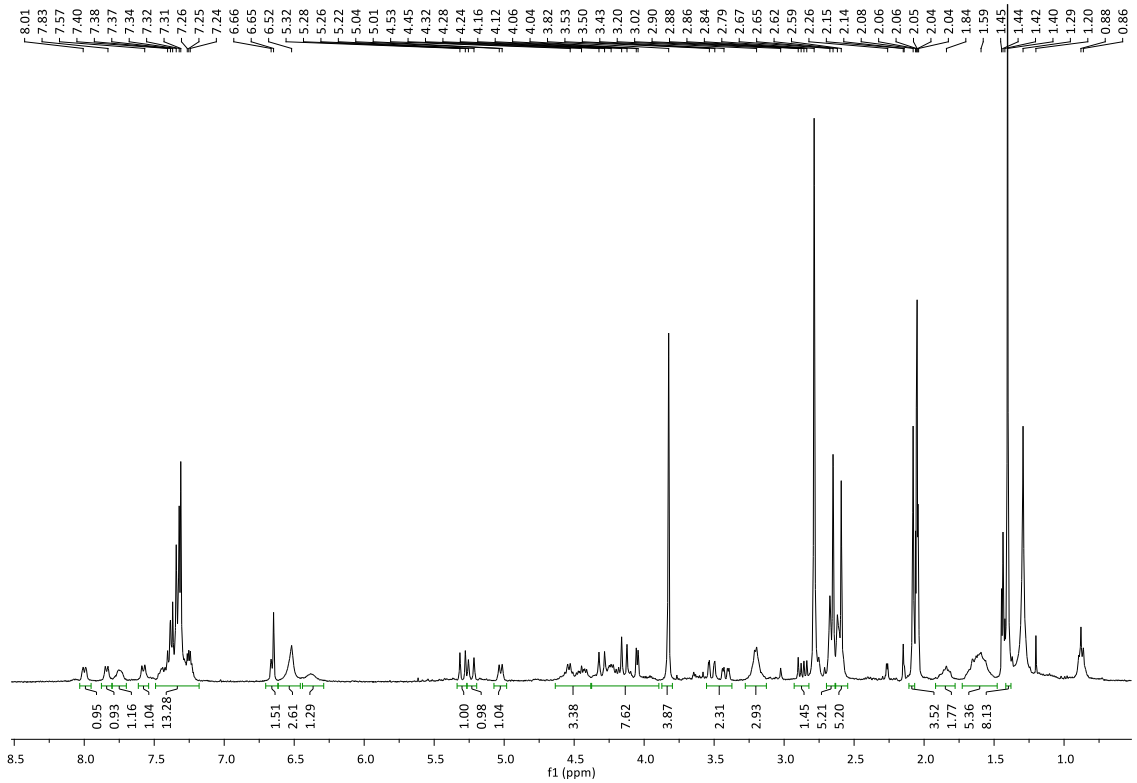

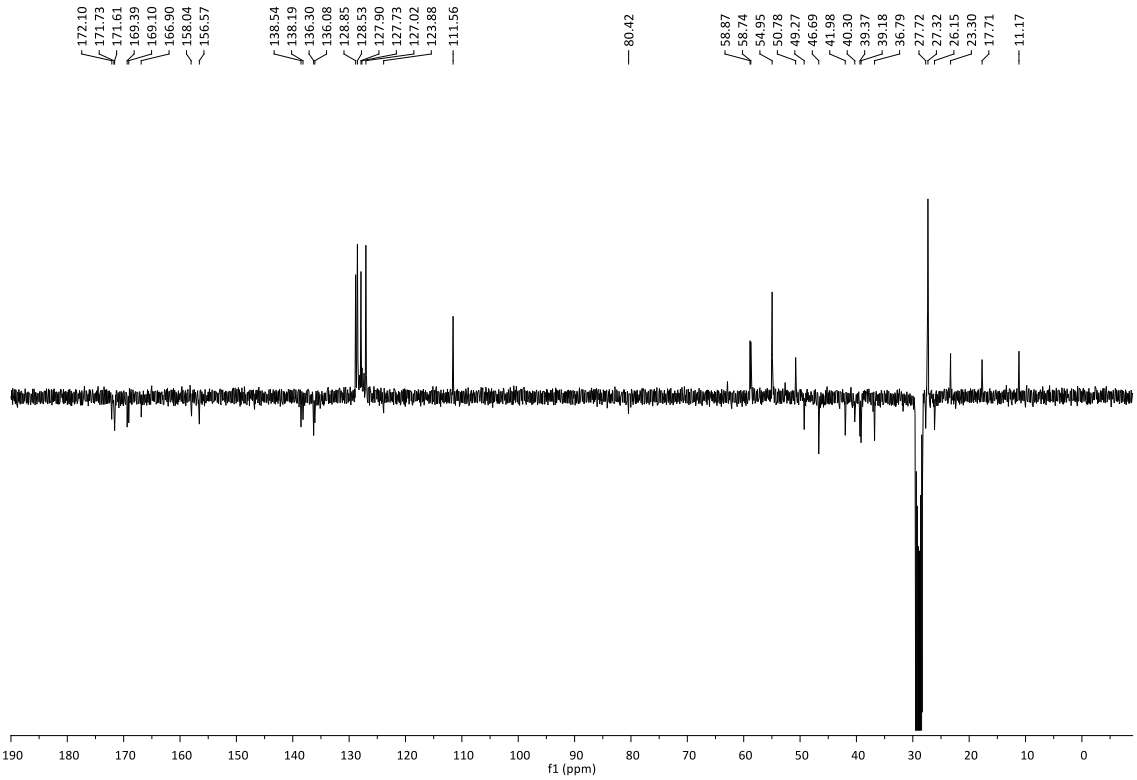

Cyclo[Arg(Mtr)-Gly-Asp(O*t*Bu)-DKP6] 83d

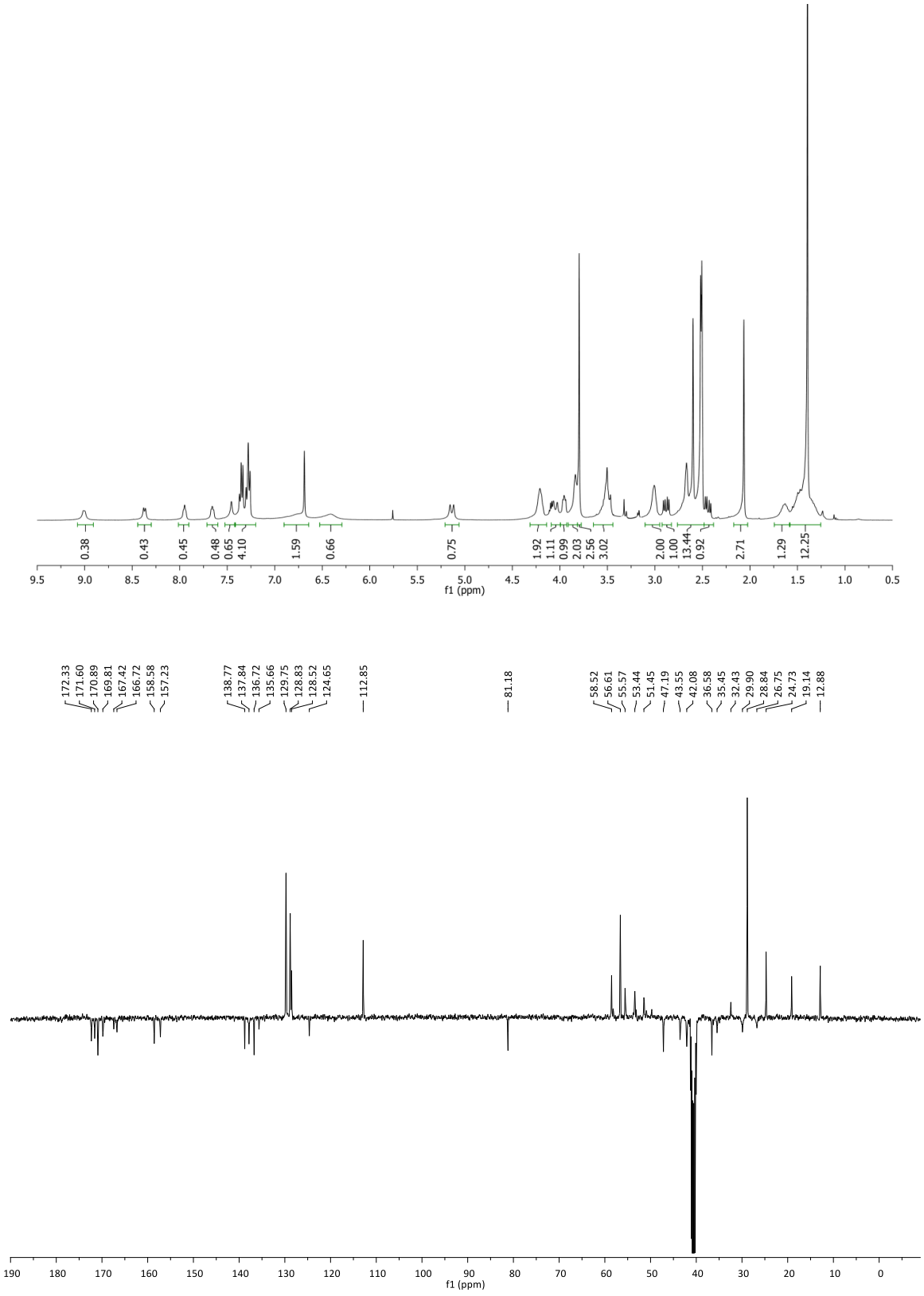

Cyclo[Arg(Mtr)-Gly-Asp(O*t*Bu)-DKP7] 83e

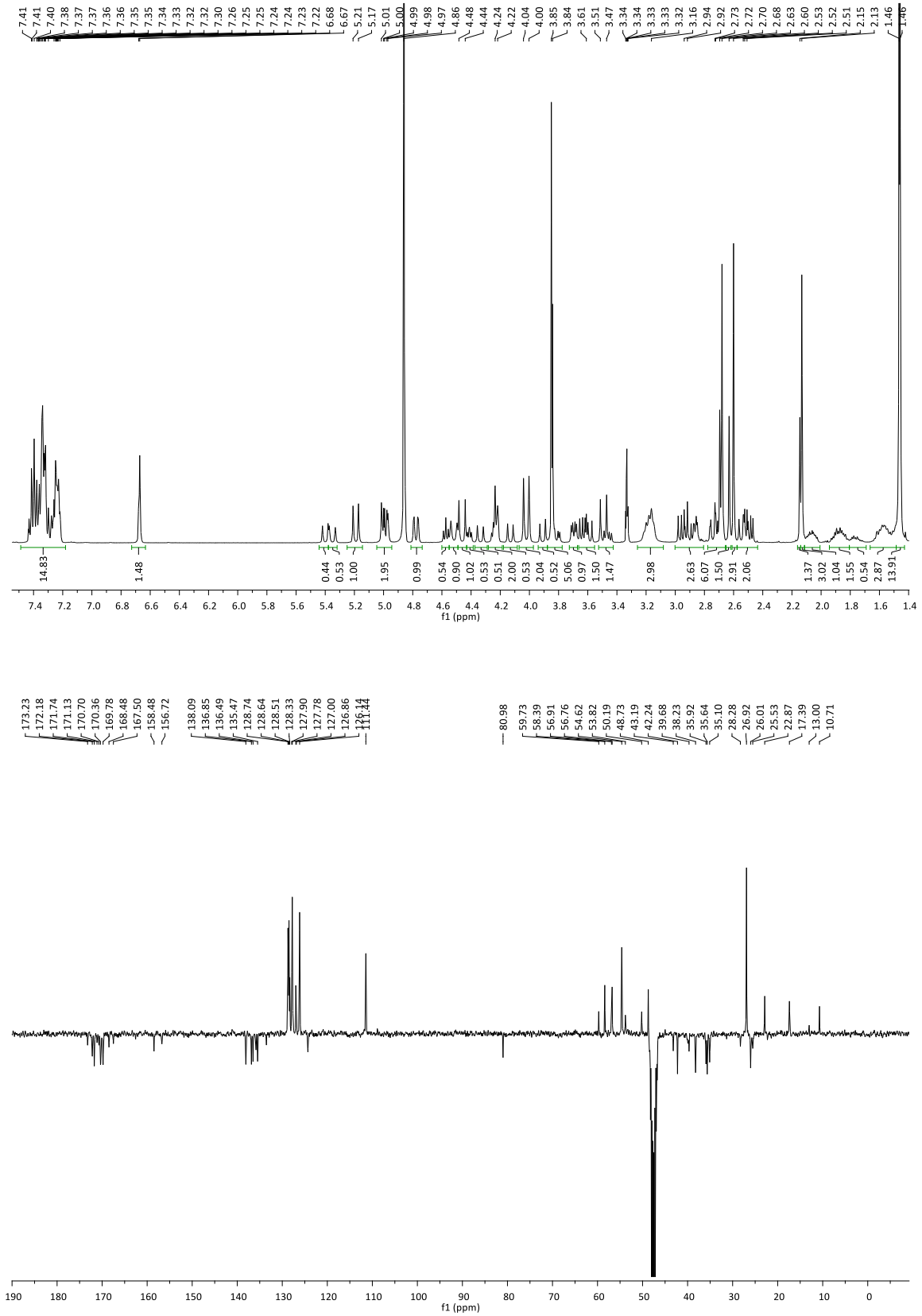

Cyclo[Arg(Mtr)-Gly-Asp(O*t*Bu)-DKP8] 83f

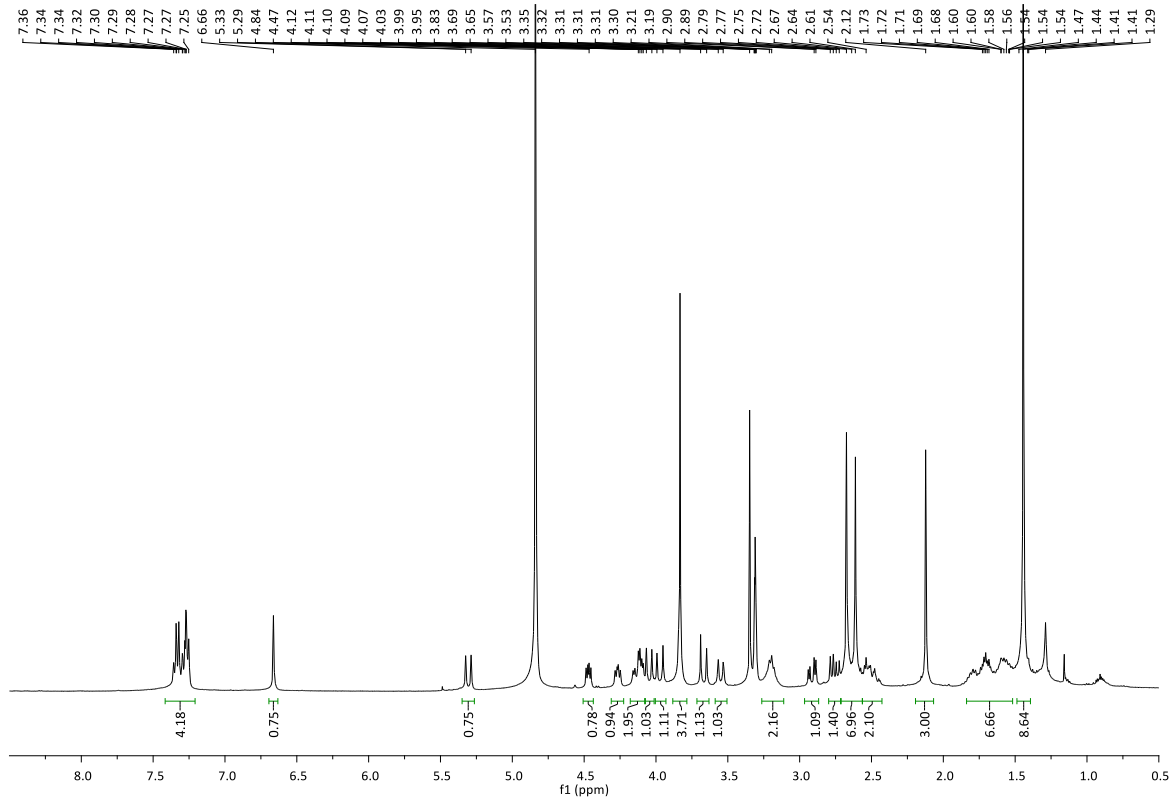

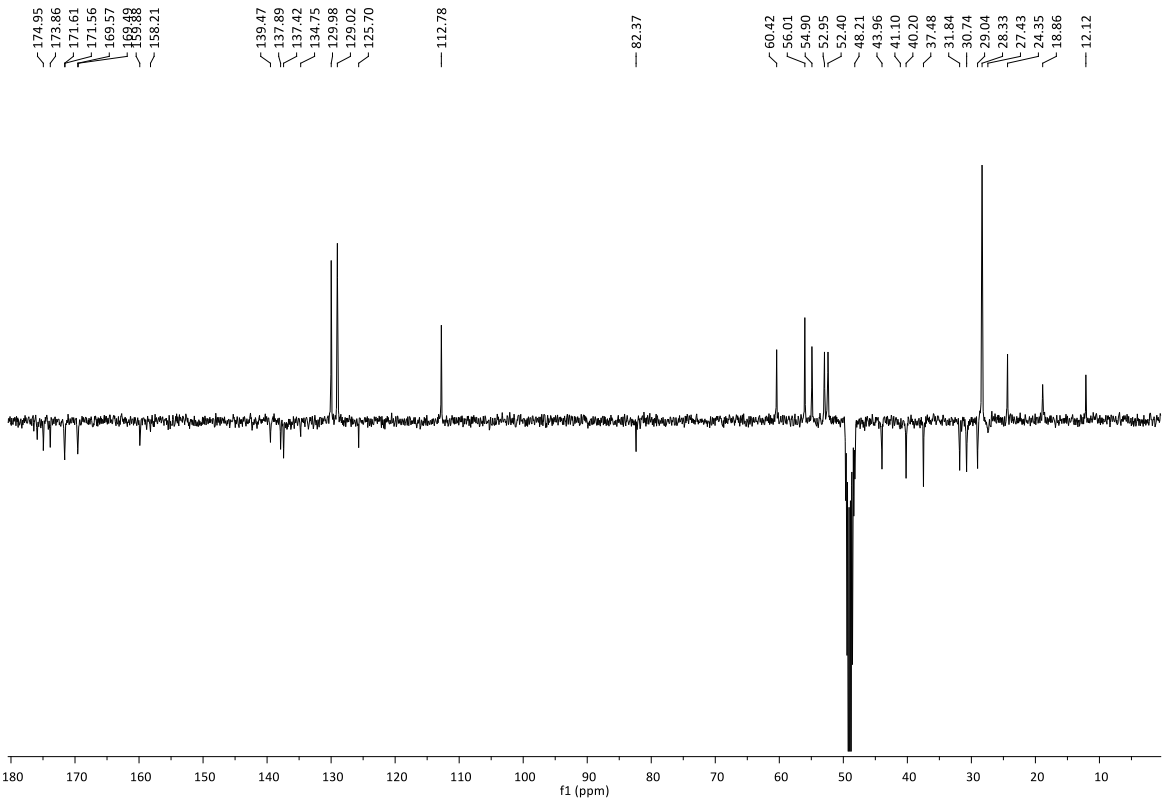

Cyclo[Arg-Gly-Asp-DKP-3] 18

^{1}H NMR (600 MHz, H_2O/D_2O 9:1)

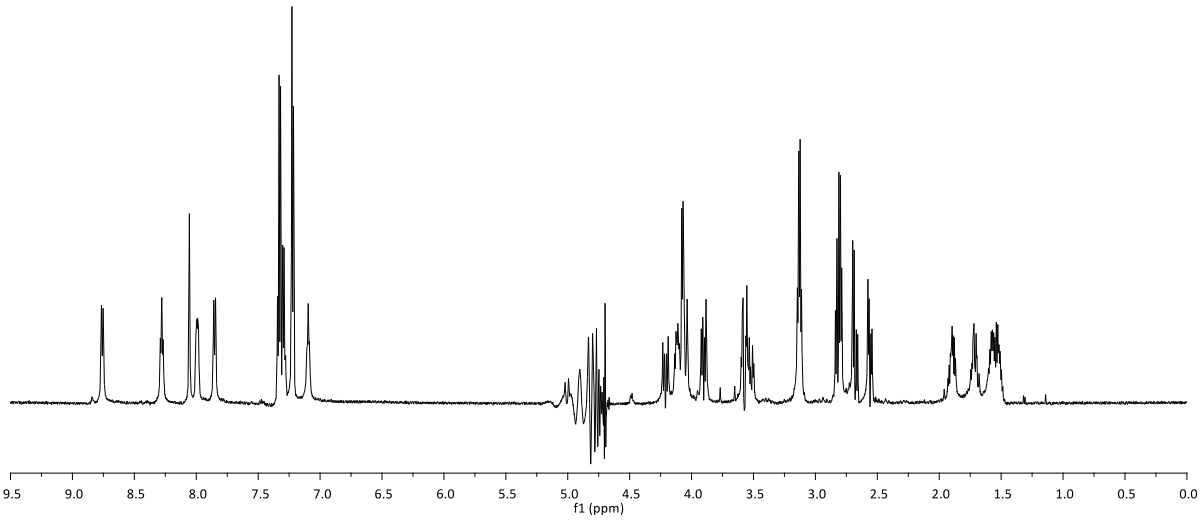

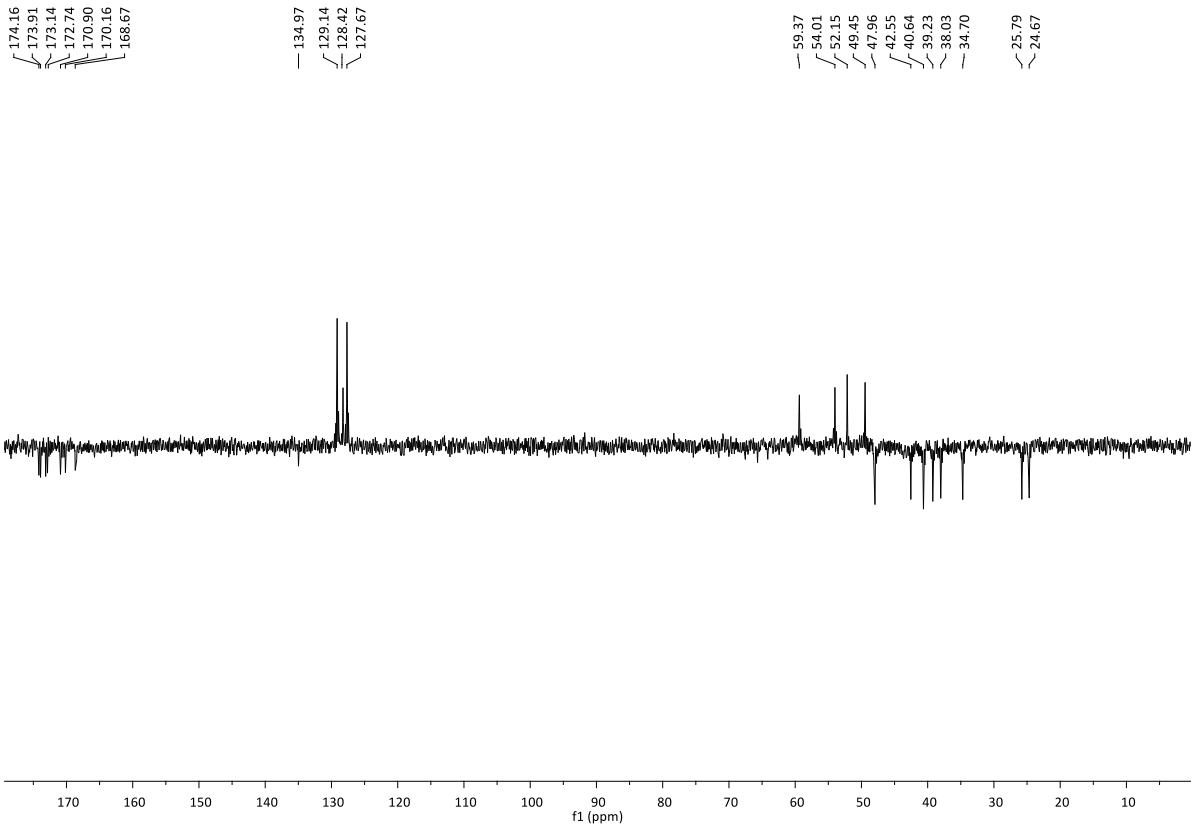

Cyclo[Arg-Gly-Asp-DKP4] 19

^{1}H NMR (400 MHz, H_2O/D_2O 9:1)

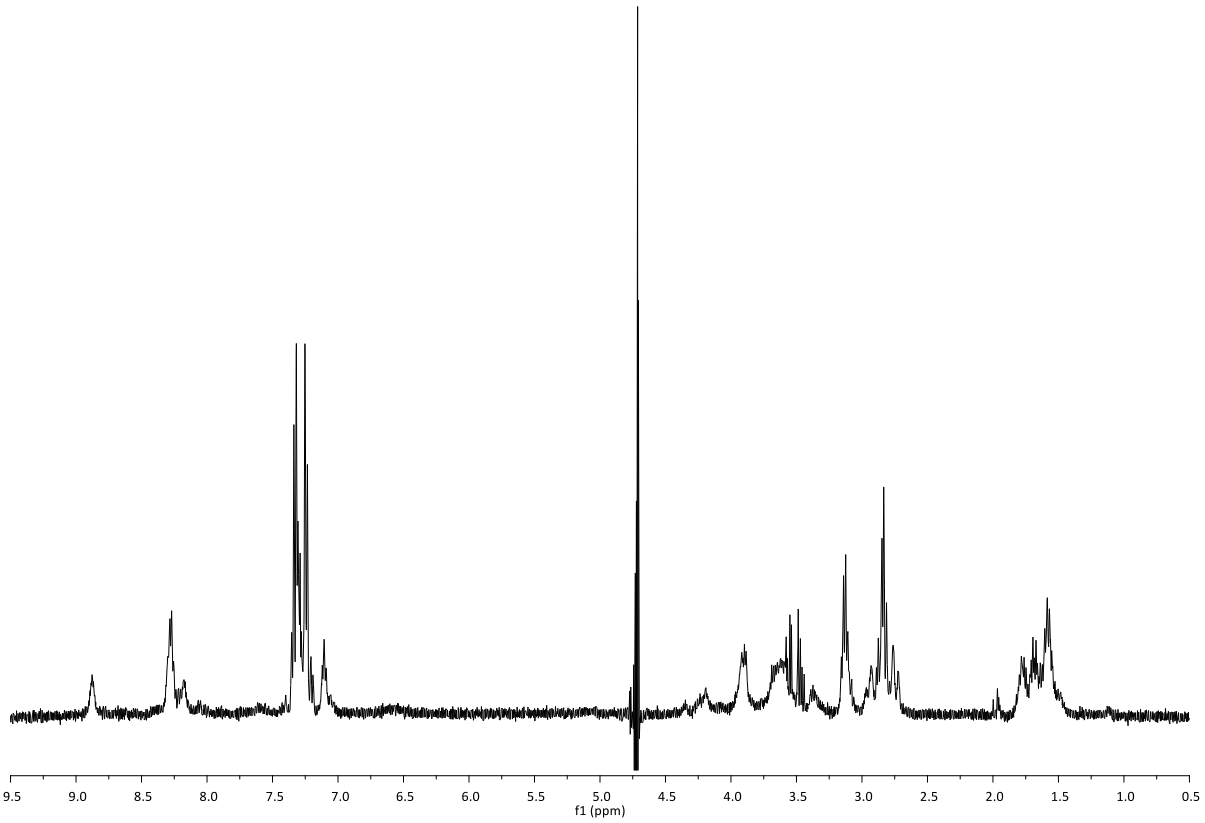

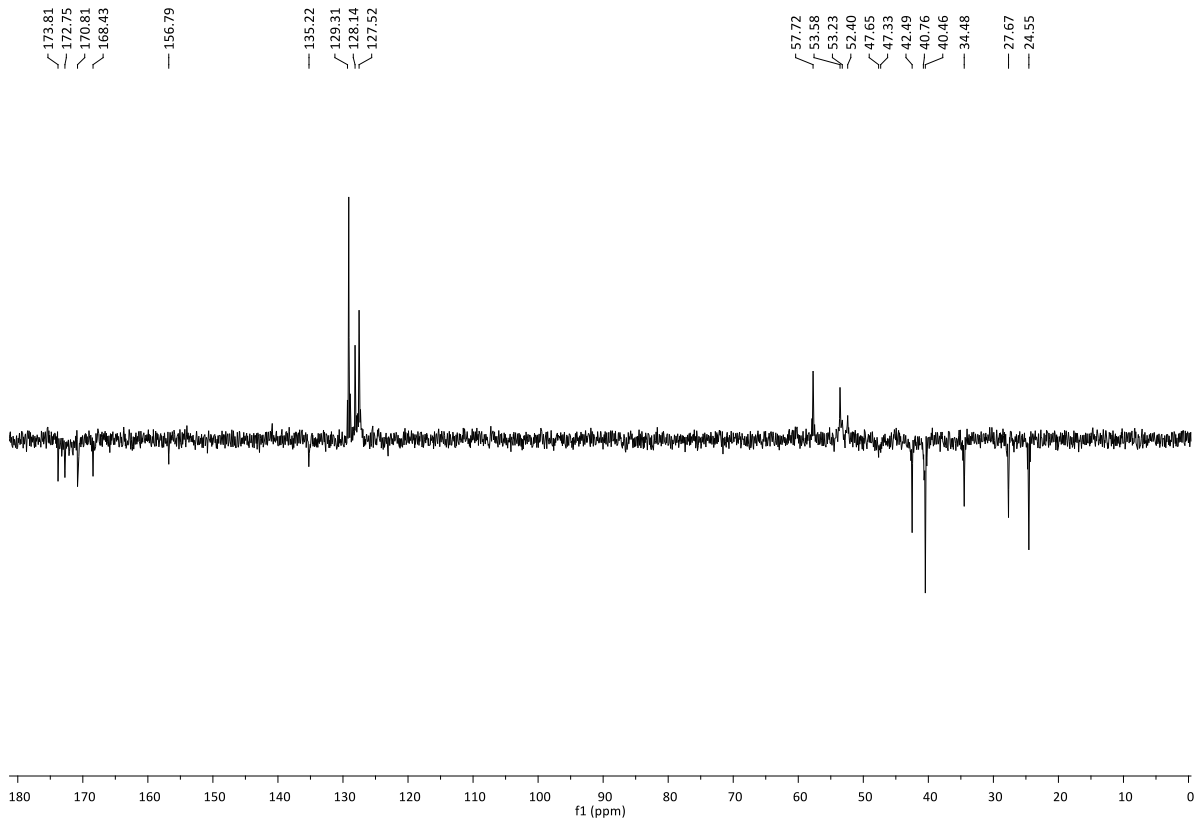

Cyclo[Arg-Gly-Asp-DKP5] 20

^{1}H NMR (400 MHz, H_2O/D_2O 9:1)

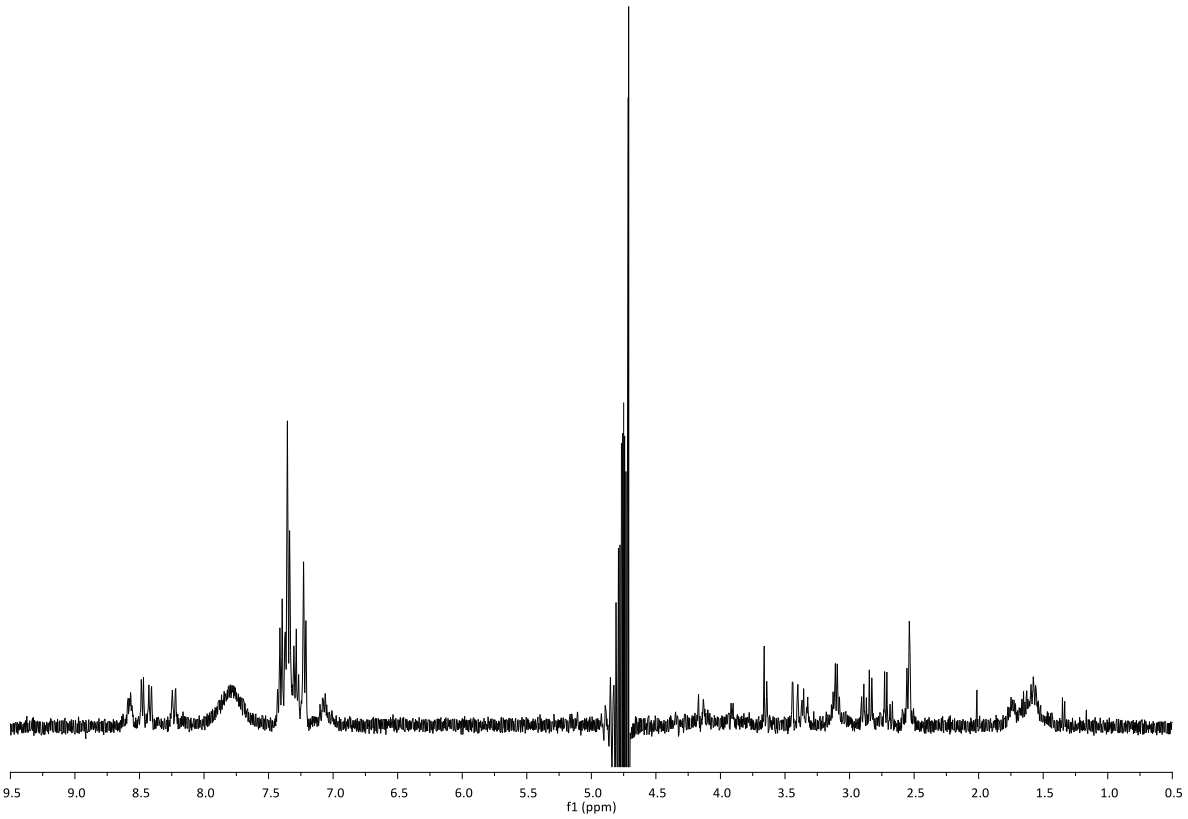

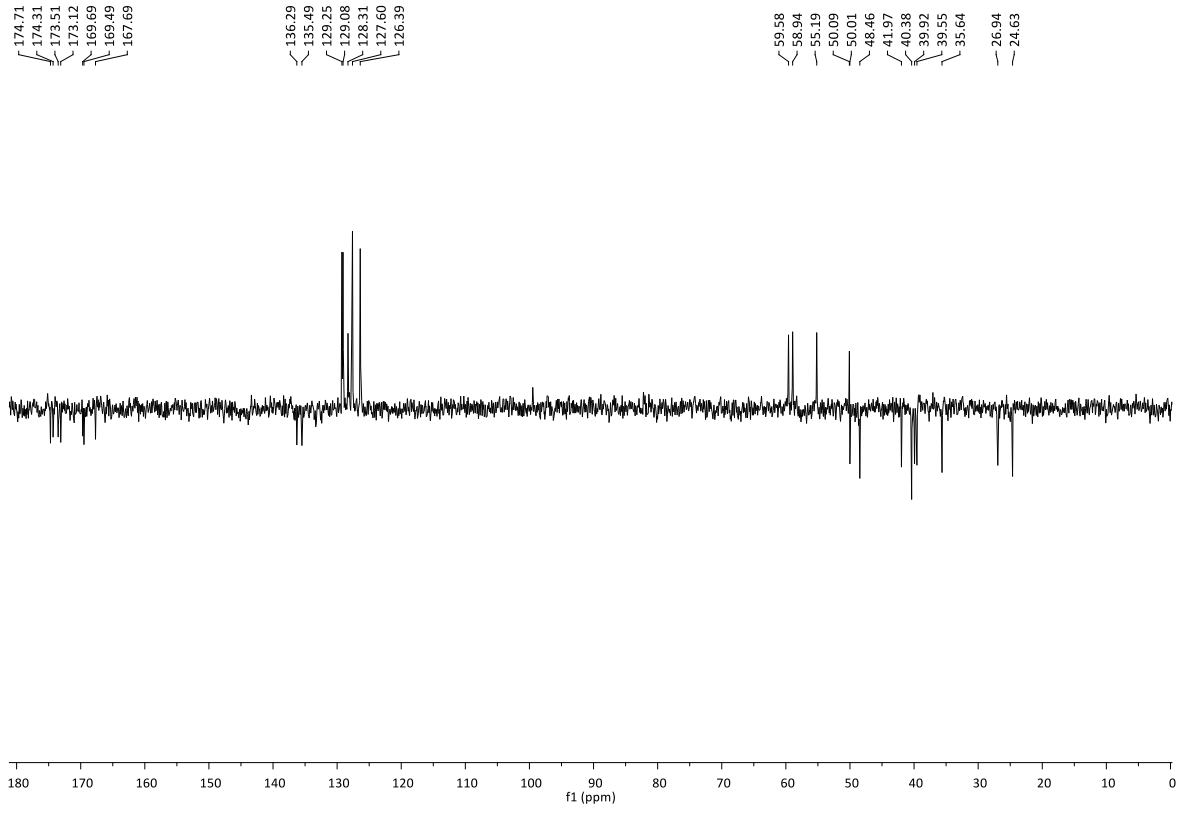

Cyclo[Arg-Gly-Asp-DKP6] 21

^{1}H NMR (400 MHz, H_2O/D_2O 9:1)

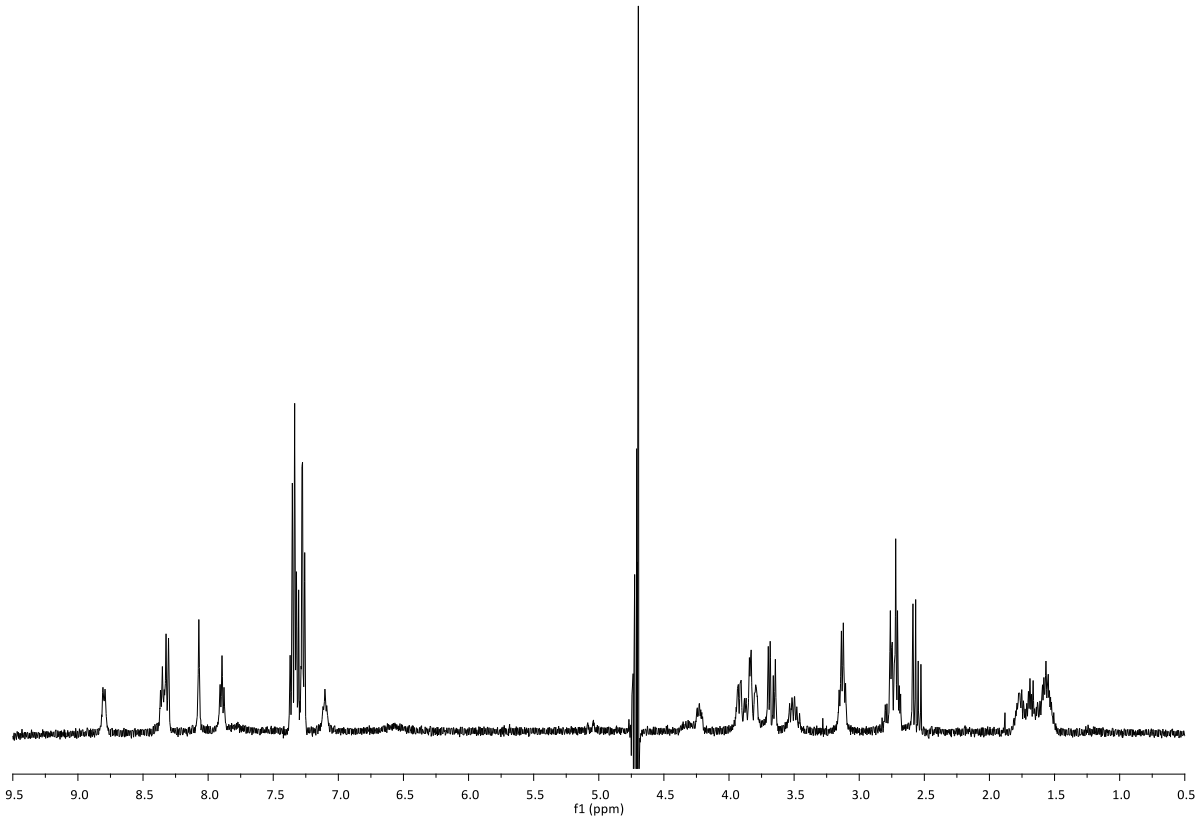

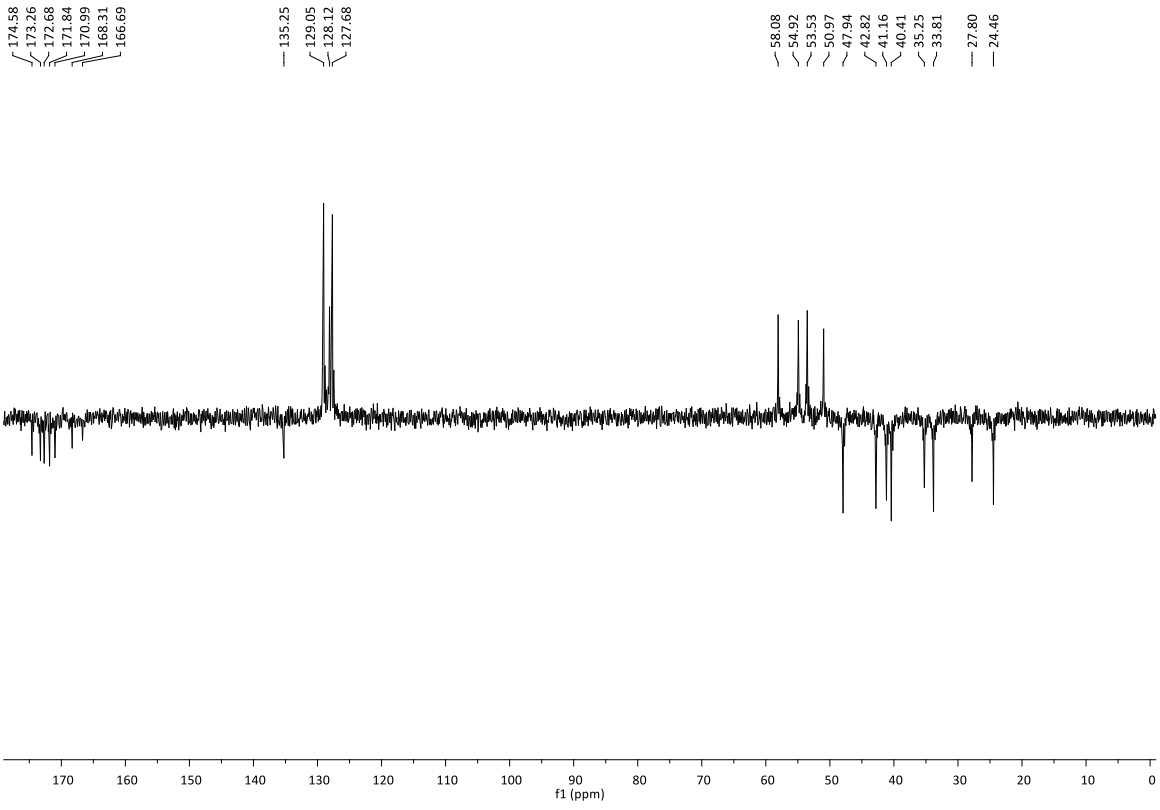

Cyclo[Arg-Gly-Asp-DKP7-A] 22A

^{1}H NMR (400 MHz, H_2O/D_2O 9:1)

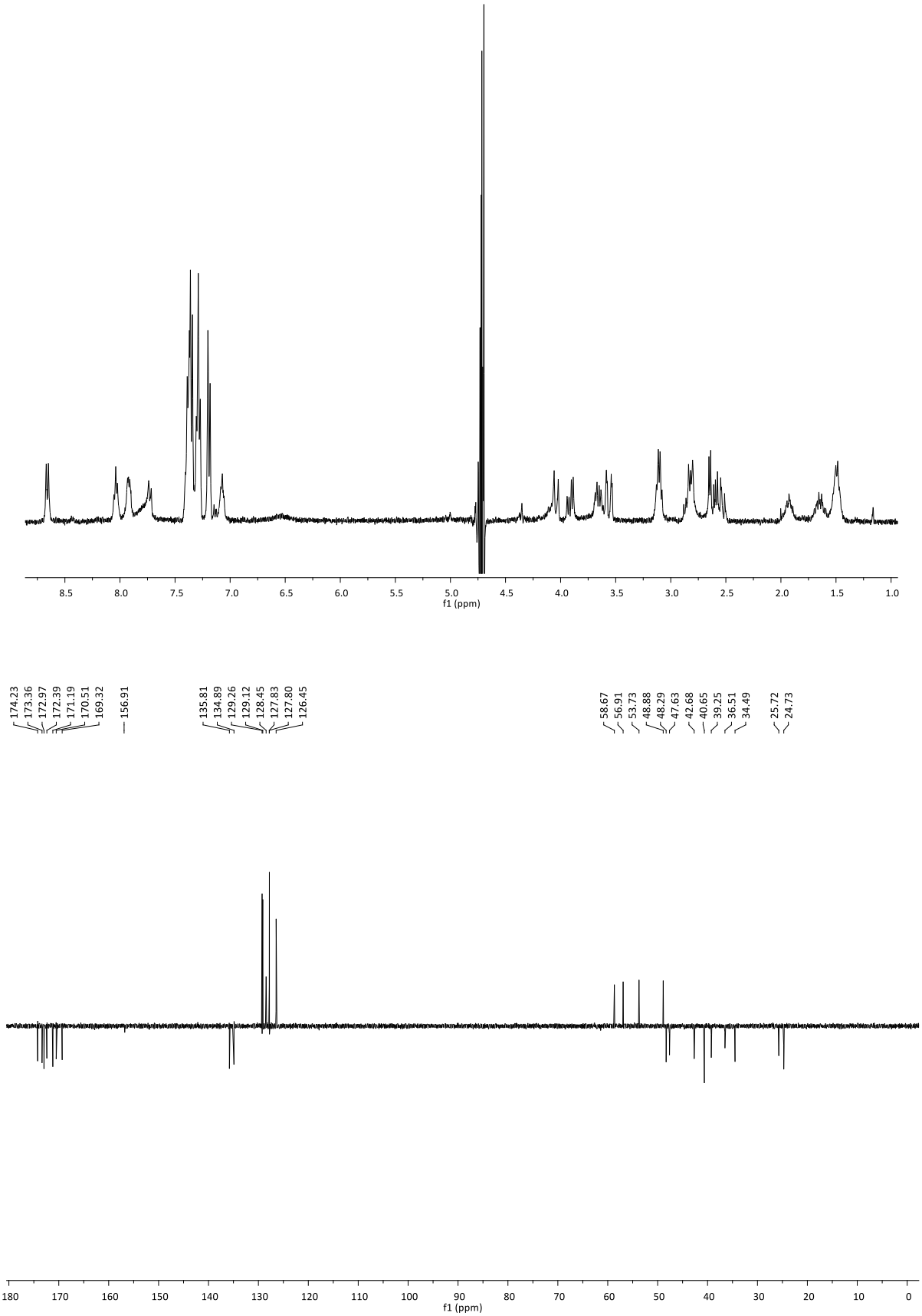

Cyclo[Arg-Gly-Asp-DKP7-B] 22B

^{1}H NMR (400 MHz, H_2O/D_2O 9:1)

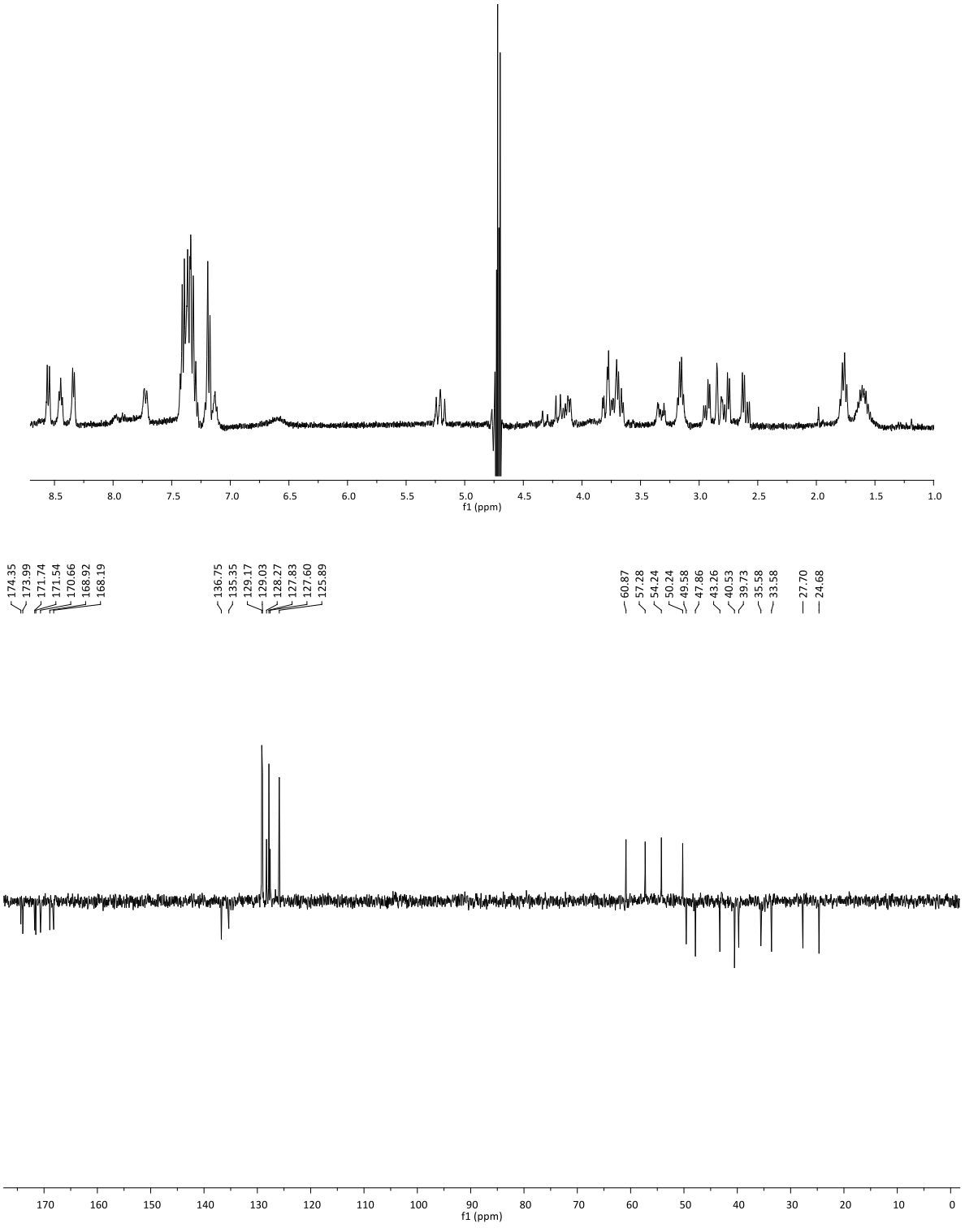

Cyclo[Arg-Gly-Asp-DKP8] 23

^{1}H NMR (400 MHz, D_2O):

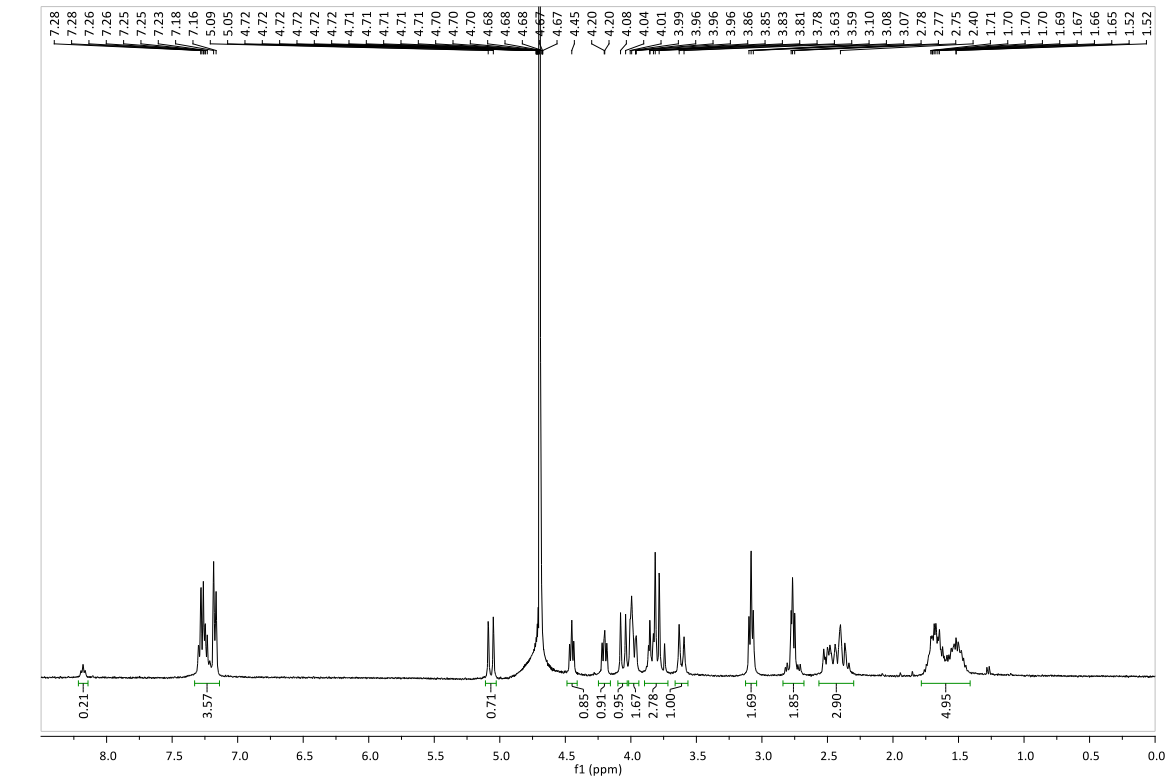

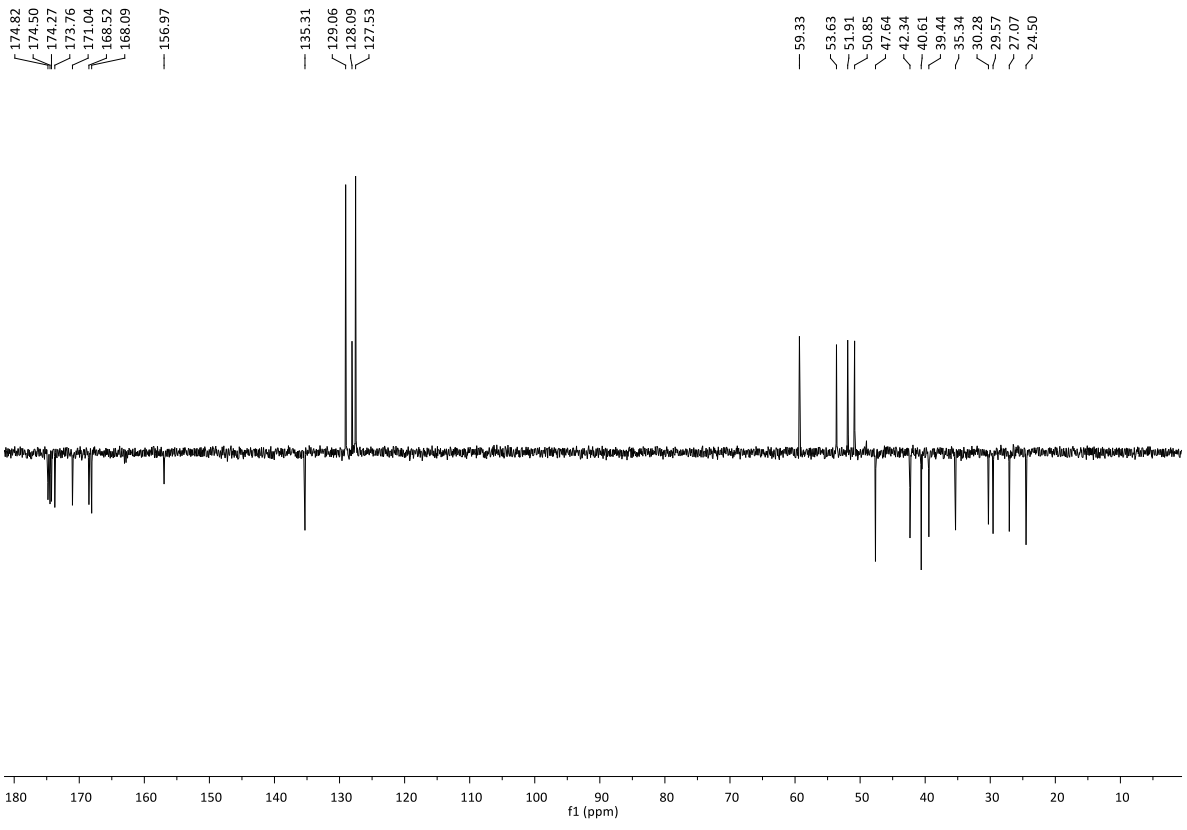

4-((4-methoxy-2,3,6-trimethylphenylsulfonyl)aminomethyl)benzylic alcohol

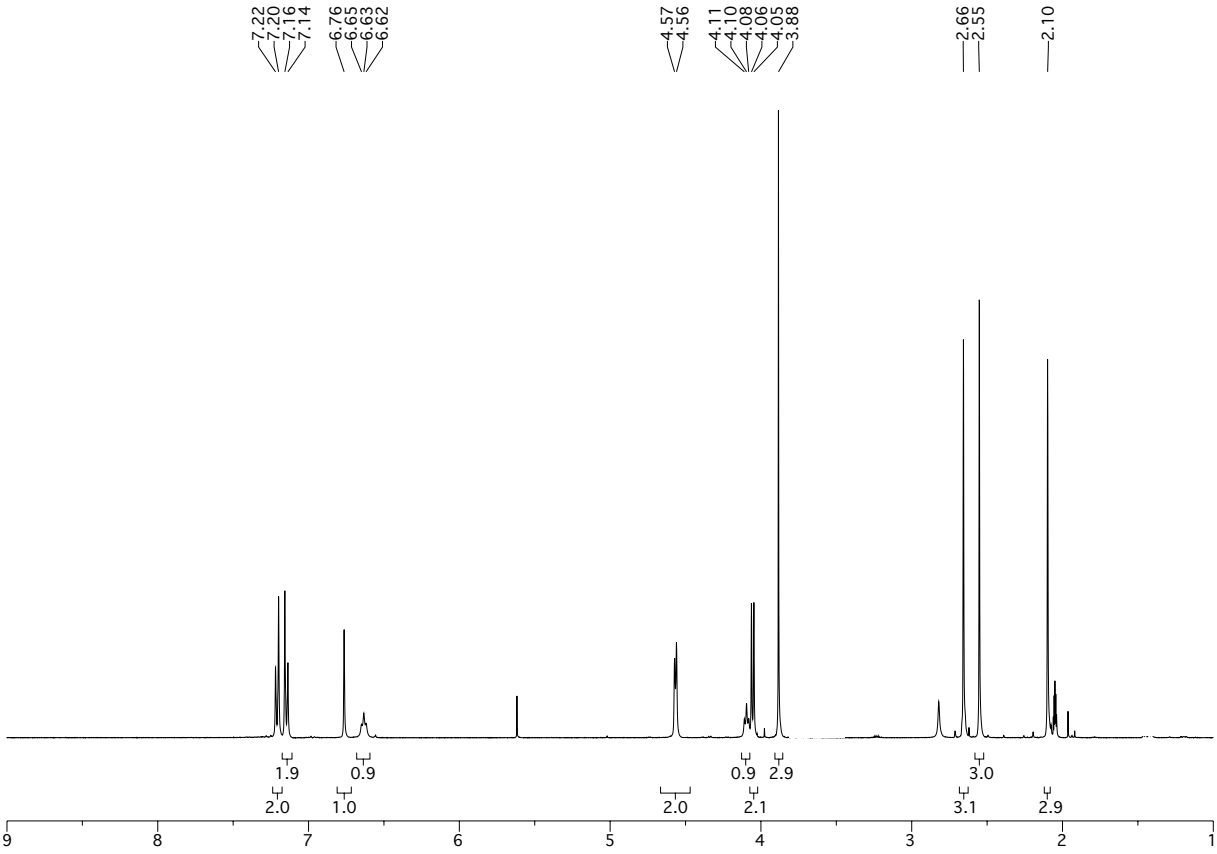

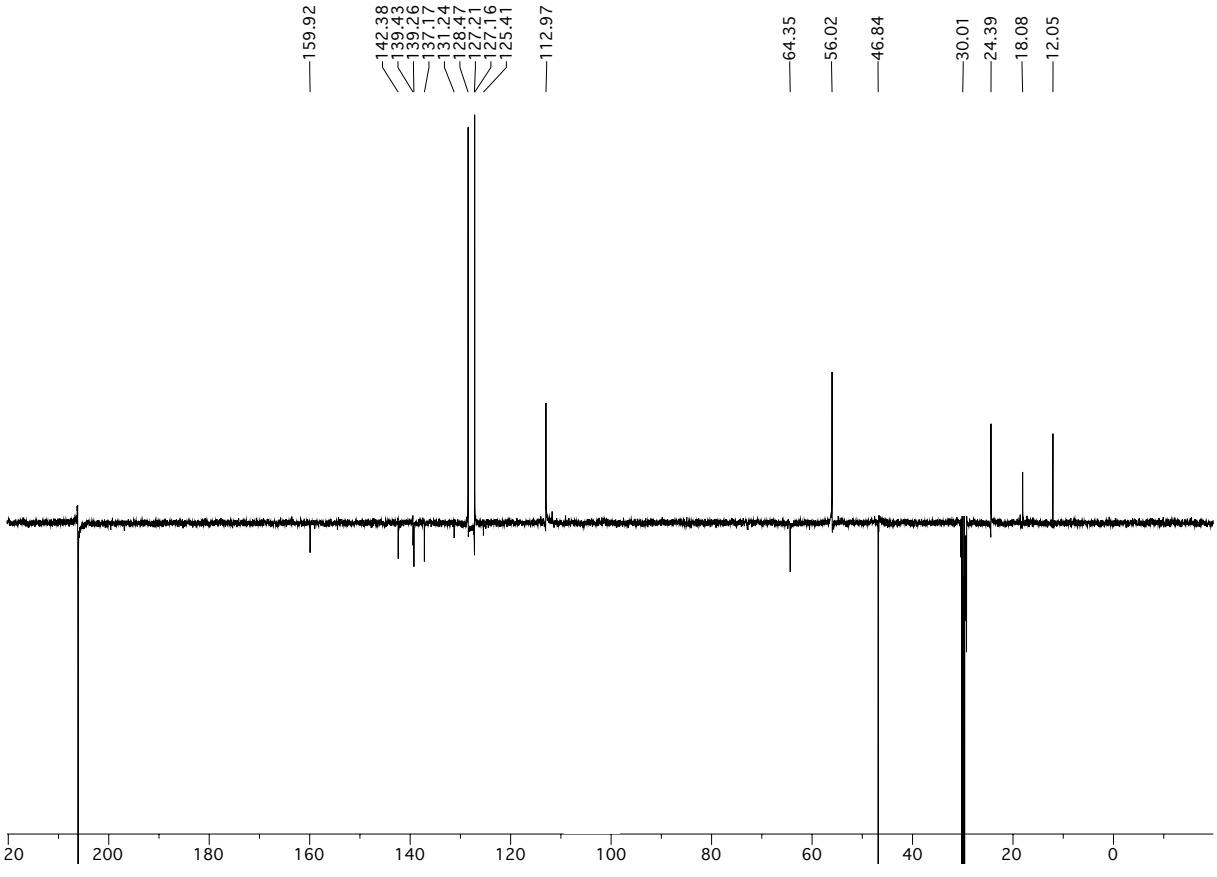

Compound **94**

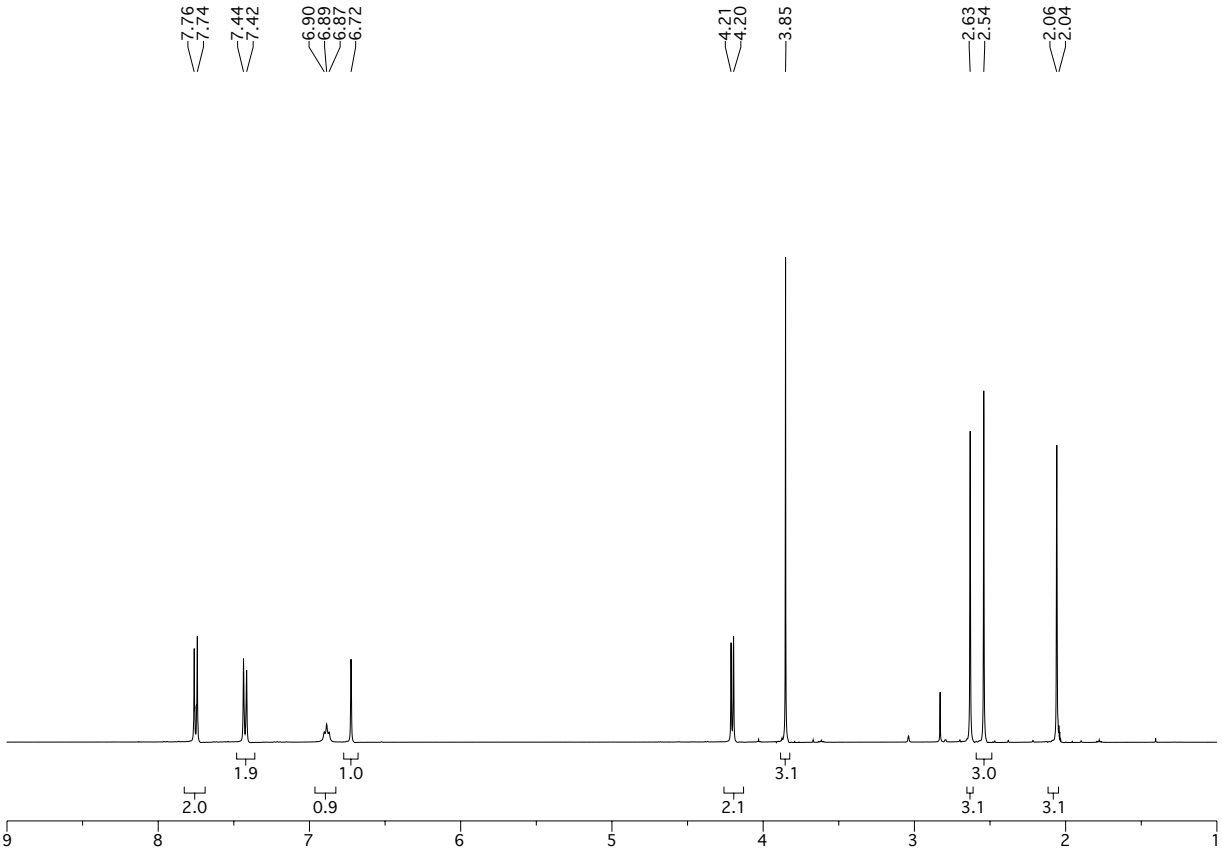
7.76
7.74
7.44
7.42
6.90
6.89
6.87
6.72
4.21
4.20
3.85
2.63
2.54
2.06
2.04
1.9
1.0
3.1
3.0
2.0
0.9
2.1
3.1
3.1
9
8
7
6
5
4
3
2
1

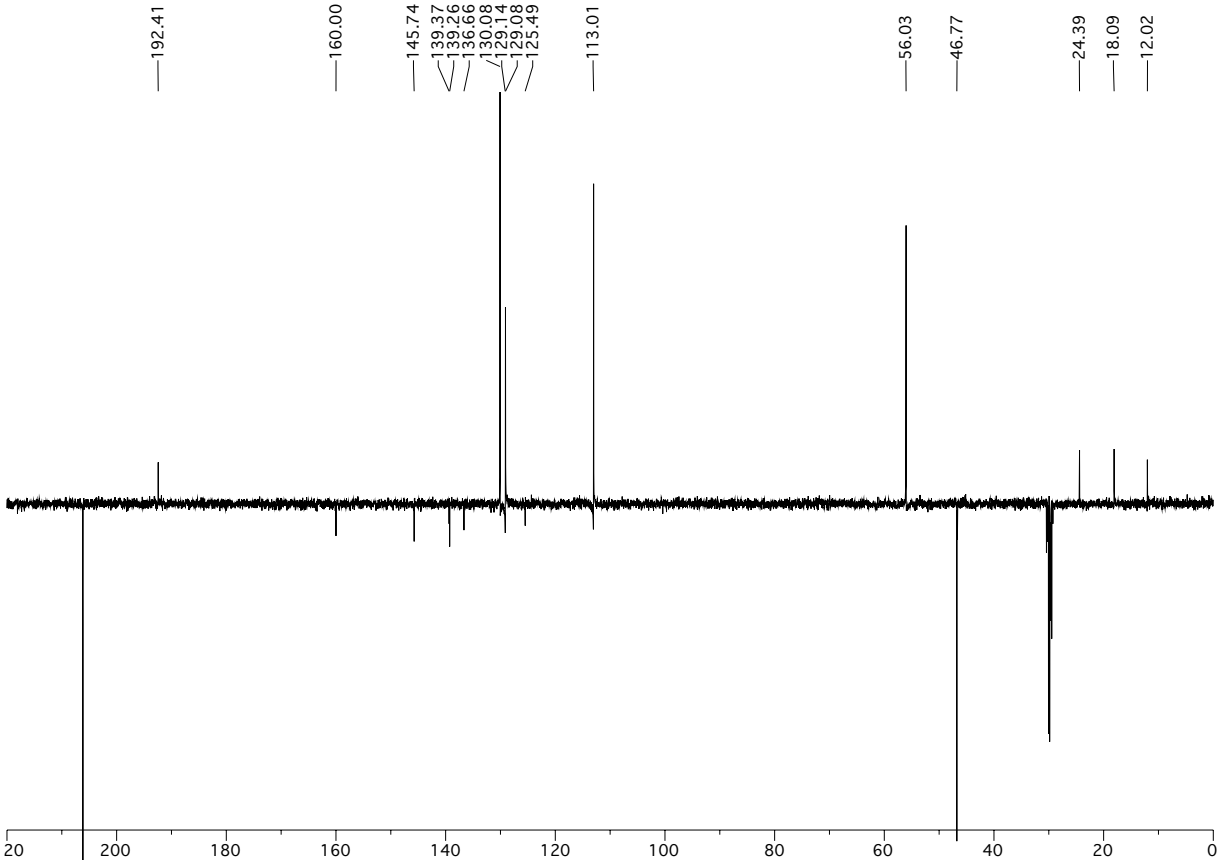
192.41
160.00
145.74
139.37
139.26
136.66
130.08
129.14
129.08
125.49
113.01
56.03
46.77
24.39
18.09
12.02
20
200
180
160
140
120
100
80
60
40
20
0

Enantiomeric compounds (*R*)-**97** and (*S*)-**98**

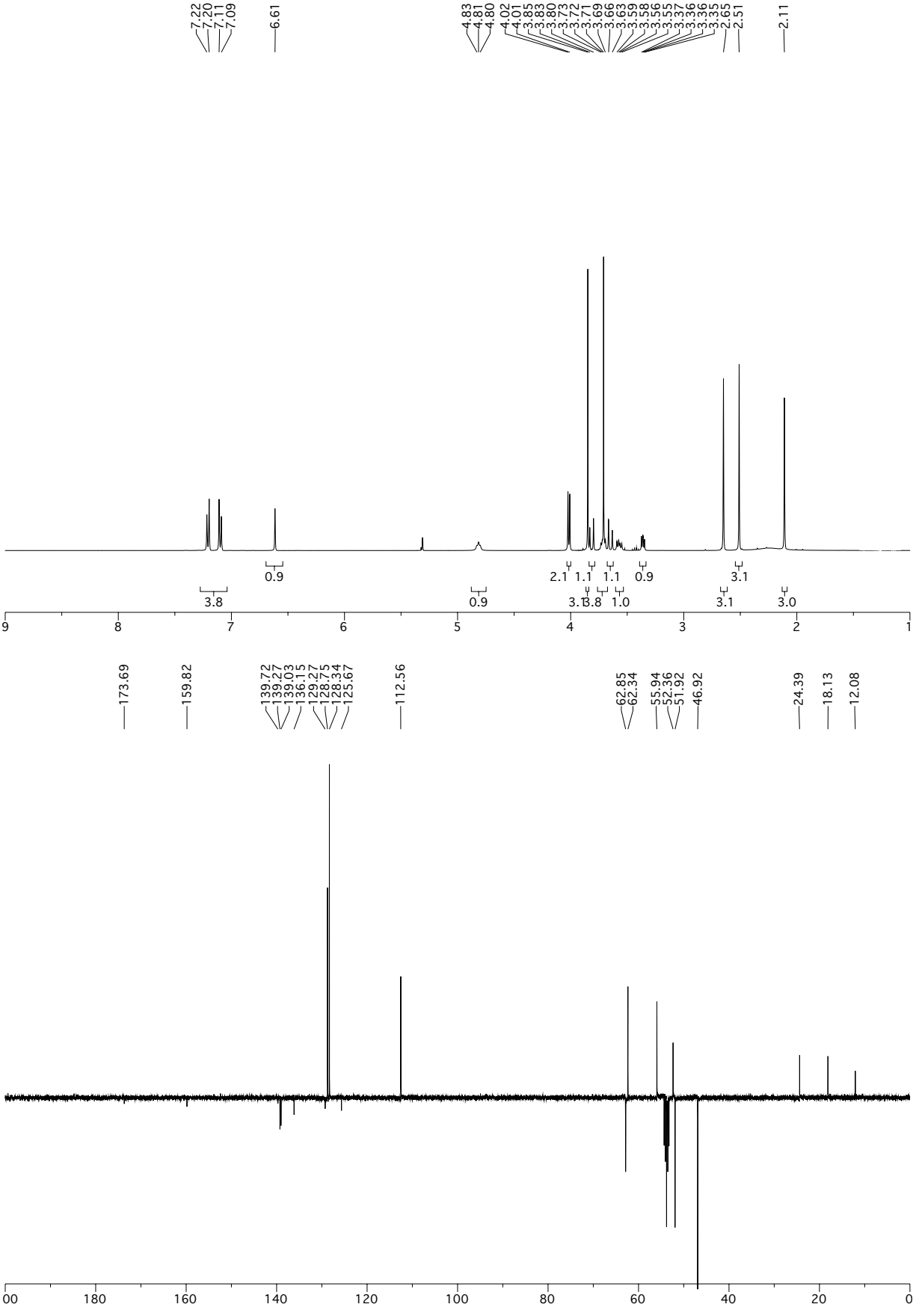

Enantiomeric compounds (*S*,*R*)-**99** and (*R*,*S*)-**100**

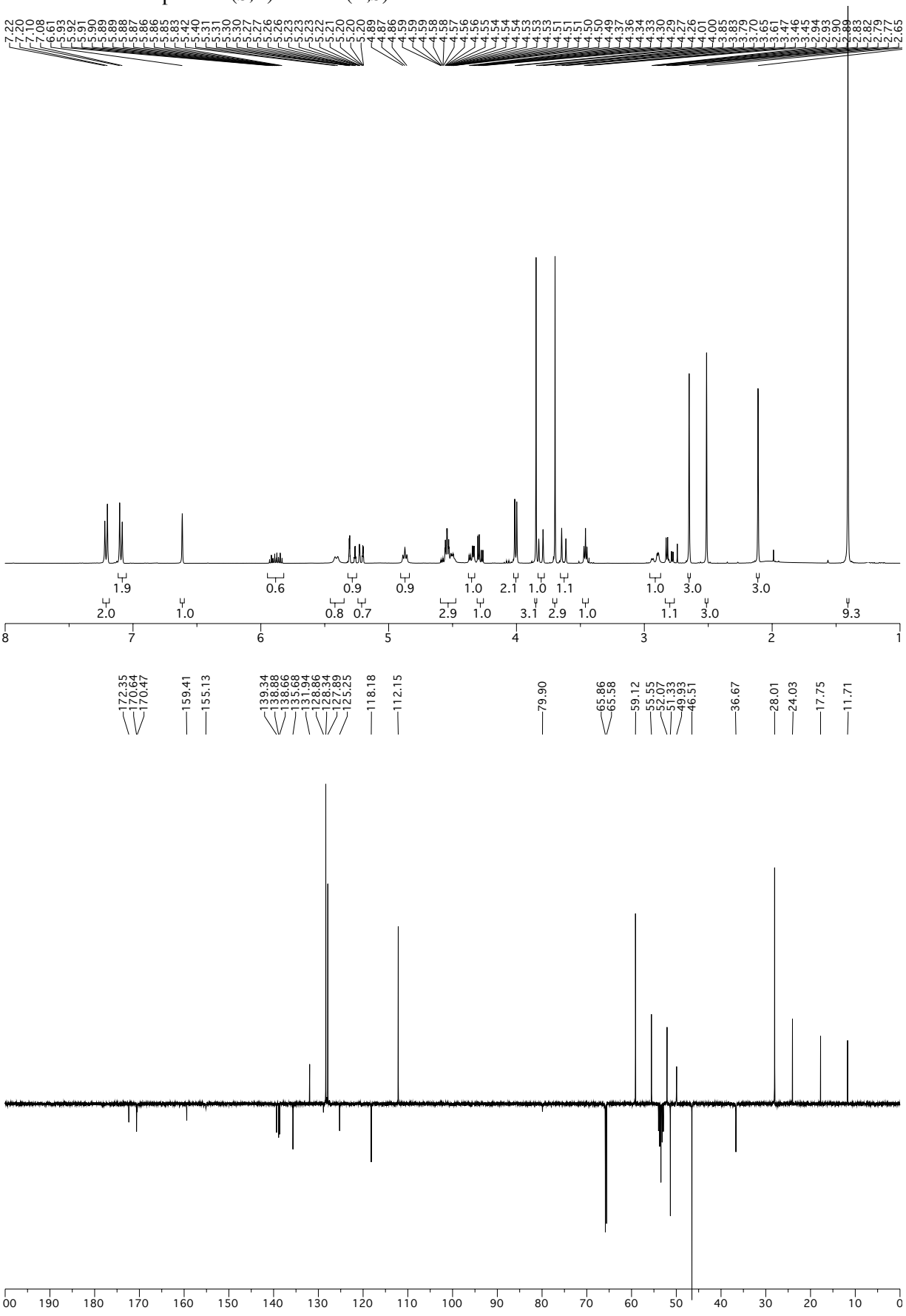

Enantiomeric compounds (3*R*,6*S*)-**101** and (3*S*,6*R*)-**102**

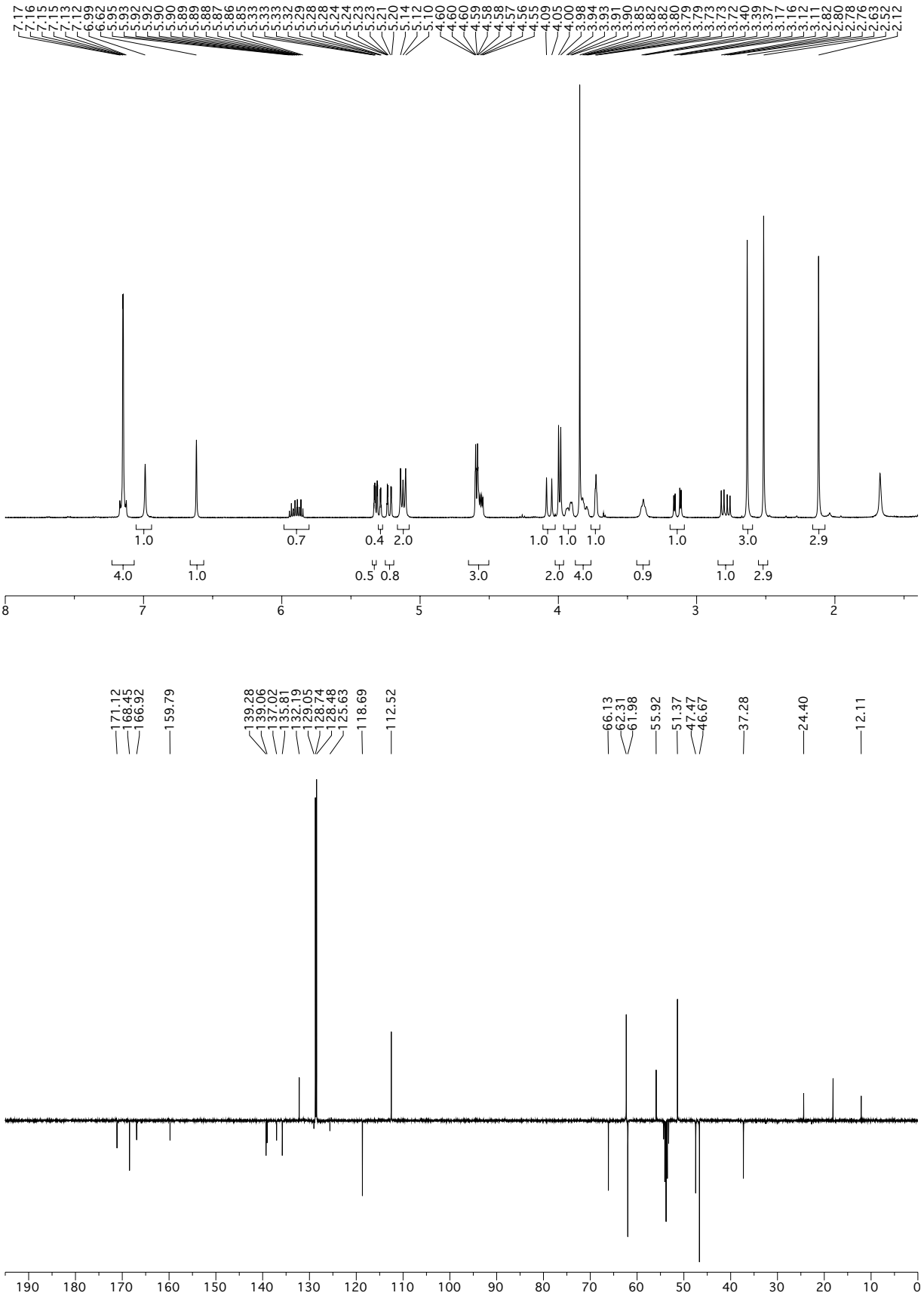

Enantiomeric compounds (3*R*,6*S*)-**103** and (3*S*,6*R*)-**104**

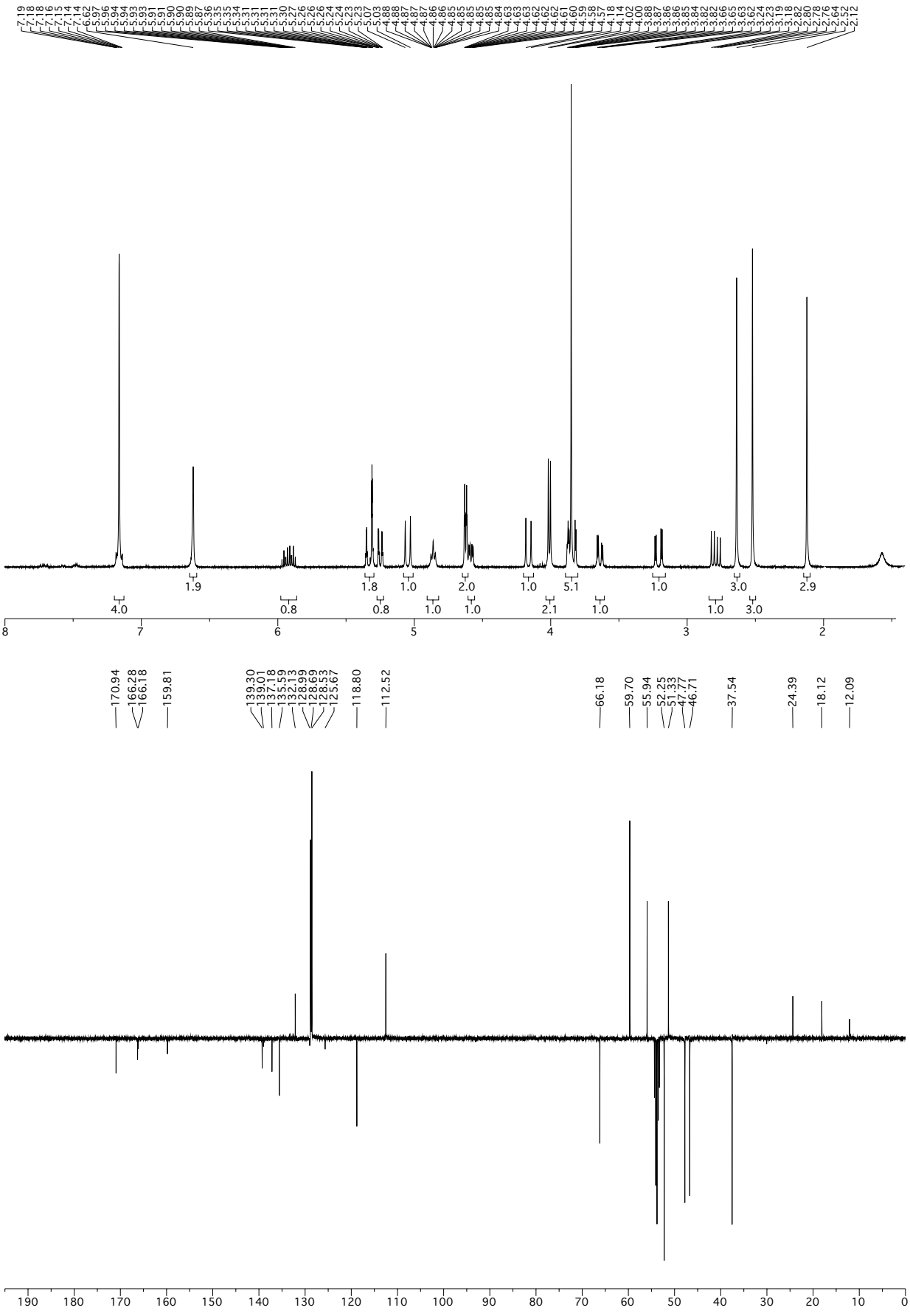

Enantiomeric compounds (3*R*,6*S*)-**105** and (3*S*,6*R*)-**106**

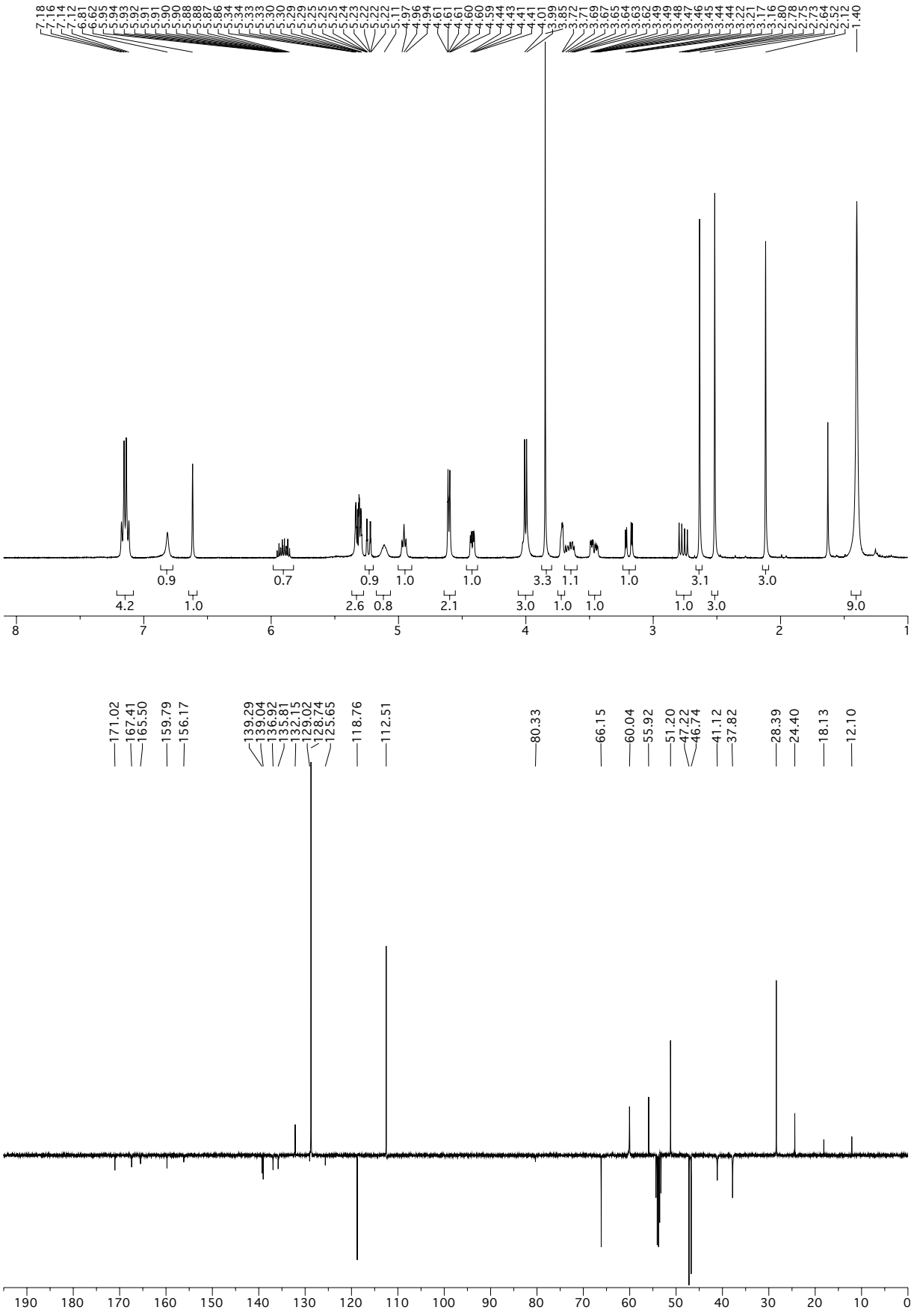

Enantiomeric compounds (*S*)-**109** and (*R*)-**110**

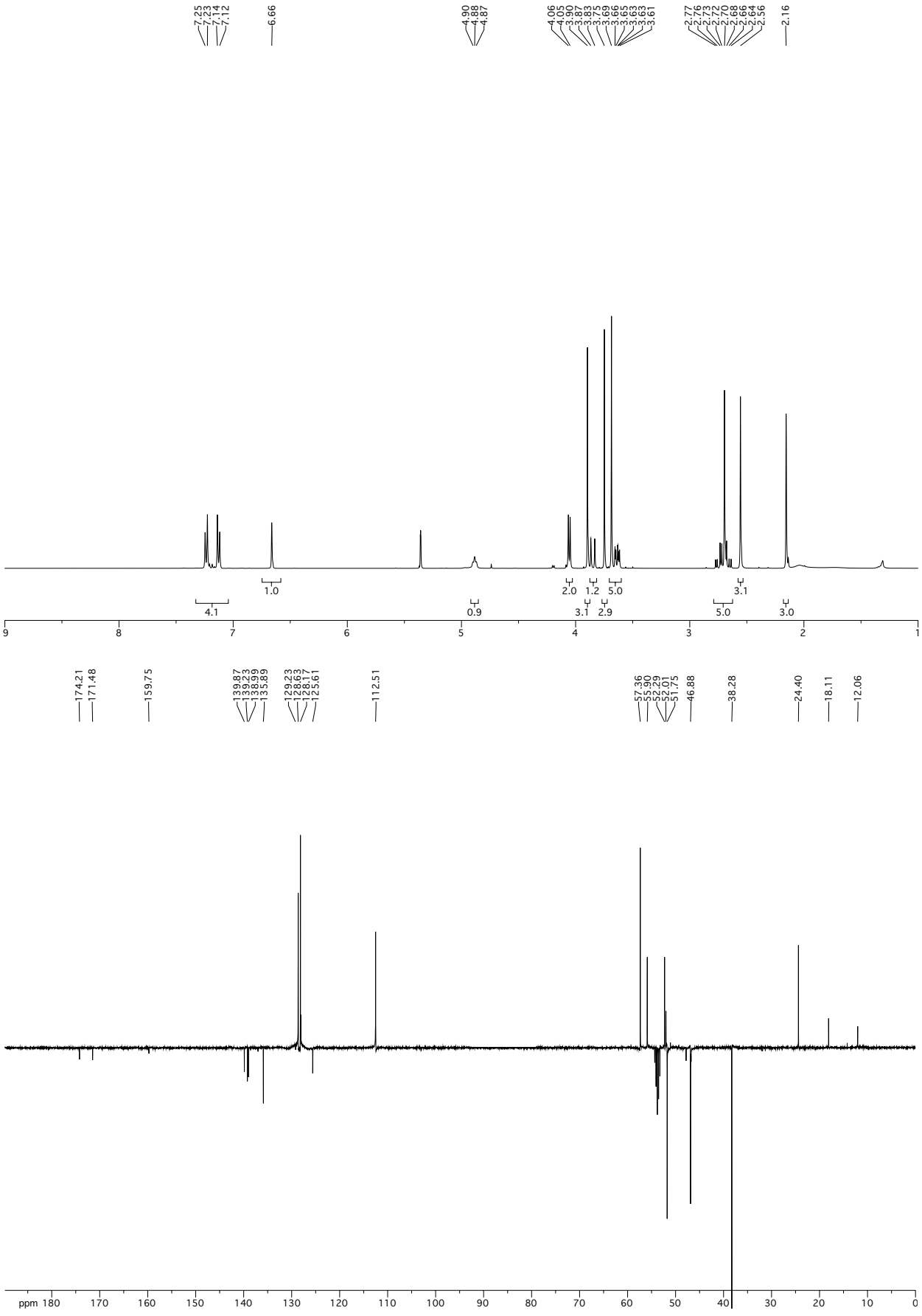

Enantiomeric compounds (*S*,*R*)-**115** and (*R*,*S*)-**116**

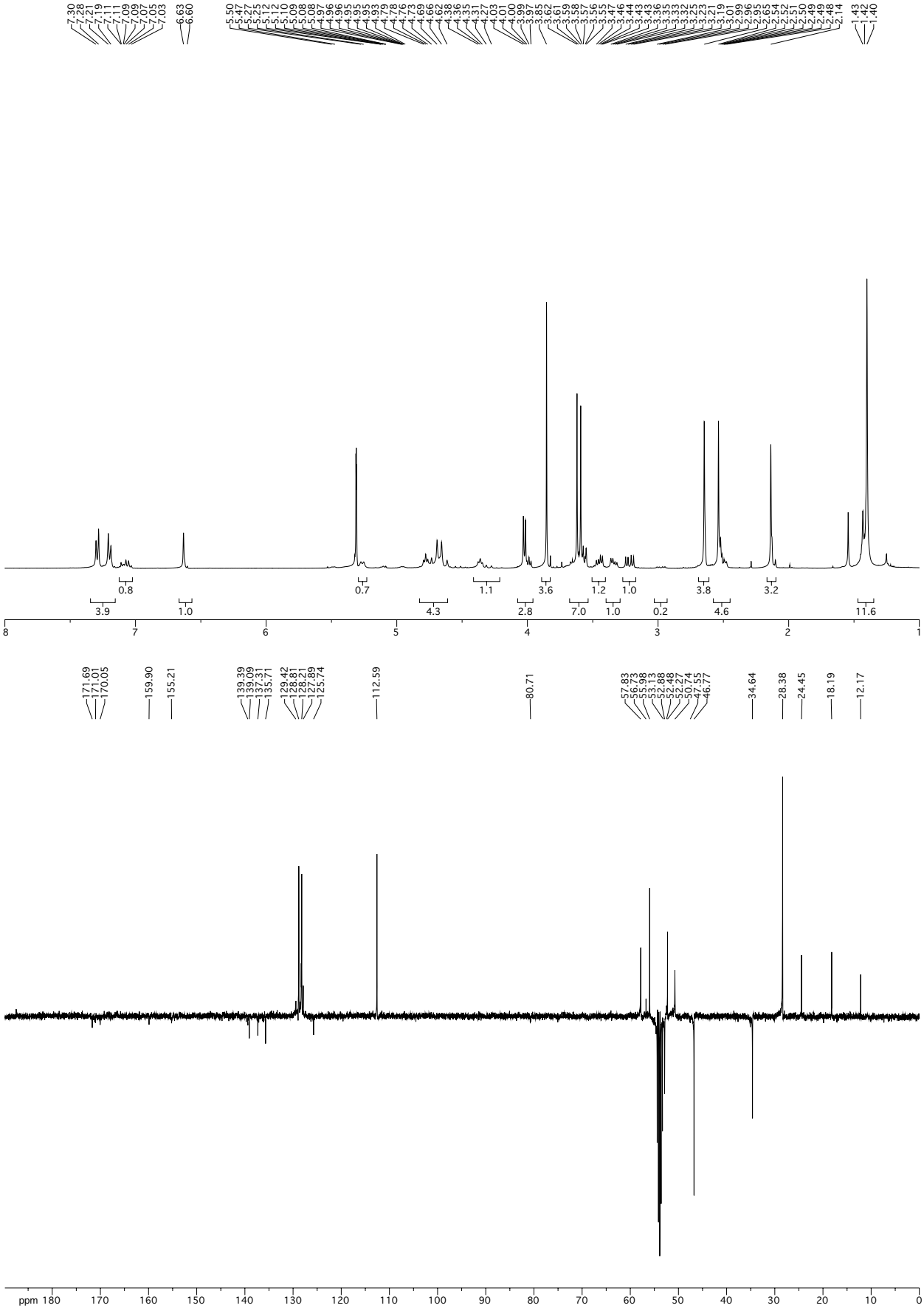

Enantiomeric compounds (3*R*,6*S*)-**117** and (3*S*,6*R*)-**118**

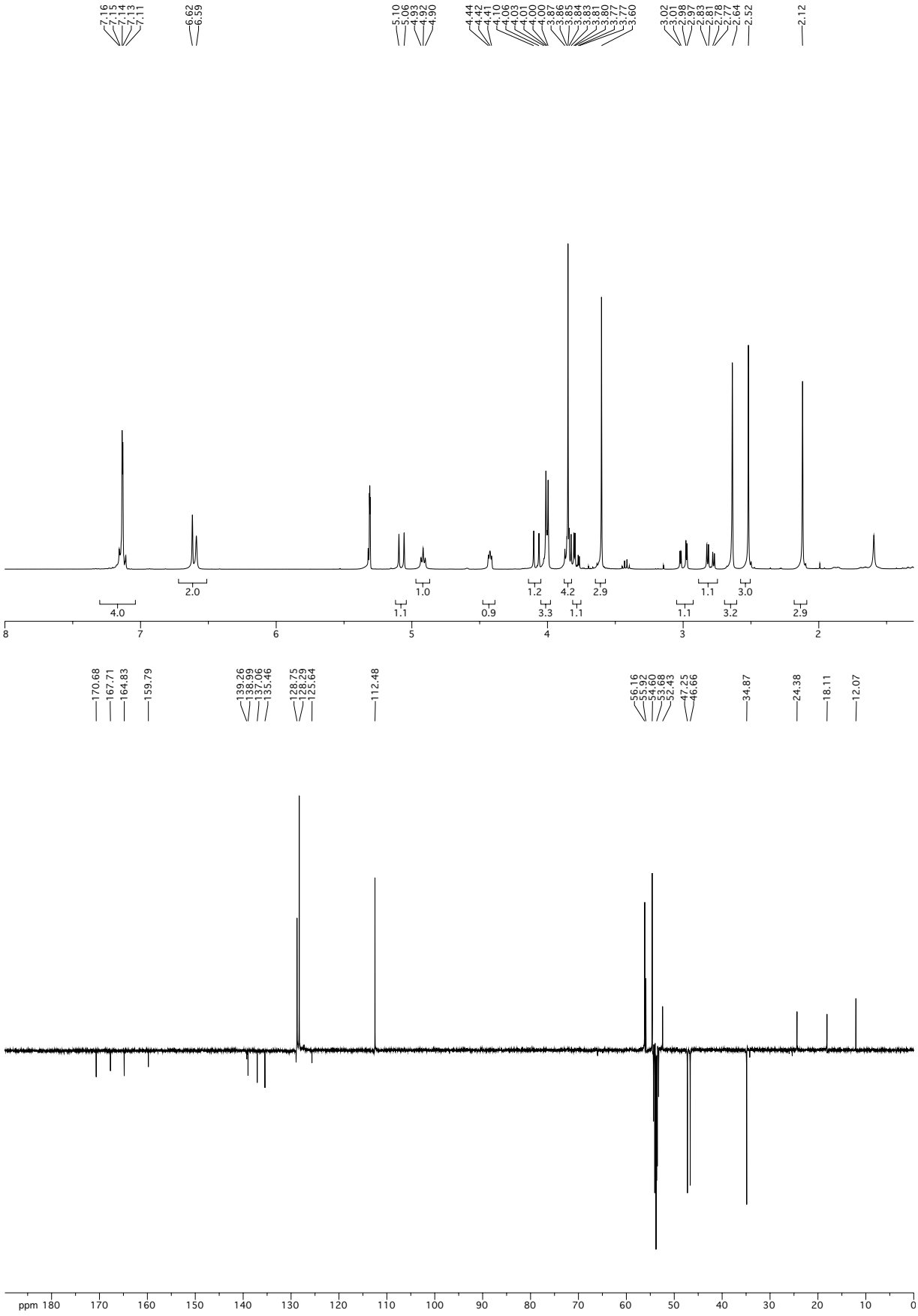

Enantiomeric compounds (3*R*,6*S*)-**119** and (3*S*,6*R*)-**120**

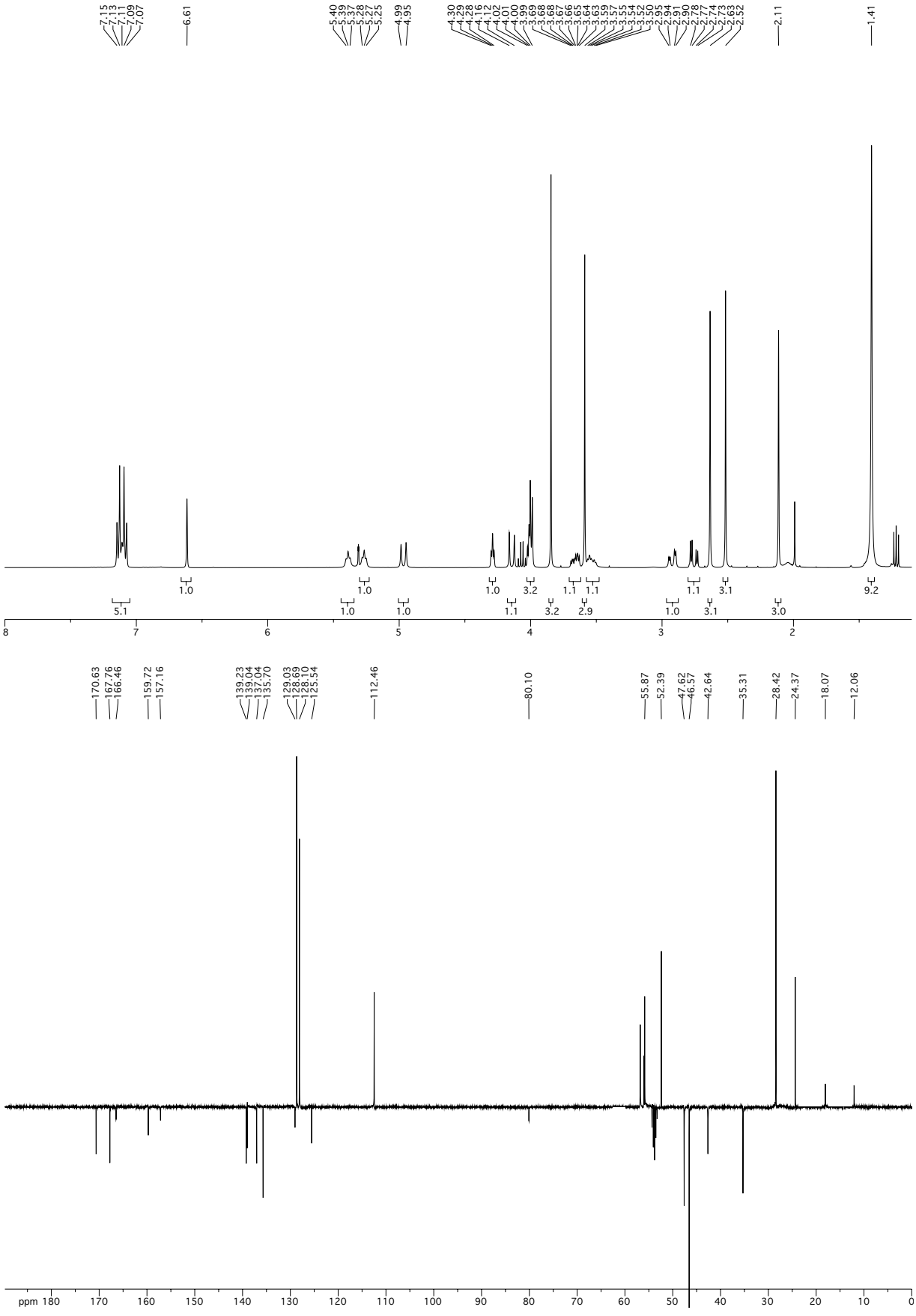

Boc-DKP-*f*2-Arg(Mtr)-Gly-OBn 123 [(3*R*, 6*S*), R^1= H, R^2= $CH_2C_6H_4CH_2NHMtr$]

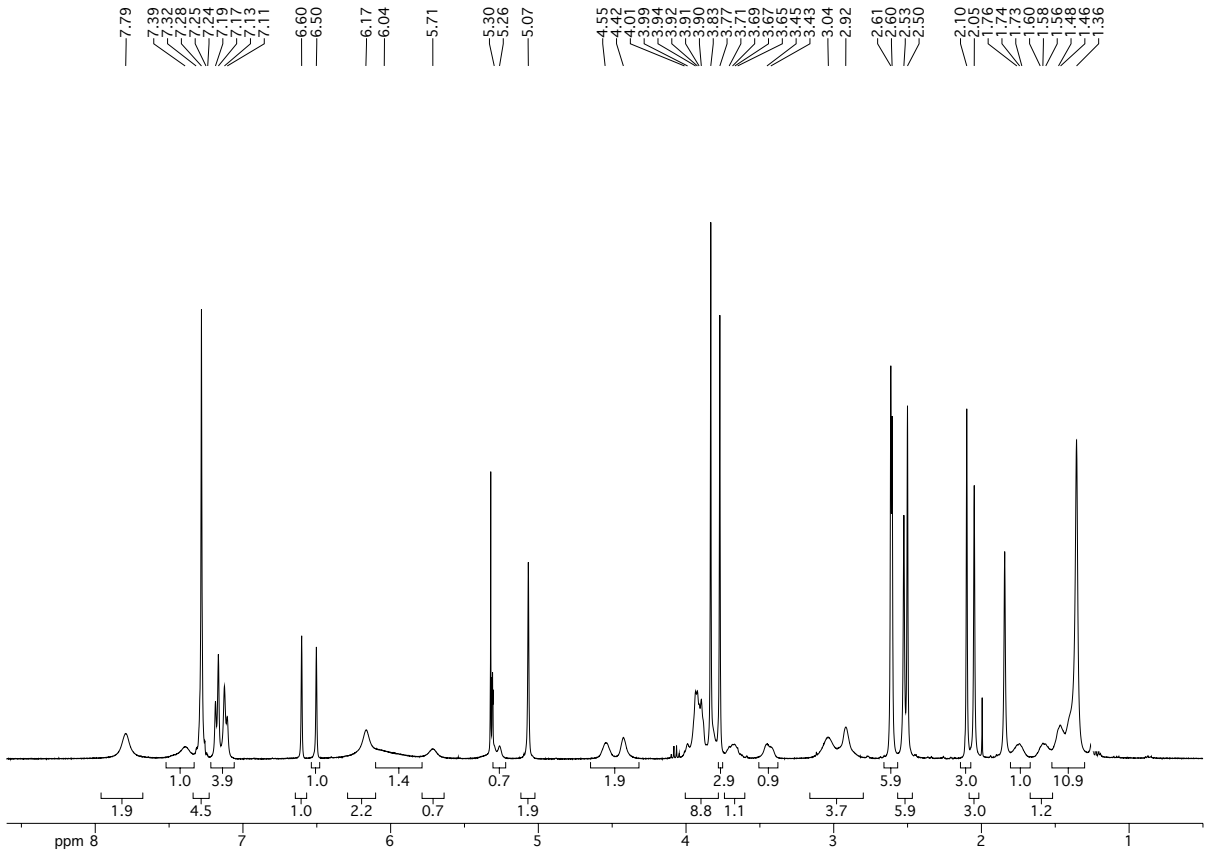

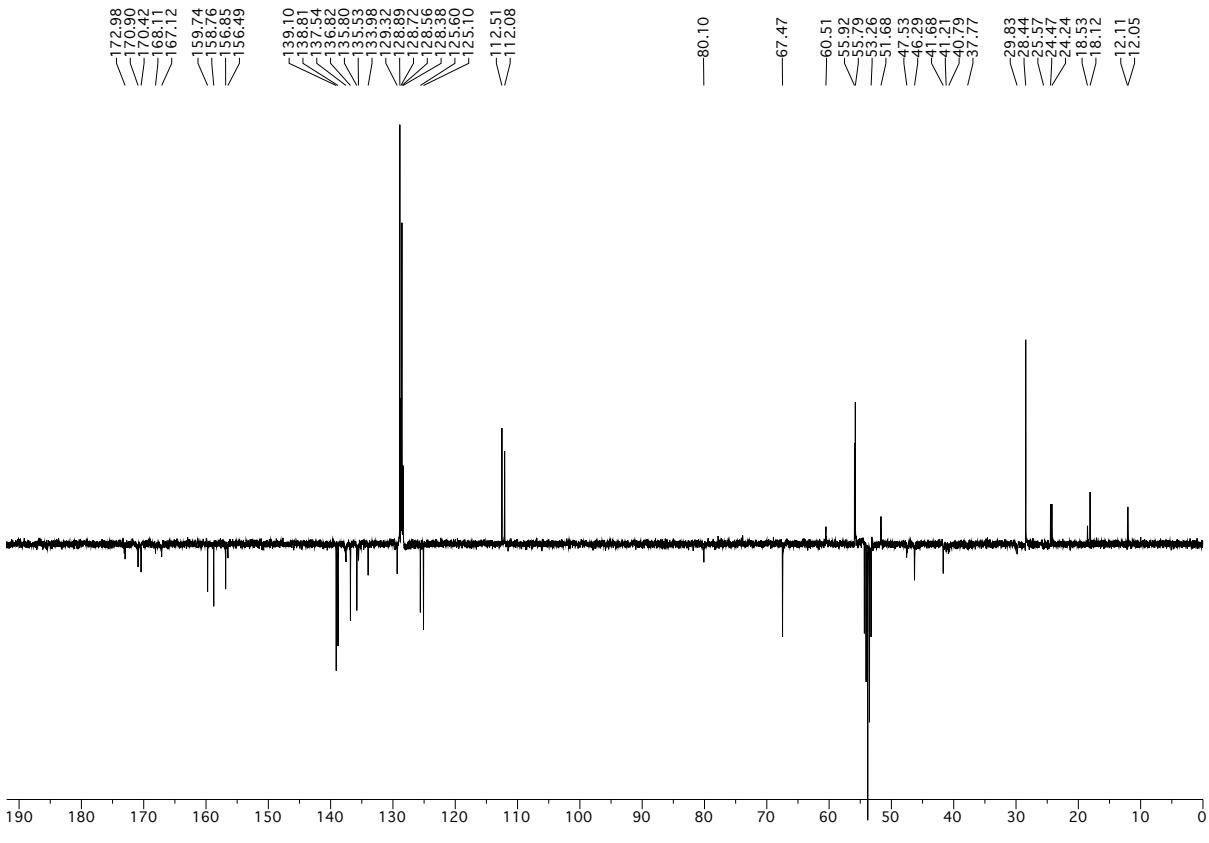

Boc-DKP-*f*3-Arg(Mtr)-Gly-OBn 124 [(3*S*, 6*R*), R^1= H, R^2= $CH_2C_6H_4CH_2NHMtr$]

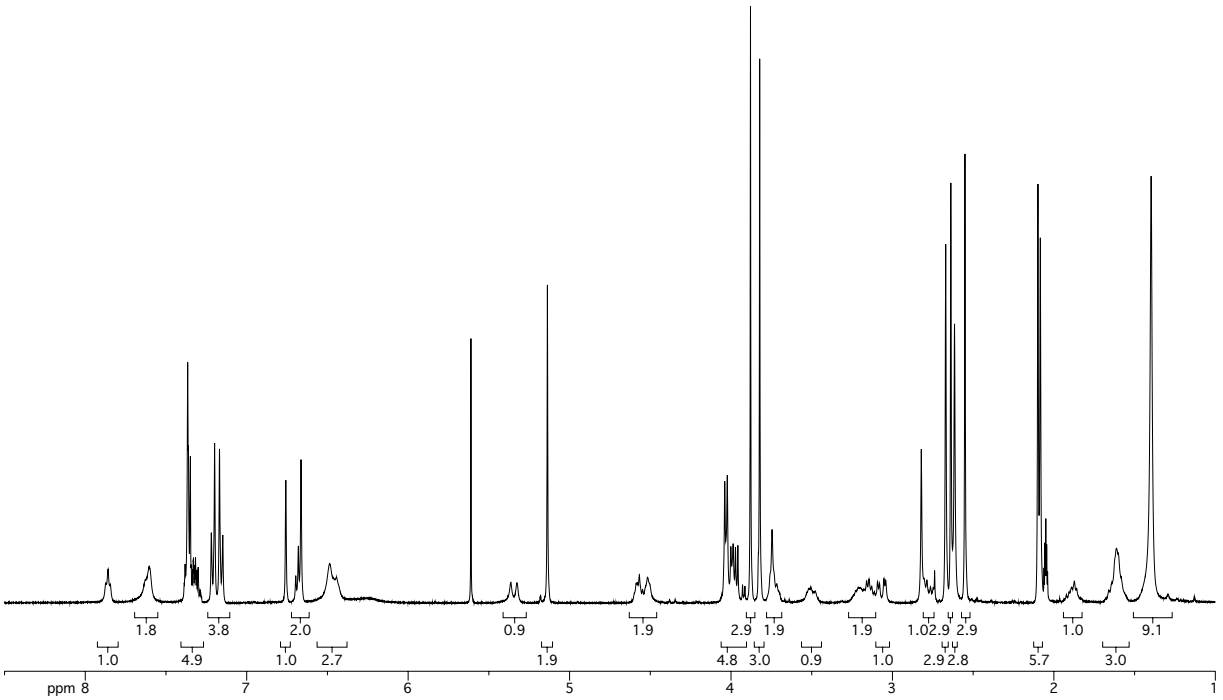

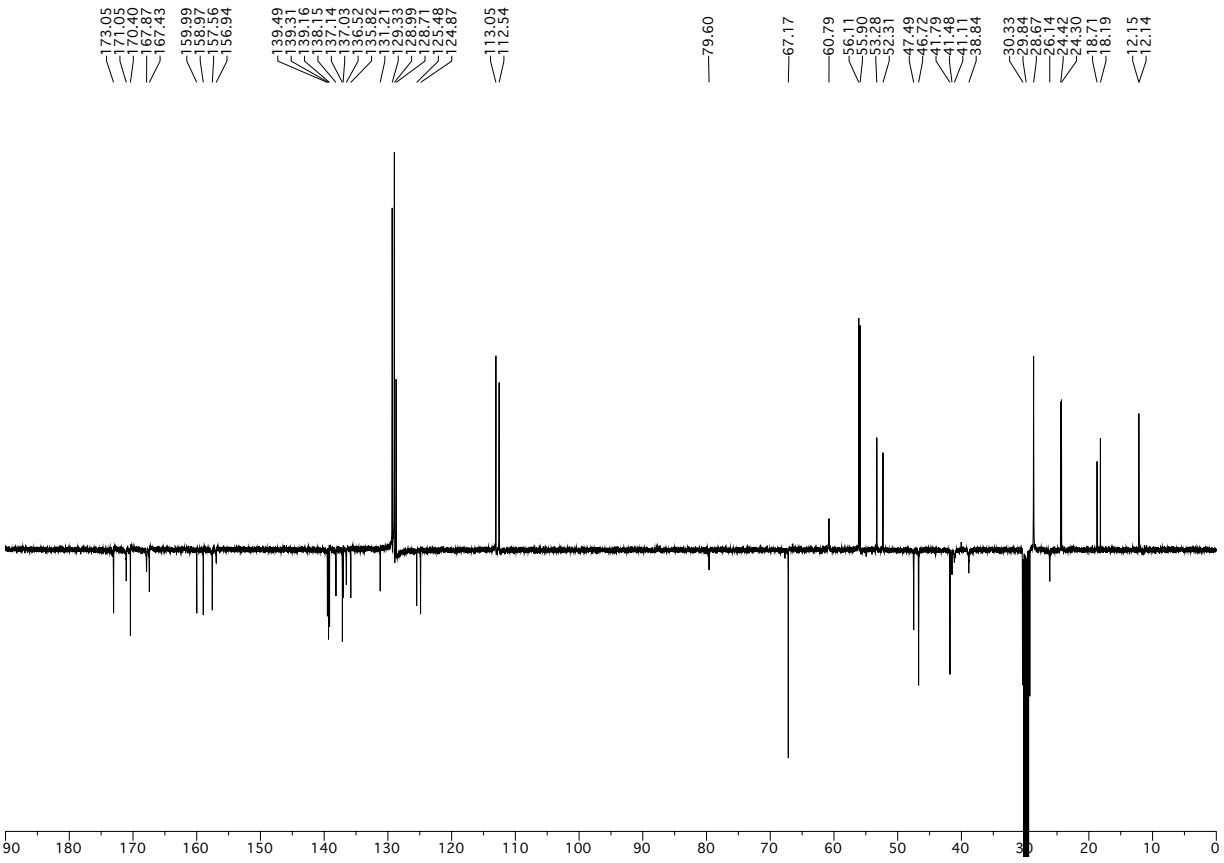

Boc-DKP-*f*4-Arg(Mtr)-Gly-OBn 125 [(3*R*, 6*S*), R^1= $CH_2C_6H_4CH_2NHMtr$, R^2= H]

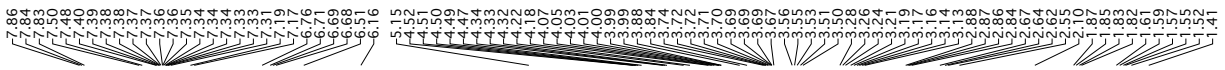

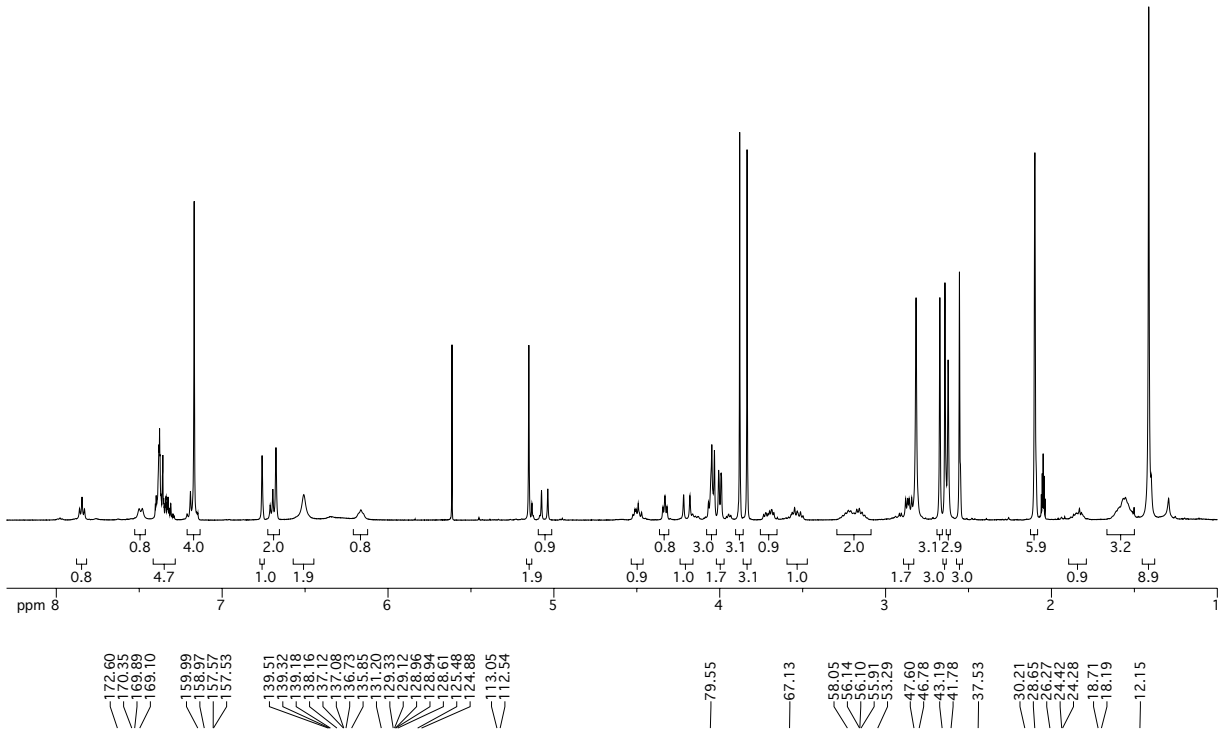

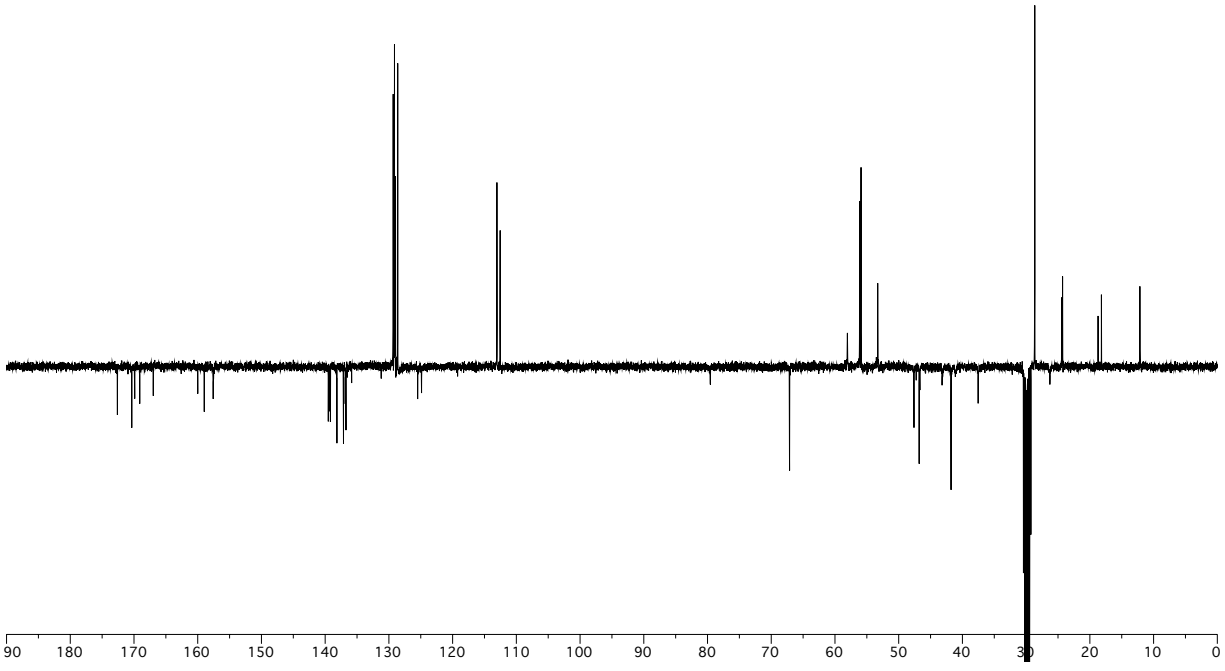

Boc-DKP-*f*6-Arg(Mtr)-Gly-OBn 126 [(3*S*, 6*R*), R^1= $CH_2C_6H_4CH_2NHMtr$, R^2= H]

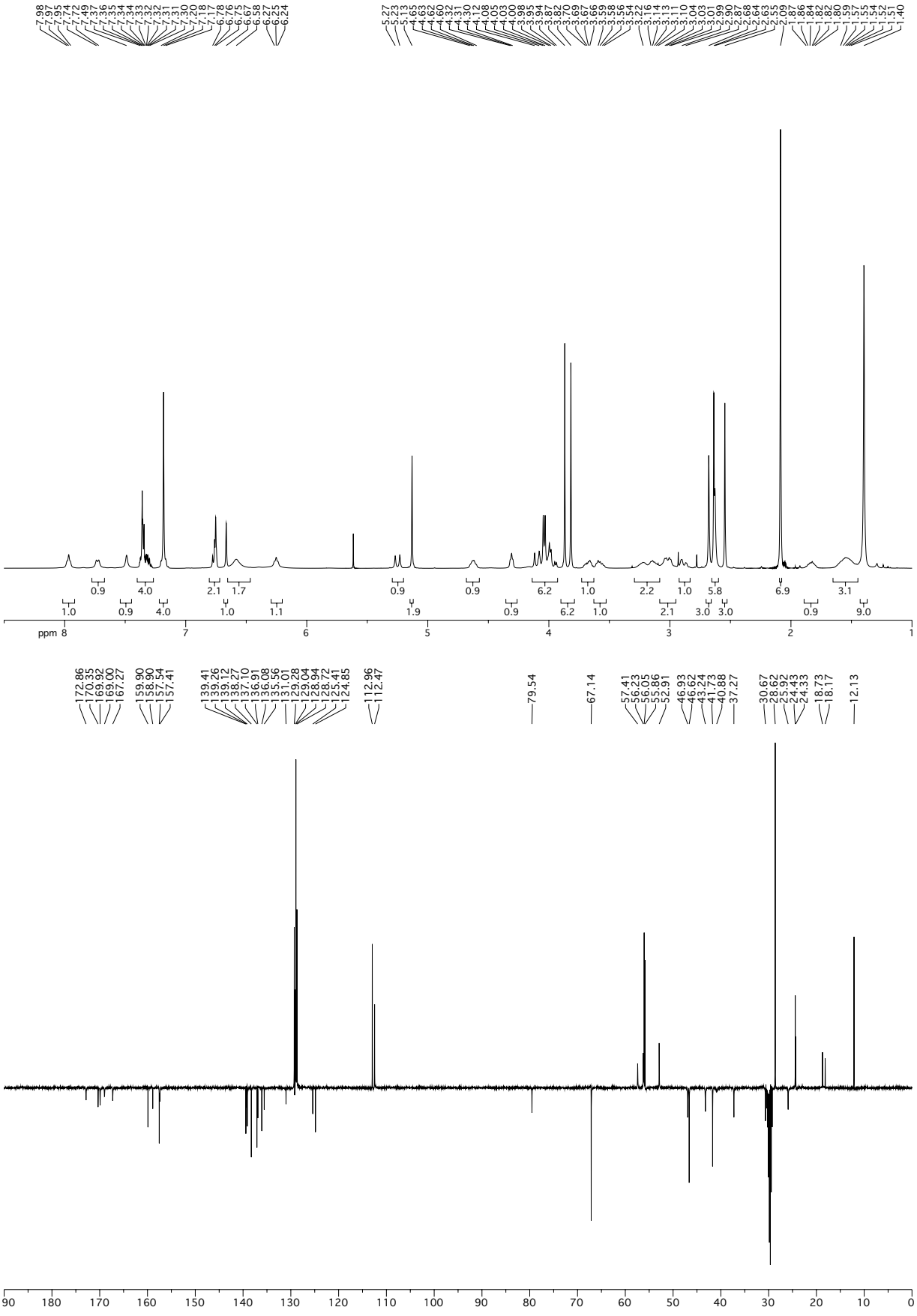

Cbz-Asp(O*t*Bu)-DKP-*f*2-Arg(Mtr)-Gly-OBn 131 [(3*R*, 6*S*), R^1= H, R^2= $CH_2C_6H_4CH_2NHMtr$]

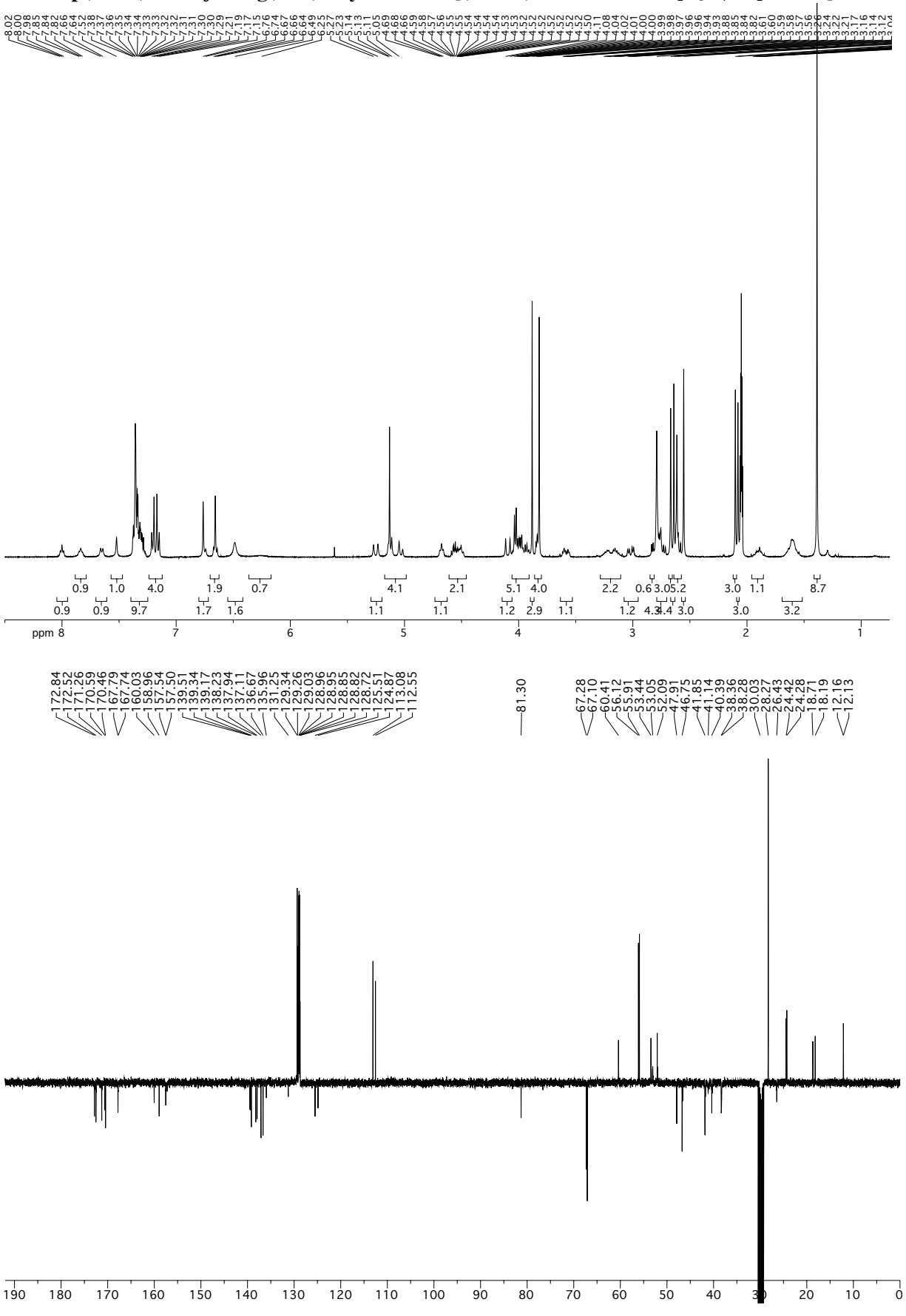

Cbz-Asp(O*t*Bu)-DKP-*f*3-Arg(Mtr)-Gly-OBn 132 [(3*S*, 6*R*), R^1= H, R^2= $CH_2C_6H_4CH_2NHMtr$]

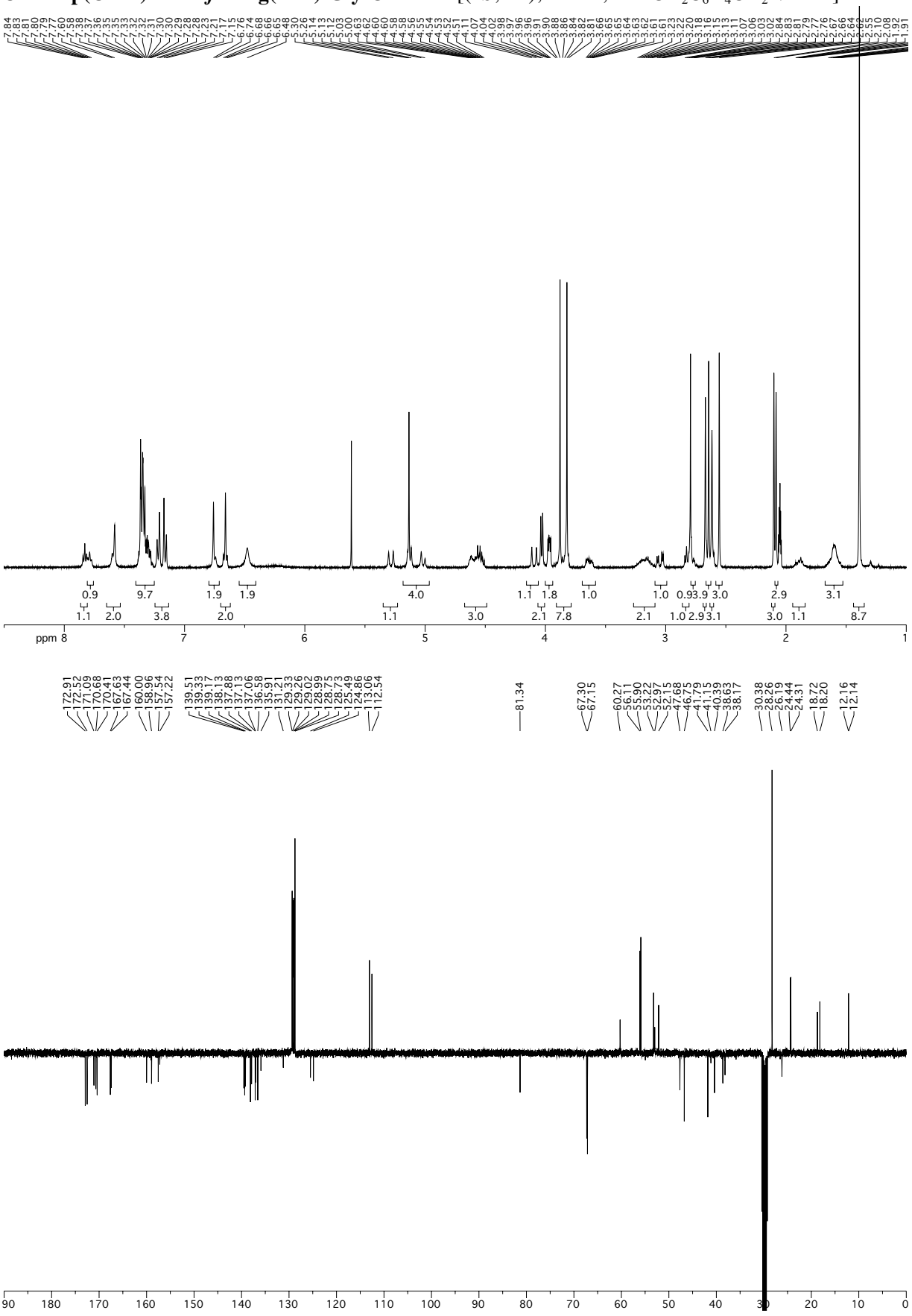

Cbz-Asp(O*t*Bu)-DKP-*f*4-Arg(Mtr)-Gly-OBn 133 [(3*R*, 6*S*), R^1= $CH_2C_6H_4CH_2NHMtr$, R^2= H]

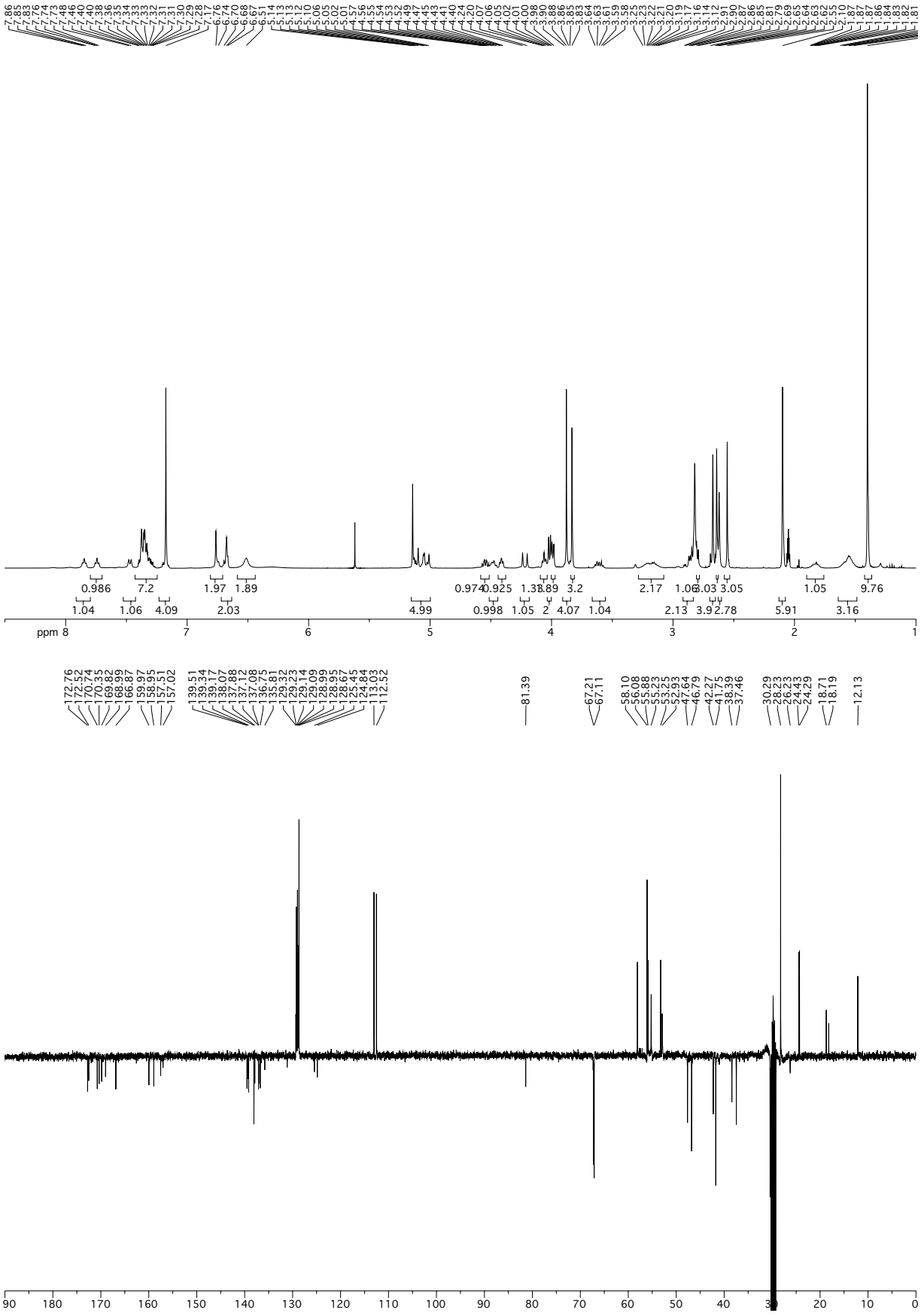

Cbz-Asp(O*t*Bu)-DKP-*f*6-Arg(Mtr)-Gly-OBn 134 [(3*S*, 6*R*), R^1= $CH_2C_6H_4CH_2NHMtr$, R^2= H]

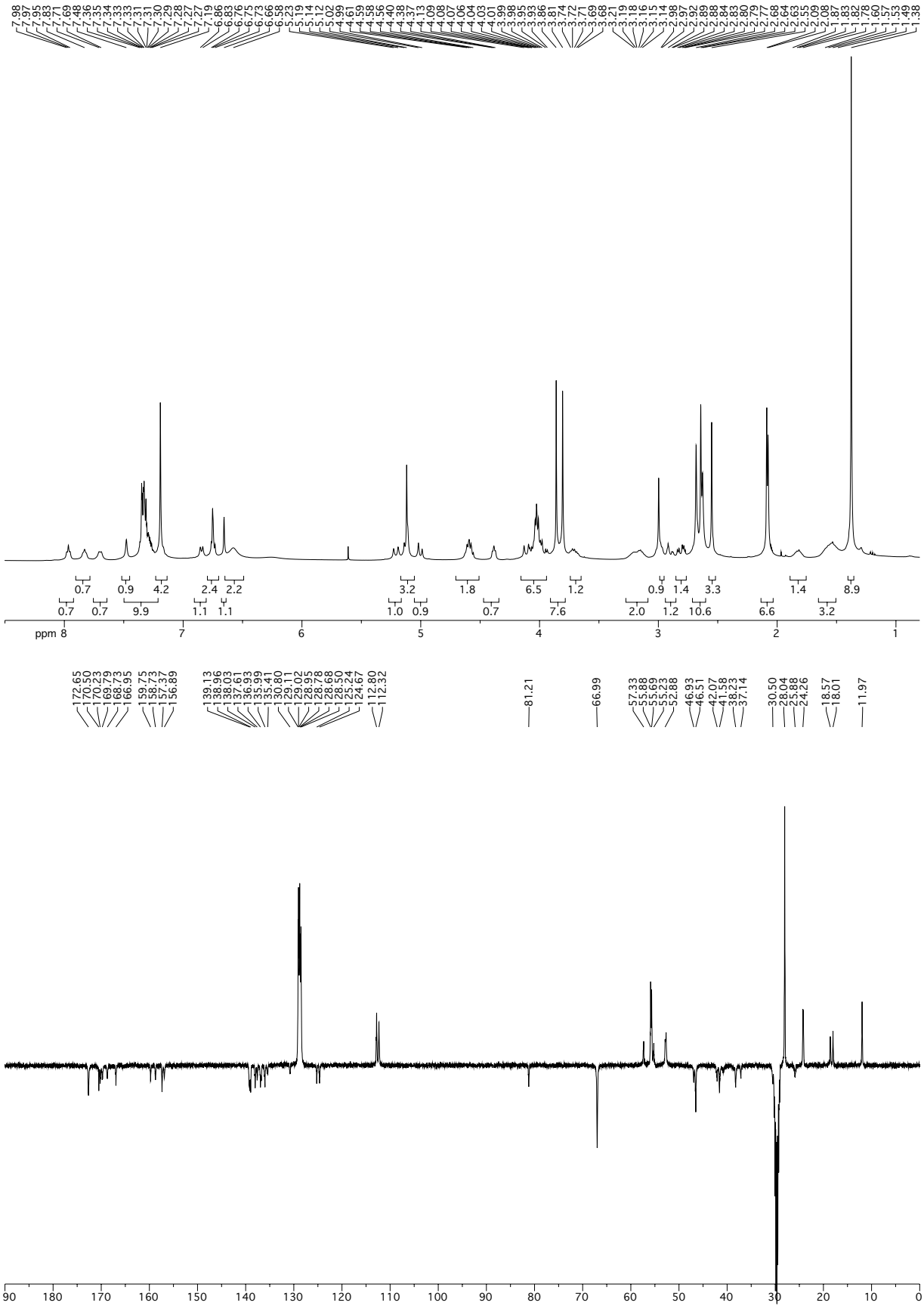

***Cyclo*[DKP-*f*2-Arg(Mtr)-Gly-Asp(O*t*Bu)] 139** [(3*R*, 6*S*), R^1= H, R^2= $CH_2C_6H_4CH_2NHMtr$]

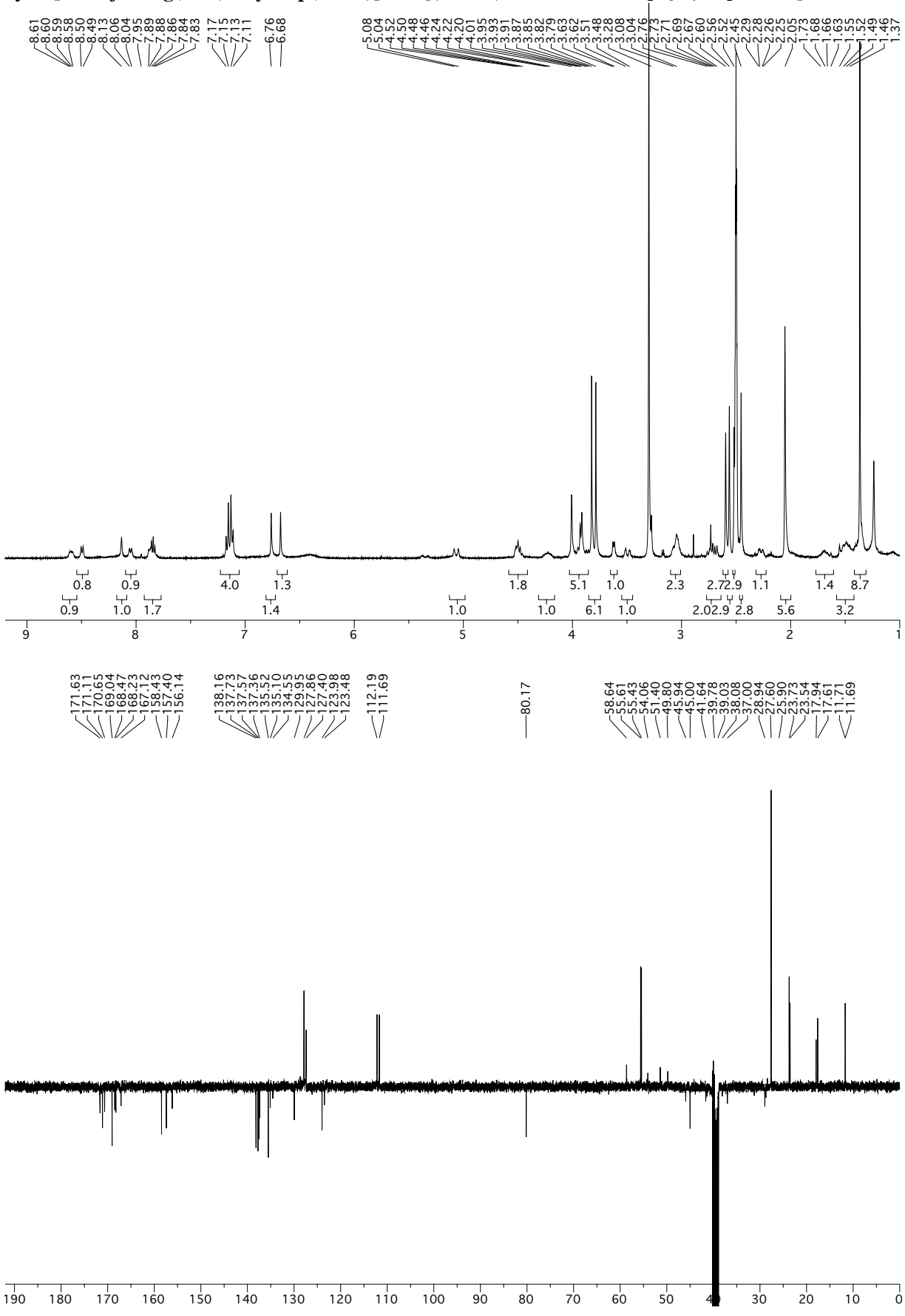

***Cyclo*[DKP-*f*3-Arg(Mtr)-Gly-Asp(O*t*Bu)] 140** [(3*S*, 6*R*), R^1= H, R^2= $CH_2C_6H_4CH_2NHMtr$]

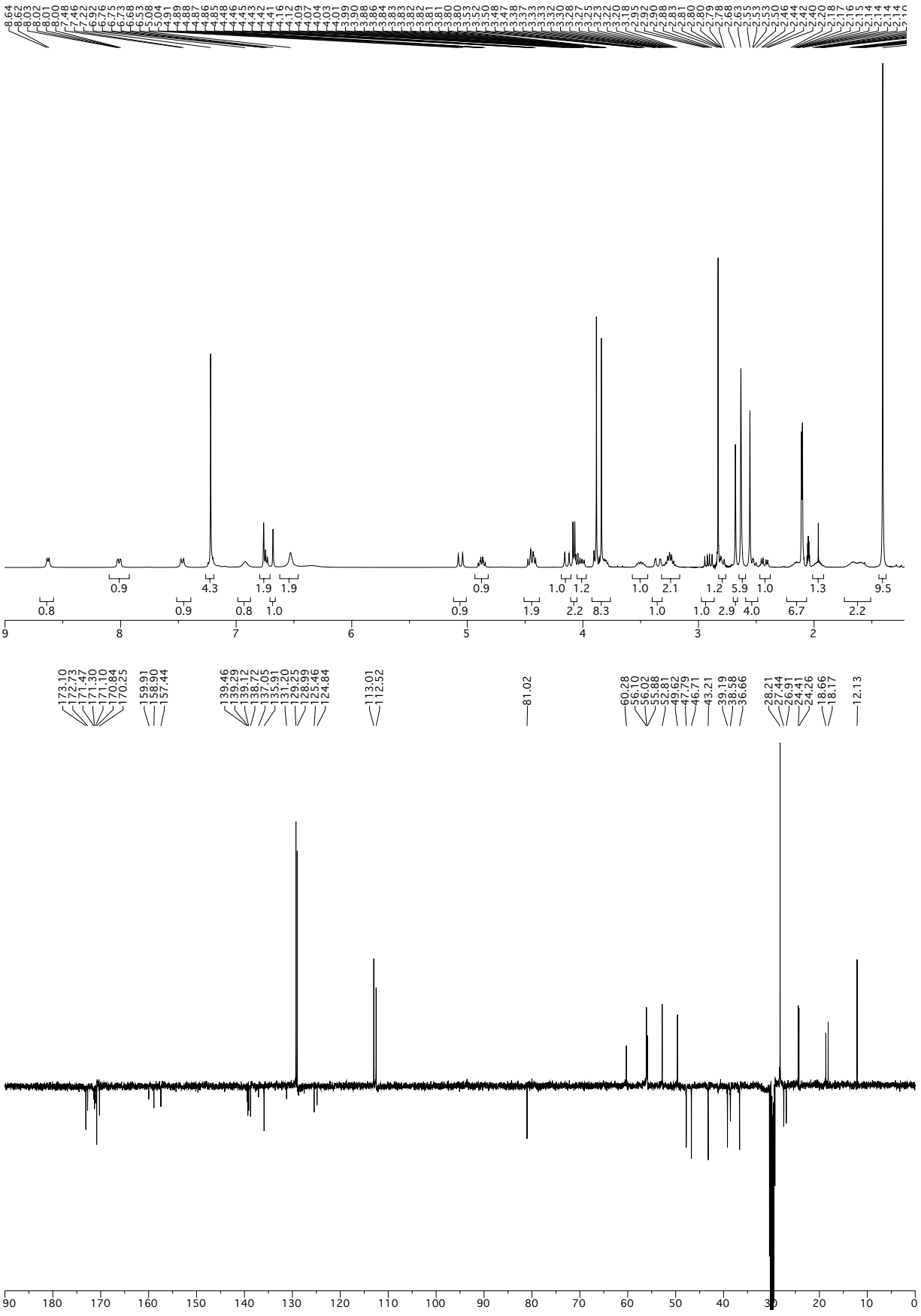

***Cyclo*[DKP-*f*4-Arg(Mtr)-Gly-Asp(O*t*Bu)] 141** [(3*R*, 6*S*), R^1= $CH_2C_6H_4CH_2NHMtr$, R^2= H]

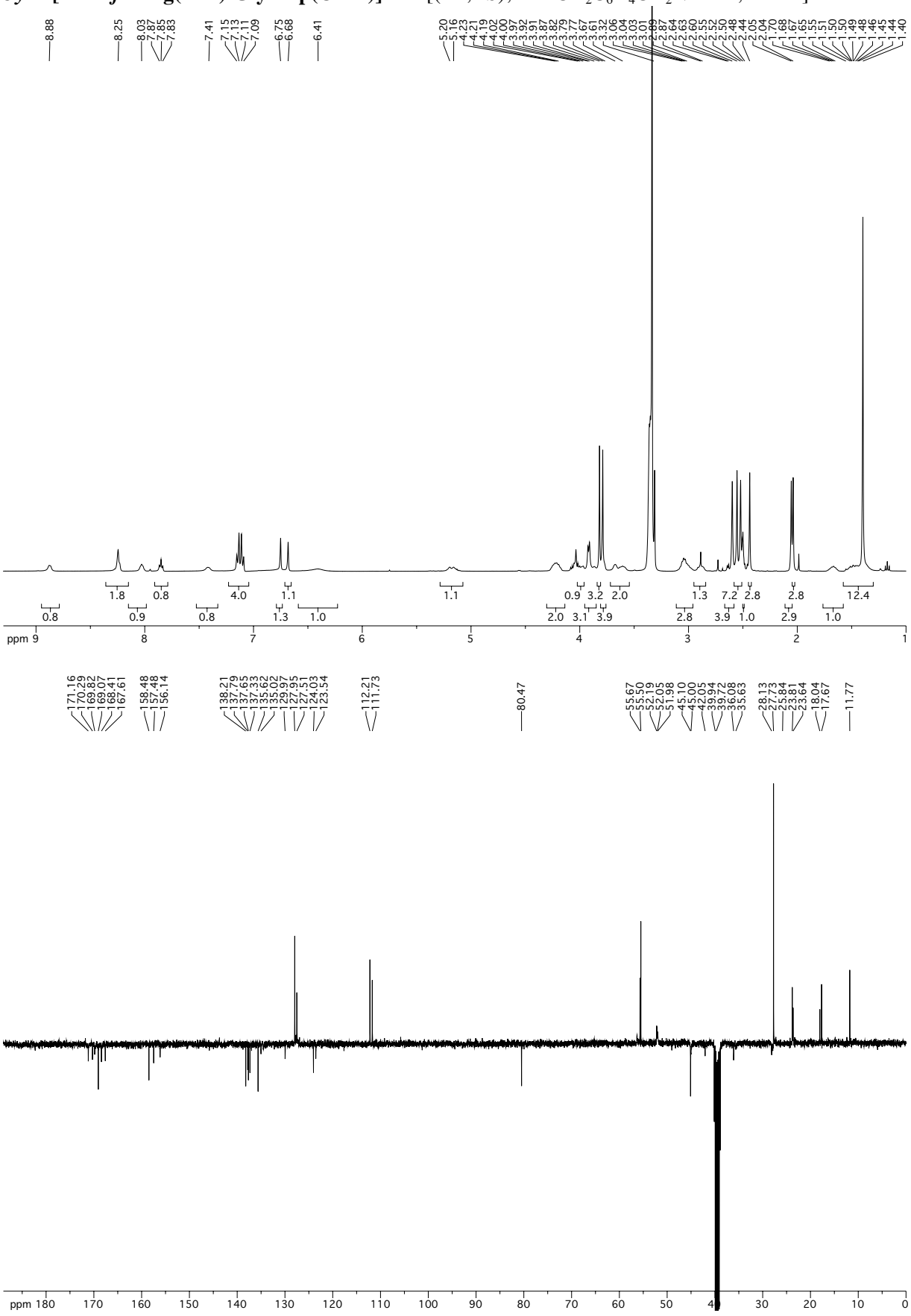

***Cyclo*[DKP-*f*6-Arg(Mtr)-Gly-Asp(O*t*Bu)] 142** [(3*S*, 6*R*), R^1= $CH_2C_6H_4CH_2NHMtr$, R^2= H]

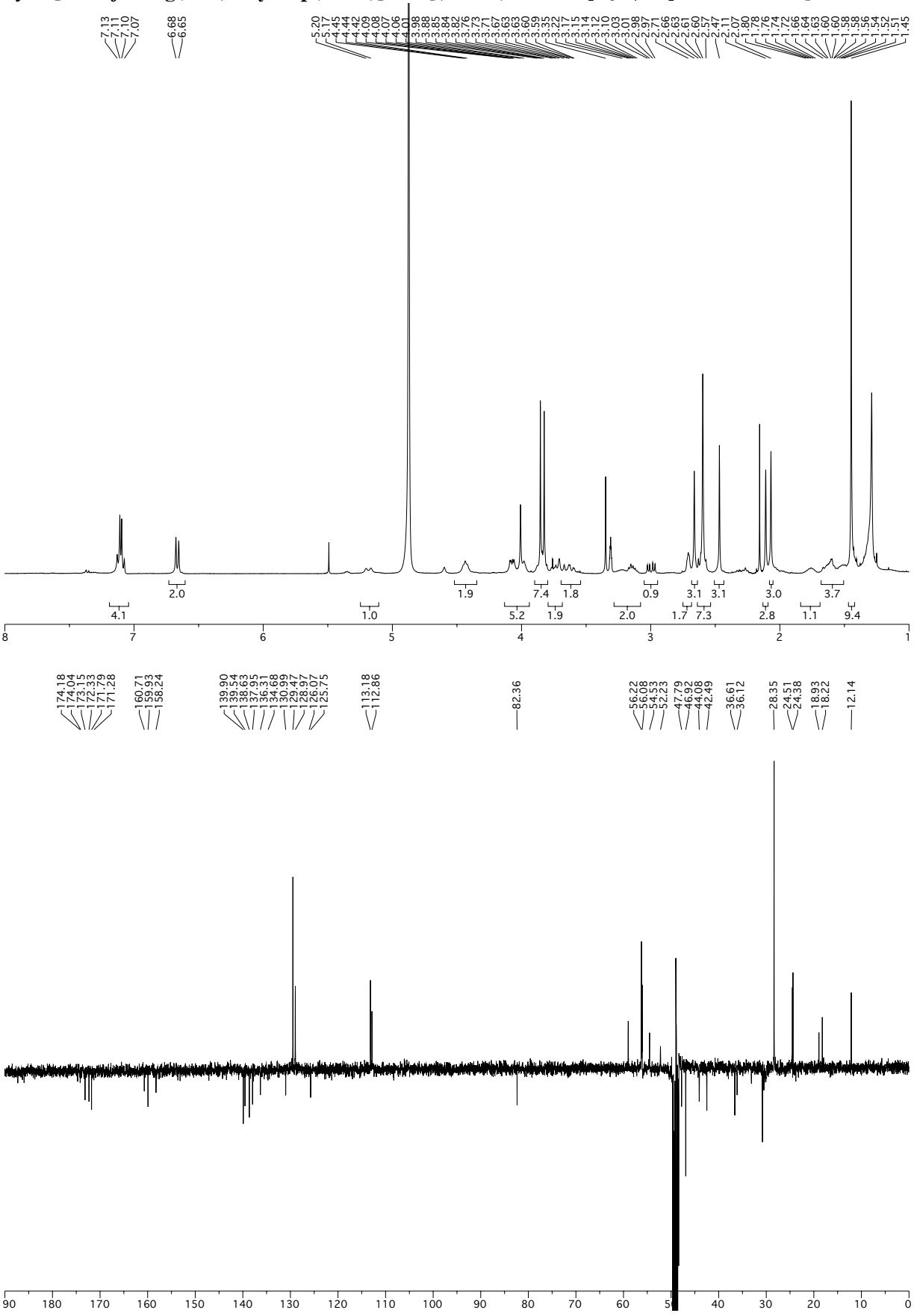

***Cyclo*[DKP-*f*2-Arg-Gly-Asp] 143** [(3*R*, 6*S*), R^1= H, R^2= $CH_2C_6H_4CH_2NH_2$]

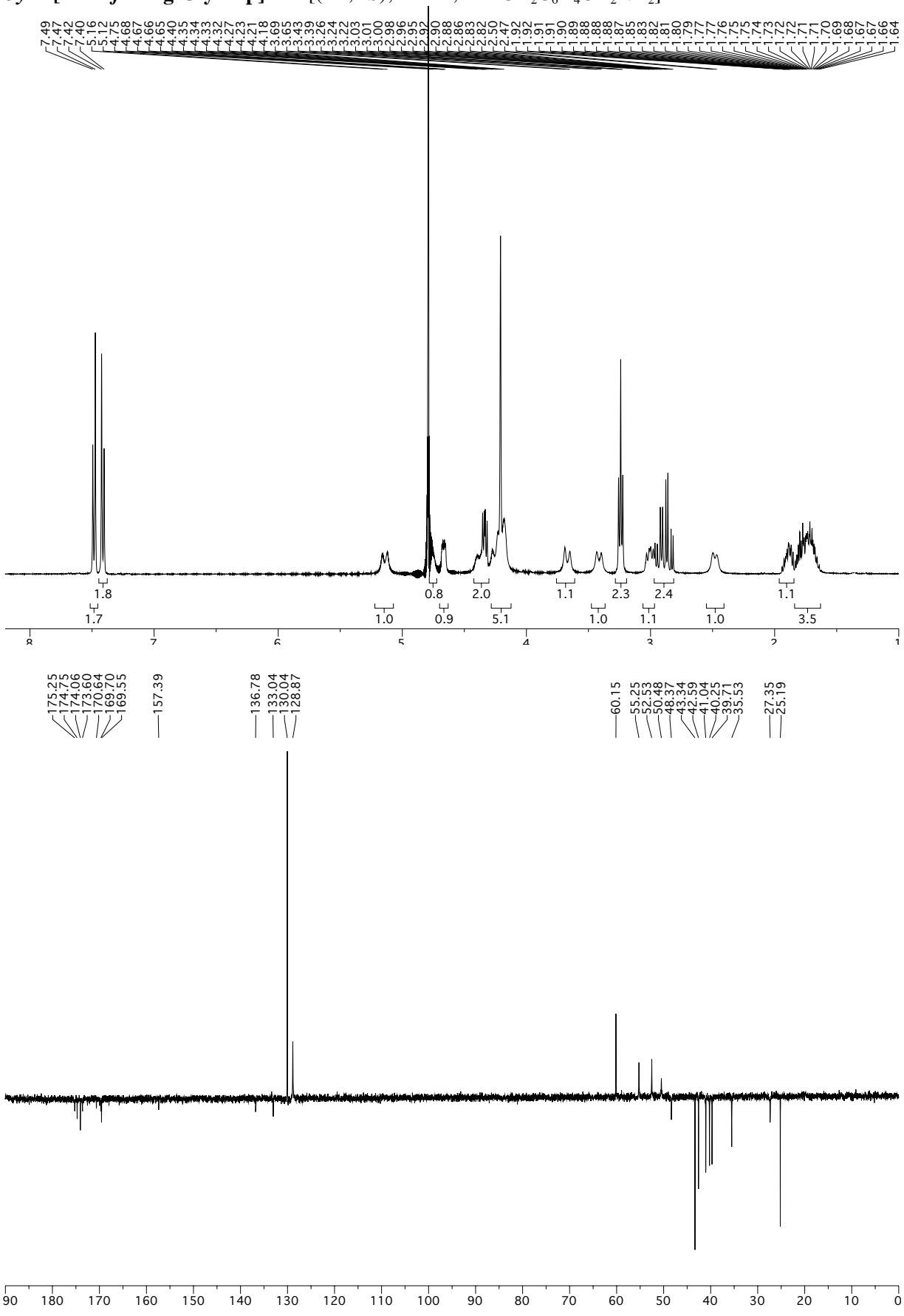

***Cyclo*[DKP-*f*3-Arg-Gly-Asp] 144** [(3*S*, 6*R*), R^1= H, R^2= $CH_2C_6H_4CH_2NH_2$]

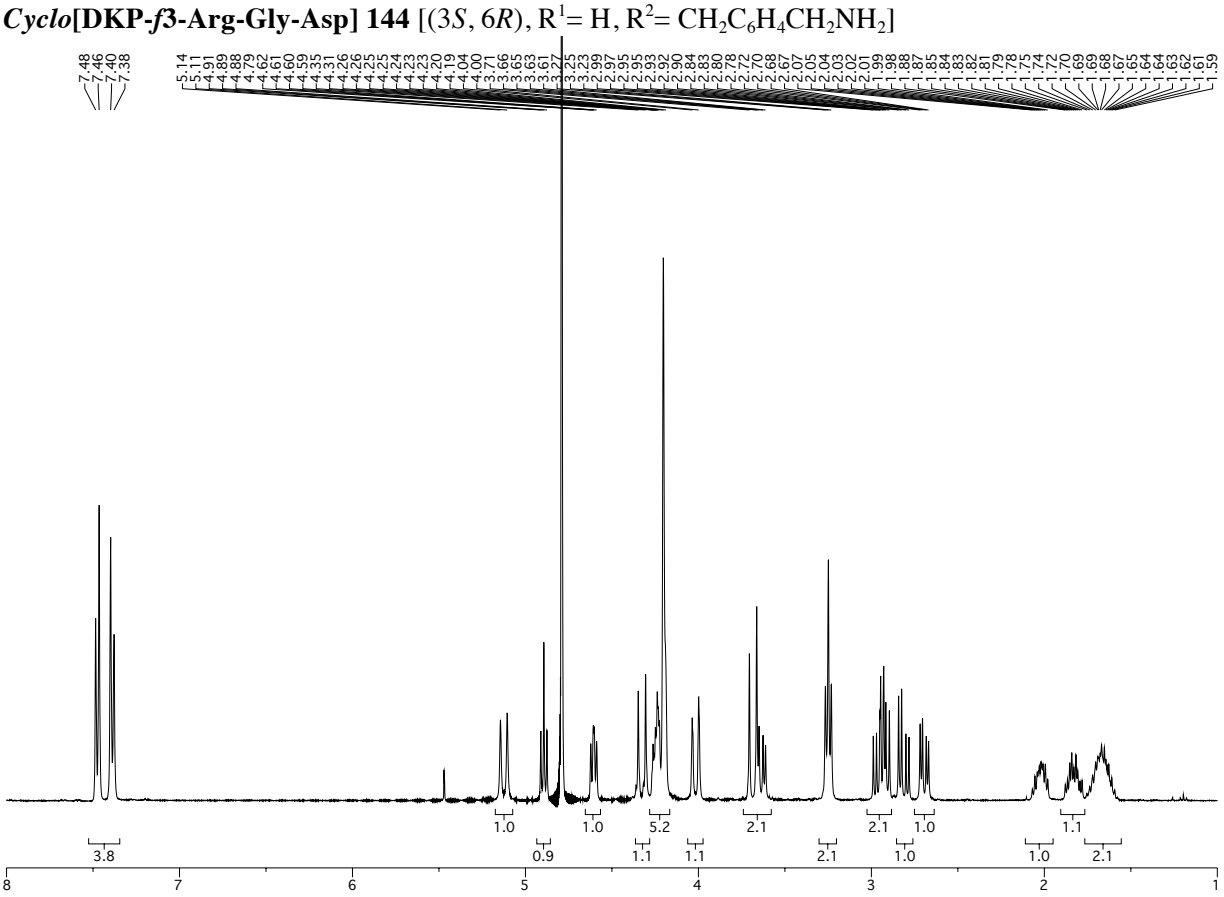

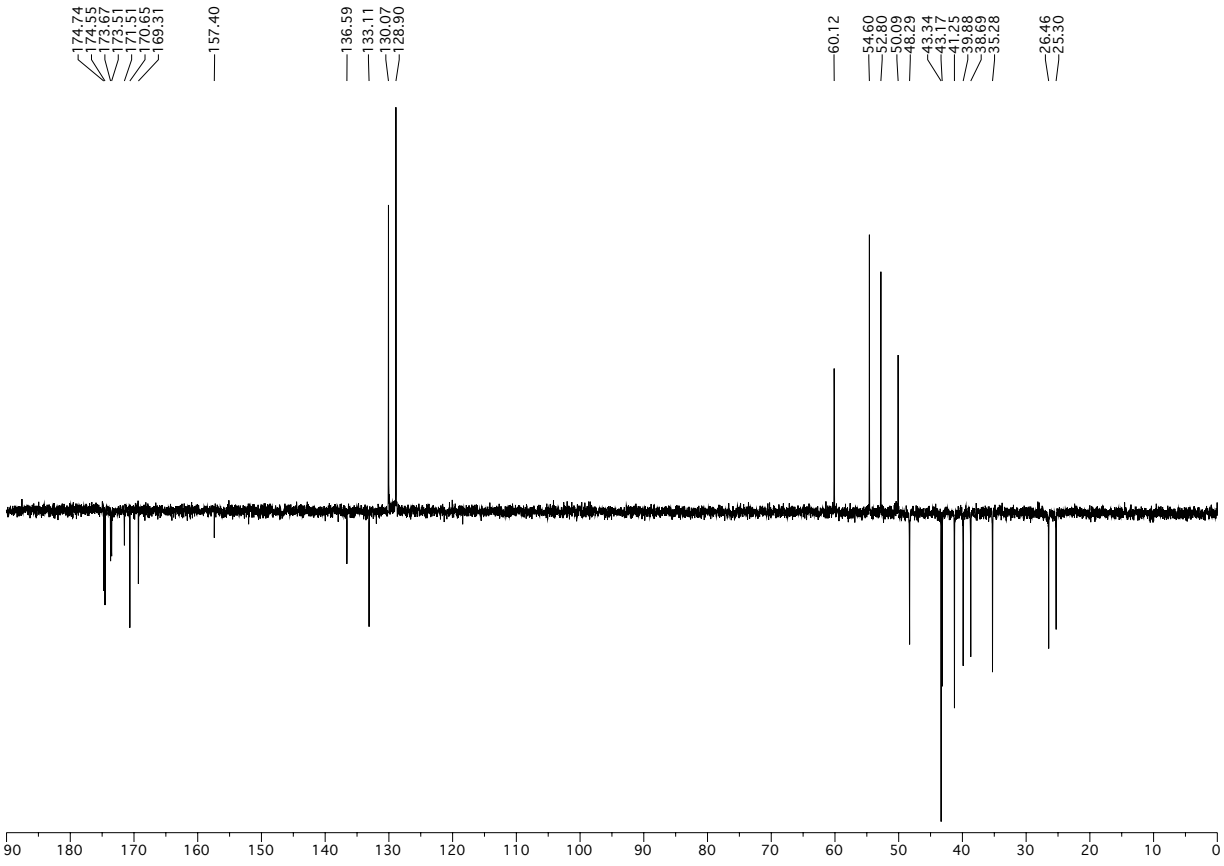

***Cyclo*[DKP-*f*4-Arg-Gly-Asp] 145** [(3*R*, 6*S*), R^1= $CH_2C_6H_4CH_2NH_2$, R^2= H]

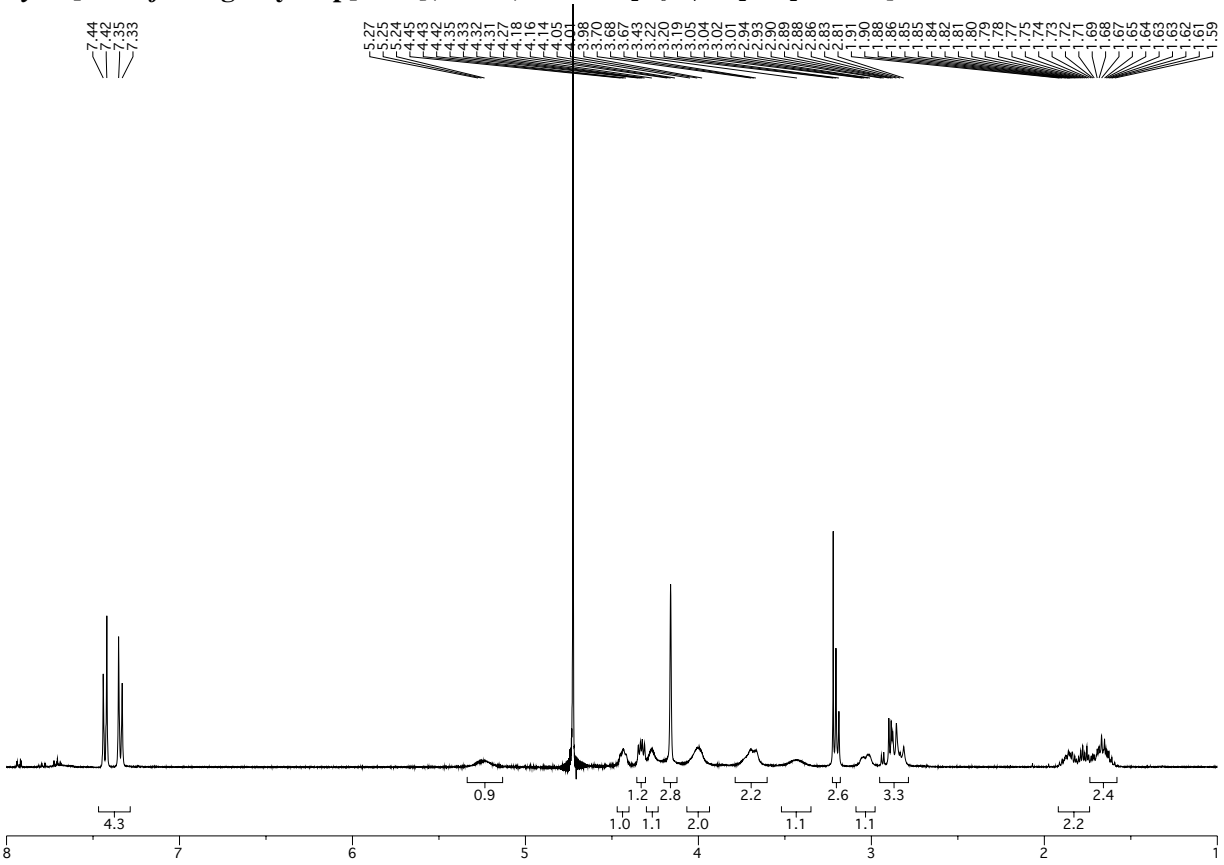

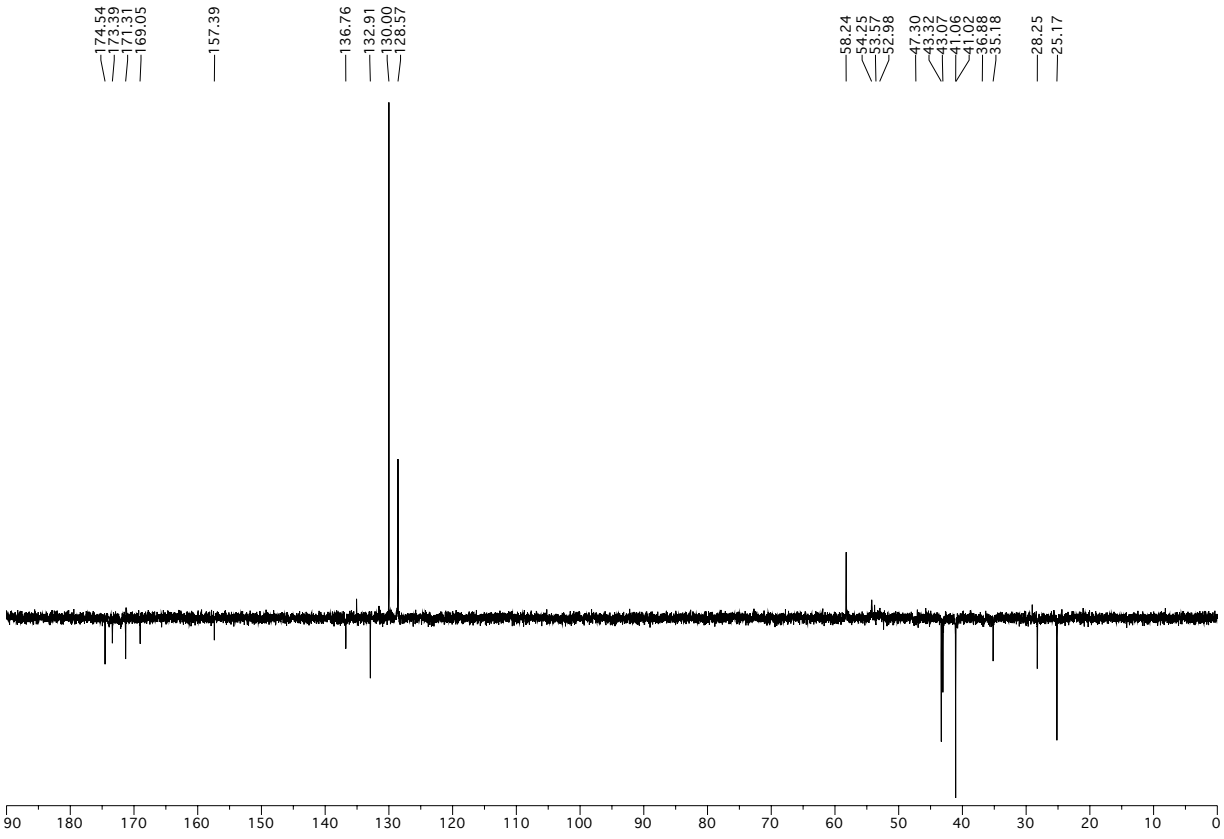

***Cyclo*[DKP-*f*6-Arg-Gly-Asp] 146** [(3*S*, 6*R*), R^1= $CH_2C_6H_4CH_2NH_2$, R^2= H]

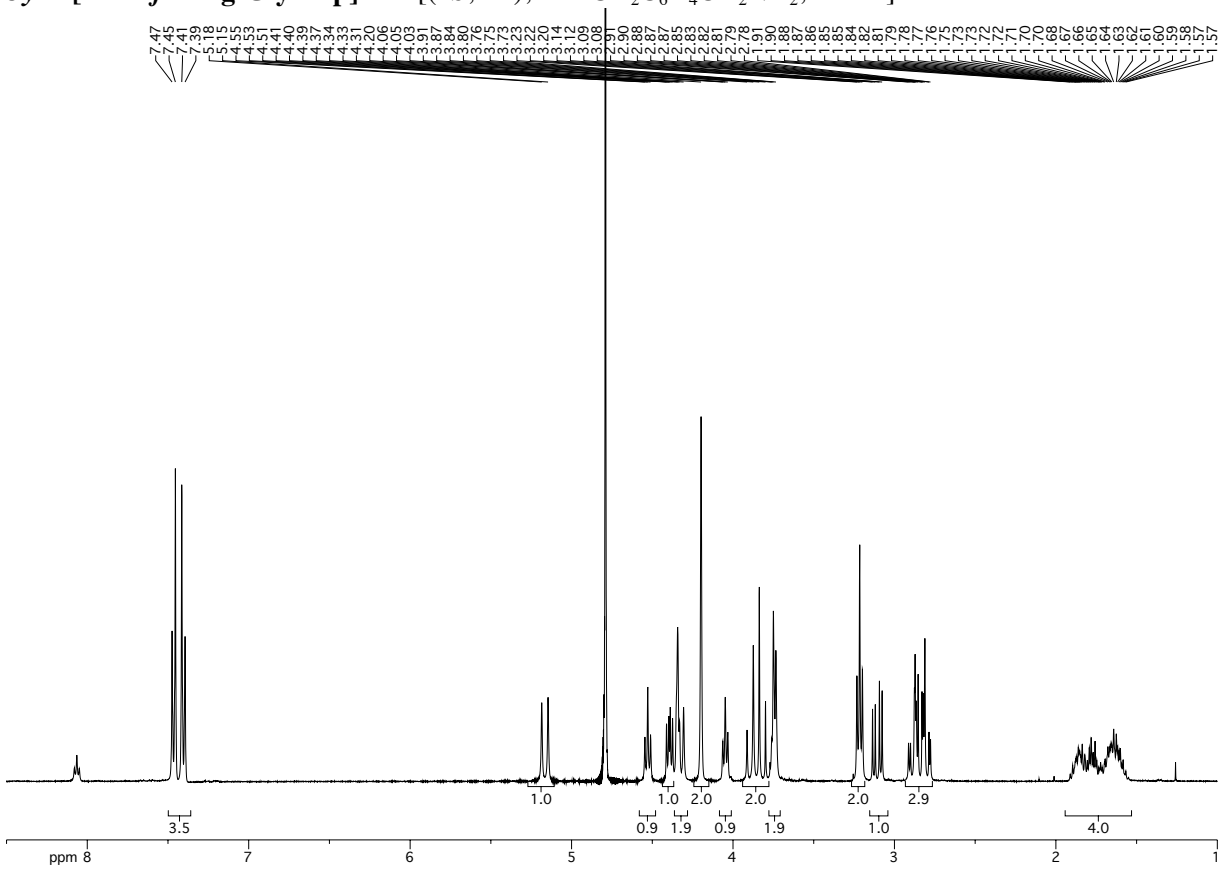

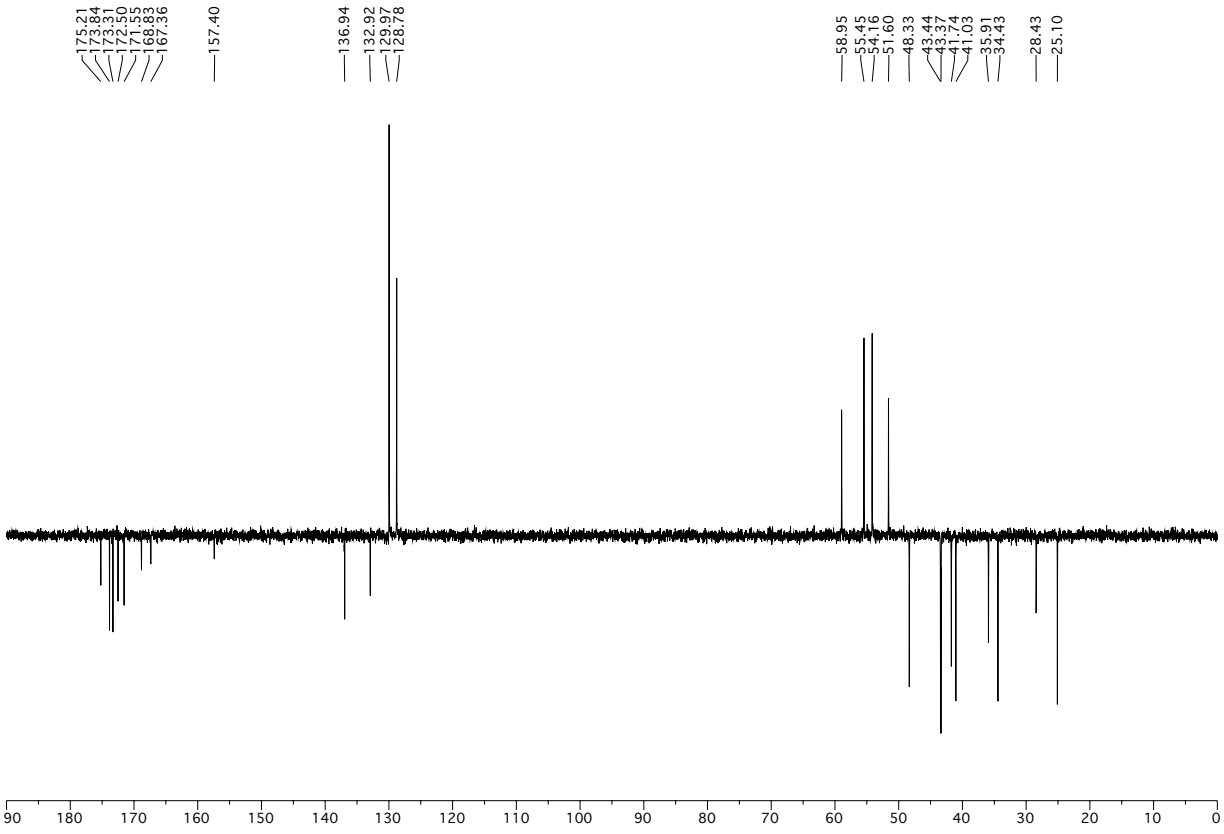

cyclo[DKP-*f*2-RGD]-PTX 90

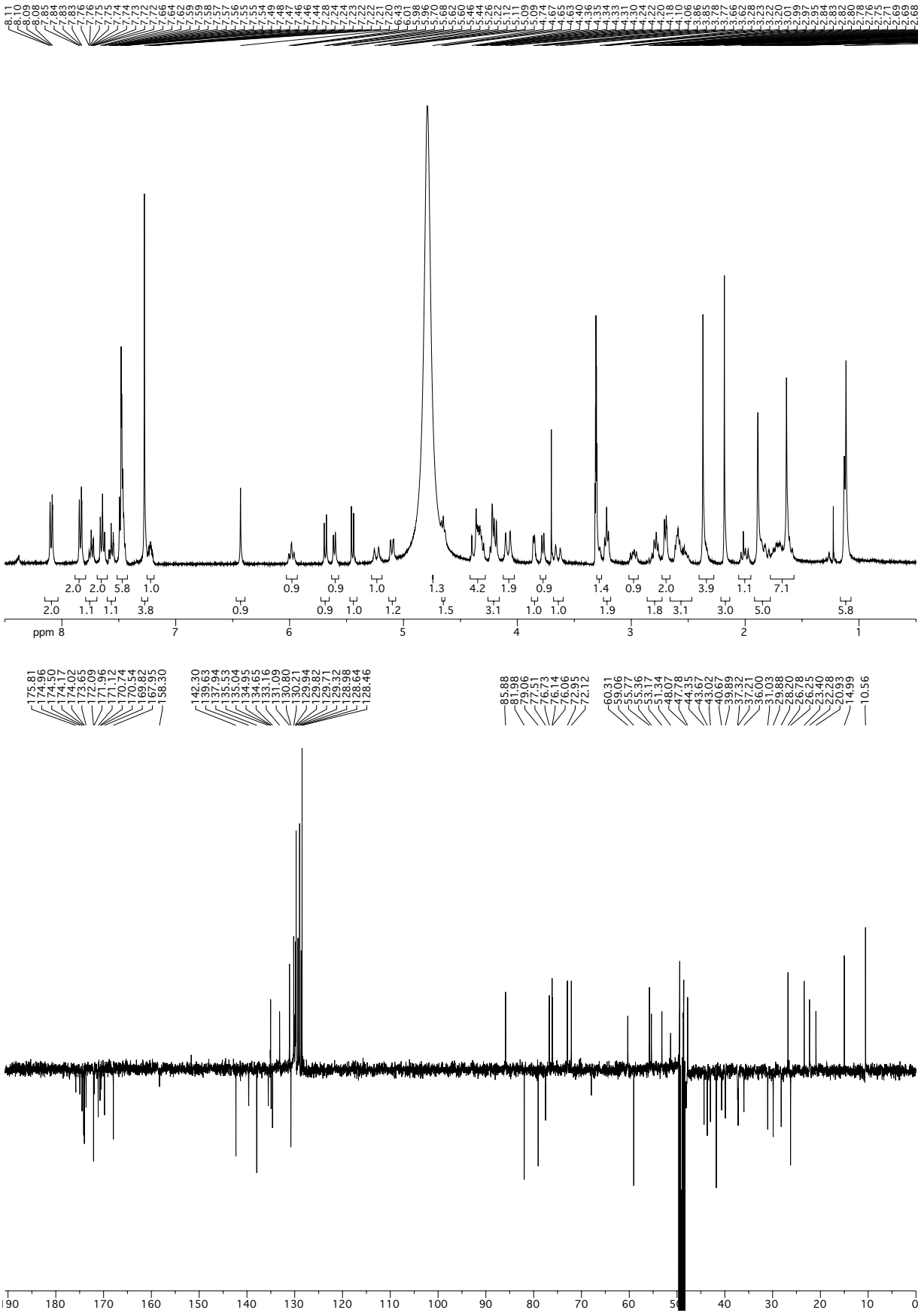

cyclo[DKP-*f*3-RGD]-PTX 91

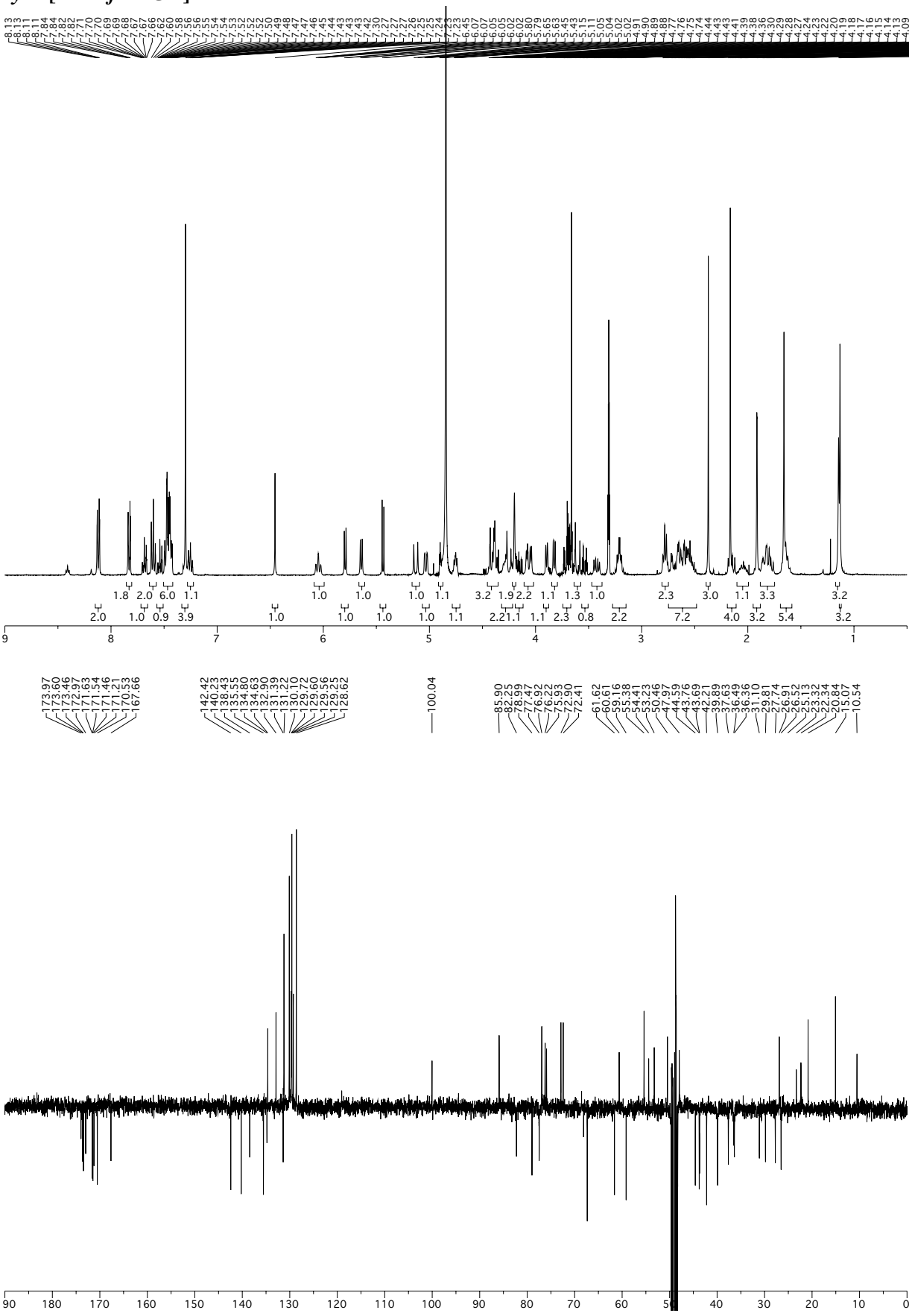

cyclo[DKP-*f*4-RGD]-PTX 92

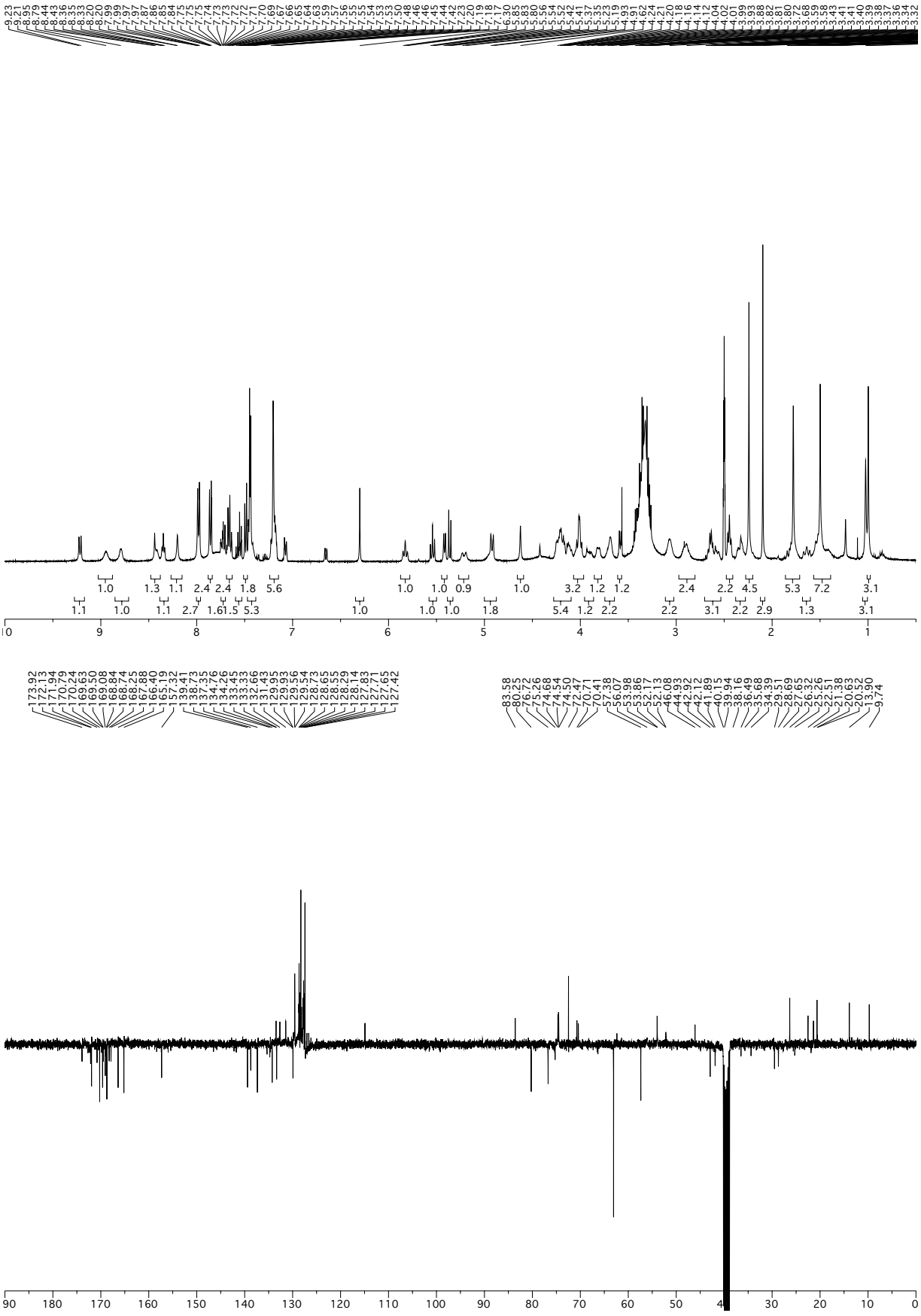

cyclo[DKP-*f*6-RGD]-PTX 93

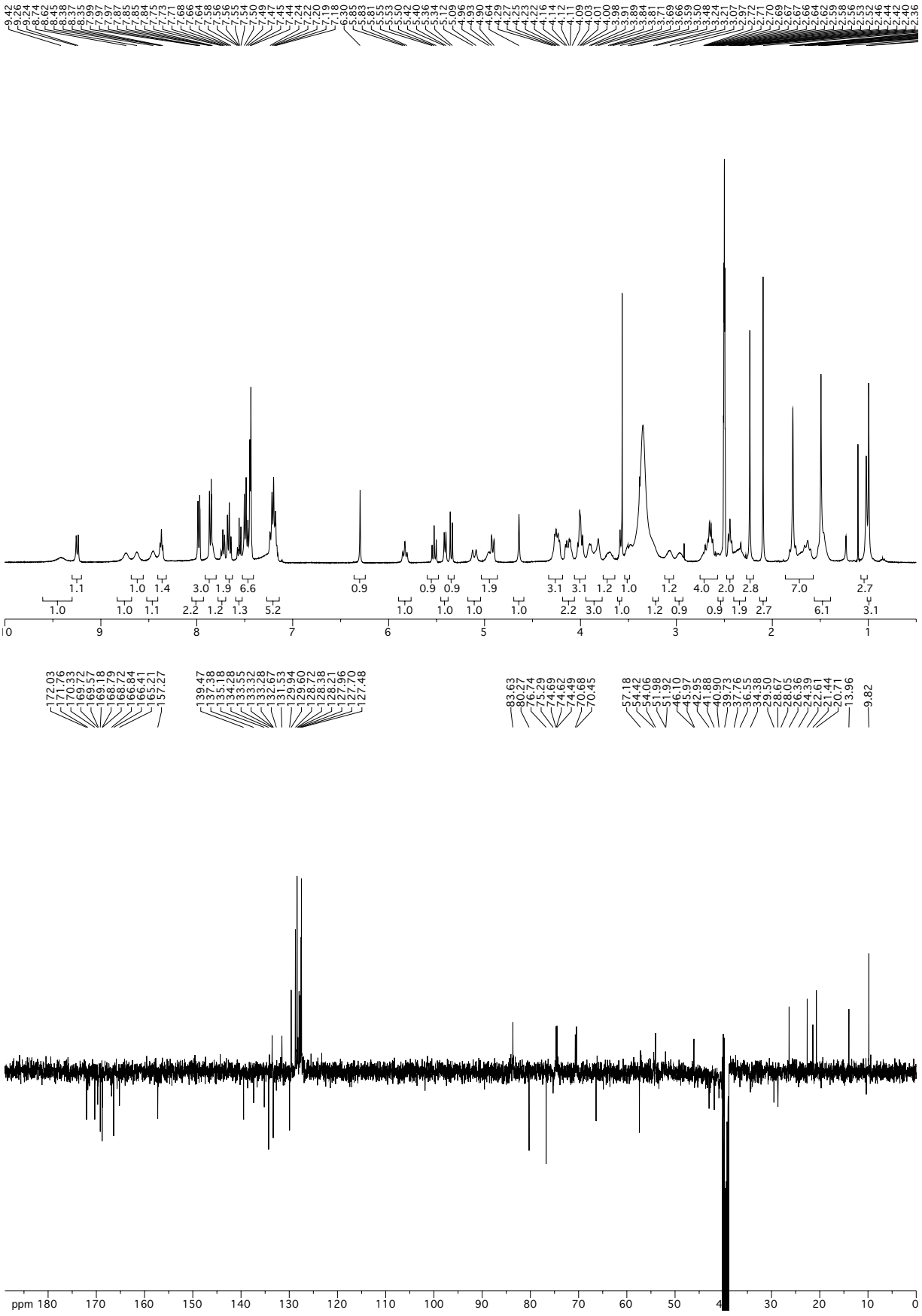

cyclo[DKP-*f*3-RGD] – hemisuccinate 148